SENSING THE WORLD THROUGH PREDICTIONS AND ERRORS

EDITED BY: Ryszard Auksztulewicz, Marta I. Garrido, Manuel S. Malmierca, Alessandro Tavano, Juanita Todd and István Winkler

PUBLISHED IN: Frontiers in Human Neuroscience

frontiers Research Topics

frontiers

ISSN 1664-8714
ISBN 978-2-88976-137-1
DOI 10.3389/978-2-88976-137-1

About Frontiers

Frontiers is more than just an open-access publisher of scholarly articles: it is a pioneering approach to the world of academia, radically improving the way scholarly research is managed. The grand vision of Frontiers is a world where all people have an equal opportunity to seek, share and generate knowledge. Frontiers provides immediate and permanent online open access to all its publications, but this alone is not enough to realize our grand goals.

Frontiers Journal Series

The Frontiers Journal Series is a multi-tier and interdisciplinary set of open-access, online journals, promising a paradigm shift from the current review, selection and dissemination processes in academic publishing. All Frontiers journals are driven by researchers for researchers; therefore, they constitute a service to the scholarly community. At the same time, the Frontiers Journal Series operates on a revolutionary invention, the tiered publishing system, initially addressing specific communities of scholars, and gradually climbing up to broader public understanding, thus serving the interests of the lay society, too.

Dedication to Quality

Each Frontiers article is a landmark of the highest quality, thanks to genuinely collaborative interactions between authors and review editors, who include some of the world's best academicians. Research must be certified by peers before entering a stream of knowledge that may eventually reach the public - and shape society; therefore, Frontiers only applies the most rigorous and unbiased reviews.
Frontiers revolutionizes research publishing by freely delivering the most outstanding research, evaluated with no bias from both the academic and social point of view. By applying the most advanced information technologies, Frontiers is catapulting scholarly publishing into a new generation.

What are Frontiers Research Topics?

Frontiers Research Topics are very popular trademarks of the Frontiers Journals Series: they are collections of at least ten articles, all centered on a particular subject. With their unique mix of varied contributions from Original Research to Review Articles, Frontiers Research Topics unify the most influential researchers, the latest key findings and historical advances in a hot research area! Find out more on how to host your own Frontiers Research Topic or contribute to one as an author by contacting the Frontiers Editorial Office: frontiersin.org/about/contact

SENSING THE WORLD THROUGH PREDICTIONS AND ERRORS

Topic Editors:
Ryszard Auksztulewicz, City University of Hong Kong, Hong Kong, SAR China
Marta I. Garrido, Other, Australia
Manuel S. Malmierca, University of Salamanca, Spain
Alessandro Tavano, Max Planck Institute for Empirical Aesthetics, Max Planck Society, Germany
Juanita Todd, The University of Newcastle, Australia
István Winkler, Research Centre for Natural Sciences, Hungarian Academy of Sciences (MTA), Hungary

Citation: Auksztulewicz, R., Garrido, M. I., Malmierca, M. S., Tavano, A., Todd, J., Winkler, I., eds. (2022). Sensing the World Through Predictions and Errors. Lausanne: Frontiers Media SA. doi: 10.3389/978-2-88976-137-1

Table of Contents

frontiers | Frontiers in Human Neuroscience

EDITORIAL
published: 21 April 2022
doi: 10.3389/fnhum.2022.899529

Editorial: Sensing the World Through Predictions and Errors

Ryszard Auksztulewicz[1,2], *Marta I. Garrido*[3], *Manuel S. Malmierca*[4,5,6], *Alessandro Tavano*[7], *Juanita Todd*[8] *and István Winkler*[9]*

[1] Department of Neuroscience, City University of Hong Kong, Kowloon, Hong Kong SAR, China, [2] European Neuroscience Institute Göttingen, University Medical Center Göttingen and the Max Planck Society, Göttingen, Germany, [3] Melbourne School of Psychological Sciences, The University of Melbourne, Melbourne, VIC, Australia, [4] Cognitive and Auditory Neuroscience Laboratory (CANELAB), Institute for Neuroscience of Castilla y León (INCYL), University of Salamanca, Salamanca, Spain, [5] Department of Cell Biology and Pathology, The Faculty of Medicine, University of Salamanca, Salamanca, Spain, [6] The Salamanca Institute of Biomedical Research, Salamanca, Spain, [7] Department of Neuroscience, Max Planck Institute for Empirical Aesthetics, Frankfurt, Germany, [8] School of Psychology, The University of Newcastle, Callaghan, NSW, Australia, [9] Institute of Cognitive Neuroscience and Psychology, Research Centre for Natural Sciences, Budapest, Hungary

Keywords: perception, sensory attenuation, prediction error, predictive coding, computational modeling, depression, altered state of consciousness, aging

Editorial on the Research Topic

Sensing the World Through Predictions and Errors

One of the critical functions of the brain is to prepare for future states and events. Over the past 40 years, several new theories and mounting empirical evidence have emerged in support of predictive information processing in the brain. Arguably, one the most popular theories is that the brain's computational goal is to minimize prediction errors—the difference between predictions and actual sensory inputs. Thus, "errors" are inseparable from prediction itself. In fact, evidence for predictive processing often comes from measuring prediction errors, which reflect sensory deviance detection (with or without awareness). The current Research Topic pulls together theoretical, empirical, and modeling studies on the role of prediction in perception, often tested by how deviation from what is predictable is processed in the brain. As a teaser for potential readers of this Research Topic, we shortly summarize each paper and their wealth of results, from measuring the response to simple forms of sensory deviation, through testing features of the putative predictive coding framework, to assessing how predictive processes of perception operate in different states of the organism, aging, clinical groups, and in conjunction with behavior.

Prediction error signaling is most commonly studied in oddball paradigms, in which an occasional presentation of an unexpected stimulus, deviating from a sequence of expected standard stimuli, evokes a mismatch response. Such unexpected deviant stimuli can differ from the standards based on multiple sensory features. In an electroencephalography (EEG) based study, An et al. tested whether mismatch responses depend on the sensory features constituting auditory deviants. The study manipulated four acoustic features and identified robust mismatch responses which, in a univariate analysis, were indistinguishable across features. However, the features could be decoded from response topography in a multivariate manner, although at relatively late latencies. These results suggest that mismatch detection may occur prior to deviant feature processing. In a magnetoencephalographic study, Xu et al. focused on the somatosensory modality and manipulated deviant stimuli such that they could be unpredictable (replacing a randomly selected standard) or predictable (presented directly after the unpredictable stimuli). The study identified an early activity component that differentiated between unpredictable and predictable deviants, implying its role in prediction error signaling.

OPEN ACCESS

Edited and reviewed by:
Lutz Jäncke,
University of Zurich, Switzerland

***Correspondence:**
István Winkler
winkler.istvan@ttk.mta.hu

Specialty section:
This article was submitted to Cognitive Neuroscience, a section of the journal Frontiers in Human Neuroscience

Received: *18 March 2022*
Accepted: *28 March 2022*
Published: *21 April 2022*

Citation:
Auksztulewicz R, Garrido MI, Malmierca MS, Tavano A, Todd J and Winkler I (2022) Editorial: Sensing the World Through Predictions and Errors. Front. Hum. Neurosci. 16:899529. doi: 10.3389/fnhum.2022.899529

In contrast, a later activity component differentiated between the deviants and standards, but not between unpredictable and predictable rare stimuli, suggesting that it reflects rareness-related signaling rather than prediction error signaling. Using direct recordings from the cortical surface in rodents, Shiramatsu et al. investigated the relationship between mismatch responses and multisensory integration. Deviant stimuli could be presented in either the auditory or visual modality alone or accompanied by congruent/incongruent stimulation in the other modality. A comparison of mismatch responses across conditions revealed a non-linear relationship between single-modal and cross-modal mismatch responses. Furthermore, local blockage of N-methyl-D-aspartate receptors in the visual cortex diminished mismatch responses to single-modal visual deviants as well as to congruent cross-modal deviants, suggesting cross-modal influences on mismatch signaling.

Going beyond classical oddball paradigm, Kimura investigated visual predictive processing in the context of a phenomenon called representational momentum, which corresponds to a predictive perceptual displacement of a position or rotation of a visual stimulus along its recent regular pattern. By quantifying the amplitude of EEG-based visual event-related potentials (vERP) to a regularly rotated visual bar, the study established an across-participant correlation between the vERP amplitude and subsequent behavioral representational momentum, stressing the role of individual differences in the neural and behavioral correlates of predictive processing.

A corollary of the predictive coding framework is that the saliency of an improbable event increases with the precision of the predictive model, which in turn depends on the variability of the regular features of sound sequences. Increasing the variability of the acoustic regularity reduces the predictive strength of one's internal generative models about the auditory environment. This, in turn is expected to lead to lower precision of predictions and thus a reduced prediction error, indexed by smaller mismatch negativity (MMN) amplitude. Three studies within the current Research Topic of articles tested this hypothesis. SanMiguel et al. demonstrated this empirically by varying regularity stability with ramping the probability of the standard tone and assessing the ERP elicited by the deviant tone. They showed that for the same deviant probability, the MMN amplitude is greater when the probability of the standard increases (i.e., regularity variability decreased). Brace and Sussman found that when two auditory features carry separate regularities, predictions are created for both, irrespective of whether either or none are attended/task relevant. Bader et al. increased the variability of the regularity by replacing one tone within a six-tone pattern with either a white-noise segment (less precise pattern) or a different pitch tone (even less precise pattern). While MMN was similar across conditions, the P3a ERP component was greater for violations of patterns with less regularity variability (greater model precision). In addition, using trial-by-trial modeling of electrocorticographic (ECoG) data, Lecaignard et al. showed that MMN indeed reflects a precision-weighted prediction error that is time-dependent at electrodes located more posteriorly over the scalp than the main MMN response.

How robust, and the same time how flexible, is prediction error as an index of sensory function integrity? The answer to this fundamental question has proven very difficult to provide, as evidenced by Gilbert et al.s' review on disrupted predictions in Major Depression Disorder as far as both sensory deviance detection and reward processing are concerned. To begin casting that picture, Tivadar et al.s' review the evidence for changes in prediction error responses under altered states of consciousness. While the absence of consciousness (e.g., anesthesia and coma) changes the morphology and reduces the amplitude of responses, deviancy may still be registered by sensory-specific neural circuits, e.g., the core auditory cortex. This is confirmed by the study of Nourski et al., who used intracranial electroencephalography (iEEG) to test patients under wake, sedated, and unresponsive stages of anesthesia induction. Using high gamma activity as a dependent measure, they found that core sensory neural circuits (auditory cortex) reflect the positive interaction of local deviant responses generated by short-term stimulation, and global deviant responses generated when stimulation lasts several seconds. Such interaction is reduced but still measurable in sedated participants.

Another often-tacit assumption is that the magnitude of prediction error response should explain a sizeable portion of variance in a tested function, so that a decay in said function would be indexed by a proportionate reduction in deviance detection processes. Said assumption may be difficult to verify. Neubert et al. studied healthy elderly individuals (60–75 years) by correlating the amplitude of the pre-attentive MMN response to violations of predictable sound sequences, with the ability of participants to ignore the same sound sequences used as a behavioral distractor. The absence of a correlation suggests that predictability extraction does not drive the effect of age on predictability-based sensory inhibition. Similarly, Csizmadia et al. found a discontinuity between visual MMN amplitude and the ability to automatically register age of photographed individuals: only in older adults was the visual MMN sensitive to age changes, suggesting the mediation of a familiarity factor. However, if one widens the clinical applications from decay to resilience and expands the dependent measures from ERPs to prediction error-related movements, such as blinks, as was done by Tavano and Kotz, then the relationship between deviancy and behavior may become strong again and reveal novel ways to compose a more complete picture of extensively studied syndromes such as Parkinson's disease.

In sensory attenuation self-generated sensory input is perceived as less intense than the same stimuli generated externally. In a review of this phenomenon in the auditory modality, Kiepe et al. question the traditional explanations based on motor-based forward models and discuss alternative hypotheses regarding the mechanisms underlying sensory attenuation, such as those based on the predictive coding framework. The review also addresses the challenge of isolating Sensory attenuation from other predictive mechanisms.

Predictive coding appeared to have put to bed the longstanding debate around the role of neuronal adaptation

in MMN generation, modeled simply as the result of release from repetition suppression. However, in this Research Topic, an updated adaptation model revives the controversy (May) by showing that recurrent interactions *via* feedforward and feedback short-range connections within the auditory cortex can beautifully simulate MMN to omissions and surprising repetitions, which were critical in ruling out previous hypotheses of adaptation as a plausible mechanism of MMN generation. Hence, physiologically-informed modeling forces the reader to rethink the very implementation of prediction error in the brain.

The wide variety of topics emerging in this article Research Topic demonstrates how deeply the notion of predictive processing permeates current scientific thinking of perception. While even some of the basic assumptions for the role of prediction in perception require further testing, significant advances have been made on mapping out a neural system based on predictive principles. Understanding how these predictive principles are implemented in the brain will have critical implication for our fundamental understanding of altered states of consciousness, as well as neurological and psychiatric conditions.

AUTHOR CONTRIBUTIONS

All authors listed have made a substantial, direct, and intellectual contribution to the work and approved it for publication.

FUNDING

The financial support to MM was provided by the Spanish Agencia Estatal de Investigación (AEI; PID2019-104570RB-I00), the European Union's Horizon 2020 research and innovation programme (grant agreement No 952378 - BrainTwin), and the Foundation Ramón Areces and the Consejería de Educación de la Junta de Castilla y León (SA252P20). JT was supported by the Australian Research Council (DP200102346). IW was supported by the National Research Development and Innovation Office, Hungary (K132642).

Conflict of Interest: The authors declare that the research was conducted in the absence of any commercial or financial relationships that could be construed as a potential conflict of interest.

Publisher's Note: All claims expressed in this article are solely those of the authors and do not necessarily represent those of their affiliated organizations, or those of the publisher, the editors and the reviewers. Any product that may be evaluated in this article, or claim that may be made by its manufacturer, is not guaranteed or endorsed by the publisher.

frontiers in Human Neuroscience

BRIEF RESEARCH REPORT
published: 01 February 2021
doi: 10.3389/fnhum.2021.613903

Do Auditory Mismatch Responses Differ Between Acoustic Features?

HyunJung An[1], *Shing Ho Kei*[1], *Ryszard Auksztulewicz*[1,2*†] *and Jan W. H. Schnupp*[1*†]

[1] *Department of Neuroscience, City University of Hong Kong, Kowloon, Hong Kong,* [2] *Department of Neuroscience, Max Planck Institute for Empirical Aesthetics, Frankfurt, Germany*

Mismatch negativity (MMN) is the electroencephalographic (EEG) waveform obtained by subtracting event-related potential (ERP) responses evoked by unexpected deviant stimuli from responses evoked by expected standard stimuli. While the MMN is thought to reflect an unexpected change in an ongoing, predictable stimulus, it is unknown whether MMN responses evoked by changes in different stimulus features have different magnitudes, latencies, and topographies. The present study aimed to investigate whether MMN responses differ depending on whether sudden stimulus change occur in pitch, duration, location or vowel identity, respectively. To calculate ERPs to standard and deviant stimuli, EEG signals were recorded in normal-hearing participants ($N = 20$; 13 males, 7 females) who listened to roving oddball sequences of artificial syllables. In the roving paradigm, any given stimulus is repeated several times to form a standard, and then suddenly replaced with a deviant stimulus which differs from the standard. Here, deviants differed from preceding standards along one of four features (pitch, duration, vowel or interaural level difference). The feature levels were individually chosen to match behavioral discrimination performance. We identified neural activity evoked by unexpected violations along all four acoustic dimensions. Evoked responses to deviant stimuli increased in amplitude relative to the responses to standard stimuli. A univariate (channel-by-channel) analysis yielded no significant differences between MMN responses following violations of different features. However, in a multivariate analysis (pooling information from multiple EEG channels), acoustic features could be decoded from the topography of mismatch responses, although at later latencies than those typical for MMN. These results support the notion that deviant feature detection may be subserved by a different process than general mismatch detection.

Keywords: electroencephalography, mismatch negativity, predictive coding, auditory processing, multivariate decoding

OPEN ACCESS

Edited by:
Martin Sommer,
University of Göttingen, Germany

Reviewed by:
Lavinia Slabu,
Université Côte d'Azur, France
Erich Schröger,
Leipzig University, Germany

***Correspondence:**
Jan W. H. Schnupp
wschnupp@cityu.edu.hk
Ryszard Auksztulewicz
rikismo@gmail.com

† These authors have contributed equally to this work

Specialty section:
This article was submitted to Cognitive Neuroscience, a section of the journal Frontiers in Human Neuroscience

Received: *04 October 2020*
Accepted: *07 January 2021*
Published: *01 February 2021*

Citation:
An H, Ho Kei S, Auksztulewicz R and Schnupp JWH (2021) Do Auditory Mismatch Responses Differ Between Acoustic Features? Front. Hum. Neurosci. 15:613903. doi: 10.3389/fnhum.2021.613903

INTRODUCTION

Neural activity is typically suppressed in response to expected stimuli and enhanced following novel stimuli (Carbajal and Malmierca, 2018). This effect is often summarized as a mismatch response, calculated by subtracting the neural response waveform to unexpected deviant stimuli from the response to expected standard stimuli. Auditory deviance detection has been associated with a human auditory-evoked potential, the mismatch negativity, occurring at about 150–250 ms from sound change onset (Naatanen, 2007; Garrido et al., 2008). The principal neural sources of the MMN are thought to be superior temporal regions adjacent to the primary auditory cortex, as

well as frontoparietal areas (Doeller et al., 2003; Chennu et al., 2013). Initially, the MMN was interpreted as a correlate of pre-attentive encoding of physical features between standard and deviant sounds (Doeller et al., 2003). However, more recent studies have led to substantial revisions of this hypothesis, and currently, the most widely accepted explanation of the MMN is that it reflects a prediction error response.

An important theoretical question remains whether mismatch signaling has a domain-general or domain-specific (feature-dependent) implementation in the auditory processing pathway. A recent study using invasive recordings from the cortical surface (Auksztulewicz et al., 2018) demonstrated that neural mechanisms of predictions regarding stimulus contents ("what") and timing ("when") can be dissociated in terms of their topographies and latencies throughout the frontotemporal network, and that activity in auditory regions is sensitive to interactions between different kinds of predictions. Additionally, biophysical modeling of the measured signals has shown that predictions of contents and timing are best explained either by short-term plasticity or by classical neuromodulation, respectively, suggesting separable mechanisms for signaling different kinds of predictions. However, these dissociations might be specific to predictions of contents vs. timing, which may have fundamentally different roles in processing stimulus sequences (Friston and Buzsaki, 2016).

Interestingly, an earlier magnetoencephalography (MEG) study (Phillips et al., 2015) provided evidence for a hierarchical model, whereby violations of sensory predictions regarding different stimulus contents were associated with similar response magnitudes in auditory cortex, but different connectivity patterns at hierarchically higher levels of the frontotemporal network. This result is consistent with the classical predictive coding hypothesis in which reciprocal feedforward and feedback connections at the lower levels of the hierarchy are thought to signal prediction errors and predictions regarding simple sensory features, but hierarchically higher levels are thought to signal more complex predictions and prediction errors, integrating over multiple features (Kiebel et al., 2008). Several studies, however, reported independent processing of prediction violations along different acoustic features or sound dimensions. An earlier study (Giard et al., 1995) investigated the neural correlates of mismatch processing across three different acoustic features (frequency, intensity, and duration). Mismatch responses to each feature were source-localized by fitting equivalent current dipoles to EEG signals, and the results indicated that violations of different features can be linked to dissociable sources, suggesting the involvement different underlying populations. Similar conclusions have been reached in another set of studies (Schroger, 1995; Paavilainen et al., 2001), which quantified the additivity of MMN to changes along different acoustic features, either in isolation or by combining two or more features. In these studies, the MMN response to violating two features could largely be reproduced by adding the MMN responses to violating two single features, suggesting that the latter are mutually independent. A more recent study has combined these two approaches (source localization and additivity analyses), demonstrating partial independence of three different timbre dimensions (Caclin et al., 2006). The notion that mismatch responses to violations of different features are mediated by independent mechanisms is also supported by studies showing that MMN (as well as the later P3a component) typically decreases following two identical deviants presented in direct succession, but remains stable following two deviants which vary from the standard along different features (for a review, see Rosburg et al., 2018).

However, in most previous studies (Giard et al., 1995; Schroger, 1995; Paavilainen et al., 2001; Phillips et al., 2015; Rosburg et al., 2018), physical differences between deviants and standards were not behaviorally matched across different features or participants, raising the possibility that differences in mismatch-evoked activity might to some extent be explained by differences in stimulus salience (Shiramatsu and Takahashi, 2018). This was also the case in the more recent studies on MMN responses to multiple acoustic features (Phillips et al., 2015) or in previous roving paradigms (Garrido et al., 2008). Interestingly, a recent study investigating the MMN to acoustic violations along multiple independent features in the auditory cortex of anesthetized rats (An et al., 2020) revealed that the topography of MMN signals was highly diverse across not only acoustic features but also individual animals, even though several sources of inter-subject variability (e.g., electrode placement) were better controlled than in typical non-invasive studies, suggesting that the spatial resolution of non-invasive methods such as EEG or MEG might not be sufficient for mapping more subtle differences between mismatch responses to violations of different features. The few EEG studies that did use behaviourally matched deviant sounds across different features either used very small sample sizes ($N = 8$; Deouell and Bentin, 1998) or were limited to relatively specialized perceptual characteristics (e.g., different timbre features; Caclin et al., 2006). In contrast, our study used a larger sample size ($N = 20$) and manipulated relatively general sound dimensions (location, pitch, duration, and syllable identity). Our primary goal was to test whether mismatch responses to violations of different features differ in magnitude or latency, in an attempt to replicate previous studies (Deouell and Bentin, 1998). However, in addition to testing the effects of acoustic feature on the MMN time-course in a mass-univariate analysis (i.e., on an electrode-by-electrode basis), we also aimed at decoding acoustic features from differences in MMN topography in a multivariate analysis (i.e., pooling signals from multiple electrodes).

MATERIALS AND METHODS

Participants

Twenty volunteers (13 males and 7 females; mean age 23.9 years old) enrolled in the study upon written informed consent. All participants self-reported as having normal hearing and no history of neurological disorders, and all but two were right-handed. All participants but one were native Hong Kong residents, and their mother tongue was Cantonese. A musical training questionnaire indicated that 16 participants had no musical training, and the remaining participants had <4 years' experience in playing a musical instrument. Participants were

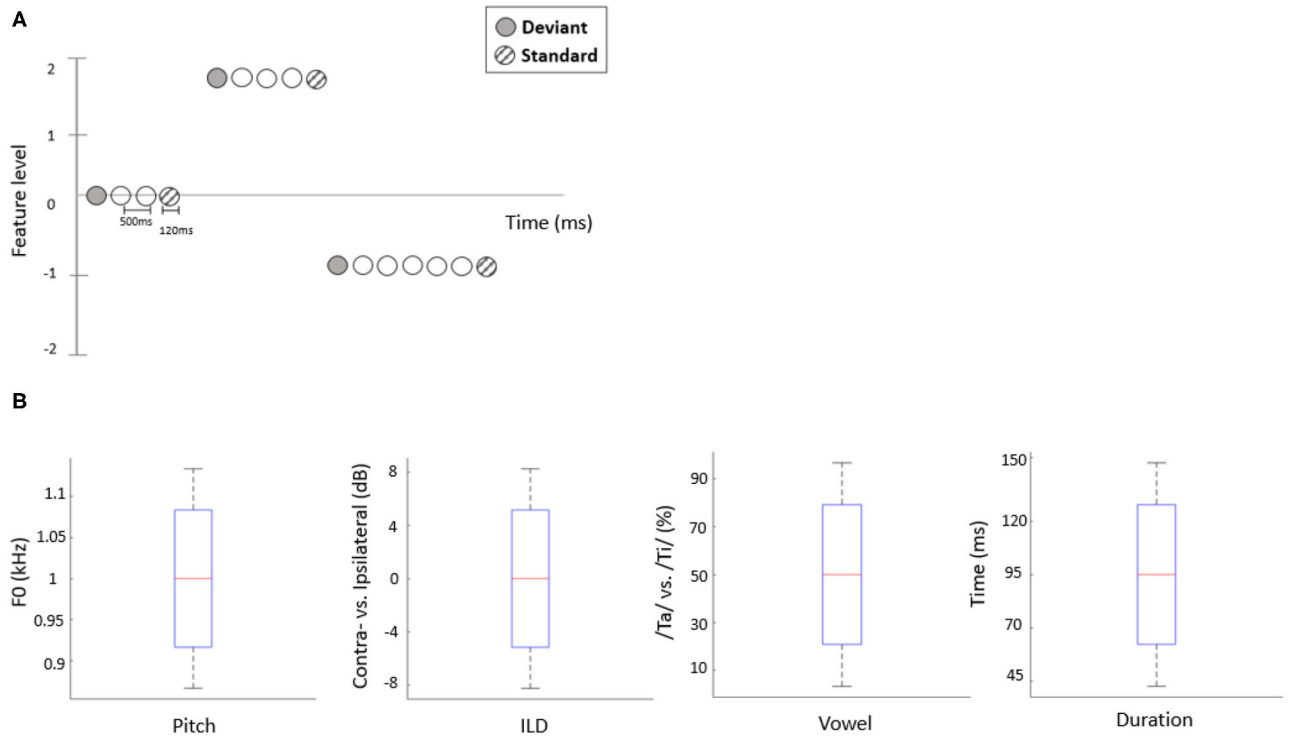

FIGURE 1 | (A) Schematic representation of the stimulation sequences. The first stimulus in each train (solid circles) represents a deviant sound, while the last (hatched circles) represents a standard sound. **(B)** The range of each acoustic feature used to construct stimuli in the EEG experiment. Red line indicates the median value of each feature (across participants), blue bars and black whiskers represent mean and SD of upper and lower ranges across participants.

seated in a sound-attenuated and electrically shielded room in front of a computer screen. They were instructed to fixate on a fixation cross displayed on the screen during the acoustic stimulation. All experimental procedures were approved by the Human Subjects Ethics Sub-Committee of the City University of Hong Kong.

Stimuli

The present study employed a roving oddball paradigm in which auditory deviants could differ from preceding standards along one of four independent acoustic features. Specifically, we manipulated two consonant-vowel (CV) syllable stimuli, /ta/ and /ti/ (Retsa et al., 2018), along the following independent acoustic features: duration, pitch, interaural level difference (ILD) or vowel (An et al., 2020). Prior to the EEG recording, per participant, we estimated the feature interval yielding ∼80% behavioral performance by employing a 1-up-3-down staircase procedure. In each staircase trial, two out of three stimuli, chosen at random, were presented at a mean level of a given feature (e.g., a 50/50 vowel mixture or a 0 dB ILD) while the third stimulus was higher or lower than the mean level by a certain interval. Participants had to indicate which stimulus was the "odd one out." Following three consecutive hits, the interval decreased by 15%; following a mistake, the interval increased by 15%. Each participant performed 30 staircase trials for each feature (**Figure 1B**). For the roving oddball stimulus sequences, the stimulus duration was set to 120 ms and the inter-stimulus intervals (ISIs) were fixed at 500 ms. Stimuli formed a roving oddball sequence: after 4–35 repetitions of a given stimulus (forming a standard), it was replaced with another (deviant) stimulus, randomly drawn from the set of 5 possible levels (**Figure 1A**). Roving oddball sequences corresponding to different features were administered in separate blocks, in a randomized order across participants. The total number of stimuli in each block was ∼2,000, including 200 deviant stimuli and 200 corresponding (immediately preceding) standards.

Experimental Procedure

We recorded signals from 64 EEG channels in a 10–20 system using an ANT Neuro EEG Sports amplifier. EEG channels were grounded at the nasion and referenced to the Cpz electrode. Participants were seated in a quiet room and fitted with Brainwavz B100 earphones, which delivered the audio stimuli via a MOTU Ultralite MK3 USB soundcard at 44.1 kHz. EEG signals were pre-processed using the SPM12 Toolbox for MATLAB. The continuous signals were first notch-filtered between 48 and 52 Hz and band-pass filtered between 0.1 and 90 Hz (both filters: 5th order zero-phase Butterworth), and then downsampled to 300 Hz. Eye blinks were automatically detected using the Fp1 channel, and the corresponding artifacts were removed by subtracting the two principal spatiotemporal components associated with each eye blink from all EEG channels (Ille

et al., 2002). Then, data were re-referenced to the average of all channels, segmented into epochs ranging from −100 ms before to 400 ms after each stimulus onset, baseline-corrected to the average pre-stimulus voltage, and averaged across trials to obtain ERPs for deviants and standards for each of the four acoustic features.

Data Analyses

First, to establish the presence of the MMN response, we converted the EEG time-series into 3D images (2D spatial topography × 1D time-course) and entered them into a general linear model (GLM) with two factors (random effect of mismatch: deviant vs. standard; fixed effect of participant), corresponding to a paired *t*-test. Statistical parametric maps were thresholded at an uncorrected $p < 0.005$, and the resulting spatiotemporal clusters of main effects were tested for statistical significance at the family-wise error corrected threshold pFWE < 0.05, taking into account the spatiotemporal correlations and multiple comparisons across channels and time points.

In an additional control analysis, we have tested whether the mismatch responses observed in this study were modulated by adaptation effects, which have been shown to be especially prominent in the N1 range (Baldeweg et al., 2004). To this end, per standard stimulus (i.e., the last stimulus in a sequence of identical stimuli), we have calculated the number of stimuli separating it from the preceding deviant (i.e., the first stimulus in a sequence of identical stimuli). If our results were indeed confounded by adaptation, the difference between responses evoked by deviants vs. standards should be modulated by the number of stimuli preceding each deviant. To test this hypothesis, we have regressed out the number of preceding stimuli from single-trial standard-evoked responses (using two regressors: a linear regressor, coding for the actual number of preceding stimuli, and a log-transformed regressor, approximating empirically observed adaptation effects; (e.g., Baldeweg et al., 2004), and subjected the residuals to the remaining univariate analysis steps (i.e., averaging the single-trial responses to obtain ERPs, and performing statistical inference while correcting for multiple comparisons across channels and time points).

Then, to test whether MMN amplitudes differed between stimulus features, ERP data were entered into a flexible-factorial GLM with one random factor (participant) and two fixed factors (mismatch: deviant vs. standard; feature: pitch, duration, ILD, and vowel), corresponding to a repeated-measures 2 × 4 ANOVA. Statistical significance thresholds were set as above.

Finally, to test whether mismatch responses can be used to decode the violated acoustic features, we subjected the data to a multivariate analysis. Prior to decoding, we calculated single-trial mismatch response signals by subtracting the EEG signal evoked by each standard from the signal evoked by the subsequent deviant. Data dimensionality was reduced using PCA (principal component analysis), resulting in spatial principal components (describing channel topographies) and temporal principal components (describing voltage time-series), sorted by the ratio of explained variance. Only those top components which, taken together, explained 95% of the original variance, were retained for further analysis. In decoding acoustic features, we adopted a sliding window approach, integrating over the relative voltage changes within a 100 ms window around each time-point (Wolff et al., 2020). To this end, per channel and trial, the time segments within 100 ms of each analyzed time-point were down-sampled by binning the data over 10 ms bins, resulting in a vector of 10 average voltage values per component. Next, the data were de-meaned by removing the component-specific average voltage over the entire 100 ms time window from each component and time bin. These steps ensured that the multivariate analysis approach was optimized for decoding transient activation patterns (voltage fluctuations around a zero mean) at the expense of more stationary neural processes (overall differences in mean voltage) (Wolff et al., 2020).

The binned single-trial mismatch fluctuations were then concatenated across components for subsequent leave-one-out cross-validation decoding. Per trial and time point, we calculated the Mahalanobis distance (De Maesschalck et al., 2000) (scaled by the noise covariance matrix of all components) between the vector of concatenated component fluctuations of this trial (test trial) and four other vectors, obtained from the remaining trials, and corresponding to the concatenated component fluctuations averaged across trials, separately for each of the four features. The resulting Mahalanobis distance values were averaged across trials, separately for each acoustic feature, resulting in 4 × 4 distance matrices. These distance matrices were summarized per time point and participant as a single decoding estimate, by subtracting the mean off-diagonal from diagonal terms (**Figure 3A**).

In a final analysis, since we have observed univariate mismatch responses as well as multivariate mismatch-based feature decoding at similar latencies (see Results), we have tested whether these two effects are related. To this end, we performed a correlation analysis between single-trial decoding estimates (i.e., the relative Mahalanobis distance values between EEG topography corresponding to mismatch responses following violations of the same vs. different features), and single-trial MMN amplitudes. We calculated Pearson correlation coefficients across single trials, per channel, time point, and participants. The resulting correlation coefficients were subject to statistical inference using statistical parametric mapping (one-sample *t*-test; significance thresholds as in the other univariate analysis, corrected for multiple comparisons across time points and channels using family-wise error).

RESULTS

Taken together, in this study, we tested whether auditory mismatch responses are modulated by violations of independent acoustic features. First, consistent with previous literature (Doeller et al., 2003; Garrido et al., 2008), we observed overall differences between the ERPs evoked by deviant stimuli vs. standard stimuli, in a range typical for MMN responses as well as at longer latencies (**Figure 2A**). Specifically, the univariate ERP analysis confirmed that EEG amplitudes differed significantly between deviants and standards when pooling over

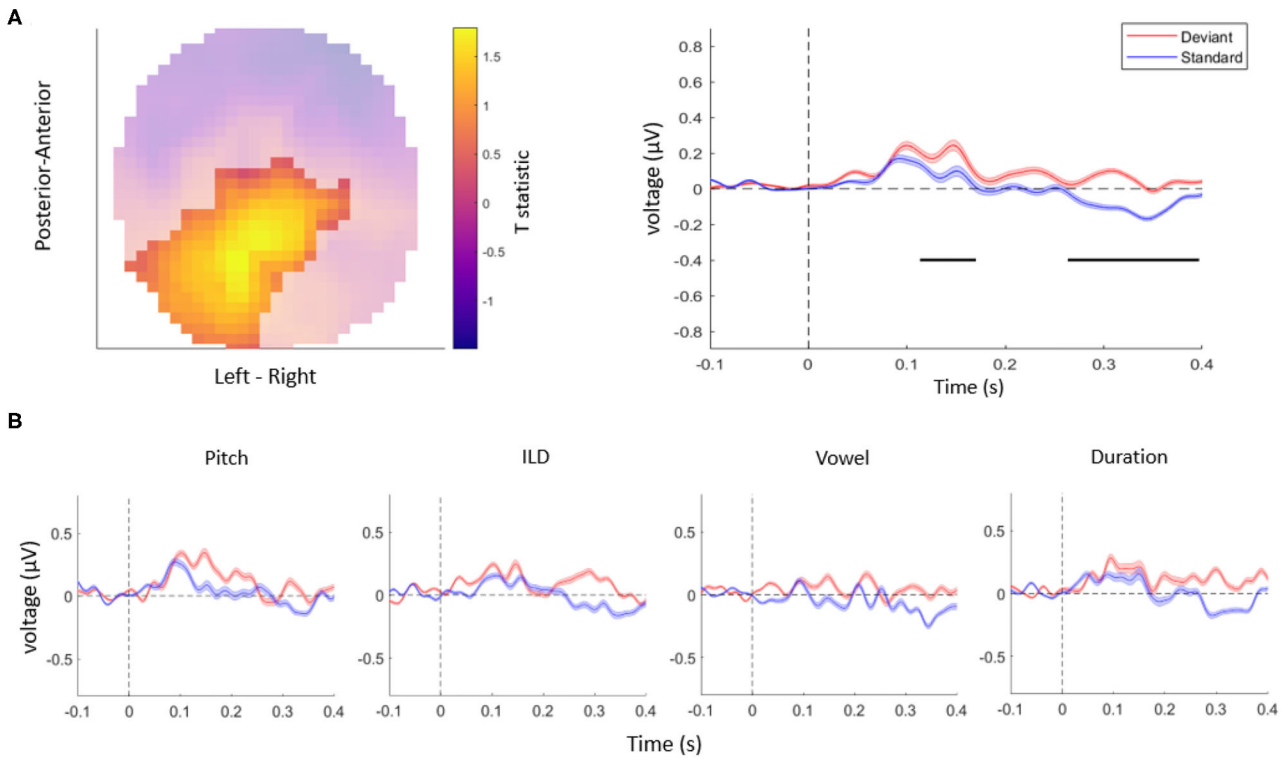

FIGURE 2 | (A) The topography (left) and time-course (right) of the mismatch response. The highlighted topography cluster represents the significant difference between deviants and standards. Based on this cluster, the average waveform of the evoked response is plotted separately for auditory standards (blue) and deviants (red). The horizontal bars (black) indicate time points with a significant difference between deviants and standards. Shaded areas denote SEM (standard error of the mean) across participants. **(B)** The average response to acoustic standards (blue) and deviants (red) for different feature conditions, extracted from the same cluster as in **(A)**. No interaction effects were significant after correcting for multiple comparisons across channels and time points.

all the acoustic features tested. This effect was observed over two clusters: the central EEG channels showed a significant mismatch response between 115 and 182 ms (cluster-level pFWE < 0.001, Tmax $= 3.94$), while posterior channels showed a significant mismatch response between 274 and 389 ms (cluster-level pFWE < 0.001, Tmax $= 5.46$), within the range of a P3b component. A control analysis, in which we controlled for single-trial adaptation effect to the standard tones, yielded a virtually identical pattern of results as the original analysis (two significant clusters of differences between responses to deviants vs. standards: an earlier cluster between 130 and 143 ms over central channels, cluster-level pFWE < 0.001, Tmax $= 15.48$, and a later cluster between 317 and 327 ms over posterior channels, cluster-level pFWE < 0.001, Tmax $= 17.48$).

Although the ERP time-courses differed between deviant and standard stimuli when pooling over violations of different acoustic features, a univariate (channel-by-channel) analysis revealed no significant differences in the amplitudes or time-courses of mismatch responses between independent stimulus features (**Figure 2B**). These results are consistent with a previous study (Phillips et al., 2015) which found that multiple deviant stimulus features (frequency, intensity, location, duration, and silent gap) were not associated with differences in activity in the auditory regions, but instead were reflected in more distributed activity patterns (frontotemporal connectivity estimates).

The resulting decoding time-courses of each participant were entered into a GLM and subject to one-sample t-tests, thresholded at an uncorrected $p < 0.05$ and correcting for multiple comparisons across time points at a cluster-level pFWE < 0.05. In this analysis, significant acoustic feature decoding was observed between 247 and 350 ms relative to tone onset (cluster-level pFWE $= 0.000$, Tmax $= 2.77$) (**Figure 3B**). Thus, when pooling information from multiple EEG channels, acoustic features could be decoded from the topography of mismatch responses, although at later latencies than typical for MMN.

Since we have observed both univariate mismatch responses and multivariate mismatch-based feature decoding at late latencies (univariate: 274–389 ms; multivariate: 247–350 ms), we have performed an additional single-trial correlation analysis to test whether these two effects are related. This analysis (**Figure 3C**) has yielded no significant clusters of correlation coefficients between single-trial mismatch amplitudes and decoding estimates, while correcting for multiple comparisons across channels and time points (Tmax $= 3.74$, all pFWE > 0.005).

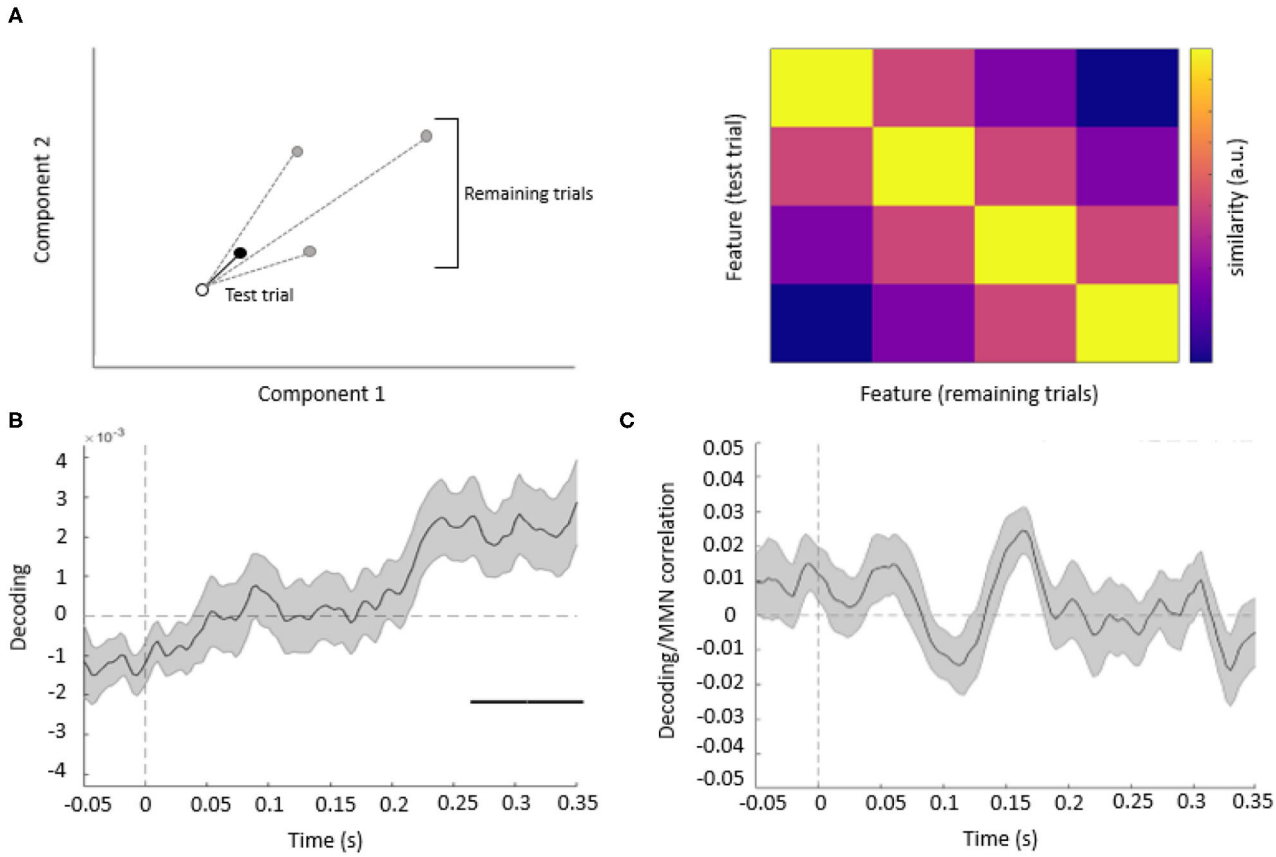

FIGURE 3 | (A) Decoding methods. Left panel: for each trial, we calculated the Mahalanobis distance, based on multiple EEG components (here shown schematically for two components), between the mismatch response in a given (test) trial (empty circle) and the average mismatch responses based on the remaining trials (black circle: same feature as test trial; gray circles: different features). Right panel: after averaging the distance values across all trials, we obtained 4 by 4 similarity matrices between all features, such that high average Mahalanobis distance corresponded to low similarity between features. Based on these matrices, we summarized feature decoding as the difference between the diagonal and off-diagonal terms. **(B)** Multivariate analysis. The average time course of the decoding of acoustic features based on single-trial mismatch response. The gray-shaded area denotes the SEM across participants, and the horizontal bar (black) shows the significant time window. **(C)** Decoding vs. MMN correlation analysis. Plot shows the time-series of mean correlation coefficients between single-trial decoding estimates and single-trial MMN amplitudes, calculated for Cz/Cpz channels and averaged across participants (shaded areas: SEM across participants). No significant correlations were observed when correcting for multiple comparisons across channels and time points.

DISCUSSION

In this study, since a univariate analysis of interactions between mismatch signals and acoustic features might not be sensitive enough to reveal subtle and distributed amplitude differences between conditions, we adopted a multivariate analysis aiming at decoding the violated acoustic feature from single-trial mismatch response topographies. This demonstrated that acoustic features could be decoded from the topography of mismatch responses, although at later latencies than typical for MMN (**Figure 3B**). An earlier oddball study (Leung et al., 2012) examined ERP differences to violations of four features (frequency, duration, intensity, and interaural difference). The study found that frequency deviants were associated with a significant amplitude change in the middle latency range. This result indicated that deviant feature detection may be subserved by a different process than general mismatch detection. Consistent with this notion, another study has used magnetoencephalography to identify mid-latency effects of local prediction violations of simple stimulus features, and contrasted them with later effects of global prediction violations of stimulus patterns (Recasens et al., 2014). Taken together, these studies would suggest that, in paradigms where multiple acoustic features vary independently (such as here), a plausible pattern of results would be that independent feature predictions should be mismatched at relatively early latencies, since an integrated representation is not required. Here, however, we found feature-specificity in the late latency range, rather than in the mid-latency range. The discrepancy between our results and the previous studies might be explained by different stimulus types. While the previous studies used simple acoustic stimuli, here we used complex syllable stimuli, possibly tapping into the later latencies of language-related mismatch responses, as compared to MMN following violations of non-speech sounds.

Speech sounds have been hypothesized to be processed in separate streams which independently derive semantic information ("what" processing) and sound location ("where" processing) (Kaas and Hackett, 2000; Tian et al., 2001; Schubotz et al., 2003; Camalier et al., 2012; Kusmierek and Rauschecker, 2014). In most animal studies, the hierarchical organization of the auditory cortex has been linked to a functional distribution of stimulus processing, such that core (hierarchically lower) regions respond preferentially to simple stimuli, whereas belt and other downstream (hierarchically higher) regions respond to more complex stimuli such as band-passed noise and speech (Rauschecker et al., 1995; Recanzone et al., 2000; Rauschecker and Tian, 2004; Kusmierek and Rauschecker, 2009; Rauschecker and Scott, 2009). This is supported by evidence functional magnetic resonance imaging (fMRI) studies in humans (Binder et al., 2000) showing that earlier auditory regions (Heschl's gyrus and surrounding fields) respond preferentially to unstructured noise stimuli, while progressively more complex stimuli such as frequency-modulated tones show more lateral response activation patterns. In that study, speech sounds showed most pronounced activations spreading ventrolaterally into the superior temporal sulcus. This result supports a hierarchical model of auditory speech processing in the human auditory cortex based on complexity and integration of temporal and spectral features. Based on this notion, the relatively long latency of neural responses compared to previous studies using pure tones might be partially explained by the fact that we used spectrally and temporally complex speech stimuli.

However, our results can also be explained in terms of a hierarchical deviance detection system based on predictive coding (Kiebel et al., 2008). On this account, neural responses supporting the lower and higher hierarchical stages communicate continuously through reciprocal pathways. When exposed to repetitive stimuli, the bottom-up (ascending) sensory inputs can be "explained away" by top-down (descending) connections mediating prediction signaling, resulting in weaker prediction error signaling back to the hierarchically higher regions. Substituting the predicted standard with unpredicted deviant results in a failure of top-down suppression by prior predictions. This leads to an increased prediction error signaling back to higher regions, providing an update for subsequent predictions. As a result, the later and more distributed activity patterns might reflect higher-order prediction errors, signaled to regions integrating multiple stimulus features and representing the entire range of stimuli likely to appear in a particular context.

In conclusion, the present study identified functional dissociations between deviance detection and deviance feature detection. First, while mismatch responses were observed at latencies typical for the MMN as well as at longer latencies, channel-by-channel analyses revealed no robust differences between mismatch responses following violations of different acoustic features. However, we demonstrate that acoustic features could be decoded at longer latencies based on fine-grained spatiotemporal patterns of mismatch responses. This finding suggests that deviance feature detection might be mediated by later and more distributed neural responses than deviance detection itself.

DATA AVAILABILITY STATEMENT

The raw data supporting the conclusions of this article will be made available by the authors, without undue reservation.

ETHICS STATEMENT

The studies involving human participants were reviewed and approved by Human Subjects Ethics Sub-Committee of the City University of Hong Kong. The patients/participants provided their written informed consent to participate in this study. Written informed consent was obtained from the individual(s) for the publication of any potentially identifiable images or data included in this article.

AUTHOR CONTRIBUTIONS

HA: formal analysis, writing original draft, conceptualization, and conducted experiment. SH: conducted experiment and formal analysis. RA: formal analysis, supervision, project administration, and conceptualization. JS: project administration, conceptualization, investigation, and supervision. All authors contributed to the article and approved the submitted version.

FUNDING

This work has been supported by the European Commission's Marie Skłodowska-Curie Global Fellowship (750459 to RA), the Hong Kong General Research Fund (11100518 to RA and JS), and a grant from European Community/Hong Kong Research Grants Council Joint Research Scheme (9051402 to RA and JS).

REFERENCES

An, H., Auksztulewicz, R., Kang, H., and Schnupp, J. W. H. (2020). Cortical mapping of mismatch responses to independent acoustic features. *Hear. Res.* 399:107894. doi: 10.1016/j.heares.2020.107894

Auksztulewicz, R., Schwiedrzik, C. M., Thesen, T., Doyle, W., Devinsky, O., Nobre, A. C., et al. (2018). Not all predictions are equal: "What" and "When" predictions modulate activity in auditory cortex through different mechanisms. *J. Neurosci.* 38, 8680–8693. doi: 10.1523/JNEUROSCI.0369-18.2018

Baldeweg, T., Klugman, A., Gruzelier, J., and Hirsch, S. R. (2004). Mismatch negativity potentials and cognitive impairment in schizophrenia. *Schizophr. Res.* 69, 203–217. doi: 10.1016/j.schres.2003.09.009

Binder, J. R., Frost, J. A., Hammeke, T. A., Bellgowan, P. S., Springer, J. A., Kaufman, J. N., et al. (2000). Human temporal lobe activation by speech and nonspeech sounds. *Cereb. Cortex* 10, 512–528. doi: 10.1093/cercor/10.5.512

Caclin, A., Brattico, E., Tervaniemi, M., Naatanen, R., Morlet, D., Giard, M. H., et al. (2006). Separate neural processing of timbre dimensions in auditory sensory memory. *J. Cogn. Neurosci.* 18, 1959–1972. doi: 10.1162/jocn.2006.18.12.1959

Camalier, C. R., D'Angelo, W. R., Sterbing-D'Angelo, S. J., de la Mothe, L. A., and Hackett, T. A. (2012). Neural latencies across auditory cortex of macaque support a dorsal stream supramodal timing advantage in primates. *Proc. Natl. Acad. Sci. U.S.A.* 109, 18168–18173. doi: 10.1073/pnas.1206387109

Carbajal, G. V., and Malmierca, M. S. (2018). The neuronal basis of predictive coding along the auditory pathway: from the subcortical roots to cortical deviance detection. *Trends Hear.* 22:2331216518784822. doi: 10.1177/2331216518784822

Chennu, S., Noreika, V., Gueorguiev, D., Blenkmann, A., Kochen, S., Ibanez, A., et al. (2013). Expectation and attention in hierarchical auditory prediction. *J. Neurosci.* 33, 11194–11205. doi: 10.1523/JNEUROSCI.0114-13.2013

De Maesschalck, R., Jouan-Rimbaud, D., and Massart, D. L. (2000). The Mahalanobis distance. *Chemomet. Intellig. Lab. Syst.* 50, 1–18. doi: 10.1016/S0169-7439(99)00047-7

Deouell, L. Y., and Bentin, S. (1998). Variable cerebral responses to equally distinct deviance in four auditory dimensions: a mismatch negativity study. *Psychophysiology* 35, 745–754. doi: 10.1111/1469-8986.3560745

Doeller, C. F., Opitz, B., Mecklinger, A., Krick, C., Reith, W., and Schroger, E. (2003). Prefrontal cortex involvement in preattentive auditory deviance detection: neuroimaging and electrophysiological evidence. *Neuroimage* 20, 1270–1282. doi: 10.1016/S1053-8119(03)00389-6

Friston, K., and Buzsaki, G. (2016). The functional anatomy of time: what and when in the brain. *Trends Cogn. Sci.* 20, 500–511. doi: 10.1016/j.tics.2016.05.001

Garrido, M. I., Friston, K. J., Kiebel, S. J., Stephan, K. E., Baldeweg, T., and Kilner, J. M. (2008). The functional anatomy of the MMN: a DCM study of the roving paradigm. *Neuroimage* 42, 936–944. doi: 10.1016/j.neuroimage.2008.05.018

Giard, M. H., Lavikahen, J., Reinikainen, K., Perrin, F., Bertrand, O., Pernier, J., et al. (1995). Separate representation of stimulus frequency, intensity, and duration in auditory sensory memory: an event-related potential and dipole-model analysis. *J. Cogn. Neurosci.* 7, 133–143. doi: 10.1162/jocn.1995.7.2.133

Ille, N., Berg, P., and Scherg, M. (2002). Artifact correction of the ongoing EEG using spatial filters based on artifact and brain signal topographies. *J. Clin. Neurophysiol.* 19, 113–124. doi: 10.1097/00004691-200203000-00002

Kaas, J. H., and Hackett, T. A. (2000). Subdivisions of auditory cortex and processing streams in primates. *Proc. Natl. Acad. Sci. U.S.A.* 97, 11793–11799. doi: 10.1073/pnas.97.22.11793

Kiebel, S. J., Daunizeau, J., and Friston, K. J. (2008). A hierarchy of time-scales and the brain. *PLoS Comput. Biol.* 4:e1000209. doi: 10.1371/journal.pcbi.1000209

Kusmierek, P., and Rauschecker, J. P. (2009). Functional specialization of medial auditory belt cortex in the alert rhesus monkey. *J. Neurophysiol.* 102, 1606–1622. doi: 10.1152/jn.00167.2009

Kusmierek, P., and Rauschecker, J. P. (2014). Selectivity for space and time in early areas of the auditory dorsal stream in the rhesus monkey. *J. Neurophysiol.* 111, 1671–1685. doi: 10.1152/jn.00436.2013

Leung, S., Cornella, M., Grimm, S., and Escera, C. (2012). Is fast auditory change detection feature specific? An electrophysiological study in humans. *Psychophysiology* 49, 933–942. doi: 10.1111/j.1469-8986.2012.01375.x

Naatanen, R. (2007). The mismatch negativity - where is the big fish? *J. Psychophysiol.* 21, 133–137. doi: 10.1027/0269-8803.21.34.133

Paavilainen, P., Valppu, S., and Naatanen, R. (2001). The additivity of the auditory feature analysis in the human brain as indexed by the mismatch negativity: 1+1 approximate to 2 but 1+1+1 < 3. *Neurosci. Lett.* 301, 179–182. doi: 10.1016/S0304-3940(01)01635-4

Phillips, H. N., Blenkmann, A., Hughes, L. E., Bekinschtein, T. A., and Rowe, J. B. (2015). Hierarchical organization of frontotemporal networks for the prediction of stimuli across multiple dimensions. *J. Neurosci.* 35, 9255–9264. doi: 10.1523/JNEUROSCI.5095-14.2015

Rauschecker, J. P., and Scott, S. K. (2009). Maps and streams in the auditory cortex: nonhuman primates illuminate human speech processing. *Nat. Neurosci.* 12, 718–724. doi: 10.1038/nn.2331

Rauschecker, J. P., and Tian, B. (2004). Processing of band-passed noise in the lateral auditory belt cortex of the rhesus monkey. *J. Neurophysiol.* 91, 2578–2589. doi: 10.1152/jn.00834.2003

Rauschecker, J. P., Tian, B., and Hauser, M. (1995). Processing of complex sounds in the macaque nonprimary auditory cortex. *Science* 268, 111–114. doi: 10.1126/science.7701330

Recanzone, G. H., Guard, D. C., and Phan, M. L. (2000). Frequency and intensity response properties of single neurons in the auditory cortex of the behaving macaque monkey. *J. Neurophysiol.* 83, 2315–2331. doi: 10.1152/jn.2000.83.4.2315

Recasens, M., Grimm, S., Wollbrink, A., Pantev, C., and Escera, C. (2014). Encoding of nested levels of acoustic regularity in hierarchically organized areas of the human auditory cortex. *Hum. Brain Mapp.* 35, 5701–5716. doi: 10.1002/hbm.22582

Retsa, C., Matusz, P. J., Schnupp, J. W. H., and Murray, M. M. (2018). What's what in auditory cortices? *Neuroimage* 176, 29–40. doi: 10.1016/j.neuroimage.2018.04.028

Rosburg, T., Weigl, M., Thiel, R., and Mager, R. (2018). The event-related potential component P3a is diminished by identical deviance repetition, but not by non-identical repetitions. *Exp. Brain Res.* 236, 1519–1530. doi: 10.1007/s00221-018-5237-z

Schroger, E. (1995). Processing of auditory deviants with changes in one versus two stimulus dimensions. *Psychophysiology* 32, 55–65. doi: 10.1111/j.1469-8986.1995.tb03406.x

Schubotz, R. I., von Cramon, D. Y., and Lohmann, G. (2003). Auditory what, where, and when: a sensory somatotopy in lateral premotor cortex. *Neuroimage* 20, 173–185. doi: 10.1016/S1053-8119(03)00218-0

Shiramatsu, T. I., and Takahashi, H. (2018). Mismatch negativity in rat auditory cortex represents the empirical salience of sounds. *Front. Neurosci.* 12:924. doi: 10.3389/fnins.2018.00924

Tian, B., Reser, D., Durham, A., Kustov, A., and Rauschecker, J. P. (2001). Functional specialization in rhesus monkey auditory cortex. *Science* 292, 290–293. doi: 10.1126/science.1058911

Wolff, M. J., Kandemir, G., Stokes, M. G., and Akyurek, E. G. (2020). Unimodal and bimodal access to sensory working memories by auditory and visual impulses. *J. Neurosci.* 40, 671–681. doi: 10.1523/JNEUROSCI.1194-19.2019

Conflict of Interest: The authors declare that the research was conducted in the absence of any commercial or financial relationships that could be construed as a potential conflict of interest.

frontiers in Human Neuroscience

ORIGINAL RESEARCH
published: 14 April 2021
doi: 10.3389/fnhum.2021.641273

Magnetoencephalography Responses to Unpredictable and Predictable Rare Somatosensory Stimuli in Healthy Adult Humans

Qianru Xu[1,2], Chaoxiong Ye[1,2], Jarmo A. Hämäläinen[2], Elisa M. Ruohonen[3], Xueqiao Li[2] and Piia Astikainen[2]*

[1] Institute of Brain and Psychological Sciences, Sichuan Normal University, Chengdu, China, [2] Jyväskylä Centre for Interdisciplinary Brain Research, Department of Psychology, Faculty of Education and Psychology, University of Jyväskylä, Jyväskylä, Finland, [3] Human Information Processing Laboratory, Psychology, Faculty of Social Sciences, Tampere University, Tampere, Finland

OPEN ACCESS

Edited by:
Manuel S. Malmierca, University of Salamanca, Spain

Reviewed by:
Chia-Hsiung Cheng, Chang Gung University, Taiwan
Gilles Naeije, Université libre de Bruxelles, Belgium

***Correspondence:**
Chaoxiong Ye
cxye1988@163.com

Specialty section:
This article was submitted to Cognitive Neuroscience, a section of the journal Frontiers in Human Neuroscience

Received: *14 December 2020*
Accepted: *19 February 2021*
Published: *14 April 2021*

Citation:
Xu Q, Ye C, Hämäläinen JA, Ruohonen EM, Li X and Astikainen P (2021) Magnetoencephalography Responses to Unpredictable and Predictable Rare Somatosensory Stimuli in Healthy Adult Humans. Front. Hum. Neurosci. 15:641273. doi: 10.3389/fnhum.2021.641273

Mismatch brain responses to unpredicted rare stimuli are suggested to be a neural indicator of prediction error, but this has rarely been studied in the somatosensory modality. Here, we investigated how the brain responds to unpredictable and predictable rare events. Magnetoencephalography responses were measured in adults frequently presented with somatosensory stimuli (FRE) that were occasionally replaced by two consecutively presented rare stimuli [unpredictable rare stimulus (UR) and predictable rare stimulus (PR); p = 0.1 for each]. The FRE and PR were electrical stimulations administered to either the little finger or the forefinger in a counterbalanced manner between the two conditions. The UR was a simultaneous electrical stimulation to both the forefinger and the little finger (for a smaller subgroup, the UR and FRE were counterbalanced for the stimulus properties). The grand-averaged responses were characterized by two main components: one at 30–100 ms (M55) and the other at 130–230 ms (M150) latency. Source-level analysis was conducted for the primary somatosensory cortex (SI) and the secondary somatosensory cortex (SII). The M55 responses were larger for the UR and PR than for the FRE in both the SI and the SII areas and were larger for the UR than for the PR. For M150, both investigated areas showed increased activity for the UR and the PR compared to the FRE. Interestingly, although the UR was larger in stimulus energy (stimulation of two fingers at the same time) and had a larger prediction error potential than the PR, the M150 responses to these two rare stimuli did not differ in source strength in either the SI or the SII area. The results suggest that M55, but not M150, can possibly be associated with prediction error signals. These findings highlight the need for disentangling prediction error and rareness-related effects in future studies investigating prediction error signals.

Keywords: deviance detection, magnetoencephalography, predictability, prediction error, somatosensory

INTRODUCTION

The ability to detect changes in the stimulus environment is crucial to an organism's survival. Equally important is the capacity to learn contingencies between stimuli and to anticipate future events based on learned patterns in stimuli. Accurate predictions of future events can advance cognitive functioning related to perception and action in a fundamentally important manner (Bar, 2007).

According to the predictive coding theory (Friston, 2005), neural networks constantly learn the statistical regularities of the surrounding stimulus environment and make predictions of future events. When the input information does not match with the prediction, the lower sensory areas send a prediction error signal into the higher cortical areas (recent findings also extend this hierarchical pattern of predictive coding framework to subcortical structures, see Parras et al., 2017; Carbajal and Malmierca, 2018) and modify the prediction (Friston, 2005; Garrido et al., 2009; Stefanics et al., 2014). This new prediction is then sent backward to the lower areas, where it is again compared with the new sensory input signals.

In experimental research, an oddball stimulus condition, wherein a standard stimulus is rarely and randomly replaced by a deviant stimulus, is a feasible tool for studying predictive coding. An event-related potential, called mismatch negativity [MMN or MMNm when investigating with magnetoencephalography (MEG)] (Näätänen et al., 1978, 2010), is elicited by the deviant stimulus and is suggested to reflect prediction error (Friston, 2005; Garrido et al., 2009; Wacongne et al., 2012; Stefanics et al., 2014; Carbajal and Malmierca, 2018). MMN was originally found in the auditory modality (Näätänen et al., 1978) but was later reported as well for deviant stimuli in the visual (e.g., Stefanics et al., 2012; Astikainen et al., 2013; Xu et al., 2018; for reviews, see Czigler, 2007; Kimura et al., 2011; Stefanics et al., 2014; Kremláček et al., 2016), olfactory (e.g., Krauel et al., 1999; for a review, see Pause and Krauel, 2000), and somatosensory (e.g., Shinozaki et al., 1998; Spackman et al., 2007; Strömmer et al., 2014, 2017; for a review, see Näätänen, 2009) modalities.

Here, we focus on the somatosensory mismatch response [sMMR, instead of MMN due to its positive polarity in some previous electroencephalography (EEG) measurements], which is less studied than its auditory and visual counterparts. The sMMR has been observed for changes in stimulus location (Shinozaki et al., 1998; Huang et al., 2005; Restuccia et al., 2009; Strömmer et al., 2014, 2017; Yamashiro et al., 2014; Shen et al., 2018; Hautasaari et al., 2019; for animal models, see: Astikainen et al., 2001; Musall et al., 2017), duration (Akatsuka et al., 2005; Spackman et al., 2007, 2010; Zhao et al., 2014), intensity (Mima et al., 1998; Ostwald et al., 2012), frequency (Kekoni et al., 1997; Spackman et al., 2007), and omissions of the stimuli (Tesche and Karhu, 2000; Naeije et al., 2018). However, one critical confounder should be considered in the context of all the previously mentioned studies, namely, that the probability of the rare stimulus in the traditional oddball paradigm is always smaller than the probability of the standard stimulus and that probability, as such, affects the brain responses (Hari et al., 1990). One possible neural mechanism underlying probability effects is neural adaptation (May et al., 1999; May and Tiitinen, 2010), in which the neural populations responding to frequently presented standard stimuli can be more adapted than those responding to the rare deviant stimuli. Therefore, larger responses can be elicited for deviant stimuli than for standard stimuli (May and Tiitinen, 2010).

For auditory and, to some extent, for visual experiments as well, several different control conditions have been developed to control for possible adaptation effects for MMN elicitation. The many-standards condition (also called the equal-probability condition) is currently the most frequently used (Schröger and Wolff, 1996; Jacobsen and Schröger, 2001). In human auditory oddball studies, the results from the many-standards control condition suggest that the differential responses found in the oddball paradigm (MMN) may not be explained by adaptation alone (Jacobsen and Schröger, 2001; Jacobsen et al., 2003; Maess et al., 2007; Lohvansuu et al., 2013), but this has been less well resolved in animal studies (for supportive evidence in animal models, see, e.g., Astikainen et al., 2011; Nakamura et al., 2011; Parras et al., 2017; Kurkela et al., 2018; Polterovich et al., 2018; for no support or partial support, see, e.g., Fishman and Steinschneider, 2012; Lipponen et al., 2019; Yang et al., 2019). In the many-standards control condition, in addition to the original deviant and standard stimuli, other stimuli with different stimulus features than those in the standard and deviant stimuli are randomly presented but without consecutive repetitions. Each stimulus's probability is the same as the probability of the deviant stimulus in the oddball paradigm. The many-standards condition is more difficult to design for the somatosensory than for the auditory and visual modality. For instance, with a deviant probability of 10%, this condition would require 10 different stimulation locations for a location-change paradigm in the somatosensory modality, and different skin locations have also different sensitivities. However, to our knowledge, no previous studies have applied this type of experiment in the somatosensory domain in human participants, and only one study in animals is reported (whisker stimulation in rats: Musall et al., 2017).

Here, we introduce a novel modified oddball paradigm that approaches the topic from a different angle. Because it is more difficult in the somatosensory than in the auditory studies to produce several feature levels (such as different frequencies of tones) for application in the many-standards condition, we developed a stimulus condition in which somatosensory responses to equally rare unpredictable and predictable stimuli can be investigated. In this stimulus paradigm, the frequently presented standard stimulus (the frequent stimulus, FRE) is rarely and randomly replaced by a deviant stimulus (the unpredictable rare stimulus, UR), as in the classical oddball paradigm. However, another deviant stimulus (the predictable rare stimulus, PR) immediately follows each UR. Therefore, these two rare somatosensory events are different in their prediction error value, but similar in rareness (probability). The UR should thus show increased responses in comparison to the FRE and PR due to its larger prediction error potential.

In this study, the stimulation is presented as electrical stimulations of fingers, and the three stimulus types differ in location of the stimulation. Consistent with previous studies

investigating the location deviance detection and where the fingers or hands have been stimulated in an ignore condition (Shinozaki et al., 1998; Akatsuka et al., 2005, 2007a,b; Restuccia et al., 2007; Strömmer et al., 2014, 2017; Hautasaari et al., 2019), we expect that the stimulation will elicit activity in two main time windows at approximately 30–70 and 100–200 ms after the stimulus onset. We also expect both the early and later responses to show a larger amplitude to rare stimuli in comparison to standard stimuli (Mima et al., 1998; Akatsuka et al., 2005, 2007a,b; Strömmer et al., 2017; Hautasaari et al., 2019). Since previous studies have not controlled for stimulus rarity (for example, by using the many-standards control condition), we cannot predict whether increased responses in comparison to the FRE will be elicited by the UR alone or by both the UR and the PR. However, larger responses specific to the UR will reflect prediction error, while larger responses to both the UR and the PR would reflect stimulus rarity in comparison to the FRE.

MATERIALS AND METHODS

Participants

Fifteen healthy participants (12 females and 3 males, aged 21–43 years old) were recruited via email lists and notice boards within the University of Jyväskylä and by an announcement in a local newspaper. Inclusion criteria were an age of 18–45 years, right-handedness, and self-reported normal senses (vision corrected with eyeglasses was allowed). Hearing ability for 1,000 and 500 Hz sounds was measured in the laboratory with an audiometer to ensure proper hearing because we also collected another dataset in the auditory sensory modality, not reported here. Exclusion criteria were pregnancy, breastfeeding, current or previous neurological or psychiatric diseases, brain damage, alcohol abuse or use of illegal drugs, and current depressive symptoms. A Finnish-language version of the Beck Depression Inventory II (BDI-II) questionnaire (Beck et al., 1996) was filled in by participants, and a maximum score of 10 in the BDI-II was allowed for included participants. In addition, participants with contraindications for MEG measurement such as a pacemaker, hearing aid, or dental implant were excluded. Before the experiment, a phone interview was conducted to confirm the inclusion and exclusion criteria. Each participant received one movie ticket as compensation for their participation. The experiment complied with the Declaration of Helsinki and was approved by the ethics committee of the University of Jyväskylä. Written informed consent was signed by each participant upon their arrival to the laboratory.

Stimulus and Task Procedure

Stimuli were electrical pulses (Stimulator: DeMeTec SCG30, DeMeTec GmbH, Langgöns, Germany) of 200 μs in duration, delivered via flexible, non-magnetic metal ring electrodes (Technomed Europe Ltd., Maastricht, Netherlands) to the left forefinger and little finger and stimulating the cathode above the proximal phalanx and the anode above the distal phalanx. All the ring electrodes were moistened with conductive jelly (Technomed Europe Ltd., Maastricht, Netherlands) to reduce impedance. A piece of gauze was tied to the stimulated finger between the two electrodes to prevent conduction between the two electrodes on the same finger. The stimulation intensity was adjusted separately according to the threshold of each finger for each subject. The threshold was determined by the participants' oral reports when they sensed an electrical pulse. The stimulation started from very low intensity and gradually continued to a higher intensity in increments of 0.1 mA until the participant reported feeling the stimulation. This process was repeated three times and applied to the two stimulated fingers. The intensity applied in the experiment was 1.5 times the subjective sensory threshold intensity.

The stimulus procedure was a modified oddball paradigm. A frequently presented stimulus was occasionally replaced by two different rare stimuli: the first one, which was unpredictable, was always followed by another one that was predictable. The experiment had two main stimulus conditions (condition A and condition B, **Figure 1**), which had counterbalanced stimulus features for the FRE and the PR. In condition A, the FRE was stimulation to the little finger, and the PR was stimulation to the forefinger. In condition B, the stimulus assignment was reversed for the FRE and PR. The unpredictable rare stimulus (UR) was a double stimulation (forefinger and little finger, simultaneously). The double stimulation was selected because we did not want to stimulate an additional finger, which would have been necessarily adjacent to either little finger or forefinger. This is because it is not known whether stimulation of adjacent fingers elicits differential responses, but we know from our previous studies that stimulation of the little finger and forefinger can elicit a differential response between the deviant and the standard stimuli (Strömmer et al., 2014, 2017). In addition, not stimulating additional fingers can also avoid the potential boundary effect. This is because previous studies have shown a significantly larger sMMR contrast between the middle finger and the thumb than between the middle finger and the little finger (Shen et al., 2018). Therefore, applying stimulation to additional fingers could also introduce other possible stimulus features variance.

In order to counterbalance the physical features of the stimuli for sMMR assessment, an additional experiment with condition C was conducted for four participants after the presentation of conditions A and B. In condition C, the FRE was a stimulation of the forefinger and little finger, simultaneously, whereas the UR and PR were stimulations to the forefinger and little finger, respectively (see **Supplementary Material 1** for the experimental setting and results). Therefore, when averaging the responses of conditions B and C, the stimulus features were counterbalanced for the FRE and the UR.

Each condition consisted of 1,000 trials presented in two runs for each participant. The probability of an FRE was 80%, and the probability of a UR or PR was 10%. The presentation order of the runs was counterbalanced between the participants, and a short break was provided after each run. The interstimulus interval (ISI, offset-to-onset) was 500 ms under all conditions. The stimulus presentation was controlled by Presentation® software (Neurobehavioral Systems, Inc., Berkeley, CA, United States). Participants were instructed to ignore the somatosensory stimuli and focus on a silent movie. The movie was projected onto

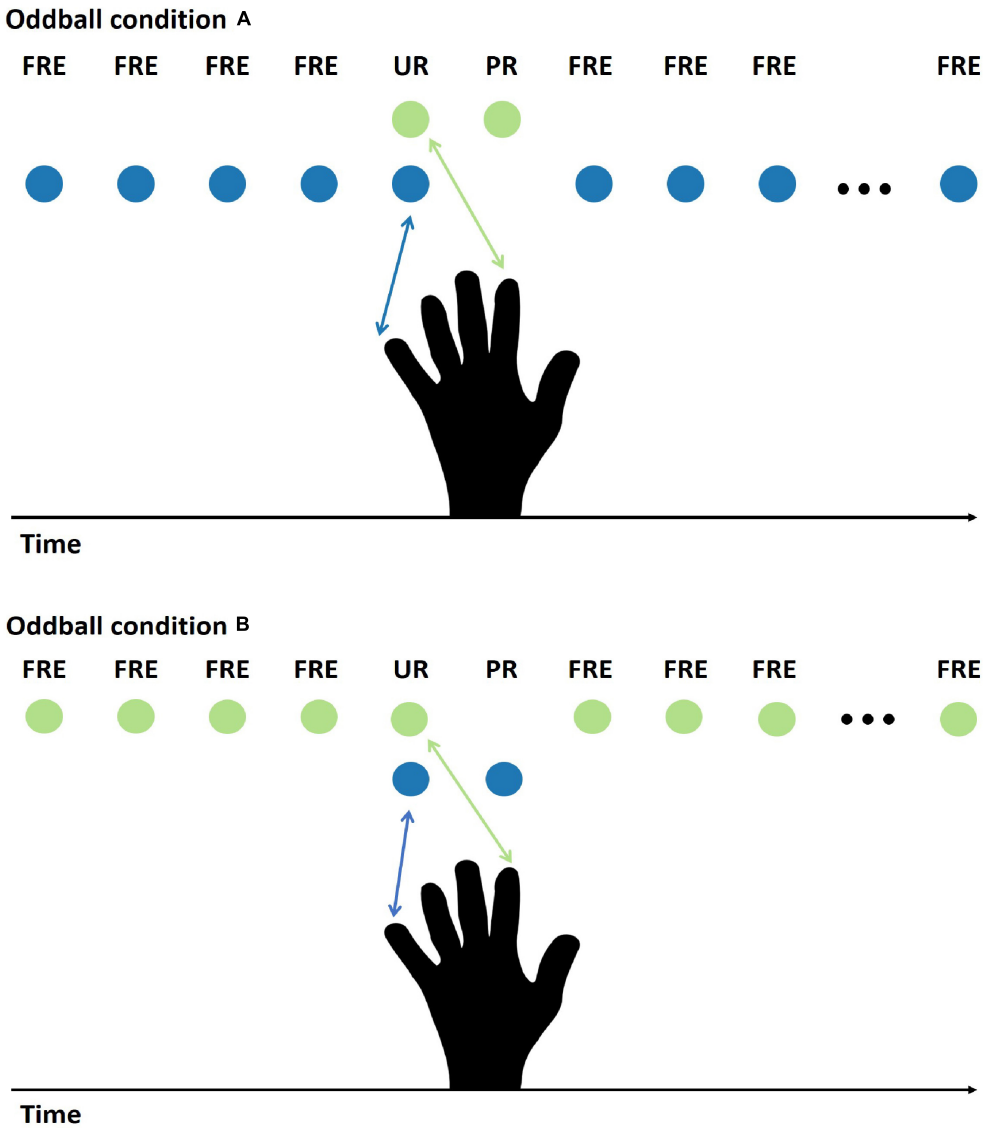

FIGURE 1 | Illustration of the stimulus presentation for conditions A and B. Under condition A, stimulation to the little finger (blue ball symbol) served as the FRE, stimulation to the forefinger (green ball symbol) as the PR, and simultaneous pulses to the forefinger and the little finger as the UR. Under condition B, the opposite assignment between the FRE and the PR was applied. In the analysis, conditions A and B were averaged; therefore, the physical features of the FRE and the PR are controlled. FRE, frequent stimulus; UR, unpredictable rare stimulus; PR, predictable rare stimulus.

the center of the screen at a distance of about 1 m from the participant (video projector: Barco FL35 projector; native resolution 1,920 × 1,080 pixels).

Data Acquisition

The somatosensory evoked related magnetic fields were recorded with a 306-channel whole-head system (Elekta Neuromag TRIUX^{TM} system, Elekta AB, Stockholm, Sweden) in a magnetically shielded, dimly lit room at the MEG Laboratory, University of Jyväskylä.

During the MEG recording, the participant was seated on the chair with their head inside the helmet-shaped device at a 68° upright position. The head position with respect to the sensors in the helmet was determined at the beginning of the task according to the magnetic fields produced by currents fed into five indicator coils at predetermined locations on the scalp. Two HPI coils were placed on both sides behind each ear; another three were placed on the forehead. The locations of these coils in relation to the anatomical location of preauricular points and nasion were determined with an Isotrak 3D digitizer (Polhemus^{TM}, United States) before the experiment started. More than 100 additional points were digitized over the scalp to provide an accurate representation of the individual head shape and for co-registration with a magnetic resonance imaging (MRI) template. The continuous MEG signal was recorded with an online bandpass filter of 0.1–330 Hz and a sampling frequency

of 1,000 Hz. The electrooculogram (EOG) and electrocardiogram (ECG) signals were recorded by detecting eye movements and heartbeat artifacts, respectively. The vertical EOG was recorded by two electrodes attached above and below the right eye; the horizontal EOG was recorded by two electrodes placed on the outer canthi of both eyes. One ECG electrode was placed below the collar bone on the right side, and the other was placed in the middle of the two collar bones. A ground wristband was wrapped around the participant's left-hand carpal bone.

Data Analysis

The Maxfilter 3.0 (Elekta AB) was first applied to reduce the artifacts and transform the mean head positions across different recording sessions. Bad channels were marked manually. The spatiotemporal signal space separation (tSSS) method (Taulu et al., 2004), with a buffer of 30 s and a subspace correlation limit of 0.98, was used to remove external interference from the data. The head position was estimated for head movement compensation with the default setting (HPI amp window: 200 ms; HPI amp step: 10 ms).

The MEG data were then preprocessed and analyzed using the Brainstorm software (Tadel et al., 2011). First, a notch filter of 50 Hz (3 dB notch bandwidth: 2 Hz) and a low-bandpass filter of 60 Hz were applied, as described previously (Hautasaari et al., 2019). Cardiac and eye blink artifacts were attenuated with signal space projection (SSP) in Brainstorm by visually inspecting and removing the corresponding SSP components separately for gradiometers and magnetometers. Additionally, data with EOG amplitudes exceeding 200 μV were marked as bad. The data were then made into epochs according to the stimulus events from a 100 ms pre-stimulus baseline to 500 ms from the stimuli onset. A DC offset baseline correction of -100 to 0 ms was calculated and removed for each epoch. Epochs that included a segment in which the EOG amplitudes exceeded 200 μV were rejected.

The responses were then averaged for each stimulus type over condition A and condition B (weighted average with the number of trials in each condition). Only FRE responses immediately preceding the UR were applied in the analysis because this allowed an equal number of trials for each stimulus type. Conditions A and B were then combined to counterbalance the physical properties of the FRE and the PR. More specifically, a weighted average based on the number of trials was calculated for the rare (both UR and PR) and the FRE responses across conditions A and B for each participant.

For sensor-level comparisons, planar gradiometer channel pairs were combined using root mean squares (RMSs) at each sensor location. For source-level analysis, because individual MRI data were not available, the FSAverage_2016 anatomy template from Brainstorm was used for the MRI co-registration and further source analysis. To make the template better match each participant's head shape, we warped the anatomy templates to match the shape defined by the digitized points. The noise covariance matrix was estimated from an empty room recording made on the same day or on neighboring days. For the MEG forward model, the sensor-weighted overlapping sphere model (one per sensor, in a total of 306 local spheres) (Huang et al., 1999) was used for the representation of the cortical surface with 45,000 dipoles (3 orientations × 15,000 vertices). The inverse solution was performed using the unconstrained depth-weighted minimum-norm estimates (wMNE) implemented in Brainstorm. The unconstrained wMNE were used to avoid the possible noisy and discontinuous current maps since we used the anatomy template instead of individual MRI data for the source estimate. The source localization results were then normalized with a *Z*-score based on the baseline from -100 to 0 ms relative to the stimulus onset. The norm of the three orientations for the unconstrained source was used in the subsequent analysis.

Statistical Analysis

Sensor-level analyses were carried out in Brainstorm by calling the spatiotemporal cluster-based permutation test functions from the Fieldtrip toolbox (Maris and Oostenveld, 2007). Since the results were similar to the source-level results, the detailed statistical analysis and main results of the sensor-level data are reported in **Supplementary Material 2**. Previous MEG studies in the ignore condition have suggested that sMMR is mainly elicited in the primary somatosensory cortex (SI) and the secondary somatosensory cortex (SII) (e.g., Akatsuka et al., 2007a,b; Naeije et al., 2016, 2018; Hautasaari et al., 2019). Thus, based on these prior findings and verified in our grand-averaged source maps of the UR and PR (**Figure 2**), we defined two regions of interest (ROIs), namely, SI (G_postcentral: postcentral gyrus) and SII (Lat_Fis-post: posterior ramus of the lateral fissure), based on the Destrieux atlas (Destrieux et al., 2010). Moreover, only the regions on the right hemisphere, which mean the contralateral SI (cSI) and the contralateral SII (cSII), were used since little or no activation occurs in the corresponding brain regions on the left hemisphere (**Figure 2**) (for previous studies in which only the contralateral side was activated, see, e.g., Strömmer et al., 2014, 2017; Naeije et al., 2016, 2018). The norms of the three orientations for an unconstrained source within the same time windows (30–100 and 130–230 ms after stimulus onset) used in the sensor-level analysis were exported from Brainstorm into the SPSS program for further analysis. For each identified ROI and time window, a separate one-way repeated-measures analysis of variance (ANOVA), with stimulus type (FRE, UR, and PR) as the within-subjects factor, was conducted. The Greenhouse–Geisser correction [*p*-value after Greenhouse–Geisser correction (p_{corr})] was applied when the assumption of sphericity was not met. For significant ANOVA results, *post hoc* analyses were conducted by using a two-tailed paired *t*-test with different stimulus type pairs. Partial eta squared (η^2_p) measures were used for effect size estimates in ANOVA. Bonferroni correction was used for both ANOVA and *post hoc* analysis to control for the multiple comparison problem [*p*-value after Bonferroni correction (p_{corr})]. Cohen's (1988) *d* was computed with pooled standard deviations for the effect size estimate in the *t*-test.

RESULTS

Descriptive Results

Figure 2 illustrates the grand-averaged sensor-level responses and the source estimates for the FRE, UR, and PR. **Figures 3A,B**

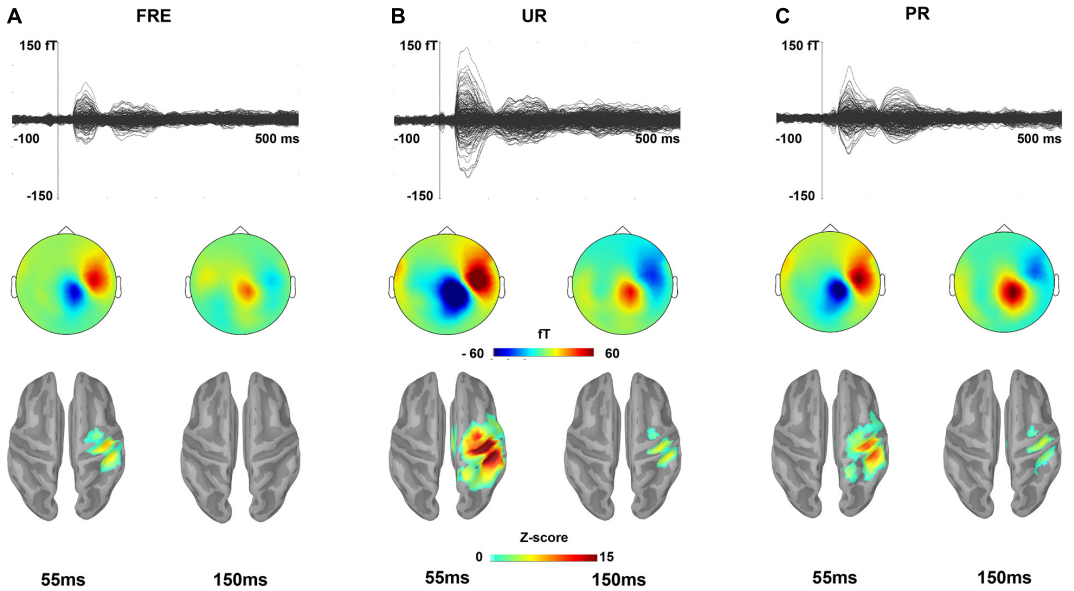

FIGURE 2 | The grand-averaged responses for **(A)** FRE, **(B)** UR, and **(C)** PR. The upper panel shows a butterfly view of the grand-averaged response for each stimulus type from all 306 sensors. For visualization purposes, gradiometer values are multiplied by 0.04 due to the differing units for magnetometers (T) and gradiometers (T/m). The middle and lower panels show the topographies of the sensor-level activity based on magnetometers and source activation, respectively, at a time point of 55 and 150 ms for each stimulus type. In the lower panel, only the sources that have a value > 40% of the color bar maximum are displayed. FRE, frequent stimulus; UR, unpredictable rare stimulus; PR, predictable rare stimulus.

illustrate the source activity waveform on both ROIs for each stimulus type (UR, PR, and FRE) and differential responses (UR–FRE and PR–FRE), respectively. As shown in **Figures 2**, **3A**, the response waveforms are characterized by two main components: one at approximately 30–100 ms latency (M55) and the other at approximately 130–230 ms latency (M150). The corresponding topography and source activation for each component are also presented in **Figure 2**. The sensor-level results are reported in **Supplementary Material 2**.

Source Activations

M55

For the results of the mean source activation value in 30–100 ms latency, one-way repeated-measures ANOVA showed main effects of stimulus type in both the cSI and cSII: in the cSI, $F(2,28) = 32.049$, $p_{corr} < 0.001$, $\eta^2_p = 0.696$); in the cSII, $F(2,28) = 18.126$, $p_{corr} < 0.001$, $\eta^2_p = 0.564$. *Post hoc* paired *t*-tests with Bonferroni-corrected *p*-values are reported in **Table 1** and **Figure 3C**. *Post hoc* tests revealed that both the PR and UR showed increased activation compared to the FRE in both the cSI and the cSII areas. In addition, both ROIs showed an increased source strength for the UR compared to the PR. The line graph of individuals' source strength to the three stimulus types are illustrated in **Figure 3D**. The grand-averaged source activations for different stimuli from the right-side view are illustrated in **Figure 4**.

M150

For M150, significant main effects for the stimulus type were found in both ROIs; cSI: $F(2,28) = 11.355$, $p < 0.001$, $\eta^2_p = 0.448$); cSII: $F(2,28) = 14.798$, $p < 0.001$, $\eta^2_p = 0.514$. *Post hoc* *t*-tests are reported in **Table 2** and **Figure 3C**. The results showed that in both ROIs, both the PR and the UR induced larger activity compared to the FRE. However, no difference was found between the UR and the PR in either the cSI or the cSII areas. The line graph of individuals' source strength to the three stimulus types are illustrated in **Figure 3D**. The grand-averaged source activations for the different stimuli from the right-side view are illustrated in **Figure 4**.

DISCUSSION

In the present study, we introduced a new oddball stimulus protocol for investigating brain responses to unpredictable and predictable rare somatosensory events. Use of this stimulus protocol allowed us to control for the rarity (probability) of the unpredictable and predictable stimuli. We found two main components, M55 and M150, for each stimulus type: the frequent stimulus (FRE), unpredictable rare stimulus (UR), and predictable rare stimulus (PR). The sources of both components were located on the contralateral somatosensory cortices. The sensor-level (see **Supplementary Material 2** for a detailed report) and the source-level results showed a similar pattern: both components elicited a larger activity for the UR and PR than for the FRE. A larger response was observed for the UR than for the PR only for M55, whereas no difference was found in response amplitudes between the UR and the PR for M150. This pattern of results suggests that M55, but not M150, possibly signals the prediction error.

The latencies of the components, one at 30–100 ms latency (M55) and the other at 130–230 ms latency (M150), were

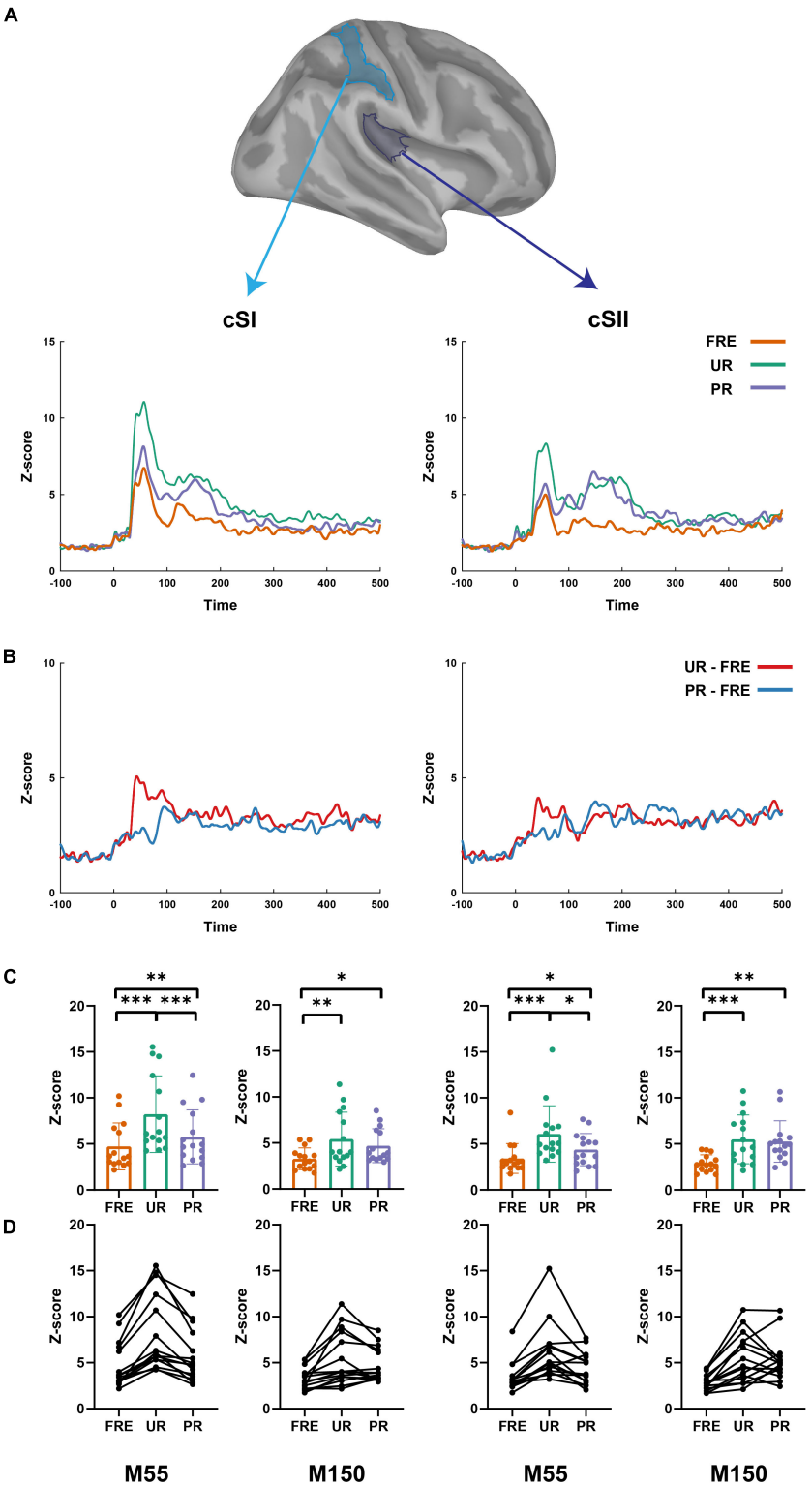

FIGURE 3 | The summary of the results from the source-level analysis. **(A)** The cortical time series for all three conditions (UR, PR, and FRE) in the cSI (left panel) and cSII (right panel). **(B)** The cortical time series for the differential responses (UR–FRE and PR–FRE) in the cSI (left panel) and cSII (right panel). **(C)** The bar graph of the source strength comparison of the FRE, UR, and PR in the cSI (left panel) and cSI (right panel). Error bars represent the standard error of the mean, and the dots represent the values of the individual participants. **(D)** Line graphs of the individual participant's source strengths to the three stimulus types in the cSI (left panel) and cSII (right panel). FRE, frequent stimulus; UR, unpredictable rare stimulus; PR, predictable rare stimulus; $^{*}p < 0.05$, $^{**}p < 0.01$, and $^{***}p < 0.001$.

well in line with the previous MEG studies that have found an early component approximately at 30–70 ms latency and a later component at approximately 100–200 ms after stimulus onset (Mima et al., 1998; Akatsuka et al., 2007a,b; Hautasaari et al., 2019). Some EEG studies that applied the somatosensory oddball paradigm have also found two components with similar latencies as M55 and M150 here (Shinozaki et al., 1998; Akatsuka et al., 2005; Restuccia et al., 2007; Strömmer et al., 2014, 2017). Consistent with previous MEG oddball studies that applied source localization (Mima et al., 1998; Akatsuka et al., 2007a,b; Naeije et al., 2016, 2018; Hautasaari et al., 2019), both components were elicited on the sensory cortices (SI and/or SII).

Our results resemble those of the previous somatosensory studies that applied a traditional oddball paradigm to elicit the sMMR; however, our data raise questions regarding the interpretation of the previous studies that the responses to rare unpredictable stimuli (here UR) at 100–200 ms latency reflect a prediction error (e.g., Mima et al., 1998; Shinozaki et al., 1998; Akatsuka et al., 2005, 2007a; Strömmer et al., 2014, 2017; Hautasaari et al., 2019). Namely, when we used equally rare stimuli with different types of predictability (UR and PR), the responses to these two stimuli did not show any amplitude difference for M150, but they did for M55. Although several studies have found larger responses to deviant than to standard stimuli at early latency (within the 100 ms post-stimulus latency, Mima et al., 1998; Shinozaki et al., 1998; Akatsuka et al., 2005, 2007a,b; Strömmer et al., 2014, 2017; Yamashiro et al., 2014; Hautasaari et al., 2019), these studies have usually considered only the later response (between 100 and 200 ms post stimulus), but not the earlier one (before 100 ms) as being analogous to sMMR (e.g., Mima et al., 1998; Shinozaki et al., 1998; Akatsuka et al., 2005, 2007a; Strömmer et al., 2014, 2017; Hautasaari et al., 2019). However, they did not provide any empirical evidence for the assumption of the specificity of the later response to a prediction error, nor did they rule out the effect of stimulus rareness (for example, by applying the many-standards control condition). Therefore, the previous findings of differential responses to deviant stimuli at 100–200 ms post-stimulus latency may possibly have reflected merely the rareness of the deviant stimulus. Conversely, the differential responses at the earlier latency (before 100 ms) reported in the previous studies (Mima et al., 1998; Shinozaki et al., 1998; Akatsuka et al., 2005, 2007a,b; Strömmer et al., 2014, 2017; Yamashiro et al., 2014; Hautasaari et al., 2019) could reflect a prediction error. Notably, the results from a previous MEG study indicated that two components, one at 30–70 ms and the other at 150–250 ms latency, showed increased amplitudes to deviant stimuli presented at 10%, but not at 30 or 50% probability (Akatsuka et al., 2007b). The results of this previous study, together with those of our study in which the predictability of the rare stimulus was manipulated, suggest that the earlier MEG component (here M55) could be specific to the prediction error and that the later responses (here M150) might reflect merely the stimulus rareness. Furthermore, studies that used a global/local paradigm to verify the hierarchical processing network of the sMMR at different levels found that a response peaking at 70–100 ms over the posterior bank of the postcentral sulcus reflected the prediction error (Naeije et al., 2016, 2018). In rabbits, similar and even earlier latencies (i.e., 20–40 and 80–100 ms) for somatosensory deviance detection have been found in recordings of local-field potentials from the somatosensory cortex (deviant-alone control condition, Astikainen et al., 2001).

Not only some of the previous studies in the somatosensory modality but also those in the auditory modality have reported deviance detection at early latencies. For example, the auditory middle latency responses (MLRs), elicited within 50 ms latency after the stimulus onset, have been studied in the context of predictive coding (e.g., Althen et al., 2011; Grimm et al., 2011; Recasens et al., 2014). These responses have their source generator possibly in the sensory cortex (Recasens et al., 2014), and a recently suggested view (Grimm et al., 2016) is that the MLRs could be correlates of stimulus-specific adaptation (SSA, Ulanovsky et al., 2003), which also occurs in a similar latency range. SSA (i.e., adaptation to repeated sounds that do not generalize to other sounds) is widely studied in animals with single-cell recordings. Although the name of the phenomenon refers to adaptation, release from SSA can also support genuine deviance detection (e.g., Parras et al., 2017; for a review, see Carbajal and Malmierca, 2018). Interestingly, a rat study that contrasted the auditory cortical responses to patterns of periodic (predictable) and random (unpredictable) changes in sounds found larger intracellular and extracellular responses to random than to periodic changes (Yaron et al., 2012). Future studies using both single-cell and neural network-level recordings are needed to understand whether the early latency brain responses (e.g., MLRs and the M55 reported here) in the auditory and somatosensory modalities have functional similarities and

TABLE 1 | *Post hoc* paired-samples *t*-tests investigating the main effect of the stimulus type found in the repeated-measures ANOVA for M55.

Conditions	cSI			cSII		
	t	p_{corr}	*d*	*t*	p_{corr}	*d*
PR vs. FRE	4.121	0.003	0.376	3.199	0.019	0.576
UR vs. FRE	6.612	<0.001	1.014	6.175	<0.001	1.086
UR vs. PR	4.816	<0.001	0.685	2.977	0.030	0.677

PR, predictable rare stimulus; FRE, frequent stimulus; UR, unpredictable rare stimulus; cSI, contralateral primary somatosensory cortex; cSII, contralateral secondary somatosensory cortex; p_{corr}, p-value after Bonferroni correction; d, Cohen's d. The degrees of freedom for all comparisons are 14.

TABLE 2 | *Post hoc* paired-samples *t*-tests investigating the main effect of stimulus type found in the repeated-measures of ANOVA for M150.

Conditions	cSI			cSII		
	t	p_{corr}	*d*	*t*	p_{corr}	*d*
PR vs. FRE	3.528	0.010	0.921	4.357	0.002	1.381
UR vs. FRE	3.768	0.006	0.962	5.161	<0.001	1.315
UR vs. PR	1.905	0.232	0.294	0.434	1.000	0.095

PR, predictable rare stimulus; FRE, frequent stimulus; UR, unpredictable rare stimulus; cSI, contralateral primary somatosensory cortex; cSII, contralateral secondary somatosensory cortex; p_{corr}, p-value after Bonferroni correction; d, Cohen's d. The degrees of freedom for all comparisons are 14.

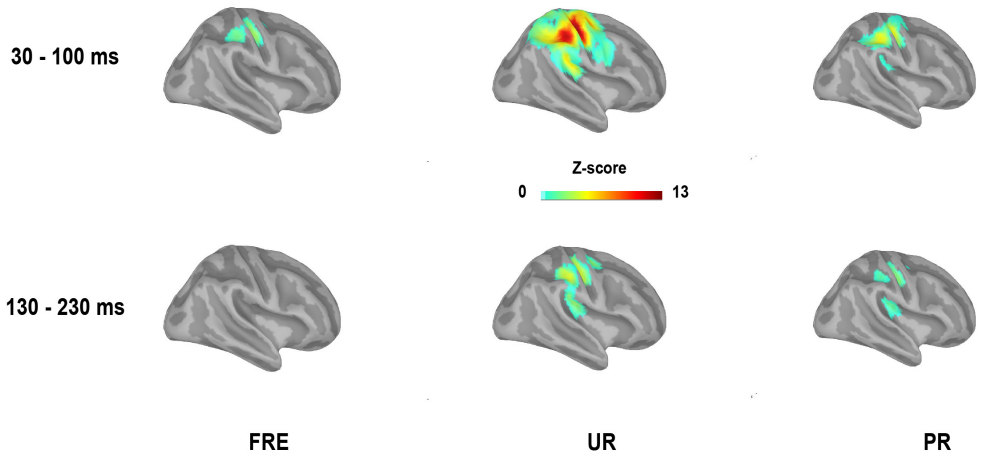

FIGURE 4 | Grand-averaged source activation for the time window of 30–100 ms (M55) and 130–230 ms (M150) after stimulus onset for each stimulus type from the right-side view (mean values of the time windows presented). For visualization purposes, only the sources with a value > 40% of the color bar maximum are displayed here. FRE, frequent stimulus, UR, unpredictable rare stimulus; PR, predictable rare stimulus.

whether they share neural mechanisms for rareness and/or deviance detection.

Here, the activity for both the UR and the PR was most pronounced on the sensory cortices (i.e., the SI and SII). Although some discrepancies exist regarding whether the activity has been found from the SI, the SII, or both, previous studies applying the somatosensory oddball condition have mainly located deviance detection-related responses in the SI and/or SII. Akatsuka et al. (2007a,b), who first applied the source localization method for the sMMR, suggested that the early component (30–70 ms) originates mainly from the SI. The later component (150–250 ms) was located mainly in the SI, but the data from some individuals showed the generators in the SII (Akatsuka et al., 2007a,b). Later, areas 1 and 3b of the SI, as well as the posterior parietal cortex (PPC), were linked to the deviance detection at approximately 50–120 ms post-stimulus latency. Deviance detection-related activity was also found on the bilateral SII cortex in a few participants (Yamashiro et al., 2014). Both the electrical and tactile stimuli also elicited SI activity for the early component (40–58 ms), and SII activity for the later component (110–185 ms) (Hautasaari et al., 2019). Some studies have also found simultaneous SI and SII responses as early as 20–30 ms (Karhu and Tesche, 1999) instead of a strict hierarchical or serial manner, suggesting that the SI and SII could process somatosensory stimuli in a parallel manner. Taken together with our results, the available evidence indicates a likelihood that the SI and SII could both contribute to the deviance detection and could also possibly be linked to the prediction error.

Even if our study strongly suggests that the increased response amplitude for M150 does not reflect a prediction error, the current study is limited in its interpretation regarding M55. The M55 was larger in amplitude for the UR than for the FRE and PR; however, whether the increased response amplitude reflects the prediction error or a larger stimulus energy for the UR in comparison to the PR and FRE is unclear. This is because the low-level stimulus features were not counterbalanced for all the stimulus types, but only between the FRE and PR. The stimulus energy for the UR (stimulation of two fingers at the same time) was larger than for the PR and FRE (stimulation of one finger) when the data combined from conditions A and B were analyzed. Therefore, we conducted an additional measurement (condition C) for a small subsample of participants (n = 4). In this measurement, the physical characteristics of the UR and FRE were reversed for condition B (**Supplementary Material 1**). Thus, when the data were combined from conditions B and C, the responses to the UR and FRE were counterbalanced for their low-level features. Visual observation of the data suggests that three of the four participants showed numerically larger activity for the UR than for the FRE in the M55 time range, and two of the four participants showed the same for M150. This suggests that the difference in low-level physical features was probably not the only reason for the larger responses to the UR than to the FRE in the larger sample, and this tentatively associates M55 with the prediction error.

Our paradigm may also be applied to the other sensory modalities. In the auditory modality, the many-standards control condition has recently been the most commonly used protocol to control for the effect of stimulus probability (e.g., Jacobsen and Schröger, 2001, 2003). However, the results may be affected by the cross-frequency adaptation (Taaseh et al., 2011) between the oddball and control condition sounds. The cross-frequency adaptation is usually observed as a reduced response amplitude to consecutive sounds of nearby frequencies. Because more sounds are present, and usually with smaller frequency differences in the control than in the oddball condition, the responses can be larger to the oddball deviant sounds than to the control sounds merely for this reason (see discussion in Yang et al., 2019, where the oddball and many-standards conditions have the same frequency separation in rats). The novel paradigm introduced in the present study can avoid this problem, because it does not require many different stimuli, and the stimuli can also be clearly distinct in frequency (or other changing feature). However, all three stimulus conditions (here conditions A and B in **Figure 1**

and condition C in **Supplementary Material 1**) are required to fully counterbalance the physical features of the three stimuli.

In summary, our results suggest that the processing of a stimulus site change in the electrical stimuli on the fingers induces two main components: M55 and M150. M55 was larger for the UR than for the FRE and PR over both the SI and SII. Surprisingly, although the UR had a larger prediction error potential and an even larger stimulus energy than the PR, it did not show an increased M150 amplitude when compared to the PR. Our data therefore tentatively link M55, but not M150, to signaling of the prediction error. The results also highlight the need for controlling the stimulus rareness or for disentangling stimulus rareness and predictability in future studies.

DATA AVAILABILITY STATEMENT

The raw data supporting the conclusions of this article will be made available by the authors, without undue reservation.

ETHICS STATEMENT

The studies involving human participants were reviewed and approved by the Ethical Committee of the University of Jyväskylä. The patients/participants provided their written informed consent to participate in this study.

AUTHOR CONTRIBUTIONS

QX and PA conceived the experiments. QX, ER, and XL performed the data acquisition. QX analyzed the data. JH contributed to data analysis. QX, CY, JH, and PA interpreted the data. QX, CY, and PA drafted the manuscript. JH, ER, and XL provided critical revisions. All authors revised and approved the manuscript.

FUNDING

This work was supported by grants from the National Natural Science Foundation of China (No. 31700948 to CY) and the Academy of Finland (No. 333649 to CY). The National Natural Science Foundation of China provided funding for the open-access publication fee. All authors had full independence from the funding sources.

ACKNOWLEDGMENTS

The authors thank Simo Monto and Viki-Veikko Elomaa for providing technical help with the MEG measurements and Weiyong Xu, Haoran Dou, and Brainstorm Engineer Francois Tadel for their help in data analysis.

SUPPLEMENTARY MATERIAL

The Supplementary Material for this article can be found online at: https://www.frontiersin.org/articles/10.3389/fnhum.2021.641273/full#supplementary-material

REFERENCES

Akatsuka, K., Wasaka, T., Nakata, H., Inui, K., Hoshiyama, M., and Kakigi, R. (2005). Mismatch responses related to temporal discrimination of somatosensory stimulation. *Clin. Neurophysiol.* 116, 1930–1937. doi: 10.1016/j.clinph.2005.04.021

Akatsuka, K., Wasaka, T., Nakata, H., Kida, T., Hoshiyama, M., Tamura, Y., et al. (2007a). Objective examination for two-point stimulation using a somatosensory oddball paradigm: an MEG study. *Clin. Neurophysiol.* 118, 403–411. doi: 10.1016/j.clinph.2006.09.030

Akatsuka, K., Wasaka, T., Nakata, H., Kida, T., and Kakigi, R. (2007b). The effect of stimulus probability on the somatosensory mismatch field. *Exp. Brain Res.* 181, 607–614. doi: 10.1007/s00221-007-0958-4

Althen, H., Grimm, S., and Escera, C. (2011). Fast detection of unexpected sound intensity decrements as revealed by human evoked potentials. *PLoS One* 6:e28522. doi: 10.1371/journal.pone.0028522

Astikainen, P., Cong, F., Ristaniemi, T., and Hietanen, J. K. (2013). Event-related potentials to unattended changes in facial expressions: detection of regularity violations or encoding of emotions? *Front. Hum. Neurosci.* 7:557. doi: 10.3389/fnhum.2013.00557

Astikainen, P., Ruusuvirta, T., and Korhonen, T. (2001). Somatosensory event-related potentials in the rabbit cerebral and cerebellar cortices: a correspondence with mismatch responses in humans. *Neurosci. Lett.* 298, 222–224. doi: 10.1016/S0304-3940(00)01747-X

Astikainen, P., Stefanics, G., Nokia, M., Lipponen, A., Cong, F., Penttonen, M., et al. (2011). Memory-based mismatch response to frequency changes in rats. *PLoS One* 6:e24208. doi: 10.1371/journal.pone.0024208

Bar, M. (2007). The proactive brain: using analogies and associations to generate predictions. *Trends Cogn. Sci.* 11, 280–289. doi: 10.1016/j.tics.2007.05.005

Beck, A. T., Steer, R. A., and Brown, G. K. (1996). *Manual for the Beck Depression Inventory-II*. San Antonio, TX: Psychological Corporation, 82.

Carbajal, G. V., and Malmierca, M. S. (2018). The neuronal basis of predictive coding along the auditory pathway: from the subcortical roots to cortical deviance detection. *Trends Hear.* 22:2331216518784822. doi: 10.1177/2331216518784822

Cohen, J. (1988). *Statistical Power Analysis for the Behavioral Sciences*, 2nd Edn. Hillsdale, NJ: Lawrence Erlbaum Associates.

Czigler, I. (2007). Visual mismatch negativity: violation of nonattended environmental regularities. *J. Psychophysiol.* 21, 224–230. doi: 10.1027/0269-8803.21.34.224

Destrieux, C., Fischl, B., Dale, A., and Halgren, E. (2010). Automatic parcellation of human cortical gyri and sulci using standard anatomical nomenclature. *Neuroimage* 53, 1–15. doi: 10.1016/j.neuroimage.2010.06.010

Fishman, Y. I., and Steinschneider, M. (2012). Searching for the mismatch negativity in primary auditory cortex of the awake monkey: deviance detection or stimulus specific adaptation? *J. Neurosci.* 32, 15747–15758. doi: 10.1523/JNEUROSCI.2835-12.2012

Friston, K. (2005). A theory of cortical responses. *Philos. Trans. R. Soc. B Biol. Sci.* 360, 815–836. doi: 10.1098/rstb.2005.1622

Garrido, M. I., Kilner, J. M., Stephan, K. E., and Friston, K. J. (2009). The mismatch negativity: a review of underlying mechanisms. *Clin. Neurophysiol.* 120, 453–463. doi: 10.1016/j.clinph.2008.11.029

Grimm, S., Escera, C., and Nelken, I. (2016). Early indices of deviance detection in humans and animal models. *Biol. Psychol.* 116, 23–27. doi: 10.1016/j.biopsycho.2015.11.017

Grimm, S., Escera, C., Slabu, L., and Costa-Faidella, J. (2011). Electrophysiological evidence for the hierarchical organization of auditory change detection in the human brain. *Psychophysiology* 48, 377–384. doi: 10.1111/j.1469-8986.2010.01073.x

Hari, R., Hämäläinen, H., Hämäläinen, M., Kekoni, J., Sams, M., and Tiihonen, J. (1990). Separate finger representations at the human second somatosensory cortex. *Neuroscience* 37, 245–249. doi: 10.1016/0306-4522(90)90210-U

Hautasaari, P., Kujala, U. M., and Tarkka, I. M. (2019). Detecting differences with magnetoencephalography of somatosensory processing after tactile and electrical stimuli. *J. Neurosci. Methods* 311, 331–337. doi: 10.1016/j.jneumeth.2018.09.014

Huang, M., Lee, R. R., Miller, G. A., Thoma, R. J., Hanlon, F. M., Paulson, K. M., et al. (2005). A parietal–frontal network studied by somatosensory oddball MEG responses, and its cross-modal consistency. *Neuroimage* 28, 99–114. doi: 10.1016/j.neuroimage.2005.05.036

Huang, M. X., Mosher, J. C., and Leahy, R. M. (1999). A sensor-weighted overlapping-sphere head model and exhaustive head model comparison for MEG. *Phys. Med. Biol.* 44, 423–440. doi: 10.1088/0031-9155/44/2/010

Jacobsen, T., Horenkamp, T., and Erich, S. (2003). Preattentive memory-based comparison of sound intensity. *Audiol. Neurootol.* 8, 338–346. doi: 10.1159/000073518

Jacobsen, T., and Schröger, E. (2001). Is there pre-attentive memory-based comparison of pitch? *Psychophysiology* 38, 723–727. doi: 10.1017/S0048577201000993

Jacobsen, T., and Schröger, E. (2003). Measuring duration mismatch negativity. *Clin. Neurophysiol.* 114, 1133–1143. doi: 10.1016/S1388-2457(03)00043-9

Karhu, J., and Tesche, C. D. (1999). Simultaneous early processing of sensory input in human primary (SI) and secondary (SII) somatosensory cortices. *J. Neurophysiol.* 81, 2017–2025. doi: 10.1152/jn.1999.81.5.2017

Kekoni, J., Hämäläinen, H., Saarinen, M., Gröhn, J., Reinikainen, K., Lehtokoski, A., et al. (1997). Rate effect and mismatch responses in the somatosensory system: ERP-recordings in humans. *Biol. Psychol.* 46, 125–142. doi: 10.1016/s0301-0511(97)05249-6

Kimura, M., Schröger, E., and Czigler, I. (2011). Visual mismatch negativity and its importance in visual cognitive sciences. *Neuroreport* 22, 669–673. doi: 10.1097/WNR.0b013e32834973ba

Krauel, K., Schott, P., Sojka, B., Pause, B. M., and Ferstl, R. (1999). Is there a mismatch negativity analogue in the olfactory event-related potential? *J. Psychophysiol.* 13, 49–55. doi: 10.1027//0269-8803.13.1.49

Kremláček, J., Kreegipuu, K., Tales, A., Astikainen, P., Põldver, N., Näätänen, R., et al. (2016). Visual mismatch negativity (vMMN): a review and meta-analysis of studies in psychiatric and neurological disorders. *Cortex* 80, 76–112. doi: 10.1016/j.cortex.2016.03.017

Kurkela, J. L. O., Lipponen, A., Kyläheiko, I., and Astikainen, P. (2018). Electrophysiological evidence of memory-based detection of auditory regularity violations in anesthetized mice. *Sci. Rep.* 8:3027. doi: 10.1038/s41598-018-21411-z

Lipponen, A., Kurkela, J. L. O., Kyläheiko, I., Hölttä, S., Ruusuvirta, T., Hämäläinen, J. A., et al. (2019). Auditory-evoked potentials to changes in sound duration in urethane-anaesthetized mice. *Eur. J. Neurosci.* 50, 1911–1919. doi: 10.1111/ejn.14359

Lohvansuu, K., Hämäläinen, J. A., Tanskanen, A., Bartling, J., Bruder, J., Honbolygó, F., et al. (2013). Separating mismatch negativity (MMN) response from auditory obligatory brain responses in school-aged children. *Psychophysiology* 50, 640–652. doi: 10.1111/psyp.12048

Maess, B., Jacobsen, T., Schröger, E., and Friederici, A. D. (2007). Localizing pre-attentive auditory memory-based comparison: magnetic mismatch negativity to pitch change. *Neuroimage* 37, 561–571. doi: 10.1016/j.neuroimage.2007.05.040

Maris, E., and Oostenveld, R. (2007). Nonparametric statistical testing of EEG- and MEG-data. *J. Neurosci. Methods* 164, 177–190. doi: 10.1016/j.jneumeth.2007.03.024

May, P., Tiitinen, H., Ilmoniemi, R. J., Nyman, G., Taylor, J. G., and Näätänen, R. (1999). Frequency change detection in human auditory cortex. *J. Comput. Neurosci.* 6, 99–120. doi: 10.1023/A:1008896417606

May, P. J. C., and Tiitinen, H. (2010). Mismatch negativity (MMN), the deviance-elicited auditory deflection, explained. *Psychophysiology* 47, 66–122. doi: 10.1111/j.1469-8986.2009.00856.x

Mima, T., Nagamine, T., Nakamura, K., and Shibasaki, H. (1998). Attention modulates both primary and second somatosensory cortical activities in humans: a magnetoencephalographic study. *J. Neurophysiol.* 80, 2215–2221. doi: 10.1152/jn.1998.80.4.2215

Musall, S., Haiss, F., Weber, B., and von der Behrens, W. (2017). Deviant processing in the primary somatosensory cortex. *Cereb. Cortex* 27, 863–876. doi: 10.1093/cercor/bhv283

Näätänen, R. (2009). Somatosensory mismatch negativity: a new clinical tool for developmental neurological research? *Dev. Med. Child Neurol.* 51, 930–931. doi: 10.1111/j.1469-8749.2009.03386.x

Näätänen, R., Astikainen, P., Ruusuvirta, T., and Huotilainen, M. (2010). Automatic auditory intelligence: an expression of the sensory–cognitive core of cognitive processes. *Brain Res. Rev.* 64, 123–136. doi: 10.1016/j.brainresrev.2010.03.001

Näätänen, R., Gaillard, A. W. K., and Mäntysalo, S. (1978). Early selective-attention effect on evoked potential reinterpreted. *Acta Psychol. (Amst).* 42, 313–329. doi: 10.1016/0001-6918(78)90006-9

Naeije, G., Vaulet, T., Wens, V., Marty, B., Goldman, S., and De Tiège, X. (2016). Multilevel cortical processing of somatosensory novelty: a magnetoencephalography study. *Front. Hum. Neurosci.* 10:259. doi: 10.3389/fnhum.2016.00259

Naeije, G., Vaulet, T., Wens, V., Marty, B., Goldman, S., and De Tiège, X. (2018). Neural basis of early somatosensory change detection: a magnetoencephalography study. *Brain Topogr.* 31, 242–256. doi: 10.1007/s10548-017-0591-x

Nakamura, T., Michie, P. T., Fulham, W. R., Todd, J., Budd, T. W., Schall, U., et al. (2011). Epidural auditory event-related potentials in the rat to frequency and duration deviants: evidence of mismatch negativity? *Front. Psychol.* 2:367. doi: 10.3389/fpsyg.2011.00367

Ostwald, D., Spitzer, B., Guggenmos, M., Schmidt, T. T., Kiebel, S. J., and Blankenburg, F. (2012). Evidence for neural encoding of Bayesian surprise in human somatosensation. *Neuroimage* 62, 177–188. doi: 10.1016/j.neuroimage.2012.04.050

Parras, G. G., Nieto-Diego, J., Carbajal, G. V., Valdés-Baizabal, C., Escera, C., and Malmierca, M. S. (2017). Neurons along the auditory pathway exhibit a hierarchical organization of prediction error. *Nat. Commun.* 8:2148. doi: 10.1038/s41467-017-02038-6

Pause, B. M., and Krauel, K. (2000). Chemosensory event-related potentials (CSERP) as a key to the psychology of odors. *Int. J. Psychophysiol.* 36, 105–122. doi: 10.1016/S0167-8760(99)00105-1

Polterovich, A., Jankowski, M. M., and Nelken, I. (2018). Deviance sensitivity in the auditory cortex of freely moving rats. *PLoS One* 13:e0197678. doi: 10.1371/journal.pone.0197678

Recasens, M., Grimm, S., Capilla, A., Nowak, R., and Escera, C. (2014). Two sequential processes of change detection in hierarchically ordered areas of the human auditory cortex. *Cereb. Cortex* 24, 143–153. doi: 10.1093/cercor/bhs295

Restuccia, D., Marca, G., Della Valeriani, M., Leggio, M. G., and Molinari, M. (2007). Cerebellar damage impairs detection of somatosensory input changes. A somatosensory mismatch-negativity study. *Brain* 130, 276–287. doi: 10.1093/brain/awl236

Restuccia, D., Zanini, S., Cazzagon, M., Del Piero, I., Martucci, L., and Della Marca, G. (2009). Somatosensory mismatch negativity in healthy children. *Dev. Med. Child Neurol.* 51, 991–998. doi: 10.1111/j.1469-8749.2009.03367.x

Schröger, E., and Wolff, C. (1996). Mismatch response of the human brain to changes in sound location. *Neuroreport* 7, 3005–3008. doi: 10.1097/00001756-199611250-00041

Shen, G., Smyk, N. J., Meltzoff, A. N., and Marshall, P. J. (2018). Neuropsychology of human body parts: exploring categorical boundaries of tactile perception using somatosensory mismatch responses. *J. Cogn. Neurosci.* 30, 1858–1869. doi: 10.1162/jocn

Shinozaki, N., Yabe, H., Sutoh, T., Hiruma, T., and Kaneko, S. (1998). Somatosensory automatic responses to deviant stimuli. *Cogn. Brain Res.* 7, 165–171. doi: 10.1016/S0926-6410(98)00020-2

Spackman, L. A., Boyd, S. G., and Towell, A. (2007). Effects of stimulus frequency and duration on somatosensory discrimination responses. *Exp. Brain Res.* 177, 21–30. doi: 10.1007/s00221-006-0650-0

Spackman, L. A., Towell, A., and Boyd, S. G. (2010). Somatosensory discrimination: an intracranial event-related potential study of children with refractory epilepsy. *Brain Res.* 1310, 68–76. doi: 10.1016/j.brainres.2009.10.072

Stefanics, G., Csukly, G., Komlósi, S., Czobor, P., and Czigler, I. (2012). Processing of unattended facial emotions: a visual mismatch negativity study. *Neuroimage* 59, 3042–3049. doi: 10.1016/j.neuroimage.2011.10.041

Stefanics, G., Kremláček, J., and Czigler, I. (2014). Visual mismatch negativity: a predictive coding view. *Front. Hum. Neurosci.* 8:666. doi: 10.3389/fnhum.2014.00666

Strömmer, J. M., Põldver, N., Waselius, T., Kirjavainen, V., Järveläinen, S., Björksten, S., et al. (2017). Automatic auditory and somatosensory brain responses in relation to cognitive abilities and physical fitness in older adults. *Sci. Rep.* 7:13699. doi: 10.1038/s41598-017-14139-9

Strömmer, J. M., Tarkka, I. M., and Astikainen, P. (2014). Somatosensory mismatch response in young and elderly adults. *Front. Aging Neurosci.* 6:293. doi: 10.3389/fnagi.2014.00293

Taaseh, N., Yaron, A., and Nelken, I. (2011). Stimulus-specific adaptation and deviance detection in the rat auditory cortex. *PLoS One* 6:e23369. doi: 10.1371/journal.pone.0023369

Tadel, F., Baillet, S., Mosher, J. C., Pantazis, D., and Leahy, R. M. (2011) Brainstorm: a user-friendly application for MEG/EEG analysis. *Comput. Intell. Neurosci.* 2011:879716. doi: 10.1155/2011/879716

Taulu, S., Simola, J., and Kajola, M. (2004). Clinical applications of the signal space separation method. *Int. Congr. Ser.* 1270, 32–37. doi: 10.1016/j.ics.2004.05.004

Tesche, C. D., and Karhu, J. J. T. (2000). Anticipatory cerebellar responses during somatosensory omission in man. *Hum. Brain Mapp.* 9, 119–142. doi: 10.1002/(SICI)1097-0193(200003)9

Ulanovsky, N., Las, L., and Nelken, I. (2003). Processing of low-probability sounds by cortical neurons. *Nat. Neurosci.* 6, 391–398. doi: 10.1038/nn1032

Wacongne, C., Changeux, J. P., and Dehaene, S. (2012). A neuronal model of predictive coding accounting for the mismatch negativity. *J. Neurosci.* 32, 3665–3678. doi: 10.1523/JNEUROSCI.5003-11.2012

Xu, Q., Ruohonen, E. M., Ye, C., Li, X., Kreegipuu, K., Stefanics, G., et al. (2018). Automatic processing of changes in facial emotions in dysphoria: a magnetoencephalography study. *Front. Hum. Neurosci.* 12:186. doi: 10.3389/fnhum.2018.00186

Yamashiro, K., Sato, D., Onishi, H., Sugawara, K., Nakazawa, S., Kameyama, S., et al. (2014). Effect of changes in stimulus site on activation of the posterior parietal cortex. *Brain Topogr.* 28, 261–268. doi: 10.1007/s10548-014-0378-2

Yang, T., Hämäläinen, J. A., Lohvansuu, K., Lipponen, A., Penttonen, M., and Astikainen, P. (2019). Deviance detection in sound frequency in simple and complex sounds in urethane-anesthetized rats. *Hear. Res.* 399:107814. doi: 10.1016/j.heares.2019.107814

Yaron, A., Hershenhoren, I., and Nelken, I. (2012). Sensitivity to complex statistical regularities in rat auditory cortex. *Neuron* 76, 603–615. doi: 10.1016/j.neuron.2012.08.025

Zhao, C., Valentini, E., and Hu, L. (2014). Functional features of crossmodal mismatch responses. *Exp. Brain Res.* 233, 617–629. doi: 10.1007/s00221-014-4141-4

Conflict of Interest: The authors declare that the research was conducted in the absence of any commercial or financial relationships that could be construed as a potential conflict of interest.

frontiers in Human Neuroscience

ORIGINAL RESEARCH
published: 09 July 2021
doi: 10.3389/fnhum.2021.682820

Auditory Pattern Representations Under Conditions of Uncertainty—An ERP Study

Maria Bader, Erich Schröger and Sabine Grimm*

Cognitive and Biological Psychology, Institute of Psychology—Wilhelm Wundt, Faculty of Life Sciences, Leipzig University, Leipzig, Germany

The auditory system is able to recognize auditory objects and is thought to form predictive models of them even though the acoustic information arriving at our ears is often imperfect, intermixed, or distorted. We investigated implicit regularity extraction for acoustically intact versus disrupted six-tone sound patterns *via* event-related potentials (ERPs). In an exact-repetition condition, identical patterns were repeated; in two distorted-repetition conditions, one randomly chosen segment in each sound pattern was replaced either by white noise or by a wrong pitch. In a roving-standard paradigm, sound patterns were repeated 1–12 times (standards) in a row before a new pattern (deviant) occurred. The participants were not informed about the roving rule and had to detect rarely occurring loudness changes. Behavioral detectability of pattern changes was assessed in a subsequent behavioral task. Pattern changes (standard vs. deviant) elicited mismatch negativity (MMN) and P3a, and were behaviorally detected above the chance level in all conditions, suggesting that the auditory system extracts regularities despite distortions in the acoustic input. However, MMN and P3a amplitude were decreased by distortions. At the level of MMN, both types of distortions caused similar impairments, suggesting that auditory regularity extraction is largely determined by the stimulus statistics of matching information. At the level of P3a, wrong-pitch distortions caused larger decreases than white-noise distortions. Wrong-pitch distortions likely prevented the engagement of restoration mechanisms and the segregation of disrupted from true pattern segments, causing stronger informational interference with the relevant pattern information.

Keywords: auditory processing, P3a, complex sound patterns, event-related potentials, mismatch negativity

OPEN ACCESS

Edited by:
István Winkler, Hungarian Academy of Sciences (MTA), Hungary

Reviewed by:
Anne Caclin, Institut National de la Santé et de la Recherche Médicale (INSERM), France
Dean F. Salisbury, University of Pittsburgh, United States
Petri Paavilainen, University of Helsinki, Finland

****Correspondence:***
Maria Bader
maria.bader@uni-leipzig.de

Specialty section:
This article was submitted to Cognitive Neuroscience, a section of the journal Frontiers in Human Neuroscience

Received: *19 March 2021*
Accepted: *11 June 2021*
Published: *09 July 2021*

Citation:
Bader M, Schröger E and Grimm S (2021) Auditory Pattern Representations Under Conditions of Uncertainty— An ERP Study. Front. Hum. Neurosci. 15:682820. doi: 10.3389/fnhum.2021.682820

INTRODUCTION

Acoustic information, which arrives at ours ears and informs us about objects in the outer world, is often imperfect. Parts of the relevant object information might be obscured by extraneous noise from concurrent auditory sources, for instance, from some sudden, interfering background sounds like a honking car or a barking dog. In other instances, parts of the relevant auditory objects can be missing. Furthermore, particularly in the domains of speech and music, mistakes in production might lead to imperfect recurrences of the same object, for instance, when a familiar melody is played with a missing or a wrong note or a word is uttered with an incorrect phoneme. Such

occurrences can intermix with or distort the acoustic input we are currently paying attention to, and might impede its intelligibility.

Our ability to deal with such distortions and to interpret the acoustic environment, even if it is degraded to a certain degree, is a remarkable asset. One should note that, on the one hand, our auditory system is able to detect even slight variations in the acoustic input. Previous studies found that the auditory system is sensitive to very subtle acoustic changes (e.g., in sound frequency), particularly if the respective varying sound event occurs after a row of invariant repetitions (Sams et al., 1985; Winkler et al., 1990). On the other hand, our brain must be able to tolerate variation to some extent. That is, we need to neglect input variation that is irrelevant for the current task or we need to compensate for missing or distorted information. Usually, we are well able to maintain a stable representation of objects in the environment, even if we encounter them occasionally in a degraded form. In fact, mechanisms of perceptual prediction and restoration help us to fill in and reconstruct occluded or obscured information. This occurs not only in the visual world (e.g., in the case of the blind spot; Walls, 1954; Ramachandran, 1992; De Weerd, 2006; Spillmann et al., 2006) but also in the auditory domain. Studies on the continuity illusion show that a tone or a word containing a short gap may be perceived as continuous if the gap is filled with noise. The listener then perceives the missing information, suggesting that the auditory system predicts and interpolates through the absent information (Warren et al., 1997; Micheyl et al., 2003; Riecke et al., 2007; Shahin et al., 2009; Bendixen et al., 2014).

Especially in speech and music research, perceptual restoration and filling-in processes are attributed to top-down influences (DeWitt and Samuel, 1990; Shinn-Cunningham and Wang, 2008). When phonemes are replaced with white noise, a word utterance can still seem intact, and, oftentimes, listeners cannot say which part of the uttered sentence was missing (Warren and Warren, 1970). Although this effect is clearly influenced by knowledge and experience, part of the phenomena might occur pre-attentively on lower levels of processing (Micheyl et al., 2003; Riecke et al., 2007).

Electrophysiological markers like the mismatch negativity (MMN) can serve as an index for such implicit and automatic compensatory mechanisms of early processing stages (Micheyl et al., 2003). The MMN is elicited by sounds violating a detected regularity in a sequence of sounds, for example, when a tone differing in pitch (deviant) is presented following a sequence of tones with identical pitch (standards). MMN reflects the process of deviance detection, and its presence indirectly implies that the regularity inherent in the standard tones has been encoded (Winkler, 2007). Although early accounts interpreted the MMN as the outcome of a retrospective comparison process between regularity representations and the incoming deviant sound, newer accounts emphasize that regularity representations are part of an internal model, prospectively generating predictions about future input (Wacongne et al., 2012; Bendixen et al., 2014; Winkler and Schröger, 2015). Previous studies showed that predictions and regularity representations of standards build up even in the absence of exact repetitions of a stimulus, for instance, when using abstract regularities (Tervaniemi et al., 2000; Brattico et al., 2006; Bendixen and Schröger, 2008; Bader et al., 2017) or in the presence of noise that degrades the physical information (Muller-Gass et al., 2001; Micheyl et al., 2003; Kozou et al., 2005). All these studies demonstrate the tolerance of the MMN systems to a considerable amount of variability in the sequence of standard sounds, including cases of imperfect repetitions of standard sounds.

These findings also align with studies on auditory object segregation. For example, McDermott et al. (2011) showed that the auditory system quickly recognizes invariant patterns, even when they are embedded in a changing acoustic background of competing sounds. The authors suggest a mechanism of cross-correlating dynamic spectrotemporal input patterns, which filters for invariances between different occurrences of the same auditory event (despite its being mixed with background noise). Nevertheless, pattern recognition is impaired for sound patterns that are not identically repeated within the mixtures of changing backgrounds. In event-related potentials (ERP) studies, deviant sounds elicit an MMN of decreased amplitude and increased latency in cases where regularity formation is impeded by abstract variations or noise masking (Muller-Gass et al., 2001; Niemitalo-Haapola et al., 2015; Bader et al., 2017).

The MMN component can be followed by a P3a component distributed over fronto-central scalp regions. Typically, P3a is interpreted as signaling an involuntary attentional switch from a primary task to the deviant stimulus (Squires et al., 1975; Escera et al., 2000; Friedman et al., 2001; Wetzel and Schröger, 2007). P3a is sometimes also discussed to reflect a higher level but automatic evaluation of novelty rather than the switch of attention itself (Horvath et al., 2008; Wetzel et al., 2013; Winkler and Schröger, 2015). The P3a amplitude is modulated by cognitive and working memory demands of the task (Berti et al., 2004). P3a amplitude and latency can be modulated by experimental manipulations affecting salience, such as in the presence of abstract variations (Bader et al., 2017) and quality degradations of the regularity inherent in the standards, for example, by added noise, interruptions, or frequency distortions (Micheyl et al., 2003; Bader et al., 2017; Uhrig et al., 2017). That is, P3a amplitude might be decreased and latency increased if deviants violate a regularity that is not defined by exact sound or pattern repetitions, for instance, in the case of a new melodic pattern occasionally occurring among pattern repetitions in a transposed form (Bader et al., 2017).

In the current study, we investigated the early phase of implicit auditory pattern learning. The presented sounds were attended; however, the pattern regularity rule was irrelevant for the task at hand. Thus, learning occurred incidentally rather than intentionally (Perruchet and Pacton, 2006). During the experiment, a standard six-tone pattern is either repeated identically to the listeners or repeated, containing distortions, which leave only 5/6 of the standard pattern intact during each presentation. In particular, the three experimental conditions included (1) an exact-repetition condition (exact) in which sound patterns within a train were perfect repetitions without any distortion; (2) a white-noise-distortion condition (wn) in which one tonal segment of the repeating sound pattern was replaced randomly by Gaussian noise, and (3) a wrong-pitch-distortion

condition (wp) in which one tonal segment of the repeating sound pattern underwent a random shift in pitch. The respective distortions could affect a different tonal segment in each pattern presentation; the same segment would be intact in the next pattern presentation. Importantly, we were not measuring the ERPs to the distortions in every trial but, rather, the ERPs to occurrences of a completely new pattern, whether or not the preceding pattern learning happened with or without distortions. If the buildup of a pattern representation is (at least partly) robust against pattern variance in complex auditory stimuli, we hypothesize that MMN and P3a will be elicited in conditions with and without distortions.

However, given that a lower quantity of unambiguous information guides the initial learning process, one might expect poorer pattern representation from distorted standard sounds as indicated by decreased MMN and P3a amplitude and possible latency delays. Given that an equal portion (five out of six tones) was unambiguously informative about the identity of the standard pattern in both distortion conditions, one might expect to find similar impairments in the two distortion conditions. Nevertheless, there are certainly qualitative differences between white noise and wrong pitch distortions. Noise contains the frequencies of the "true" pattern segment and can involve filling-in or restoration processes, once an internal representation of the standard pattern has been formed; whereas wrong pitch distortions might interfere with the formation of a pattern representation. Therefore, differential effects on MMN and/or P3a could be expected in the two distortion conditions, particularly with stronger impairments in the wrong-pitch condition. If that is the case, one can conclude that potentially different mechanisms rule the formation of pattern identity representations in the context of white noise or wrong pitch distortions. This would also be compatible with masking studies, showing stronger degrading effects on speech intelligibility when it is masked by similar stimulus material, such as irrelevant speech (as in the case of informational masking), than when it is masked by noise (as in the case of energetic masking) (Cooke et al., 2008; Lidestam et al., 2014).

Furthermore, if we observed such distortion-specific effects already at the level of MMN, this would argue in favor of an impact of our manipulation on relatively early merely perceptual and automatic processing levels. In contrast, if they were confined to the P3a level, this would indicate that distortion processing occurs only at a later stage in the course of more context-dependent novelty evaluation and automatic orienting of attention.

As mentioned above, we expect MMN and P3a elicitation to full pattern changes in all conditions and a possible differentiable effect of the inserted distortions. These effects might also interact with the number of preceding standards. Therefore, the number of standard patterns (with or without distortions) preceding a deviant was varied (1, 2, 3, 6, or 12 standard patterns) in a roving-standard paradigm (Winkler et al., 1996; Bendixen and Schröger, 2008; Garrido et al., 2009). According to previous studies (Cowan et al., 1993; Winkler et al., 1996; Bendixen et al., 2007; Garrido et al., 2008; Bader et al., 2017), we expect to see a growth in MMN (and P3a) amplitude with increasing numbers of preceding standards in all conditions, if the implicit learning mechanisms are robust against the inserted distortions. Likely, both standard and deviant ERPs contribute to the MMN increase with deviant ERPs growing more negative and standard ERPs growing more positive (and *vice versa* for the P3a) as a function of the number of previous standards in a train (Baldeweg et al., 2004; Bendixen et al., 2007; Costa-Faidella et al., 2011; Bader et al., 2017). We will model the emergence and growth, using a logarithmic regression analysis, because regression coefficients can be informative of the time course and the strength of the implicit formation of pattern representations in our three distortion conditions.

MATERIALS AND METHODS

Participants

The experimental protocol was approved by the Ethical Committee of the University of Leipzig and was in accordance with the Code of Ethics of the World Medical Association (Declaration of Helsinki). The participants gave written informed consent before experimental sessions. All the subjects in the experiment participated for credit points or monetary compensation (€8 per hour). Of the 19 healthy subjects (age range: 19–40 years, 18 females) that participated in this research, all reported normal hearing and 17 out of 19 participants were right-handed. All of them were Leipzig University students, and 84% reported to have played a musical instrument for some time (M = 6.6 years, SD = 4.2 years).

Materials

As in one of our previous studies (Bader et al., 2017), auditory stimuli were composed of 300-ms sound patterns, consisting each of six concatenated 50-ms segments with randomly chosen fundamental frequencies between 220 and 880 Hz (in 25 semitone steps). Harmonics were added to each fundamental frequency until a cutoff at 6,000 Hz. Starting at 3,000 Hz, tonal segments were modulated by reducing the signal linearly resulting in 0% intensity at 6,000 Hz. For a smoother sound, odd harmonics (uneven positive integer multiples of the fundamental frequency) were additionally attenuated to 20% of their intensity. To prevent loudness differences between segments, intensities were root mean square equalized. Segments included a 5-ms rise and a 5-ms fall time, and there were no gaps introduced between the six segments when concatenating them to a sound pattern. The stimulus onset asynchrony (SOA) between patterns presented in our auditory sequences was set to 650 ms.

Design and Procedure

Sound patterns were presented in a roving-standard paradigm (Cowan et al., 1993; Winkler et al., 1996; Bendixen et al., 2007; Garrido et al., 2008) with varying train lengths; a randomly generated sound pattern was presented either 1, 2, 3, 6, or 12 times in a sequence before a newly generated pattern occurred, which started a new train of stimuli. In a single block of the experiment, each possible train length occurred 10 times in random order, resulting in 240 pattern presentations per block. As in our previous study (Bader et al., 2017), 10 additional trials

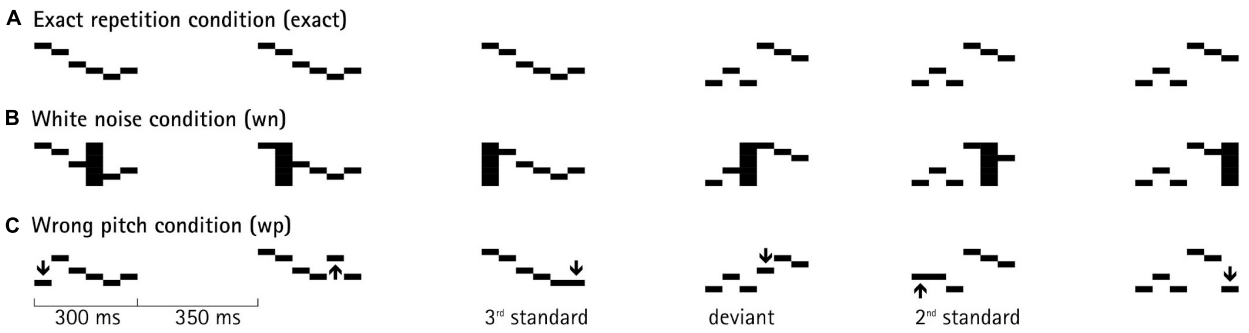

FIGURE 1 | An example of a pattern sequence, in which patterns were presented in a roving-standard paradigm. At the third position, the pattern has been presented three times; before, at the fourth position, a new train started with a new sound pattern (deviant), which, itself, is repeated within that next train. Each deviant corresponds to a first standard of a new train. Each pattern was composed of six concatenated 50-ms segments, differing in fundamental frequency (black horizontal bars). SOA (stimulus onset asynchrony) was set to 650 ms (= 300-ms pattern duration + 350-ms interstimulus interval). The *top line* **(A)** depicts the identical repetition of a sound pattern within a train in the exact-repetition condition. The *middle line* **(B)** depicts the white-noise-distortion condition, in which a randomly chosen segment of each sound pattern was replaced by white noise, marked with the black vertical bar. The *bottom line* **(C)** depicts the wrong-pitch condition, in which a randomly chosen segment of each sound pattern was replaced by a new segment of randomly chosen new pitch, indicated by the arrow.

of train length 1 were included in each block, in the way that one trial of train length 1 was directly followed by another trial of train length 1. In this context, three pattern changes always occurred in a row. This served to have pattern changes that did not follow a pattern repetition, and it ensured the investigation of memory trace formation, starting with a first pattern presentation. Here, the first pattern change served as a deviant with respect to the previous train, the second served as a "standard" of train length 1, and the third served as a "deviant" of train length 1. This terminology is consistent with the one used for other train lengths but, admittedly, arbitrary, since stimuli of train length 1 do not have an actual history of pattern repetition. Overall, for each train length, a similar number of standard and deviant patterns was available for ERP analysis (Bader et al., 2017).

The experiment consisted of two sessions with a total of 36 blocks (12 blocks × 3 conditions). In each session, six blocks of each condition were presented in random order. In the exact-repetition condition, patterns were repeated 100% identically within a train. In the white-noise condition, during each presentation of a melodic pattern, one randomly chosen segment out of the six was replaced by a 50-ms snippet of white noise. In the wrong-pitch condition, the pitch of one segment in each pattern was changed to a randomly chosen new pitch, while keeping all other characteristics of that segment (e.g., timbre) unchanged. The randomly chosen pitch for the new segment could keep the contour of the pattern intact, or violate it with equal probability. Each position of a pattern (1–6) could be affected by this manipulation with equal probability in the two distortion conditions—randomly selected from trial to trial. The intensity of the white noise segment was root-mean-square equalized to the rest of the pattern. **Figure 1** depicts an example of a train with three patterns and the beginning of the following train.

At the beginning of the first session, ability of the participants to tell whether two melodic phrases are the same or different was measured *via* the melody part of musical ear test (MET) of Wallentin et al. (2010). It contains 52 trials during which two short melodies (comprising of three to eight tones) are played with a tempo of 100 beats per minute, one after the other, with sampled piano sounds. This part of the MET lasts approximately 10 min. In half of the 52 trials, the two melodies are identical. In order to be above-chance level, the participants must score 32 out of 52 trials correctly (= 62%).

During the experimental sessions, the participants were seated in an electrically and acoustically shielded chamber in our laboratory at the Institute of Psychology of Leipzig University. To minimize eye movements, the participants fixated a cross on a computer screen placed behind a window outside the chamber 130 cm from the eyes of the participants. Auditory stimuli were presented binaurally over headphones (Sennheiser HD 25) at an intensity level of approximately 78 dB SPL. The participants were not informed about the roving rule. While listening to the presented sound patterns, the subjects performed a loudness change detection task in order to ensure their attention on the auditory stimulation. Occasionally, the sound patterns were presented with a higher volume (+ 4 dB, five sound patterns = 2% per block) or with a lower volume (–4 dB, five sound patterns = 2% per block). The participants pressed the left button of a response pad as soon as they detected a sound pattern of lower volume and the right button of the response pad as soon as they detected a sound pattern of higher volume. The targets were distributed randomly over each block with the restriction of at least two non-targets in between. After finishing a block, the participants received feedback on their performance (a ratio of hits, interchanged buttons, false alarms, and their mean reaction time). After each block, the subjects had a short break, allowing for movements.

Additionally, at the end of the second experimental session, the participants performed an active pattern change detection task to measure behavioral detectability of pattern changes. In these active blocks, the SOA was prolonged to 1,100 ms for the participants to have sufficient time for solving the task. They were instructed to detect the onset of a new train while ignoring segment distortions. They pressed a button of the response pad as

soon as they detected a change to a new sound pattern. After short training, each subject performed one block of each distortion condition, consisting of 200 trials each (8 times train lengths 2, 3, 6, and 12; 16 times train length 1). The order of conditions was counterbalanced over the participants.

Data Acquisition and Analyses

Electroencephalography data were collected continuously from 64 Ag/AgCl active electrodes. The electrodes were positioned according to the international 10–20 system in a nylon cap. The vertical and horizontal electrooculograms (EOG) were measured with external electrodes placed above and below the right eye and at the outer canthi of both eyes, respectively. As possible offline references, additional electrodes were placed on the tip of the nose and over each mastoid. All electrode signals were (DC) amplified and continuously sampled with a rate of 512 Hz (an anti-aliasing filter with –3 dB at 1/4 of the sampling frequency) by BioSemi Active-Two amplifiers. No high-pass filter was applied online. The BioSemi system uses the common mode sense (CMS) and the driven right leg (DRL) electrode—placed at different sites at the back of the head—to reference the recording to the CMS–DRL ground while minimizing the effect of external noise sources[1].

Offline, EEG data were re-referenced to the average signal of the two mastoids (Paavilainen et al., 1989; Ritter et al., 1992; Schröger, 1997) and filtered using a 0.5 Hz high pass filter (transition bandwidth of 1 Hz, filter order 1,690) and a 35 Hz low pass filter (transition bandwidth of 10 Hz, filter order 170). Both filters were Kaiser windowed sinc FIR filters (beta = 5.653, stopband attenuation = –60 dB implemented in EEGLAB (Delorme and Makeig, 2004; Widmann et al., 2015). Epochs of 650-ms duration were extracted from the continuous electroencephalography (EEG) time-locked to sound pattern onset. No baseline correction was applied to avoid the introduction of pre-stimulus neuroelectric activity in the baseline period into the post-stimulus waveforms (Urbach and Kutas, 2006). Epochs were sorted for each participant, condition, and stimulus type. Artifactual epochs with a signal range exceeding 100 μV on any recording channel (including EOG channels) were discarded from the analyses. To exclude trials containing artifacts, which are not characterized by extreme amplitude but by noise, we additionally ran a sorted averaging procedure (Muhler and von Specht, 1999; Rahne et al., 2008), during which all epochs of one condition and one participant were sorted according to their noise level (quantified by the root mean square of the voltage and sorted from lowest to highest) and successively entered the average as long as they increase the overall signal-to-noise ratio of the average. Epochs with extreme noise levels, which have a deteriorating effect on the signal to the noise ratio, were excluded. On average, 87 epochs (= 73%) remained for analysis across conditions and the participants. The data of all the participants went into analyses.

Event-related potentials were averaged for deviant sounds (the first pattern of a new train) and for standard sounds (the last corresponding pattern of the preceding train) in each condition. Difference waves were computed by subtracting the standard from the deviant ERPs. To compare ERP effects, in general, between the three conditions, we pooled the deviant and standard ERPs of train lengths 3, 6, and 12 in order to extract a general difference waveform in each condition (general analysis). Train lengths 1 and 2 were not included in the general analysis, because former studies showed that perceptual regularity extraction requires at least two repetitions (i.e., three presentations) of the standard before unexpected complex sound patterns elicit an MMN (Bendixen and Schröger, 2008; Bader et al., 2017). With non-parametric cluster-based permutation tests (Maris and Oostenveld, 2007), we tested for the presence of significant MMN and P3a components in each condition within this general analysis by comparing the whole epoch of the deviant ERP with the standard ERP (α-level for channels and clusters: Monte Carlo $p < 0.05$). About 1,000 permutations were run for each test, and dependent samples *t*-tests quantified the effect. These analyses and the creation of topographical scalp plots were run in FieldTrip (Oostenveld et al., 2011).

For the statistical assessment, amplitude measures were derived from the individual ERPs as the mean signal amplitude in the component time interval for combined conditions (MMN: 200–300 ms after the stimulus onset, P3a: 400–500 ms after the stimulus onset). An estimate of relative slope of each component at the latency for which 75% of the peak amplitude was reached was determined, using the jackknife approach (Miller et al., 1998; Kiesel et al., 2008).

The MMN and P3a amplitude were separately subjected to a repeated measures analysis of variance (ANOVA) with the factors condition (exact, wn, wp), stimulus type (deviant, standard), and train length (1, 2, 3, 6, and 12) as within-subject factors. For the MMN, maximal peak deflections were distributed over different electrodes in central-parietal regions (CPz, Pz, POz). Following a data-driven approach, we focused our MMN analyses on this region with maximal amplitude, and we discuss this rather unexpected topography later (see Discussion). To examine possible topography differences, the factor electrode (CPz, Pz, and POz) was added to the ANOVA. P3a measures were taken from electrode FCz because amplitude deflected maximally at this electrode in all conditions. Three condition-wise repeated measures ANOVAs, with the factors stimulus type (deviant, standard) and train length (1, 2, 3, 6, and 12), and two stimulus-type-wise repeated measures ANOVAs, with the factors condition (exact, wn, and wp) and train length (1, 2, 3, 6, and 12), were run to explore the three-way interactions for MMN and P3a. To investigate in more detail whether and how amplitude of MMN and P3a, as well as the contribution of deviant and standard stimuli to amplitude of both components, changed systematically as a function of train length; *post hoc* logarithmic trend analyses were run for difference waveforms, deviant and standard ERPs, separately. The standardized regression coefficient *r* and its 95% confidence interval (lower and upper bounds) were reported. All ANOVAs generalized eta squared (η^2) served as an estimate of effect size (Bakeman, 2005), and the Greenhouse–Geisser correction was applied when the assumption of sphericity was violated (corrected *df*s were reported). All parametric statistical analyses

[1]https://www.biosemi.com/faq/cms&drl.htm

and the creation of figures were run with RStudio (RStudio. PBC. Version 1.3.1073).

To ensure the participants attended to the auditory stimulation during the EEG session, we analyzed sensitivity d' according to Macmillan and Creelman (2004) to the loudness changes. Sensitivity d' was adjusted for extreme hit or false alarm rates to avoid infinite d' values by adding 0.5 to all response counts (Brown and White, 2005; Hautus and Lee, 2006). Reaction times were measured by calculating the latency between the pattern onset and the key press. Response latencies greater than two SOAs (1,300 ms) were excluded from analysis. To check further for unwanted side effects, the behavioral data in the loudness change detection task were additionally analyzed in repeated measures ANOVA with the factors session (first, second) and condition (exact, wn, and wp).

The active pattern change detection task at the end of the second EEG session was analyzed in terms of the signal detection theory, by extracting an index of sensitivity d' (Macmillan and Creelman, 2004) and correcting it for an extreme hit or false alarm rates by adding 0.5 to all response counts (Brown and White, 2005; Hautus and Lee, 2006). Reaction times were measured by calculating the latency between the pattern onset and the key press. Responses with latencies greater than the SOA (1,100 ms) were excluded from the analysis. To compare the behavioral performance between conditions, repeated measures ANOVAs and Bonferroni-corrected two-tailed *t*-tests were run. Cohen's *d* was calculated as an estimate of effect size for Student's *t*-tests. Additionally, hit rates were analyzed *via* repeated measures ANOVA with the factors condition (exact, wn, and wp) and train length (1, 2, 3, 6, and 12) and *via* logarithmic trend analysis to investigate behavioral effects condition-wise and as a function of the number of previous standard repetitions.

RESULTS

Behavioral Performance in the MET and in the Loudness Change Detection Task

In the MET, the participants scored, on average, 72% correct (range: 42–88% *SD* = 12%, 17/19 subjects scored above chance). In the loudness change detection task, which participants performed during the EEG recordings, the targets were discriminated with high accuracy. In the first session, averaged sensitivity over the participants ($N = 19$) was $d' = 3.71$ ($SD = 0.58$) in the exact-repetition condition, $d' = 3.45$ ($SD = 0.64$) in the white-noise condition, and $d' = 3.60$ ($SD = 0.70$) in the wrong-pitch condition. In the second session, averaged sensitivity over the participants ($N = 19$) was $d' = 3.92$ ($SD = 0.52$) in the exact-repetition condition, $d' = 3.80$ ($SD = 0.51$) in the white-noise condition, and $d' = 3.92$ ($SD = 0.58$) in the wrong-pitch condition. A repeated measures ANOVA with the factors session (first, second) and condition (exact, wn, and wp) revealed the main effect of session [$F(1, 18) = 39.17$, $p < 0.001$, $\eta^2 = 0.69$] but no significant effect of condition [$F(2, 36) = 3.07$, $p = 0.060$, $\eta^2 = 0.15$]. No interaction between condition and sessions was found [$F(2, 36) = 0.52$, $p < 0.60$, $\eta^2 = 0.03$].

In the first session, reaction times for correctly detected target sounds were $M = 634$ ms ($SD = 50$ ms) in the exact-repetition condition, $M = 664$ ms ($SD = 53$ ms) in the white-noise condition, and $M = 631$ ms ($SD = 49$ ms) in the wrong-pitch condition. In the second session, reaction times for correctly detected target sounds were $M = 609$ ms ($SD = 59$ ms) in the exact-repetition condition, $M = 628$ ms ($SD = 58$ ms) in the white-noise condition, and $M = 617$ ms ($SD = 54$ ms) in the wrong-pitch condition. A two-way repeated measures ANOVA revealed a significant effect of condition [$F(2, 36) = 13.99$, $p < 0.001$, $\eta^2 = 0.04$] and of session [$F(1, 18) = 14.08$, $p = 0.001$, $\eta^2 = 0.05$]. These main effects were not qualified by an additional interaction [$F(2, 36) = 1.32$, $p = 0.28$, $\eta^2 = 0.01$]. Bonferroni-corrected two-tailed *t*-tests showed that, across the sessions, the reaction times in the white-noise condition differed significantly from the exact-repetition condition and the wrong-pitch condition [exact vs. wn: $t(37) = -3.59$, $p = 0.003$ $d = -1.18$; wn vs. wp: $t(37) = 3.09$, $p = 0.001$, $d = 1.02$; exact vs. wp: $t(37) = -0.43$, $p = 1.000$, $d = -0.14$].

The participants showed a high sensitivity in the active pattern change detection task at the end of the EEG recordings in the exact-repetition condition [$d' = 3.12$ ($SD = 0.77$)]. The sensitivity in the white-noise condition was $d' = 1.90$ ($SD = 0.47$) and in the wrong-pitch condition $d' = 0.96$ ($SD = 0.28$). Repeated measures ANOVA comparing the three conditions revealed a significant effect of condition [$F(0.96, 34.53) = 125.68$, $p < 0.001$, $\eta^2 = 0.74$]. Bonferroni-corrected two-tailed *t*-tests showed significant differences between each condition pair [exact vs. wn: $t(18) = 8.47$, $p < 0.001$, $d = 3.99$; wn vs. wp: $t(18) = 10.12$, $p < 0.001$, $d = 4.77$; exact vs. wp: $t(18) = 13.31$, $p < 0.001$, $d = 6.27$].

On average, reaction times for correctly detected target sounds were $M = 578$ ms ($SD = 34$ ms) in the exact-repetition condition, $M = 610$ ms ($SD = 39$ ms) in the white-noise condition, and $M = 617$ ms ($SD = 50$ ms) in the wrong-pitch condition. A one-way repeated measures ANOVA revealed a significant effect of condition [$F(2, 36) = 12.54$, $p < 0.001$, $\eta^2 = 0.15$]. Bonferroni-corrected two-tailed *t*-tests revealed significant differences between exact vs. wn: $t(18) = -3.94$, $p = 0.003$, $d = -1.86$ and exact vs. wp: $t(18) = -3.90$, $p < 0.003$, $d = 1.84$. The difference in reaction times between the white noise and the wrong-pitch condition was not significant [$t(18) = -1.08$, $p = 0.88$, $d = 0.51$]. The results of sensitivity and reaction time analysis can be seen in **Figures 2A,B**.

A repeated measures ANOVA on the hit rates, including the factors condition (exact, wn, and wp) and train length (1, 2, 3, 6, and 12) showed a significant main effect of condition [$F(2, 36) = 103.98$, $p < 0.001$, $\eta^2 = 0.48$] and a significant main effect of train length [$F(4, 72) = 51.36$, $p < 0.001$, $\eta^2 = 0.35$]. These main effects were qualified by an additional interaction [$F(8, 144) = 5.11$, $p < 0.001$, $\eta^2 = 0.08$]. A highly significant logarithmic trend for the train length effect was revealed for each condition [exact: $F(1, 18) = 22.52$, $p < 0.001$, $\eta^2 = 0.56$; wn: $F(1, 18) = 228.30$, $p < 0.001$, $\eta^2 = 0.93$; wp: $F(1, 18) = 35.10$, $p < 0.001$, $\eta^2 = 0.66$]. Logarithmic regression analyses revealed a steeper increase of the hit rates with increasing train length in the white-noise condition than in the wrong-pitch condition, as

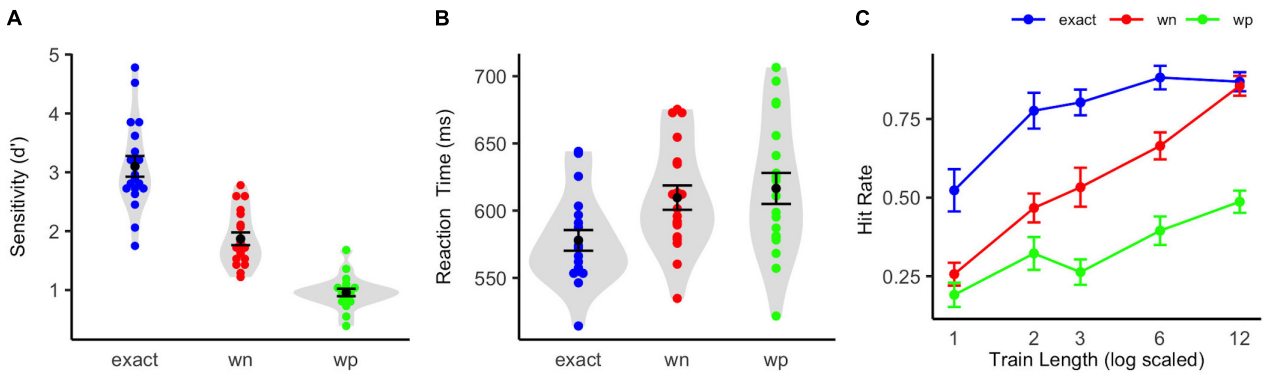

FIGURE 2 | Behavioral performance in the active pattern change detection task. **(A)** Violin plots show participants sensitivity index *d'* when actively detecting pattern changes in the exact-repetition condition (exact: blue), in the white-noise condition (wn: red), and in the wrong-pitch condition (wp: green). **(B)** Violin plots show participants reaction times in the active pattern change detection task. The colored dots indicate the results of each single participant (N = 19). The black dots show the mean of all the participants, and whiskers indicate the corresponding standard error of the mean. The shapes (gray) show the distribution of results over all the participants. **(C)** Mean proportion of hits for the exact-repetition condition (exact: blue), the white-noise condition (wn: red), and the wrong-pitch condition (wp: green) on deviant sound patterns as a function of the number of preceding standard sound patterns are shown. Whiskers indicate standard errors of mean.

confidence intervals did not overlap (wn: r = 0.23; CI: 0.19–0.28, wp: r = 0.11; CI: 0.07–0.16). A ceiling effect in the exact-repetition condition caused a non-optimal fit of the logarithmic regression and, therefore, an overlap with the confidence interval of the wrong-pitch condition, but not so with the white-noise condition (r = 0.13; CI: 0.08–0.18). Mean hit rates are depicted in **Figure 2C**.

EEG Data

The non-parametric cluster-based permutation tests (see **Figure 3**) showed that grand-averaged difference waveforms (collapsed for train length 3, 6, and 12) elicited negative deflections prior to 300 ms after the stimulus onset in all conditions, likely reflecting MMN, even though its amplitudes were largest at central-parietal and parietal electrodes (exact: Pz: M = –1.81 μV at 252 ms; wn: CPz: M = –1.01 μV at 240 ms; wp: POz: M = –0.91 μV at 211 ms). This negative component was followed by a positive deflection in all conditions, peaking at electrode FCz (exact: M = 3.90 μV at 402 ms; wn: M = 1.83 μV at 475 ms; wp: M = 1.79 μV at 488 ms), reflecting P3a (see **Figure 4B**).

MMN Latency

Jackknife estimates of the MMN slope latency of the grand-averaged difference waves (at collapsed electrodes CPz, Pz, and POz), using the relative 75% peak amplitude criterion of the grand-averaged difference waves were M_{jack} = 223 ms (SD_{jack} = 3.12 ms) for the exact-repetition condition, M_{jack} = 175 ms (SD_{jack} = 14.38 ms) for the white-noise condition and M_{jack} = 194 ms (SD_{jack} = 2.31 ms) for the wrong-pitch condition. A one-way repeated measures ANOVA did not reveal a significant effect of condition: F_{adj} (1.11, 19.93) = 0.44, p = 0.51, η^2 = 0.09.

P3a Latency

Jackknife estimates of the P3a slope latency at electrode FCz of relative 75% peak amplitude criteria of the difference were M_{jack} = 369 ms (SD_{jack} = 2.46 ms) for the exact-repetition condition, M_{jack} = 402 ms (SD_{jack} = 1.19 ms) for the white-noise condition and M_{jack} = 428 ms (SD_{jack} = 7.08 ms) for the wrong-pitch condition. A one-way repeated measures ANOVA did not reveal a significant condition effect: F_{adj} (1.19, 21.45) = 2.68, p = 0.12, $\eta^2 < 0.001$.

MMN Mean Amplitudes

ERP difference waves and scalp distributions of MMN (and P3a) can be seen in **Figure 4**.

A four-way repeated measures ANOVA with the factors condition (exact, wn, wp), stimulus type (dev, stand), train length (1, 2, 3, 6, and 12) and electrode (CPz, Pz, and POz) for mean amplitudes in the MMN time window (200 to 300 ms after the stimulus onset) neither revealed a significant 4-way interaction [F(6.36, 114.44) = 1.50 p = 0.18 $\eta^2 < 0.001$] nor any three-way interaction, including the factors electrode and condition [condition × type × electrode: F(2.76, 49.64) = 1.05, p = 0.38, $\eta^2 < 0.001$; condition × train length × electrode: F(5.48, 98.59) = 1.12, p = 0.36, $\eta^2 < 0.001$] that would point to topographical differences between conditions.

Instead, the ANOVA revealed significant main effects [condition: F(2, 36) = 17.74, $p < 0.001$, η^2 = 0.05; stimulus type: F(1, 18) = 41.47, $p < 0.001$, η^2 = 0.07; train length: F(4, 72) = 3.70, p = 0.01, η^2 = 0.02] and significant two-way interactions [condition × stimulus type: F(2, 36) = 4.37, p = 0.02, η^2 = 0.02; condition × train length: F(8, 144) = 4.53, $p < 0.001$, η^2 = 0.03; stimulus type × train length: F(4, 72) = 26.05, $p < 0.001$, η^2 = 0.11]. All those effects were qualified by a three-way interaction condition × stimulus type × train length: F(8, 144) = 2.54, p = 0.01, η^2 = 0.03.

Subsequently, we first tested whether in each of the three conditions the deviant ERP differed from the standard ERP (main effect of stimulus type) and whether this difference developed with increasing train length (interaction stimulus type × train length). Both the stimulus type effect [exact: F(1, 18) = 25.40,

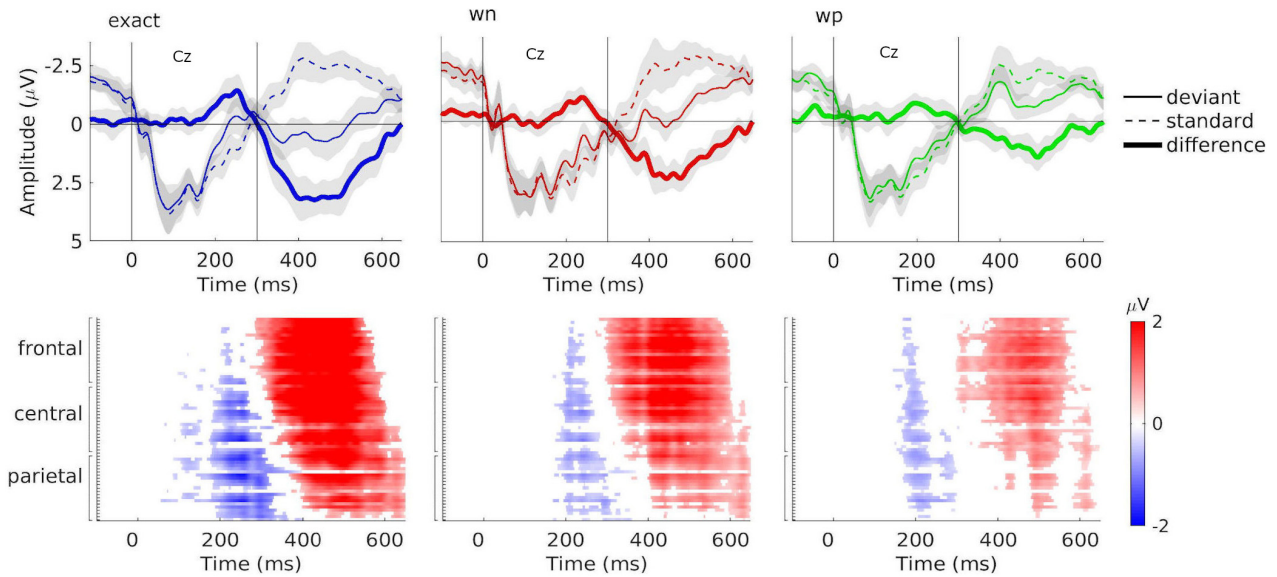

FIGURE 3 | Grand-averaged event-related potentials (ERPs), difference waveforms, and results of the cluster-based permutation test. *Top:* Grand-averaged ERPs at electrode Cz for combined train lengths 3, 6, and 12 in the exact-repetition condition (exact: blue), in the white-noise condition (wn: red), and in the wrong-pitch condition (wp: green). ERPs were elicited by standards (dashed line) and deviants (solid line). Difference waves of the grand-averaged ERPs (deviants minus standards) are shown as thick solid lines. Vertical solid lines indicate the pattern onset at 0 ms and the pattern offset at 300 ms. *Bottom:* Plots are illustrating significant differences (cluster $p < 0.05$) between ERPs to deviants and standards according to cluster-based permutation tests for combined train lengths 3, 6, and 12. Red and blue portions indicate time points/electrodes in which the ERPs to deviants are more positive and negative, respectively. Color brightness indicates the amplitude of the difference. White portions indicate time points/electrodes at which no significant differences were found. Negative deflections (blue) can be seen around 200–300 ms, and positive deflections (red) are found between 300 and 600 ms after the stimulus onset.

$p < 0.001$, $\eta^2 = 0.16$; wn: $F(1, 18) = 5.54$, $p = 0.03$, $\eta^2 = 0.03$; wp: $F(1, 18) = 5.76$, $p = 0.03$, $\eta^2 = 0.03$] and the interaction stimulus type × train length [exact: $F(4, 72) = 19.25$, $p < 0.001$, $\eta^2 = 0.20$; wn: $F(4, 72) = 5.17$, $p = 0.001$, $\eta^2 = 0.10$; wp: $F(4, 72) = 4.05$, $p = 0.01$, $\eta^2 = 0.06$] were significant in each condition. Particularly, the stimulus type × train length interactions resulted from increasingly negative MMN amplitudes of the deviant minus standard difference with train length (see **Figure 5A**).

To further explore the origin of the condition × stimulus type × train length interaction, we analyzed deviant and standard amplitudes at the centro-parietal electrodes in separate two-way ANOVAs for possible train length effects and interactions with condition. Here, we found for the deviants a significant condition [$F(2, 36) = 12.03$, $p < 0.001$, $\eta^2 = 0.11$] and train length effect [$F(4, 72) = 20.92$, $p < 0.001$, $\eta^2 = 0.16$] and a significant condition × train length interaction [$F(8, 144) = 4.97$, $p < 0.001$, $\eta^2 = 0.08$]. However, for standards, the two-way ANOVA revealed only a train length effect [$F(4, 72) = 8.05$, $p < 0.001$, $\eta^2 = 0.07$]. The condition effect [$F(2, 36) = 2.41$, $p = 0.10$, $\eta^2 = 0.01$] and the condition × train length interaction [$F(8, 144) = 1.19$, $p = 0.31$, $\eta^2 = 0.02$] were not significant. This indicates a similar development of the standard amplitudes with train length independently of condition and a different development of deviant amplitudes with train length in dependence of condition. Furthermore, we observed a significant logarithmic trend for the increase in deviant negativity with increasing train length in all three conditions [exact: $F(1, 18) = 67.48$, $p < 0.001$, $\eta^2 = 0.79$; wn: $F(1, 18) = 13.22$, $p = 0.002$, $\eta^2 = 0.42$; wp: $F(1, 18) = 5.20$, $p = 0.04$, $\eta^2 = 0.22$] (see **Table 1**). Logarithmic regression analyses revealed a steeper increase in negativity for deviants in the exact-repetition condition ($r = -0.82$; CI: −1.05 to −0.59) than in the white noise ($r = -0.28$; CI: −0.49 to −0.06) and wrong-pitch condition ($r = -0.20$; CI: −0.39 to −0.02) (see **Table 1** and **Figure 5B**).

P3a Mean Amplitudes

A repeated measures ANOVA with the factors condition (exact, wn, and wp), stimulus type (dev, stand) and train length (1, 2, 3, 6, and 12) for mean amplitudes in the P3a time window (400 to 500 ms after the stimulus onset) revealed a significant main effect of condition [$F(2, 36) = 6.47$, $p = 0.004$, $\eta^2 = 0.01$]. Furthermore, the main effect of stimulus type [$F(1, 18) = 122.86$, $p < 0.001$, $\eta^2 = 0.36$] and the main effect of train length [$F(4, 72) = 4.64$, $p = 0.002$, $\eta^2 = 0.01$] were found. The two-way interactions condition × stimulus type [$F(1.50, 26.97) = 28.57$, $p < 0.001$, $\eta^2 = 0.07$] and train length × stimulus type [$F(2.76, 49.70) = 38.45$, $p < 0.001$, $\eta^2 = 0.09$], as well as the interaction condition × train length [$F(8, 144) = 2.18$, $p = 0.03$, $\eta^2 = 0.01$], were significant. However, the main effects and the two-way interactions were qualified by an additional three-way interaction of the factors condition × stimulus type × train length: [$F(8, 144) = 5.13$, $p < 0.001$, $\eta^2 = 0.02$].

Two-way repeated measures ANOVAs with the factors stimulus type (dev, stand) and train length (1, 2, 3, 6, and 12) revealed the main effect of stimulus type [exact: $F(1, 18) = 95.95$, $p < 0.001$, $\eta^2 = 0.52$; wn: $F(1, 18) = 86.24$, $p < 0.001$, $\eta^2 = 0.31$; wp:

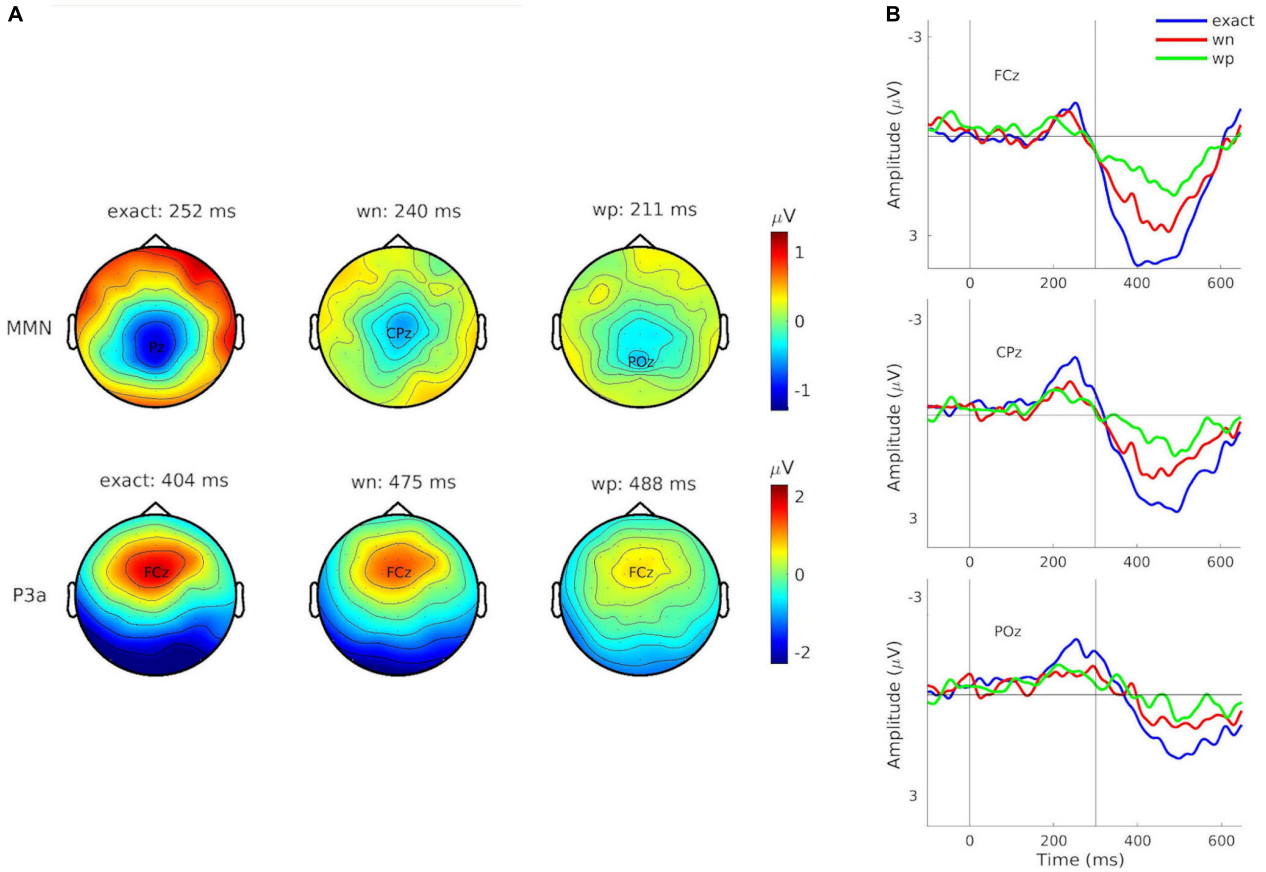

FIGURE 4 | (A) Potential topographies of the grand-averaged event-related potential (ERP) differences for combined train lengths 3, 6, and 12 for the components of interest mismatch negativity (MMN) (*top*) and P3a (*bottom*), depending on condition (*left*: exact-repetition condition, exact; *middle*: white-noise condition, wn; *right*: wrong-pitch condition—wp). Topographies show the time point with the maximal amplitude deflections. Corresponding electrodes are highlighted. **(B)** Difference waves of the grand-averaged ERPs (deviants minus standards) for combined train lengths 3, 6, and 12 at electrodes FCz (*top*), CPz (*middle*), and POz (*bottom*). Conditions are indicated by different colors (exact: blue, wn: red, and wp: green). Vertical solid lines indicate the pattern onset at 0 ms and the pattern offset at 300 ms.

$F(1, 18) = 57.71$, $p < 0.001$, $\eta^2 = 0.20$] and an interaction between stimulus type and train length [exact: $F(4, 72) = 26.51$, $p < 0.001$, $\eta^2 = 0.16$; wn: $F(4, 72) = 20.31$, $p < 0.001$, $\eta^2 = 0.11$; wp: $F(4, 72) = 4.09$, $p = 0.005$, $\eta^2 = 0.04$] for each experimental condition. Particularly, the stimulus type × train length interactions resulted from increasing positive P3a amplitudes of the deviant minus standard difference with train length (see **Figure 5A**).

To further explore the origin of the condition × stimulus type × train length interaction, we analyzed deviants and standards in separate two-way ANOVAs for possible train length effects and interactions with conditions. Here, we found for the deviants a significant condition [$F(2, 36) = 24.56$, $p < 0.001$, $\eta^2 = 0.15$] and train length effect [$F(4, 72) = 31.84$, $p < 0.001$, $\eta^2 = 0.16$], which was qualified by a significant condition × train length interaction [$F(8, 144) = 3.90$, $p < 0.001$, $\eta^2 = 0.04$]. For standards, the two-way ANOVA revealed a train length effect [$F(4, 72) = 11.76$, $p < 0.001$, $\eta^2 = 0.06$] and a condition effect [$F(2, 36) = 10.07$, $p < 0.001$, $\eta^2 = 0.03$]. Also, the condition × train length interaction [$F(8,144) = 3.78$, $p < 0.001$, $\eta^2 = 0.02$] was significant. Despite significant effects and interactions for deviants and standards, the effects differed between conditions in their strength as *post hoc* logarithmic trend analysis shows (see **Table 1**). We observed a significant logarithmic trend for the increase in deviant positivity with increasing train length in all three conditions [exact: $F(1, 18) = 47.90$, $p < 0.001$, $\eta^2 = 0.73$; wn: $F(1, 18) = 75.38$, $p < 0.001$, $\eta^2 = 0.81$; wp: $F(1, 18) = 6.51$, $p = 0.02$, $\eta^2 = 0.27$]. Logarithmic regression analyses revealed a steeper increase in positivity for deviants in the exact-repetition condition ($r = 0.95$; CI: 0.57–1.32) compared with the wrong-pitch condition ($r = 0.29$; CI: 0.01–0.56). Confidence intervals in the white-noise condition ($r = 0.67$; CI: 0.38–0.96) overlapped with the increase in the exact-repetition condition and the wrong-pitch condition. For standards, we did not find a significant logarithmic trend in the wrong-pitch condition [$F(1, 18) = 1.65$, $p = 0.22$, $\eta^2 = 0.08$] in contrast to the exact-repetition condition [$F(1, 18) = 11.70$, $p < 0.001$, $\eta^2 = 0.40$] and the white-noise condition [$F(1, 18) = 18.03$, $p < 0.001$, $\eta^2 = 0.50$]. The difference waves of the wrong-pitch condition also developed less steeply than in the exact-repetition condition and in the white-noise

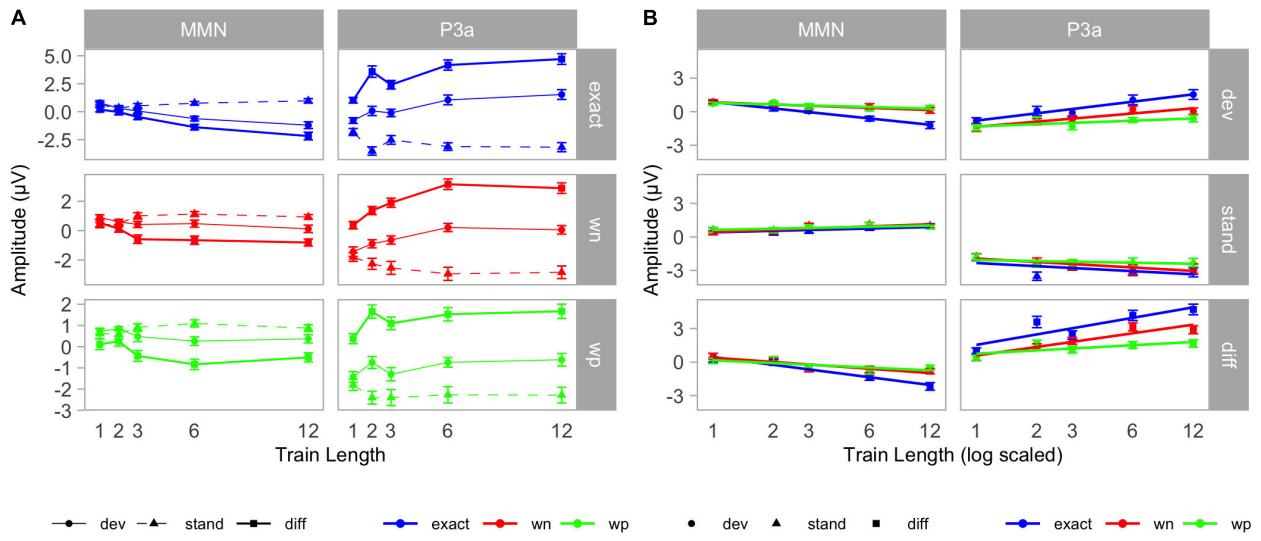

FIGURE 5 | (A) Grand-averaged mean amplitudes in the mismatch negativity (MMN) (*left*) and P3a (*right*) time windows. ERPs were elicited by standards (triangles/dashed lines) and deviants (points/solid thin lines). Difference wave amplitudes (deviant minus standard) are shown by rectangles and solid thick lines. Results are plotted condition-wise (*top*: exact/blue, *middle*: wn/red, *bottom*: wp/green). Whiskers denote standard errors of the mean. **(B)** Logarithmic regression analysis. Mean amplitudes in the MMN (*left*) and P3a (*right*) time windows. Results are plotted stimulus-type wise (*top*: deviants/points; *middle*: standards/triangles; *bottom:* differences/rectangle). Conditions are indicated by colors (exact: blue, wn: red, and wp: green). Whiskers denote standard errors of the mean. Train lengths are scaled logarithmically, and trend lines indicate the lines of the best fit.

condition as confidence intervals did not overlap (exact: $r = 1.35$; CI: 0.91–1.80, wn: $r = 1.11$; CI: 0.79–1.44, wp: $r = 0.42$; CI: 0.11–0.73) (see **Table 1** and **Figure 5B**).

DISCUSSION

In this study, we investigated the implicit memory formation for repeated auditory objects in situations in which single occurrences of the same object were subject to variability. More specifically, in three conditions, we studied how repetitions of unfamiliar short sound patterns lead to the formation of pattern-specific auditory sensory memory representations when single instances of pattern repetitions are identical (exact) or when they contain small distortions by replacing a segment of the pattern information either by white noise (wn) or by a wrong pitched segment (wp). The participants were not explicitly focusing on the pattern-repetition rule and, instead, performed the task of detecting occasionally occurring loudness changes in the auditory sequence. They performed this task with high accuracy and in the second session of the experiment with increased sensitivity and faster reaction times, likely due to familiarity and learning effects. Sensitivity of the participants to detect loudness changes was not affected by condition. However, the reaction times were significantly slower in the white-noise condition. It is possible the white-noise insertions were stronger distractors from the task, because these segments differed in sound quality from all the other segments of the sound pattern.

As expected, the occurrence of a new sound pattern elicited an MMN and a subsequent P3a; both of which appeared with their typical time course according to previous studies, using an auditory oddball (Alho et al., 1997; Schröger and Wolff, 1998b; Roeber et al., 2003; Debener et al., 2005) and roving-standard paradigms (Cowan et al., 1993; Baldeweg et al., 2004; Bendixen and Schröger, 2008; Garrido et al., 2008). However, the central-parietal distribution of an MMN seems rather untypical, since it can usually be observed at fronto-central recording sites (Näätänen et al., 2001, 2007; Winkler, 2007). We already observed rather posterior MMN topography in a previous study, using similar stimulus material in a comparable experimental procedure (Bader et al., 2017). An explanation for this topography could be the fact that the participants attended the sound sequence (although the pattern changes themselves were task irrelevant). That is, attention might have modulated the otherwise automatic mismatch detection process, potentially allowing for the contribution of an N2b-like component. Yet, even in this case, a more central but not a posterior distribution is expected (e.g., Woods, 1992). Furthermore, the task irrelevance of the pattern changes, and the early latency of the negative peak argues rather against an N2b. Coy et al. (2021) indicate that N2b for task-relevant pattern changes occurs later and can be dissociated from MMN, since, in their data, N2b latency is modulated by the difficulty of the deviant discrimination, whereas MMN latency is not. An alternative explanation could be that the auditory task increased the distracting nature of the deviants (Schröger and Wolff, 1998a). This could evoke a prominent and early P3a in the current paradigm (compared with the more typical passive listening situation). An early emergence of a frontally distributed P3a might partly overlap with the MMN time window and shift the topography toward more posterior sites. Nevertheless, more posterior distributions of the MMN have also been reported in other studies in which the participants

TABLE 1 | Logarithmic trend and regression analysis for the main effect of train length on MMN and P3a amplitudes.

	MMN				P3a			
	$F(1, 18)$	P	η^2	β (upper bound - lower bound)	$F(1, 18)$	P	η^2	β (upper bound - lower bound)
standards								
exact	4.82	0.04	0.21	0.19 (−0.00 to 0.38)	11.70	0.00	0.40	−0.41 (−0.79 to −0.03)
wn	14.25	0.00	0.44	0.28 (0.09 to 0.46)	18.03	0.00	0.50	−0.45 (−0.84 to −0.05)
wp	4.12	0.06	0.19	0.16 (−0.03 to 0.35)	1.65	0.22	0.08	−0.14 (−0.48 to 0.21)
deviants								
exact	67.48	0.00	0.79	−0.82 (−1.05 to −0.59)	47.90	0.00	0.73	0.95 (0.57 to 1.32)
wn	13.22	0.00	0.42	−0.28 (−0.49 to −0.06)	75.38	0.00	0.81	0.67 (0.38 to 0.96)
wp	5.20	0.04	0.22	−0.20 (−0.39 to −0.02)	6.51	0.02	0.27	0.29 (0.01 to 0.56)
difference								
exact	52.36	0.00	0.74	−1.01 (−1.27 to −0.75)	70.57	0.00	0.80	1.35 (0.91 to 1.80)
wn	20.18	0.00	0.53	−0.55 (−0.82 to −0.29)	58.64	0.00	0.77	1.11 (0.79 to 1.44)
wp	7.07	0.02	0.28	−0.36 (−0.61 to −0.12)	7.04	0.02	0.28	0.42 (0.11 to 0.73)

watched a silent movie, suggesting that the complexity of the auditory stimuli (e.g., speech and action words) could also result in such atypical MMN topography, indicating activation of a more global network (Shtyrov et al., 2004; Hasting et al., 2007).

Sensory Memory Trace Formation as Indexed by MMN

The MMM implies that the regularity of repeated complex sound patterns was encoded into a predictive model, and that a change in the overall pattern was detected (Denham and Winkler, 2006; Bendixen et al., 2012; Winkler and Schröger, 2015). This was the case for exact pattern repetitions as well as patterns containing distortions of quality of one segment (white noise) or pitch. We conclude that the auditory system quickly forms pattern representations, even when distortions introduce uncertainty into the implicit learning process. Nevertheless, the amplitude of the MMM was smaller with standard variability, suggesting diminished precision of the predictive model.

Yet MMN amplitude was larger in the condition without distortions compared with the conditions with distortions in the standard patterns. This suggests that the certainty about the repetition regularity must be higher in the exact-repetition condition, which results in more pronounced deviant-related negativity. In particular, MMN amplitudes increased as a function of preceding number of standards, following a logarithmic trend in all conditions, suggesting a fast buildup of pattern representations, particularly with the initial pattern repetitions (see also Baldeweg et al., 2004; Costa-Faidella et al., 2011; Bader et al., 2017). In general, two effects caused the growth in MMN: an increasing positivity for standard ERPs and an increasing negativity for deviant ERPs in the respective MMN time window as a function of train length. The steepness, with which MMN amplitudes grew with increasing train length, was modulated by condition. This effect was mainly driven by the deviant responses, which yielded a steeper growth function in the exact repetition condition than in the conditions containing distortions. The train length effects on standard responses were not modulated by condition, yet, already, their size was smaller than those for deviants.

While change detection was affected by whether distortions were introduced or not, it was not modulated by the type of distortion (noise or wrong pitch information). It seems to be mainly the number of intact segments within the sound patterns, guiding the fundamental process of extracting pattern identity representations as generative predictors under uncertainty, at least on this early processing stage.

The Role of Exact and Distorted Pitch Code on Evaluation Processes as Indexed by P3a and Behavior in an Active Pattern Change Detection Task

Subsequent to the MMN, a P3a component with typical fronto-central distribution was elicited, and systematic repetition-related modulations of amplitudes were found in all the conditions (see also Bendixen et al., 2007; Horvath et al., 2008; Bader et al., 2017). P3a amplitude increased logarithmically as a function of the number of preceding standard stimuli in all the conditions. This is congruent with studies showing that the P300 amplitude for task-irrelevant deviants is increased, if they occur with lower probability (Squires et al., 1975; Katayama and Polich, 1996) since, in our study, decreased local deviant probability (resulting from longer train lengths) led to an increase of P3a. Overall, P3a magnitude is associated with the degree of novelty and constitutes a marker of the evaluative processing of the contextual novelty (Friedman et al., 2001; Bendixen and Schröger, 2008). Even though attention was focused on a rule-independent task, deviant stimuli likely captured involuntarily attention and were evaluated on the basis of their underlying pattern structure in all conditions.

The growth of P3a as a function of train length resulted from both an increasing positivity for deviant ERPs and an increasing negativity for standard ERPs in the respective P3a time window. For both stimulus types, the growth function was modulated by condition. At the level of the difference waveform, the steepest logarithmic increase in P3a amplitudes with train length was found in the exact-repetition condition. The logarithmic

growth of P3a amplitudes in the wrong-pitch condition was distinctly less steep compared with the white noise and the exact-repetition condition. Thus, the growth of P3a activity with increasing number of preceding standards seems to be lowest in the condition with wrong pitch information. Consequently, pattern changes in the context of exact repetitions and white noise distortions might need fewer standard presentations to evaluate deviants as potential novels or targets and to trigger a call for attention of equal strength than pattern changes occurring among repetitions with wrong pitch distortions. Condition differences between P3a growths were partly due to the processing of the standard events. In the wrong-pitch condition, standard responses in the P3a time window did not show a logarithmic repetition-related modulation as opposed to the exact repetition and the white-noise-distortion condition. The amplitude decreases with the number of repetitions seems relatively flat, but confidence intervals overlapped with the exact repetition and the white-noise-distortion condition. Overall, the processing of deviating events had a stronger contribution to the condition differences on the P3a level (similar to what we found for the MMN). In the exact-repetition condition, the logarithmic trend of systematic amplitude modulations was much steeper than in the wrong-pitch condition.

Despite the pronounced differences in P3a amplitude, estimated component latencies were not affected by our experimental manipulation. The time needed to internally evaluate pattern identity seems not higher with noise or wrong pitch insertions. Here, the auditory system seems equally quick in classifying the stimuli, in evaluating the novelty of the deviance, and in automatically orienting attention toward the task-irrelevant novel patterns (Polich, 2007; Horvath et al., 2008; Wetzel et al., 2013; Winkler and Schröger, 2015).

The behavioral performance in the active pattern change detection task showed highest accuracy in the exact-repetition condition, less accuracy in the white-noise condition, and least accuracy in the wrong pitch segment condition. The development of the hit rates as a function of train length also followed a logarithmic trend in all conditions with the hit rates in the exact-repetition condition, developing quickly toward a ceiling effect and most slowly in the wrong-pitch condition, mirroring the pattern of results at the level of P3a.

Effects of the Different Types of Distortion at the Levels of Sensory Memory Formation and Contextual Stimulus Evaluation

Effects in the MMN time range did not distinguish between the two types of distortions that we introduced in the sequences. In both cases, when a pattern segment was occasionally replaced by white noise or by a differently pitched segment, the typical negativity observed for deviant responses grew less steeply compared with the condition with exact pattern repetitions. As the portion of matching pattern segments was similar for both conditions (five out of six), one could speculate that, at this early processing stage, the strength of regularity encoding mainly depends on the probability of matching information in spectrotemporal space. A previous study revealed that object representations can be retrieved from repetitions embedded in different backgrounds and suggested the correlation of input spectrograms between several non-perfect repetitions as a potential mechanism to achieve this (McDermott et al., 2011).

In contrast to the MMN findings, the type of distortion (white noise or wrong pitch information) seems to have a greater impact on evaluation processes at the stage of P3a. Here, we observed a clear disadvantage for the wrong pitch compared with the exact-repetition condition, whereas the response pattern in the white-noise condition resembled that of the exact-repetition condition. This suggests that the higher cognitive evaluation process and the attentional switch toward a deviant pattern are not substantially impaired in the white-noise condition. This could be explained by processes related to stream segregation or perceptual filling-in. Firstly, the white noise segments differed substantially from the other five segments in their spectral composition, leading to a vastly different timbre percept. This could have assisted the segregation of pattern and distracter information, allowing the later stages of evaluating a newly incoming pattern to be less disturbed. Secondly, white noise insertions could even lead to a partial restoration of the perceptual continuity of an intact standard pattern (Warren et al., 1997, 1988), particularly since the pitch forming spectral components of the replaced pattern segment can physically be found in the 50-ms white noise segment. This could explain similar processing of standards and deviants in the exact and the white-noise condition. The processing of wrong pitch information might have prevented segregation and restoration processes. Here, the similar timbre of the distorted segment promoted the percept of a continuous sound pattern, and a segregation mechanism cannot take an effect. Also, the wrong pitch information is simply misleading, and there is no option for a perceptual restoration of erased or ambiguous information. This might have led to the greater disadvantage for the wrong-pitch condition and is compatible with explanations of failed segregation in informational masking studies (Kidd et al., 2008).

Overall, our two types of manipulations might remind of energetic and informational masking. During energetic masking, the processing of a sensory event is degraded typically by a noise masker, where, mainly, the energy relation between the signal and the masker determines their separability and the amount of difficulty in perceiving the signal (Muller-Gass et al., 2001; Darwin, 2008; Moore, 2008; Wilson et al., 2012). During informational masking, it is, additionally, the similarity (either the acoustic or the semantic similarity) between the target and masker sound that deteriorates segregation and perception of the signal sound, such as when a speech signal is masked by speech (Dirks and Bower, 1969; Durlach et al., 2003; Scott et al., 2004; Gutschalk et al., 2008; Kidd et al., 2008; Mattys et al., 2012). In masking studies, it has been found that irrelevant information is easier to suppress when energetic masking is dominant, thus facilitating the processing of relevant sensory information (Lidestam et al., 2014). In contrast, when informational masking is dominant, a widespread general attentional network is activated to distinguish distracter and target information (Szalárdy et al., 2019). In our study, the wrong

pitch segment is due to its spectral profile acoustically highly similar to the pattern elements themselves. The uncertainty about which are the five relevant (intact) segments of the tonal pattern is maximally high, and segregation between the true pattern and the replaced distracting element will not be as easy as in the white-noise condition. In that sense, replacing valid pattern information by white noise or by wrong pitch information could lead to distinct forms of interference that might be resolved at different processing levels and even distinguishable neural circuits (Scott et al., 2004).

CONCLUSION

In the present study, we demonstrated that the auditory system is able to form pattern representations and predictions even in the context of uncertainty. MMN and P3a were elicited in response to deviants in all conditions at similar latency estimations. Independent of distorted segments, an implicit and automatic buildup of regularity representations and deviance detection, with a following call for attention toward the stimuli, can be assumed. However, we found a general advantage for the exact-repetition condition over the two distorted repetition conditions. This is shown by steeper logarithmic amplitude changes on MMN and the P3a level, with increasing number of repetitions, as well as in the behavioral performance in the active pattern change detection task. The processing on the MMN level does not seem to differentiate between the qualities of the distortions but reacts to general (mis-)matching statistics between the sound patterns. At the level of P3a, we observed an influence of the type of distortion. On this processing stage, white-noise distortions may not have impeded stimulus processing to such an extent as wrong pitch distortions did. This is evidenced by the distinct degradation of the P3a, which also goes along with the behavioral findings in the active pattern change detection task. Additionally, our results revealed that deviant processing is more affected by our experimental manipulations compared with standard processing.

To sum up, our findings indicate that the auditory system is able to quickly extract regularities and generate reliable predictions, even when the to-be-extracted patterns contain distortions. However, higher cognitive processing and the involvement of an attentional network might give the basis for the subtler evaluation of the acoustic input with regard to the type of distortion. The segregation between informative pattern segments and the distorting element, as well as the accessibility of a possible interpolation mechanism (like the one discussed for the continuity illusion), might explain the facilitated processing of white noise compared with wrong-pitch distortions on later processing stages that govern the elicitation of P3a and guide behavioral responses.

DATA AVAILABILITY STATEMENT

The raw data supporting the conclusions of this article will be made available by the authors, without undue reservation.

ETHICS STATEMENT

This studies involving human participants were reviewed and approved by the Ethics Committee of the University of Leipzig, Germany. The patients/participants provided their written informed consent to participate in this study.

AUTHOR CONTRIBUTIONS

SG and ES: conceptualization, supervision, and resources. MB: data curation, visualization, and writing—original draft. MB and SG: formal analysis, investigation, software, and project administration. SG: funding acquisition. SG, ES, and MB: methodology, writing, review, and editing, and validation. All authors contributed to the article and approved the submitted version.

FUNDING

The study was funded by the German Research Foundation (www.dfg.de) with the project number GR 3412/2-1. Furthermore, we acknowledge support from the German Research Foundation (DFG) and the Leipzig University within the program of Open Access Publishing. The funders had no role in study design, data collection and analysis, decision to publish, or preparation of the manuscript.

ACKNOWLEDGMENTS

We wish to thank Nina Coy for helping with the data acquisition and Robert P. O'Shea for commenting helpfully on the previous draft of the manuscript.

REFERENCES

Alho, K., Escera, C., Diaz, R., Yago, E., and Serra, J. M. (1997). Effects of involuntary auditory attention on visual task performance and brain activity. *Neuroreport* 8, 3233–3237. doi: 10.1097/00001756-199710200-00010

Bader, M., Schröger, E., and Grimm, S. (2017). How regularity representations of short sound patterns that are based on relative or absolute pitch information establish over time: an EEG study. *PLoS One* 12:e0176981. doi: 10.1371/journal.pone.0176981

Bakeman, R. (2005). Recommended effect size statistics for repeated measures designs. *Behav. Res. Methods* 37, 379–384. doi: 10.3758/bf03192707

Baldeweg, T., Klugman, A., Gruzelier, J., and Hirsch, S. R. (2004). Mismatch negativity potentials and cognitive impairment in schizophrenia. *Schizophr. Res.* 69, 203–217. doi: 10.1016/j.schres.2003.09.009

Bendixen, A., Roeber, U., and Schröger, E. (2007). Regularity extraction and application in dynamic auditory stimulus sequences. *J. Cogn. Neurosci.* 19, 1664–1677. doi: 10.1162/jocn.2007.19.10.1664

Bendixen, A., SanMiguel, I., and Schröger, E. (2012). Early electrophysiological indicators for predictive processing in audition: a review. *Int. J. Psychophysiol.* 83, 120–131. doi: 10.1016/j.ijpsycho.2011.08.003

Bendixen, A., Scharinger, M., Strauss, A., and Obleser, J. (2014). Prediction in the service of comprehension: modulated early brain responses to omitted speech segments. *Cortex* 53, 9–26. doi: 10.1016/j.cortex.2014.01.001

Bendixen, A., and Schröger, E. (2008). Memory trace formation for abstract auditory features and its consequences in different attentional contexts. *Biol. Psychol.* 78, 231–241. doi: 10.1016/j.biopsycho.2008.03.005

Berti, S., Roeber, U., and Schröger, E. (2004). Bottom-up influences on working memory: behavioral and electrophysiological distraction varies with distractor strength. *Exp. Psychol.* 51, 249–257. doi: 10.1027/1618-3169.51.4.249

Brattico, E., Tervaniemi, M., Näätänen, R., and Peretz, I. (2006). Musical scale properties are automatically processed in the human auditory cortex. *Brain Res.* 1117, 162–174. doi: 10.1016/j.brainres.2006.08.023

Brown, G. S., and White, K. G. (2005). The optimal correction for estimating extreme discriminability. *Behav. Res. Methods* 37, 436–449.

Cooke, M., Garcia Lecumberri, M. L., and Barker, J. (2008). The foreign language cocktail party problem: energetic and informational masking effects in non-native speech perception. *J. Acoust. Soc. Am.* 123, 414–427. doi: 10.1121/1.2804952

Costa-Faidella, J., Baldeweg, T., Grimm, S., and Escera, C. (2011). Interactions between "What" and "When" in the auditory system: temporal predictability enhances repetition suppression. *J. Neurosci.* 31, 18590–18597. doi: 10.1523/Jneurosci.2599-11.2011

Cowan, N., Winkler, I., Teder, W., and Näätänen, R. (1993). Memory prerequisites of mismatch negativity in the auditory event-related potential (Erp). *J. Exp. Psychol. Learn. Mem. Cogn.* 19, 909–921. doi: 10.1037/0278-7393.19.4.909

Coy, N., Bader, M., Schröger, E., and Grimm, S. (2021). Change detection of auditory tonal patterns defined by absolute versus relative pitch information. A combined behavioural and EEG study. *PLoS One* 16:e0247495. doi: 10.1371/journal.pone.0247495

Darwin, C. J. (2008). Listening to speech in the presence of other sounds. *Philos. Trans. R. Soc. Lond. B Biol. Sci.* 363, 1011–1021. doi: 10.1098/rstb.2007.2156

De Weerd, P. (2006). Perceptual filling-in: more than the eye can see. *Prog. Brain Res.* 154, 227–245. doi: 10.1016/S0079-6123(06)54012-9

Debener, S., Makeig, S., Delorme, A., and Engel, A. K. (2005). What is novel in the novelty oddball paradigm? Functional significance of the novelty P3 event-related potential as revealed by independent component analysis. *Cogn. Brain Res.* 22, 309–321. doi: 10.1016/j.cogbrainres.2004.09.006

Delorme, A., and Makeig, S. (2004). EEGLAB: an open source toolbox for analysis of single-trial EEG dynamics including independent component analysis. *J. Neurosci. Methods* 134, 9–21. doi: 10.1016/j.jneumeth.2003.10.009

Denham, S. L., and Winkler, I. (2006). The role of predictive models in the formation of auditory streams. *J. Physiol. Paris* 100, 154–170. doi: 10.1016/j.jphysparis.2006.09.012

DeWitt, L. A., and Samuel, A. G. (1990). The role of knowledge-based expectations in music perception: evidence from musical restoration. *J. Exp. Psychol. Gen.* 119, 123–144. doi: 10.1037//0096-3445.119.2.123

Dirks, D. D., and Bower, D. R. (1969). Masking effects of speech competing messages. *J. Speech Hear. Res.* 12, 229–245. doi: 10.1044/jshr.1202.229

Durlach, N. I., Mason, C. R., Kidd, G. Jr., Arbogast, T. L., Colburn, H. S., and Shinn-Cunningham, B. G. (2003). Note on informational masking (L). *J. Acoust. Soc. Am.* 113, 2984–2987. doi: 10.1121/1.1570435

Escera, C., Alho, K., Schröger, E., and Winkler, I. W. (2000). Involuntary attention and distractibility as evaluated with event-related brain potentials. *J. Audiol. Otol.* 5, 151–166.

Friedman, D., Cycowicz, Y. M., and Gaeta, H. (2001). The novelty P3: an event-related brain potential (ERP) sign of the brain's evaluation of novelty. *Neurosci. Biobehav. Rev.* 25, 355–373. doi: 10.1016/S0149-7634(01)00019-7

Garrido, M. I., Friston, K. J., Kiebel, S. J., Stephan, K. E., Baldeweg, T., and Kilner, J. M. (2008). The functional anatomy of the MMN: a DCM study of the roving paradigm. *Neuroimage* 42, 936–944. doi: 10.1016/j.neuroimage.2008.05.018

Garrido, M. I., Kilner, J. M., Kiebel, S. J., Stephan, K. E., Baldeweg, T., and Friston, K. J. (2009). Repetition suppression and plasticity in the human brain. *Neuroimage* 48, 269–279. doi: 10.1016/j.neuroimage.2009.06.034

Gutschalk, A., Micheyl, C., and Oxenham, A. J. (2008). Neural correlates of auditory perceptual awareness under informational masking. *PLoS Biol.* 6:e138. doi: 10.1371/journal.pbio.0060138

Hasting, A. S., Kotz, S. A., and Friederici, A. D. (2007). Setting the stage for automatic syntax processing: the mismatch negativity as an indicator of syntactic priming. *J. Cogn. Neurosci.* 19, 386–400. doi: 10.1162/jocn.2007.19.3.386

Hautus, M., and Lee, A. (2006). Estimating sensitivity and bias in a yes/no task. *Br. J. Math. Stat. Psychol.* 59, 257–273. doi: 10.1348/000711005X65753

Horvath, J., Winkler, I., and Bendixen, A. (2008). Do N1/MMN, P3a, and RON form a strongly coupled chain reflecting the three stages of auditory distraction? *Biol. Psychol.* 79, 139–147. doi: 10.1016/j.biopsycho.2008.04.001

Katayama, J., and Polich, J. (1996). P300, probability, and the three-tone paradigm. *Evoked Potent. Electroencephalogr. Clin. Neurophysiol.* 100, 555–562. doi: 10.1016/S0168-5597(96)95171-0

Kidd, G., Mason, C. R., Richards, V. M., Gallun, F. J., and Durlach, N. I. (2008). "Informational Masking," in *Auditory Perception of Sound Sources*, eds W. A. Yost, A. N. Popper, and R. R. Fay (Boston, MA: Springer), 143–189.

Kiesel, A., Miller, J., Jolicoeur, P., and Brisson, B. (2008). Measurement of ERP latency differences: a comparison of single-participant and jackknife-based scoring methods. *Psychophysiology* 45, 250–274. doi: 10.1111/j.1469-8986.2007.00618.x

Kozou, H., Kujala, T., Shtyrov, Y., Toppila, E., Starck, J., Alku, P., et al. (2005). The effect of different noise types on the speech and non-speech elicited mismatch negativity. *Hear. Res.* 199, 31–39. doi: 10.1016/j.heares.2004.07.010

Lidestam, B., Holgersson, J., and Moradi, S. (2014). Comparison of informational vs. energetic masking effects on speechreading performance. *Front. Psychol.* 5:639. doi: 10.3389/fpsyg.2014.00639

Macmillan, N. A., and Creelman, C. D. (2004). *Detection Theory: A User's Guide*. London: Psychology press.

Maris, E., and Oostenveld, R. (2007). Nonparametric statistical testing of EEG- and MEG-data. *J. Neurosci. Methods* 164, 177–190. doi: 10.1016/j.jneumeth.2007.03.024

Mattys, S. L., Davis, M. H., Bradlow, A. R., and Scott, S. K. (2012). Speech recognition in adverse conditions: a review. *Lang. Cogn. Process.* 27, 953–978. doi: 10.1080/01690965.2012.705006

McDermott, J. H., Wrobleski, D., and Oxenham, A. J. (2011). Recovering sound sources from embedded repetition. *Proc. Natl. Acad. Sci. U.S.A.* 108, 1188–1193. doi: 10.1073/pnas.1004765108

Micheyl, C., Carlyon, R. P., Shtyrov, Y., Hauk, O., Dodson, T., and Pullvermuller, F. (2003). The neurophysiological basis of the auditory continuity illuion: a mismatch negativity study. *J. Cogn. Neurosci.* 15, 747–758. doi: 10.1162/089892903322307456

Miller, J., Patterson, T., and Ulrich, R. (1998). Jackknife-based method for measuring LRP onset latency differences. *Psychophysiology* 35, 99–115.

Moore, B. C. (2008). Basic auditory processes involved in the analysis of speech sounds. *Philos. Trans. R. Soc. Lond. B, Biol. Sci.* 363, 947–963. doi: 10.1098/rstb.2007.2152

Muhler, R., and von Specht, H. (1999). Sorted averaging–principle and application to auditory brainstem responses. *Scand. Audiol.* 28, 145–149. doi: 10.1080/010503999424716

Muller-Gass, A., Marcoux, A., Logan, J., and Campbell, K. B. (2001). The intensity of masking noise affects the mismatch negativity to speech sounds in human subjects. *Neurosci. Lett.* 299, 197–200. doi: 10.1016/S0304-3940(01)01508-7

Näätänen, R., Paavilainen, P., Rinne, T., and Alho, K. (2007). The mismatch negativity (MMN) in basic research of central auditory processing: a review. *Clin. Neurophysiol.* 118, 2544–2590. doi: 10.1016/j.clinph.2007.04.026

Näätänen, R., Tervaniemi, M., Sussman, E., Paavilainen, P., and Winkler, I. (2001). 'Primitive intelligence'in the auditory cortex. *Trends Neurosci.* 24, 283–288. doi: 10.1016/S0166-2236(00)01790-2

Niemitalo-Haapola, E., Haapala, S., Jansson-Verkasalo, E., and Kujala, T. (2015). Background noise degrades central auditory processing in toddlers. *Ear. Hear.* 36, E342–E351. doi: 10.1097/Aud.0000000000000192

Oostenveld, R., Fries, P., Maris, E., and Schoffelen, J. M. (2011). FieldTrip: open source software for advanced analysis of MEG, EEG, and invasive electrophysiological data. *Comput. Intell. Neurosci.* 2011:156869. doi: 10.1155/2011/156869

Paavilainen, P., Karlsson, M. L., Reinikainen, K., and Näätänen, R. (1989). Mismatch negativity to change in spatial location of an auditory stimulus. *Electroencephalogr. Clin. Neurophysiol.* 73, 129–141. doi: 10.1016/0013-4694(89)90192-2

Perruchet, P., and Pacton, S. (2006). Implicit learning and statistical learning: one phenomenon, two approaches. *TiCS* 10, 233–238. doi: 10.1016/j.tics.2006.03.006

Polich, J. (2007). Updating p300: an integrative theory of P3a and P3b. *Clin. Neurophysiol.* 118, 2128–2148. doi: 10.1016/j.clinph.2007.04.019

Rahne, T., von Specht, H., and Muhler, R. (2008). Sorted averaging–application to auditory event-related responses. *J. Neurosci. Methods* 172, 74–78. doi: 10.1016/j.jneumeth.2008.04.006

Ramachandran, V. S. (1992). Filling in the blind spot. *Nature* 356, 115–115. doi: 10.1038/356115a0

Riecke, L., van Opstal, A. J., Goebel, R., and Formisano, E. (2007). Hearing illusory sounds in noise: sensory-perceptual transformations in primary auditory cortex. *J. Neurosci.* 27, 12684–12689. doi: 10.1523/Jneurosci.2713-07.2007

Ritter, W., Paavilainen, P., Lavikainen, J., Reinikainen, K., Alho, K., Sams, M., et al. (1992). Event-related potentials to repetition and change of auditory-stimuli. *Electroencephalogr. Clin. Neurophysiol.* 83, 306–321. doi: 10.1016/0013-4694(92)90090-5

Roeber, U., Berti, S., and Schröger, E. (2003). Auditory distraction with different presentation rates: an event-related potential and behavioral study. *Clin. Neurophysiol.* 114, 341–349. doi: 10.1016/S1388-2457(02)00377-2

Sams, M., Paavilainen, P., Alho, K., and Näätänen, R. (1985). Auditory frequency discrimination and event-related potentials. *Electroencephalogr. Clin. Neurophysiol.* 62, 437–448. doi: 10.1016/0168-5597(85)90054-1

Schröger, E. (1997). On the detection of auditory deviations: a pre-attentive activation model. *Psychophysiology* 34, 245–257. doi: 10.1111/j.1469-8986.1997.tb02395.x

Schröger, E., and Wolff, C. (1998a). Attentional orienting and reorienting is indicated by human event-related brain potentials. *Neuroreport* 9, 3355–3358. doi: 10.1097/00001756-199810260-00003

Schröger, E., and Wolff, C. (1998b). Behavioral and electrophysiological effects of task-irrelevant sound change: a new distraction paradigm. *Cogn. Brain Res.* 7, 71–78.

Scott, S. K., Rosen, S., Wickham, L., and Wise, R. J. S. (2004). A positron emission tomography study of the neural basis of informational and energetic masking effects in speech perception. *J. Acoust. Soc. Am.* 115, 813–821. doi: 10.1121/1.1639336

Shahin, A. J., Bishop, C. W., and Miller, L. M. (2009). Neural mechanisms for illusory filling-in of degraded speech. *Neuroimage* 44, 1133–1143. doi: 10.1016/j.neuroimage.2008.09.045

Shinn-Cunningham, B. G., and Wang, D. J. (2008). Influences of auditory object formation on phonemic restoration. *J. Acoust. Soc. Am.* 123, 295–301. doi: 10.1121/1.2804701

Shtyrov, Y., Hauk, O., and Pulvermüller, F. (2004). Distributed neuronal networks for encoding category-specific semantic information: the mismatch negativity to action words. *Eur. J. Neurosci.* 19, 1083–1092. doi: 10.1111/j.1460-9568.2004.03126.x

Spillmann, L., Otte, T., Hamburger, K., and Magnussen, S. (2006). Perceptual filling-in from the edge of the blind spot. *Vis. Res.* 46, 4252–4257. doi: 10.1016/j.visres.2006.08.033

Squires, N. K., Squires, K. C., and Hillyard, S. A. (1975). Two varieties of long-latency positive waves evoked by unpredictable auditory stimuli in man. *Electroen. Clin. Neurol.* 38, 387–401. doi: 10.1016/0013-4694(75)90263-1

Szalárdy, O., Tóth, B., Farkas, D., György, E., and Winkler, I. (2019). Neuronal correlates of informational and energetic masking in the human brain in a multi-talker situation. *Front. Psychol.* 10:786. doi: 10.3389/fpsyg.2019.00786

Tervaniemi, M., Schröger, E., Saher, M., and Näätänen, R. (2000). Effects of spectral complexity and sound duration on automatic complex-sound pitch processing in humans - a mismatch negativity study. *Neurosci. Lett.* 290, 66–70. doi: 10.1016/S0304-3940(00)01290-8

Uhrig, S., Arndt, S., Möller, S., and Voigt-Antons, J. N. (2017). Perceptual references for independent dimensions of speech quality as measured by electroencephalography. *Q. User Exp.* 2:10. doi: 10.1007/s41233-017-0011-8

Urbach, T. P., and Kutas, M. (2006). Interpreting event-related brain potential (ERP) distributions: implications of baseline potentials and variability with application to amplitude normalization by vector scaling. *Biol. Psychol.* 72, 333–343. doi: 10.1016/j.biopsycho.2005.11.012

Wacongne, C., Changeux, J. P., and Dehaene, S. (2012). A neuronal model of predictive coding accounting for the mismatch negativity. *J. Neurosci.* 32, 3665–3678. doi: 10.1523/JNEUROSCI.5003-11.2012

Wallentin, M., Nielsen, A. H., Friis-Olivarius, M., Vuust, C., and Vuust, P. (2010). The Musical Ear Test, a new reliable test for measuring musical competence (vol 20, pg 188, 2010). *Learn. Individ. Diff.* 20, 705–705. doi: 10.1016/j.lindif.2010.10.001

Walls, G. L. (1954). The filling-in process. *Optom. Vis. Sci.* 31, 329–341.

Warren, R. M., Hainsworth, K. R., Brubaker, B. S., Bashford, J. A., and Healy, E. W. (1997). Spectral restoration of speech: intelligibility is increased by inserting noise in spectral gaps. *Percept. Psychophys.* 59, 275–283. doi: 10.3758/Bf03211895

Warren, R. M., and Warren, R. P. (1970). Auditory illusions and confusions. *Sci. Am.* 223, 30–36. doi: 10.1038/scientificamerican1270-30

Warren, R. M., Wrightson, J. M., and Puretz, J. (1988). Illusory continuity of tonal and infratonal periodic sounds. *J. Acoust. Soc. Am.* 84, 1338–1342. doi: 10.1121/1.396632

Wetzel, N., and Schröger, E. (2007). Modulation of involuntary attention by the duration of novel and pitch deviant sounds in children and adolescents. *Biol. Psychol.* 75, 24–31. doi: 10.1016/j.biopsycho.2006.10.006

Wetzel, N., Schröger, E., and Widmann, A. (2013). The dissociation between the P 3a event-related potential and behavioral distraction. *Psychophysiology* 50, 920–930. doi: 10.1111/psyp.12072

Widmann, A., Schröger, E., and Maess, B. (2015). Digital filter design for electrophysiological data–a practical approach. *J. Neurosci. Methods* 250, 34–46. doi: 10.1016/j.jneumeth.2014.08.002

Wilson, R. H., Trivette, C. P., Williams, D. A., and Watts, K. L. (2012). The effects of energetic and informational masking on the Words-in-Noise Test (WIN). *J. Am. Acad. Audiol.* 23, 522–533. doi: 10.3766/jaaa.23.7.4

Winkler, I. (2007). Interpreting the mismatch negativity. *J. Psychophysiol.* 21, 147–163. doi: 10.1027/0269-8803.21.3.147

Winkler, I., Cowan, N., Csepe, V., Czigler, I., and Näätänen, R. (1996). Interactions between transient and long-term auditory memory as reflected by the mismatch negativity. *J. Cogn. Neurosci.* 8, 403–415. doi: 10.1162/jocn.1996.8.5.403

Winkler, I., Paavilainen, P., Alho, K., Reinikainen, K., Sams, M., and Näätänen, R. (1990). The effect of small variation of the frequent auditory stimulus on the event-related brain potential to the infrequent stimulus. *Psychophysiology* 27, 228–235. doi: 10.1111/j.1469-8986.1990.tb00374.x

Winkler, I., and Schröger, E. (2015). Auditory perceptual objects as generative models: setting the stage for communication by sound. *Brain Lang.* 148, 1–22. doi: 10.1016/j.bandl.2015.05.003

Woods, D. L. (1992). Auditory selective attention in middle-aged and elderly subjects: an event-related brain potential study. *Electroencephalogr. Clin. Neurophysiol.* 84, 456–468. doi: 10.1016/0168-5597(92)90033-8

Conflict of Interest: The authors declare that the research was conducted in the absence of any commercial or financial relationships that could be construed as a potential conflict of interest.

frontiers in Human Neuroscience

REVIEW
published: 18 August 2021
doi: 10.3389/fnhum.2021.702520

Automatic Sensory Predictions: A Review of Predictive Mechanisms in the Brain and Their Link to Conscious Processing

*Ruxandra I. Tivadar[1], Robert T. Knight[2,3] and Athina Tzovara[1,2,4]**

[1] Institute of Computer Science, University of Bern, Bern, Switzerland, [2] Helen Wills Neuroscience Institute, University of California, Berkeley, Berkeley, CA, United States, [3] Department of Psychology, University of California, Berkeley, Berkeley, CA, United States, [4] Sleep-Wake Epilepsy Center | NeuroTec, Department of Neurology, Inselspital, Bern University Hospital, University of Bern, Bern, Switzerland

The human brain has the astonishing capacity of integrating streams of sensory information from the environment and forming predictions about future events in an automatic way. Despite being initially developed for visual processing, the bulk of predictive coding research has subsequently focused on auditory processing, with the famous mismatch negativity signal as possibly the most studied signature of a surprise or prediction error (PE) signal. Auditory PEs are present during various consciousness states. Intriguingly, their presence and characteristics have been linked with residual levels of consciousness and return of awareness. In this review we first give an overview of the neural substrates of predictive processes in the auditory modality and their relation to consciousness. Then, we focus on different states of consciousness - wakefulness, sleep, anesthesia, coma, meditation, and hypnosis - and on what mysteries predictive processing has been able to disclose about brain functioning in such states. We review studies investigating how the neural signatures of auditory predictions are modulated by states of reduced or lacking consciousness. As a future outlook, we propose the combination of electrophysiological and computational techniques that will allow investigation of which facets of sensory predictive processes are maintained when consciousness fades away.

Keywords: prediction error, mismatch negativity, coma, sleep, anesthesia, P300

OPEN ACCESS

Edited by:
Ryszard Auksztulewicz, City University of Hong Kong, SAR China

Reviewed by:
Umberto Olcese, University of Amsterdam, Netherlands
Martina G. Vilas, Max Planck Institute for Empirical Aesthetics, Max Planck Society (MPG), Germany

****Correspondence:***
Athina Tzovara
Athina.tz@gmail.com

Specialty section:
This article was submitted to Cognitive Neuroscience, a section of the journal Frontiers in Human Neuroscience

Received: *29 April 2021*
Accepted: *12 July 2021*
Published: *18 August 2021*

Citation:
Tivadar RI, Knight RT and Tzovara A (2021) Automatic Sensory Predictions: A Review of Predictive Mechanisms in the Brain and Their Link to Conscious Processing. Front. Hum. Neurosci. 15:702520. doi: 10.3389/fnhum.2021.702520

INTRODUCTION

Learning information from our environment and forming predictions about future events is a key skill for survival. Stimuli from the world around us contain repetitive rules and patterns, as for example music, or speech. Being able to form predictions about future events facilitates perception and increases chances of survival, as a deviation from an expected pattern can signal danger.

The human brain has the astonishing capacity to formulate predictions about future events, relying on internal models that generate automatic predictions (generative models) about the most plausible states of the environment given prior information. Neural predictions are generated not only in the case of active perception (SanMiguel et al., 2013), but also when conscious access to

the environment is diminished, such as in sleep, anesthesia, or coma (**Figure 1**). The study of predictive processes has pervaded neuroscientific publications in the last three decades and painted a new view of the brain as a predictive organ (Dayan et al., 1995; Friston, 2005). Prediction provides explanation of phenomena at both the macro- and the micro-scales of brain functioning, including psychology (perception, cognition) and electrophysiology (neuronal processes). The study of predictive processes, which was first hinted to in the later 1800s (Lotze, 1852; Von Helmholtz, 1867) has been concretely formalized by statistics, information theory and machine learning. This review will focus on how sensory predictions have been used to probe different states of consciousness, and on what unknowns they have revealed about brain dynamics and functioning in these different states. By summarizing research done in both humans and animals, we examine the different components of the predictive network, and how these are modulated by conscious perception.

INTRODUCTION TO AUDITORY PREDICTIVE MECHANISMS

Paradigms for Studying Sensory Predictions and Consciousness

The most common sensory modality for studying predictive processes in the absence of consciousness is the auditory modality. Auditory stimulation is relatively straightforward to achieve, and it can reach the brain even in the absence of attention, or under conditions where eyes are closed, such as for example during sleep. The most famous paradigm for studying sensory predictions is the oddball paradigm (Näätänen and Alho, 1995; Garrido et al., 2009b), where a stream of identical repeated sounds (standards) is broken by an oddball, or a different sound (deviant), that is occasionally presented. In this paradigm, a regularity is built by repeating stimuli or sequences of stimuli. Prediction errors (PE) are signaled when deviations from the established regularity occur (Mumford, 1992; Rao and Ballard, 1999; Friston, 2005), by comparing neural responses to predicted (standard) versus observed (deviant) stimuli. Other experimental paradigms consist of the roving paradigm, where the oddball sound is followed by a stream of identical sounds, which at some point become standards, and are then followed by another stream of oddball sounds that turn into standards, with this pattern repeating (Garrido et al., 2009b); and the local-global paradigm (Bekinschtein et al., 2009), which is used to study local and global deviance effects. In the local-global paradigm, two forms of regularities are created – a local and a global one. These two types of regularities are built over single sounds (local), or groups of sounds (global). For local deviance, a standard sound is repeated a few times, followed by a deviant sound (e.g., aaaaB). This is similar to the deviance effect in a standard oddball paradigm. The global deviance effect is built by repeating this classic oddball structure, and then breaking this sequence by replacing the deviant in the third repetition with a standard (aaaaB aaaaB aaaaa).

Mechanisms Underlying Auditory Predictions

Stimulus Specific Adaptation and Deviance Detection

To formulate a prediction, first a regularity needs to be established, often through repetition. Repeating a given stimulus, for example a sound, results in a reduced response at the neural level, commonly referred to as stimulus specific adaptation (SSA) in animal research (Carbajal and Malmierca, 2018; Sikkens et al., 2019), and repetition suppression (RS) in human research (Rangarajan et al., 2020). SSA quantifies the change in the firing rate of a neuron when a certain tone is frequently or infrequently presented (Ulanovsky et al., 2004; Khouri and Nelken, 2015). The SSA was first recorded in the cortex of anesthetized cats (Condon and Weinberger, 1991), where small but precise reductions in the responses to standard, tones were demonstrated, appearing minutes after the first presentation of the standard, and lasting for an hour or more. Neurons along the auditory pathway and in frontal and subcortical areas (see section "Cortical and Subcortical Generators") show progressively reduced responses to repetitive stimuli, possibly as a result of short-term plasticity (Carbajal and Malmierca, 2018). Interestingly, neurons along the auditory processing pathway can express SSA, which in mice include parts of the inferior colliculus (IC), the dorsal and medial divisions of the medial geniculate body (MGB) and parts of the auditory cortex (Carbajal and Malmierca, 2018). This pathway is thought to carry predictions and prediction error signals (Carbajal and Malmierca, 2018).

A second crucial component of formulating a prediction is being able to detect violations from an established regularity. A deviant event may result in an increased neuronal response compared to the response to regular events, a phenomenon referred to as Deviance Detection (DD; Sikkens et al., 2019). For DD to occur, the increased neural response to deviant stimuli needs to be stronger than the neural response to standard stimuli, over and above SSA. DD is considered a correlate of error signaling (Sikkens et al., 2019). Although SSA occurs at early latencies, generally within the first 80 ms after stimulus onset, DD occurs at later latencies, around 120–240 ms post-stimulus onset (Sikkens et al., 2019). Macroscopically, these two processes of SSA and DD are thought to be contributors to a human EEG signature of regularity detection, the MMN (Sikkens et al., 2019).

Mismatch Negativity

The Mismatch Negativity (MMN) signal was first discovered in the late 1970's (Näätänen et al., 1978). The MMN manifests as a negative component of a *difference wave* peaking at about 100–250 milliseconds (ms) post-deviance onset, obtained by subtracting responses to standard stimuli from responses to deviant stimuli (Näätänen, 2003; Garrido et al., 2009b). MMN was originally thought to be elicited based on a previously created sensory memory trace (Näätänen, 2003), thus offering an observation window into the central auditory system and its functioning (Näätänen and Escera, 2000). This is known as the "trace-mismatch" explanation of MMN (Winkler, 2007), where MMN is seen as a signal of mismatch or surprise between a *retrospective* memory trace and the current input. Another

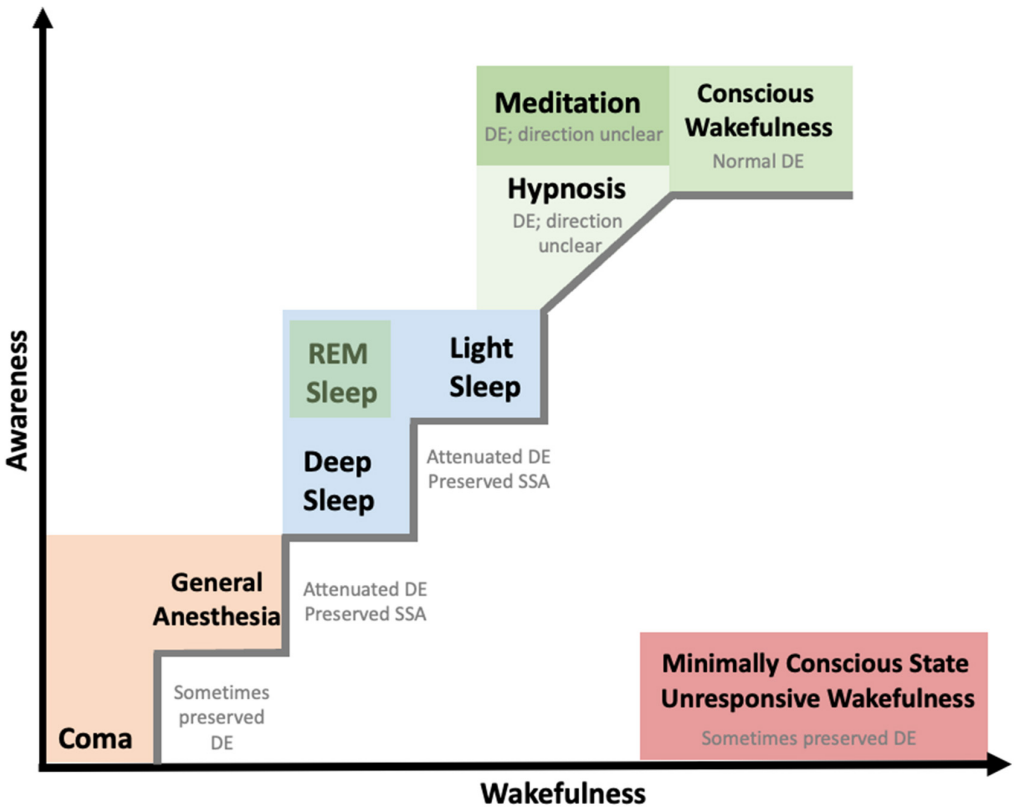

FIGURE 1 | Manifestation of auditory predictive processes in different consciousness states. States of consciousness are placed according to the observed level of wakefulness and awareness, adapted from Laureys, 2005. The colors represent similarities or overarching groupings of states of consciousness. While there is a continuum from coma to conscious wakefulness, minimally conscious state and unresponsive wakefulness syndrome do not lie on the same continuum; neither do REM sleep, meditation, and hypnosis. The positioning of different consciousness states is following previous studies (e.g., Laureys, 2005) when possible and is an approximate estimate for consciousness states that were not originally included in previous studies (e.g., hypnosis, meditation). *DE: deviance effects, grouping together mainly effects observed at scalp EEG level. For more fine-grained information for each consciousness state we refer readers to **Tables 1–4**.

interpretation of MMN is found in the adaptation hypothesis (May et al., 1999; Jääskeläinen et al., 2004). According to this hypothesis, cells tuned to standard sounds adapt, while cells tuned to more infrequent deviant sounds do not adapt and thus elicit higher responses (May et al., 1999). More recently, the MMN has been examined under the lens of predictive coding, which suggests that the MMN is a neural signature of a sensory prediction error signal, and that it represents an 'error' response that is elicited by deviant sounds (Garrido et al., 2009b). This view is supported by computational modeling studies, which have linked trial by trial changes in the MMN signal with the adjustment of an internal probabilistic model of the environment (Lieder et al., 2013). Under predictive processing, MMN is a signal of mismatch between sensory input and, contrary to the "trace-mismatch" hypothesis, a *prospective* and not retrospective sensory stimulus.

Interestingly, the MMN is described as a pre-attentive, automatic response, which can be elicited despite variations in states of wakefulness (Sculthorpe et al., 2009), such as during sleep or anesthesia, coma, or states of altered awareness, including hypnosis and meditation (Cahn and Polich, 2009; Chennu and Bekinschtein, 2012; Morlet and Fischer, 2014; Jamieson, 2016). In addition to extensive research in humans, MMN responses have also been recorded in cats (Csépe et al., 1987; Pincze et al., 2001), monkeys (Javitt et al., 1992, 1994), rabbits (Ruusuvirta et al., 1995, 1996a,b), guinea pigs (Kraus et al., 1994), and rats (Shiramatsu et al., 2013; Harms et al., 2014), via epidural EEG electrodes or cortical surface microelectrode arrays. Results are comparable, but not completely identical. For example, MMN responses in cats appear with shorter latencies due to the smaller size of cat cortex (Pincze et al., 2001). In summary, the MMN is an event-related potential (ERP) component that represents a scalp EEG signature of predictive processing, and is observed across species and states of consciousness.

P300

The P300 component is a positive deflection in the human ERP, with a peak latency at about 300 ms post-stimulus onset in response to a novel or task-relevant stimulus (Sutton et al., 1965). The P300 is usually elicited in an oddball paradigm when behavioral responses to deviants are demanded – thus, as a response to a target deviant stimulus (Picton, 1992). It has been proposed that the P300 reflects contextual updating (Donchin, 1981; Donchin and Coles, 1988) driven by attentional processes

(Polich, 2007), namely updating of a stimulus or of task-related (working) memory and expectancies (Verleger, 1988). The P300 has two main subcomponents, the P3a and P3b, which have different topographies and functional implications. While the P3a is fronto-centrally distributed and appears as a response to novel and distracting stimuli, the P3b is maximal over parietal recording sites in response to conscious detection of target and novel stimuli (Squires et al., 1975; Polich, 2007).

Neural Circuits Underlying Auditory Predictions

Predictive neural traces manifest in multiple stages of sensory processing. The most prevalent view is that higher level regions in a processing hierarchy generate and propagate sensory predictions to lower level regions, which compare these predictions to the actual sensory input (Rao and Ballard, 1999; Friston, 2005). Predictions flow 'down' the processing stream from higher level areas to lower level areas, while the opposite is true for error signaling, meaning that errors are signaled 'upward' by lower level areas detecting a mismatch with the current prediction (Rao and Ballard, 1999; Bastos et al., 2012). Importantly, the signaling of predictions and errors is posited to underlie multiple stages of information processing, so that sensory processing would, at each processing level, have to resolve the correspondence between predictions and sensory input (Friston, 2005; Summerfield and Egner, 2009). For this reason, some argue that predictive coding theories go beyond the standard bottom-up and top-down dichotomy (Rauss and Pourtois, 2013), as higher levels do not only modulate activity at lower levels of processing, but have the chance to initiate such activity (Mumford, 1992), in addition to lower level stages of the hierarchy being able to generate predictions for higher-level error signals (Kok and de Lange, 2015). There are multiple models of predictive processing (e.g., Spratling, 2008a,b; Bastos et al., 2012), which deviate from standard models with regards to where the error units are situated (i.e., in middle and not superficial cortical layers), and how predictions flow (i.e., not only 'downward' through the processing stream, but also 'upward'). Nevertheless, most models posit that error and predictive units have different laminar profiles (see Heilbron and Chait, 2018 for a detailed review).

Cortical and Subcortical Generators of Sensory Predictions

Sensory predictions are supported by distributed circuits in the brain, including sensory and prefrontal, but also subcortical regions, which may compute different variables related to predictions (Johnson et al., 2020). Predictive mechanisms are not only inherent properties of microcircuits in the brain, but also find expression through cortical connectivity (Johnson et al., 2020). Connected regions in the cortical hierarchy interact recurrently in a joint effort to find the world model that best explains the sensory inputs in the prediction units, and thereby reduce the activity of these units (Kok and de Lange, 2015).

In the auditory modality, magnetoencephalography (MEG) studies first showed that the MMN is generated in the auditory cortex (Hari et al., 1984). Later, using functional Magnetic Resonance Imaging (fMRI) and EEG, it was discovered that frontal regions are also involved in MMN generation (Alho, 1995; Opitz et al., 2002). Specifically, Opitz et al. (2002) used fMRI and EEG to study the temporal and frontal generators of the MMN and showed that responses to deviant stimuli of medium and large, but not small amplitude are found in the superior temporal gyrus (STG) bilaterally, and in the inferior frontal gyrus (IFG). Since then, these areas were often studied using EEG and fMRI combined with dynamic causal modeling (Garrido et al., 2007, 2008, 2009a; Boly, 2011; Chennu et al., 2016), and were also confirmed by multiunit activity (MUA) recordings (Nieto-Diego and Malmierca, 2016) and local field potential (LFP) measurements of SSA in rats (Imada et al., 2013). The neural correlates of the P300 component have been localized to multiple brain regions. The generators of the P3a include frontal cortical generators, the cingulate cortex, the supramarginal gyrus, and the hippocampus, while the generators of the scalp P3b include mainly temporo-parietal and frontal regions (Fonken et al., 2019).

Intracranial EEG (iEEG) recordings in humans have further advanced our understanding of the neural underpinnings of the predictive circuit (Johnson et al., 2020), by confirming the involvement of temporal and frontal regions in responding to deviant events (e.g., Rosburg et al., 2005). Additionally, Durschmid and colleagues showed that the temporal cortex detects deviations at the level of single stimuli, while prefrontal regions are sensitive to whether these deviations were predictable (Dürschmid et al., 2016), as well as to the likelihood of a deviant sound to occur (Dürschmid et al., 2019). Intracranial recordings have also implicated the posterior cingulate and parietal lobe (Halgren et al., 1995; Clarke et al., 1999), limbic structures such as the hippocampus, the amygdala (Halgren et al., 1980), and basal ganglia and thalamic circuits such as the caudate nucleus (Kropotov et al., 2000) and nucleus accumbens (Zaehle et al., 2013; Dürschmid et al., 2016) in supporting the auditory predictive network.

In addition, Cacciaglia et al. (2015) used event-related fMRI during an oddball task and found evidence of involvement of human inferior colliculus (IC) and MGB of the thalamus (Cacciaglia et al., 2015), confirming previous similar results found using SSA in animals for the occurrence of infrequent speech-like stimuli (Kraus et al., 1994), as well as for sounds with different binaural phases (King et al., 1995). fMRI studies further involved the amygdala (Kropotov et al., 2000; Czisch et al., 2009; Blackford et al., 2010) and hippocampal (Blackford et al., 2010) structures in deviance detection. Subsequent single unit recordings, and fMRI implicated the IC (Pérez-González et al., 2005; Malmierca et al., 2009; Patel et al., 2012; Gao et al., 2014) and the MGB (Anderson et al., 2009; Antunes et al., 2010; Richardson et al., 2013) in SSA (see also, Duque et al., 2015 for an extensive review on subcortical structures implicated in SSA generation).

In summary, sensory predictions rely on a distributed network of brain regions, expressed in low-level sensory processing areas, cortico-thalamic circuits involving subcortical thalamic and basal ganglia structures together with the amygdala and hippocampus, as well as higher-level parietal and frontal areas. This complex distributed network involved in sensory processing

and PE generation works in concert to allow learning of sensory regularities and the formation of predictions.

Attention

The role of attention in MMN generation was initially investigated in auditory tasks, where the ear to be attended was manipulated (Näätänen et al., 1993; Trejo et al., 1995; Alain and David, 1997). The debate was initiated when Näätänen proposed that the MMN was unaffected by manipulations of attention (see Näätänen, 1990 for a review). This view was challenged by research showing attentional effects on MMN (Woldorff and Hillyard, 1991; Szymanski et al., 1999; Auksztulewicz and Friston, 2015). There is now a plethora of studies showing that attention enhances the amplitude of MMN (Woldorff and Hillyard, 1991; Alain and David, 1997; Szymanski et al., 1999; Chennu et al., 2013; Auksztulewicz and Friston, 2015) and P300 (Chennu et al., 2013) responses. Electrophysiologically, manipulations of attention have been shown to predominantly affect the detection of oddball stimuli in prefrontal, but not temporal, regions, and to increase effects of oddball detection (Kam et al., 2020).

Later views suggested that the MMN response can be considered as a two-step process, composed of both standard formation and deviance detection (Sussman, 2007). The standard formation phase consists of auditory processes such as scene analysis and is susceptible to attentional effects. In contrast, the deviance detection phase, which depends on the standard formation phase, is independent of attentional manipulations. From a computational perspective, attention is thought to increase the precision of PEs, leading to more reliable estimates and a more accurate update of an environmental model (Auksztulewicz and Friston, 2015).

Although attention is not the focus of the present review, it can be argued that inattentive states represent states where sensory signals and predictions are elicited in an automatic way, as in unconscious states. We therefore mentioned these key findings in the field to emphasize that the brain not only produces predictions about the features of a signal (i.e., intensity, frequency, etc.), but also about the signal's reliability or precision (i.e., how predictable is the signal). When signal reliability is low, such as in inattentive conditions, deviations are down-weighted; when it is high, deviations are amplified and prioritized for further processing (Heilbron and Chait, 2018). In this view, predictive processes and attentive processes are distinct, independent processes which can interact. The role of predictive mechanisms is making inferences about what causes the sensory input and how precise this input is, whereas attention optimizes the precision of this input and regulates the gain of feedforward PEs (Schröger et al., 2015).

SENSORY PREDICTIONS IN REDUCED CONSCIOUSNESS STATES

Automatic sensory predictions manifest during wakefulness, but also when conscious access to the environment is lost, as will be subsequently reviewed. The interest for studying how neural responses are elicited during various awareness states first appeared when it was discovered that the MMN was evoked in the absence of attention (Näätänen, 1990), albeit with a much lower amplitude. MMN responses were even observed when subjects were engaged in other tasks, such as reading a book (Näätänen et al., 1993). Early studies recording MMN responses in animals anesthetized with barbiturates also confirmed MMN responses (Csépe et al., 1987; Javitt et al., 1992; Kraus et al., 1994). MMN responses were also observed during sleep in humans (Nielsen-Bohlman et al., 1991) and animals (Csépe et al., 1987). These studies indicated a great potential for studying auditory predictions in the absence of conscious access to the environment. Therefore, the value of the MMN response as a diagnostic tool for patients with disorders of consciousness (Chennu and Bekinschtein, 2012), or with psychiatric disorders (e.g., depersonalisation and derealisation) became evident (Lew et al., 2003; Kotchoubey et al., 2005; Wijnen et al., 2007).

Understanding the neural underpinnings that are associated with the emergence of conscious experience is of one of the main unresolved questions in neuroscience, with a first major challenge consisting in the clarification of the experimental definition of the term consciousness (Dehaene and Changeux, 2011). This is a fundamental challenge, due to the implications it brings for patients in coma, anesthesia, and those suffering from disorders of consciousness. Here, we adopt a widely used, non-exhaustive, functional definition of consciousness, which assesses conscious states by their expressed level of consciousness (wakefulness) on the one hand, and content of consciousness (awareness) on the other hand (Laureys, 2005; and **Figure 1**). This clinical definition of consciousness is also used to diagnose disorders of consciousness (see Giacino et al., 2014 for a review), characterized by a disrupted relationship between awareness and wakefulness (Gosseries et al., 2011), where observations of spontaneous and stimulus-evoked behaviors are used. Predictive processing was recently characterized as a "neural motif," which is present in many computations in the brain (Aitchison and Lengyel, 2017), but how does it relate to our conscious wakefulness and awareness? In fact, auditory predictive coding is commonly used to assess residual brain functions in patients with disorders of consciousness, often through scalp EEG components that are considered as neural signatures of predictive processing (Chennu and Bekinschtein, 2012; Gosseries et al., 2014a).

In the next sections we will provide an overview of findings from the last 30 years studying the extent to which the neural markers of predictive processes are altered by reduced or absent consciousness. We will present findings from studies in sleep, anesthesia, disorders of consciousness, or altered states of consciousness, in humans and animals. In particular, we will focus on different neural signatures of auditory predictive processes, such as MMN and P3, or SSA, and we will review how these are modulated by the absence or reduction of consciousness. When possible, we will elaborate on neural mechanisms and circuits of auditory predictions, for example, in the case of studies using techniques with a high spatial resolution (e.g., iEEG or source localization techniques). In other cases, we will discuss findings based on neural markers of predictive processing at a more macroscopic level such as scalp EEG components and their possible clinical applications.

SLEEP

Sleep represents a naturally occurring and rapidly reversible state of reduced consciousness (Campbell and Colrain, 2002). Sleep electrophysiology is altered with respect to wakefulness (Destexhe et al., 2007; Cox et al., 2014), but is well-characterized and relatively uniform across individuals (Steriade, 2006). In terms of the physiology of sleep, we distinguish paradoxical sleep or rapid eye-movement sleep (REM), and non-REM (NREM) sleep, which is further divided into three stages. NREM1 is the sleep onset period, NREM2 is light sleep, and NREM3 sleep is slow-wave-sleep. Different sleep stages have been associated with reduced consciousness or arousal (Goupil and Bekinschtein, 2012; Lendner et al., 2020).

Research in Humans

Several studies have investigated the neural correlates of MMN during sleep (Camman et al., 1987; Csépe et al., 1987; Näätänen and Lyytinen, 1994; Sallinen et al., 1994; Winter et al., 1995; Loewy et al., 1996; Atienza et al., 1997; Sallinen and Lyytinen, 1997; to name a few). After the wave of research in the 90's, which employed standard intensity or duration oddball paradigms, the consensus was that MMN and P300 components appeared in REM sleep, but not in NREM2 (see e.g., Winter et al., 1995; Loewy et al., 1996, 2000; Cote, 2002; Colrain and Campbell, 2007; Sculthorpe et al., 2009). The main evoked potentials were K-complexes and late potentials that were functionally different from the classic deviance response (Wesensten and Badia, 1988; Nielsen-Bohlman et al., 1991; Van Sweden et al., 1994; Nordby et al., 1996). Nevertheless, some studies still indicated differential processing of auditory information even during deeper sleep stages (Nielsen-Bohlman et al., 1991; Winter et al., 1995). Laboratories therefore modified their paradigms in order to have more sensitive tests, and presented either rapidly succeeding stimuli (every 150 ms) (Sabri et al., 2003), or used "hyper-salient" stimuli (Chennu and Bekinschtein, 2012) – i.e., very rare, very deviant stimuli, as used for example by Loewy and colleagues, with low probability and 1000 Hz difference between the standard and the deviant stimuli. In some of these studies, MMN responses were elicited during NREM1 and NREM2 (Sabri et al., 2003; Sabri and Campbell, 2005), whereas in others they were only evoked during REM sleep (Loewy et al., 1996; see **Table 1A** for a summary).

A more recent study employed MEG and EEG recordings during sleep and used a local-global paradigm (Strauss et al., 2015). Results showed a disrupted global response in NREM2 sleep, associated with an absence of the P300 response together with a simultaneous absence of behavioral responses, despite retained local mismatch responses across all sleep stages (Strauss et al., 2015). Moreover, authors used an additional manipulation where expectation was induced by alternating different sounds (aBaBa and aBaBB sequences), instead of repeating the same stimulus (aaaaa). In this case, the differential response that was observed between predicted and unpredicted sequences during wakefulness vanished during NREM2 sleep. This was interpreted as evidence that predictive processing during sleep could be explained with an adaptation framework (through repetition of the same stimuli) and not by using prediction error (through repetitions of different stimuli) mechanisms.

Even when MMN responses are present during sleep, their characteristics (i.e., amplitude or latency) are typically attenuated with respect to awake conditions (Atienza et al., 2001). It is, however, unclear whether predictive processes during sleep are altered because the underlying predictive computations are fundamentally different compared to wakefulness, or because the sleep electrophysiology is modified (Sabri and Campbell, 2002). Apart from detecting deviant events, there is an ongoing debate whether new information can be learned during sleep, and if so, under which conditions (Andrillon et al., 2017). A large body of literature reports no evidence for learning new rules

TABLE 1 | Studies in sleep.

(A) Humans

Study	Paradigm	Phase	Deviance effects
Wesensten and Badia, 1988	Pitch oddball	REM	Yes
		NREM2	Yes
Nielsen-Bohlman et al., 1991	Pitch oddball	NREM2	Yes
Van Sweden et al., 1994	Pitch oddball	REM	Yes
		NREM	Yes
Winter et al., 1995	Pitch oddball	NREM	Yes
Nordby et al., 1996	Pitch oddball	REM	No
		NREM	No
Loewy et al., 1996	Pitch oddball	REM	Yes
		NREM 2	No
		NREM 3	No
Loewy et al., 2000	Intensity oddball	REM	No
		NREM 2	No
Sabri and Campbell, 2002	Pitch oddball	NREM 3	Yes
Sabri et al., 2003	Pitch oddball	NREM 2	Yes
		NREM 1	Yes
Sabri and Campbell, 2005	Pitch oddball	REM	Yes
		NREM 1	Yes
		NREM 3	Yes
Sculthorpe et al., 2009	Repetition oddball	REM	Yes
		NREM	No
Strauss et al., 2015	Local-global	REM	Only local
		NREM 1	Only local
		NREM 2	Only local

(B) Animals

Study	Paradigm	Phase	Deviance effects	Species
Csépe et al., 1987	Pitch oddball	NREM	Yes	Cats
Nir et al., 2015	Pitch oddball	REM	SSA	Rats
		NREM	SSA	

**NREM, non-rapid eye movement sleep; REM, rapid eye movement; SSA, stimulus-specific adaptation.*

in deep NREM sleep, but more recent findings show that semantic associations can be learned if these are presented during peaks (i.e., "up" states) of slow-wave activity (Züst et al., 2019), which are characterized by similar conditions of cortical excitability as wakefulness (Destexhe et al., 2007; Cox et al., 2014). Moreover, other studies have shown that sleep facilitates encoding of previously learned generative models, improving sensory predictions (Lutz et al., 2018).

Research in Animals

Animal sleep research has investigated evoked responses in sensory systems (Hennevin et al., 2007). From a physiological viewpoint, two states of sleep are classically categorized in animals, paradoxical or REM sleep, and NREM sleep. Physiological studies in sleep further demonstrate preserved auditory processing (Edeline et al., 2000; Issa and Wang, 2008), with reported decreases in the amount and quality of information reaching the higher-level cortices (for an extensive review, see Coenen and Drinkenburg, 2002; see also Murata and Kameda, 1963). This reduction in information transmission is thought to be due to thalamic gating (McCormick and Bal, 1994), with sensory input to the cortex partially blocked at the thalamus (Hall and Borbely, 1970; Edeline et al., 2000). Pre-thalamic processing is thought to be *mostly* maintained (Steriade, 1991). Nevertheless, relevant stimuli can have some form of impact on the functional state of the sleeping animal, suggesting that the sleeping brain is still able to judge the meaningfulness of stimuli (Nielsen-Bohlman et al., 1991). Sophisticated paradigms suggest that simple forms of learning are also still possible, as for example in extinction (where a pre-conditioned association between two stimuli is erased) and pre-exposure (when animals are exposed to the to-be-conditioned stimulus before actual conditioning) experiments; and there is evidence that new associations can be formed with lower quality than the ones formed during waking (Coenen and Drinkenburg, 2002).

An early study in cats reported that the MMN can be elicited during all sleep stages (Csépe et al., 1987). Auditory evoked potentials were elicited by standard and deviant tones of different probabilities during wakefulness and sleep. A large MMN response was elicited by deviant tones, with MMN amplitude inversely proportional to deviants' probability. MMN during slow-wave sleep exhibited longer latency and was only evoked by deviant tones at the lowest probabilities. Another more recent study in rats used an oddball paradigm and found comparable SSA responses across REM, NREM and wake cycles in the core auditory region, defined by the authors as the core auditory fields receiving input from the ventral division of the medial geniculate nucleus of the thalamus (Nir et al., 2015; **Figure 2B**; see also **Table 1B**, for a summary). This suggests that evoked activity in low-level sensory cortices during sleep is driven by external stimuli with little modulation by the vigilance state, and that the disconnection of cortical processing during sleep may occur at a later stage, thus corroborating the physiological findings described above.

Conclusion

In conclusion, the majority of sleep studies suggest that auditory predictive processing may be retained during sleep, in particular within core auditory areas (Nir et al., 2015). There is consensus that scalp EEG components related to predictive processes can manifest during REM sleep, with similar characteristics as during wakefulness. For NREM, the question of whether auditory predictions can occur remains actively debated. One key factor that will need to be taken into account in the design of new experiments and during data analysis is the complex and dynamic brain physiology of sleep.

Different sleep stages are characterized by multiple local disruptions (Drummond et al., 2004; Magnin et al., 2010), leading to qualitatively different epochs with differences in sensory processing (Hennevin et al., 2007). Additionally, different stages of sleep are not homogeneous, as they are characterized by tonic and phasic fluctuations of arousal, of the background EEG activity, and of neuromodulator release (Hobson et al., 2000). As a result, cortico-thalamic long-range connectivity is affected, while some basic cortico-cortical connectivity might be preserved, as for example in the default mode network (Koike et al., 2011).

These fluctuations in sleep physiology might explain the attenuated MMN responses measured during sleep, and might mirror the decreasing thalamic activity, by indicating an impaired bottom-up component of MMN elicitation (Atienza et al., 2002). The impaired top-down component might stem from prefrontal lobe deactivation during sleep (Atienza et al., 2002). The cortico-thalamic network during REM sleep seems to be characterized by general activations in thalamic and posterior areas including temporo-occipital cortices (Maquet et al., 1996; Braun et al., 1997; Maquet, 2000; Portas et al., 2000), while frontal area activity is reduced (Maquet, 2000; Portas et al., 2000). All these areas are deactivated during NREM sleep (Maquet, 2000). Alternatively, connectivity at a later stage of information processing has also been reported during sleep (Massimini et al., 2005; Horovitz et al., 2009; Tagliazucchi et al., 2013), with preserved activation of primary sensory cortices in both animals (Peña et al., 1999; Edeline et al., 2001; Issa and Wang, 2008) and humans (Portas et al., 2000; Czisch et al., 2002; Dang-Vu et al., 2011).

Future research investigating predictive processing in sleep is crucial, given the sparseness of the current literature. Auditory paradigms are particularly important for assessing brain processing during sleep, as well as associations between sleep disorders and generalized reduced cognitive performance (Pilcher and Huffcutt, 1996; Banks and Dinges, 2007), or impaired auditory processing (Raz et al., 2001; Key et al., 2009; Bortoletto et al., 2011; Liberalesso et al., 2012; Leite et al., 2017).

ANESTHESIA

Phenomenologically and behaviorally, anesthetic states can be described as a continuum ranging between mild sedation, "a pharmacologically induced, reversible state, characterized by dose-related impairment of cognitive functions, including attention and memory, but during which consciousness and awareness are maintained" (Stamatakis et al., 2010), to complete anesthesia, "a drug-induced loss of consciousness during which patients are not rousable, even by painful stimulation" (Anesthesiologists Task Force on Intraoperative Awareness, 2006).

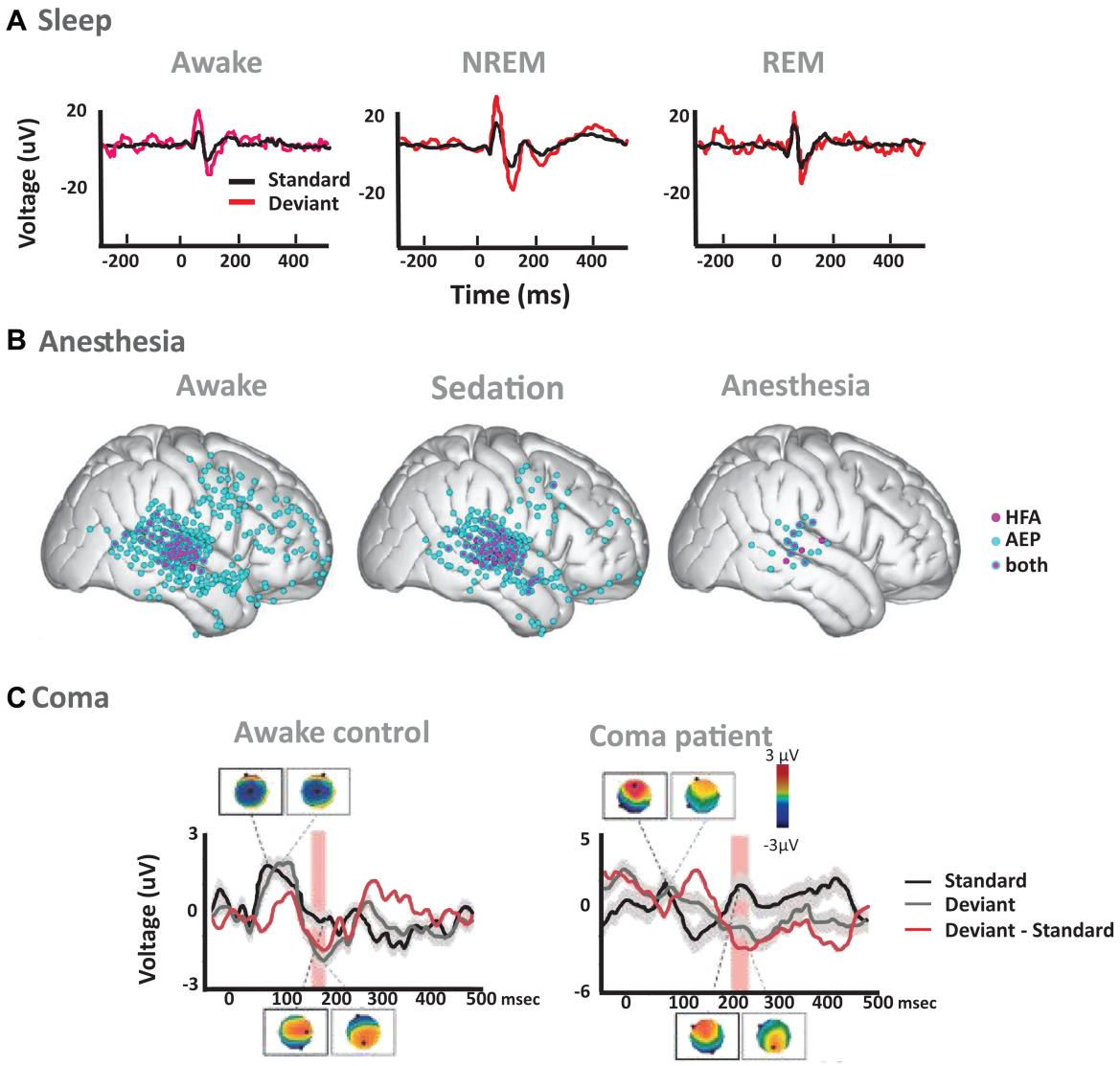

FIGURE 2 | Examples of auditory predictive processes across states of reduced consciousness. **(A)** Auditory averaged ERP responses to standard (black) and deviant (red) tones during normal wakefulness (left), NREM sleep (middle) and REM sleep (right) from EEG recordings in rats. Figure adapted from Nir et al. (2015). EEG recordings showed weaker responses following standard compared to deviant tones in wakefulness, NREM and REM sleep, an effect that was additionally quantified by the authors as SSA in single unit activity of the primary auditory cortex (Nir et al., 2015). **(B)** Local Deviance effects in electrocorticography (ECoG) recordings of patients with epilepsy (Figure adapted from Nourski et al., 2018). Pink dots show electrodes with significant differences between responses to standard and deviant sounds in high frequency activity (HFA; 70–150 Hz); blue dots show electrodes with differences in evoked potentials (AEP); and pink and blue dots show electrodes with significant AEP and HFA effects. Local deviance was defined as significant increases in response to the deviant versus standard stimuli along a 0–800 ms post 5th stimulus window: (aaaaB – aaaaa) or (BBBBa – BBBBB). Stimuli were vowels /ɑ/ and /i/, extracted from a female voice uttering the words h/ɑ/d and h/i/d. Significant electrodes are shown for the awake state (left), for sedation (middle) and for the anesthesia state (right). **(C)** Auditory evoked potentials (AEP) and scalp topographies for an exemplar awake control and a coma patient, measured over frontal electrodes to standard (black) and duration deviant (gray) sounds, as well as the difference of the two responses (red; Figure adapted from Tzovara et al., 2013). The awake control shows a typical N100 response to auditory stimuli, manifesting as a central negativity in the AEP topography, and an MMN response starting around 170 ms post-stimuli onset. The exemplar patient shows differential responses between standard and deviant sounds at later latencies, after 220 ms post-stimuli onset. Red rectangles signify periods of significant difference in response to standard vs. deviant sounds.

Anesthetics have complex effects on neural activity, such as alterations in the activity of wide-spread cortico-thalamic networks (Rudolph and Antkowiak, 2004; Scheinin et al., 2021), and disruptions of cortico-thalamic connectivity (Guldenmund et al., 2017). Interestingly, general anesthesia and NREM sleep share similarities, such as slow oscillatory activity, a disruption of cortico-cortical connections (Massimini et al., 2005; Pal et al., 2016), and changes in non-oscillatory neural dynamics (Lendner et al., 2020). During anesthesia and NREM, thalamocortical hyperpolarized neurons are alternating between active and silent

periods. By contrast, during wakefulness and REM sleep, the thalamocortical system is depolarized with awake-like low-voltage activity, and with tonic firing in neurons (Steriade et al., 2001). At high doses, general anesthesia during surgery can approximate brain stem death, where patients are unconscious, have inhibited brain stem reflexes, do not respond to nociceptive stimuli, and require cardiorespiratory and thermoregulatory support (Brown et al., 2010). These levels of anesthesia can be accompanied by isoelectric (i.e., almost a flat line) EEG activity (Brown et al., 2010).

In terms of cerebral metabolism, most anesthetics result in a general reduction in cortical brain activity, with certain regions, including cortical association areas, the thalamus, and the midbrain showing a higher decrease in cerebral metabolism (Heinke and Koelsch, 2005). In human studies, anesthesia is typically induced using either propofol (Plourde and Picton, 1991; Reinsel et al., 1995; Koelsch et al., 2006) or opioids (Plourde and Boylan, 1991). Propofol is an agonist at the GABA receptor and exerts a hypnotic and sedative effect through this mechanism (Rudolph and Antkowiak, 2004). Light propofol anesthesia, as administered in surgery, causes stage 2 sleep-like brain electrophysiological activity, with sleep and sleep-like spindles appearing during deep propofol anesthesia (Stamatakis et al., 2010; see Purdon et al., 2015, for a review). Opioids such as fentanyl are mostly used in cardiovascular surgery due to limited fluctuations in cardiovascular dynamics (Saidman et al., 1984). The EEG trace during opioid anesthesia is characterized by high amplitude slow delta waves (Wauquier et al., 1984). Opioids provide anesthesia, analgesia and unconsciousness after premedication with other anesthetic agents such as benzodiazepines (Sebel et al., 1981).

Research in Humans

Early human anesthesia studies did not compute the MMN response, but rather examined the P300 response, due to its suspected association with conscious awareness (Plourde and Boylan, 1991; Plourde and Picton, 1991; Reinsel et al., 1995). These studies report a decrease in amplitude of the P300 response with progressive sedation and abolishment when unconsciousness is reached (Plourde and Boylan, 1991; Plourde and Picton, 1991; Sneyd et al., 1994; Reinsel et al., 1995), accompanied by absent behavioral responses to deviant stimuli (Plourde and Picton, 1991).

Later studies carried out in the 2000's (Simpson et al., 2002; Yppärilä et al., 2002; Heinke et al., 2004; Koelsch et al., 2006) started to measure MMN responses alongside the P300 responses. These studies reported a dose-dependent incremental breakdown of MMN and P300 (Yppärilä et al., 2002; Heinke et al., 2004; Koelsch et al., 2006). As patients transition from wakefulness to anesthesia, AEPs tend to decrease in amplitude: Simpson et al. (2002) reported that N100 (thought to reflect the early processing of acoustic features of a stimulus; Näätänen and Picton, 1987) responses to auditory stimuli disappear when patients become unconscious, and MMN is no longer elicited right before consciousness is lost, at the point of highest propofol concentration at which patients are still responsive. Yppärilä et al. (2002) complemented these findings by showing that the amplitudes of AEPs including N100 and MMN gradually decrease, and latencies gradually increase as patients transition from light to deep sedation. Notably, a small subset of patients retains both MMN and P300 responses even in deep sedation (Yppärilä et al., 2002). Similar findings were reported by Heinke et al. (2004), who showed decreasing amplitudes and increasing latencies for MMN as propofol sedation progresses, and an abolishment of P300 responses in deeper sedation levels (Heinke et al., 2004).

Koelsch et al. (2006) measured MMN and P300 responses in healthy volunteers undergoing propofol sedation in a state of sedation shallower than surgical anesthesia, as participants were still arousable by loud and repeated utterances of their own name or by mild prodding. The authors noted reduced, but existent, MMN and P3a responses during propofol sedation, with a missing P3b response. With recovery from deep propofol sedation, MMN recovered quickly to wake levels, but not the P300 response. Lastly, Zhang et al. (2018) report that MMN is abolished during deep anesthesia. The authors used source localization techniques to investigate how the network underlying the MMN response during awake conditions is altered by anesthesia. Deviant stimuli during anesthesia induced less long-distance connections between frontal and temporal-parietal regions than in an awake state (Zhang et al., 2018).

More recent studies have employed the local-global paradigm (Shirazibeheshti et al., 2018; Witon et al., 2020) with high-density EEG or iEEG recordings (Nourski et al., 2018) to test this hypothesis directly. Specifically, Shirazibeheshti et al. (2018) measured high-density EEG during a local-global paradigm in wakefulness, propofol sedation, and recovery. During sedation, both local and global deviance responses were recorded, but their amplitude was reduced with respect to wakefulness. The authors observed an interaction between effects of local and global deviance, namely that effects of local deviance exacerbate effects of global deviance. Nevertheless, under anesthesia this interaction was reduced. The authors posited that the coincidence of local and global deviance had a facilitatory effect on global deviance responses, which was reduced when individuals were sedated. Witon et al. (2020) further examined the neural circuits of this effect and observed effects of sedation on local deviance responses during early (100–150 ms post-stimulus onset) and middle (250–350 ms) time periods, indicative of modulations of evoked power responses early in the processing pathway. The interaction between the local and global effects was significant in a late time window (400–600 ms). The authors found a locally mediated acceleration of global deviance responses (Witon et al., 2020) during sedation and recovery. The second important interaction – the local standard global deviant, representing the pure global deviance effect – was reduced in anesthesia compared to recovery. Here, deviance processing is thought to be instantiated by more higher-level than low-level predictions. Key findings during sedation included a reduction in amplitude of the responses, and a slowing of the responses to deviant stimuli, specifically in global deviance.

Nourski et al. (2018) examined the neural networks that are preserved for local and global deviance responses in iEEG recordings. High frequency activity responses, which correlate

with local infragranular multi-unit activity and superficial dendritic potentials (Leszczynski et al., 2020), and intracranial auditory evoked potentials were recorded. Authors used vowels instead of pure tones in patients implanted in temporal and inferior frontal regions, as well as in the amygdala, under propofol sedation. This study reported retained local deviance effects under loss of consciousness in auditory regions, but not outside of these regions, indicating intact low-level sensory predictive processing independent of the state of consciousness (**Figure 2**). By contrast, local deviance responses in frontal regions began to reduce during initial sedation and vanished during anesthesia. Global deviance was completely abolished with anesthesia, and in some patients, it was abolished even during a sedated state in which they were still responsive (Nourski et al., 2018). The authors concluded that the presence of a global deviance effect is indicative of conscious processing, while its absence is not necessarily linked to loss of consciousness (see **Table 2A** for a summary).

Research in Animals

In animals, anesthesia is *mostly* induced using ketamine, urethane, or halothane (see **Table 2B** for summary). Anesthesia in general, whether with barbiturates or ketamine, seems to have more wide-spread effects in animals than in humans. Specifically, inhibition of auditory cortical units was reported 70 years ago (Thomas and Jenkner, 1952). Anesthetics are known to affect the entire central auditory pathway, from the dorsal cochlear nucleus (Young and Brownell, 1976) to core auditory regions (Gaese and Ostwald, 2001), such as the primary auditory cortex (A1). A1 neurons demonstrate reduced mean bandwidth in anesthesia than when animals are awake, with reductions up to threefold (Qin et al., 2003). In particular, ketamine anesthesia depth modulates not only average evoked responses but also response variability, which is highest under medium anesthesia, where ongoing cortical activity exhibits rhythmic bursting activity (Kisley and Gerstein, 1999). Importantly, this observed variability in shape and amplitude can be accounted for by the background ongoing activity, which speaks for transitions in thalamocortical excitability modulating these effects (Zurita et al., 1994). Specifically, stronger excitatory responses are observed in the thalamus after ketamine injection, despite decreasing overall cortical and thalamic firing rates (Kisley and Gerstein, 1999). Halothane, a gas anesthetic, shows a weaker suppressive effect on auditory-evoked responses (Johnson and Taylor, 1998; Moshitch et al., 2006), with responses found to sometimes resemble those in awake animals. Auditory working memory was found to be active for hundreds of ms after stimulus onset (Moshitch et al., 2006). Urethane causes moderate cardiovascular depression, with long duration of anesthesia (greater than 24 h), excellent anesthesia depth, and analgesia (Field et al., 1993). During urethane anesthesia auditory neurons show higher minimum thresholds, lower spontaneous firing rates, longer response latencies, and more frequent occurrence of tuning alterations, with stronger inhibition (Huang et al., 2013).

Because anesthesia facilitates experimental procedures, there are a multitude of deviance studies done in different species of anesthetized animals. Most of the studies have been carried out in rats (Ruusuvirta et al., 1998; Lazar and Metherate, 2003; Eriksson and Villa, 2005; Astikainen et al., 2006; Nakamura et al., 2011; Taaseh et al., 2011; Xu et al., 2014; Takahashi et al., 2015; Ahnaou et al., 2017; Parras et al., 2017; Rui et al., 2018; Cappotto et al., 2021), and mice (Ehrlichman et al., 2008; Chen et al., 2015; Duque and Malmierca, 2015; Duque et al., 2018; Lipponen et al., 2019), with a few studies in non-human primates (Uhrig et al., 2014), guinea pigs (Kraus et al., 1994; Christianson et al., 2014), gerbils (Bäuerle et al., 2011), and songbirds (Beckers and Gahr, 2012). These studies mainly report successful recordings of SSA or MMN-like responses in auditory cortices, especially under urethane anesthesia (Astikainen et al., 2006; Taaseh et al., 2011; Duque et al., 2015; Rui et al., 2018). Nevertheless, depending on the used anesthetic, higher-level deviance responses are attenuated or eliminated, despite retained low-level responses to deviant stimuli, as for example under ketamine anesthesia (Ehrlichman et al., 2008; Uhrig et al., 2016). Uhrig et al. (2016) anesthetized macaque monkeys with propofol and ketamine and presented a local-global auditory task during anesthesia. The authors observed no local deviance responses during light propofol sedation and deep anesthesia. By contrast, the global effect was preserved in core auditory areas bilaterally and the MGN, as well as in the anterior cingulate and prefrontal areas, albeit with diminished activations compared to wakefulness. During anesthesia, the global effect was reduced compared to wakefulness in all brain regions.

Thalamic SSA responses were recorded during ketamine anesthesia in gerbils (Bäuerle et al., 2011). In order to control for auditory cortical regulatory effects on subcortical regions, the authors pharmacologically inactivated cortical regions using muscimol, which preserves subcortical auditory processing. Interestingly, this led to a reduction of responses in the MGB of the thalamus of the anesthetized gerbil. The authors interpreted their findings as a demonstration that SSA in subcortical structures is mainly regulated by the descending corticofugal system, highlighting a more general function in information processing than just novelty detection. Finally, another interesting study in anesthetized zebra finches (Beckers and Gahr, 2012) used a switching oddball paradigm with naturalistic short-range contact zebra finch social calls, different to usual zebra finch background vocalizations. Birds were anesthetized with isoflurane gas, which produces behavioral and physiological effects through binding at multiple targets in the brain and central nervous system (binding to GABAa receptors and enhancing GABAergic inhibition; blocking glutamate release by binding to NMDA receptors), and shows similar effects on EEG as propofol (Purdon et al., 2015). Results indicate deviance processing in secondary, but not primary, cortices, suggesting that deviant events, more than just stimulating a larger part of a single sensory processing network, may activate a different network compared to standards, eliciting more widespread activity. It is worth noting that social calls are more complex than the pure tones generally used in the majority of oddball paradigms, and thus might recruit more complex predictive mechanisms.

TABLE 2 | Studies in anesthesia.

(A) Humans

Study	Paradigm	Agents	Anesthesia (A)/ sedation (S)	Surgical A/S	Deviance effects
Plourde and Picton, 1991	Pitch oddball	Thiopental, fentanyl, and isoflurane ± nitrous oxide	A	Yes	No
Plourde and Boylan, 1991	Pitch oddball	Sufentanil with lorazepam premedication	A	Yes	No
Reinsel et al., 1995	Pitch oddball	Propofol	S	No	Yes
Sneyd et al., 1994	Pitch oddball	Propofol	S	No	Yes
Simpson et al., 2002	Pitch oddball	Propofol	S - conscious	No	Yes
			S - unconscious		no
	Duration oddball		S - conscious		no
			S - unconscious		no
Yppärilä et al., 2002	Pitch oddball	Propofol	S	Yes	Yes
Heinke et al., 2004		Propofol	S - light	Yes	Yes
			S - deep		Yes
			S - unconscious		No
Koelsch et al., 2006	Pitch oddball	Propofol	S	No	Yes
Zhang et al., 2018	Pitch oddball	Propofol	S - deep	No	No
Nourski et al., 2018	Local-global	Propofol	A - conscious	Yes	Only local
			A - unconscious		Only local
Shirazibeheshti et al., 2018	Local-global	Propofol	S - unconscious	No	Local and global
Witon et al., 2020	Local-global	Propofol	S - moderate	No	Local and global

(B) Animals

Study	Paradigm	Agents	Deviance effects	Species
Ruusuvirta et al., 1998	Pitch oddball	Urethane	Yes	Rats
Lazar and Metherate, 2003	Pitch-frequency oddball	Urethane-xylazine	SSA	Rats
Eriksson and Villa, 2005	Pitch oddball	Ketamine-xylazine	No	Rats
Astikainen et al., 2006	Pitch-intensity oddball	Urethane	Yes	Rats
Nakamura et al., 2011	Pitch-duration oddball	Fentanyl-medetomidine-isoflurane	Yes	Rats
Taaseh et al., 2011	Pitch oddball	Halothane	Yes	Rats
Xu et al., 2014	Aurality-specific noise	Sodium pentobarbital	SSA	Rats
Takahashi et al., 2015	Pitch oddball	Isoflurane	SSA	Rats
Ahnaou et al., 2017	Pitch oddball	Ketamine	Yes	Rats
Rui et al., 2018	Pitch oddball	Urethane	SSA	Rats
Ehrlichman et al., 2008	Pitch oddball	Ketamine	No	Mice
Chen et al., 2015	Pitch oddball	Isoflurane	SSA	Mice
Duque and Malmierca, 2015	Pitch oddball	Urethane ± acepromazine	SSA	Mice
Duque et al., 2018	Pitch oddball	Ketamine-xylazine	SSA	Mice
Lipponen et al., 2019	Duration oddball	Urethane	No	Mice
Uhrig et al., 2016	Local-global	Propofol	Only global, no local	Primates
		Ketamine	Only local, no global	
Kraus et al., 1994	Pitch oddball	Ketamine-xylazine	Yes	Guinea pigs
Christianson et al., 2014	Roving standard	Urethane-buprenorphine	SSA	Guinea pigs
Bäuerle et al., 2011	Roving standard	Ketamine-xylazine	SSA	Gerbils
Beckers and Gahr, 2012	Naturalistic oddball	Isoflurane	Yes	Songbirds

**SSA, stimulus-specific adaptation; Yes, effects other than SSA.*

Conclusion

Overall, studies in humans and animals suggest that auditory predictions are reduced but may still be present in conditions of sedation and anesthesia. Interestingly, scalp EEG components corresponding to auditory predictive processes like the MMN or P3a may be preserved in anesthesia but are altered with respect to wakefulness. The latencies of scalp level auditory and deviance components are longer, and their amplitudes decrease. Moreover, the processing of deviant events at a local level is spatially restricted as shown via iEEG and source localization studies (Nourski et al., 2018; Zhang et al., 2018). Global deviance effects seem to be further restricted or even absent as the depth of anesthesia progresses in humans (Nourski et al., 2018; Shirazibeheshti et al., 2018), although they may be preserved in core auditory areas, at least in non-human primates (Uhrig et al., 2016). Importantly, similar to sleep, SSA is preserved also in anesthesia. These findings suggest that predictive processes are maintained to some degree under anesthesia, although they involve limited brain regions and sub-networks as compared to wakefulness.

DISORDERS OF CONSCIOUSNESS

One important application of auditory deviance paradigms has been the prognosis of patients with disorders of consciousness (DOC; Lew et al., 2003; Kotchoubey, 2005; Wijnen et al., 2007; Tzovara et al., 2013). DOCs are defined as a disrupted relationship between the two components clinically defining consciousness – wakefulness/arousal and awareness (Laureys, 2005). Coma is characterized by the absence of arousal and awareness. The vegetative state (VS) or unresponsive wakefulness syndrome (UWS; Laureys et al., 2010) is described by some degree of arousal in the absence of awareness, and the minimally conscious state (MCS) is characterized by preserved arousal with varying signs of awareness (Gosseries et al., 2011; **Figure 1**). In contrast, in the locked-in syndrome, often a consequence of brainstem damage, patients are fully aware and awake, but suffer from complete paralysis of all voluntary muscles except for vertical eye movements, as in amyotrophic lateral sclerosis (Bauer et al., 1979; Sharma, 2011). The famous American case of patient Terri Schiavo (see e.g., Perry et al., 2005) is a good example of the important and nuanced medical, ethical, religious, social, familial, philosophical, and political debates around retained awareness and prognosis in patients suffering from DOC.

About 50% of patients emerging from coma are expected to evolve into a MCS (Giacino et al., 2006), which is difficult to differentially diagnose from UWS because of intermittent signs of consciousness in MCS patients (Fins et al., 2007). Despite the immense societal importance, DOCs remain among the most poorly understood conditions of modern neurology (Boly et al., 2012). For many years, clinical and behavioral examinations were the leading approaches to diagnosing retained consciousness (Plum and Posner, 1982), but this approach has high rates of misdiagnosis (Laureys, 2005). Electrophysiology typically using ERPs is currently used in the majority of studies investigating patients with DOC (see Giacino et al., 2006; Owen and Coleman, 2007; Demertzi et al., 2008; Boly, 2011; Boly et al., 2012; Gosseries et al., 2014b), and is applied to the search for a "consciousness marker" to be used in diagnosis of DOC.

Auditory Predictions and Their Link to Coma Outcome

Despite the heterogeneity of coma aetiologies and types of brain injury, several studies suggest that some patients in a coma can detect environmental deviant events at a neural level (Laureys et al., 2004; see also **Table 3A** for a summary). For instance, scalp EEG components such as the MMN and P300 correlate with patients' outcome (Fischer et al., 1999; Kane et al., 2000; Luauté et al., 2005; Daltrozzo et al., 2007). Studies undertaken in the 90s have shown that some, but not all, coma patients may have preserved N100 (thought to reflect the early processing of acoustic features of a stimulus; Näätänen and Picton, 1987) and MMN responses, indicative of intact auditory deviance processing (Fischer et al., 1999; Daltrozzo et al., 2007). Interestingly, the presence of a MMN response was more frequently observed in patients who later awoke from coma (Fischer et al., 2004; Naccache et al., 2005), suggesting that the MMN is a predictor of patients' chances of awakening. This hypothesis was driven by the fact that non-survivors generally did not show a MMN response (Fischer et al., 2004). However, these studies were performed several weeks or months after coma onset (Fischer et al., 2004; Boly, 2011).

More recent studies, performed in post-anoxic coma patients, have examined deviance processing in the acute coma phase, within the first 36 h of coma (Tzovara et al., 2013, 2016; Juan et al., 2016). In order to overcome the inherent difficulties associated with the detection of ERP components over single electrodes, these studies applied a multivariate decoding analysis (Tzovara et al., 2013) which models topographies of single-trial EEG activity. The model estimation was performed on a portion of the data (the training data set) and then used to decode the category of sounds (standard/deviant) in a separate portion of data. An above chance decoding performance implied a differential scalp EEG response to standard vs. deviant stimuli, focusing on the most discriminative time-windows within the trial. These studies have shown that during acute coma, even patients who do not survive show differential patterns of EEG activity in response to standard vs. deviant stimuli. Moreover, discrimination between standard and deviant sounds deteriorates from the first to the 2nd day of coma in non-survivors, while an improvement in auditory discrimination is observed for patients who later awake from coma (Tzovara et al., 2013, 2016).

More work in the acute coma phase using a local-global paradigm has shown that the global deviance effects, assessed via topographic patterns on scalp EEG, were preserved in 10 out of 24 patients (Tzovara et al., 2015). Moreover, while the global effect was not in itself predictive of the patient's outcome, an improvement in decoding global standard vs. global deviant stimuli over the first 2 days of coma was informative of survival and return of consciousness (Tzovara et al., 2015).

TABLE 3 | Studies in disorders of consciousness.

(A) Coma

Study	Paradigm	Time of testing	Patients showing deviance effects
Fischer et al., 1999	Duration oddball	8.7 ± 11 days	33/128 patients
Fischer et al., 2004	Duration oddball	10.3 ± 11.4 days	88/346 patients
Luauté et al., 2005	Duration oddball	10.3 ± 11.4 days	Yes
Naccache et al., 2005	Pitch oddball	4–96 days	10/33 patients
Tzovara et al., 2013	Pitch, duration, location oddball	First 48 h	9/30 patients
Tzovara et al., 2015	Local-global	First 48 h	Global in 10/24 patients
Pfeiffer et al., 2018	Duration, location, pitch oddball	First 48 h	25/66 in 1st and 31/66 patients in 2nd day of coma
	Somatosensory oddball		16/66 patients in 1st and 23/66 in 2nd day of coma

(B) UWS/MCS

Study	Paradigm	Deviance effects	Patients showing deviance effects
Perrin et al., 2006	Personal name oddball	Yes	6 MCS; 3/5 UWS; 4 LIS
Wijnen et al., 2007	Pitch oddball	Yes	10 UWS at first measurement
Bekinschtein et al., 2009	Local-global	Local	3/4 UWS, 4/4 MCS
		Global	3/4 MCS
Risetti et al., 2013	Pitch-duration oddball with own name; active counting of name	Yes	UWS: active < passive; MCS: passive > active
	Passive	Yes	10/11 patients
King et al., 2013	Local-global	Local	All
		Global	Only MCS, not UWS
Faugeras et al., 2011	Local-global	Yes	2/22 patients
Faugeras et al., 2012	Local-global	Local	Only CS and MCS
		Global	Only controls
Perez et al., 2021	Local-global	Local	N/A
		Global	43 (E)MCS/ 23 UWS out of 236 total

**N/A not reported; MCS, minimally conscious state; (E)MSC, (exit) MCS; UWS, unresponsive wakefulness syndrome; LIS, Locked-in Syndrome; CS, conscious ± paralysis.*

The vast majority of deviance studies in coma target the auditory pathway, with the exception of one study comparing auditory and somatosensory stimuli, using the same oddball paradigm (Pfeiffer et al., 2018). Interestingly, this study found that discrimination between deviant and standard events at the EEG level is preserved in acute coma for both the auditory and somatosensory modalities. However, only the auditory modality was informative of coma outcome, with an improvement in auditory discrimination being indicative of survival. The specificity of deviance mechanisms for outcome prognosis is also highlighted by a study performed on the same type of patients, examining discrimination of naturalistic sounds, which, albeit preserved in some patients, was not informative of coma outcome (Cossy et al., 2014). Overall, these studies show that sensory deviance effects can be preserved in acute coma, suggesting a fundamental role for auditory predictions in relation to consciousness.

Auditory Predictions Differentiating Consciousness Levels

Unresponsive wakefulness syndrome is typically characterized by spared brainstem activity with widespread severe damage to gray and white matter in both cerebral hemispheres (Laureys et al., 2004). Although brainstem metabolism can be spared in UWS, preserving arousal and autonomic functions, several cortical regions, including prefrontal regions, parietotemporal and posterior parietal cortices, and the precuneus, are typically impaired (see Laureys et al., 2004 for a detailed review). Regarding patients, spared medial parietal cortex (precuneus) and adjacent posterior cingulate cortex metabolism seem to differentiate MCS from UWS (Laureys et al., 2004). Overall cortical metabolism is slightly higher in MCS than in UWS patients (Laureys, 2005).

Deviance effects are posited to correlate with retained consciousness in UWS and MCS patients (e.g., Wijnen et al., 2007; see **Table 3B** for a summary). While MMN and P300 can be recorded in both clinical groups, global deviance effects in active tasks (e.g., counting the number of deviant stimuli, but without behavioral responses) are only recorded in MCS, and thus are associated with the presence of residual levels of consciousness. A study using a passive and active oddball paradigm (i.e., where participants had to count the deviant stimulus) in MCS and UWS patients recorded MMN (between standard and deviant tones) and P300 (in response to the patients' own name) responses in all but one patient (Risetti et al., 2013). Nevertheless, only in MCS did the P300 increase in amplitude during the active condition, corroborating the possible advantage of using this paradigm for probing awareness by bypassing the motor response. In a similar paradigm, Perrin et al. (2006) observed the P300 response to patients' own name in 3 out of 5 UWS patients, and in all MCS patients, concluding that this ERP component is not specific enough to differentiate UWS ad MCS patients.

When regularities are established over groups of sounds, past studies have shown a link between global deviance effects in UWS patients and the presence of residual consciousness (Faugeras et al., 2011, 2012; King et al., 2013). Particularly, global deviance effects have been linked to conscious perception, mainly supported by the absence of evidence for a global deviance effect in UWS patients (Bekinschtein et al., 2009; Faugeras et al., 2012;

King et al., 2013). Bekinschtein et al. (2009) measured local deviance effects in UWS/VS and MCS patients, but no global effects. King et al. (2013), observed a global effect in 14 % of UWS and 31 % of MCS patients. A more recent study reported that the presence of a global deviance effect in UWS patients is related to an eventual return of consciousness, while its absence is not informative of patients' outcome (Perez et al., 2021). In particular, the majority of patients that showed a global effect eventually regained consciousness, while amongst patients that did not show a global effect some regained consciousness, and some did not, paralleling findings based on MMN (Fischer et al., 2004).

When investigated during recovery from UWS, the MMN was found to be an important predictor of recovery ability (Wijnen et al., 2007), as MMN amplitudes increased with recovery. Moreover, a sudden increase in amplitudes preceding overt external communication was interpreted as consolidation of the networks and mechanism supporting this ability. The study of functional connectivity supports this hypothesis (Boly et al., 2011). Boly et al. (2011) used a roving MMN paradigm in MCS and UWS patients and modeled cortical source activity using scalp EEG data to quantify backward and forward connections between temporal and frontal cortices during MMN generation. The authors found that compared to MCS and healthy controls, UWS patients had impaired connections from frontal to superior temporal cortex, but no impairments in connectivity within temporal cortical networks.

Conclusion

Taken together, studies in patients in a coma or with DOC show that scalp level EEG signatures of auditory predictive processes, including the MMN, may be preserved. An improvement of differential responses between standard and deviant stimuli over the 1st days of coma, or the presence of MMN responses in later coma stages, are frequently observed in patients that eventually regain consciousness.

Investigations of the neural circuits of predictive processes in patients with DOC remain sparse, and report that an impairment in predictive mechanisms may be accompanied by an impairment in backward connections from frontal to temporal cortical regions (Boly et al., 2011). One main challenge in studies with patients is pathological heterogeneity, for example relating to the cause of coma or DOC, to whether a focal lesion is present or not, or to the time of recording, as this may be followed by reconfigurations of brain networks supporting processing of environmental stimuli. Further studies of circuit level mechanisms are needed to better disentangle impaired and retained sensory predictive processes in patients with DOC, and link those to disease etiology and outcome.

ALTERED STATES OF CONSCIOUSNESS

Altered states of consciousness were first defined in the late 60's as "any mental state(s), induced by various physiological, psychological, or pharmacological maneuvers or agents. An altered state of consciousness can be recognized subjectively by the individual [...] as representing a sufficient deviation in subjective experience or psychological functioning from certain general norms for that individual during alert, waking consciousness" (Ludwig, 1966). Despite the fact that all the above-mentioned states can be considered altered states of consciousness, we here focus on those states induced by hypnosis and meditation (see e.g., Vaitl et al., 2005, for a review) due to availability of research using MMN paradigms in these states.

The psychological mechanisms that hypnosis and meditation engage are distinct: while hypnotic suggestions are utilized to elicit changes in experience, meditation may be considered as a form of mental training that induces alterations in attention and self-regulation (Jamieson, 2016). A common feature of hypnosis and meditation is that both processes involve self-regulation, including attentional control and self-awareness. These involve sensory and frontal-parietal attentional systems that also support predictive processing (Tang et al., 2015; Jamieson, 2016). The human brain is hypothesized to use both perceptual and active inference to maximize the effectiveness of predictive processing: for perceptual inference internal models are adjusted to best fit perception using predictions that best explain the experienced sensory information, whereas active inference consists of performing actions that produce sensory input conforming to predictions (Martin and Pacherie, 2019). Perception in itself can be divided into exteroception (perception of the external world), proprioception (perception of one's own motion and one's body in space), and interoception (perception of one's own homeostatically regulated physiological states) (Jamieson, 2016), all of which are used to generate predictive models of the world, our bodies and our mental states. As discussed below, the processes of perceptual and active inference are altered during both meditation and hypnosis through modified priors as well as through altered perception. Despite sparse research into the topic of auditory deviance processing in hypnosis and meditation, the few existing studies are worth discussing, due to insights they might offer into mechanisms of self-regulation.

Meditation

Meditation describes practices of self-regulation (Kabat-Zinn, 1982) and modulates the awareness component of consciousness (Brown and Ryan, 2004). Predictive processing during mindfulness meditation is thought to correspond to reductions in active inference and in the influence of priors (Pagnoni, 2019), as well as reduced stimulus salience weighting (Jamieson, 2016) – leading to reduced PEs, and thus reduced updating of expectancies, with parallel enhanced precision of proprioceptive and interoceptive predictions (Pagnoni, 2019). Collectively, these processes might lead to enhanced matching of interoceptive predictions and feedback (Jamieson, 2016), and thus to meta-awareness (Pagnoni, 2019).

Several ERP studies have investigated auditory oddball paradigms in mindfulness meditation (Cahn and Polich, 2009; Atchley et al., 2016; Biedermann et al., 2016; Fucci et al., 2018; see **Table 4A** for a summary). Cahn and colleagues compared a passive oddball task to a control thought period in expert meditators. They observed reduced amplitudes of the N1 and P2 components, representing early processing of acoustic features

TABLE 4 | Studies in altered states of consciousness.

(A) Meditation

Study	Paradigm	When	Deviance effects
Cahn and Polich, 2009	Pitch oddball with distractor	During meditation	Yes
Atchley et al., 2016	Active pitch oddball with distractor	Before meditation	Meditators > controls
	Passive pitch oddball with distractor (meditation)	During meditation	Controls > meditators
Biedermann et al., 2016	Pitch oddball	Imaginative task	Meditators > controls
		During meditation	Meditators > controls
Fucci et al., 2018	Pitch oddball	Open presence meditation	Meditators = controls
		Focused attention meditation	Meditators > controls
		Reading	Meditators = controls

(B) Hypnosis

Study	Paradigm	When	Deviance effects
Csépe et al., 1997	Phoneme oddball	During hypnosis	Hypnposis < baseline
Kallio et al., 1999	Pitch oddball	During hypnosis	Hypnosis > baseline (one virtuoso)
Jamieson et al., 2005	Roving standard	Before hypnosis	Yes
		During hypnosis	Yes
		After hypnosis	Yes
Hiltunen et al., 2019	Pitch oddball	Before hypnosis	Yes
		During hypnosis	Yes
		After hypnosis	Yes

of a stimulus, and later P300 components to deviant tones and distractors (white noise), but not to standards (Cahn and Polich, 2009). Another study showed reductions in amplitudes of N1 and P2 components for all types of stimuli (standards, deviant, distractor), but not later P300, during mindfulness as compared to a tone detection task in expert and novice meditators versus controls (Atchley et al., 2016). A recent study in novice and expert meditators compared MMN responses during mindfulness meditation to a reading control condition (Biedermann et al., 2016). MMN amplitude was larger for both reading and meditation conditions in meditators as compared to controls. In novices, MMN responses were also increased during meditation as compared to reading. Taken together, these results indicate that mindfulness meditation might be associated with larger early sensory detection peaks for standard events, larger MMN responses and reduced P3a responses compared to normal wakefulness, which might be interpreted as greater environmental monitoring abilities, then applied to disengaging from distracting stimuli (supported by smaller early sensory detection peaks for distractors).

Hypnosis

Individuals who are susceptible to hypnosis are reported to experience changes in subjective awareness (Kihlstrom, 2005; Pekala, 2015). Hypnosis is thought to affect both active and perceptual inference, as well as perception, per se through attentional modulation (Jamieson, 2016, 2018; Martin and Pacherie, 2019). There are only a handful of studies investigating auditory predictive processes during hypnosis (Csépe et al., 1997; Kallio et al., 1999; Jamieson et al., 2005; Hiltunen et al., 2019; summarized in **Table 4B**). Perhaps the earliest systematic studies of this type were conducted by Gruzelier and colleagues (see Gruzelier, 1998, for a summary). In brief, medium-high hypnosis susceptible participants, but not low, showed decreased P300 to auditory oddballs and reduced MMN amplitudes during and following a hypnotic induction compared to pre-induction. By contrast, participants with low susceptibility showed an increase in MMN amplitudes following hypnotic induction. Measuring deviance responses in a passive oddball paradigm before the hypnotic induction and during neutral hypnosis (Kallio et al., 1999), as well as after the hypnosis in highly hypnotisable subjects (Jamieson et al., 2005; Hiltunen et al., 2019), and sometimes also using phonemes and participants with different levels of hypnotic suggestibility (Csépe et al., 1997), different studies demonstrate either increases or decreases of MMN amplitudes during hypnosis as compared to pre- or post-hypnosis. Another study found suppressed MMN amplitudes during hypnosis in highly hypnotisable subjects and no differences during waking between high, middle and low hypnotisable subjects (Csépe et al., 1997). While no changes were found in a recent study focusing on mean amplitude of ERP components from responses to standard and deviant sounds (Hiltunen et al., 2019), Jamieson et al. (2005) found increases in amplitude for MMN over frontal electrodes during hypnosis as compared to pre- and post-hypnosis in high suggestible participants (Jamieson et al., 2005). This trend was observed for these participants in temporal electrodes, too, but not for low suggestible participants, who showed linear increases in these electrodes from pre- to during to post-hypnosis. One possible interpretation for these results is that precision of deviance processing was enhanced, despite the engagement of attentional control with another active task.

Conclusion

As a general conclusion, it is hypothesized that both meditation and hypnosis modulate predictive processes manifesting through scalp EEG components. For meditation, the results are too sparse and heterogeneous to draw firm conclusions, highlighting the need for more research. To address these heterogeneous results, predictive processing theories offer testable hypotheses to assess these changes in awareness and subjective perception that are at the core of these states. Some of the seemingly inconsistent results in hypnosis and meditation emphasize the limitations of this literature: the focus on analysis of ERP components at single electrodes, the heterogeneity of instructions, high inter-individual variations,

and the differences in statistical analyses and dependent variables, making it difficult to draw consistent conclusions. Future research can address these issues by focusing on replication studies using similar task instructions, and moving beyond analysis of single EEG electrodes, to measures that quantify the whole electrical field at the scalp level (see e.g., Michel and Murray, 2012).

DISCUSSION AND FUTURE OUTLOOK

A large body of literature has shown that sensory predictive signals manifest in the absence of consciousness. Here, we approached consciousness via states where consciousness is reduced or absent (sleep, anesthesia, disorders of consciousness), or altered (hypnosis, meditation). In the absence or alteration of consciousness, predictive processes can be preserved for predictions built over simple and long-lasting regularities. At the level of scalp EEG, evoked components associated with auditory predictions tend to have a reduced amplitude with decreasing levels of consciousness. At the level of generators, several studies suggest that the network underlying the generation of sensory predictions is restricted when conscious access and behavioral reactivity to the environment is lost. In the absence of consciousness, core auditory areas can preserve their capacities for generating deviance effects, while such effects in areas that are 'higher' in the sensory processing hierarchy (i.e., frontal areas) are abolished, likely as a result of disruption of connections from higher to lower regions.

However, as the generation of sensory predictions extends well beyond a two-node circuit of frontal-sensory areas, it remains an open question how each of the regions and the corresponding networks involved in sensory predictions is altered by the loss of consciousness. Importantly, the brain is a complex system, where mental states arise through the principle of emergence, and thus through an interaction of multiple functional, structural, and computational levels (Bassett and Gazzaniga, 2011). Within these computations, sensory predictive processes appear as a necessary, but not sufficient, condition for consciousness.

From an electrophysiological viewpoint, the loss of consciousness is accompanied by a plethora of changes in neural activity, such as the disruption of thalamo-cortical and cortico-cortical long-range connections, and changes in non-oscillatory components of the EEG (Magnin et al., 2010; Lendner et al., 2020, to name a few. These electrophysiological alterations may in turn affect circuit level mechanisms underlying predictions. Future studies should take into account these fundamental changes in neural activity when designing new experiments to study predictions in the absence of consciousness, and can choose to selectively stimulate specific states of neural activity, such as "up" or "down" sleep states.

In this review, we focused on neural signatures of predictive processes both at the neuronal level (e.g., SSA) and at the scalp EEG level (e.g., MMN or P300). The neural signals that can be recorded with scalp EEG have limited interpretation about the precise circuit or mechanisms underlying auditory predictions, because of the poor spatial resolution of EEG responses. Nevertheless, these scalp EEG components have strong clinical applications because of their relatively straightforward implementation (i.e., no invasive recordings are needed) that can facilitate their integration with other clinical measures to detect residual levels of consciousness.

From Electrophysiology to Computational Models

As the loss of consciousness engenders drastic changes to the predictive circuit, another important future question is how these changes affect the neural computations that lead to a predictive signal. Although theoretical modeling has been widely applied in the field of threat predictions (e.g., Tzovara et al., 2018), or reward learning (Abbott and Dayan, 2005), attempts to model sensory predictions are limited. This is important given the fact that scalp EEG responses associated with deviance processing such as the MMN are compound responses, reflecting multiple and complex processes from multiple brain regions and neural computations. Distinguishing which neural computations of deviance processing (e.g., adaptation, PEs, update of an internal model) are performed in different cortical and subcortical structures involved in the sensory predictive network is a crucial future necessity.

Previous studies have tested various theories of auditory PE generation, and have shown that trial-by-trial changes in deviance EEG responses are compatible with a Bayesian updating of a probabilistic model of the environment in the auditory (Lieder et al., 2013), somatosensory (Ostwald et al., 2012), and visual modalities (Stefanics et al., 2018). Modeling work has also supported claims that deviance effects reflect PE signals, weighted by the precision of predictions (Stefanics et al., 2018), with attention increasing the precision of PEs (Smout et al., 2019). Nevertheless, the MMN still remains opaque in terms of which computational components it represents, and which changes these components undergo when consciousness is lost.

A principled way to model PE signals comes from the field of reinforcement learning (see e.g., Hoy et al., 2021). When studying reward PEs, past studies have applied an axiomatic model developed in the field of economics to assess whether responses indeed reflect PEs (Caplin and Dean, 2008; Rutledge et al., 2010). Developed for testing dopamine-related hypotheses, namely whether the firing rate of midbrain dopamine neurons reflect PEs, these axioms represent necessary and sufficient conditions for a brain response to be considered a true PE signal. Given theoretical work drawing similarities between reward and sensory PEs (Gardner et al., 2018), future studies can investigate computational approaches to offer more objective means to disentangle complex constructs such as the MMN.

Regarding the ambiguity as to which computational components are altered when consciousness is lost, some first attempts to resolve this question have used ketamine, which was shown to diminish model quantities that correspond to PE signals related to higher order predictions, like transition probabilities (Weber et al., 2020). Another recent study examined how awareness and task-relevance affect the neural computations

of the MMN component (Schlossmacher et al., 2021). When stimuli were task-irrelevant, both in unaware and aware conditions, the MMN was best explained by an adaptation model, whereas when stimuli were aware and task-relevant, the MMN was best explained by a precision-weighted prediction error. Interestingly, although the trial-by-trial N100 amplitude of the EEG response to repeated tones in UWS patients has been shown to change (Kotchoubey et al., 2006), indicative of cortical learning, to date there are no attempts to formally model such changes. Future studies will need to link the electrophysiological alterations that are observed in sensory predictions during sleep, coma or anesthesia to computational models, in order to obtain a mechanistic understanding of the neural computations underlying sensory predictions in the absence of consciousness.

An important future question is whether the presence or absence of consciousness can be linked to specific computations that result in the generation of prediction signals. It has been proposed that one of the main functions of consciousness is the generation of internal representations from incoming sensory input (Kanai et al., 2019) so that we can act meaningfully on this input (Hohwy, 2012). Under standard predictive theories, the influence of PEs depends on their precision (Auksztulewicz and Friston, 2015; Kanai et al., 2015), and, as explained previously, this is the effect of attentional selection. This means that ascending PEs with higher precision have more model-updating power than those with lower precision (Witon et al., 2020). Future studies can evaluate whether a similar computational role can be attributed to different states of consciousness and, in particular, according to their arousal and awareness contents.

Conclusion

In this review, we summarized studies investigating sensory predictions and their modulations by the loss of consciousness. We reviewed studies of animal and human physiology, from the fields of sleep, anesthesia, disorders of consciousness, hypnosis and meditation. Predictive processes represent a key, cross-species mechanism of perception, that manifests in an automatic way, and is embedded in distributed neuronal circuits. Refining our understanding of the neural networks and computations that underly sensory predictions in the physiological absence of consciousness (i.e., sleep or anesthesia) can advance our understanding of its pathological loss, and lead to improved, theory-driven strategies for diagnosis and prognostication in patients with disorders of consciousness.

AUTHOR CONTRIBUTIONS

RT, RK, and AT wrote sections of the manuscript. All authors read and approved the submitted version.

FUNDING

This work was supported by the Interfaculty Research Cooperation "Decoding Sleep: From Neurons to Health and Mind" of the University of Bern and the Swiss National Science Foundation #320030_188737, NINDS Grant R37NS21135, and NIMH CONTE Center P50MH109429.

ACKNOWLEDGMENTS

We hereby wish to gratefully thank Graham Jamieson (University of New England) for his very helpful comments on the section "Altered States of Consciousness."

REFERENCES

Abbott, L. F., and Dayan, P. (2005). *Theoretical Neuroscience: Computational and Mathematical Modeling of Neural Systems*. Cambridge: MIT press.

Ahnaou, A., Huysmans, H., Biermans, R., Manyakov, N. V., and Drinkenburg, W. (2017). Ketamine: differential neurophysiological dynamics in functional networks in the rat brain. *Transl. Psych.* 7, e1237–e1237. doi: 10.1038/tp.2017.198

Aitchison, L., and Lengyel, M. (2017). With or without you: predictive coding and bayesian inference in the brain. *Curr. Opin. Neurobiol.* 46, 219–227. doi: 10.1016/j.conb.2017.08.010

Alain, C., and David, L. W. (1997). Attention modulates auditory pattern memory as indexed by event-related brain potentials. *Psychophysiology* 34, 534–546. doi: 10.1111/j.1469-8986.1997.tb01740.x

Alho, K. (1995). Cerebral generators of mismatch negativity (MMN) and its magnetic counterpart (MMNM) elicited by sound changes. *Ear Hearing* 16, 38–51. doi: 10.1097/00003446-199502000-00004

Anderson, L. A., Christianson, G. B., and Linden, J. F. (2009). Stimulus-specific adaptation occurs in the auditory thalamus. *J. Neurosci.* 29, 7359–7363. doi: 10.1523/jneurosci.0793-09.2009

Andrillon, T., Pressnitzer, D., Léger, D., and Kouider, S. (2017). Formation and suppression of acoustic memories during human sleep. *Nat. Commun.* 8:179. doi: 10.1038/s41467-017-00071-z

Anesthesiologists Task Force on Intraoperative Awareness (2006). Practice advisory for intraoperative awareness and brain function monitoring: a report by the american society of anesthesiologists task force on intraoperative awareness. *Anesthesiology* 104, 847–864.

Antunes, F. M., Nelken, I., Covey, E., and Malmierca, M. S. (2010). Stimulus-specific adaptation in the auditory thalamus of the anesthetized rat. *PLoS One* 5:e14071. doi: 10.1371/journal.pone.0014071

Astikainen, P., Ruusuvirta, T., Wikgren, J., and Penttonen, M. (2006). Memory-based detection of rare sound feature combinations in anesthetized rats. *Neuroreport* 17, 1561–1564. doi: 10.1097/01.wnr.0000233097.13032.7d

Atchley, R., Klee, D., Memmott, T., Goodrich, E., Wahbeh, H., and Oken, B. (2016). Event-related potential correlates of mindfulness meditation competence. *Neuroscience* 320, 83–92. doi: 10.1016/j.neuroscience.2016.01.051

Atienza, M., Cantero, J. L., and Dominguez-Marin, E. (2002). Mismatch negativity (MMN): an objective measure of sensory memory and long-lasting memories during sleep. *Int. J. Psychophysiol.* 46, 215–225. doi: 10.1016/s0167-8760(02)00113-7

Atienza, M., Cantero, J. L., and Escera, C. (2001). Auditory information processing during human sleep as revealed by event-related brain potentials. *Clin. Neurophysiol.* 112, 2031–2045. doi: 10.1016/S1388-2457(01)00650-2

Atienza, M., Cantero, J. L., and Gómez, C. M. (1997). The mismatch negativity component reveals the sensory memory during rem sleep in humans. *Neurosci. Lett.* 237, 21–24. doi: 10.1016/s0304-3940(97)00798-2

Auksztulewicz, R., and Friston, K. (2015). Attentional enhancement of auditory mismatch responses: a DCM/MEG study. *Cerebral Cortex* 25, 4273–4283. doi: 10.1093/cercor/bhu323

Banks, S., and Dinges, D. F. (2007). Behavioral and physiological consequences of sleep restriction. *J. Clin. Sleep Med.* 3, 519–528. doi: 10.5664/jcsm.26918

Bassett, D. S., and Gazzaniga, M. S. (2011). Understanding complexity in the human brain. *Trends Cogn. Sci.* 15, 200–209. doi: 10.1016/j.tics.2011.03.006

Bastos, A. M., Usrey, W. M., Adams, R. A., Mangun, G. R., Fries, P., and Friston, K. J. (2012). Canonical microcircuits for predictive coding. *Neuron* 76, 695–711. doi: 10.1016/j.neuron.2012.10.038

Bauer, G., Gerstenbrand, F., and Rumpl, E. (1979). Varieties of the locked-in syndrome. *J. Neurol.* 221, 77–91. doi: 10.1007/bf00313105

Bäuerle, P., von, der Behrens, W., Kössl, M., and Gaese, B. H. (2011). Stimulus-specific adaptation in the gerbil primary auditory thalamus is the result of a fast frequency-specific habituation and is regulated by the corticofugal system. *J. Neurosci.* 31, 9708–9722. doi: 10.1523/jneurosci.5814-10.2011

Beckers, G. J. L., and Gahr, M. (2012). Large-scale synchronized activity during vocal deviance detection in the zebra finch auditory forebrain. *J. Neurosci.* 32, 10594–10608. doi: 10.1523/jneurosci.6045-11.2012

Bekinschtein, T. A., Dehaene, S., Rohaut, S., Tadel, F., Cohen, L., and Naccache, L. (2009). Neural signature of the conscious processing of auditory regularities. *Proc. Natl. Acad. Sci. U.S.A* 106, 1672–1677. doi: 10.1073/pnas.0809667106

Biedermann, B., De Lissa, P., Mahajan, Y., Polito, V., Badcock, N., Connors, M. H., et al. (2016). Meditation and auditory attention: an ERP study of meditators and non-meditators. *Int. J. Psychophysiol.* 109, 63–70. doi: 10.7287/peerj.preprints.2318

Blackford, J. U., Buckholtz, J. W., Avery, S. N., and Zald, D. H. (2010). A unique role for the human amygdala in novelty detection. *Neuroimage* 50, 1188–1193. doi: 10.1016/j.neuroimage.2009.12.083

Boly, M. (2011). Measuring the fading consciousness in the human brain. *Curr. Opin. Neurol.* 24, 394–400. doi: 10.1097/wco.0b013e328347da94

Boly, M., Garrido, M. I., Gosseries, O., Bruno, M. A., Boveroux, P., Schnakers, C., et al. (2011). Preserved feedforward but impaired top-down processes in the vegetative state. *Science* 332, 858–862. doi: 10.1126/science.1202043

Boly, M., Massimini, M., Garrido, M. I., Gosseries, O., Noirhomme, Q., Laureys, S., et al. (2012). Brain connectivity in disorders of consciousness. *Brain Connectivity* 2, 1–10. doi: 10.1089/brain.2011.0049

Bortoletto, M., Tona, G. D. M., Scozzari, S., Sarasso, S., and Stegagno, L. (2011). Effects of sleep deprivation on auditory change detection: a N1-mismatch negativity study. *Int. J. Psychophysiol.* 81, 312–316. doi: 10.1016/j.ijpsycho.2011.07.017

Braun, A. R., Balkin, T. J., Wesenten, N. J., Carson, R. E., Varga, M., Baldwin, P. I., et al. (1997). Regional cerebral blood flow throughout the sleep-wake cycle. An H2(15)O PET study. *Brain* 120, 1173–1197. doi: 10.1093/brain/120.7.1173

Brown, E. N., Lydic, R., and Schiff, N. D. (2010). General anesthesia, sleep, and coma. *N. Engl. J. Med.* 363, 2638–2650. doi: 10.1056/nejmra0808281

Brown, K. W., and Ryan, R. M. (2004). Perils and promise in defining and measuring mindfulness: observations from experience. *Clin. Psychol.* 11, 242–248. doi: 10.1093/clipsy.bph078

Cacciaglia, R., Escera, C., Slabu, L., Grimm, S., Sanjuán, A., Ventura-Campos, N., et al. (2015). Involvement of the human midbrain and thalamus in auditory deviance detection. *Neuropsychologia* 68, 51–58.

Cahn, B. R., and Polich, J. (2009). Meditation (vipassana) and the P3a event-related brain potential. *Int. J. Psychophysiol.* 72, 51–60. doi: 10.1016/j.ijpsycho.2008.03.013

Camman, R., Paavilainen, P., Alho, K., Näätänen, R., Reinikainen, K., and Sams, S. (1987). Disappearence of mismatch negativity during sleep. *Int. J. Neurosci.* 34, 154–155.

Campbell, K. B., and Colrain, I. M. (2002). Event-related potential measures of the inhibition of information processing: II. The sleep onset period. *Int. J. Psychophysiol.* 46, 197–214. doi: 10.1016/s0167-8760(02)00112-5

Caplin, A., and Dean, M. (2008). Axiomatic methods, dopamine and reward prediction error. *Curr. Opin. Neurobiol.* 18, 197–202. doi: 10.1016/j.conb.2008.07.007

Cappotto, D., Auksztulewicz, R., Kang, H., Poeppel, D., Melloni, L., and Schnupp, J. (2021). Decoding the content of auditory sensory memory across species. *Cerebral Cortex.* 31, 3226–3236. doi: 10.1093/cercor/bhab002

Carbajal, G. V., and Malmierca, M. S. (2018). The neuronal basis of predictive coding along the auditory pathway: from the subcortical roots to cortical deviance detection. *Trends Hearing* 22:2331216518784822. doi: 10.1177/2331216518784822

Chen, I.-W., Helmchen, F., and Lütcke, H. (2015). Specific early and late oddball-evoked responses in excitatory and inhibitory neurons of mouse auditory cortex. *J. Neurosci.* 35, 12560–12573. doi: 10.1523/jneurosci.2240-15.2015

Chennu, S., and Bekinschtein, T. A. (2012). Arousal modulates auditory attention and awareness: insights from sleep, sedation, and disorders of consciousness. *Front. Psychol.* 3:65. doi: 10.3389/fpsyg.2012.00065

Chennu, S., Noreika, V., Gueorguiev, D., Blenkmann, A., Kochen, S., Ibánez, A., et al. (2013). Expectation and attention in hierarchical auditory prediction. *J. Neurosci.* 33, 11194–11205. doi: 10.1523/jneurosci.0114-13.2013

Chennu, S., Noreika, V., Gueorguiev, D., Shtyrov, Y., Bekinschtein, T. A., and Henson, R. (2016). Silent expectations: dynamic causal modeling of cortical prediction and attention to sounds that weren't. *J. Neurosci.* 36, 8305–8316. doi: 10.1523/jneurosci.1125-16.2016

Christianson, G. B., Chait, M., de Cheveigné, A., and Linden, J. F. (2014). Auditory evoked fields measured noninvasively with small-animal meg reveal rapid repetition suppression in the guinea pig. *J. Neurophysiol.* 112, 3053–3065. doi: 10.1152/jn.00189.2014

Clarke, J. M., Halgren, E., and Chauvel, P. (1999). Intracranial erps in humans during a lateralized visual oddball task: II. Temporal, parietal, and frontal recordings. *Clin. Neurophysiol.* 110, 1226–1244. doi: 10.1016/s1388-2457(99)00064-4

Coenen, A. M. L., and Drinkenburg, W. H. I. M. (2002). Animal models for information processing during sleep. *Int. J. Psychophysiol.* 46, 163–175. doi: 10.1016/s0167-8760(02)00110-1

Colrain, I. M., and Campbell, K. B. (2007). The use of evoked potentials in sleep research. *Sleep Med. Rev.* 11, 277–293. doi: 10.1016/j.smrv.2007.05.001

Condon, C. D., and Weinberger, N. M. (1991). Habituation produces frequency-specific plasticity of receptive fields in the auditory cortex. *Behav. Neurosci.* 105:416. doi: 10.1037/0735-7044.105.3.416

Cossy, N., Tzovara, A., Simonin, A., Rossetti, A. O., and De Lucia, M. (2014). Robust discrimination between eeg responses to categories of environmental sounds in early coma. *Front. Psychol.* 5:155. doi: 10.3389/fpsyg.2014.00155

Cote, K. A. (2002). Probing awareness during sleep with the auditory odd-ball paradigm. *Int. J. Psychophysiol.* 46, 227–241. doi: 10.1016/s0167-8760(02)00114-9

Cox, R., van Driel, J., de Boer, M., and Talamini, L. M. (2014). Slow oscillations during sleep coordinate interregional communication in cortical networks. *J. Neurosci.* 34, 16890–16901. doi: 10.1523/jneurosci.1953-14.2014

Csépe, V., Bányai, E. I., and Mády, K. (1997). Changes of phoneme contrast sensitivity in hypnosis: an Erp study. *Int. J. Psychophysiol.* 1:79. doi: 10.1016/s0167-8760(97)85567-5

Csépe, V., Karmos, G., and Molnar, M. (1987). Evoked potential correlates of stimulus deviance during wakefulness and sleep in cat—animal model of mismatch negativity. *Electroencephalogr. Clin. Neurophysiol.* 66, 571–578. doi: 10.1016/0013-4694(87)90103-9

Czisch, M., Wehrle, R., Stiegler, A., Peters, H., Andrade, K., Holsboer, F., et al. (2009). Acoustic oddball during NREM sleep: a combined EEG/fMRI study. *PLoS One* 4:e6749. doi: 10.1371/journal.pone.0006749

Czisch, M., Wetter, T. C., Kaufmann, C., Pollmächer, T., Holsboer, F., and Auer, D. P. (2002). Altered processing of acoustic stimuli during sleep: reduced auditory activation and visual deactivation detected by a combined fMRI/Eeg study. *Neuroimage* 16, 251–258. doi: 10.1006/nimg.2002.1071

Daltrozzo, J., Wioland, N., Mutschler, V., and Kotchoubey, B. (2007). Predicting coma and other low responsive patients outcome using event-related brain potentials: a meta-analysis. *Clin. Neurophysiol.* 118, 606–614. doi: 10.1016/j.clinph.2006.11.019

Dang-Vu, T. T., Bonjean, M., Schabus, M., Boly, M., Darsaud, A., Desseilles, M., et al. (2011). Interplay Between spontaneous and induced brain activity during human non-rapid eye movement sleep. *Proc. Natl. Acad. Sci. U.S. A.* 108, 15438–15443. doi: 10.1073/pnas.1112503108

Dayan, P., Hinton, G. E., Neal, R. N., and Zemel, R. S. (1995). The helmholtz machine. *Neural Comput.* 7, 889–904. doi: 10.1162/neco.1995.7.5.889

Dehaene, S., and Changeux, J. P. (2011). Experimental and theoretical approaches to conscious processing. *Neuron* 70, 200–227. doi: 10.1016/j.neuron.2011.03.018

Demertzi, A., Vanhaudenhuyse, A., Bruno, M.-A., Schnakers, C., Boly, M., Boveroux, P., et al. (2008). Is there anybody in there? detecting awareness in

disorders of consciousness. *Exp. Rev. Neurother.* 8, 1719–1730. doi: 10.1586/14737175.8.11.1719

Destexhe, A., Hughes, S. W., Rudolph, M., and Crunelli, V. (2007). Are corticothalamic 'up' states fragments of wakefulness? *Trends Neurosci.* 30, 334–342. doi: 10.1016/j.tins.2007.04.006

Donchin, E. (1981). Surprise!? *Surprise?. Psychophysiology* 18, 493–513. doi: 10.1111/j.1469-8986.1981.tb01815.x

Donchin, E., and Coles, M. G. H. (1988). Is the p300 component a manifestation of context updating? *Behav. Brain Sci.* 11:357. doi: 10.1017/s0140525x00058027

Drummond, S. P. A., Smith, M. T., Orff, H. J., Chengazi, V., and Perlis, M. L. (2004). Functional imaging of the sleeping brain: review of findings and implications for the study of insomnia. *Sleep Med. Rev.* 8, 227–242. doi: 10.1016/j.smrv.2003.10.005

Duque, D., and Malmierca, M. S. (2015). Stimulus-specific adaptation in the inferior colliculus of the mouse: anesthesia and spontaneous activity effects. *Brain Struct. Funct.* 220, 3385–3398. doi: 10.1007/s00429-014-0862-1

Duque, D., Ayala, Y. A., and Malmierca, M. S. (2015). Deviance detection in auditory subcortical structures: what can we learn from neurochemistry and neural connectivity? *Cell Tissue Res.* 361, 215–232. doi: 10.1007/s00441-015-2134-7

Duque, D., Pais, R., and Malmierca, M. S. (2018). Stimulus-specific adaptation in the anesthetized mouse revealed by brainstem auditory evoked potentials. *Hearing Res.* 370, 294–301. doi: 10.1016/j.heares.2018.08.011

Dürschmid, S., Reichert, C., Hinrichs, H., Heinze, H. J., Kirsch, H. E., Knight, R. T., et al. (2019). Direct evidence for prediction signals in frontal cortex independent of prediction error. *Cerebral Cortex* 29, 4530–4538. doi: 10.1093/cercor/bhy331

Dürschmid, S., Zaehle, T., Hinrichs, H., Heinze, H.-J., Voges, J., Garrido, M. I., et al. (2016). Sensory deviancy detection measured directly within the human nucleus accumbens. *Cerebral Cortex* 26, 1168–1175. doi: 10.1093/cercor/bhu304

Edeline, J. M., Manunta, Y., and Hennevin, E. (2000). Auditory thalamus neurons during sleep: changes in frequency selectivity, threshold, and receptive field size. *J. Neurophysiol.* 84, 934–952. doi: 10.1152/jn.2000.84.2.934

Edeline, J.-M., Dutrieux, G., Manunta, Y., and Hennevin, E. (2001). Diversity of receptive field changes in auditory cortex during natural sleep. *Eur. J. Neurosci.* 14, 1865–1880. doi: 10.1046/j.0953-816x.2001.01821.x

Ehrlichman, R. S., Maxwell, C. R., Majumdar, S., and Siegel, S. J. (2008). Deviance-elicited changes in event-related potentials are attenuated by ketamine in mice. *J. Cogn. Neurosci.* 20, 1403–1414. doi: 10.1162/jocn.2008.20097

Eriksson, J., and Villa, A. E. P. (2005). Event-related potentials in an auditory oddball situation in the rat. *Biosystems* 79, 207–212. doi: 10.1016/j.biosystems.2004.09.017

Faugeras, F., Rohaut, B., Weiss, N., Bekinschtein, T. A., Galanaud, D., Puybasset, L., et al. (2011). Probing consciousness with event-related potentials in the vegetative state. *Neurology* 77, 264–268. doi: 10.1212/wnl.0b013e3182217ee8

Faugeras, F., Rohaut, B., Weiss, N., Bekinschtein, T., Galanaud, D., Puybasset, L., et al. (2012). Event related potentials elicited by violations of auditory regularities in patients with impaired consciousness. *Neuropsychologia* 50, 403–418. doi: 10.1016/j.neuropsychologia.2011.12.015

Field, K. J., White, W. J., and Lang, M. C. (1993). Anaesthetic effects of chloral hydrate, pentobarbitone and urethane in adult male rats. *Lab. Anim.* 27, 258–269. doi: 10.1258/002367793780745471

Fins, J. J., Master, M. G., Gerber, L. M., and Giacino, J. T. (2007). The minimally conscious state: a diagnosis in search of an epidemiology. *Archiv. Neurol.* 64, 1400–1405. doi: 10.1001/archneur.64.10.1400

Fischer, C., Luaute, J., Adeleine, P., and Morlet, D. (2004). Predictive value of sensory and cognitive evoked potentials for awakening from coma. *Neurology* 63, 669–673. doi: 10.1212/01.wnl.0000134670.10384.e2

Fischer, C., Morlet, D., Bouchet, P., Luaute, J., Jourdan, C., and Salord, F. (1999). Mismatch negativity and late auditory evoked potentials in comatose patients. *Clin. Neurophysiol.* 110, 1601–1610. doi: 10.1016/s1388-2457(99)00131-5

Fonken, Y. M., Kam, J. W. Y., and Knight, R. T. (2019). A differential role for human hippocampus in novelty and contextual processing: implications for P300. *Psychophysiology* 57:400. doi: 10.1111/psyp.13400

Friston, K. (2005). A theory of cortical responses. *Philosoph. Transact. Roy. Soc. B* 360, 815–836. doi: 10.1098/rstb.2005.1622

Fucci, E., Abdoun, O., Caclin, A., Francis, A., Dunne, J. D., Ricard, M. R. J., et al. (2018). Differential Effects of non-dual and focused attention meditations on the formation of automatic perceptual habits in expert practitioners. *Neuropsychologia* 119, 92–100. doi: 10.1016/j.neuropsychologia.2018.07.025

Gaese, B. H., and Ostwald, J. (2001). Anesthesia changes frequency tuning of neurons in the rat primary auditory cortex. *J. Neurophysiol.* 86, 1062–1066. doi: 10.1152/jn.2001.86.2.1062

Gao, P. P., Zhang, J. W., Cheng, J. S., Zhou, I. Y., and Wu, E. X. (2014). The inferior colliculus is involved in deviant sound detection as revealed by bold fMRI. *Neuroimage* 91, 220–227. doi: 10.1016/j.neuroimage.2014.01.043

Gardner, M. P. H., Schoenbaum, G., and Gershman, S. J. (2018). Rethinking dopamine as generalized prediction error. *Proc. Roy. Soc. B* 285:20181645. doi: 10.1098/rspb.2018.1645

Garrido, M. I., Friston, K. J., Kiebel, S. J., Stephan, K. E., Baldeweg, T., and Kilner, J. M. (2008). The functional anatomy of the MMN: a DCM study of the roving paradigm. *Neuroimage* 42, 936–944. doi: 10.1016/j.neuroimage.2008.05.018

Garrido, M. I., Kilner, J. M., Kiebel, S. J., and Friston, K. J. (2009a). Dynamic causal modeling of the response to frequency deviants. *J. Neurophysiol.* 101, 2620–2631. doi: 10.1152/jn.90291.2008

Garrido, M. I., Kilner, J. M., Kiebel, S. J., Stephan, K. E., and Friston, K. J. (2007). Dynamic causal modelling of evoked potentials: a reproducibility study. *Neuroimage* 36, 571–580. doi: 10.1016/j.neuroimage.2007.03.014

Garrido, M. I., Kilner, J. M., Stephan, K. E., and Friston, K. J. (2009b). The mismatch negativity: a review of underlying mechanisms. *Clin. Neurophysiol.* 120, 453–463. doi: 10.1016/j.clinph.2008.11.029

Giacino, J. T., Fins, J. J., Laureys, S., and Schiff, N. D. (2014). Disorders of consciousness after acquired brain injury: the state of the science. *Nat. Rev. Neurol.* 10:99. doi: 10.1038/nrneurol.2013.279

Giacino, J. T., Hirsch, J., Schiff, N., and Laureys, S. (2006). Functional neuroimaging applications for assessment and rehabilitation planning in patients with disorders of consciousness. *Archiv. Phys. Med. Rehabilitat.* 87, 67–76. doi: 10.1016/j.apmr.2006.07.272

Gosseries, O., Di, H., Laureys, S., and Boly, M. (2014a). Measuring consciousness in severely damaged brains. *Annu. Rev. Neurosci.* 37, 457–478. doi: 10.1146/annurev-neuro-062012-170339

Gosseries, O., Vanhaudenhuyse, A., Bruno, M.-A., Demertzi, A., Schnakers, C., Boly, M. M., et al. (2011). *Disorders of Consciousness: Coma, Vegetative and Minimally Conscious States*. Netherland: Springer, 29–55. doi: 10.1007/978-3-642-18047-7_2

Gosseries, O., Zasler, N. D., and Laureys, S. (2014b). Recent advances in disorders of consciousness: focus on the diagnosis. *Brain INJ.* 28, 1141–1150. doi: 10.3109/02699052.2014.920522

Goupil, L., and Bekinschtein, T. (2012). Cognitive processing during the transition to sleep. *Archiv. Ital. Biol.* 150, 140–154. doi: 10.4449/aib.v150i2.1247

Gruzelier, J. (1998). A working model of the neurophysiology of hypnosis: a review of evidence. *Contemp. Hypn.* 15, 3–21. doi: 10.1002/ch.112

Guldenmund, P., Vanhaudenhuyse, A., Sanders, R. D., Sleigh, J., Bruno, M. A., Demertzi, A., et al. (2017). Brain functional connectivity differentiates dexmedetomidine from propofol and natural sleep. *Br. J. Anaesth.* 119, 674–684. doi: 10.1093/bja/aex257

Halgren, E., Patrick, B., Clarke, J. M., Heit, G., Liégeois, C., Chauvel, P., et al. (1995). Intracerebral potentials to rare target and distractor auditory and visual stimuli. I. superior temporal plane and parietal lobe. *Electroencephalogr. Clin. Neurophysiol.* 94, 191–220. doi: 10.1016/0013-4694(94)00259-n

Halgren, E., Squires, N. K., Wilson, C. L., Rohrbaugh, J. W., Babb, T. L., and Crandall, P. H. (1980). Endogenous potentials generated in the human hippocampal formation and amygdala by infrequent events. *Science* 210, 803–805. doi: 10.1126/science.7434000

Hall, R. D., and Borbely, A. A. (1970). Acoustically evoked potentials in the rat during sleep and waking. *Exp. Brain Res.* 11, 93–110. doi: 10.1007/bf00234203

Hari, R., Hämäläinen, H., Ilmoniemi, R., Kaukoranta, E., Reinikainen, K., Salminen, J., et al. (1984). Responses of the primary auditory cortex to pitch changes in a sequence of tone pips: neuromagnetic recordings in man. *Neurosci. Lett.* 50, 127–132. doi: 10.1016/0304-3940(84)90474-9

Harms, L., Fulham, W. R., Todd, J., Budd, T. W., Hunter, M., Meehan, C., et al. (2014). Mismatch negativity (mmn) in freely-moving rats with several

experimental controls. *PLoS One* 9:e110892. doi: 10.1371/journal.pone.0110892

Heilbron, M., and Chait, M. (2018). Great expectations: is there evidence for predictive coding in auditory cortex? *Neuroscience* 389, 54–73. doi: 10.1016/j.neuroscience.2017.07.061

Heinke, W., and Koelsch, S. (2005). The effects of anesthetics on brain activity and cognitive function. *Curr. Opin. Anesthesiol.* 18, 625–631. doi: 10.1097/01.aco.0000189879.67092.12

Heinke, W., Kenntner, R., Gunter, T. C., Sammler, D., Olthoff, D., and Koelsch, S. (2004). Sequential effects of increasing propofol sedation on frontal and temporal cortices as indexed by auditory event-related potentials. *J. Am. Soc. Anesthesiol.* 100, 617–625. doi: 10.1097/00000542-200403000-00023

Hennevin, E., Huetz, C., and Edeline, J. M. (2007). Neural representations during sleep: from sensory processing to memory traces. *Neurobiol. Learn. Mem.* 87, 416–440. doi: 10.1016/j.nlm.2006.10.006

Hiltunen, S., Virta, M., Kallio, S., and Paavilainen, P. (2019). The effects of hypnosis and hypnotic suggestions on the mismatch negativity in highly hypnotizable subjects. *Int. J. Clin. Exp. Hypn.* 67, 192–216. doi: 10.1080/00207144.2019.1580966

Hobson, J. A., Pace-Schott, E. F., and Stickgold, R. (2000). Dreaming and the brain: toward a cognitive neuroscience of conscious states. *Behav. Brain Sci.* 23, 793–842. doi: 10.1017/s0140525x00003976

Hohwy, J. (2012). Attention and conscious perception in the hypothesis testing brain. *Front. Psychol.* 3:96. doi: 10.3389/fpsyg.2012.00096

Horovitz, S. G., Braun, A. R., Carr, W. S., Picchioni, D., Balkin, T. J., Fukunaga, M., et al. (2009). Decoupling of the brain's default mode network during deep sleep. *Proc. Natl. Acad. Sci. U.S. A.* 106, 11376–11381. doi: 10.1073/pnas.0901435106

Hoy, C. W., Steiner, S. C., and Knight, R. T. (2021). Single-trial modeling separates multiple overlapping prediction errors during reward processing in human EEG. *Commun. Biol.* 4:910. doi: 10.1038/s42003-021-02426-1

Huang, L., Bai, L., Zhao, Y., and Xiao, Z. (2013). Comparison of tonal response properties of primary auditory cortex neurons of adult rats under urethane and ketamine anesthesia. *J. South. Med. Univ.* 33, 785–793. doi: 10.1016/j.heares.2016.06.012

Imada, A., Morris, A., and Wiest, M. C. (2013). Deviance detection by a P3-like response in rat posterior parietal cortex. *Front. Integr. Neurosci.* 6:127. doi: 10.3389/fnint.2012.00127

Issa, E. B., and Wang, X. (2008). Sensory responses during sleep in primate primary and secondary auditory cortex. *J. Neurosci.* 28, 14467–14480. doi: 10.1523/jneurosci.3086-08.2008

Jääskeläinen, I. P., Ahveninen, J., Bonmassar, G., Dale, A. M., Ilmoniemi, R. J., Levänen, S., et al. (2004). Human posterior auditory cortex gates novel sounds to consciousness. *Proc. Natl. Acad. Sci. U.S.A.* 101, 6809–6814. doi: 10.1073/pnas.0303760101

Jamieson, G. A. (2016). "A unified theory of hypnosis and meditation states: the interoceptive predictive coding approach," in *Hypnosis and meditation: Towards an integrative science of conscious planes*, eds A. Raz and M. Lifshitz (Oxford: Oxford University Press), 313–342.

Jamieson, G. A. (2018). Expectancies of the future in hypnotic suggestions. *Psychol. Consci.* 5, 258–277. doi: 10.1037/cns0000170

Jamieson, G. A., Dwivedi, P., and Gruzelier, J. H. (2005). Changes in mismatch negativity across pre-hypnosis, hypnosis and post-hypnosis conditions distinguish high from low hypnotic susceptibility groups. *Brain Res. Bull.* 67, 298–303. doi: 10.1016/j.brainresbull.2005.06.033

Javitt, D. C., Schroeder, C. E., Steinschneider, M., Arezzo, J. C., and Vaughan, H. G. Jr. (1992). Demonstration of mismatch negativity in the monkey. *Electroencephalogr. Clin. Neurophysiol.* 83, 87–90. doi: 10.1016/0013-4694(92)90137-7

Javitt, D. C., Steinschneider, M., Schroeder, C. E., Vaughan, H. G. Jr., and Arezzo, J. C. (1994). Detection of stimulus deviance within primate primary auditory cortex: intracortical mechanisms of mismatch negativity (MMN) generation. *Brain Res.* 667, 192–200. doi: 10.1016/0006-8993(94)91496-6

Johnson, C. B., and Taylor, P. M. (1998). Comparison of the effects of halothane, isoflurane and methoxyflurane on the electroencephalogram of the horse. *Br. J. Anaesth.* 81, 748–753. doi: 10.1093/bja/81.5.748

Johnson, E., Kam, J., Tzovara, A., Robert, T., and Knight, R. T. (2020). Insights into human cognition from intracranial eeg: a review of audition, memory, internal cognition, and causality. *J. Neural Engin.* 17:051001. doi: 10.1088/1741-2552/abb7a5

Juan, E., De Lucia, M., Tzovara, A., Beaud, V., Oddo, M., Clarke, S., et al. (2016). Prediction of cognitive outcome based on the progression of auditory discrimination during coma. *Resuscitation* 106, 89–95. doi: 10.1016/j.resuscitation.2016.06.032

Kabat-Zinn, J. (1982). An outpatient program in behavioral medicine for chronic pain patients based on the practice of mindfulness meditation: theoretical considerations and preliminary results. *Gener. Hosp. Psych.* 4, 33–47. doi: 10.1016/0163-8343(82)90026-3

Kallio, S., Revonsuo, A., Lauerma, H., Hämäläinen, H., and Lang, H. (1999). The MMN amplitude increases in hypnosis: a case study. *NeuroReport* 10, 3579–3582. doi: 10.1097/00001756-199911260-00021

Kam, J. W. Y., Helfrich, R. F., Solbakk, A.-K., Endestad, T., Larsson, P. G., Lin, J. J., et al. (2020). Top- down attentional modulation in human frontal cortex: differential engagement during external and internal attention. *Cerebral Cortex* 31, 873–883. doi: 10.1093/cercor/bhaa262

Kanai, R., Chang, A., Yu, Y., Magrans, de Abril, I., Biehl, M., et al. (2019). Information generation as a functional basis of consciousness. *Neurosci. Conscious.* 2019:niz016. doi: 10.1093/nc/niz016

Kanai, R., Komura, Y., Shipp, S., and Friston, K. (2015). Cerebral hierarchies: predictive processing, precision and the pulvinar. *Philosoph. Transact. Roy. Soc. B* 370:20140169. doi: 10.1098/rstb.2014.0169

Kane, N. M., Butler, S. R., and Simpson, T. (2000). Coma outcome prediction using event-related potentials: P3 and mismatch negativity. *Audiol. Neurotol.* 5, 186–191. doi: 10.1159/000013879

Key, A. P. F., Molfese, D. L., O'Brien, L., and Gozal, D. (2009). Sleep-disordered breathing affects auditory processing in 5–7-year-old children: evidence from brain recordings. *Devel. Neuropsychol.* 34, 615–628. doi: 10.1080/87565640903133608

Khouri, L., and Nelken, I. (2015). Detecting the unexpected. *Curr. Opin. Neurobiol.* 35, 142–147. doi: 10.1016/j.conb.2015.08.003

Kihlstrom, J. F. (2005). Is hypnosis an altered state of consciousness or what? *Contemp. Hypnosis* 22, 34–38. doi: 10.1002/ch.20

King, C., McGee, T., Rubel, E. W., Nicol, T., and Kraus, N. (1995). Acoustic features and acoustic change are represented by different central pathways. *Hearing Res.* 85, 45–52.

King, J.-R., Faugeras, F., Gramfort, A., Schurger, A., El Karoui, I., Sitt, J. D., et al. (2013). Single-trial decoding of auditory novelty responses facilitates the detection of residual consciousness. *Neuroimage* 83, 726–738. doi: 10.1016/j.neuroimage.2013.07.013

Kisley, M. A., and Gerstein, G. L. (1999). Trial-to-trial variability and state-dependent modulation of auditory-evoked responses in cortex. *J. Neurosci.* 19, 10451–10460. doi: 10.1016/0378-5955(95)00028-3

Koelsch, S., Heinke, W., Sammler, D., and Olthoff, D. (2006). Auditory processing during deep propofol sedation and recovery from unconsciousness. *Clin. Neurophysiol.* 117, 1746–1759. doi: 10.1016/j.clinph.2006.05.009

Koike, T., Kan, S., Misaki, M., and Miyauchi, S. (2011). Connectivity pattern changes in default-mode network with deep non-REM and REM sleep. *Neurosci. Res.* 69, 322–330. doi: 10.1016/j.neures.2010.12.018

Kok, P., and de Lange, F. P. (2015). Predictive coding in sensory cortex. *Introduct. Model Based Cogn. Neurosci.* 18, 221–244. doi: 10.1007/978-1-4939-2236-9_11

Kotchoubey, B. (2005). Event-related potential measures of consciousness: two equations with three unknowns. *Progr. Brain Res.* 150, 427–444. doi: 10.1016/s0079-6123(05)50030-x

Kotchoubey, B., Jetter, U., Lang, S., Semmler, A., Mezger, G., Schmalohr, D., et al. (2006). Evidence of cortical learning in vegetative state. *J. Neurol.* 253, 1374–1376. doi: 10.1007/s00415-006-0221-0

Kotchoubey, B., Lang, S., Mezger, G., Schmalohr, D., Schneck, M., Semmler, A., et al. (2005). Information processing in severe disorders of consciousness: vegetative state and minimally conscious state. *Clin. Neurophysiol.* 116, 2441–2453. doi: 10.1016/j.clinph.2005.03.028

Kraus, N., McGee, T., Littman, T., Nicol, T., and King, C. (1994). Nonprimary auditory thalamic representation of acoustic change. *J. Neurophysiol.* 72, 1270–1277. doi: 10.1152/jn.1994.72.3.1270

Kropotov, J. D., Alho, K., Näätänen, R., Ponomarev, V. A., Kropotova, O. V., Anichkov, A. D., et al. (2000). Human auditory-cortex mechanisms of

preattentive sound discrimination. *Neurosci. Lett.* 280, 87–90. doi: 10.1016/s0304-3940(00)00765-5

Laureys, S. (2005). The neural correlate of (un) awareness: lessons from the vegetative state. *Trends Cogn. Sci.* 9, 556–559. doi: 10.1016/j.tics.2005.10.010

Laureys, S., Celesia, G. G., Cohadon, F., Lavrijsen, J., León-Carrión, J., Sannita, W. G., et al. (2010). Unresponsive wakefulness syndrome: a new name for the vegetative state or apallic syndrome. *BMC Medicine* 8:68. doi: 10.1186/1741-7015-8-68

Laureys, S., Owen, A. M., and Schiff, N. D. (2004). Brain function in coma, vegetative state, and related disorders. *Lancet Neurol.* 3, 537–546. doi: 10.1016/s1474-4422(04)00852-x

Lazar, R., and Metherate, R. (2003). Spectral interactions, but no mismatch negativity, in auditory cortex of anesthetized rat. *Hearing Res.* 181, 51–56. doi: 10.1016/s0378-5955(03)00166-7

Leite, F. A. C., da Silva, F. F., Pradella-Hallinan, M., Xavier, S. D., Miranda, M. C., and Pereira, L. D. (2017). Auditory behavior and auditory temporal resolution in children with sleep-disordered breathing. *Sleep Med.* 34, 90–95. doi: 10.1016/j.sleep.2017.03.009

Lendner, J. D., Helfrich, R. F., Mander, B. A., Romundstad, L., Lin, J. J., Walker, et al. (2020). An electrophysiological marker of arousal level in humans. *eLife* 9:e55092. doi: 10.7554/eLife.55092

Leszczynski, M., Barczak, A., Kajikawa, Y., Ulbert, I., Falchier, A., Tal, I., et al. (2020). Dissociation of broadband high-frequency activity and neuronal firing in the neocortex. *Scient. Adv.* 6:eabb0977. doi: 10.1101/531368

Lew, H. L., Dikmen, S., Slimp, J., Temkin, N., Lee, E. H., Newell, D., et al. (2003). Use of somatosensory-evoked potentials and cognitive event-related potentials in predicting outcomes of patients with severe traumatic brain injury. *Am. J. Phys. Med. Rehabil.* 82, 53–61. doi: 10.1097/00002060-200301000-00009

Liberalesso, P. B. N., D'Andrea, K. F. K., Cordeiro, M. L., Zeigelboim, B. S., Marques, J. M., and Jurkiewicz, A. L. (2012). Effects of sleep deprivation on central auditory processing. *BMC Neuroscience* 13:83. doi: 10.1186/1471-2202-13-83

Lieder, F., Daunizeau, J., Garrido, M. I., Friston, K. J., and Stephan, K. E. (2013). Modelling trial-by-trial changes in the mismatch negativity. *PLoS Comput. Biol.* 9:e1002911. doi: 10.1371/journal.pcbi.1002911

Lipponen, A., Kurkela, J. L. O., Kyläheiko, I., Hölttä, S., Ruusuvirta, T., Hämäläinen, J. A., et al. (2019). Auditory-evoked potentials to changes in sound duration in urethane-anaesthetized mice. *Eur. J. Neurosci.* 50, 1911–1919. doi: 10.1111/ejn.14359

Loewy, D. H., Campbell, K. B., and Bastien, C. (1996). The mismatch negativity to frequency deviant stimuli during natural sleep. *Electroencephalogr. Clin. Neurophysiol.* 98, 493–501. doi: 10.1016/0013-4694(96)95553-4

Loewy, D. H., Campbell, K. B., de Lugt, D. R., Elton, M., and Kok, A. (2000). The mismatch negativity during natural sleep: intensity deviants. *Clin. Neurophysiol.* 111, 863–872.

Lotze, R. H. (1852). Medizinische psychologie oder physiologie der seele.

Luauté, J., Fischer, C., Adeleine, P., Morlet, D., Tell, L., and Boisson, D. (2005). Late auditory and event-related potentials can be useful to predict good functional outcome after coma. *Archiv. Phys. Med. Rehabil.* 86, 917–923. doi: 10.1016/j.apmr.2004.08.011

Ludwig, A. M. (1966). Altered states of consciousness. *Archiv. Gener. Psych.* 15, 225–234. doi: 10.1001/archpsyc.1966.01730150001001

Lutz, N. D., Wolf, I., Hübner, S., Born, J., and Rauss, K. (2018). Sleep strengthens predictive sequence coding. *J. Neurosci.* 38, 8989–9000. doi: 10.1523/jneurosci.1352-18.2018

Magnin, M., Rey, M., Bastuji, H., Guillemant, P., Mauguière, F., and Garcia-Larrea, L. (2010). Thalamic deactivation at sleep onset precedes that of the cerebral cortex in humans. *Proc. Natl. Acad. Sci.* 107, 3829–3833. doi: 10.1073/pnas.0909710107

Malmierca, M. S., Cristaudo, S., Pérez-González, D., and Covey, E. (2009). Stimulus-specific adaptation in the inferior colliculus of the anesthetized rat. *J. Neurosci.* 29, 5483–5493. doi: 10.1523/jneurosci.4153-08.2009

Maquet, P. (2000). Functional neuroimaging of normal human sleep by positron emission tomography. *J. Sleep Res.* 9, 207–232. doi: 10.1046/j.1365-2869.2000.00214.x

Maquet, P., Péters, J.-M., Aerts, J., Delfiore, G., Degueldre, C., Luxen, A., et al. (1996). Functional neuroanatomy of human rapid-eye-movement sleep and dreaming. *Nature* 383, 163–166. doi: 10.1038/383163a0

Martin, J.-R., and Pacherie, E. (2019). Alterations of agency in hypnosis: a new predictive coding model. *Psychol. Rev.* 126:133. doi: 10.1037/rev0000134

Massimini, M., Ferrarelli, F., Huber, R., Esser, S. K., Singh, H., and Tononi, G. (2005). Breakdown of cortical effective connectivity during sleep. *Science* 309, 2228–2232. doi: 10.1126/science.1117256

May, P., Tiitinen, H., Ilmoniemi, R. J., Nyman, G., Taylor, J. G., and Näätänen, R. (1999). Frequency change detection in human auditory cortex. *J. Comput. Neurosci.* 6, 99–120. doi: 10.1023/a:1008896417606

McCormick, D. A., and Bal, T. (1994). Sensory gating mechanisms of the thalamus. *Curr. Opin. Neurobiol.* 4, 550–556. doi: 10.1016/0959-4388(94)90056-6

Michel, C. M., and Murray, M. M. (2012). Towards the utilization of eeg as a brain imaging tool. *NeuroImage* 61, 371–385. doi: 10.1016/j.neuroimage.2011.12.039

Morlet, D., and Fischer, C. (2014). MMN and novelty P3 in coma and other altered states of consciousness: a review. *Brain Topogr.* 27, 467–479. doi: 10.1007/s10548-013-0335-5

Moshitch, D., Las, L., Ulanovsky, N., Bar-Yosef, O., and Nelken, I. (2006). Responses of neurons in primary auditory cortex (A1) to pure tones in the halothane-anesthetized cat. *J. Neurophysiol.* 95, 3756–3769. doi: 10.1152/jn.00822.2005

Mumford, D. (1992). On the computational architecture of the neocortex. *Biol. Cybernet.* 66, 241–251. doi: 10.1007/bf00198477

Murata, K., and Kameda, K. (1963). The activity of single cortical neurones of unrestrained cats during sleep and wakefulness. *Archiv. Ital. Biol.* 156, 127–136. doi: 10.12871/00039829201834

Näätänen, R. (1990). The role of attention in auditory information processing as revealed by event-related potentials and other brain measures of cognitive function. *Behav. Brain Sci.* 13, 201–233. doi: 10.1017/s0140525x00078407

Näätänen, R. (2003). Mismatch negativity: clinical research and possible applications. *Int. J. Psychophysiol.* 48, 179–188. doi: 10.1016/s0167-8760(03)00053-9

Näätänen, R., and Alho, K. (1995). Mismatch negativity – a unique measure of sensory processing in audition. *Int. J. Neurosci.* 80, 317–337. doi: 10.3109/00207459508986107

Näätänen, R., and Escera, C. (2000). Mismatch negativity: clinical and other applications. *Audiol. Neurotol.* 5, 105–110. doi: 10.1159/000013874

Näätänen, R., and Lyytinen, H. (1994). Mismatch negativity in sleep. *Sleep Onset* 20, 339–349. doi: 10.1037/10166-020

Näätänen, R., and Picton, T. (1987). The N1 wave of the human electric and magnetic response to sound: a review and an analysis of the component structure. *Psychophysiology* 24, 375–425. doi: 10.1111/j.1469-8986.1987.tb00311.x

Näätänen, R., Gaillard, A. W. K., and Mäntysalo, S. (1978). Early selective-attention effect on evoked potential reinterpreted. *Acta Psychol.* 42, 313–329. doi: 10.1016/0001-6918(78)90006-9

Näätänen, R., Paavilainen, P., Titinen, H., Jiang, D., and Alho, K. (1993). Attention and mismatch negativity. *Psychophysiology* 30, 436–450.

Naccache, L., Puybasset, L., Gaillard, R., Serve, E., and Willer, J.-C. (2005). Auditory mismatch negativity is a good predictor of awakening in comatose patients: a fast and reliable procedure. *Clin. Neurophysiol.* 116, 988–989. doi: 10.1016/j.clinph.2004.10.009

Nakamura, T., Michie, P. T., Fulham, W. R., Todd, J., Budd, T. W., Schall, U., et al. (2011). Epidural auditory event-related potentials in the rat to frequency and duration deviants: evidence of mismatch negativity? *Front. Psychol.* 2:367. doi: 10.3389/fpsyg.2011.00367

Nielsen-Bohlman, L., Knight, R. T., Woods, D. L., and Woodward, K. (1991). Differential auditory processing continues during sleep. *Electroencephalogr. Clin. Neurophysiol.* 79, 281–290. doi: 10.1016/0013-4694(91)90124-m

Nieto-Diego, J., and Malmierca, M. S. (2016). Topographic distribution of stimulus-specific adaptation across auditory cortical fields in the anesthetized rat. *PLoS Biol.* 14:e1002397. doi: 10.1371/journal.pbio.1002397

Nir, Y., Vyazovskiy, V. V., Cirelli, C., Banks, M. I., and Tononi, G. (2015). Auditory responses and stimulus-specific adaptation in rat auditory cortex are preserved

across NREM and REM sleep. *Cerebral Cortex* 25, 1362–1378. doi: 10.1093/cercor/bht328

Nordby, H., Hugdahl, K., Stickgold, R., Bronnick, S. K., and Hobson, J. A. (1996). Event-related potentials (ERPS) to deviant auditory stimuli during sleep and waking. *Neuroreport* 7, 1082–6. doi: 10.1097/00001756-199604100-00026

Nourski, K. V., Steinschneider, M., Rhone, A. E., Kawasaki, H., Howard, M. A., and Banks, M. I. (2018). Auditory predictive coding across awareness states under anesthesia: an intracranial electrophysiology study. *J. Neurosci.* 38, 8441–8452. doi: 10.1523/jneurosci.0967-18.2018

Opitz, B., Rinne, T., Mecklinger, A., Von Cramon, D. Y., and Schröger, E. (2002). Differential contribution of frontal and temporal cortices to auditory change detection: fMRI and ERP results. *Neuroimage* 15, 167–174. doi: 10.1006/nimg.2001.0970

Ostwald, D., Spitzer, B., Guggenmos, M., Schmidt, T. T., Kiebel, S. J., and Blankenburg, F. (2012). Evidence for neural encoding of bayesian surprise in human somatosensation. *NeuroImage* 62, 177–188. doi: 10.1016/j.neuroimage.2012.04.050

Owen, A. M., and Coleman, M. R. (2007). Functional MRI in disorders of consciousness: advantages and limitations. *Curr. Opin. Neurol.* 20, 632–637. doi: 10.1097/wco.0b013e3282f15669

Pagnoni, G. (2019). The contemplative exercise through the lenses of predictive processing: a promising approach. *Progr. Brain Res.* 22, 299–322. doi: 10.1016/bs.pbr.2018.10.022

Pal, D., Silverstein, B. H., Lee, H., and Mashour, G. A. (2016). Neural correlates of wakefulness, sleep, and general anesthesia. *Anesthesiology* 125, 929–942.

Parras, G. G., Nieto-Diego, J., Carbajal, G. V., Valdés-Baizabal, C., Escera, C., and Malmierca, M. S. (2017). Neurons along the auditory pathway exhibit a hierarchical organization of prediction error. *Nat. Commun.* 8, 1–17. doi: 10.1038/s41467-017-02038-6

Patel, C. R., Redhead, C., Cervi, A. L., and Zhang, H. (2012). Neural sensitivity to novel sounds in the rat's dorsal cortex of the inferior colliculus as revealed by evoked local field potentials. *Hearing Res.* 286, 41–54. doi: 10.1016/j.heares.2012.02.007

Pekala, R. J. (2015). Hypnosis as a 'state of consciousness': how quantifying the mind can help us better understand hypnosis. *Am. J. Clin. Hypn.* 57, 402–424. doi: 10.1080/00029157.2015.1011480

Peña, J. L., Pérez-Perera, L., Bouvier, M., and Velluti, R. A. (1999). Sleep and wakefulness modulation of the neuronal firing in the auditory cortex of the guinea pig. *Brain Res.* 816, 463–470. doi: 10.1016/s0006-8993(98)01194-9

Perez, P., Valente, M., Hermann, B., Sitt, J., Faugeras, F., Demeret, S., et al. (2021). Auditory event-related "global effect" predicts recovery of overt consciousness. *Front. Neurol.* 11:233. doi: 10.3389/fneur.2020.588233

Pérez-González, D., Malmierca, M. S., and Covey, E. (2005). Novelty detector neurons in the mammalian auditory midbrain. *Eur. J. Neurosci.* 22, 2879–2885. doi: 10.1111/j.1460-9568.2005.04472.x

Perrin, F., Schnakers, C., Schabus, M., Degueldre, C., Goldman, S., Brédart, S., et al. (2006). Brain response to one's own name in vegetative state, minimally conscious state, and locked-in syndrome. *Arch. Neurol.* 63, 562–569. doi: 10.1001/archneur.63.4.562

Perry, J. E., Churchill, L. R., and Kirshner, H. S. (2005). The terri schiavo case: legal, ethical, and medical perspectives. *Anna. Int. Med.* 143:744. doi: 10.7326/0003-4819-143-10-200511150-00012

Pfeiffer, C., Nguissi, N. A. N., Chytiris, M., Bidlingmeyer, P., Haenggi, M., Kurmann, R., et al. (2018). Somatosensory and auditory deviance detection for outcome prediction during postanoxic coma. *Anna. Clin. Transl. Neurol.* 5, 1016–1024. doi: 10.1002/acn3.600

Picton, T. W. (1992). The P300 wave of the human event-related potential. *J. Clin. Neurophysiol.* 9, 456–479. doi: 10.1097/00004691-199210000-00002

Pilcher, J. J., and Huffcutt, A. I. (1996). Effects of sleep deprivation on performance: a meta-analysis. *Sleep* 19, 318–326. doi: 10.1093/sleep/19.4.318

Pincze, Z., Lakatos, P., Rajkai, C., Ulbert, I., and Karmos, G. (2001). Separation of mismatch negativity and the N1 wave in the auditory cortex of the cat: a topographic study. *Clin. Neurophysiol.* 112, 778–784. doi: 10.1016/s1388-2457(01)00509-0

Plourde, G., and Boylan, J. F. (1991). The long-latency auditory evoked potential as a measure of the level of consciousness during sufentanil anesthesia. *J. Cardioth. Vasc. Anesth.* 5, 577–583. doi: 10.1016/1053-0770(91)90010-q

Plourde, G., and Picton, T. W. (1991). Long-latency auditory evoked potentials during general anesthesia: N1 and P3 components. *Anesthes. Anal.* 72, 342–350. doi: 10.1213/00000539-199103000-00011

Plum, F., and Posner, J. B. (1982). *The Diagnosis of Stupor and Coma*, Vol. 19. Oxford, USA: Oxford University Press.

Polich, J. (2007). Updating P300: an integrative theory of P3a and P3b. *Clin. Neurophysiol.* 118, 2128–2148. doi: 10.1016/j.clinph.2007.04.019

Portas, C. M., Krakow, K., Allen, P., Josephs, O., Armony, J. L., and Frith, C. D. (2000). Auditory processing across the sleep-wake cycle: simultaneous EEG and fMRI monitoring in humans. *Neuron* 28, 991–999. doi: 10.1016/s0896-6273(00)00169-0

Purdon, P. L., Sampson, A., Pavone, K. J., and Brown, E. N. (2015). Clinical electroencephalography for anesthesiologists: Part I: background and basic signatures. *Anesthesiology* 123, 937–960. doi: 10.1097/aln.0000000000000841

Qin, L., Kitama, T., Chimoto, S., Sakayori, S., and Sato, Y. (2003). Time course of tonal frequency-response-area of primary auditory cortex neurons in alert cats. *Neurosci. Res.* 46, 145–152. doi: 10.1016/s0168-0102(03)00034-8

Rangarajan, V., Jacques, C., Knight, R. T., Weiner, K. S., and Grill-Spector, K. (2020). Diverse temporal dynamics of repetition suppression revealed by intracranial recordings in the human ventral temporal cortex. *Cerebral Cortex* 30, 5988–6003. doi: 10.1093/cercor/bhaa173

Rao, R. P. N., and Ballard, D. H. (1999). Predictive coding in the visual cortex: a functional interpretation of some extra-classical receptive-field effects. *Nat. Neurosci.* 2, 79–87. doi: 10.1038/4580

Rauss, K., and Pourtois, G. (2013). What is bottom-up and what is top-down in predictive coding? *Front. Psychol.* 4:276. doi: 10.3389/fpsyg.2013.00276

Raz, A., Deouell, L. Y., and Bentin, S. (2001). Is pre-attentive processing compromised by prolonged wakefulness? effects of total sleep deprivation on the mismatch negativity. *Psychophysiology* 38, 787–795. doi: 10.1111/1469-8986.3850787

Reinsel, R. A., Veselis, R. A., Wronski, M., and Marino, P. (1995). The P300 event-related potential during propofol sedation: a possible marker for amnesia? *Br. J. Anaesth.* 74, 674–680. doi: 10.1093/bja/74.6.674

Richardson, B. D., Hancock, K. E., and Caspary, D. M. (2013). Stimulus-specific adaptation in auditory thalamus of young and aged awake rats. *J. Neurophysiol.* 110, 1892–1902. doi: 10.1152/jn.00403.2013

Risetti, M., Formisano, R., Toppi, J., Quitadamo, L. R., Bianchi, L., Astolfi, L., et al. (2013). On ERPs detection in disorders of consciousness rehabilitation. *Front. Hum. Neurosci.* 7:775. doi: 10.3389/fnhum.2013.00775

Rosburg, T., Trautner, P., Dietl, T., Korzyukov, O. A., Boutros, N. N., Schaller, C., et al. (2005). Subdural recordings of the mismatch negativity (MMN) in patients with focal epilepsy. *Brain* 128, 819–828. doi: 10.1093/brain/awh442

Rudolph, U., and Antkowiak, B. (2004). Molecular and neuronal substrates for general anaesthetics. *Nat. Rev. Neurosci.* 5, 709–720. doi: 10.1038/nrn1496

Rui, Y.-Y., He, J., Zhai, Y.-Y., Sun, Z.-H., and Yu, X. (2018). Frequency-dependent stimulus-specific adaptation and regularity sensitivity in the rat auditory thalamus. *Neuroscience* 392, 13–24. doi: 10.1016/j.neuroscience.2018.09.015

Rutledge, R. B. M., Caplin, D. A., and Glimcher, P. W. (2010). Testing the reward prediction error hypothesis with an axiomatic model. *J. Neurosci.* 30, 13525–13536. doi: 10.1523/jneurosci.1747-10.2010

Ruusuvirta, T., Korhonen, T., Arikoski, J., and Kivirikko, J. (1996a). ERPs to pitch changes: a result of reduced responses to standard tones in rabbits. *Neuroreport* 7, 413–416. doi: 10.1097/00001756-199601310-00009

Ruusuvirta, T., Korhonen, T., Arikoski, J., and Kivirikko, J. (1996b). Multiple-unit responses to pitch changes in rabbits. *Neuroreport* 7, 1266–1268. doi: 10.1097/00001756-199605170-00009

Ruusuvirta, T., Korhonen, T., Penttonen, M., and Arikoski, J. (1995). Hippocampal evoked potentials to pitch deviances in an auditory oddball situation in the rabbit: no human mismatch-like dependence on standard stimuli. *Neurosci. Lett.* 185, 123–126. doi: 10.1016/0304-3940(94)11240-j

Ruusuvirta, T., Penttonen, M., and Korhonen, T. (1998). Auditory cortical event-related potentials to pitch deviances in rats. *Neurosci. Lett.* 248, 45–48. doi: 10.1016/s0304-3940(98)00330-9

Sabri, M., and Campbell, K. B. (2002). The effects of digital filtering on mismatch negativity in wakefulness and slow-wave sleep. *J. Sleep Res.* 11, 123–127. doi: 10.1046/j.1365-2869.2002.00292.x

Sabri, M., and Campbell, K. B. (2005). Is the failure to detect stimulus deviance during sleep due to a rapid fading of sensory memory or a degradation of stimulus encoding? *J. Sleep Res.* 14, 113–122. doi: 10.1111/j.1365-2869.2005.00446.x

Sabri, M., Labelle, S., Gosselin, A., and Campbell, K. B. (2003). Effects of sleep onset on the mismatch negativity (MMN) to frequency deviants using a rapid rate of presentation. *Cogn. Brain Res.* 17, 164–176. doi: 10.1016/s0926-6410(03)00090-9

Saidman, L. J., Bovill, J. G., Sebel, P. S., and Stanley, T. H. (1984). Opioid analgesics in anesthesia: with special reference to their use in cardiovascular anesthesia. *J. Am. Soc. Anesthesiol.* 61, 731–755. doi: 10.1097/00000542-198412000-00018

Sallinen, M., and Lyytinen, H. (1997). Mismatch negativity during objective and subjective sleepiness. *Psychophysiology* 34, 694–702. doi: 10.1111/j.1469-8986.1997.tb02144.x

Sallinen, M., Kaartinen, J., and Lyytinen, H. (1994). Is the appearance of mismatch negativity during stage 2 sleep related to the elicitation of K-complex? *Electroencephalogr. Clin. Neurophysiol.* 91, 140–148. doi: 10.1016/0013-4694(94)90035-3

SanMiguel, I., Widmann, A., Bendixen, A., Trujillo-Barreto, N., and Schroger, E. (2013). Hearing silences: human auditory processing relies on preactivation of sound-specific brain activity patterns. *J. Neurosci.* 33, 8633–8639. doi: 10.1523/jneurosci.5821-12.2013

Scheinin, A., Kantonen, O., Alkire, M., Långsjö, J., Kallionpää, R. E., Kaisti, K., et al. (2021). Foundations of human consciousness: imaging the twilight zone. *J. Neurosci.* 41, 1769–1778. doi: 10.1523/jneurosci.0775-20.2020

Schlossmacher, I., Lucka, F., Bruchmann, M., and Straube, T. (2021). Effects of awareness and task relevance on neurocomputational models of mismatch negativity generation. *bioRxiv* [preprint] doi: 10.1101/2021.02.03.429421

Schröger, E., Marzecová, A., and SanMiguel, I. (2015). Attention and prediction in human audition: a lesson from cognitive psychophysiology. *Eur. J. Neurosci.* 41, 641–664. doi: 10.1111/ejn.12816

Sculthorpe, L. D., Ouellet, D. R., and Campbell, K. B. (2009). MMN elicitation during natural sleep to violations of an auditory pattern. *Brain Res.* 1290, 52–62. doi: 10.1016/j.brainres.2009.06.013

Sebel, P. S., Bovill, J. G., Wauquier, A., and Rog, P. (1981). Effects of high-dose fentanyl anesthesia on the electroencephalogram. *J. Am. Soc. Anesthesiol.* 55, 203–211. doi: 10.1097/00000542-198109000-00004

Sharma, R. (2011). Oculomotor dysfunction in amyotrophic lateral sclerosis. *Archiv. Neurol.* 68:857. doi: 10.1001/archneurol.2011.130

Shiramatsu, T. I., Kanzaki, R., and Takahashi, H. (2013). Cortical mapping of mismatch negativity with deviance detection property in rat. *PLoS One* 8:e82663. doi: 10.1371/journal.pone.0082663

Shirazibeheshti, A., Cooke, J., Chennu, S., Adapa, R., Menon, D. K., Hojjatoleslami, S. A., et al. (2018). Placing meta-stable states of consciousness within the predictive coding hierarchy: the deceleration of the accelerated prediction error. *Conscious. Cogn.* 63, 123–142. doi: 10.1016/j.concog.2018.06.010

Sikkens, T., Bosman, C. A., and Olcese, U. (2019). The role of top-down modulation in shaping sensory processing across brain states: implications for consciousness. *Front. Syst. Neurosci.* 13:31. doi: 10.3389/fnsys.2019.00031

Simpson, T. P., Manara, A. R., Kane, N. M., Barton, R. L., Rowlands, C. A., and Butler, S. R. (2002). Effect of propofol anaesthesia on the event-related potential mismatch negativity and the auditory-evoked potential N1. *Br. J. Anaesth.* 89, 382–388. doi: 10.1093/bja/89.3.382

Smout, C. A., Tang, M. F., Garrido, M. I., and Mattingley, J. B. (2019). Attention promotes the neural encoding of prediction errors. *PLoS Biol.* 17:e2006812. doi: 10.1371/journal.pbio.2006812

Sneyd, J. R., Samra, S. K., Davidson, B., Kishimoto, T., Kadoya, C., and Domino, E. F. (1994). Electrophysiologic effects of propofol sedation. *Anesth. Anal.* 79, 1151–1158. doi: 10.1213/00000539-199412000-00022

Spratling, M. W. (2008a). Predictive coding as a model of biased competition in visual attention. *Vision Res.* 48, 1391–1408. doi: 10.1016/j.visres.2008.03.009

Spratling, M. W. (2008b). Reconciling predictive coding and biased competition models of cortical function. *Front. Comput. Neurosci.* 2:4. doi: 10.3389/neuro.10.004.2008

Squires, N. K., Squires, K. C., and Hillyard, S. A. (1975). Two varieties of long-latency positive waves evoked by unpredictable auditory stimuli in man. *Electroencephalogr. Clin. Neurophysiol.* 38, 387–401. doi: 10.1016/0013-4694(75)90263-1

Stamatakis, E. A., Adapa, R. M., Absalom, A. R., and Menon, D. K. (2010). Changes in resting neural connectivity during propofol sedation. *PLoS One* 5:e14224. doi: 10.1371/journal.pone.0014224

Stefanics, G., Heinzle, J., Horváth, A. A., and Stephan, K. E. (2018). Visual mismatch and predictive coding: a computational single-trial ERP study. *J. Neurosci.* 38, 4020–4030. doi: 10.1523/jneurosci.3365-17.2018

Steriade, M. (1991). Alertness, quiet sleep, dreaming. *Norm. Altered Stat. Funct.* 8, 279–357. doi: 10.1007/978-1-4615-6622-9_8

Steriade, M. (2006). Grouping of brain rhythms in corticothalamic systems. *Neuroscience* 137, 1087–1106. doi: 10.1016/j.neuroscience.2005.10.029

Steriade, M., Timofeev, I., and Grenier, F. (2001). Natural waking and sleep states: a view from inside neocortical neurons. *J. Neurophysiol.* 85, 1969–1985. doi: 10.1152/jn.2001.85.5.1969

Strauss, M., Sitt, J. D., King, J.-R., Elbaz, M., Azizi, L., Buiatti, M., et al. (2015). Disruption of hierarchical predictive coding during sleep. *Proc. Natl. Acad. Sci. U.S.A.* 112, E1353–E1362. doi: 10.1073/pnas.1501026112

Summerfield, C., and Egner, T. (2009). Expectation (and attention) in visual cognition. *Trends Cogn. Sci.* 13, 403–409. doi: 10.1016/j.tics.2009.06.003

Sussman, E. S. (2007). A new view on the MMN and attention debate. *J. Psychophysiol.* 21:164. doi: 10.1027/0269-8803.21.34.164

Sutton, S., Braren, M., Zubin, J., and John, E. R. (1965). Evoked-potential correlates of stimulus uncertainty. *Science* 150, 1187–1188. doi: 10.1126/science.150.3700.1187

Szymanski, M. D., Yund, E. W., and Woods, D. L. (1999). Phonemes, intensity and attention: differential effects on the mismatch negativity (MMN). *J. Acoust. Soc. Am.* 106, 3492–3505. doi: 10.1121/1.428202

Taaseh, N., Yaron, A., and Nelken, I. (2011). Stimulus-specific adaptation and deviance detection in the rat auditory cortex. *PLoS One* 6:e23369. doi: 10.1371/journal.pone.0023369

Tagliazucchi, E., von Wegner, F., Morzelewski, A., Brodbeck, V., Jahnke, K., and Laufs, H. (2013). Breakdown of long-range temporal dependence in default mode and attention networks during deep sleep. *Proc. Natl. Acad. Sci. U.S.A.* 110, 15419–15424. doi: 10.1073/pnas.1312848110

Takahashi, H., Tokushige, H., Shiramatsu, T. I, Noda, T., and Kanzaki, R. (2015). Covariation of pupillary and auditory cortical activity in rats under isoflurane anesthesia. *Neuroscience* 300, 29–38. doi: 10.1016/j.neuroscience.2015.05.004

Tang, Y.-Y., Hölzel, B. K., and Posner, M. I. (2015). The neuroscience of mindfulness meditation. *Nat. Rev. Neurosci.* 16, 213–225. doi: 10.1038/nrn3916

Thomas, L. B., and Jenkner, F. L. (1952). The effects of asphyxia and certain drugs on the activity of single cortical cells. *Transact. Am. Neurol. Assoc.* 56, 47–51. doi: 10.1002/9780470751466.ch23

Trejo, L. J., David, L. R. J., and Kramer, A. (1995). Attentional modulation of the mismatch negativity elicited by frequency differences between binaurally presented tone bursts. *Psychophysiology* 32, 319–328. doi: 10.1111/j.1469-8986.1995.tb01214.x

Tzovara, A., Korn, C. W., and Bach, D. R. (2018). Human pavlovian fear conditioning conforms to probabilistic learning. *PLoS Comput. Biol.* 14:e1006243. doi: 10.1371/journal.pcbi.1006243

Tzovara, A., Rossetti, A. O., Juan, E., Suys, T., Viceic, D., Rusca, M., et al. (2016). Prediction of awakening from hypothermic postanoxic coma based on auditory discrimination. *Anna. f Neurol.* 79, 748–757. doi: 10.1002/ana.24622

Tzovara, A., Rossetti, A. O., Spierer, L., Grivel, J., Murray, M. M., Oddo, M., et al. (2013). Progression of auditory discrimination based on neural decoding predicts awakening from coma. *Brain* 136, 81–89. doi: 10.1093/brain/aws264

Tzovara, A., Simonin, A., Oddo, M., Rossetti, A. O., and De Lucia, M. (2015). Neural detection of complex sound sequences in the absence of consciousness. *Brain* 138, 1160–1166. doi: 10.1093/brain/awv041

Uhrig, L., Dehaene, S., and Jarraya, B. (2014). A hierarchy of responses to auditory regularities in the macaque brain. *J. Neurosci.* 34, 1127–1132. doi: 10.1523/jneurosci.3165-13.2014

Uhrig, L., Janssen, D., Dehaene, S., and Jarraya, B. (2016). Cerebral responses to local and global auditory novelty under general anesthesia. *Neuroimage* 141, 326–340. doi: 10.1016/j.neuroimage.2016.08.004

Ulanovsky, N., Las, L., Farkas, D., and Nelken, I. (2004). Multiple time scales of adaptation in auditory cortex neurons. *J. f Neurosci.* 24, 10440–10453. doi: 10.1523/jneurosci.1905-04.2004

Vaitl, D., Birbaumer, N., Gruzelier, J., Jamieson, G. A., Kotchoubey, B., Kübler, et al. (2005). Psychobiology of altered states of consciousness. *Psychol. Bull.* 131:98. doi: 10.1037/0033-2909.131.1.98

Van Sweden, B., Van Dijk, J. G., and Caekebeke, J. F. V. (1994). Auditory information processing in sleep: late cortical potentials in an oddball paradigm. *Neuropsychobiology* 29, 152–156. doi: 10.1159/000119078

Verleger, R. (1988). Event-related potentials and cognition: a critique of the context updating hypothesis and an alternative interpretation of P3. *Behav. Brain Sci.* 11:343. doi: 10.1017/s0140525x00058015

Von Helmholtz, H. (1867). *Handbuch Der Physiologischen Optik: Mit 213 in Den Text Eingedruckten Holzschnitten Und 11 Tafeln*, Vol. 9. Leipzig: Leopold Voss.

Wauquier, A., Bovill, J. G., and Sebel, P. S. (1984). Electroencephalographic effects of fentanyl-, sufentanil-and alfentanil anaesthesia in man. *Neuropsychobiology* 11, 203–206. doi: 10.1159/000118078

Weber, L. A., Diaconescu, A. O., Mathys, C., Schmidt, A., Kometer, M., Vollenweider, F., et al. (2020). Ketamine affects prediction errors about statistical regularities: a computational single-trial analysis of the mismatch negativity. *J. Neurosci.* 40, 5658–5668. doi: 10.1523/jneurosci.3069-19.2020

Wesensten, N. J., and Badia, P. (1988). The P300 component in sleep. *Physiol. Behav.* 44, 215–220. doi: 10.1016/0031-9384(88)90141-2

Wijnen, V. J. M., Van Boxtel, G. J. M., Eilander, H. J., and De Gelder, B. (2007). Mismatch negativity predicts recovery from the vegetative state. *Clin. Neurophysiol.* 118, 597–605. doi: 10.1016/j.clinph.2006.11.020

Winkler, I. (2007). Interpreting the mismatch negativity. *J. Psychophysiol.* 21, 147–163. doi: 10.1027/0269-8803.21.34.147

Winter, O., Kok, A., Kenernans, J. L., and Elton, M. (1995). Auditory event-related potentials to deviant stimuli during drowsiness and stage 2 sleep. *Electroencephalogr. Clin. Neurophysiol.* 96, 398–412. doi: 10.1016/0168-5597(95)00030-v

Witon, A., Shirazibehehsti, A., Cooke, J., Aviles, A., Adapa, R., Menon, D. K., et al. (2020). Sedation modulates frontotemporal predictive coding circuits and the double surprise acceleration effect. *Cerebral Cortex* 30, 5204–5217. doi: 10.1093/cercor/bhaa071

Woldorff, M. G., and Hillyard, S. A. (1991). Modulation of early auditory processing during selective listening to rapidly presented tones. *Electroencephalogr. Clin. Neurophysiol.* 79, 170–191. doi: 10.1016/0013-4694(91)90136-r

Xu, X., Yu, X., He, J., and Nelken, I. (2014). Across-ear stimulus-specific adaptation in the auditory cortex. *Front. Neural Circuits* 8:89. doi: 10.3389/fncir.2014.00089

Young, E. D., and Brownell, W. E. (1976). Responses to tones and noise of single cells in dorsal cochlear nucleus of unanesthetized cats. *J. Neurophysiol.* 39, 282–300. doi: 10.1152/jn.1976.39.2.282

Yppärilä, H., Karhu, J., Westerén-Punnonen, S., Musialowicz, T., and Partanen, J. (2002). Evidence of auditory processing during postoperative propofol sedation. *Clin. Neurophysiol.* 113, 1357–1364. doi: 10.1016/s1388-2457(02)00158-x

Zaehle, T., Bauch, E. M., Hinrichs, H., Schmitt, F. C., Voges, J., Heinze, H.-J., et al. (2013). Nucleus accumbens activity dissociates different forms of salience: evidence from human intracranial recordings. *J. Neurosci.* 33, 8764–8771. doi: 10.1523/jneurosci.5276-12.2013

Zhang, Y., Yan, F., Wang, L., Wang, Y., Wang, C., Wang, Q., et al. (2018). Cortical areas associated with mismatch negativity: a connectivity study using propofol anesthesia. *Front. Hum. Neurosci.* 2:392. doi: 10.3389/fnhum.2018.00392

Zurita, P., Villa, A. E. P., De Ribaupierre, Y., De Ribaupierre, F., and Rouiller, E. M. (1994). Changes of single unit activity in the cat's auditory thalamus and cortex associated to different anesthetic conditions. *Neurosci. Res.* 19, 303–316. doi: 10.1016/0168-0102(94)90043-4

Züst, M. A., Ruch, S., Wiest, R., and Henke, K. (2019). Implicit vocabulary learning during sleep is bound to slow-wave peaks. *Curr. Biol.* 29, 541–553.e7. doi: 10.1016/j.cub.2018.12.038

Conflict of Interest: The authors declare that the research was conducted in the absence of any commercial or financial relationships that could be construed as a potential conflict of interest.

frontiers in Human Neuroscience

ORIGINAL RESEARCH
published: 20 August 2021
doi: 10.3389/fnhum.2021.707702

Older Adults Automatically Detect Age of Older Adults' Photographs: A Visual Mismatch Negativity Study

Petra Csizmadia[1,2], Bela Petro[1], Petia Kojouharova[1], Zsófia Anna Gaál[1], Katalin Scheiling[1], Boglárka Nagy[1,2] and István Czigler[1]*

[1] Institute of Cognitive Neuroscience and Psychology, Research Centre for Natural Sciences, Budapest, Hungary, [2] Doctoral School of Psychology (Cognitive Science), Budapest University of Technology and Economics, Budapest, Hungary

The human face is one of the most frequently used stimuli in vMMN (visual mismatch negativity) research. Previous studies showed that vMMN is sensitive to facial emotions and gender, but investigations of age-related vMMN differences are relatively rare. The aim of this study was to investigate whether the models' age in photographs were automatically detected, even if the photographs were not parts of the ongoing task. Furthermore, we investigated age-related differences, and the possibility of different sensitivity to photographs of participants' own versus different ages. We recorded event-related potentials (ERPs) to faces of young and old models in younger (N = 20; 18–30 years) and older groups (N = 20; 60–75 years). The faces appeared around the location of the field of a tracking task. In sequences the young or the old faces were either frequent (standards) or infrequent (deviants). According to the results, a regular sequence of models' age is automatically registered, and faces violating the models' age elicited the vMMN component. However, in this study vMMN emerged only in the older group to same-age deviants. This finding is explained by the less effective inhibition of irrelevant stimuli in the elderly, and corresponds to own-age bias effect of recognition studies.

Keywords: oddball, visual mismatch negativity (vMMN), facial stimuli, aging, own-age bias

OPEN ACCESS

Edited by:
Juanita Todd,
The University of Newcastle, Australia

Reviewed by:
Motohiro Kimura,
National Institute of Advanced Industrial Science and Technology (AIST), Japan
Marta Zimmer,
Budapest University of Technology and Economics, Hungary

****Correspondence:***
Petra Csizmadia
csizmadia.petra@ttk.hu

Specialty section:
This article was submitted to Cognitive Neuroscience, a section of the journal Frontiers in Human Neuroscience

Received: *10 May 2021*
Accepted: *21 July 2021*
Published: *20 August 2021*

Citation:
Csizmadia P, Petro B, Kojouharova P, Gaál ZA, Scheiling K, Nagy B and Czigler I (2021) Older Adults Automatically Detect Age of Older Adults' Photographs: A Visual Mismatch Negativity Study. Front. Hum. Neurosci. 15:707702. doi: 10.3389/fnhum.2021.707702

INTRODUCTION

The information content of the human face encompasses various important pieces of information such as identity, gender, race, age, and emotional state. This set has utmost importance in interpersonal and social behavior. In this study our aim was to investigate the possibility of automatic registration of age by using the visual mismatch negativity (vMMN) component of the event-related potentials (ERPs) of the brain electric activity.

Visual mismatch negativity emerges to visual events that violate the regularities of a stimulus sequence, even if the eliciting stimuli are unrelated to an ongoing task (for reviews see Kimura et al., 2011; Stefanics et al., 2015). VMMN is usually investigated in the passive oddball paradigm. In this paradigm participants perform a visual (or sometimes auditory) task, while the vMMN-related events are presented outside the task's context as unattended stimuli. The characteristics of the frequent (standard) events of stimulus sequences may acquire representation, even if the characteristics are simple visual features such as color, orientation, spatial frequency, etc. VMMN

also emerges to perceptual categories like symmetry (Kecskés-Kovács et al., 2013b) and orderliness (Durant et al., 2017).

The human face is one of the most frequently used stimuli in vMMN research. VMMN is especially sensitive to facial emotions, i.e., rare (deviant) faces expressing a different emotion from the frequent (standard) faces within the same sequence (e.g., Astikainen and Heitanen, 2009; Li et al., 2012; Stefanics et al., 2012; for a review see Kovarski et al., 2017). In case of gender as another facial feature, Kecskés-Kovács et al. (2013a) recorded vMMN to faces of female models within sequences of male faces, and *vice versa*.

In the present study we investigated the possibility of a similar effect, automatic detection of age by showing photographs of faces of models with different ages. Furthermore, we compared vMMN differences between older and younger participants. Investigations of age-related vMMN differences are relatively rare. Nevertheless, this is an important topic, because vMMN provides direct evidence about the sensitivity of automatic registration of environmental regularities, and the putative change of sensitivity with aging. So far in the context of age differences the majority of vMMN studies applied low-level deviancies, and the results are equivocal. Lorenzo-López et al. (2004) investigated vMMN to horizontally drifting sinusoidal gratings and obtained a long-lasting posterior negativity. Whereas in the older group the negativity was different from zero only at the Oz electrode site, it had a broader distribution in younger participants. Tales et al. (2002) presented single and double bars as standard and deviant stimuli. VMMN in the younger group emerged in the 250–400 ms range, but in the older group they obtained vMMN only in the later part of this range. However, using the same method, Stothart et al. (2013) obtained no age-related differences. Recently, we compared older and younger groups in three studies (Gaál et al., 2017; Sulykos et al., 2017, 2018). In our laboratory Sulykos et al. (2017) investigated vMMN to the offset of parts of continuously presented objects. Age-related vMMN difference emerged in the 180–220 ms range, but there was no vMMN difference in the earlier part of this component. In the Sulykos et al. (2018) study checkerboard stimuli were presented. VMMN appeared in the 100–300 ms range in both age groups, but in the later part of vMNN the amplitude was smaller in the older group. In contrast with the simple stimuli of the above studies, Gaál et al. (2017) investigated category-related vMMN, i.e., letters and pseudo-letters. The stimuli were presented in pairs of subsequent fragments, and the two fragments together constituted the stimuli as wholes. The main variable was the duration between the onset of the fragments, therefore the integration effects on vMMN were investigated in the two age groups. The integration period of the fragments was longer in the older group, showing longer stimulus persistence in the elderly. As this review of previous studies shows, with the exception of the Gaál et al. (2017) study, only low-level features were investigated in the context of age-related differences. One of the aims of the present study is to investigate age-related effects of automatic detection in the case of complex stimuli violating sequential regularities. As far as we know, this is the first vMMN study that investigated the sensitivity of an older and a younger group in the domain of human faces.

As another aim of this study, we investigated vMMNs to deviant photographs showing models of the same age as or a different age than the age of the participants. This issue is related to the phenomenon of own-age bias (OAB). As a considerable body of research shows, people are more efficient in recognizing photographs depicting faces of their own age than faces depicting different ages (for reviews see Rhodes and Anastasi, 2012; Wiese et al., 2013). Theories about the OAB proposed that people have more practice in processing faces of others with age similar to their own. This view emphasizes the importance of the different frequency of encounters for people with different ages (He et al., 2011). As an argument for the importance of encounter frequency, the OAB effect is reduced or even absent in groups with considerable experience with other age-groups (Harrison and Hole, 2009; Wiese et al., 2012). It is possible that in a multidimensional system of perception (Valentine, 1991), as an effect of less frequent experience, other-age faces are farther away from the more discriminative central regions on various dimensions. However, besides the frequency of encounter, motivational and social group relations have also been suggested as underlying mechanisms of OAB. This type of theory was originally proposed for the own-race bias (ORB) in face recognition, an effect stronger than OAB (Mukudi and Hills, 2019). Sporer (2001) supposed that ingroup-outgroup differentiation is an automatic process. The categorization-individualization model (Hugenberg et al., 2010) proposed that in an initial processing stage face processing is categorical, and individualization is a process at a subsequent stage. In the case of faces of a different age, processing is frequently restricted to the first stage. However, across different age groups OAB is not perfectly symmetrical. According to results by Bartlett and Leslie (1986) and Wiese et al. (2008), in groups of older participants no OAB emerged.

As results of some OAB studies show, both stages of the hypothesized processes are automatic. This is because following incidental learning of faces (attractiveness or friendliness rating or age estimation, search for a non-facial target feature), subsequent face recognition is similar to the effect of intentional (attentional) learning (Randall et al., 2012; Neumann et al., 2014). To investigate the possibility of automaticity of OAB-related effects and of age-related sensitivity differences, we compared a younger and an older group of participants in a vMMN paradigm with sequences of young standard – old deviant and old standard – young deviant photographs. We applied the method developed by Stefanics et al. (2012) for emotion-related vMMN. Accordingly, we presented four photographs around a central task field. As a modification of the method, to ensure continuous attentional engagement to the task-field, we introduced a tracking task. What did we expect in the present study? On a general level we expected the automatic perception of the models' age, that is, the appearance of a negative deviant *minus* standard difference potential (vMMN) over the posterior locations within the 200–400 ms post-stimulus latency range. As a more specific possibility, we expected to find an OAB by registering a vMMN difference between the age groups in the young standard – old deviant and old standard – young deviant conditions. According to the categorization-individualization model of

OAB (Hugenberg et al., 2010), only the own-age photographs are processed at the level of individual features. Such age-related difference may lead to increased sensitivity to own-age deviants, and accordingly, a larger deviant *minus* standard ERP difference for photographs of models of the same age as that of the participants.

Age difference of photographs *per se* elicits ERP differences. As an example, in a gender categorization task a larger anterior positivity and a smaller anterior negativity emerged to old faces in a younger group, and in the same group a larger late positivity emerged to old faces in a later latency range (Ebner et al., 2011). Therefore, in the present study we compared the ERPs to stimuli of the same age as deviants and standards (inverse control procedure). Face processing is dependent on the orientation of the photographs. Upside-down presentation of faces decreases the effectiveness of face-specific processing (Yin, 1969; for a review see Rossion, 2009). Low-level visual differences are preserved in upside-down photographs, therefore vMMN differences between original and upside-down presentation argue against the role of age-related low-level feature differences. Accordingly, we did not expect deviant *minus* standard ERP difference for upside-down faces.

In summary, our main goal was to study the possibility of automatic registration of age and to investigate age related sensitivity differences by using the visual mismatch negativity. We compared a younger and an older group of participants in a passive oddball paradigm with sequences of young standard – old deviant and old standard – young deviant photographs. According to results of previous vMMN studies with facial features, we expected the appearance of a negative deviant *minus* standard difference potential (vMMN) over the posterior locations within the 200–400 ms post-stimulus latency range and we expected to find an OAB, a larger deviant *minus* standard ERP difference for photographs of models of the same age as that of the participants.

MATERIALS AND METHODS

Participants

Twenty older (60–75 years) participants were selected from a larger pool of available participants. This selection was independent of the potential difference between the deviant *minus* standard ERPs difference, but they had discernible P1 and N1/N170 exogenous components. In the younger (18–30 years) group seven participants were excluded from a starting sample of 27 participants because they had no discernable exogenous components. This way there were 20 participants in each age group (younger adults: 10 women; mean age: 22.0 years, *SD* = 2.34 years, older adults: 11 women; mean age: 68.45 years, *SD* = 3.62 years). Cognitive functions were measured by four subtests (Similarities, Digit Span, Matrix Reasoning, and Digit Symbol-Coding) of the Hungarian version of WAIS-IV (Rózsa et al., 2010). The aggregated mean points were 43.65 (*SD* = 5.85) in the younger group and 52.45 (*SD* = 8.31) in the older group. All participants were right-handed, had normal or corrected-to-normal vision (measured via a Hungarian version of Snellen card), and were free of any kind of neurological or psychiatric disease. Older adults were paid for participation. Younger adults participated in the experiment for course credit, except two paid participants, who were no longer college students. Written informed consent was obtained from all participants prior to the experimental procedure.

The study was conducted in accordance with the Declaration of Helsinki and approved by the United Ethical Review Committee for Research in Psychology in Hungary (EPKEB).

Stimuli and Procedure

The stimuli were presented on a 24″ LCD monitor (Asus VS229na, 60-Hz refresh rate) on a gray (44.48 cd/m^2) background at a viewing distance of 1.44 m. ERP-related stimuli consisted of black and white photographs of 16 young and 16 old male models taken from the database constructed by Minear and Park (2004). Using Adobe Photoshop CS3 Extended 10.0 (Adobe Systems Inc. San Jose, CA, United States) the photographs were converted to grayscale (8 bit) and inserted onto a gray background. Each stimulus screen consisted of images of four different individuals, either four young male faces or four old male faces. The photographs appeared on the upper-left, upper-right, lower-left, and lower-right sides from the center of the screen. The average luminance of the faces was 62 cd/m^2 (*SE* = 1.2 cd/m^2). The size of the images was 260 × 360 pixels (2.9° × 4.0°). The center of each image was at a 2.7° horizontal and 2.7° vertical viewing angle from the center of the screen. Stimulus duration was 150 ms, the inter-stimulus intervals were between 366 and 416 ms with a jitter in steps of 16.67 ms.

There were four conditions in the experiment in separate blocks (i.e., inverted and upright faces were presented in separate sequences). Photographs were presented either in the original position or inverted (Position: upright, inverted). Either the photographs of young or old models were deviant stimuli (Photographs: young, old). In the sequences 20% of the stimuli were deviants. The order of presentation of conditions was counterbalanced across participants. There were 400 stimuli (320 standards and 80 deviants) within a condition. The presentation order of the models was random with the restriction that a photograph of the same model was not presented at subsequent stimuli, that is, faces changed trial-by-trial. (The photograph of a model as standard face was repeated 80 times, a deviant one was repeated 20 times within a condition).

The task-relevant stimuli appeared on the central area of the screen and consisted of two disks. A red disk served as a fixation point (0.19° visual angle), and a green disk (0.38°) made horizontal pseudorandom movements around the red disk. The participant's task was to keep the green disk as close to the fixation point as possible using the S (left) and É (right) keys of the keyboard. Errors occurred when the distance of the two disks exceeded 0.77° in either direction. In case of an error, the color of the green disk changed to blue providing online visual feedback. Performance (the sum of the errors in one block) was reported on the screen at the end of each block. **Figure 1** shows examples of the stimulus display. The experiment started with a practice block (252 trials) to ensure that the participant fully understood the task. In the practice sequence an equal number of young

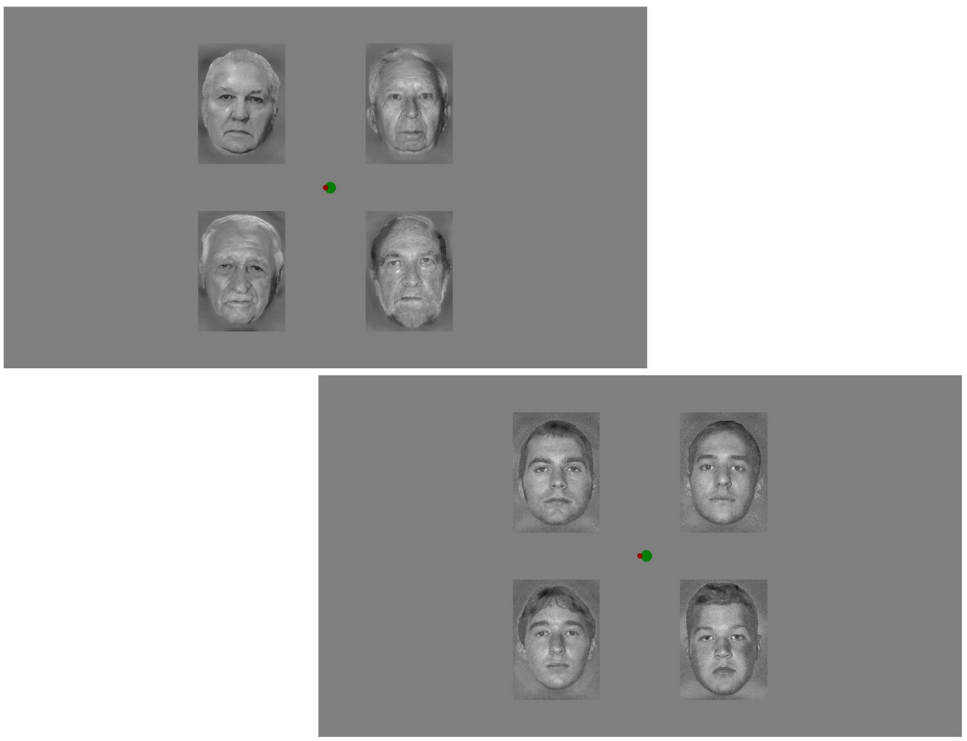

FIGURE 1 | Examples of the stimulus display. At the center there is the task-field with the target and moving circles is at the center.

and old faces were mixed within the sequence. EEG was not recorded in this block.

Measurement of Brain Electric Activity

Electrophysiological recording was performed in an electrically and acoustically shielded room. Electrical brain activity was recorded from 32 locations according to the extended 10–20 system (BrainVision Recorder 1.21.0303, ActiChamp amplifier, Ag/AgCl active electrodes, EasyCap (Brain Products GmbH), sampling rate: 1000 Hz, DC-70 Hz online filtering). The ground electrode was placed on the forehead (AFz) and the reference electrode was on the nose tip. Both horizontal and vertical electrooculogram signals (HEOG and VEOG) were recorded with bipolar configurations between two electrodes (placed lateral to the outer canthi of the two eyes and above and below the left eye, respectively). The EEG signal was bandpass filtered offline with a non-causal Kaiser-windowed Finite Impulse Response filter (low pass filter parameters: 30 Hz of cutoff frequency, beta of 12.2653, a transition bandwidth of 10 Hz; high pass filter parameters: 0.1 Hz of cut off frequency, a transition bandwidth of 0.2 Hz). Epochs ranging from −100 to 600 ms relative to the onset of stimuli were extracted for all deviants and for those standards that immediately preceded a deviant. The first 100 ms of each epoch served as the baseline. Epochs with larger than 100 μV or smaller than 2 μV voltage change were considered artifacts and rejected from further processing. ERPs were calculated by averaging the extracted epochs (separately for standards and deviants for young and old faces). Difference waveforms were created by subtracting the ERPs to standards from the ERPs to deviants, separately for the two age category of the models (inverse control procedure), i.e., deviant and standard responses to physically identical stimuli were compared (deviant old face vs. standard old face and deviant young face vs. standard young face).

Analyses and Comparisons

Exogenous Components

P1 latency was measured at POz and Oz locations as the largest positivity within the 60–130 ms range, and P1 amplitude was measured as the average of $a \pm 10$ ms range around the group averages. Amplitude and latency values were calculated in repeated measure ANOVAs with between group factor of *Group* (younger, older), and within group factors of *Photograph* (young, old), *Stimulus* (deviant, standard), and *Position* (upright, inverted). N1/N170 latency was measured at PO7 and PO8 locations as the largest negative/smallest positive value in the 100–200 ms range, and N1/N170 amplitude was measured as the average of $a \pm 10$ ms range around the group averages. In the ANOVAs on latencies and amplitudes, *Location* (left, right) was included as an additional factor. P2 latency (as the largest positive value) was measured within the 170–270 and 190–290 ms latency ranges (younger and older group, respectively), and amplitude was measured as the average of a $\pm$ 10 ms range around the group averages at P7 and P8 locations. In the ANOVAs the between group factor was *Group* (younger, older), and within group factors were *Photograph* (young, old), *Stimulus* (deviant,

standard), *Position* (upright, inverted), and *Location* (left, right). We report here only age-related differences, because other aspects of exogenous activity are beyond the scope of this study[1].

Difference Potentials

To explore the possibility of deviant *minus* standard differences, as the first step we calculated consecutive *t*-tests (difference from zero as null-hypothesis) at PO7, PO3, POz, PO4, PO8, O1, Oz, and O2 locations on the deviant *minus* standard difference potentials at all points within the 200–400 ms latency range, i.e., in the expected range of vMMN. As criteria we considered significant t-values ($p < 0.05$) at least over two adjacent locations and 20 subsequent significant points (20 ms per location). Afterward we investigated the difference potentials in two epochs: in 230–270 and 330–370 ms, respectively, i.e., the middle part of the 200–300 and 300–400 ms latency ranges. These investigations were conducted in a posterior ROI, containing PO7, PO3, POz, PO4, PO8, O1, Oz, and O2 locations. These tests were conducted only if there were significant results in the exploratory analyzes. In the two epochs we calculated Benjamini-Hochberg corrected *t*-tests, comparing the difference potentials to zero. In these calculations the Statistica 13 (TIBCO Software Inc.) was applied. In case of tendencies of deviant *minus* standard differences, we conducted Bayesian statistics (JASP Team, 2018) to control the reliability of null effects (this calculation was not planned *a priori*). We used the default prior option for the *t*-tests, a Cauchy distribution with spread r set to 0.707. All tests were two-tailed[2].

In case of reliable differences between the ERPs to deviant and standard stimuli, we conducted a source analysis using the sLORETA method. These results, along with the applied calculations are presented in **Supplementary Materials**.

RESULTS

Behavioral Results

The number of errors (the circle outside the target field) was larger in the older group (36.1, $SE = 11.9$) than in the younger group (2.10, $SE = 0.60$), according to the Mann-Whitney test, $p < 0.001$. The task was easier in the younger group, however, as we noted, participants of the older group attempted to concentrate on the task.

Event-Related Potentials

Exogenous Components

As **Figure 2** shows, ERPs were different in the two age-groups. Following the P1 component, in the older group the ERP returned to the baseline, and the N1 component was followed by the P2. In the younger group N1 did not reach the baseline. This is because the negativity superimposed on a positive wave, and this positivity peaked as P2. **Table 1** shows the latency and amplitude values of these components.

On the P1 latency values we obtained a significant main effect of *Group*, $F(1,38) = 14.66$, $\eta_p^2 = 0.28$, $p < 0.001$, showing shorter P1 latency in the older group. For the P1 amplitude, despite the apparent difference we obtained no age-related difference. For the N1 latency we obtained no age-related differences. It is worth noting that the latencies were below 150 ms, which is shorter than the usual N170 latency. As it is evident from **Figure 2**, N1 amplitude was larger in the older group, accordingly, this difference was significant, $F(1,38) = 11.42$, $\eta_p^2 = 0.23$, $p < 0.01$. P2 latency was longer in the older group, $F(1,38) = 33.60$, $\eta_p^2 = 0.47$, $p < 0.001$, and P2 amplitude was larger in the younger group, $F(1,38) = 10.15$, $\eta_p^2 = 0.21$, $p = 0.003$.

Difference Potentials

In the inverted condition the difference potentials failed to pass the criteria of the exploratory analysis, therefore we did not analyze this condition further. In the younger group the deviant *minus* standard difference just failed the criteria (at the photography with young models, in the 200–300 ms range there were negativities of 28 and 16 ms long epochs at O2 and Oz locations, respectively), therefore we further analyzed the earlier range in this age group. In the older group significant negativity emerged within the 343–374 ms latency range at all locations for the photographs depicting old models.

Figure 3 shows the difference potentials, and **Figure 4** shows the surface distribution of the difference potentials in the 230–270 and 330–370 ms ranges to upright photographs in the two age-groups for the two ages of models. **Table 2** shows the mean amplitude values of the above ranges. In the *t*-tests significant differences appeared in the older group in the 330–370 ms range for the photographs of old models, $t(19) = 3.76$, $d = 0.79$, $p < 0.05$ (Benjamini-Hochberg corrected), and there was a tendency for the negativity for young models $t(19) = 2.05$, $d = 0.46$, $p < 0.06$ (uncorrected). In the younger group we obtained a tendency of young deviant-related negativity in the 230–270 ms range, $t(19) = 1.85$, $d = 0.41$, $p < 0.08$ (uncorrected). No other comparison approached significance.

In the Bayesian analyses we obtained strong evidence for the negative difference potential in the older group for upright old models in the 330–370 ms range ($BF_{10} = 15.93$). In this condition an anecdotal evidence appeared in the 330–370 ms range for young models ($BF_{10} = 1.31$). In the younger group the apparent negativity for the young models in the 230–270 ms range was unreliable ($BF_{10} = 0.97$).

DISCUSSION

The aim of the present study was to investigate the possibility of automatic identification of models' age in photographs. To this end, in a passive oddball sequence of photographs some model's age were different (deviants) from the frequent age of the models (standards). We investigated a group of younger and

[1]The complete data set is available in the **Supplementary Material**.

[2]It should be noted, that in a formal sense an ANOVA with factors of *Group* (younger, older), *Photograph* (young, old), *Stimulus* (deviant, standard), and *ROI* (parieto-occipital, occipital) corresponds to the design. However, due to the lack of significant differences in the younger group, it is equivocal to select a proper latency range of measurements. Results of an ANOVA using the range of significant difference between young and old photographs in the older group show only significant Group × Picture interaction: $F(1,38) = 4.13$, $p < 0.05$, $\eta_p^2 = 0.10$.

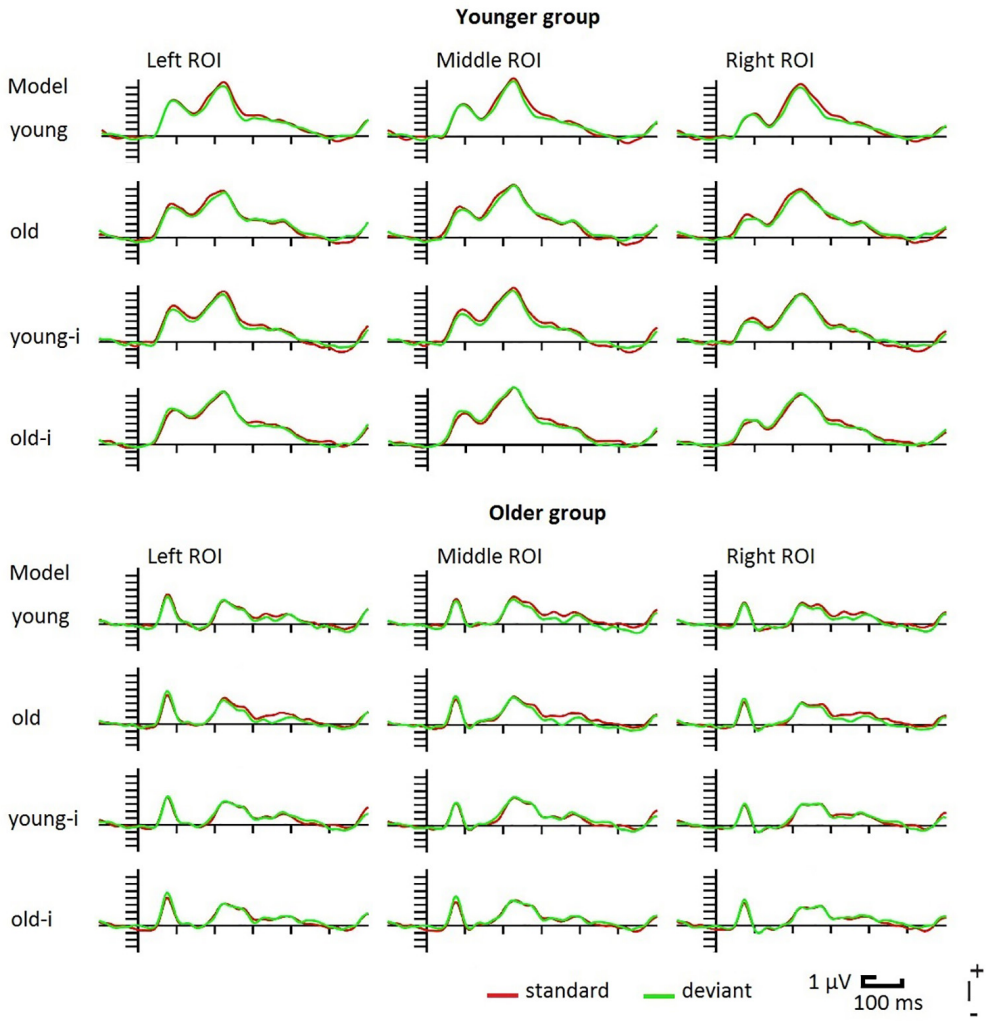

FIGURE 2 | Event-related potentials in the younger and older groups to upright and inverted (-i) photographs of young and old models. For illustrative reasons the posterior ROI is divided into left (PO7, PO3, O1) middle (POz, Oz) and right (PO8, PO4, O2) parts.

TABLE 1 | Mean amplitude (μV) and latency (ms) values of the P1, N1, and P2 components for upright and inverted photographs in the younger and older groups to the standard stimuli. P1 was measured at POz, N1 was measured at PO8 and P2 was measured at P7 (S.E.M. in parenthesis).

Photo	Younger group				Older group			
	Upright		Inverted		Upright		Inverted	
	Young	Old	Young	Old	Young	Old	Young	Old
Latency								
P1	96 (3.42)	91 (3.43)	91 (3.18)	94 (3.87)	83 (3.00)	79 (2.00)	80 (2.48)	81 (2.90)
N1	139 (4.40)	146 (4.66)	146 (5.34)	149 (4.21)	144 (7.41)	138 (6.84)	139 (6.37)	140 (6.51)
P2	213 (5.06)	207 (4.85)	213 (5.09)	217 (5.12)	247 (6.29)	243 (6.09)	250 (6.17)	244 (6.10)
Amplitude								
P1	5.2 (0.74)	4.8 (0.94)	5.1 (0.82)	5.0 (0.91)	3.7 (0.46)	3.7 (0.50)	3.3 (0.43)	3.4 (0.54)
N1	1.4 (0.55)	1.8 (0.60)	1.8 (0.63)	2.1 (0.63)	−0.7 (0.53)	−0.2 (0.90)	−0.4 (0.78)	−0.4 (0.80)
P2	4.2 (0.57)	3.5 (0.66)	3.9 (0.66)	4.0 (0.69)	1.7 (0,55)	2.0 (0.56)	1.7 (0.53)	1.3 (0.62)

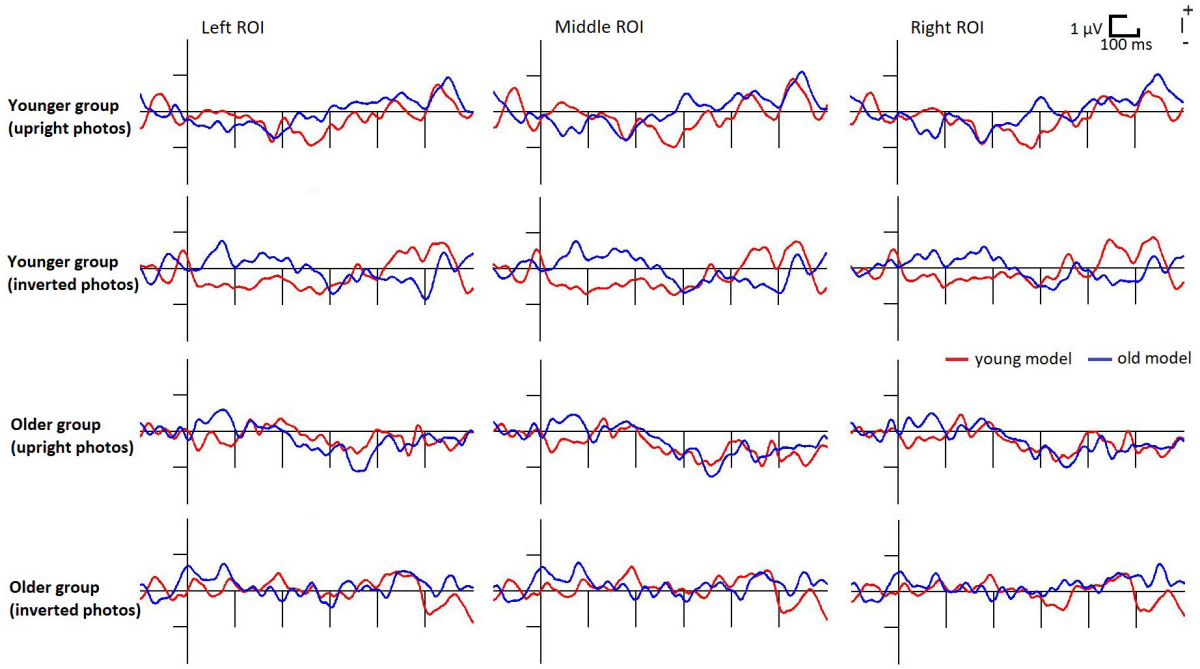

FIGURE 3 | Deviant *minus* standard difference potentials in the younger and older groups to upright photographs of young and old models. For illustrative reasons the posterior ROI is divided into left (PO7, PO3, O1) middle (POz, Oz) and right (PO8, PO4, O2) parts.

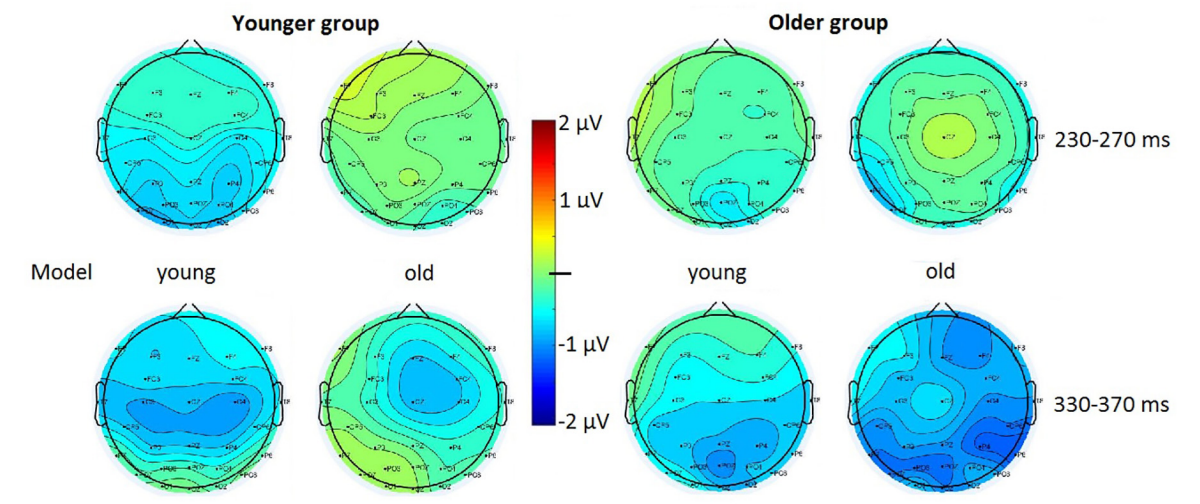

FIGURE 4 | Surface distribution of the deviant *minus* standard difference potentials in the 230–270 and 330–370 ms latency ranges in the younger and older groups to upright photographs of young and old models.

a group of older participants with deviant photographs of old and young models, and expected deviant *minus* standard event-related activity, the visual mismatch negativity (vMMN). As a specific expectation, we anticipated different effects to own-age vs. other-age deviancies.

Reliable deviant *minus* standard negativity (using traditional and Bayesian methods) appeared only in the older group to upright photographs of old models. This difference emerged in the 330–370 ms latency range, and it can be identified as vMMN. Although there was a tendency for similar posterior negativity to photographs of young models, the above results are a hint of the own-age effect, i.e., increased sensitivity to infrequent photographs of faces of age similar to that of the participants. Another tendency in the younger group for deviant *minus* standard difference at photographs of young models (in the 230–270 ms range) does not contradict the possibility of

TABLE 2 | Mean amplitude of the difference potentials (μV) in the younger and older groups in the 230–270 and 330–370 ms ranges to upright photographs of young and old models (S.E.M. in parenthesis).

	Younger group		Older group	
	Young model	Old model	Young model	Old model
230–270 ms	−0.83 (0.45)	−0.24 (0.29)	−0.36 (0.33)	−0.20 (0.37)
330–370 ms	−0.05 (0.67)	0.09 (0.46)	−0.70 (0.34)	−1.10 (0.31)

larger sensitivity to own-age faces. While the results in the older group corresponded to our expectation, as one of the reviewers noted, another way of thinking leads to different expectation. If participants have higher sensitivity to same-age faces, then it is likely that participants form a more robust standard representation for same-age standards, and as a result, different-age deviants elicit greater vMMN. However, we obtained no results in this direction.

Visual mismatch negativity to face-related stimuli have been reported in various post-stimulus latency ranges. The 320–370 ms range is relatively late, but it is within the range reported in previous studies (e.g., Susac et al., 2004, 2010; Gayle et al., 2012; Kimura, 2012; Vogel et al., 2015) and also within the vMMN range for other complex stimuli like right vs. left hands (Stefanics and Czigler, 2012). Due to the dependence of the position (upright vs. inverted) the effect seems to depend on holistic face processing, instead of the effect of low-level physical differences (e.g., Yin, 1969; Maurer et al., 2002; for review see Rossion, 2009). Our inverse control method, i.e., the comparison of faces of identical age in the role of deviant and standard, underscores this statement.

Using a similar method (four photographs in eccentric positions) Stefanics et al. (2012) obtained much more robust vMMN to emotional deviancy, showing that facial age difference is a less salient characteristic than facial emotion. Being an unexpected result, the sensitivity to deviant photographs in the older group deserves discussion. As a specificity of the present design, four photographs were presented at eccentric locations, and the task in the center of the screen required continuous fixation to the task field. This arrangement required stronger focal attention than other studies in the field of age-related vMMN differences. As a possibility, younger participants concentrated more effectively on the task-field, e.g., they were more efficient in inhibiting the task-irrelevant part of the visual field. On the one hand, this explanation corresponds to the compromised inhibitory processes in some fields of aging research (e.g., Hasher and Zacks, 1988), the larger effect of age-related distraction (e.g., Karthaus et al., 2020), and increased ERP effects of irrelevant stimuli (Kojouharova et al., 2020). On the other hand, spatial attention is relatively preserved in the elderly (for a discussion see Lawrence et al., 2018), and as an example, in the flanker task there is no robust age-related difference (De Bruin and Della Sala, 2018). Furthermore, less effective processing of events appearing at parafoveal regions in older participants is also against the above possibility. As an example, younger participants outperformed older participants in detection of motion direction at parafoveal areas (Park et al., 2020). However, according to some results, irrelevant stimuli outside the focus of attention have larger effects in older adults (Porter et al., 2012; Tsvetanov et al., 2013). As for the vMMN research, in a recent study with younger participants File and Czigler (2019) obtained considerable spatial attention effects on vMMN. In the only study with complex stimuli (meaningful vs. meaningless letter strings; Gaál et al., 2017) the advantage of older participants was due to the longer aftereffect of stimulus appearance. Longer aftereffect may facilitate the more elaborate processing of stimuli. The relatively long vMMN latency supports this assumption. The less efficient filtering of the task-irrelevant stimuli together with the possible advantage in stimulus coding seems to be a favorable condition for our older group for the emergence of vMMN.

As the more specific aim of the present study, the investigation of own-age bias (OAB) in the field of automatic change detection, in the older group we obtained positive results. In this group the magnitude of the reliable vMMN to photographs of old models was similar to the vMMN amplitude in younger groups to emotional face deviants (e.g., Chang et al., 2010; Wang et al., 2014; Sel et al., 2016). As an apparent controversy, in some studies OAB was less pronounced or even absent in older participants (e.g., Harrison and Hole, 2009; Wiese et al., 2012). However, our automatic change-detection procedure is different from the recognition paradigm of OAB studies, apart from a methodological similarity of a certain task that required task-irrelevant coding of facial age (Randall et al., 2012; Neumann et al., 2014). However, even in these studies participants had to attend to other aspects of the faces (e.g., gender, aesthetic value). As results on object-related attention (Duncan, 1984; Scholl, 2001) indicate, even if the ages of the models were task-irrelevant, faces were not "unattended." On the contrary, in the present study the faces were outside the focus of attention, therefore the faces were not only task-irrelevant, but they were also "unattended." As the results of the present study show, in the age group with relevant vMMN (i.e., the older group), photographs of their own age were automatically registered as deviant stimuli among the photographs of models of other ages. This way our results show that OAB has a component of automatic sensitivity. On a theoretical (but speculative) level, vMMN is considered as an index of predictive coding mechanism (Stefanics et al., 2014). According to this account, the representation of incoming stimuli is compared to the model of expected events. In case of mismatch, an error signal is compared to gradually updated models throughout a cascade of processes. As Hugenberg et al. (2010) proposed, other-age photographs are processed only at categorical level, whereas for own-age photographs there is an attempt at processing at individual level. The attempt at processing at a deeper level may contribute to a larger discrepancy (surprise) effect and accordingly, to a stronger activity of the match-mismatch mechanism.

Besides the deviant-related ERP differences, we obtained robust age-related differences in the exogenous ERP activities (P1, N1, and P2), i.e., earlier P1 in the older group, and larger and earlier P2 in the younger group. In previous studies the results on age-related differences on P1 are equivocal. Čeponiené et al. (2008) obtained smaller visual P1 in the older group, and

this difference was especially large over the occipital regions. In contrast, after controlling for visual acuity (similar to that in the present study), Daffner et al. (2013) obtained larger P1 in older participants. Our results on P1 can be interpreted as preserved early processing in the older group. It is important to remind that the stimuli of the present study were human faces. P1 sensitivity to faces, especially to non-cropped photographs has been reported earlier (e.g., Dering et al., 2011). However, unlike in some studies (e.g., Pesciarelli et al., 2011), in the present study we found no P1 amplitude difference between the upright and inverted faces, showing that in the present study P1 had no strong connection to a face-specific processing stage. Facial stimuli typically elicit the posterior N170 component (e.g., Bentin et al., 1996). The N1 component of the present study was earlier than the usual latency of N170. Furthermore (like in case of P1), we obtained no N1 difference between the upright and inverted faces, e.g., longer N170 latency to inverted faces (Rossion et al., 2000). In an earlier study with similar stimulus presentation (four photographs at the four corners of the visual field) we got characteristic N170 components (Stefanics et al., 2012). As a marked difference between the studies, in the Stefanics et al. (2012) study the target-stimuli appeared intermittently as a change of the fixation cross, whereas the tracking task of the present study required continuous attentive processing. The strict attentional control might diminish the recordable negativity within the 100–200 ms latency range.

In the younger group N1 superimposed on a positivity peaked in the usual P2 range. The function of the processes underlying P2 is unclear, but their role is implicated at different stages of face processing (Itier and Taylor, 2004; Boutsen et al., 2006). Amplitude changes of P2 (P200) appeared in studies that investigated face-related decisions. Wiese et al. (2008) obtained amplitude decrease for old faces at older participants, and they interpreted the difference as deeper or more extensive processing at stimulus ambiguity. Faerber et al. (2015) obtained P2 (P200) amplitude reduction as a priming effect in younger participants, supporting this interpretation. In a passive task, i.e., without intentional decision demand, we obtained no such amplitude difference.

In summary, sequences of photographs showing models of particular age acquire memory representation for this regularity, even if the photographs are irrelevant (unattended). Photographs violating this regularity (deviants) elicit the vMMN component. This process is more effective in older adults, especially for deviant photographs of old models. Exogenous visual components are markedly different in younger and older groups, but little is known about the functional aspects of these differences.

DATA AVAILABILITY STATEMENT

The original contributions presented in the study are included in the article/**Supplementary Material**, further inquiries can be directed to the corresponding author/s.

ETHICS STATEMENT

The studies involving human participants were reviewed and approved by United Ethical Review Committee for Research in Psychology (EPKEB). The patients/participants provided their written informed consent to participate in this study.

AUTHOR CONTRIBUTIONS

PC, IC, and ZG designed the study. PC, BN, and ZG collected the data. PC, BP, PK, KS, and IC analyzed the data. PC, PK, and IC wrote the manuscript. All authors contributed to the article and approved the submitted version.

FUNDING

This study was supported by the National Research, Development and Innovation Office (Hungary), grant number: 119587.

ACKNOWLEDGMENTS

We thank Zsuzsanna D'Albini for her technical help.

SUPPLEMENTARY MATERIAL

The Supplementary Material for this article can be found online at: https://www.frontiersin.org/articles/10.3389/fnhum.2021.707702/full#supplementary-material

REFERENCES

Astikainen, P., and Heitanen, J. K. (2009). Event-related potentials to irrelevant changes in facial expressions. *Behav. Brain Funct.* 5:30. doi: 10.1186/1744-9081-5-30

Bartlett, J. C., and Leslie, J. E. (1986). Aging and memory for faces versus single view of faces. *Mem. Cognit.* 14, 371–381. doi: 10.3758/bf03197012

Bentin, S., Allison, T., Puce, A., Perez, E., and McCarthy, G. (1996). Electrophysiological studies of face perception in humans. *J. Cogn. Neurosci.* 8, 551–565. doi: 10.1162/jocn.1996.8.6.551

Boutsen, L., Humphreys, G. W., Praamstra, P., and Warbrick, T. (2006). Comparing neural correlates of configural processing in faces and objects: an ERP study of the Thacher illusion. *Neuroimage* 32, 352–367. doi: 10.1016/j.neuroimage.2006.03.023

Čeponienė, R., Westerfield, M., Torki, M., and Townsend, J. (2008). Modality-specificity of sensory aging in vision and audition. Evidence from event-related potential. *Brain Res.* 1215, 53–68. doi: 10.1016/j.brainres.2008.02.010

Chang, Y., Xu, J., Shi, B. N., Zhang, B., and Zhao, L. (2010). Dysfunction of processing task-irrelevant emotional faces in major depressive disorder patients revealed by expression-related visual MMN. *Neurosci. Lett.* 472, 33–77. doi: 10.1016/j.neulet.2010.01.050

Daffner, K. R., Haring, A. E., Alpert, B. R., Zhuravleva, T. Y., Mott, K. K., and Holcomb, P. J. (2013). The impact of visual acuity on age-related differences in neural markers of early visual processing. *Neuroimage* 15, 127–136. doi: 10.1016/j.neuroimage.2012.10.089

De Bruin, A., and Della Sala, S. (2018). Effects of age on inhibitory control are affected by task-specific features. *Q. J. Exp. Psychol.* 71, 1219–1233. doi: 10.1080/17470218.2017.1311352

Dering, B., Martin, C. D., Moro, S., Pegna, A. J., and Thierry, G. (2011). Face-sensitive processes one hundred millisecond after picture onset. *Front. Hum. Neurosci.* 15:93. doi: 10.3389/fnhum.2011.00093

Duncan, J. (1984). Selective attention and the organization of visual information. *J. Exp. Psychol. Gen.* 113, 501–517. doi: 10.1037/0096-3445.113.4.501

Durant, S., Sulykos, I., and Czigler, I. (2017). Automatic deviation of orientation variance. *Neurosci. Lett.* 658, 43–47. doi: 10.1016/j.neulet.2017.08.027

Ebner, N. C., He, Y., Fichtenholtz, H. M., McCarthy, G., and Johnson, M. K. (2011). Electrophysiological correlates of processing faces of younger and older individuals. *Soc. Cogn. Affect. Neurosci.* 6, 526–535. doi: 10.1093/scan/nsq074

Faerber, S. J., Kaufmann, J. M., and Schweinberger, S. R. (2015). Early temporal negativity is sensitive to perceived (rather than physical) facial identity. *Neuropsychologia* 75, 132–142. doi: 10.1016/j.neuropsychologia.2015.05.023

File, D., and Czigler, I. (2019). Automatic detection of violations of statistical regularities in the periphery is affected by the focus of spatial attention: a visual mismatch negativity study. *Eur. J. Neurosci.* 49, 1348–1356.

Gaál, Z. A., Bodnár, F., and Czigler, I. (2017). When elderly outperform young adults – integration in vision revealed by the visual mismatch negativity event-related component. *Front. Aging Neurosci.* 9:5. doi: 10.3389/fnagi.2017.00015

Gayle, L. C., Gal, D. E., and Kieffaber, P. D. (2012). Measuring affective reactivity in individuals with autism spectrum personality traits using the visual mismatch negativity event-related brain potential. *Front. Hum. Neurosci.* 6:334. doi: 10.3389/fnhum.2012.00334

Harrison, V., and Hole, G. (2009). Evidence for a contact.based explanation of the own-age bias in face recognition. *Psychon. Bull. Rev.* 16, 264–296. doi: 10.3758/pbr.16.2.264

Hasher, L., and Zacks, R. T. (1988). "Working memory, comprehension, and aging: a review and a new view," in *The Psychology of Learning and Motivation*, ed. G. Bower (San Diego, CA: Academic Press), 193–225. doi: 10.1016/s0079-7421(08)60041-9

He, Y., Ebner, N., and Johnson, M. K. (2011). What predicts the own-age bias in in face recognition? *Soc. Cogn.* 29, 97–109. doi: 10.1521/soco.2011.29.1.97

Hugenberg, K., Yiung, S. G., Bernstein, M. J., and Sacco, D. F. (2010). The organization-individualization model: an integrative accoubt of the other-race recognition deficit. *Psychol. Rev.* 117, 1168–1187. doi: 10.1037/a0020463

Itier, R. J., and Taylor, M. J. (2004). N170 or N1? Spatiotemporal differences between object and face processing using ERPs. *Cereb. Cortex* 14, 132–142. doi: 10.1093/cercor/bhg111

JASP Team (2018). *JASP (Version 0.9.2) [Computer Software]*.

Karthaus, M., Wascher, E., Falkenstein, M., and Getzmann, S. (2020). The ability of young, middle-aged and older drivers to inhibit visual and auditory distraction in a driving simulator task. *Transp. Res. F* 68, 272–284. doi: 10.1016/j.trf.2019.11.007

Kecskés-Kovács, K., Sulykos, I., and Czigler, I. (2013b). Visual mismatch negativity is sensitive to symmetry as a perceptual category. *Eur. J. Neurosci.* 37, 662–667. doi: 10.1111/ejn.12061

Kecskés-Kovács, K., Sulykos, I., and Czigler, I. (2013a). Is it a face of a woman or a man? Visual mismatch negativity is sensitive to gender category. *Front. Hum. Neurosci.* 7:532. doi: 10.3389/fnhum.2013.00532

Kimura, M. (2012). Visual mismatch negativity and unintentional temporal context-based prediction in vision. *Int. J. Psychophysiol.* 83, 144–155. doi: 10.1016/j.ijpsycho.2011.11.010

Kimura, M., Schröger, E., and Czigler, I. (2011). Visual mismatch negativity and its importance in visual cognitive sciences. *Neuroreport* 22, 669–673. doi: 10.1097/wnr.0b013e32834973ba

Kojouharova, P., Gaál, Z. A., Nagy, B., and Czigler, I. (2020). Age effects on distraction in a visual task requiring fast reactions: an event-related potential study. *Front. Aging Neurosci.* 7:596047. doi: 10.3389/fnagi.2020.596047

Kovarski, K., Latinus, M., Charpentier, J., Clery, H., Roux, S., Houy-Durand, E., et al. (2017). Expression related vMMN: disentangling emotional from neutral change. *Front. Hum. Neurosci.* 11:18. doi: 10.3389/fnhum.2017.00018

Lawrence, R. K., Edwards, M., and Goodhew, S. C. (2018). Changes in the spatial spread of attention with ageing. *Acta Psychol.* 188, 188–199. doi: 10.1016/j.actpsy.2018.06.009

Li, X., Lu, Y., Sun, G., Gao, L., and Zhao, L. (2012). Visual mismatch negativity elicited by facial expressions: new evidence from the equiprobable paradigm. *Behav. Brain Funct.* 8:7. doi: 10.1186/1744-9081-8-7

Lorenzo-López, L., Amenedo, E., Pazo-Alvarez, P., and Cadaveira, F. (2004). Pre-attentive detection of motion direction changes in normal aging. *Neuroreport* 15, 2633–2636. doi: 10.1097/00001756-200412030-00015

Maurer, D., Grand, I. R., and Mondloch, C. J. (2002). The many faces of configural processing. *Trends Cogn. Sci.* 6, 255–260. doi: 10.1016/s1364-6613(02)01903-4

Minear, M., and Park, D. C. (2004). A lifespan database of adult facial stimuli. *Behav. Res. Methods Instrum. Comput.* 36, 630–633. doi: 10.3758/bf03206543

Mukudi, P. B. L., and Hills, P. J. (2019). The combined influence of the own-age, -genfer, and –ethnicity bias on face recognition. *Acta Psychol.* 194, 1–6. doi: 10.1016/j.actpsy.2019.01.009

Neumann, M. F., End, E., Luttmann, S., Schweinberger, S. R., and Wiese, H. (2014). The own-age bias in face memory is unrelated to differences in attention – Evidence from event-related potentials. *Cogn. Affect. Behav. Neurosci.* 15, 180–194. doi: 10.3758/s13415-014-0306-7

Park, S., Nguyen, B. N., and McKendrick, A. M. (2020). Ageing elevates peripheral spatial suppression of motion regardless of divided attention. *Ophthalmic Physiol. Opt.* 40, 117–127. doi: 10.1111/opo.12674

Pesciarelli, F., Sarlo, M., and Leo, I. (2011). The time course of implicit processing of facial features: an event-related potential study. *Neuropsychologia* 49, 1154–1161. doi: 10.1016/j.neuropsychologia.2011.02.003

Porter, G., Wright, A., Tales, A., and Gilchrist, I. D. (2012). Stimulus onsets and distraction in younger and older adults. *Psychol. Aging* 27, 1111–1119. doi: 10.1037/a0028486

Randall, J. L., Tabernik, H. E., Aguilra, A. M., Anastasi, J. S., and Valk, K. V. (2012). Effects of encoding task on the own-age face recognition bias. *J. Gen. Psychol.* 139, 55–67. doi: 10.1080/00221309.2012.657266

Rhodes, M. G., and Anastasi, J. S. (2012). The own-age bias in face recognition: a meta-analytic and theoretical review. *Psychol. Bull.* 138, 146–174. doi: 10.1037/a0025750

Rossion, B. (2009). Distinguishing the cause and consequence of face inversion: the perceptual field hypothesis. *Acta Psychol. (Amst.)* 132, 300–312. doi: 10.1016/j.actpsy.2009.08.002 Epub 2009 Sep 10.

Rossion, B., Gauthier, I., Tarr, M. J., Despland, P., Bruyer, R., Linotte, S., et al. (2000). The N170 occipito-temporal component is delayed and enhanced to inverted faces but not to inverted objects: an electrophysiological account of face-specific processes in the human brain. *Neuroreport* 11, 69–74. doi: 10.1097/00001756-200001170-00014

Rózsa, S., Kő, N., Kuncz, E., Mészáros, A., and Mlinkó, R. (2010). *WAIS-IV. Wechsler Adult Intelligence Scale – Fourth Edition. Tesztfelvételi és pontozási kézikönyv. Magyar adaptáció: OS-Hungary Tesztfejlesztő Kft*. Available online at: http://www.oshungary.hu/hu/tesztkatalogus-oshungary/wais-iv/

Scholl, B. J. (2001). Objects and attention: the state of the art. *Cognition* 80, 1–46. doi: 10.1016/s0010-0277(00)00152-9

Sel, A., Harding, R., and Tsakiris, M. (2016). Elecrophysiological correlates of self-specific prediction error int he human brain. *Neuroimage* 125, 13–24. doi: 10.1016/j.neuroimage.2015.09.064

Sporer, S. L. (2001). Recognizing faces of other ethnic groups: an integration of theories. *Psychol. Public Policy Law* 7, 36–97. doi: 10.1037/1076-8971.7.1.36

Stefanics, G., Astikainen, P., and Czigler, I. (2015). Visual mismatch negativity (vMMN): a prediction error signal in the visual modality. *Front. Hum. Neurosci.* 8:1074. doi: 10.3389/fnhum.2014.01074

Stefanics, G., Csukly, G., Komlosi, S., Czobor, P., and Czigler, I. (2012). Processing of unattended facial emotions: a visual mismatch negativity study. *Neuroimage* 59, 3042–3049. doi: 10.1016/j.neuroimage.2011.10.041

Stefanics, G., and Czigler, I. (2012). Automatic prediction error responses to hands with unexpected laterality: an electrophysiological study. *Neuroimage* 63, 253–261. doi: 10.1016/j.neuroimage.2012.06.068

Stefanics, G., Kremlacek, J., and Czigler, I. (2014). Visual mismatch negativity: a predictive coding view. *Front. Hum. Neurosci.* 8:666. doi: 10.3389/fnhum.2014.00666

Stothart, G., Tales, A., and Kazanina, N. (2013). Evoked po¬tentials reveal age-related compensatory mechanisms in early visual processing. *Neurobiol. Aging* 34, 1302–1308. doi: 10.1016/j.neurobiolaging.2012.08.012

Sulykos, I., Gaál, Z. A., and Czigler, I. (2017). Visual mismatch negativity to vanishing parts of objects in younger and older adults. *PLoS One* 12:e0188929. doi: 10.1371/journal.pone.0188929

Sulykos, I., Gaál, Z. A., and Czigler, I. (2018). Automatic change detection in older and younger women: a visual mismatch negativity study. *Gerontology* 64, 318–325. doi: 10.1159/000488588

Susac, A., Ilmoniemi, R. J., Pihko, E., Ranken, D., and Supek, S. (2010). Early cortical responses are sensitive to changes in face stimuli. *Brain Res.* 1346, 155–164. doi: 10.1016/j.brainres.2010.05.049

Susac, A., Ilmoniemi, R. J., Pihko, E., and Supek, S. (2004). Neurodynamic studies on emotional and inverted faces in an oddball paradigm. *Brain Topogr.* 16, 265–268. doi: 10.1023/b:brat.0000032863.39907.cb

Tales, A., Troscianko, T., Wilcock, G. K., Newton, P., and Butler, S. R. (2002). Age-related changes in the preattentional detection of visual change. *Neuroreport* 13, 969–972. doi: 10.1097/00001756-200205240-00014

Tsvetanov, K. A., Mevorach, C., Allen, H., and Humphreys, G. W. (2013). Age-related differences in selection by visual saliency. *Atten. Percept. Psychophys.* 75, 1382–1394. doi: 10.3758/s13414-013-0499-9

Valentine, T. (1991). A unified account of the effects of distinctiveness, inversion, and race in face recognition. *Q. J. Exp. Psychol.* 43A, 161–204. doi: 10.1080/14640749108400966

Vogel, B. O., Shen, C., and Neuhaus, A. H. (2015). Emotional context facilitates cortical prediction error responses. *Hum. Brain Mapp.* 36, 3641–3652. doi: 10.1002/hbm.22868

Wang, W., Miao, D., and Zhao, L. (2014). Automatic detection of orientation change of faces versus non-face objects: a visual MMN study. *Biol. Psychol.* 100, 71–78. doi: 10.1016/j.biopsycho.2014.05.004

Wiese, H., Comes, J., and Schweinberger, S. R. (2012). Daily-life contact affects the own-age bias and neural correlates of face memory in elderly participants. *Neuropsychologia* 50, 3496–3508. doi: 10.1016/j.neuropsychologia.2012.09.022

Wiese, H., Komes, J., and Schweinberger, S. R. (2013). Ageing faces in aging mind: a review ont he own-age bias in face recognition. *Vis. Cogn.* 21, 1337–1663. doi: 10.1080/13506285.2013.823139

Wiese, H., Schweinberger, S. R., and Hansen, K. (2008). The age of the beholder: ERP evidence of an own-age bias in face memory. *Neuropsychologia* 46, 2973–2985. doi: 10.1016/j.neuropsychologia.2008.06.007

Yin, R. K. (1969). Looking at upside-down faces. *J. Exp. Psychol.* 81, 141–145. doi: 10.1037/h0027474

Conflict of Interest: The authors declare that the research was conducted in the absence of any commercial or financial relationships that could be construed as a potential conflict of interest.

The reviewer MZ declared a shared affiliation, with no collaboration, with several of the authors (PC and BN) to the handling editor at the time of the review.

frontiers in Human Neuroscience

ORIGINAL RESEARCH
published: 25 August 2021
doi: 10.3389/fnhum.2021.730962

Prediction, Suppression of Visual Response, and Modulation of Visual Perception: Insights From Visual Evoked Potentials and Representational Momentum

*Motohiro Kimura**

Department of Information Technology and Human Factors, National Institute of Advanced Industrial Science and Technology (AIST), Tsukuba, Japan

When a visual object changes its position along with certain sequential regularities, the visual system rapidly and automatically forms a prediction regarding the future position of the object based on the regularities. Such prediction can drastically alter visual perception. A phenomenon called representational momentum (RM: a predictive displacement of the perceived final position of a visual object along its recent regular pattern) has provided extensive evidence for the predictive modulation of visual perception. The purpose of the present study was to identify neural effects that could explain individual differences in the strength of the predictive modulation of visual perception as measured by RM. For this purpose, in two experiments with a conventional RM paradigm where a bar was discretely presented in a regular rotation manner (with a step of 18° in Experiment 1 and a step of 20° in Experiment 2), visual evoked potentials (VEPs) in response to the regularly rotated bar were measured, and correlations between the magnitudes of RM and VEPs were examined. The results showed that the magnitudes of RM and central P2 were negatively correlated, consistently in both experiments; participants who showed a smaller central P2 tended to exhibit greater RM. Together with a previous proposal that central P2 would represent delayed reactivation of lower visual areas around the striate and prestriate cortices via reentrant feedback projections from higher areas, the present results suggest that greater suppression of delayed reactivation of lower visual areas (as indicated by smaller central P2) may underlie stronger predictive modulation of visual perception (as indicated by greater RM).

Keywords: visual evoked potentials (VEPs), representational momentum, visual perception, prediction suppression, central P2, individual difference

OPEN ACCESS

Edited by:
István Winkler,
Hungarian Academy of Sciences (MTA), Hungary

Reviewed by:
István Czigler,
Hungarian Academy of Sciences (MTA), Hungary
Kairi Kreegipuu,
University of Tartu, Estonia

***Correspondence:**
Motohiro Kimura
m.kimura@aist.go.jp

Specialty section:
This article was submitted to Cognitive Neuroscience, a section of the journal Frontiers in Human Neuroscience

Received: *25 June 2021*
Accepted: *27 July 2021*
Published: *25 August 2021*

Citation:
Kimura M (2021) Prediction, Suppression of Visual Response, and Modulation of Visual Perception: Insights From Visual Evoked Potentials and Representational Momentum. Front. Hum. Neurosci. 15:730962. doi: 10.3389/fnhum.2021.730962

INTRODUCTION

Visual objects in the environment (e.g., a flying ball) dynamically change their positions. However, when an object's image hits an observer's eyes, the observer cannot perceive the image instantaneously; it takes about a tenth of a second after the image hits the eyes. Therefore, by the time the observer has perceived the object at a certain position, its actual position has already

changed. Despite this fundamental problem, an observer can effortlessly interact with such objects in real time (e.g., by catching a flying ball). A possible solution to the problem of how the visual system can bridge the gap between perception and action is to form a prediction about the future position of the object, based on sequential regularities in the recent past (i.e., recent trajectory of the ball) (Mackay, 1958; Freyd, 1992; Nijhawan, 1994; Hubbard, 1995, 2005).

A phenomenon known as representational momentum (RM: Freyd and Finke, 1984, 1985) provides strong evidence for the existence of such prediction based on sequential regularities in the recent past and demonstrates that visual perception can indeed be strongly modulated by the prediction. RM denotes predictive displacement of the perceived final position of a changing object. In a conventional RM paradigm developed by Freyd and Finke (1984, 1985), participants observe a stimulus sequence where a bar is discretely presented in a regular rotation manner (denoted "inducing stimuli": e.g., 10°/30°/50°). Participants are required to compare the orientation of the final inducing stimulus (i.e., 50°) to that of a subsequent bar (denoted "probe"). It has been shown that participants report "same" with higher probability when the probe is slightly shifted forward along the regular direction of rotation (e.g., 52°) than when it is truly the same (50°) or shifted backward (e.g., 48°) (Freyd and Finke, 1985). RM is thought to reflect predictive displacement of the sensory representation of an object along its recent change pattern (Freyd, 1992; Hubbard, 1995, 2005). RM can be observed based on sequential regularities in position or orientation but also in other visual features (Kelly and Freyd, 1987; Hayes and Freyd, 2002) and sequential regularities in auditory features (Freyd et al., 1990), suggesting that the predictive displacement of sensory representation would be a general phenomenon across visual features and sensory modalities. Also, RM can occur without the observer paying much attention to the object (Hayes and Freyd, 2002; for related findings, see Finke and Freyd, 1985), suggesting that the predictive displacement of sensory representation can occur in an automatic and obligatory manner.

Representational momentum is a robust phenomenon that is stably observed across participants (Freyd and Finke, 1985). However, there seem to be large individual differences in the magnitude of RM (Finke et al., 1986; Verfaillie and d'Ydewalle, 1991), which leads to the assumption that there may be large individual differences in the strength of the predictive modulation of visual perception. The purpose of the present study was to identify neural effects that could explain individual differences in the strength of predictive modulation of visual perception as measured by RM. For this purpose, the present study measured visual evoked potentials (VEPs) with a conventional RM paradigm (Freyd and Finke, 1984, 1985). In two experiments, a bar was discretely presented in a regular rotation manner (i.e., inducing stimuli); with a step of 18° in Experiment 1 (**Figure 1**) and 20° in Experiment 2 (**Figure 2**). Participants were required to compare the orientation of the final (i.e., tenth) inducing stimulus to that of a subsequent probe. VEPs in response to inducing stimuli were measured, and correlations were examined between the magnitudes of RM and VEPs: (1) occipito-temporal P1 at around 110 ms, (2) frontal N1 at around 140 ms, (3) occipito-temporal N1 at around 170 ms, and (4) central P2 at around 200 ms after stimulus onset (Clark et al., 1995; Di Russo et al., 2002; Capilla et al., 2016).[1]

No previous study has examined the relationship between the magnitudes of RM and VEPs in response to inducing stimuli. However, based on a previous VEP finding on automatic prediction based on sequential regularities (Kimura and Takeda, 2015), the neural effect that is most likely to correlate with RM is central P2. To identify neural effects that specifically emerge when the current position of an object successfully matches the predicted position of the object based on sequential regularities, Kimura and Takeda (2015) compared VEPs elicited by bars that were discretely presented in a regular rotation manner (e.g., 10°/30°/50°/70°/90°. . ., where the upcoming orientation of the bar could be predicted, as in the RM paradigm) to VEPs elicited by the same bars that were discretely presented in a random manner (e.g., 70°/10°/30°/90°/50°. . ., where a prediction of the upcoming orientation of the bar could not be formed). It was found that central P2 at around 200 ms after stimulus onset was selectively suppressed when the upcoming orientation could be predicted compared to when a prediction could not be formed. Contrary to central P2, no difference in this comparison was found for occipito-temporal P1 at around 110 ms, frontal N1 at around 140 ms, and occipito-temporal N1 at around 170 ms; instead, occipito-temporal P1 and N1 (but not frontal N1) were found to be suppressed only when bars were presented in a repetitive manner (e.g., 10°/10°/10°/10°/10°. . .) compared to when bars were presented in a random manner (e.g., 70°/10°/30°/90°/50°. . .), suggesting that these P1 and N1 effects represent repetition suppression attributable to stimulus-specific adaptation or neural refractoriness rather than prediction suppression (cf. Todorovic and de Lange, 2012). Therefore, at least when a regularly rotating bar was used as stimuli, the suppression of central P2 is thought to be a unique neural effect that could emerge when the current position of a visual object successfully matches the predicted position of the object based on sequential regularities.

The neural sources of central P2 at around 200 ms were previously localized in lower visual areas around the striate and prestriate cortices (Capilla et al., 2016); although the neural

[1]In general, VEPs time-locked to visual stimulus onset are comprised of (1) occipital C1 that peaks at around 60 ms, (2) occipito-temporal P1 that peaks at around 110 ms, (3) frontal N1 that peaks at around 140 ms, (4) occipito-temporal N1 that peaks at around 170 ms, and (5) central P2 that peaks at around 200 ms after stimulus onset (Clark et al., 1995; Di Russo et al., 2002; Capilla et al., 2016). The main neural sources of these VEPs were localized in the visual areas and the related areas belonging to the dorsal and ventral processing streams: (1) C1 in the striate cortex (i.e., V1), (2) P1 in the dorsal and ventral extrastriate cortices (e.g., V3 and V4), (3) frontal N1 in the parieto-occipital cortex, (4) occipito-temporal N1 in the dorsal extrastriate cortex (e.g., V3), and (5) P2 in the striate and prestriate cortices (i.e., V1 and V2) (Clark et al., 1995; Di Russo et al., 2002, 2003, 2008; Capilla et al., 2016). Although tentative, occipital C1, occipito-temporal P1, and frontal N1 may mainly represent early bottom-up activation, whereas occipito-temporal N1 and central P2 may mainly represent delayed reactivation of visual areas via reentrant feedback projections from higher areas (Di Russo et al., 2003, 2008; Capilla et al., 2016; for related findings, see Olson et al., 2001; Noesselt et al., 2002). Note that occipital C1 was not analyzed in the present study, since centrally presented visual stimuli (see **Figures 1**, **2**) were not suitable to observe C1; retinotopically specific single-quadrant stimulation is required to observe C1 (Clark et al., 1995).

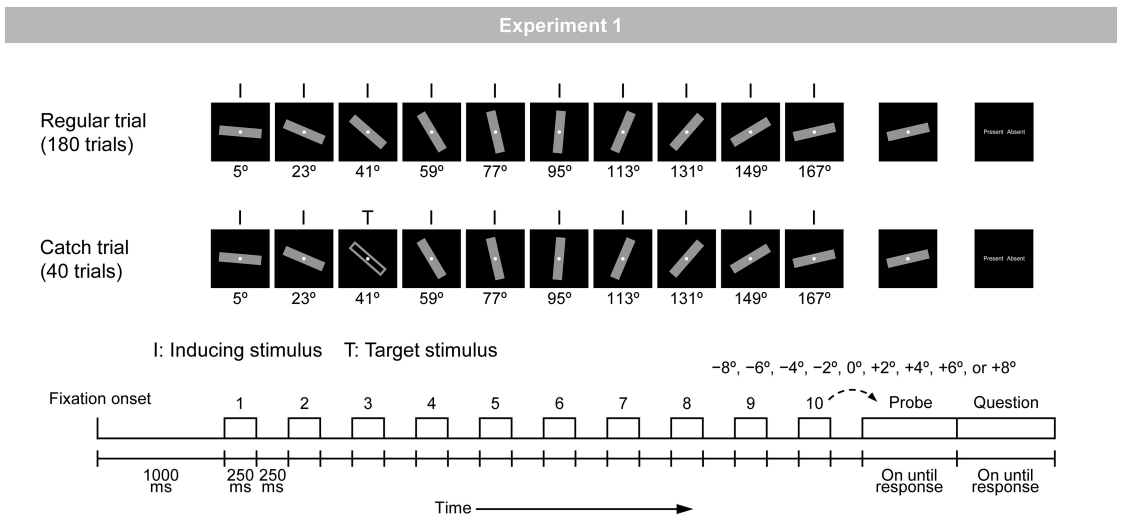

FIGURE 1 | Schematic illustration of the regular and catch trials in Experiment 1. A bar was rotated regularly with a step of 18°.

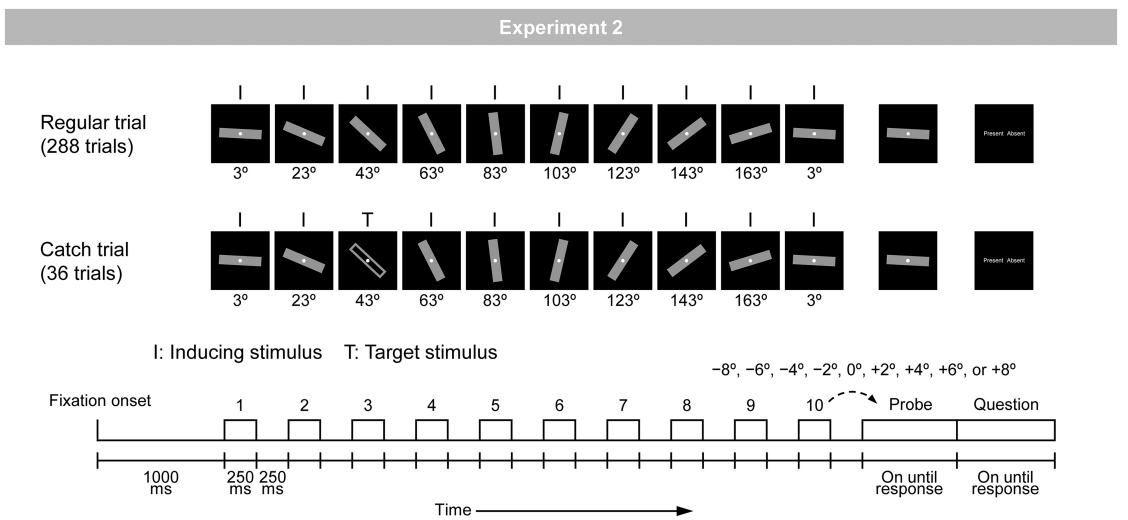

FIGURE 2 | Schematic illustration of the regular and catch trials in Experiment 2. A bar was rotated regularly with a step of 20°.

sources of P2 are still less well understood compared to those of other VEPs, this finding appears to be consistent with a non-human neuroimaging finding suggesting the involvement of lower visual areas (i.e., monkey V2) in the P2 homolog (Metha et al., 2000). The involvement of lower visual areas in P2 is interesting, since the neural sources of temporally earlier VEPs such as P1 at around 110 ms were localized in higher visual areas including the dorsal and ventral extrastriate cortices (Clark et al., 1995; Di Russo et al., 2002). To explain this paradox, P2 has proposed to be a sign of delayed reactivation of lower visual areas via reentrant feedback projections from higher areas (Di Russo et al., 2003, 2008). Based on these previous findings, prediction suppression of central P2 (Kimura and Takeda, 2015) is best assumed to represent reduced delayed reactivation of lower visual areas around the striate and prestriate cortices. This assumption is consistent with human neuroimaging findings that automatic prediction based on sequential regularities resulted in suppressed activation in lower visual areas including the striate cortex, whereas activation in higher visual areas including the dorsal extrastriate cortex was not affected (Alink et al., 2010) and non-human neuroimaging findings that automatic prediction based on sequential regularities resulted in markedly suppressed activation in lower visual areas (i.e., monkey V2) rather than higher visual areas (Vergnieux and Vogels, 2020; see also Kaposvari et al., 2018).

Taken together, the present study expected that participants who exhibited greater RM may show smaller central P2 in response to inducing stimuli; in other words, the magnitudes of RM and central P2 would show a negative correlation.

EXPERIMENT 1

The experiment reported here was conducted with multiple purposes, and included trials that were not related to the present purpose (i.e., irregular trials; see Materials and Methods). Data in the irregular trials have already been reported in another paper (Kimura, 2018). Data reported in this paper have not been reported elsewhere.

Materials and Methods

Participants

Thirty-five healthy adults (32 males, 3 females; mean age 22.5 years; age range 19–32 years) participated in this experiment. All participants had normal or corrected-to-normal vision. Thirty-three participants were right-handed and two were left-handed. Written informed consent was obtained from each participant after the nature of the study had been explained. The experiment was approved by the Safety and Ethics committee of the National Institute of Advanced Industrial Science and Technology (AIST).

Stimuli and Procedure

The experiment was controlled by MATLAB (MathWorks) on Mac OSX with the Psychophysics Toolbox (Brainard, 1997; Pelli, 1997). All visual stimuli were presented on a 17-inch cathode ray tube display (Sony, Trinitron Multiscan G220) at a viewing distance of about 57 cm.

The experiment consisted of three types of trials (i.e., regular, irregular, and catch trials). **Figure 1** shows an illustration of the regular and catch trials; the irregular trials are not related to the present purpose and therefore are not illustrated in **Figure 1**. The regular trial was included to measure RM and the catch trial was included to ensure that participants kept observing the stimulus sequence. Each trial began with the onset of a gray fixation circle (42.3 cd/m^2; diameter of 0.3°), which was continuously visible on the display. At 1000 ms after fixation onset, a stimulus sequence consisting of 10 presentations of a bar appeared. In the regular trial, a gray-filled bar (9.2 cd/m^2; width of 0.9° × height of 5.7°) was rotated regularly with a step of 18° (i.e., inducing stimuli). In the catch trial, a gray-filled bar was rotated regularly, but at any of the 10 positions, it was replaced with a gray-unfilled bar (i.e., target stimuli). In all trials, each stimulus was presented for 250 ms and the inter-stimulus interval, where only the fixation circle was presented, was 250 ms. Note that 10 presentations of inducing stimuli would not necessarily be needed to obtain RM, given that three, four, or at most five presentations of inducing stimuli are common in RM studies. In the present study, 10 presentations were adopted to ensure that prediction had been fully stabilized by the time probe was presented.

This stimulus sequence was followed by a probe. The orientation of the probe was either the same as or slightly different than that of the final (i.e., tenth) inducing stimulus (i.e., −8°, −6°, −4°, −2°, 0°, +2°, +4°, +6°, or +8°). Here, the participants judged whether the orientations of the final inducing stimulus and the probe were the same or different, by pressing either the left or right response button. Mapping of same/different judgments and left/right buttons was fixed throughout the experiment for each participant and counterbalanced across participants. The probe was presented until the participant's response.

The participant's response was immediately followed by a question display consisting of the words "Present" and "Absent." Here, the participants judged whether the target stimulus (i.e., a gray-unfilled bar presented only in the catch trial) was presented or not, by pressing either the left or right response button beside the words on the display. The side on which the words were presented was varied randomly across trials, with a constraint that two possible arrangements (i.e., "Present" on the left and "Absent" on the right, and vice versa) were equally presented within an experiment. The question display was presented until the participant's response, which was immediately followed by a blank screen for 2000 ms.

The experiment included 180 regular trials and 40 catch trials, which were arranged in random order. In the 180 regular trials, 20 trial types, defined by the combination of 10 orientations of the first inducing stimulus (i.e., from 5° to 167° with a step of 18°) and two directions of regular rotation (i.e., clockwise and counterclockwise), were presented in nine trials each. In these 180 trials, nine angular differences between the final inducing stimulus and the probe (i.e., −8°, −6°, −4°, −2°, 0°, +2°, +4°, +6°, and +8°) were assigned with equal probabilities. Note that the 10 orientations of the first inducing stimulus were used to keep the physical attributes of inducing stimuli presented at each of the 10 positions in a stimulus sequence on average the same. That is, at each of 10 positions, 10 orientations were presented 18 times each.

In the 40 catch trials, the same 20 trial types, defined by the combination of 10 orientations of the first inducing stimulus (i.e., from 5° to 167° with a step of 18°) and two directions of regular rotation (i.e., clockwise and counterclockwise), were presented in two trials each. In these 40 trials, the target stimulus was presented at each of 10 positions with equal probability. The orientations of the final inducing stimulus and the probe were always the same.

The participants performed the task while seated in a chair in a sound-attenuated, dimly lit room. Before the start of the experiment, the participants were given instructions about the same/different judgment. They were instructed to judge whether the orientations of the tenth stimulus and a subsequent probe were the same or different, as accurately as possible. They were also instructed to count stimuli so that the tenth stimulus could be properly compared with the probe. The speed of their response was not stressed. Here, they were explicitly informed that the angular difference would be −8°, −6°, −4°, −2°, 0°, +2°, +4°, +6°, or +8°; this was intended to help the participants understand that the angular difference would be quite small. However, they were not informed about the ratio of "same" and "different" trials. Information regarding the nine angular differences might have led participants to expect the probability of each angular difference to be about 11%. However, such expectation is unlikely to significantly affect the magnitude of RM, although it may affect the overall probability of making a "same" response (Hubbard and Lange, 2010). Finally, it was emphasized that they should make a "same" response only

when they believed that the orientations were exactly the same (Freyd and Finke, 1985).

Next, the participants were given instructions about the present/absent judgment. They were instructed to judge whether or not an unfilled stimulus was presented, as accurately as possible. The speed of their response was not stressed. Here, they were explicitly informed that the unfilled stimulus could appear at any of 10 positions in the stimulus sequence. However, they were not informed about the ratio of "present" and "absent" trials. It was emphasized that they should keep observing the stimulus sequence to perform this task adequately.

Finally, the participants were instructed to minimize any eye movements and blinks when the stimulus sequence was presented. After these instructions, the participants performed 20–40 practice trials, and then started the experiment.

Recordings

The electroencephalogram (EEG) was recorded with a digital amplifier (Nihon-Kohden, Neurofax EEG1200) and silver-silver chloride electrodes placed at 27 scalp sites (Fp1, Fp2, F7, F3, Fz, F4, F8, FCz, T7, C3, Cz, C4, T8, CPz, P7, P3, Pz, P4, P8, PO7, PO3, POz, PO4, PO8, O1, Oz, and O2 according to the extended International 10–20 System). All electrodes were referenced to the nose tip. To monitor blinks and eye movements, vertical and horizontal electrooculograms (EOGs) were also recorded with two electrodes above and below the right eye and two electrodes at the right and left outer canthi of the eyes, respectively. The ground electrode was attached to the forehead. The impedance of all electrodes was kept below 5 kΩ. The EEG and EOG signals were bandpass-filtered online at 0.016–300 Hz and digitized at a sampling rate of 1000 Hz.

The digitized signals were then analyzed by MATLAB (MathWorks) with EEGLAB toolbox (Delorme and Makeig, 2004) and ERPLAB Toolbox (Lopez-Calderon and Luck, 2014). The EEG and EOG signals were bandpass-filtered using a non-causal Butterworth infinite impulse response filter with half-amplitude cutoffs at 0.1 and 30 Hz and a roll-off of 12 dB/octave. The EEG and EOG signals time-locked to the onset of inducing stimuli were extracted. The extracted epochs were 600 ms (i.e., from −100 to 500 ms relative to the onset of inducing stimuli). An independent component analysis (Delorme and Makeig, 2004) was performed to remove artifacts derived from blinks and eye movements. The epochs were then baseline-corrected relative to the initial 100-ms interval (i.e., from −100 to 0 ms relative to the onset of inducing stimuli).

For each participant, the EEG signals in the regular trials were averaged for four categories: i.e., inducing stimuli (1) at the first position, (2) at the second, third, and fourth positions, (3) at the fifth, sixth, and seventh positions, and (4) at the eighth, ninth, and tenth positions. VEPs elicited by inducing stimuli at the first position were separately averaged, in consideration of their special morphologies reflecting initial-orienting reaction (Kenemans et al., 1989). VEPs elicited by inducing stimuli at the second–tenth positions were separated for three categories, to explore the time course of the correlation of RM and VEPs, while meeting ideal averaging numbers for VEPs (i.e., about 400 times, Luck, 2005). Note that the physical attributes of the inducing stimuli for these four position categories were on average kept the same. Epochs during which the signal change exceeded ± 80 μV on any of the EEG or EOG electrodes were excluded from averaging. As a result, the number of epochs averaged for the first, second–fourth, fifth–seventh, and eighth–tenth positions was, on average, 170.8 (*SD* = 10.2), 524.5 (20.9), 530.1 (14.7), and 532.8 (10.4), respectively.

Data Analysis

Magnitude of RM

For each participant, the percentages of "same" responses in the regular trials were calculated for nine position categories defined by the angular difference between the final inducing stimulus and the probe and its relation to the direction of regular rotation (i.e., backward 8°, backward 6°, backward 4°, backward 2°, same, forward 2°, forward 4°, forward 6°, and forward 8°). Next, for each participant, the magnitude of RM was estimated by a standard formula for calculating the mean position of a probe judged as "same" (Freyd and Jones, 1994; Hayes and Freyd, 2002; Munger and Minchew, 2002). In this calculation, each "same" response was weighted by the position of the probe, and the average of these weighted "same" responses was estimated to be the magnitude of RM.[2] To confirm the occurrence of RM, the measured values were compared to zero with a one-tailed *t*-test; the statistical threshold was $p < 0.05$.

Target detection

For each participant, the percentage of "present" responses in the catch trials (i.e., hit rate) and those of "absent" responses in the regular trials (i.e., correct rejection rates) were calculated.

Magnitude of VEPs

For each participant, the magnitudes of VEPs elicited by inducing stimuli in the regular trials were estimated by calculating the mean amplitudes of the occipito-temporal P1, frontal N1, occipito-temporal N1, and central P2 for the four position categories (i.e., first, second–fourth, fifth–seventh, and eighth–tenth positions). The time windows of these VEPs for the second–fourth, fifth–seventh, and eighth–tenth positions were determined to be the 40-ms windows centered on the peaks in the grand-average VEPs in which the three position categories were collapsed; this procedure was chosen to avoid possible biases among the three position categories (Luck, 2014). As a result, the time windows were determined as follows: within the 90–130 ms time window at the PO8 electrode site for occipito-temporal P1, within the 118–158 ms time window at the Fz electrode site for frontal N1, within the 148–188 ms time window at the PO8 electrode site for occipito-temporal N1, and within the 178–218 ms time window at the Cz electrode site for central P2

[2]In a certain participant, if the mean percentages of "same" response in the backward 8°, backward 6°, backward 4°, backward 2°, same, forward 2°, forward 4°, forward 6°, and forward 8°conditions were 0, 9, 12, 53, 87, 90, 78, 45, and 12%, respectively, then the sum of the products of the percentage of "same" responses and the distance of the probe from true-same was calculated (i.e., 0*(−8) + 9*(−6) + 12*(−4) + 53*(−2) + 87*(0) + 90*(+2) + 78*(+4) + 45*(+6) + 12*(+8) = 650), and the obtained value (i.e., 650) was divided by the sum of the percentages of the same responses (i.e., 0 + 9 + 12 + 53 + 87 + 90 + 78 + 45 + 12 = 386). This resulted in the magnitude of RM of 1.68°.

(**Table 1**). The time windows for the first position were separately determined as the 40-ms windows centered on the peaks in the grand-average VEPs for the first position. As a result, the time windows were determined as follows: within the 94–134 ms time window at the PO8 electrode site for occipito-temporal P1, within the 119–159 ms time window at the Fz electrode site for frontal N1, within the 150–190 ms time window at the PO8 electrode site for occipito-temporal N1, and within the 212–252 ms time window at the Cz electrode site for central P2 (**Table 1**).

Correlations between RM and VEPs

The correlation between the magnitudes of RM and VEPs (i.e., occipito-temporal P1, frontal N1, occipito-temporal N1, and central P2 for the four position categories) were assessed by Spearman's correlation analyses (two-tailed); the statistical threshold was $p < 0.05$. Spearman's correlation analysis was chosen here, since the relationship between RM and VEPs was assumed to be not necessarily linear.

Results

Figure 3A shows the mean (black line) and individual (gray lines) percentages of "same" responses. **Figure 3B** shows the mean (black line) and individual (gray lines) magnitudes of RM. The individual magnitudes of RM ranged from 0.55° to 3.02°. The mean magnitude of RM was 1.86° ($SD = 0.68$). A one-tailed t-test revealed a significant occurrence of RM [$t(34) = 16.31$, $p < 0.001$, $d = 2.76$].

The mean hit rate in the catch trial was 95.1% ($SD = 8.4$). The mean correct rejection rate in the regular trial was 98.9% ($SD = 1.1$).

Figure 4A shows VEPs elicited by the inducing stimuli in the regular trials for the first (red lines), second–fourth (blue lines), fifth–seventh (green lines), and eighth–tenth positions (purple lines). **Figure 4B** shows topographical maps of VEPs within the time windows listed in **Table 1**. Typical waveforms consisting of occipito-temporal P1, frontal N1, occipito-temporal N1, and central P2 were observed. **Figure 4C** shows the mean (black lines) and individual (gray lines) magnitudes of these VEPs, calculated as the mean amplitude according to the time windows and electrodes sites listed in **Table 1**.

Figure 5 shows the relationship between the magnitudes of RM and VEPs (i.e., occipito-temporal P1, frontal N1, occipito-temporal N1, and central P2 for the four position categories). Spearman's correlation analysis (two-tailed) revealed significant negative correlations between the magnitudes of RM and central P2 for the fifth–seventh ($\rho = -0.35$; $p < 0.05$) and eighth–tenth positions ($\rho = -0.39$; $p < 0.05$).[3]

TABLE 1 | Time windows for calculating mean amplitudes of VEPs in Experiment 1.

	Position 1	Positions 2–4, 5–7, and 8–10
Occipito-temporal P1	94–134 ms (PO8)	90–130 ms (PO8)
Frontal N1	119–159 ms (Fz)	118–158 ms (Fz)
Occipito-temporal N1	150–190 ms (PO8)	148–188 ms (PO8)
Central P2	212–252 ms (Cz)	178–218 ms (Cz)

Discussion

The results regarding the same/different judgment showed that RM robustly occurred in the regular trials. This is highly consistent with previous RM findings (Freyd and Finke, 1984, 1985). The results regarding target detection showed that the hit rates in the catch trial as well as the correct rejection rates in the regular trial were high, ensuring that the participants kept observing the stimulus sequence. The results regarding VEPs showed that inducing stimuli elicited occipito-temporal P1, frontal N1, occipito-temporal N1, and central P2 that were comparable to those obtained with regularly rotated bars (Kimura and Takeda, 2015). For the correlation between RM and VEPs, the magnitude of RM was negatively correlated with the magnitude of central P2; participants who showed a smaller P2 tended to exhibit greater RM. This seems to be consistent with a previous finding that the suppression of central P2 would be a neural effect that would specifically emerge when the current and predicted positions of an object successfully matched (Kimura and Takeda, 2015). In contrast to central P2, the magnitude of RM was not correlated with the magnitude of occipito-temporal P1, frontal N1, and occipito-temporal N1. Given a previous finding that these VEPs were not sensitive to successful matching between the current and predicted positions of a visual object (Kimura and Takeda, 2015), the null correlation seems to be reasonable.

EXPERIMENT 2

To test the replicability and robustness of the negative correlation between the magnitudes of RM and central P2, the same analyses were performed on data obtained in another experiment where a bar was regularly rotated with a different angular step (i.e., 20°; cf. 18° in Experiment 1). Similar to Experiment 1, the experiment reported here was conducted with multiple purposes, and included trials that were not related to the present purpose (i.e., irregular trials; see Materials and Methods). Data in the irregular condition will be reported elsewhere. Data reported in this paper have not been reported elsewhere.

Materials and Methods

Participants

Thirty-seven healthy adults (26 males, 11 females; mean age 23.3 years; age range 20–33 years) participated in this experiment; three participants had also participated in Experiment 1. All

[3]Given that VEPs for the first position showed a large and sustained occipito-temporal positivity at around 200–400 ms (see **Figures 4A,B**), one may be interested in the relationship between RM and the occipito-temporal positivity. So, an exploratory analysis was made for the correlation between the magnitudes of RM and the occipito-temporal positivity (mean amplitudes were calculated with the time window of 240–280 ms at PO8 electrode). The results showed that the magnitude of the positivity was not significantly correlated with the magnitude of RM; the first ($rho = 0.06$, $p = 0.74$), second–forth ($rho = 0.10$, $p = 0.57$), fifth–seventh ($rho = 0.00$, $p = 0.99$), and eighth–tenth positions ($rho = -0.06$, $p = 0.72$).

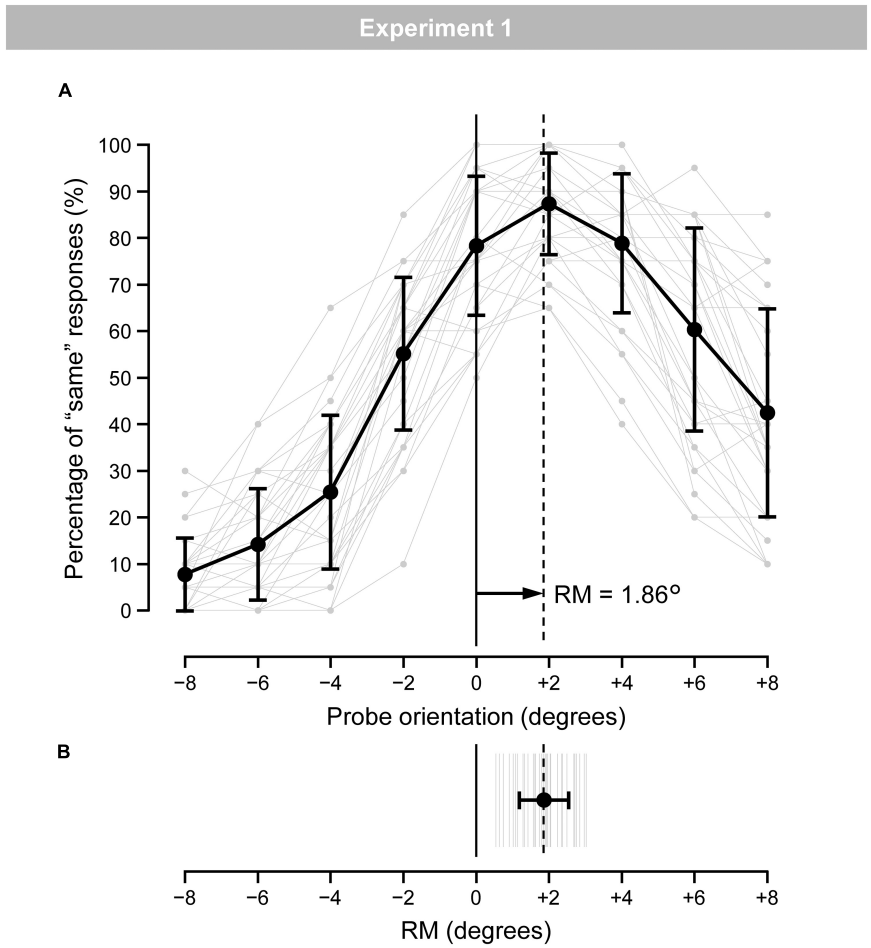

FIGURE 3 | (A) Mean (black) and individual (gray) percentages of "same" responses for the nine probe-orientation categories in the regular trials. Error bars indicate *SD*. **(B)** Mean (black) and individual (gray) magnitudes of RM. Error bars indicate *SD*.

participants had normal or corrected-to-normal vision. Thirty-six participants were right-handed and one was left-handed. Written informed consent was obtained from each participant after the nature of the study had been explained. The experiment was approved by the Safety and Ethics committee of the National Institute of Advanced Industrial Science and Technology (AIST).

Stimuli and Procedure

The stimuli and procedure were the same as those in Experiment 1, except for the following points. The experiment was comprised of three types of trials (i.e., regular, irregular, and catch trials). **Figure 2** shows an illustration of the regular and catch trials. In the regular trial, a gray-filled bar was rotated regularly with a step of 20° (i.e., inducing stimuli). In the catch trial, a gray-filled bar was rotated regularly, but at any of the 10 positions, it was replaced by a gray-unfilled bar (i.e., target stimuli).

The experiment included 288 regular trials and 36 catch trials, which were arranged in random order. The direction of regular rotation was fixed throughout the experiment for each participant and counterbalanced across the participants; for half of the participants (i.e., 18 participants), the direction of regular rotation was clockwise, and for the other half of the participants (i.e., 19 participants), the direction of regular rotation was counterclockwise.

In the 288 regular trials, 36 trial types that were defined by 36 orientations of the first inducing stimulus (i.e., from 3° to 178° with a step of 5°) were presented in eight trials each. In these 288 trials, nine angular differences between the final inducing stimulus and the probe (i.e., −8°, −6°, −4°, −2°, 0°, +2°, +4°, +6°, and +8°) were assigned with equal probabilities. Note that the 36 orientations of the first stimulus were used to keep the physical attributes of inducing stimuli presented at each of the 10 positions in a stimulus sequence on average the same. Thus, at each of the 10 positions, 36 orientations were presented eight times each.

In the 36 catch trials, the same 36 trial types that were defined by 36 orientations of the first stimulus (i.e., from 3° to 178° with a step of 5°) were presented in one trial each. In these 36 trials, the target stimulus was presented at each of 10 positions with almost equal probability.

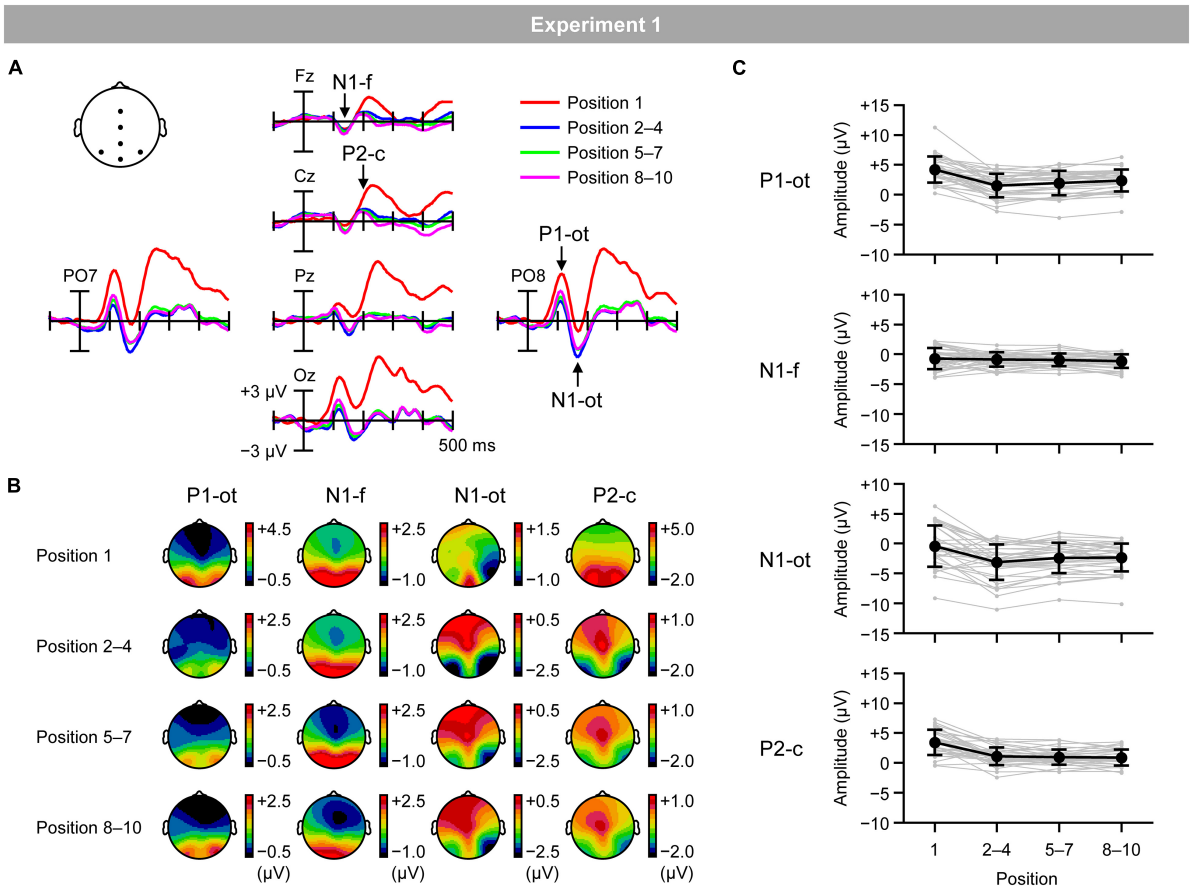

FIGURE 4 | (A) VEPs elicited by inducing stimuli presented at the first position (red lines), second, third, and fourth positions (blue lines), fifth, sixth, and seventh positions (green lines), and eighth, ninth, and tenth positions (purple lines) in the regular trials. **(B)** Topographical maps of VEPs. **(C)** Mean (black) and individual (gray) magnitudes of VEPs. P1-ot: occipito-temporal P1, N1-f: frontal N1, N1-ot: occipito-temporal N1, P2-c: central P2. Error bars indicate *SD*.

Recordings

The recording parameters were the same as those in Experiment 1. As a result, the number of epochs averaged for the first, second–fourth, fifth–seventh, and eighth–tenth positions was, on average, 280.4 (*SD* = 12.1), 851.2 (29.8), 856.2 (21.1), and 857.8 (10.7), respectively.

Data Analysis

Magnitude of RM

The data analysis was the same as that in Experiment 1.

Target detection

The data analysis was the same as that in Experiment 1.

Magnitude of VEPs

The data analysis was the same as that in Experiment 1, except for the time windows for calculating the mean amplitudes of VEPs. The time windows of VEPs for the second–fourth, fifth–seventh, and eighth–tenth positions were determined as follows: within the 89–129 ms time window at the PO8 electrode site for occipito-temporal P1, within the 111–151 ms time window at the Fz electrode site for frontal N1, within the 146–186 ms time window at the PO8 electrode site for occipito-temporal N1, and within the 174–214 ms time window at the Cz electrode site for central P2 (**Table 2**). The time windows of VEPs for the first position were determined as follows: within the 100–140 ms time window at the PO8 electrode site for occipito-temporal P1, within the 114–154 ms time window at the Fz electrode site for frontal N1, within the 151–191 ms time window at the PO8 electrode site for occipito-temporal N1, and within the 200–240 ms time window at the Cz electrode site for central P2 (**Table 2**).

Correlations between RM and VEPs

The analysis was the same as that in Experiment 1.

Results

Figure 6A shows the mean (black line) and individual (gray lines) percentages of "same" responses. **Figure 6B** shows the mean (black line) and individual (gray lines) magnitudes of RM. The individual magnitudes of RM ranged from 0.07° to 3.65°. The mean magnitude of RM was 2.06° (*SD* = 0.80). A one-tailed *t*-test revealed a significant occurrence of RM [$t(36) = 15.73$, $p < 0.001$, $d = 2.59$].

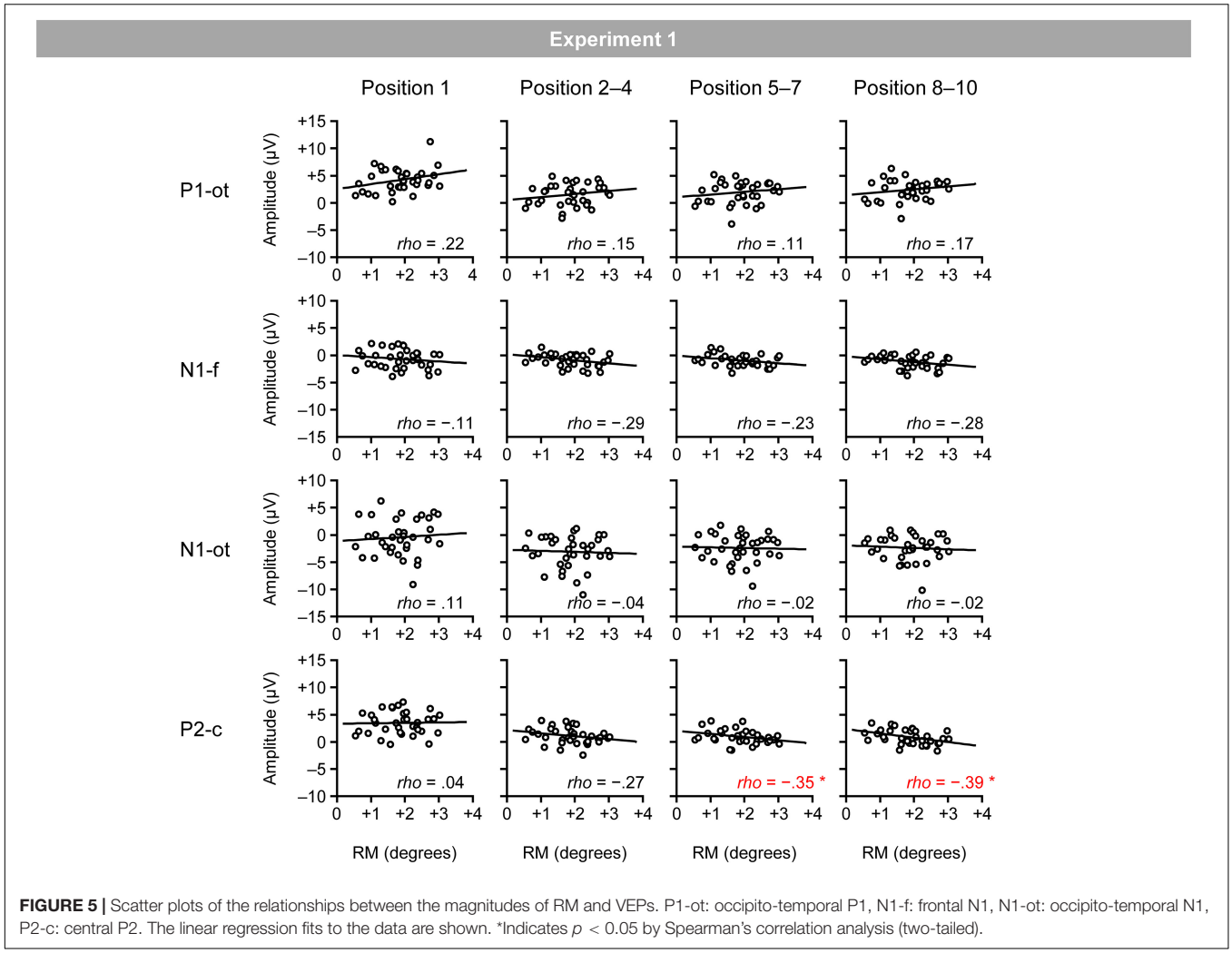

FIGURE 5 | Scatter plots of the relationships between the magnitudes of RM and VEPs. P1-ot: occipito-temporal P1, N1-f: frontal N1, N1-ot: occipito-temporal N1, P2-c: central P2. The linear regression fits to the data are shown. *Indicates $p < 0.05$ by Spearman's correlation analysis (two-tailed).

The mean hit rate in the catch trial was 94.7% (SD = 6.2). The mean correct rejection rate in the regular trial was 98.6% (SD = 1.1).

Figure 7A shows VEPs elicited by the inducing stimuli in the regular trials for the first (red lines), second–fourth (blue lines), fifth–seventh (green lines), and eighth–tenth positions (purple lines). **Figure 7B** shows topographical maps of VEPs within the time windows listed in **Table 2**. **Figure 7C** shows the mean (black lines) and individual (gray lines) magnitudes of VEPs, calculated as the mean amplitude according to the time windows and electrodes sites listed in **Table 2**.

TABLE 2 | Time windows for calculating mean amplitudes of VEPs in Experiment 2.

	Position 1	Positions 2–4, 5–7, and 8–10
Occipito-temporal P1	100–140 ms (PO8)	89–129 ms (PO8)
Frontal N1	114–159 ms (Fz)	111–151 ms (Fz)
Occipito-temporal N1	151–191 ms (PO8)	146–186 ms (PO8)
Central P2	200–240 ms (Cz)	174–214 ms (Cz)

Figure 8 shows the relationship between the magnitudes of RM and VEPs. Spearman's correlation analysis (two-tailed) revealed significant negative correlations between the magnitudes of RM and central P2 for the second–fourth ($\rho = -0.39$; $p < 0.05$), fifth–seventh ($\rho = -0.40$; $p < 0.05$), and eighth–tenth positions ($\rho = -0.54$; $p < 0.01$), as well as a significant negative correlation between the magnitudes of RM and occipito-temporal P1 for the first position ($\rho = -0.38$; $p < 0.05$).[4]

Discussion

As in Experiment 1, RM robustly occurred in the regular trials, and the inducing stimuli elicited occipito-temporal P1, frontal N1, occipito-temporal N1, and central P2. The magnitude of RM was again negatively correlated with the magnitude of

[4]As in Experiment 1, an exploratory analysis for the correlation between the magnitudes of RM and the occipito-temporal positivity (mean amplitudes were calculated with the time window of 240–280 ms at PO8 electrode) showed that the magnitude of the positivity was not significantly correlated with the magnitude of RM; the first (rho = 0.05, p = 0.76), second–forth (rho = 0.13, p = 0.46), fifth–seventh (rho = 0.16, p = 0.34), and eighth–tenth positions (rho = 0.03, p = 0.87).

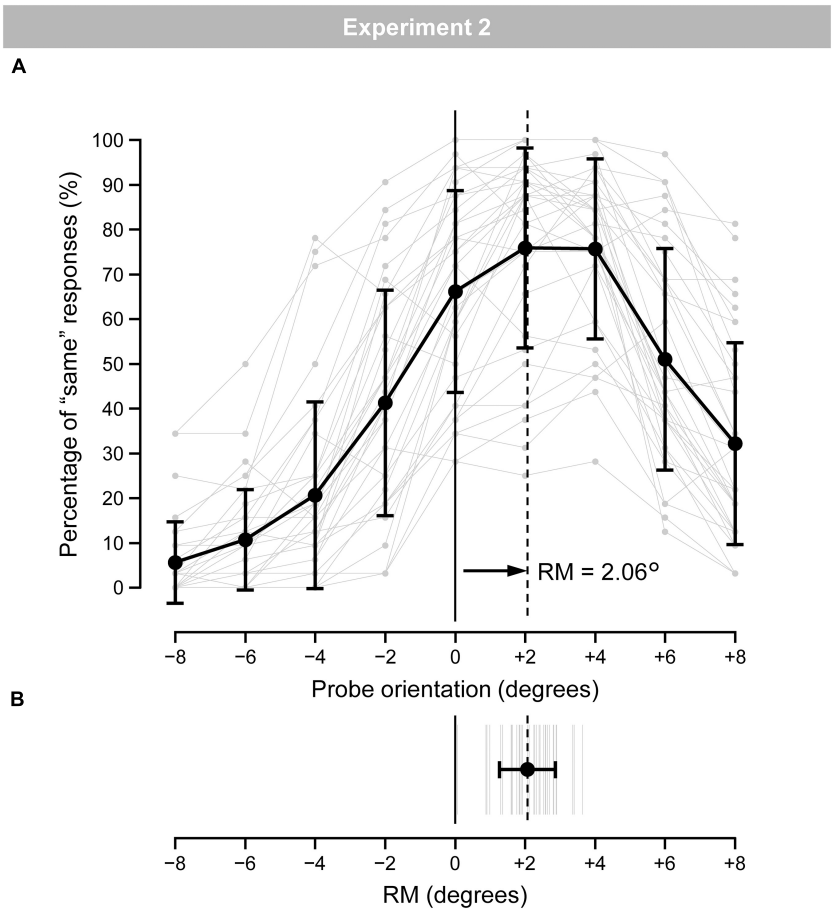

FIGURE 6 | (A) Mean (black) and individual (gray) percentages of "same" responses for the nine probe-orientation categories in the regular trials. Error bars indicate *SD*. **(B)** Mean (black) and individual (gray) magnitudes of RM. Error bars indicate *SD*.

central P2; participants who showed a smaller P2 tended to exhibit greater RM. Thus, the negative correlation between the magnitudes of RM and central P2 observed in Experiment 1 was clearly replicated in Experiment 2, ensuring the replicability and robustness of the negative correlation between RM and central P2. In addition to central P2, the magnitude of occipito-temporal P1 for the first position was negatively correlated with the magnitude of RM. However, given that such negative correlation was not observed in Experiment 1 (rather, a tendency of an opposite, positive correlation was observed in Experiment 1), no conclusion could be drawn about this effect.

GENERAL DISCUSSION

In Experiments 1 and 2, the results regarding the same/different judgment showed that RM clearly occurred in regular trials. This is highly consistent with the previous findings with the conventional RM paradigm with regular rotations of a bar (Freyd and Finke, 1984, 1985) as well as with other types of changes (Kelly and Freyd, 1987; Hayes and Freyd, 2002). The magnitude of RM in Experiment 2 (mean of 2.06°) was numerically greater than that in Experiment 1 (mean of 1.86°). This could be mainly attributed to the step size of a regular rotations of a bar (i.e., 18° in Experiment 1 and 20° in Experiment 2), since the magnitude of RM is proportional to the implied velocity of regular rotations of a bar (Freyd and Finke, 1985; Finke et al., 1986).

In Experiments 1 and 2, the magnitude of RM was negatively correlated with the magnitude of central P2 at around 200 ms after bar onset; that is, participants who showed a smaller P2 tended to exhibit greater RM. This is consistent with the expectation based on a previous finding that the suppression of central P2 is a neural effect that specifically emerges when the current position of a visual object successfully matches the predicted position of the object based on sequential regularities (Kimura and Takeda, 2015). The negative correlations between the magnitudes of RM and central P2 showed a similar time course in Experiments 1 and 2. That is, the magnitudes of RM and central P2 were not initially correlated at the first position, and they started to be negatively correlated at later positions. These results support the idea that the correlation would be associated with the individual's ability to automatically form a prediction based on sequential regularities and contradict the idea that the correlation between the magnitudes of RM and P2 merely

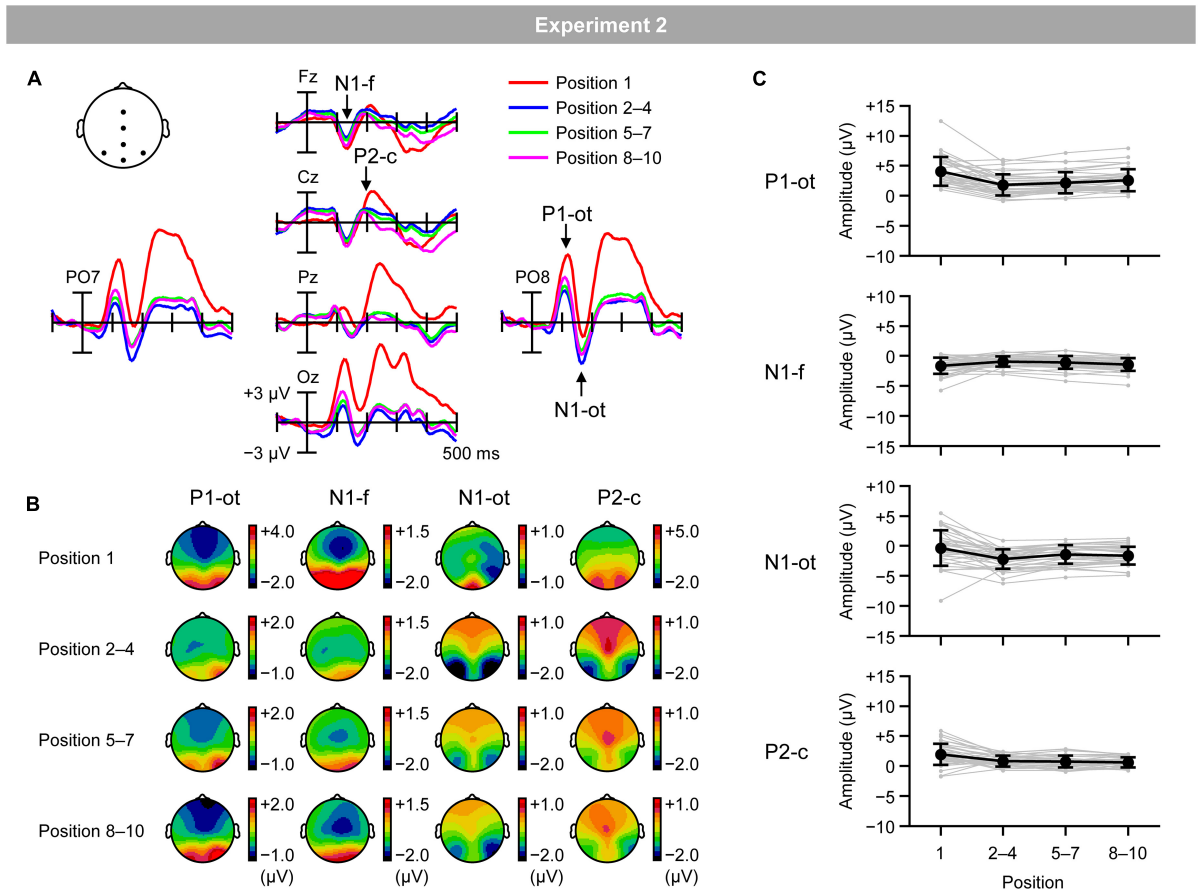

FIGURE 7 | (A) VEPs elicited by inducing stimuli presented at the first position (red lines), second, third, and fourth positions (blue lines), fifth, sixth, and seventh positions (green lines), and eighth, ninth, and tenth positions (purple lines) in the regular trials. **(B)** Topographical maps of VEPs. **(C)** Mean (black) and individual (gray) magnitudes of VEPs. P1-ot: occipito-temporal P1, N1-f: frontal N1, N1-ot: occipito-temporal N1, P2-c: central P2. Error bars indicate *SD*.

reflects the individual's inherent strength of neural activations represented by P2.

Although the negative correlations between the magnitudes of RM and central P2 were highly similar between Experiments 1 and 2, there were slight differences between Experiments 1 and 2. The negative correlation appeared earlier in Experiment 2 (i.e., the second–fourth positions) than in Experiment 1 (i.e., the fifth–seventh positions). Also, the negative correlation between the magnitudes of RM and central P2 was more robust (at least in terms of the correlation coefficient) in Experiment 2 than in Experiment 1. These differences would be mainly attributed to two differences in the experimental design. First, they may be attributed to the greater step size of the regular rotation of a bar in Experiment 2 (i.e., 20°) than in Experiment 1 (i.e., 18°). Second, they may be attributed to the arrangement of directions of regular rotation. In Experiment 1, directions of regular rotation (i.e., clockwise and counterclockwise) were changed trial-by-trial in a random manner; therefore, only after the second inducing stimulus was presented, the participants could recognize whether the current regular rotation was clockwise or counterclockwise and could predict the orientation of the upcoming inducing stimuli. In contrast, in Experiment 2, the direction of regular rotation (i.e., clockwise or counterclockwise) was fixed for each participant throughout the experiment; therefore, immediately after the first inducing stimulus was presented, the participants could predict the orientation of the upcoming inducing stimuli.

It appears difficult to attribute the negative correlation between RM and central P2 to factors other than prediction. For example, one might consider that the negative correlation may be involved in visual attention to inducing stimuli. However, if the negative correlation was involved in the degree of visual attention, then significant correlations should have also been observed between RM and occipito-temporal P1/N1, since visual attention predominantly affects occipito-temporal P1/N1 (Hillyard and Anllo-Vento, 1998; Luck et al., 2000). The present results of the almost null correlation between RM and P1/N1 are incongruent with this expectation. One might also consider that the negative correlation may be associated with some strategic processes. It has been shown that RM is primarily determined by automatic predictive processes. However, due to the essential requirements of the task (i.e., the same/different judgment), RM may not be free from the effects of strategic

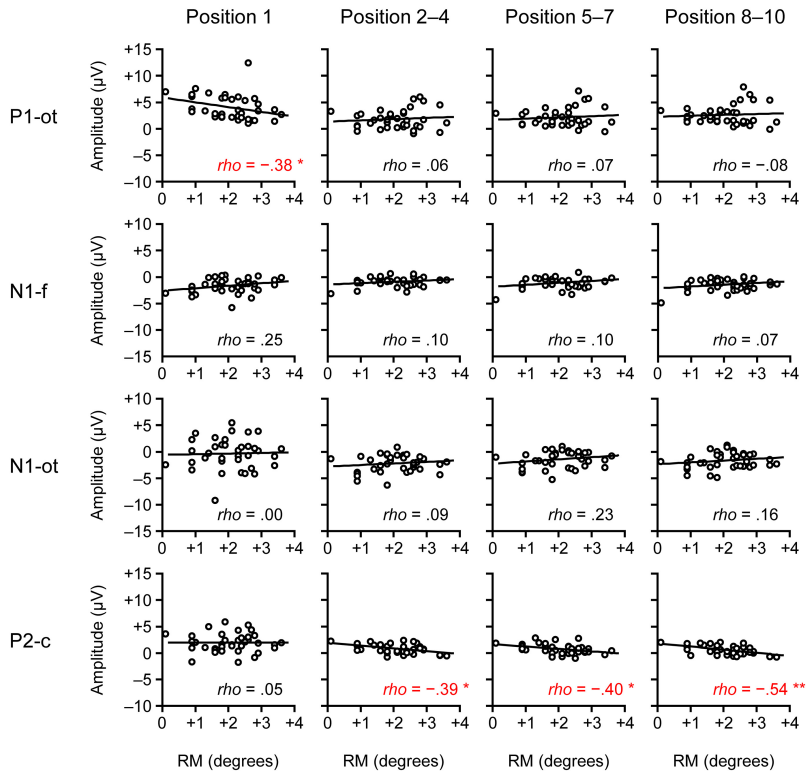

FIGURE 8 | Scatter plots of the relationships between the magnitudes of RM and VEPs. P1-ot: occipito-temporal P1, N1-f: frontal N1, N1-ot: occipito-temporal N1, P2-c: central P2. The linear regression fits to the data are shown. *Indicates $p < 0.05$ and **indicates $p < 0.01$ by Spearman's correlation analysis (two-tailed).

processes such as "cognitive resistance" (i.e., to intentionally stop the forward displacement of a sensory representation to improve the same/different judgment; Finke et al., 1986) and "opposite-acting compensation" (i.e., to strategically change the judgment to compensate for a likely perceptual bias; Joordens et al., 2004). Although such effects of strategic processes could not be completely ruled out, given that the present negative correlation was not limited to the eighth–tenth positions where such strategic processes are expected to be operated, it seems unlikely that the presented negative correlation was related to such strategic processes.

Taken together, the present results suggest that the greater sensory suppression as indicated by smaller central P2 underlies stronger predictive modulation of visual perception as indicated by greater RM. Given the previous findings that neural sources of central P2 were localized around lower visual areas around the striate and prestriate cortices (Capilla et al., 2016; see also Metha et al., 2000) and P2 may be a sign of delayed reactivation of lower visual areas via reentrant feedback projections from higher areas (Di Russo et al., 2003, 2008; see also Olson et al., 2001; Noesselt et al., 2002), the present results would support the notion that the strength of prediction suppression of delayed reactivation of lower visual areas determines the strength of predictive modulation of visual perception. This notion is consistent with that in a human neuroimaging study which demonstrated that successful matching between current visual inputs and predicted visual inputs based on sequential regularities drives less neural activation in the striate cortex, probably via feedback projections from higher visual areas (Alink et al., 2010). From a broader perspective, the present findings appear to be in line with previous findings that the strength of delayed reactivation of lower visual areas such as striate cortex via reentrant feedback projections critically determines perceptual experience and awareness (Lamme et al., 1998; Lamme and Roelfsema, 2000; Tong, 2003; Pak et al., 2020) as well as the hierarchical predictive coding framework which proposes that prior expectations about an upcoming stimulus act as top-down signals that predict the bottom-up input (Rao and Ballard, 1999; Friston, 2005; Summerfield and de Lange, 2014).

The present findings should be treated with caution in three respects. First, the present study used a simple stimulus (i.e., a bar) that changed along with a simple regularity (i.e., rotation). It seems possible that, when observing a more complex stimulus (e.g., face) that changes along with a more complex regularity (e.g., changes in facial features), the main loci of prediction suppression might change (e.g., from lower visual areas to higher areas such as face-responsible inferior temporal cortex,

Haxby et al., 2000), and the prediction suppression in such higher areas may mainly determine the predictive modulation of visual perception. Second, the present study applied a conventional RM paradigm (Freyd and Finke, 1984, 1985), but there are several different RM paradigms such as those with a still photograph of an object in motion (Freyd, 1983) or a smooth animated motion of an object (Hubbard and Bharucha, 1988). To capture the overall picture of the relationship between prediction suppression based on sequential regularities and predictive modulation of visual perception, the accumulation of studies with a variety of paradigm should be required. Third, the present study did not directly examine the neural sources of central P2. The precise source localization was not a realistic option in the present study, since central P2 was expected to be overlapped by temporally and/or spatially adjacent VEPs. Furthermore, although a previous study reported that the neural sources of central P2 were localized in lower visual areas (Capilla et al., 2016), stimuli used in the previous study (i.e., reversal of a checkerboard pattern) were different from those used in the present study (i.e., discrete presentation of a bar). In future studies, the direct examination of the neural sources should be made with an optimal experimental design by which the predictive suppression of central P2 can be isolated from other neural activities (Kimura and Takeda, 2015).

Finally, this present finding may drive the fundamental question of what factors determine the individual's ability to automatically form a prediction based on sequential regularities. For example, previous RM studies showed that the magnitude of RM can be modulated by domain-specific expertise (e.g., greater RM for road scenes in experienced compared to inexperienced automobile drivers), suggesting that prediction ability can be improved with expertise (Blättler et al., 2010, 2011). As another approach, a recent study sought clinical factors that determine the magnitude of RM in terms of autistic and schizotypal traits, although a strong factor could not be determined (Tulver et al., 2019). The quest for critical factors that determine an individual's prediction abilities would be important for better understanding the mechanisms of visual perception and for establishing possible training/intervention methods to improve prediction abilities.

CONCLUSION

By measuring VEPs with a conventional RM paradigm, the present study demonstrated the relationship between the strength of predictive modulation of visual perception (as measured by the magnitude of RM) and the strength of prediction suppression of sensory response (as measured by the magnitude of central P2, which is best assumed to represent delayed reactivation of lower visual areas around striate and prestriate cortices via reentrant feedback projections from higher areas).

DATA AVAILABILITY STATEMENT

The raw data supporting the conclusion of this article will be made available by the authors, without undue reservation.

ETHICS STATEMENT

The studies involving human participants were reviewed and approved by the Safety and Ethics Committee of the National Institute of Advanced Industrial Science and Technology (AIST). The patients/participants provided their written informed consent to participate in this study.

AUTHOR CONTRIBUTIONS

The author confirms being the sole contributor of this work and has approved it for publication.

REFERENCES

Alink, A., Schwiedrzik, C. M., Kohler, A., Singer, W., and Muckli, L. (2010). Stimulus predictability reduces responses in primary visual cortex. *J. Neurosci.* 30, 2960–2966. doi: 10.1523/jneurosci.3730-10.2010

Blättler, C., Ferrari, V., Didierjean, A., and Marméche, E. (2011). Representational momentum in aviation. *J. Exp. Psychol. Hum. Percept. Perform.* 37, 1569–1577. doi: 10.1037/a0023512

Blättler, C., Ferrari, V., Didierjean, A., van Elslande, P., and Marméche, E. (2010). Can expertise modulate representational momentum? *Vis. Cogn.* 18, 1253–1273. doi: 10.1080/13506281003737119

Brainard, D. H. (1997). The psychophysics toolbox. *Spat. Vis.* 10, 433–436. doi: 10.1163/156856897x00357

Capilla, A., Melcón, M., Kessel, D., Calderón, R., Pazo-Álvarez, P., and Carretié, L. (2016). Retinotopic mapping of visual event-related potentials. *Biol. Psychol.* 118, 114–125. doi: 10.1016/j.biopsycho.2016.05.009

Clark, V. P., Fan, S., and Hillyard, S. A. (1995). Identification of early visual evoked potential generators by retinotopic and topographic analyses. *Hum. Brain Mapp.* 2, 170–187. doi: 10.1002/hbm.460020306

Delorme, A., and Makeig, S. (2004). EEGLAB: an open source toolbox for analysis of single-trial EEG dynamics including independent component analysis. *J. Neurosci. Methods* 134, 9–21. doi: 10.1016/j.jneumeth.2003.10.009

Di Russo, F., Aprile, T., Spitoni, G., and Spinelli, D. (2008). Impaired visual processing of contralesional stimuli in neglect patients: a visual-evoked potential study. *Brain* 131, 842–854. doi: 10.1093/brain/awm281

Di Russo, F., Martínez, A., and Hillyard, S. A. (2003). Source analysis of event-related cortical activity during visuo-spatial attention. *Cereb. Cortex* 13, 486–499. doi: 10.1093/cercor/13.5.486

Di Russo, F., Martínez, A., Sereno, M. I., Pitzalis, S., and Hillyard, S. A. (2002). Cortical sources of the early components of the visual evoked potential. *Hum. Brain Mapp.* 15, 95–111. doi: 10.1002/hbm.10010

Finke, R. A., and Freyd, J. J. (1985). Transformations of visual memory induced by implied motions of pattern elements. *J. Exp. Psychol. Learn. Mem. Cogn.* 11, 780–794. doi: 10.1037/0278-7393.11.1-4.780

Finke, R. A., Freyd, J. J., and Shyi, G. C. W. (1986). Implied velocity and acceleration induced transformations of visual memory. *J. Exp. Psychol. Gen.* 115, 175–188. doi: 10.1037/0096-3445.115.2.175

Freyd, J. J. (1983). The mental representation of movement when static stimuli are viewed. *Percept. Psychophys.* 33, 575–581. doi: 10.3758/bf03202940

Freyd, J. J. (1992). "Dynamic representations guiding adaptive behavior," in *Time, Action and Cognition: Towards Bridging the Gap*, eds F. Macar, V. Pouthas, and W. J. Friedman (Dordrecht: Kluwer Academic Publishers), 309–323. doi: 10.1007/978-94-017-3536-0_32

Freyd, J. J., and Finke, R. A. (1984). Representational momentum. *J. Exp. Psychol. Learn. Mem. Cogn.* 10, 126–132.

Freyd, J. J., and Finke, R. A. (1985). A velocity effect for representational momentum. *Bull. Psychon. Soc.* 23, 443–446. doi: 10.3758/bf03329847

Freyd, J. J., and Jones, K. T. (1994). Representational momentum for a spiral path. *J. Exp. Psychol. Learn. Mem. Cogn.* 20, 968–976. doi: 10.1037/0278-7393.20.4.968

Freyd, J. J., Kelly, M. H., and DeKay, M. L. (1990). Representational momentum in memory for pitch. *J. Exp. Psychol. Learn. Mem. Cogn.* 16, 1107–1117. doi: 10.1037/0278-7393.16.6.1107

Friston, K. J. (2005). A theory of cortical responses. *Philos. Trans. R. Soc. Lond. Ser. B Biol. Sci.* 360, 815–836.

Haxby, J. V., Hoffman, E. A., and Gobbini, M. I. (2000). The distributed human neural system for face perception. *Trends Cogn. Sci.* 4, 223–233. doi: 10.1016/s1364-6613(00)01482-0

Hayes, A. E., and Freyd, J. J. (2002). Representational momentum when attention is divided. *Vis. Cogn.* 9, 8–27. doi: 10.1080/13506280143000296

Hillyard, S. A., and Anllo-Vento, L. (1998). Event-related brain potentials in the study of visual selective attention. *Proc. Natl. Acad. Sci. U.S.A.* 95, 781–787.

Hubbard, T. L. (1995). Environmental invariants in the representation of motion: implied dynamics and representational momentum, gravity, friction, and centripetal force. *Psychon. Bull. Rev.* 2, 322–338. doi: 10.3758/bf03210971

Hubbard, T. L. (2005). Representational momentum and related displacements in spatial memory: a review of the findings. *Psychon. Bull. Rev.* 12, 822–851. doi: 10.3758/bf03196775

Hubbard, T. L., and Bharucha, J. J. (1988). Judged displacement in apparent vertical and horizontal motion. *Percept. Psychophys.* 44, 211–221. doi: 10.3758/bf03206290

Hubbard, T. L., and Lange, M. (2010). Prior probabilities and representational momentum. *Vis. Cogn.* 18, 1063–1087. doi: 10.1080/13506281003665708

Joordens, S., Spalek, T. M., Razmy, S., and van Duijn, M. (2004). A clockwork orange: compensation opposing momentum in memory for location. *Mem. Cogn.* 32, 39–50. doi: 10.3758/bf03195819

Kaposvari, P., Kumar, S., and Vogels, R. (2018). Statistical learning signals in macaque inferior temporal cortex. *Cereb. Cortex* 28, 250–266. doi: 10.1093/cercor/bhw374

Kelly, M. H., and Freyd, J. J. (1987). Explorations of representational momentum. *Cogn. Psychol.* 19, 369–401. doi: 10.1016/0010-0285(87)90009-0

Kenemans, J. L., Verbaten, M. N., Roelofs, J. W., and Slangen, J. L. (1989). "Initial-" and "change-orienting reactions": an analysis based on visual single-trial event-related potentials. *Biol. Psychol.* 28, 199–226. doi: 10.1016/0301-0511(89)90001-x

Kimura, M. (2018). Visual mismatch negativity and representational momentum: their possible involvement in the same automatic prediction. *Biol. Psychol.* 139, 178–185. doi: 10.1016/j.biopsycho.2018.10.015

Kimura, M., and Takeda, Y. (2015). Automatic prediction regarding the next state of a visual object: electrophysiological indicators of prediction match and mismatch. *Brain Res.* 1626, 31–44. doi: 10.1016/j.brainres.2015.01.013

Lamme, V. A., and Roelfsema, P. R. (2000). The distinct modes of vision offered by feedforward and recurrent processing. *Trends Neurosci.* 23, 571–579. doi: 10.1016/s0166-2236(00)01657-x

Lamme, V. A., Supèr, H., and Spekreijse, H. (1998). Feedforward, horizontal, and feedback processing in the visual cortex. *Curr. Opin. Neurobiol.* 8, 529–535. doi: 10.1016/s0959-4388(98)80042-1

Lopez-Calderon, J., and Luck, S. J. (2014). ERPLAB: an open-source toolbox for the event-related potentials. *Front. Hum. Neurosci.* 8:213. doi: 10.3389/fnhum.2014.00213

Luck, S. J. (2005). *An Introduction to the Event-Related Potential Technique*. Cambridge, MA: MIT Press.

Luck, S. J. (2014). *An Introduction to the Event-Related Potential Technique*, 2nd Edn. Cambridge, MA: MIT Press.

Luck, S. J., Woodman, G. F., and Vogel, E. K. (2000). Event-related potential studies of attention. *Trends Cogn. Sci.* 4, 432–440.

Mackay, D. M. (1958). Perceptual stability of a stroboscopically lit visual field containing self-luminous objects. *Nature* 181, 507–508. doi: 10.1038/181507a0

Metha, A. D., Ulbert, I., and Schroeder, C. E. (2000). Intermodal selective attention in monkeys. II: physiological mechanisms of modulation. *Cereb. Cortex* 10, 359–370. doi: 10.1093/cercor/10.4.359

Munger, M. P., and Minchew, J. H. (2002). Parallels between remembering and predicting an object's location. *Vis. Cogn.* 9, 177–194. doi: 10.1080/13506280143000386

Nijhawan, R. (1994). Motion extrapolation in catching. *Nature* 370, 256–257. doi: 10.1038/370256b0

Noesselt, T., Hillyard, S. A., Woldorff, M. G., Schoenfeld, A., Hagner, T., Jäncke, L., et al. (2002). Delay striate cortical activation during spatial attention. *Neuron* 35, 575–587. doi: 10.1016/s0896-6273(02)00781-x

Olson, I. R., Chun, M. M., and Allison, T. (2001). Contextual guidance of attention: Human intracranial event-related potential evidence for feedback modulation in anatomically early, temporally late stages of visual processing. *Brain* 124, 1417–1425. doi: 10.1093/brain/124.7.1417

Pak, A., Ryu, E., Li, C., and Chubykin, A. A. (2020). Top-down feedback controls the cortical representation of illusory contours in mouse primary visual cortex. *J. Neurosci.* 40, 648–660. doi: 10.1523/jneurosci.1998-19.2019

Pelli, D. G. (1997). The VideoToolbox software for visual psychophysics: transforming numbers into movies. *Spat. Vis.* 10, 437–442. doi: 10.1163/156856897x00366

Rao, R. P. N., and Ballard, D. H. (1999). Predictive coding in the visual cortex: a functional interpretation of some extra-classical receptive-field effects. *Nat. Neurosci.* 2, 79–87. doi: 10.1038/4580

Summerfield, C., and de Lange, F. P. (2014). Expectation in perceptual decision making: neural and computational mechanisms. *Nat. Rev. Neurosci.* 15, 745–756. doi: 10.1038/nrn3838

Todorovic, A., and de Lange, F. P. (2012). Repetition suppression and expectation suppression are dissociable in time in early auditory evoked fields. *J. Neurosci.* 32, 13389–13395. doi: 10.1523/jneurosci.2227-12.2012

Tong, F. (2003). Primary visual cortex and visual awareness. *Nat. Rev. Neurosci.* 4, 219–229. doi: 10.1038/nrn1055

Tulver, K., Aru, J., Rutiku, R., and Bachmann, T. (2019). Individual differences in the effects of priors on perception: a multi-paradigm approach. *Cognition* 187, 167–177. doi: 10.1016/j.cognition.2019.03.008

Verfaillie, K., and d'Ydewalle, G. (1991). Representational momentum and event course anticipation in the perception of implied periodical motions. *J. Exp. Psychol. Learn. Mem. Cogn.* 17, 302–313. doi: 10.1037/0278-7393.17.2.302

Vergnieux, V., and Vogels, R. (2020). Statistical learning signals for complex visual images in macaque early visual cortex. *Front. Hum. Neurosci.* 14:789. doi: 10.3389/fnins.2020.00789

Conflict of Interest: The author declares that the research was conducted in the absence of any commercial or financial relationships that could be construed as a potential conflict of interest.

frontiers in Human Neuroscience

ORIGINAL RESEARCH
published: 17 September 2021
doi: 10.3389/fnhum.2021.721476

Auditory, Visual, and Cross-Modal Mismatch Negativities in the Rat Auditory and Visual Cortices

*Tomoyo Isoguchi Shiramatsu[1], Kanato Mori[1], Kotaro Ishizu[2] and Hirokazu Takahashi[1]**

[1] Graduate School of Information Science and Technology, The University of Tokyo, Tokyo, Japan, [2] Institute for Quantitative Biosciences, The University of Tokyo, Tokyo, Japan

When the brain tries to acquire an elaborate model of the world, multisensory integration should contribute to building predictions based on the various pieces of information, and deviance detection should repeatedly update these predictions by detecting "errors" from the actual sensory inputs. Accumulating evidence such as a hierarchical organization of the deviance-detection system indicates that the deviance-detection system can be interpreted in the predictive coding framework. Herein, we targeted mismatch negativity (MMN) as a type of prediction-error signal and investigated the relationship between multisensory integration and MMN. In particular, we studied whether and how cross-modal information processing affected MMN in rodents. We designed a new surface microelectrode array and simultaneously recorded visual and auditory evoked potentials from the visual and auditory cortices of rats under anesthesia. Then, we mapped MMNs for five types of deviant stimuli: single-modal deviants in (i) the visual oddball and (ii) auditory oddball paradigms, eliciting single-modal MMN; (iii) congruent audio-visual deviants, (iv) incongruent visual deviants, and (v) incongruent auditory deviants in the audio-visual oddball paradigm, eliciting cross-modal MMN. First, we demonstrated that visual MMN exhibited deviance detection properties and that the first-generation focus of visual MMN was localized in the visual cortex, as previously reported in human studies. Second, a comparison of MMN amplitudes revealed a non-linear relationship between single-modal and cross-modal MMNs. Moreover, congruent audio-visual MMN exhibited characteristics of both visual and auditory MMNs—its latency was similar to that of auditory MMN, whereas local blockage of *N*-methyl-D-aspartic acid receptors in the visual cortex diminished it as well as visual MMN. These results indicate that cross-modal information processing affects MMN without involving strong top-down effects, such as those of prior knowledge and attention. The present study is the first electrophysiological evidence of cross-modal MMN in animal models, and future studies on the neural mechanisms combining multisensory integration and deviance detection are expected to provide electrophysiological evidence to confirm the links between MMN and predictive coding theory.

Keywords: cross-modal information processing, deviance detection, mismatch negativity, microelectrode array, sensory cortex

OPEN ACCESS

Edited by:
Alessandro Tavano,
Max Planck Institute, Germany

Reviewed by:
Motohiro Kimura,
National Institute of Advanced Industrial Science and Technology (AIST), Japan
Flora M. Antunes,
University of Salamanca, Spain

****Correspondence:***
Hirokazu Takahashi
takahashi@i.u-tokyo.ac.jp

Specialty section:
This article was submitted to Cognitive Neuroscience, a section of the journal Frontiers in Human Neuroscience

Received: *07 June 2021*
Accepted: *24 August 2021*
Published: *17 September 2021*

Citation:
Shiramatsu TI, Mori K, Ishizu K and Takahashi H (2021) Auditory, Visual, and Cross-Modal Mismatch Negativities in the Rat Auditory and Visual Cortices. Front. Hum. Neurosci. 15:721476. doi: 10.3389/fnhum.2021.721476

INTRODUCTION

Prediction is an essential brain function required to understand the surrounding environment correctly. According to many theories, including Bayesian and Kahneman's frameworks, the brain is thought to build predictions from various types of information and update these repeatedly by observing "errors" to acquire an elaborate model of the external world (Kahneman, 2011; Clark, 2013). In this prediction-building process, multisensory integration is thought to play an important role to obtain meaningful perceptual experiences by integrating information from different sensory modalities (Tononi et al., 1998; Alais et al., 2010). The latter "updating" process is thought to be triggered by a "prediction error," recognized by using the deviance-detection system of the brain. A recent report that prediction error is hierarchically represented as deviance-detecting neural activities along the sensory pathway is in accordance with the hierarchical predictive coding framework (Friston, 2005; Stefanics et al., 2014). Additionally, previous studies demonstrating that deviance-detecting activities reflect experience and learning suggest that the deviance-detection system is deeply involved in predictions mediated by internal models of the brain, as the predictive coding framework suggests (Menning et al., 2002; Shiramatsu and Takahashi, 2018). Therefore, combination of the multisensory integration and deviance-detecting system contribute to the brain building, maintaining, and renewing a model of the external environment.

Many studies have focused on the deviance detection system of the brain, primarily because the leading candidate for its neural correlates, that is, mismatch negativity (MMN), was discovered relatively early. The first paradigm designed to observe MMN was developed for the auditory domain—an infrequent or deviant sound following a frequent or standard sound elicits auditory MMN (aMMN) (Näätänen et al., 1978). Later, MMN was also confirmed in the context of other sensory modalities (Kekoni et al., 1997; Musall et al., 2017). Currently, visual MMN (vMMN) is the second most prominent focus among MMN studies, particularly in humans (Pazo-Alvarez et al., 2003). Many previous studies have demonstrated that both aMMN and vMMN cannot be fully explained by adaptation, and unpredictable deviations from abstract rules can also elicit MMN (Czigler et al., 2002, 2006; Pazo-Alvarez et al., 2004; Astikainen and Hietanen, 2009; Kimura et al., 2009; Chang et al., 2010; Clifford et al., 2010; Stefanics and Czigler, 2012; Czigler, 2014). This deviance-detection property of MMN has stimulated a predictive coding framework that considers MMN as a type of prediction-error signal (Friston, 2005; Garrido et al., 2008, 2009; Den Ouden et al., 2012). Together with the fact that integration of visual and auditory information is essential for object recognition, the elucidation of the relationship between multisensory integration and MMN should enhance the theoretical understanding of predictive coding.

Despite its importance, very few studies have investigated how cross-modal information processing affects MMN. One reason for this is that the primary brain areas focused on in studies of MMN and multimodal integration are different. The sensory cortex is the earliest source of MMN (Scherg et al., 1989; Csépe et al., 1992; Tiitinen et al., 1993; Alho et al., 1996; Berti and Schröger, 2001; Pincze et al., 2001; Czigler et al., 2002; Shiramatsu et al., 2013), whereas the parietal and frontal cortices are assumed to be essential for multisensory integration (Calvert, 2001; Sereno and Huang, 2014). Another reason for the paucity of these studies is the difficulty in the experimental control of top-down effects, such as prior knowledge and attention. Most human studies investigating the cross-modal effect on MMN have utilized audio-visual illusions, such as the McGurk–MacDonald illusion and the ventriloquist illusion, which often depend on linguistic knowledge (Colin et al., 2002a,b; Stekelenburg et al., 2004; Saint-Amour et al., 2007; Froyen et al., 2008; Andres et al., 2011; Stekelenburg and Vroomen, 2012). Additionally, it is difficult to exclude the influence of attention on the cross-modal information processing when evaluating these illusions using linguistic stimuli. However, notwithstanding the difficulties involved, controlling these top-down effects is important when attempting to clarify the "pre-attentive" cross-modal effects on MMN.

To address this challenge, the present study used anesthetized rats as the first animal model to be used in studying cross-modal MMN. Accumulating evidence has indicated that both aMMN and vMMN in rodents exhibit characteristics similar to those in humans (Shiramatsu et al., 2013; Hamm and Yuste, 2016). Moreover, the top-down effects of prior knowledge and attention can be minimized by using simple non-linguistic stimuli and anesthesia, respectively. Thus, these controls would help reveal the most primitive cross-modal effect on MMN. We also developed a new microelectrode array to cover both the visual and auditory cortices of rats for mapping vMMN, aMMN, and audio-visual MMN. We first tested the deviance-detection property of vMMN because it has not been demonstrated in rats. We then investigated cross-modal effects on MMN by comparing the amplitudes and latencies of the single-modal and audio-visual MMNs. Lastly, we locally blocked *N*-methyl-D-aspartic acid (NMDA) receptors in the visual cortex to investigate the neural mechanisms of cross-modal MMN.

MATERIALS AND METHODS

This study was conducted in strict accordance with the "Guiding Principles for the Care and Use of Animals in the Field of Physiological Science" published by the Japanese Physiological Society. The experimental protocol was approved by the Committee on the Ethics of Animal Experiments at the Graduate School of Information Science and Technology, the University of Tokyo (Permit Number: JA20-2). All surgeries were performed under isoflurane anesthesia, and all efforts were made to minimize the suffering of animals. After the experiments, the animals were euthanized with an overdose of pentobarbital sodium (160 mg/kg, i.p.). The raw data supporting the conclusions of this manuscript will be made available by the authors, without undue reservation, to any qualified researcher.

Implantation of the Head-Fix Attachment

Eleven male Wistar rats (postnatal weeks 9–17; body weight, 260–360 g) were used for the experiments. The rats were

first implanted with a custom-made head-fix attachment (**Figures 1A,B**), which was used to fix them to the experimental neural recording setup. Briefly, the animals were anesthetized using isoflurane (Mylan Inc., PA, United States; 5% v/v in air for induction and 2–3.5% for maintenance) and were held in a stereotaxic apparatus (SR-50; Narishige Group, Tokyo, Japan). Thereafter, a skin incision was made under local anesthesia using xylocaine (1%, 0.2 ml; Aspen Japan, Tokyo, Japan) to expose part of the skull. Five screws (diameter, 1 mm; length, 3 mm) were anchored to the skull—two in the left parietal bone, two in the frontal bone, and one in the interparietal bone (**Figure 1B**). Wires were connected to two of the screws for use as the reference and ground electrodes. Specifically, the screw in the interparietal bone, in contact with the dura over the cerebellum, was used as the ground electrode, and the frontal screw in the left parietal bone, in contact with the dura over the left somatosensory cortex, was used as the reference electrode (the blue and red circles, respectively, in **Figure 1B**). Several previous studies have reported auditory evoked potentials (AEPs) and aMMN using a reference electrode on the somatosensory cortex (Shiramatsu et al., 2013; Shiramatsu and Takahashi, 2018). The screws were fixed to the skull using a dental adhesive (Super-Bond C&B; Sun Medical Co., Ltd., Shiga, Japan), after which the head-fix attachment was mounted and fixed on the skull using dental resin (Unifast TRAD; GC Corporation, Tokyo, Japan). The attachment was custom designed and 3D printed using acrylonitrile butadiene styrene plastic. Part of the right parietal and right temporal bones were covered using dental silicone (DentSilicone-V; Shofu Inc., Kyoto, Japan) rather than dental resin and sealed until we removed these bones at the time of neural recording. After the implantation procedure, an anti-inflammatory agent (Capisten; 5 mg/mL, 0.2 mL; Kissei Pharmaceutical Co., Ltd., Nagano, Japan) and an antibiotic (Bixillin; 25 mg/mL, 0.2 mL; Meiji Seika Pharma Co., Ltd., Tokyo, Japan) were injected intramuscularly to avoid infection.

Neural Recording

More than 3 days after the implantation of the head-fix attachment, the rats were anesthetized again using isoflurane (5% v/v in air for induction and 1–3.5% for maintenance) and held in place in the experimental setup for neural recording (**Figure 1A**). The dental silicone was removed, and the right temporal muscle, cranium, and dura overlying the visual and auditory cortices were locally anesthetized using xylocaine (1%, 0.1–0.3 mL). The exposed cortical surface was perfused with saline to prevent desiccation, and the cisternal cerebrospinal fluid was drained to minimize cerebral edema. A heating blanket was used to maintain body temperature at approximately 37°C. The respiration rate, heart rate, and hind-paw withdrawal reflexes were monitored throughout the experiment to ensure that an adequate and stable level of anesthesia was maintained.

A surface microelectrode array (**Figure 1C**; TU218-008; Unique Medical Co., Ltd., Tokyo, Japan) with 32 recording sites simultaneously recorded visual evoked potentials (VEPs) and AEPs from the visual and auditory cortices, respectively. This microelectrode array covered an area of 5 mm × 7 mm, with the recording sites in the upper left and bottom right quadrants, covering the visual and auditory cortices, respectively. The recording sites were made of platinum and placed between two silicon rubber sheets at a center-to-center distance of 1 mm. The diameter of the exposed surface of each recording site was 250 μm. Neural signals were obtained with an amplification gain of 1,000, a digital filter bandpass of 0.3–500 Hz, and a sampling frequency of 1 kHz (Cerebus Data Acquisition System; Blackrock Microsystems LLC, Salt Lake City, UT, United States).

Visual and Acoustic Stimulation

Visual and acoustic stimuli were provided using MATLAB (MathWorks, Natick, MA, United States) and Psychtoolbox.[1] A display monitor (LCM-T102AS; Logitec Corp., Tokyo, Japan) was positioned 20 cm from the left eye of the animal, at an axis of 60° left from the sagittal axis. A speaker (ST400 BLK; JBL Professional, Northridge, CA, United States or DLS-108X; Alpine Electronics Inc., Tokyo, Japan) was positioned 15 cm in front of the animal. Acoustic stimuli were calibrated at the pinna using a 1/4-inch microphone (4939; Brüel & Kjær, Nærum Denmark) and a spectrum analyzer (CF-5210; Ono Sokki Co., Ltd., Yokohama, Japan). The stimulus level was presented in terms of the sound pressure level in decibels with respect to 20 μPa [dB sound pressure level (SPL)]. The order of data acquisition was randomized, although not completely.

First, we recorded flash-elicited VEPs and click-elicited AEPs to demonstrate that the microelectrode array could separately map the neural activities in the visual and auditory cortices. A flash was a white circle with a 7.5-cm radius on a black background for a duration of 400 ms, and a click was a monophasic positive wave with a duration of 10 ms or 50 μs. The inter-onset interval was 900 ms, and the stimuli were separately presented 60 or 100 times. The amplitude of the middle-latency response, i.e., visual P1 (vP1) or auditory P1 (aP1), was quantified as the maximum potential within 200 ms from the onset of the stimulus.

Single-modal MMN (vMMN and aMMN) and cross-modal MMN were then obtained using several oddball paradigms. The visual test stimuli were white vertical bars (1.875-cm wide and 10-cm high) against a black background, presented for a duration of 400 ms. The bars appeared in two different horizontal positions, 22.8° apart on the viewing angle (first and seventh from the left in **Figure 1D**). The auditory test stimuli were tone bursts (8 or 16 kHz, 60 dB SPL) for a duration of 400 ms, including 5-ms rise/fall times. In the visual or auditory oddball paradigm (**Figures 1Ei,ii**), the two white bars or two pure tones served as either a frequent standard ($p = 0.9$) or a rare deviant ($p = 0.1$). The inter-onset interval between stimuli was 900 ms. After we obtained 60 or 100 deviant responses, we swapped the test position or test frequency of standard and deviant stimuli and then delivered the second oddball session. The grand-averaged deviant response was subtracted from the standard response to the same stimuli, i.e., the position of the bar and tone frequency and the MMN amplitude was quantified as the maximum potential of this difference wave between 50 and 450 ms from the onset of the stimulus. The latency of MMN was

[1] http://psychtoolbox.org/

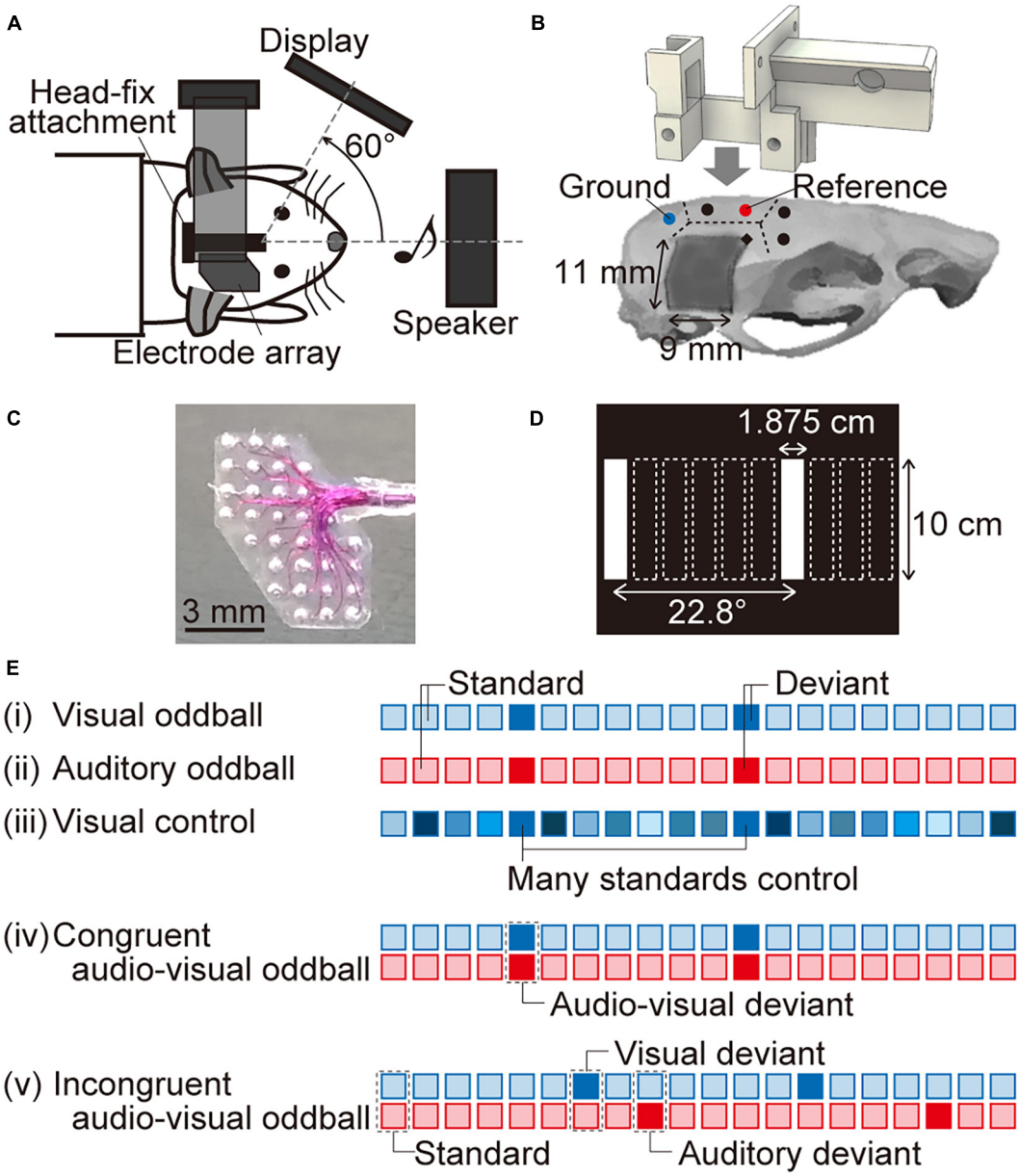

FIGURE 1 | Experimental setup. **(A)** Schema of the experimental system. A custom-designed head-fix attachment implanted on the skull of each tested animal was used to fix it to the experimental neural recording system. The animals were anesthetized using isoflurane, the right visual and auditory cortices were exposed, and an electrode array was positioned onto the surface of the brain. Visual and auditory stimuli were presented from a display monitor facing an axis 60° left from the sagittal axis and from a speaker in front of the rat, respectively. **(B)** The dotted lines indicate the boundaries of the skull. The five circles indicate where the screws (diameter, 1 mm; length, 3 mm) were anchored. Two of these screws made electrical contact with the dura mater for use as the ground and reference electrodes (indicated by the blue and red circles, respectively). The head-fix attachment was fixed on the skull using dental resin. For neural recording, we started drilling into the skull from the point indicated by a black diamond (2-mm posterior and 1.5-mm lateral to the bregma) and removed a part of the right temporal skull (approximately 11 mm × 9 mm, dark gray color). **(C)** Magnified image of the surface microelectrode array with 32 recording sites. The recording sites in the upper left and bottom right cover the visual and auditory cortices, respectively. **(D)** In the visual "many standards control" paradigm, white vertical bars (1.875-cm wide and 10-cm high) at 10 different horizontal positions were displayed on the monitor. Two of these positions (i.e., the first and seventh from the left) were also presented in the oddball paradigm. **(E)** We tested five paradigms to record visual and auditory MMNs. The blue and red squares indicate visual and auditory stimuli, respectively. In (i) the visual oddball and (ii) the auditory oddball paradigm, standard and deviant stimuli were randomly delivered at a 90 and 10% frequency, respectively. (iii) In the visual control paradigm, 10 visual stimuli at different horizontal positions were presented randomly with the same probability as the deviant in the oddball paradigm, i.e., 10%. We also tested two audio-visual oddball paradigms: (iv) in the congruent audio-visual oddball paradigm, visual and auditory deviant stimuli were always presented together, while (v) in the incongruent audio-visual oddball paradigm, they were delivered independently. When the visual and auditory deviant stimuli were presented together in the incongruent audio-visual oddball paradigm, we eliminated the corresponding responses from the analysis. We also performed a second recording for the four oddball paradigms, in which we converted the standard and deviant stimuli to quantify MMN by comparing standard and deviant responses for the same stimuli.

also obtained as the post-stimulus time when the amplitude of the MMN was quantified as the maximum potential difference.

To test whether vMMN in rats exhibited deviance detection properties, VEPs were also investigated in the "many standards control" paradigm (**Figure 1Eiii**). In this control paradigm, white bars in 10 different horizontal positions, including two stimuli used in the oddball paradigm, were presented randomly (**Figure 1D**). The inter-onset interval was 900 ms. The probability of appearance of each test stimulus was identical to that of the deviant stimuli, i.e., 10%, and 60 or 100 control responses were obtained.

To test cross-modal MMN, we delivered two types of cross-modal oddball paradigms, i.e., the congruent and incongruent audio-visual oddball paradigms (**Figures 1Eiv,v**). In these paradigms, the inter-onset interval was same as that in the single-modal oddball paradigms, i.e., 900 ms, and standard stimulus was a combination of the bar at the first position from the left ("left bar") and the 8-kHz tone burst ("low tone") in the first oddball session, or the bar at the seventh position from the left ("right bar") and the 16-kHz tone burst ("high tone") in the second oddball session. In the congruent paradigm, visual and auditory deviants were always presented together; therefore, the deviant stimulus was a combination of "right bar" and "high tone" in the first congruent oddball session. From this paradigm, we obtained the amplitude and the latency of audio-visual MMN (avMMN) in the same way as the single-modal MMN. In the incongruent paradigm, visual and auditory deviants were independently presented; therefore, the stimulus with visual deviant was a combination of "right bar" and "low tone," and the stimulus with auditory deviant was a combination of "left bar" and "high tone" in the first incongruent oddball session with the standard stimuli of "left bar" and "low tone." When the visual and auditory deviants were unexpectedly delivered together in the incongruent audio-visual oddball paradigm, we eliminated the corresponding responses from the analysis. To quantify the amplitude and latency of MMN in the incongruent oddball paradigm, the grand-averaged deviant response was subtracted from the standard response in the other session; specifically, the visual-deviant response for "right bar" and "low tone" was subtracted from the standard response for "right bar" and "high tone." Moreover, the auditory-deviant response for "left bar" and "high tone" was subtracted from the same standard response. The amplitude and latency of MMN were then obtained from the same post-stimulus time as the single-modal MMN.

Administration of an NMDA Receptor Antagonist

To investigate whether NMDA receptors in the visual cortex mediate vMMN and cross-modal MMN, MMNs were also measured following the direct administration of the NMDA receptor agonist D-(-)-2-amino-5-phosphonopentanoic acid (AP5) onto the surface of the visual cortex. Briefly, after the first recording under the oddball paradigms and control paradigm, we removed the microelectrode array and placed a 2% (20 g/L) agarose gel sheet containing 100 μM AP5 onto the surface of the visual cortex. The auditory cortex was covered with a piece of cotton soaked in saline solution to prevent AP5 infiltration. After 15 min, we removed the gel sheet and cotton, mounted the surface array, and recorded MMNs under the auditory oddball, visual oddball, and congruent audio-visual oddball paradigms.

Statistical Analysis

To confirm separate mapping from the visual and auditory cortices, multiple comparisons between the putative regions were conducted separately for vP1 and aP1 using the Kruskal-Wallis test. For *post hoc* comparison, the Wilcoxon one-sided signed-rank test with Bonferroni correction for three comparisons was used.

To demonstrate adaptation for the repetitive standard stimuli, we compared vP1 for the standard, deviant, and "many standards control" VEPs using the Kruskal-Wallis test for multiple comparisons and the Wilcoxon one-sided signed-rank test with Bonferroni correction for three comparisons as a *post hoc* test. Additionally, the Wilcoxon one-sided signed-rank test was used to investigate the deviance-detection property of vMMN by comparing the amplitude of negative deflections between the subtraction of deviant responses from the standard or control response.

To test the cross-modal effect on MMN, comparisons of MMN amplitude were assessed. The Wilcoxon one-sided signed-rank test was applied to compare (1) amplitude of vMMN in the single-modal visual oddball and amplitude of MMN for the visual deviance in the incongruent oddball, (2) amplitude of aMMN in the single-modal auditory oddball and amplitude of MMN for the auditory deviance in the incongruent oddball, and (3) amplitude of avMMN in the congruent oddball and the summation of the amplitude of vMMN and aMMN. Additionally, to reveal the propagation of MMN, we compared the latency of each MMN between the visual and auditory cortices.

Finally, to assess effect of the blockade of NMDA receptors in the visual cortex, the Wilcoxon one-sided signed-rank test was applied to compare the amplitude of each MMN before the blockade with that after the blockade.

All statistical analyses were performed using MATLAB (MathWorks).

RESULTS

Mapping of the Evoked Potentials in the Visual and Auditory Cortices

Figure 2A shows the representative cortical mapping of flash-elicited VEPs and click-elicited AEPs. Both VEPs and AEPs exhibited clear positive potentials, i.e., vP1 and aP1, and aP1 exhibited shorter latencies than vP1. We quantified the amplitude of these P1s as the maximum amplitude within 200 ms from the onset of the stimulus, then mapped them. As shown in these maps (**Figure 2B**), vP1 and aP1 had separate activation foci, which seemed to be localized in the visual and auditory cortices, that is, the upper and lower parts of the recording area, respectively. Based on this observation, we putatively divided the recording area into three regions: the visual cortex, including 15 or fewer recording sites showing a vP1 amplitude larger than 10% of the

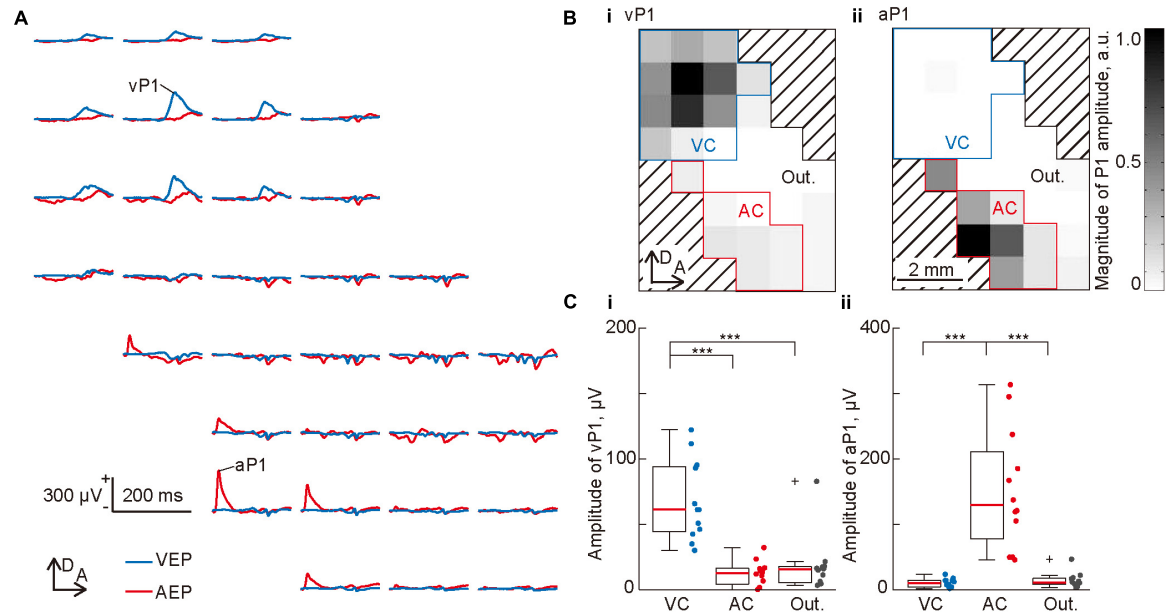

FIGURE 2 | Mapping of the evoked potentials in the visual and auditory cortices. **(A)** Representative mapping of the waveform of a flash-elicited visual evoked potential (VEP; blue lines) and click-elicited auditory evoked potential (AEP; red lines) recorded simultaneously from 32 recording sites. Each waveform is approximately aligned in the spatial coordinates of the recording sites of the surface microelectrode array. Amplitudes of the visual P1 (vP1) and auditory P1 (aP1) was quantified as the maximum amplitude within 200 ms from the onset of the stimulus. **(B)** Spatial distributions of (i) vP1 and (ii) aP1. The gray level at each grid corresponds to the P1 amplitude at each recording site. The recording sites surrounded by blue or red lines were categorized as the putative visual cortex (VC) or auditory cortex (AC), which showed a vP1 or aP1 amplitude larger than 10% of the maximum amplitude. The other recording sites were categorized as the outer region. **(C)** Regional differences in (i) vP1 and (ii) aP1. Dots indicate the mean amplitudes of vP1 and aP1 among each putative region in individual animals ($n = 12$ animals). Asterisks indicate statistical significance in the *post hoc* analysis: ***$p < 0.001$ (Wilcoxon one-sided signed-rank test with Bonferroni correction for three comparisons, following the Kruskal-Wallis test).

maximum amplitude among all the recording sites; the auditory cortex, including 10 or fewer recording sites showing an aP1 amplitude larger than 10% of the maximum amplitude among all recording sites; and the outer region, which encompassed the remaining recording sites (**Figure 2B**). Consequently, the mean amplitude of P1s in these areas was significantly different. The multiple comparison and *post hoc* analyses showed that vP1 was larger in the putative visual cortex (**Figure 2Ci**; Kruskal-Wallis test, $p = 5.6 \times 10^{-6}$; *post hoc* Wilcoxon one-sided signed-rank test with Bonferroni correction for three comparisons, $p = 0.00024$ for visual cortex vs. auditory cortex, and visual cortex vs. outer region, respectively), and that aP1 was larger in the putative auditory cortex (**Figure 2Cii**; Kruskal-Wallis test, $p = 5.6 \times 10^{-6}$; *post hoc* Wilcoxon one-sided signed-rank test with Bonferroni correction for three comparisons, $p = 0.00024$ for auditory cortex vs. visual cortex, and auditory cortex vs. outer region, respectively). These results suggest that the surface microelectrode array could separately map the evoked responses in these cortical regions. Thus, we continued to adopt these putative visual and auditory regions in the subsequent analyses.

Deviance-Detecting Property of the vMMN

We then mapped single-modal MMNs, i.e., vMMN and aMMN, and tested whether vMMN exhibited deviance-detection properties. **Figure 3A** shows the mapping of VEPs and AEPs recorded in the visual oddball, visual many standards control, and auditory oddball paradigms. Again, the first positive peaks, i.e., vP1 and aP1, appeared only in the visual and auditory cortices, respectively, and aP1 appeared earlier than vP1, as described above (**Figures 3B,C** and **Supplementary Figure 1**). In contrast, the deviant responses in both regions exhibited a significant negative deflection with a longer latency than each P1; in other words, vMMN appeared in the auditory cortex, and aMMN appeared in the visual cortex, without distinct P1s. In addition, as shown in **Figures 3B-D**, vMMN appeared earlier in the visual cortex than the auditory cortex, and aMMN appeared earlier in the auditory cortex than the visual cortex, suggesting propagation of single-modal MMN toward another sensory cortex.

Thereafter, the visual "many standards control" paradigm was applied to test the deviance detection property of vMMN. The control responses did not exhibit negative deflection as seen in the deviant responses (**Figures 3A-C**). The results also confirmed that the negative deflections in the deviant responses were significantly larger than those in the standard and control responses (**Figure 3D**). Additionally, comparison of the amplitude of vP1, i.e., the maximum potential within 200 ms from the stimulus onset, demonstrated clear adaptation in the standard responses (**Figure 3Ei**, Kruskal-Wallis test, $p = 0.0052$; *post hoc* Wilcoxon one-sided signed-rank test with

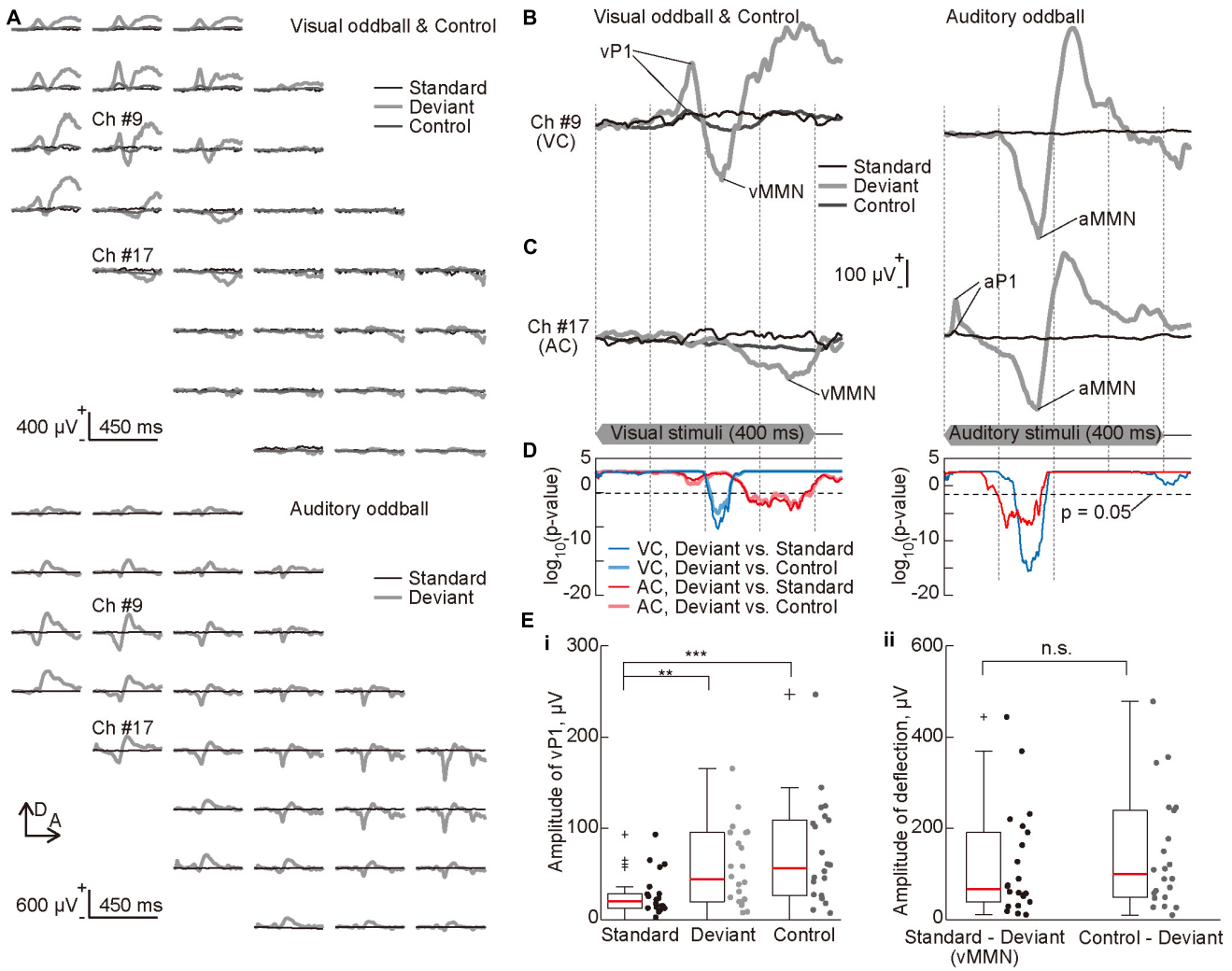

FIGURE 3 | Deviance detection properties of visual mismatch negativity (vMMN). **(A)** Representative mapping of visual evoked potential (VEP) recorded in the visual oddball and control paradigms (top) and auditory evoked potential (AEP) recorded in the auditory oddball paradigm (bottom). The standard (black lines), deviant (bold light gray lines), and the control (dark gray lines) responses were approximately aligned in the spatial coordinates of the recording sites of the surface microelectrode array. **(B,C)** Representative time courses of evoked responses in the oddball paradigms. The traces represent VEPs (left) and AEPs (right) from indicated recording sites **(B)** in the visual (#9) and **(C)** auditory cortices (#17). Prominent components of these traces, i.e., visual P1 (vP1), vMMN, auditory P1 (aP1), and auditory MMN (aMMN) are pointed. The time course of stimulus presentation is indicated at the bottom of the inset. **(D)** Statistical confirmation of MMN as a negative deflection in the deviant responses. The lines show significance level under the null hypothesis that deviant responses are larger than standard or control responses at a given post-stimulus latency time (Wilcoxon one-sided rank-sum test with Bonferroni correction for 450 comparisons). The blue and red lines indicate significance levels for comparison of deviant and standard responses, and the light blue and pink lines indicate those for comparison of deviant and control responses. The blue and light blue lines indicate the recording sites in the visual cortex, and the red and pink lines indicate the recording sites in the auditory cortex. Horizontal broken lines indicate $p = 0.05$. **(E)** The amplitude of (i) vP1 in the standard, deviant, and control responses, and (ii) the negative deflection or MMN quantified in the subtraction of deviant responses from the standard or control responses. Dots indicate the mean amplitudes in the visual cortex of each animal and for each stimulus. Asterisks indicate statistical significance in *post hoc* analysis: $^{**}p < 0.01$; $^{***}p < 0.001$ (Wilcoxon one-sided signed-rank test with Bonferroni correction for three comparisons following the Kruskal-Wallis test).

Bonferroni correction for three comparisons, $p = 0.0016$ for standard vs. deviant responses, 0.00036 for standard vs. control responses). Conversely, amplitude of the negative deflection, i.e., maximum of the difference wave between 50 and 450 ms from the stimulus onset, did not differ irrespective of whether the deviant response was subtracted from the standard response or from the control response (**Figure 3Eii**, $p = 0.63$, Wilcoxon one-sided signed-rank test). Thus, vMMN in rats exhibits deviance-detection properties, as reported for aMMN in our previous study (Shiramatsu et al., 2013).

Comparison Between Cross-Modal MMN and Single-Modal MMN

Mapping of the cross-modal MMN revealed putative cross-modal effects on deviance detection. In response to audio-visual deviant

stimuli in the congruent oddball paradigm, early P1 appeared in the auditory cortex, followed by a negative wave in both the visual and auditory cortices (purple lines in **Figures 4A,D** and **Supplementary Figure 1**). Relatively slow P1 in the visual cortex, which is similar to vP1, was often absent; therefore, we often obtained responses similar to those seen in the auditory oddball paradigm. In the incongruent oddball paradigm, the visual deviant and auditory deviant responses were similar to the deviant responses obtained in the single-modal oddball paradigm (light blue and pink lines in **Figures 4B-D**). There were distinct P1 and earlier MMN in the same modality sensory area as the deviance and late MMN in the other sensory areas. The representative difference waves in all tested oddball paradigms showed that the vMMN in the single-modal visual oddball paradigm (blue lines in **Figure 4E**) and MMN in the incongruent oddball paradigm (light blue lines) were similar and that the aMMN in the single-modal auditory oddball paradigm (red lines) and MMN in the incongruent oddball paradigm (pink lines) were similar (**Figure 4E**). The latency in which a significant MMN ($p < 0.05$ in the comparison between the deviant and standard responses) was found was earlier in the auditory oddball, in the congruent oddball, and auditory deviance in the incongruent oddball than in the visual oddball and visual deviance in the incongruent oddball.

We further investigated the cross-modal effect on MMN amplitude using pooled data. A simple test of the cross-modal

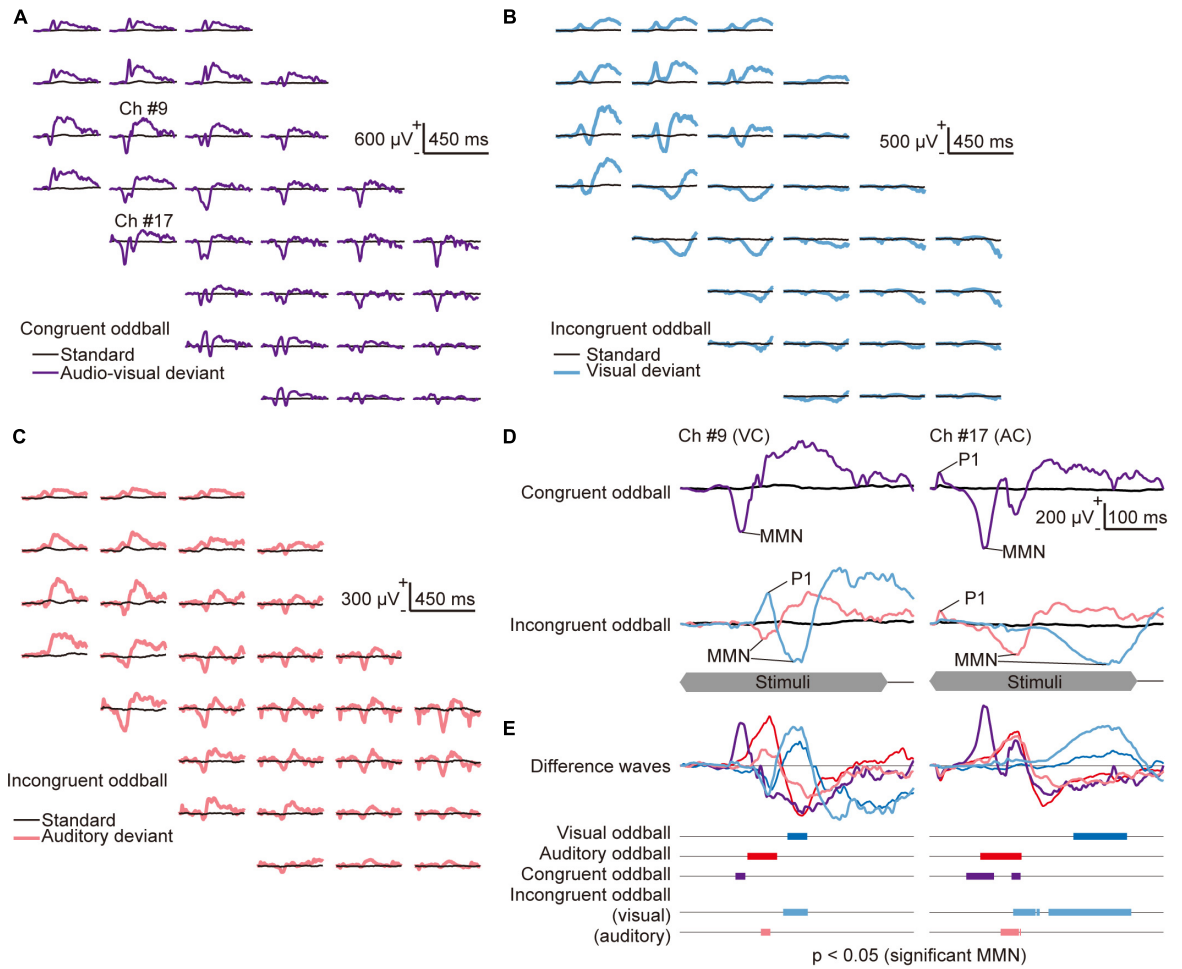

FIGURE 4 | Mapping of the congruent and incongruent audio-visual mismatch negativity (avMMN). **(A–C)** Representative mapping of responses recorded **(A)** in the congruent audio-visual oddball paradigm, where the auditory and visual deviant stimuli were always presented together (purple lines), and (**B–C)** in the incongruent audio-visual oddball paradigm, where **(B)** the visual deviant (light blue lines) and **(C)** the auditory deviant (pink lines) were delivered independently. Both incongruent oddball paradigm maps show the same standard (black lines) responses. **(D)** Responses in the congruent oddball (top) and the incongruent oddball (bottom) paradigm from the indicated recording sites in the visual (left, #9) and auditory cortices (right, #17). The time course of stimulus presentation is indicated at the bottom of the inset. **(E)** Difference waves obtained by subtracting the deviant responses from the standard responses in all tested oddball paradigms: visual oddball (blue lines), auditory oddball (red lines), and congruent audio-visual oddball (purple lines). In the incongruent audio-visual oddball paradigm, the difference wave between the standard, visual-deviant (light blue), and auditory-deviant responses (pink) are shown separately. The bars in the bottom inset represent time courses of each MMN, i.e., the latencies when significant differences were found under the null hypothesis that deviant responses are larger than standard responses (Wilcoxon one-sided rank-sum test with Bonferroni correction for 450 comparisons).

effect is to compare MMN amplitude in the cross-modal paradigm with MMN assumed to be elicited independently in each sensory modality. If there is no cross-modal effect and vMMN and aMMN are always elicited separately, then the amplitude of the MMN for the visual or auditory deviance in the incongruent oddball paradigm (light blue and pink dots in **Figure 5A**) should be the same as the amplitude of the vMMN or aMMN in the single-modal oddball paradigm (blue and red dots), respectively. Moreover, the amplitude of the avMMN in the congruent oddball paradigm (purple dots) may be the same as the summation of the vMMN and aMMN in a single-modal oddball paradigm (gray dots). We found evidence that did not support the above hypothesis. The amplitudes of MMN in the incongruent oddball were smaller than those in the single-modal oddball paradigm in some cases, and the amplitudes of avMMN in the congruent oddball were smaller than the summation of the MMN amplitude in the single-modal oddball paradigm (**Figure 5Ai**: $p = 0.018$, vMMN in single-modal oddball vs. MMN for visual deviance in incongruent oddball; $p = 7.7 \times 10^{-5}$, aMMN in single-modal oddball vs. MMN for auditory deviance in incongruent oddball; $p = 0.00014$, avMMN in congruent oddball vs. summation. **Figure 5Aii**: $p = 0.00012$, aMMN in single-modal oddball vs. MMN for auditory deviance in incongruent oddball; $p = 0.0017$, avMMN in congruent oddball vs. summation; Wilcoxon one-sided signed-rank test), indicating a cross-modal effect on deviance detection.

In analysis of the peak latency of MMN, it was obtained as the post-stimulus time when the amplitude of the MMN was quantified as the maximum and significant potential difference between 50 and 450 ms from the stimulus onset. The latency pattern of avMMN in the congruent oddball paradigm (purple dots in **Figure 5B**) resembled closely with that of aMMN (red dots) as compared to the latency pattern of vMMN (blue dots), indicating the advantage of aMMN over vMMN. Comparison of MMN latency between the visual and auditory cortices showed two types of generation and propagation of MMN. First, vMMN in the single-modal oddball and the MMN for visual deviance in the incongruent oddball (blue and light blue dots) were generated in the visual cortex and propagated with longer latency. Second, aMMN in the single-modal oddball, the MMN for auditory deviance in the incongruent oddball, and avMMN in the congruent oddball (red dots, pink dots, and purple triangles) were generated earlier in the auditory cortex and propagated to the visual cortex (**Figure 5B**: $p = 0.0020$ and 0.00017, vMMN and aMMN in the single-modal oddball paradigm; $p = 0.019$, avMMN in the congruent oddball paradigm; $p = 0.0017$, MMN for the auditory deviance in the incongruent oddball paradigm; Wilcoxon one-sided signed-rank test). Pooling the data according to the relative vertical distance from the border between the visual and auditory regions made these two types of propagation very clear (**Figure 5C**). The propagation time, i.e., the latency difference between the areas was 80–130 ms from the visual to the auditory area and 35–45 ms in the opposite direction. Taken together, these results strongly suggested that visual and auditory deviance detection did not work independently under the cross-modal oddball paradigm. Additionally, cross-modal MMN responding to single-modal deviances was mainly mediated by the corresponding sensory area, whereas avMMN responding to congruent deviance appeared to have a robust source in the auditory area.

Pharmacological Effect of NMDA Receptor Antagonist Administration in the Visual Cortex on Each MMN

Finally, we tested whether NMDA receptor antagonist administration attenuated single-modal vMMN and aMMN and cross-modal avMMN in the congruent oddball paradigm. For this analysis, data were included only when the deviant responses that were obtained before placing the agarose gel sheet exhibited a significant MMN. The antagonist caused significant reductions in the mean amplitude of single-modal vMMN in both sensory areas (**Figure 6**; $p = 0.0012$ and 0.025 for the visual and auditory cortices, respectively; Wilcoxon one-sided signed-rank test) but not of single-modal aMMN ($p = 0.33$ and 0.17 for the visual and auditory cortices, respectively). These different changes indicated that the agarose gel sheet allowed administration of AP5 to the visual cortex.

Lastly, we investigated whether avMMN elicited in the congruent oddball paradigm is mediated by the visual cortex. The mean amplitude of avMMN in the visual cortex was significantly reduced ($p = 0.038$, Wilcoxon one-sided signed-rank test). This reduction in mean amplitude was not significant in the auditory cortex ($p = 0.056$); however, the maximum amplitude in this area was significantly reduced after application of the NMDA antagonist ($p = 0.027$, data not shown). Taken together, these results show that NMDA receptor blockade in the visual cortex attenuated vMMN in the single-modal oddball paradigm and avMMN in the congruent oddball paradigm.

DISCUSSION

In this study, we investigated whether and how cross-modal information processing affects MMN in rodents. After using a surface microelectrode array to map vMMN and aMMN, we found that vMMN in rats exhibited characteristics similar to those previously reported for aMMN—a negative deflection following the P1 response, the deviance detection property, generation from the corresponding sensory area, and dependence on NMDA receptors in that area (Shiramatsu et al., 2013; Shiramatsu and Takahashi, 2021). Furthermore, we recorded three types of cross-modal MMN, that is, avMMN in the congruent oddball paradigm and MMN for the visual and auditory deviances in the incongruent oddball paradigm. Mapping of the amplitudes and latencies of the tested MMNs and administration of an NMDA blocker showed cross-modal effects on MMN. To date, cross-modal audio-visual MMN in rodents has not been reported. Our results emphasize the importance of rodents as animal models for MMN study, and future studies on the neural mechanisms combining multisensory integration and deviance detection are expected to provide electrophysiological evidence to confirm the links between MMN and predictive coding theory.

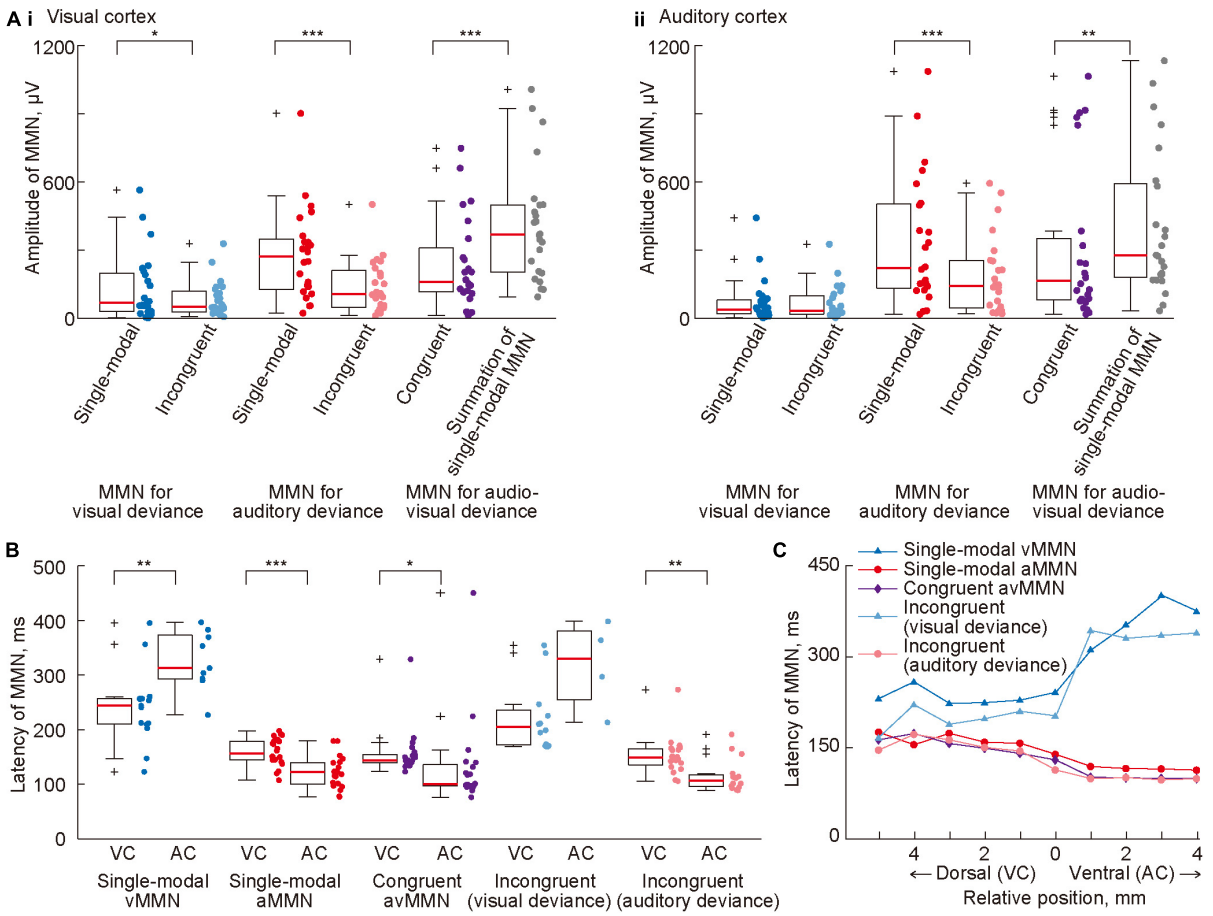

FIGURE 5 | Cross-modal effect on mismatch negativity (MMN) amplitude and latency. **(A)** Mean amplitude of MMN in (i) the visual and (ii) auditory cortices, quantified in all tested paradigms. For comparison, the sum of vMMN and aMMN in the single-modal oddball paradigm is also shown (rightmost). **(B)** Comparison of mean MMN latency in the putative visual cortex (VC) and the putative auditory cortex (AC). **(C)** Propagation of MMN. The median latency of MMN in each row of the recording site was plotted with respect to the relative vertical position from the most ventral row of the putative visual cortex. In panels **(A,B)**, dots indicate the mean amplitudes of MMN in each putative region in individual animals. Asterisks indicate statistical significance: $^{*}p < 0.05$; $^{**}p < 0.01$; $^{***}p < 0.001$ (Wilcoxon one-sided signed-rank test).

Functional Similarity of vMMN Between Rodents and Humans

This study demonstrated four functional characteristics of rat vMMN that were comparable to those of human MMN: morphological characteristics, the deviance detection property, generation in the corresponding sensory area, and dependence on NMDA receptors. First, vMMN appeared in the deviant responses as a negative deflection following vP1 responses, as reported in humans (Sams et al., 1985; Tiitinen et al., 1994; Amenedo and Escera, 2000; Näätänen et al., 2007). The peak latencies of vP1 and vMMN in the visual cortex were approximately 90 and 110–400 ms, respectively (**Figures 3A,B**, **5B**). These latencies were longer than those of the auditory responses, i.e., aP1 at 20 ms and aMMN at 70–190 ms, as reported in several physiological studies (Meredith et al., 1987; Bell et al., 2006; Jaekl et al., 2014), yet the latencies of human vMMN and aMMN are comparable, i.e., 120–300 ms (Berti and Schröger, 2001; Czigler et al., 2002; Pazo-Alvarez et al., 2003; Näätänen et al., 2007). One possible reason is the weak eyesight of rats as nocturnal animals, which sometimes exhibits different structures of the visual cortex compared to humans (Kondo et al., 2016; Maruoka et al., 2017). Our supplemental results indicated that vMMN was not sensitive to the magnitude of deviance (**Supplementary Figure 2**; there was no increase in the amplitude of vMMN for more distant deviants), which also supports the possibility of rats having different visual deviance detection from that of humans. Another possibility is that the visual stimuli used in this study induced weak activation in the rat visual cortex or its deviance detection system (Alho et al., 1992; Czigler et al., 2002; Pazo-Alvarez et al., 2003). A previous mice study reported vMMN in a similar time course with humans (Hamm and Yuste, 2016), using full-field square-wave gratings, which might cause different activation from one vertical bar used in the present study.

Second, despite the long latency, vMMN in rats exhibited a deviance detection property as well as human vMMN

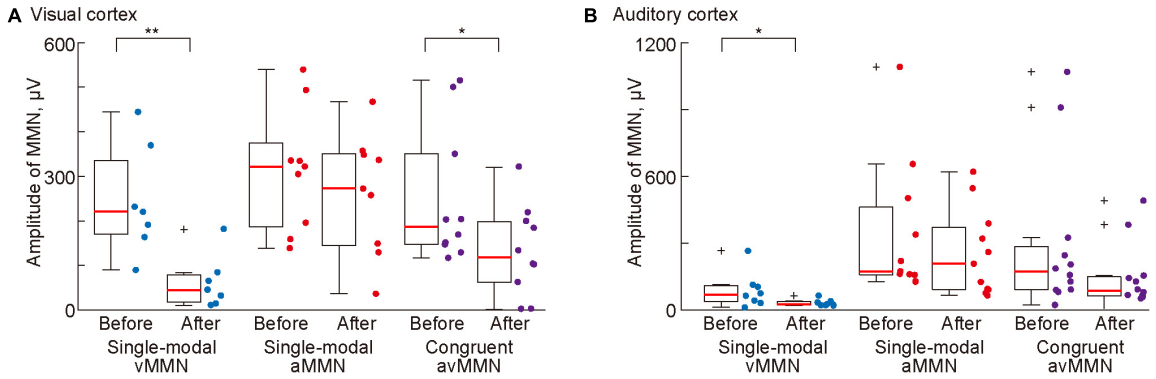

FIGURE 6 | Pharmacological effects of administration of an *N*-methyl-D-aspartic acid (NMDA) antagonist (AP5) in the visual cortex on mismatch negativity (MMN). Mean amplitude of MMN in **(A)** the visual and **(B)** auditory cortices before and after administration of AP5 to the visual cortex. Dots indicate the mean MMN amplitudes in each putative region in individual animals. Asterisks indicate statistical significance: $^{*}p < 0.05$; $^{**}p < 0.01$ (Wilcoxon one-sided signed-rank test).

(Czigler et al., 2002, 2006; Pazo-Alvarez et al., 2004; Kimura et al., 2009). It has been claimed that both vMMN and aMMN in humans represent deviance detection and are not mere effects of adaptation, because they are also elicited by complex changes, such as a violation of categorization or sequential rules (Czigler et al., 2006; Astikainen and Hietanen, 2009; Chang et al., 2010; Clifford et al., 2010; Stefanics and Czigler, 2012; Czigler, 2014). The present study applied a previously designed control paradigm and distinguished the deviance detection property in the vMMN from adaptation. To date, this is the first evidence of the deviance detection property in vMMN in rats, following the previous reports in rabbits (Astikainen et al., 2000) and in mice (Hamm and Yuste, 2016).

Third, the present mapping technique across the two sensory cortices revealed that the MMN for the deviance in one sensory modality first appeared in the corresponding sensory cortex, consistent with several electroencephalography studies (Scherg et al., 1989; Csépe et al., 1992; Tiitinen et al., 1993; Alho et al., 1996; Berti and Schröger, 2001; Czigler et al., 2002). However, because of the low spatial resolution of the present microelectrode array, we could not identify the precise MMN-generating subregion in the visual cortex. It is expected that the higher-order visual area, i.e., the secondary visual area (V2L), or both the primary and higher-order visual areas, are involved, considering that aMMN is generated from the secondary auditory cortex in cats (Pincze et al., 2001) and spreads toward the belt area in rats (Shiramatsu et al., 2013).

Lastly, the present study also demonstrated that single-modal MMN is mainly mediated by NMDA receptors in the corresponding sensory cortex, indicating the role of NMDA receptors in the MMN generation process. Accumulating evidence from both clinical and animal studies has shown that NMDA receptors mediate aMMN (Kreitschmann-Andermahr et al., 2001; Umbricht et al., 2002; Tikhonravov et al., 2010; Shiramatsu et al., 2013), and that aberrant NMDA receptor function diminish vMMN (Shelley et al., 1991; Baldeweg et al., 2004; Urban et al., 2008; Farkas et al., 2015). To date, however, no previous study has directly shown the decrease in vMMN caused by the NMDA receptor blockade, or the effect of limited, local infusion of an NMDA receptor antagonist. The present invasive recording in the rodents allowed us to demonstrate that the blocker that was locally infused into the visual area reduced vMMN in the visual and auditory areas, while aMMN remained unaffected in both areas (**Figure 6**). These results indicate that NMDA receptors contribute to the neural process of deviance detection in a modality-specific manner. However, these receptors might not directly mediate the negative deflection itself. Taken together with a recent report that another neuromodulator, i.e., somatostatin, worked with a similar time-course of MMN (Hamm and Yuste, 2016), the deviance detection process should be divided into several sub-steps, with NMDA receptors contributing to the early steps, such as the construction of prediction. Future studies using local application of blockers or genetically engineered animals could identify the step-by-step role of each neuromodulator in the MMN generation process.

Cross-Modal Effects on MMN in Rodents

The present study demonstrated cross-modal effects in the MMN elicited by three types of deviant stimuli, that is, congruent (or paired) audio-visual deviant and incongruent (or independent) visual and auditory deviant stimuli (**Figure 1E**). Cross-modal effects on the avMMN in the congruent oddball were demonstrated by three characteristics: the latencies similar to aMMN, dependence on the NMDA receptors in the visual area, and the non-linear relationship of its amplitude. First, the shorter latency of the avMMN in the auditory area (**Figures 5B,C**) indicates that some parts of the neural substrates of single-modal aMMN may also mediate avMMN. Second, after the local blockade of the NMDA receptor in the visual area, amplitudes of the avMMN and single-modal vMMN decreased, while that of the single-modal aMMN remained unchanged (**Figure 6**). This result pharmacologically demonstrated the contribution of the deviance detection system in the visual area to avMMN mediation. Lastly, the amplitude of the avMMN was not comparable to the summation of single-modal vMMN and aMMN, supporting a cross-modal effect on MMN (**Figure 5A**). When the deviant detection system manages double deviants

independently, i.e., sound frequency and intensity, the amplitude of MMN shows a linear relationship, i.e., summation of the MMNs for corresponding single deviants (Paavilainen et al., 2001; Wolff and Schröger, 2001). Taken together with the previous report that multi-modal interactions between the deviance detection systems also exhibited non-linear MMN for double-deviants (Butler et al., 2012), the present results demonstrated cross-modal interaction between visual and auditory systems on avMMN in the congruent oddball paradigm.

In the incongruent oddball paradigm, smaller MMNs than the corresponding single-modal oddball paradigm also indicated cross-modal effect (**Figure 5A**). For this non-linear relationship, there were two possible mechanisms. When both modalities were considered together, the probability of deviants was twice (20%) of that of the single-modal oddball paradigm (10%), which could elicit a smaller MMN (Sato et al., 2000; Sabri and Campbell, 2001; Näätänen et al., 2007). The second possibility is that the impact of the deviance was different in the incongruent oddball paradigm due to the multimodal feature integration—when the paired stimuli were perceived as one audio-visual object, the change in the single-modal characteristic should be a "weak deviant," possibly eliciting small MMN. Considering that even unconscious animal subjects can produce MMN based on empirically acquired information (Shiramatsu and Takahashi, 2018), the different impacts of deviance under multimodal feature integration should also affect MMN. In both cases, it can be assumed that the deviance detection functions in the visual and auditory systems were not independent but rather interacted with each other.

To date, audio-visual MMNs have been obtained in humans using experimental designs that highlight top-down effects, such as the McGurk-MacDonald illusion or pairs of specific languages, or language-replicated sounds with letters or speaking faces (Colin et al., 2002a,b; Saint-Amour et al., 2007; Froyen et al., 2008; Andres et al., 2011; Stekelenburg and Vroomen, 2012). Both stimuli need some knowledge of the corresponding language or the habituation process to integrate the appropriate auditory and visual pairs, emphasizing empirically acquired top-down effects on these MMNs. A few studies have used non-linguistic stimuli and demonstrated cross-modal effects on congruent avMMN and incongruent vMMN and aMMN (Stekelenburg et al., 2004; Horvath et al., 2013). However, one of the main interests was the ventriloquist illusion (Stekelenburg et al., 2004) and to demonstrate that MMN reflects our illusory perception; therefore, the detailed interpretation of the results differs from that in the present study. We believe that, to distinguish between top-down and bottom-up effects on audio-visual MMN for linguistic stimuli, further investigation of MMN in humans and animal models using simple stimuli, such as those employed in this study, will be beneficial.

Possible Neural Mechanisms of the Cross-Modal Effect on MMN

The present cross-modal MMN can be modified in various processing stages, i.e., the bottom-up, corticocortical, and top-down pathways (Cappe et al., 2011). Several subcortical nuclei and thalamocortical projection in the auditory ascending pathway exhibit sensitivity to visual inputs and vice versa (Budinger et al., 2006; Alvarado et al., 2007; Porter et al., 2007; Henschke et al., 2015; Kimura, 2020). These subcortical nuclei are sensitive to oddball paradigm and often exhibit strong stimulus-specific adaptation (Escera and Malmierca, 2014; Shiramatsu et al., 2016a; Parras et al., 2017; Takahashi et al., 2020); therefore, they can convey cross-modal information about repetitive inputs to cortical areas. Direct crosstalk between sensory cortices can also affect ongoing predictions and deviance detection (Falchier et al., 2002, 2010; Rockland and Ojima, 2003; Clavagnier et al., 2004; Budinger et al., 2006). Lastly, top-down information about cross-modal integration is expected to influence cortical sensory processing. The functional areas for sensory integration are widely distributed in the brain, i.e., the prefrontal and parietal cortices (Romanski, 2007; Sereno and Huang, 2014). Top-down projections from these associative areas often terminate in higher sensory regions, which are putative foci of MMN generation (Alho et al., 1996; Romanski et al., 1999; Pincze et al., 2001; Shiramatsu et al., 2013). A previous study reported that damage to the prefrontal cortex affected MMN in the auditory cortex, which supports the hypothesis that such top-down projections contribute to the generation of cross-modal MMN to some extent (Alain et al., 1998). Thus, we can expect further advancements in microscale electrophysiological and pharmacological techniques in animal models to reveal the precise neural mechanisms underlying both cross-modal MMN and pre-attentive sensory integration.

As a new phenomenon that could be the subject of future investigation in cross-modal animal MMN, we found interregional propagation of MMN between the visual and auditory cortices (**Figure 5C**). However, the present study could not clarify whether this phenomenon was similar to stimulus-induced traveling waves or transmitted signals, such as the late frontal sources of human aMMN (Rinne et al., 2000). Traveling waves are characterized in multichannel recordings and mainly mediated by long-range horizontal fibers of intracortical axons, spreading within the superficial layers of the cortex (Muller et al., 2018). Involvement of the superficial layers can explain why robust propagation was only found in MMN but not P1—MMN is thought to reflect neural components in the superficial layers, while P1 mainly reflects synaptic current to cortical layer 4 (Javitt et al., 1996; Lee et al., 2004; Fishman and Steinschneider, 2012). Moreover, smooth surface of the rat cortex might emphasize such horizontal spread. The speed of this propagation was reported to be 0.1–0.8 m/s, which is not vastly different from the present results, i.e., 0.02–0.06 m/s (**Figure 5C**; vMMN and aMMN required 80–130 and 35–45 ms, respectively, for an approximately 2-mm propagation). Another possibility is that MMN in one sensory area is transmitted to another area, where it elicits a new MMN-like deflection. In this scenario, the variation in MMN latency between sensory areas should be more significant than within a sensory area, as seen in our study (**Figure 5C**). The asymmetrical transfer rate between visual-to-auditory and auditory-to-visual propagation also supports this possibility. As the poor spatial resolution of the current recording system prevented detailed mapping of latency, we cannot reach

any definitive conclusions. However, in both scenarios, the propagation of MMN may provide cross-modal modulation in other sensory cortices by altering neuronal excitability.

Methodological Considerations

Although the present study succeeded in simultaneous recording from the visual and auditory cortices of rats, there were certain limitations in the context of the comprehensive recording. First, it was often difficult to expose the entire visual cortex surgically. In such cases, the ventral and anterior parts of the visual-related area, which is assumed to include higher-order subregions (i.e., the V2L) than the primary subregion of the visual cortex, was used for recording. Second, due to the design of the microelectrode array, we often failed to cover the higher-order auditory cortex, that is, the ventral auditory subfield (Takahashi et al., 2004, 2005; Shiramatsu et al., 2016b,c). Since our focus was on the global trends between the two sensory cortices, we preferentially covered the boundaries of these areas rather than the more distant subregions. Therefore, we could not categorize the primary and higher-order subregions of these cortices and failed to reveal different cortical maps between P1 and MMN, as in our previous report (Pincze et al., 2001; Shiramatsu et al., 2013). Third, the large inter-electrode distance of 1 mm prevented us from identifying the precise audio-visual border, which made propagation velocities ambiguous. In the future, using a microelectrode array with a higher density of recording sites and a larger coverage area toward the outer boundary of the targeted sensory areas will provide more detailed electrophysiological evidence to elucidate the cross-modal interaction under audio-visual oddball sequences.

In the analysis for the incongruent oddball paradigm, the standard and deviant responses were not derived from the identical audio-visual stimuli (see section "Materials and Methods"). Although the compared standard and deviant stimulus should be identical, its influence on the present result is thought to be small from two perspectives. First, the standard responses did not show distinct deflection in the latency of MMN (**Figures 3**, **4**); therefore, subtraction of the standard responses (almost zero potential) from the deviant responses would not affect the quantified amplitude of MMNs. Second, for the quantification of MMN, we chose the standard and deviant responses so that the stimuli of the deviant modality would be the same. The deviant stimuli would strongly stimulate the sensory system and trigger MMN, supported by the distinct P1 in the modality of deviance (**Figure 4D**); therefore, this subtraction was reasonable in the absence of an identical standard response.

Future Directions

The present study provided evidence of cross-modal effects on animal MMN, which had not been described previously and which will inform future research in this area. Accumulating evidence indicates that MMN in animal models, particularly in rodents, could be homologous to human MMN. We also believe that future studies on rodent MMN will contribute to the elucidation of neural mechanisms underlying aberrant information processing in specific psychological disorders. We previously demonstrated that aMMN in rats reflects salience processing, based on individual experience, inspired by a "naive" asymmetry of the amplitude of aMMN between upward and downward changes (Shiramatsu and Takahashi, 2018). In the present study, vMMN also exhibited similar asymmetry between forward and backward shifts of the stimulus (**Supplementary Figure 2** shows that forwarding changes elicited larger vMMNs than backward changes). This result suggests that vMMN in rats, as in human vMMN, also represents empirical salience (Sulykos et al., 2015). Taken together with the links between the small aMMN and aberrant salience processing in patients with schizophrenia (Baldeweg et al., 2004; Nelson et al., 2014), the present results raise the possibility that such aberrant salience processing can also develop in the visual domain, which could stimulate and inform further investigations into the general neural substrates of specific psychological disorders.

DATA AVAILABILITY STATEMENT

The raw data supporting the conclusions of this article will be made available by the authors, without undue reservation.

ETHICS STATEMENT

The animal study was reviewed and approved by the Committee on the Ethics of Animal Experiments at the Graduate School of Information Science and Technology, the University of Tokyo.

AUTHOR CONTRIBUTIONS

TS, KM, KI, and HT designed the study and approved the final version of the manuscript. KM and KI performed the experiments. TS and KM analyzed the data, interpreted the results, and prepared the figures. TS drafted the manuscript. KM, KI, and HT revised the manuscript. All authors contributed to the article and approved the submitted version.

FUNDING

This work is partially supported by KAKENHI grants (20H04252 and 18K18138), Japan Agency for Medical Research and Development grant (JP21dm0307009), and the Naito Foundation. The results of experiments were partly obtained from projects commissioned by NEDO (18101806-0).

SUPPLEMENTARY MATERIAL

The Supplementary Material for this article can be found online at: https://www.frontiersin.org/articles/10.3389/fnhum.2021.721476/full#supplementary-material

REFERENCES

Alain, C., Woods, D. L., and Knight, R. T. (1998). A distributed cortical network for auditory sensory memory in humans. *Brain Res.* 812, 23–37. doi: 10.1016/S0006-8993(98)00851-8

Alais, D., Newell, F. N., and Mamassian, P. (2010). Multisensory processing in review: from physiology to behaviour. *Seeing Perceiving* 23, 3–38. doi: 10.1163/187847510X488603

Alho, K., Tervaniemi, M., Huotilainen, M., Lavikainen, J., Tiitinen, H., Ilmoniemi, R. J., et al. (1996). Processing of complex sounds in the human auditory cortex as revealed by magnetic brain responses. *Psychophysiology* 33, 369–375. doi: 10.1111/j.1469-8986.1996.tb01061.x

Alho, K., Woods, D. L., Algazi, A., and Näätänen, R. (1992). Intermodal selective attention. II. Effects of attentional load on processing of auditory and visual stimuli in central space. *Electroencephalogr. Clin. Neurophysiol.* 82, 356–368. doi: 10.1016/0013-4694(92)90005-3

Alvarado, J. C., Vaughan, J. W., Stanford, T. R., and Stein, B. E. (2007). Multisensory versus unisensory integration: contrasting modes in the superior colliculus. *J. Neurophysiol.* 97, 3193–3205. doi: 10.1152/jn.00018.2007

Amenedo, E., and Escera, C. (2000). The accuracy of sound duration representation in the human brain determines the accuracy of behavioural perception. *Eur. J. Neurosci.* 12, 2570–2574. doi: 10.1046/j.1460-9568.2000.00114.x

Andres, A. J. D., Oram Cardy, J. E., and Joanisse, M. F. (2011). Congruency of auditory sounds and visual letters modulates mismatch negativity and P300 event-related potentials. *Int. J. Psychophysiol.* 79, 137–146. doi: 10.1016/j.ijpsycho.2010.09.012

Astikainen, P., and Hietanen, J. K. (2009). Event-related potentials to task-irrelevant changes in facial expressions. *Behav. Brain Funct.* 5:30. doi: 10.1186/1744-9081-5-30

Astikainen, P., Ruusuvirta, T., and Korhonen, T. (2000). Cortical and subcortical visual event-related potentials to oddball stimuli in rabbits. *Neuroreport* 11, 1515–1517. doi: 10.1097/00001756-200005150-00030

Baldeweg, T., Klugman, A., Gruzelier, J., and Hirsch, S. R. (2004). Mismatch negativity potentials and cognitive impairment in schizophrenia. *Schizophr. Res.* 69, 203–217. doi: 10.1016/j.schres.2003.09.009

Bell, A. H., Meredith, M. A., Van Opstal, A. J., and Munoz, D. P. (2006). Stimulus intensity modifies saccadic reaction time and visual response latency in the superior colliculus. *Exp. Brain Res.* 174, 53–59. doi: 10.1007/s00221-006-0420-z

Berti, S., and Schröger, E. (2001). A comparison of auditory and visual distraction effects: behavioral and event-related indices. *Cogn. Brain Res.* 10, 265–273. doi: 10.1016/S0926-6410(00)00044-6

Budinger, E., Heil, P., Hess, A., and Scheich, H. (2006). Multisensory processing via early cortical stages: connections of the primary auditory cortical field with other sensory systems. *Neuroscience* 143, 1065–1083. doi: 10.1016/j.neuroscience.2006.08.035

Butler, J. S., Foxe, J. J., Fiebelkorn, I. C., Mercier, M. R., and Molholm, S. (2012). Multisensory representation of frequency across audition and touch: high density electrical mapping reveals early sensory-perceptual coupling. *J. Neurosci.* 32, 15338–15344. doi: 10.1523/JNEUROSCI.1796-12.2012

Calvert, G. A. (2001). Crossmodal processing in the human brain: insights from functional neuroimaging studies. *Cereb. Cortex* 11, 1110–1123. doi: 10.1093/cercor/11.12.1110

Cappe, C., Rouiller, E. M., and Barone, P. (2011). "Cortical and thalamic pathways for multisensory and sensorimotor interplay," in *The Neural Bases of Multisensory Processes*, eds M. M. Murray and M. T. Wallace (Boca Raton, FL: CRC Press), 15–30. doi: 10.1201/b11092-4

Chang, Y., Xu, J., Shi, N., Zhang, B., and Zhao, L. (2010). Dysfunction of processing task-irrelevant emotional faces in major depressive disorder patients revealed by expression-related visual MMN. *Neurosci. Lett.* 472, 33–37. doi: 10.1016/j.neulet.2010.01.050

Clark, A. (2013). Whatever next? Predictive brains, situated agents, and the future of cognitive science. *Behav. Brain Sci.* 36, 181–204. doi: 10.1017/S0140525X12000477

Clavagnier, S., Falchier, A., and Kennedy, H. (2004). Long-distance feedback projections to area V1: implications for multisensory integration, spatial awareness, and visual consciousness. *Cogn. Affect. Behav. Neurosci.* 4, 117–126. doi: 10.3758/CABN.4.2.117

Clifford, A., Holmes, A., Davies, I. R. L., and Franklin, A. (2010). Color categories affect pre-attentive color perception. *Biol. Psychol.* 85, 275–282. doi: 10.1016/j.biopsycho.2010.07.014

Colin, C., Radeau, M., Soquet, A., Dachy, B., and Deltenre, P. (2002a). Electrophysiology of spatial scene analysis: the mismatch negativity (MMN) is sensitive to the ventriloquism illusion. *Clin. Neurophysiol.* 113, 507–518. doi: 10.1016/S1388-2457(02)00028-7

Colin, C., Radeau, M., Soquet, A., Demolin, D., Colin, F., and Deltenre, P. (2002b). Mismatch negativity evoked by the mcgurk-macdonald effect: a phonetic representation within short-term memory. *Clin. Neurophysiol.* 113, 495–506. doi: 10.1016/S1388-2457(02)00024-X

Csépe, V., Pantev, C., Hoke, M., Hampson, S., and Ross, B. (1992). Evoked magnetic responses of the human auditory cortex to minor pitch changes: localization of the mismatch field. *Electroencephalogr. Clin. Neurophysiol.* 84, 538–548. doi: 10.1016/0168-5597(92)90043-b

Czigler, I. (2014). Visual mismatch negativity and categorization. *Brain Topogr.* 27, 590–598. doi: 10.1007/s10548-013-0316-8

Czigler, I., Balázs, L., and Winkler, I. (2002). Memory-based detection of task-irrelevant visual changes. *Psychophysiology* 39, 869–873. doi: 10.1111/1469-8986.3960869

Czigler, I., Weisz, J., and Winkler, I. (2006). ERPs and deviance detection: visual mismatch negativity to repeated visual stimuli. *Neurosci. Lett.* 401, 178–182. doi: 10.1016/j.neulet.2006.03.018

Den Ouden, H. E. M., Kok, P., and de Lange, F. P. (2012). How prediction errors shape perception, attention, and motivation. *Front. Psychol.* 3:548. doi: 10.3389/fpsyg.2012.00548

Escera, C., and Malmierca, M. S. (2014). The auditory novelty system: an attempt to integrate human and animal research. *Psychophysiology* 51, 111–123. doi: 10.1111/psyp.12156

Falchier, A., Clavagnier, S., Barone, P., and Kennedy, H. (2002). Anatomical evidence of multimodal integration in primate striate cortex. *J. Neurosci.* 22, 5749–5759. doi: 10.1523/jneurosci.22-13-05749.2002

Falchier, A., Schroeder, C. E., Hackett, T. A., Lakatos, P., Nascimento-Silva, S., Ulbert, I., et al. (2010). Projection from visual areas V2 and prostriata to caudal auditory cortex in the monkey. *Cereb. Cortex* 20, 1529–1538. doi: 10.1093/cercor/bhp213

Farkas, K., Stefanics, G., Marosi, C., and Csukly, G. (2015). Elementary sensory deficits in schizophrenia indexed by impaired visual mismatch negativity. *Schizophr. Res.* 166, 164–170. doi: 10.1016/j.schres.2015.05.011

Fishman, Y. I., and Steinschneider, M. (2012). Searching for the mismatch negativity in primary auditory cortex of the awake monkey: deviance detection or stimulus specific adaptation? *J. Neurosci.* 32, 15747–15758. doi: 10.1523/JNEUROSCI.2835-12.2012

Friston, K. (2005). A theory of cortical responses. *Philos. Trans. R. Soc. B Biol. Sci.* 360, 815–836. doi: 10.1098/rstb.2005.1622

Froyen, D., Van Atteveldt, N., Bonte, M., and Blomert, L. (2008). Cross-modal enhancement of the MMN to speech-sounds indicates early and automatic integration of letters and speech-sounds. *Neurosci. Lett.* 430, 23–28. doi: 10.1016/j.neulet.2007.10.014

Garrido, M. I., Friston, K. J., Kiebel, S. J., Stephan, K. E., Baldeweg, T., and Kilner, J. M. (2008). The functional anatomy of the MMN: a DCM study of the roving paradigm. *Neuroimage* 42, 936–944. doi: 10.1016/j.neuroimage.2008.05.018

Garrido, M. I., Kilner, J. M., Kiebel, S. J., Stephan, K. E., Baldeweg, T., and Friston, K. J. (2009). Repetition suppression and plasticity in the human brain. *Neuroimage* 48, 269–279. doi: 10.1016/j.neuroimage.2009.06.034

Hamm, J. P., and Yuste, R. (2016). Somatostatin interneurons control a key component of mismatch negativity in mouse visual cortex. *Cell Rep.* 16, 597–604. doi: 10.1016/j.celrep.2016.06.037

Henschke, J. U., Noesselt, T., Scheich, H., and Budinger, E. (2015). Possible anatomical pathways for short-latency multisensory integration processes in primary sensory cortices. *Brain Struct. Funct.* 220, 955–977. doi: 10.1007/s00429-013-0694-4

Horvath, J. C., Schilberg, L., and Thomson, J. (2013). Does sight predominate sound? Electrophysiological evidence for multisensory mismatch negativity correlation. *Neurophysiology* 45, 459–467. doi: 10.1007/s11062-013-9394-1

Jaekl, P., Pérez-Bellido, A., and Soto-Faraco, S. (2014). On the "visual" in "audio-visual integration": a hypothesis concerning visual pathways. *Exp. Brain Res.* 232, 1631–1638. doi: 10.1007/s00221-014-3927-8

Javitt, D. C., Steinschneider, M., Schroeder, C. E., and Arezzo, J. C. (1996). Role of cortical N-methyl-D-aspartate receptors in auditory sensory memory and mismatch negativity generation: implications for schizophrenia. *Proc. Natl. Acad. Sci. U.S.A.* 93, 11962–11967. doi: 10.1073/pnas.93.21.11962

Kahneman, D. (2011). *Thinking, Fast and Slow*. New York, NY: Farrar, Straus and Giroux.

Kekoni, J., Hämäläinen, H., Saarinen, M., Gröhn, J., Reinikainen, K., Lehtokoski, A., et al. (1997). Rate effect and mismatch responses in the somatosensory system: ERP-recordings in humans. *Biol. Psychol.* 46, 125–142. doi: 10.1016/S0301-0511(97)05249-6

Kimura, A. (2020). Cross-modal modulation of cell activity by sound in first-order visual thalamic nucleus. *J. Comp. Neurol.* 528, 1917–1941. doi: 10.1002/cne.24865

Kimura, M., Katayama, J., Ohira, H., and Schröger, E. (2009). Visual mismatch negativity: new evidence from the equiprobable paradigm. *Psychophysiology* 46, 402–409. doi: 10.1111/j.1469-8986.2008.00767.x

Kondo, S., Yoshida, T., and Ohki, K. (2016). Mixed functional microarchitectures for orientation selectivity in the mouse primary visual cortex. *Nat. Commun.* 7:13210. doi: 10.1038/ncomms13210

Kreitschmann-Andermahr, I., Rosburg, T., Demme, U., Gaser, E., Nowak, H., and Sauer, H. (2001). Effect of ketamine on the neuromagnetic mismatch field in healthy humans. *Cogn. Brain Res.* 12, 109–116. doi: 10.1016/S0926-6410(01)00043-X

Lee, C. C., Schreiner, C. E., Imaizumi, K., and Winer, J. A. (2004). Tonotopic and heterotopic projection systems in physiologically defined auditory cortex. *Neuroscience* 128, 871–887. doi: 10.1016/j.neuroscience.2004.06.062

Maruoka, H., Nakagawa, N., Tsuruno, S., Sakai, S., Yoneda, T., and Hosoya, T. (2017). Lattice system of functionally distinct cell types in the neocortex. *Science* 358, 610–615. doi: 10.1126/science.aam6125

Menning, H., Imaizumi, S., Zwitserlood, P., and Pantev, C. (2002). Plasticity of the human auditory cortex induced by discrimination learning of non-native, mora-timed contrasts of the japanese language. *Learn. Mem.* 9, 253–267. doi: 10.1101/lm.49402

Meredith, M. A., Nemitz, J. W., and Stein, B. E. (1987). Determinants of multisensory integration in superior colliculus neurons. I. Temporal factors. *J. Neurosci.* 7, 3215–3229. doi: 10.1523/jneurosci.07-10-03215.1987

Muller, L., Chavane, F., Reynolds, J., and Sejnowski, T. J. (2018). Cortical travelling waves: mechanisms and computational principles. *Nat. Rev. Neurosci.* 19, 255–268. doi: 10.1038/nrn.2018.20

Musall, S., Haiss, F., Weber, B., and von der Behrens, W. (2017). Deviant processing in the primary somatosensory cortex. *Cereb. Cortex* 27, 863–876. doi: 10.1093/cercor/bhv283

Näätänen, R., Gailland, A. W. K., and Mäntysalo, S. (1978). Early selective-attention effect on evoked potential reinterpreted. *Acta Psychol.* 42, 313–329. doi: 10.1016/0001-6918(78)90006-9

Näätänen, R., Paavilainen, P., Rinne, T., and Alho, K. (2007). The mismatch negativity (MMN) in basic research of central auditory processing: a review. *Clin. Neurophysiol.* 118, 2544–2590. doi: 10.1016/j.clinph.2007.04.026

Nelson, B., Whitford, T. J., Lavoie, S., and Sass, L. A. (2014). What are the neurocognitive correlates of basic self-disturbance in schizophrenia?: integrating phenomenology and neurocognition. Part 2 (Aberrant salience). *Schizophr. Res.* 152, 20–27. doi: 10.1016/j.schres.2013.06.033

Paavilainen, P., Valppu, S., and Näätänen, R. (2001). The additivity of the auditory feature analysis in the human brain as indexed by the mismatch negativity: 1+1≈152;2 but 1+1+1<3. *Neurosci. Lett.* 301, 179–182. doi: 10.1016/S0304-3940(01)01635-4

Parras, G. G., Nieto-Diego, J., Carbajal, G. V., Valdés-Baizabal, C., Escera, C., and Malmierca, M. S. (2017). Neurons along the auditory pathway exhibit a hierarchical organization of prediction error. *Nat. Commun.* 8:2148. doi: 10.1038/s41467-017-02038-6

Pazo-Alvarez, P., Amenedo, E., and Cadaveira, F. (2004). Automatic detection of motion direction changes in the human brain. *Eur. J. Neurosci.* 19, 1978–1986. doi: 10.1111/j.1460-9568.2004.03273.x

Pazo-Alvarez, P., Cadaveira, F., and Amenedo, E. (2003). MMN in the visual modality: a review. *Biol. Psychol.* 63, 199–236. doi: 10.1016/S0301-0511(03)00049-8

Pincze, Z., Lakatos, P., Rajkai, C., Ulbert, I., and Karmos, G. (2001). Separation of mismatch negativity and the N1 wave in the auditory cortex of the cat: a topographic study. *Clin. Neurophysiol.* 112, 778–784. doi: 10.1016/s1388-2457(01)00509-0

Porter, K. K., Metzger, R. R., and Groh, J. M. (2007). Visual- and saccade-related signals in the primate inferior colliculus. *Proc. Natl. Acad. Sci. U.S.A.* 104, 17855–17860. doi: 10.1073/pnas.0706249104

Rinne, T., Alho, K., Ilmoniemi, R. J., Virtanen, J., and Näätänen, R. (2000). Separate time behaviors of the temporal and frontal mismatch negativity sources. *Neuroimage* 12, 14–19. doi: 10.1006/nimg.2000.0591

Rockland, K. S., and Ojima, H. (2003). Multisensory convergence in calcarine visual areas in macaque monkey. *Int. J. Psychophysiol.* 50, 19–26. doi: 10.1016/S0167-8760(03)00121-1

Romanski, L. M. (2007). Representation and integration of auditory and visual stimuli in the primate ventral lateral prefrontal cortex. *Cereb. Cortex* 17(Suppl. 1), i61–i69. doi: 10.1093/cercor/bhm099

Romanski, L. M., Bates, J. F., and Goldman-Rakic, P. S. (1999). Auditory belt and parabelt projections to the prefrontal cortex in the rhesus monkey. *J. Comp. Neurol.* 403, 141–157. doi: 10.1002/(SICI)1096-9861(19990111)403:2<141:AID-CNE1<3.0.CO;2-V

Sabri, M., and Campbell, K. B. (2001). Effects of sequential and temporal probability of deviant occurrence on mismatch negativity. *Cogn. Brain Res.* 12, 171–180. doi: 10.1016/S0926-6410(01)00026-X

Saint-Amour, D., De Sanctis, P., Molholm, S., Ritter, W., and Foxe, J. J. (2007). Seeing voices: high-density electrical mapping and source-analysis of the multisensory mismatch negativity evoked during the McGurk illusion. *Neuropsychologia* 45, 587–597. doi: 10.1016/j.neuropsychologia.2006.03.036

Sams, M., Paavilainen, P., Alho, K., and Näätänen, R. (1985). Auditory frequency discrimination and event-related potentials. *Electroencephalogr. Clin. Neurophysiol.* 62, 437–448. doi: 10.1016/0168-5597(85)90054-1

Sato, Y., Yabe, H., Hiruma, T., Sutoh, T., Shinozaki, N., Nashida, T., et al. (2000). The effect of deviant stimulus probability on the human mismatch process. *Neuroreport* 11, 3703–3708. doi: 10.1097/00001756-200011270-00023

Scherg, M., Vajsar, J., and Picton, T. W. (1989). A source analysis of the late human auditory evoked potentials. *J. Cogn. Neurosci.* 1, 336–355. doi: 10.1162/jocn.1989.1.4.336

Sereno, M. I., and Huang, R. S. (2014). Multisensory maps in parietal cortex. *Curr. Opin. Neurobiol.* 24, 39–46. doi: 10.1016/j.conb.2013.08.014

Shelley, A. M., Ward, P. B., Catts, S. V., Michie, P. T., Andrews, S., and McConaghy, N. (1991). Mismatch negativity: an index of a preattentive processing deficit in schizophrenia. *Biol. Psychiatry* 30, 1059–1062. doi: 10.1016/0006-3223(91)90126-7

Shiramatsu, T. I., Hitsuyu, R., Ibayashi, K., Kanzaki, R., Kawai, K., and Takahashi, H. (2016a). "Effect of vagus nerve stimulation on neural adaptation in thalamo-cortical system in rats," in *Proceedings of the Annual International Conference of the IEEE Engineering in Medicine and Biology Society, EMBS*, Orlando, FL, 1834–1837. doi: 10.1109/EMBC.2016.7591076

Shiramatsu, T. I., Noda, T., Akutsu, K., and Takahash, H. (2016b). Tonotopic and field-specific representation of long-lasting sustained activity in rat auditory cortex. *Front. Neural Circuits* 10:59. doi: 10.3389/fncir.2016.00059

Shiramatsu, T. I., Takahashi, K., Noda, T., Kanzaki, R., Nakahara, H., and Takahashi, H. (2016c). Microelectrode mapping of tonotopic, laminar, and field-specific organization of thalamo-cortical pathway in rat. *Neuroscience* 332, 38–52. doi: 10.1016/j.neuroscience.2016.06.024

Shiramatsu, T. I., Kanzaki, R., and Takahashi, H. (2013). Cortical mapping of mismatch negativity with deviance detection property in rat. *PLoS One* 8:e82663. doi: 10.1371/journal.pone.0082663

Shiramatsu, T. I., and Takahashi, H. (2018). Mismatch negativity in rat auditory cortex represents the empirical salience of sounds. *Front. Neurosci.* 12:924. doi: 10.3389/fnins.2018.00924

Shiramatsu, T. I., and Takahashi, H. (2021). Mismatch-negativity (MMN) in animal models: homology of human MMN? *Hear. Res.* 399:107936. doi: 10.1016/j.heares.2020.107936

Stefanics, G., and Czigler, I. (2012). Automatic prediction error responses to hands with unexpected laterality: an electrophysiological study. *Neuroimage* 63, 253–261. doi: 10.1016/j.neuroimage.2012.06.068

Stefanics, G., Stefanics, G., Kremláček, J., and Czigler, I. (2014). Visual mismatch negativity: a predictive coding view. *Front. Hum. Neurosci.* 8:666. doi: 10.3389/fnhum.2014.00666

Stekelenburg, J. J., and Vroomen, J. (2012). Electrophysiological evidence for a multisensory speech-specific mode of perception. *Neuropsychologia* 50, 1425–1431. doi: 10.1016/j.neuropsychologia.2012.02.027

Stekelenburg, J. J., Vroomen, J., and De Gelder, B. (2004). Illusory sound shifts induced by the ventriloquist illusion evoke the mismatch negativity. *Neurosci. Lett.* 357, 163–166. doi: 10.1016/j.neulet.2003.12.085

Sulykos, I., Kecskés-Kovács, K., and Czigler, I. (2015). Asymmetric effect of automatic deviant detection: the effect of familiarity in visual mismatch negativity. *Brain Res.* 1626, 108–117. doi: 10.1016/j.brainres.2015.02.035

Takahashi, H., Nakao, M., and Kaga, K. (2004). Cortical mapping of auditory-evoked offset responses in rats. *Neuroreport* 15, 1565–1569. doi: 10.1097/01.wnr.0000134848.63755.5c

Takahashi, H., Nakao, M., and Kaga, K. (2005). Interfield differences in intensity and frequency representation of evoked potentials in rat auditory cortex. *Hear. Res.* 210, 9–23. doi: 10.1016/j.heares.2005.05.014

Takahashi, H., Shiramatsu, T. I., Hitsuyu, R., Ibayashi, K., and Kawai, K. (2020). Vagus nerve stimulation (VNS)-induced layer-specific modulation of evoked responses in the sensory cortex of rats. *Sci. Rep.* 10:8932. doi: 10.1038/s41598-020-65745-z

Tiitinen, H., Alho, K., Huotilainen, M., Ilmoniemi, R. J., Simola, J., and Näätänen, R. (1993). Tonotopic auditory cortex and the magnetoencephalographic (MEG) equivalent of the mismatch negativity. *Psychophysiology* 30, 537–540. doi: 10.1111/j.1469-8986.1993.tb02078.x

Tiitinen, H., May, P., Reinikainen, K., and Näätänen, R. (1994). Attentive novelty detection in humans is governed by pre-attentive sensory memory. *Nature* 372, 90–92. doi: 10.1038/372090a0

Tikhonravov, D., Neuvonen, T., Pertovaara, A., Savioja, K., Ruusuvirta, T., Näätänen, R., et al. (2010). Dose-related effects of memantine on a mismatch negativity-like response in anesthetized rats. *Neuroscience* 167, 1175–1182. doi: 10.1016/j.neuroscience.2010.03.014

Tononi, G., Edelman, G. M., and Sporns, O. (1998). Complexity and coherency: integrating information in the brain. *Trends Cogn. Sci.* 2, 474–484. doi: 10.1016/S1364-6613(98)01259-5

Umbricht, D., Koller, R., Vollenweider, F. X., and Schmid, L. (2002). Mismatch negativity predicts psychotic experiences induced by NMDA receptor antagonist in healthy volunteers. *Biol. Psychiatry* 51, 400–406. doi: 10.1016/s0006-3223(01)01242-2

Urban, A., Kremláček, J., Masopust, J., and Libiger, J. (2008). Visual mismatch negativity among patients with schizophrenia. *Schizophr. Res.* 102, 320–328. doi: 10.1016/j.schres.2008.03.014

Wolff, C., and Schröger, E. (2001). Human pre-attentive auditory change-detection with single, double, and triple deviations as revealed by mismatch negativity additivity. *Neurosci. Lett.* 311, 37–40. doi: 10.1016/S0304-3940(01)02135-8

Conflict of Interest: The authors declare that the research was conducted in the absence of any commercial or financial relationships that could be construed as a potential conflict of interest.

Publisher's Note: All claims expressed in this article are solely those of the authors and do not necessarily represent those of their affiliated organizations, or those of the publisher, the editors and the reviewers. Any product that may be evaluated in this article, or claim that may be made by its manufacturer, is not guaranteed or endorsed by the publisher.

frontiers in Human Neuroscience

ORIGINAL RESEARCH
published: 28 September 2021
doi: 10.3389/fnhum.2021.734200

Standard Tone Stability as a Manipulation of Precision in the Oddball Paradigm: Modulation of Prediction Error Responses to Fixed-Probability Deviants

Iria SanMiguel[1,2,3†], Jordi Costa-Faidella[1,2,3†], Zulay R. Lugo[4], Elisabet Vilella[4,5] and Carles Escera[1,2,3]*

[1] Brainlab-Cognitive Neuroscience Research Group, Department of Clinical Psychology and Psychobiology, University of Barcelona, Barcelona, Spain, [2] Institute of Neurosciences, University of Barcelona, Barcelona, Spain, [3] Institut de Recerca Sant Joan de Déu, Esplugues de Llobregat, Spain, [4] Hospital Universitari Institut Pere Mata, Universitat Rovira i Virgili (URV), Institut d'Investigació Sanitària Pere Virgili (IISPV), Reus, Spain, [5] Centro de Investigación Biomédica en Red en Salud Mental (CIBERSAM), Madrid, Spain

OPEN ACCESS

Edited by:
Juanita Todd,
The University of Newcastle, Australia

Reviewed by:
Satu Pakarinen,
University of Helsinki, Finland
Elyse S. Sussman,
Albert Einstein College of Medicine, United States

***Correspondence:**
Iria SanMiguel
isanmiguel@ub.edu

† These authors have contributed equally to this work and share first authorship

Specialty section:
This article was submitted to Cognitive Neuroscience, a section of the journal Frontiers in Human Neuroscience

Received: *30 June 2021*
Accepted: *09 September 2021*
Published: *28 September 2021*

Citation:
SanMiguel I, Costa-Faidella J, Lugo ZR, Vilella E and Escera C (2021) Standard Tone Stability as a Manipulation of Precision in the Oddball Paradigm: Modulation of Prediction Error Responses to Fixed-Probability Deviants. Front. Hum. Neurosci. 15:734200. doi: 10.3389/fnhum.2021.734200

Electrophysiological sensory deviance detection signals, such as the mismatch negativity (MMN), have been interpreted from the predictive coding framework as manifestations of prediction error (PE). From a frequentist perspective of the classic oddball paradigm, deviant stimuli are unexpected because of their low probability. However, the amount of PE elicited by a stimulus can be dissociated from its probability of occurrence: when the observer cannot make confident predictions, any event holds little surprise value, no matter how improbable. Here we tested the hypothesis that the magnitude of the neural response elicited to an improbable sound (D) would scale with the precision of the prediction derived from the repetition of another sound (S), by manipulating repetition stability. We recorded the Electroencephalogram (EEG) from 20 participants while passively listening to 4 types of isochronous pure tone sequences differing in the probability of the S tone (880 Hz) while holding constant the probability of the D tone [1,046 Hz; p(D) = 1/11]: Oddball [p(S) = 10/11]; High confidence (7/11); Low confidence (4/11); and Random (1/11). Tones of 9 different frequencies were equiprobably presented as fillers [p(S) + p(D) + p(F) = 1]. Using a mass-univariate non-parametric, cluster-based correlation analysis controlling for multiple comparisons, we found that the amplitude of the deviant-elicited ERP became more negative with increasing S probability, in a time-electrode window consistent with the MMN (ca. 120–200 ms; frontal), suggesting that the strength of a PE elicited to an improbable event indeed increases with the precision of the predictive model.

Keywords: uncertainty, precision, prediction error, mismatch negativity (MMN), deviance detection, predictability, oddball

INTRODUCTION

According to current models that view the brain as a Bayesian inference system, our experience of the world stems from internal representations of the statistical regularities of the sensory input. These internal representations embody our experience and prior knowledge about the world, and the associated expectations. Based on these representations, internal forward models continuously make predictions regarding the sensory input (Friston, 2010). Predictions are compared with incoming sensory information and prediction error (PE) is used to adjust the internal representations. This comparison process and the ensuing generation of PE signals is also referred to as sensory deviance detection, and it is reflected in electrophysiological responses, most notably in the mismatch negativity (MMN; Garrido et al., 2009). Today, deviance detection is widely accepted as a general principle of brain function (Friston, 2010; Escera and Malmierca, 2014; Malmierca et al., 2014).

An aspect of this process which is much less well-established in the deviance detection literature is the proposal that it is flexibly adjusted depending on the estimated precision of the sensory signals, or in other words, the confidence that can be placed in the current internal models and the predictions derived from them. Specifically, it is proposed that the gain of the PE signals is modulated ("precision-weighted") by their expected precision, thereby adjusting the impact that the PE has in terms of updating the internal representations (Feldman and Friston, 2010; Schröger et al., 2015). This is critical for the proper formation and updating of predictive models under different contexts and levels of noise, avoiding issues like overfitting, and allowing a dynamic adjustment of the balance between the weight placed on priors and the weight placed on sensory evidence when interpreting sensory input. Precision-weighting of the gain of the PE signal is also proposed to be the mechanism through which attention operates to modulate sensory responses (Feldman and Friston, 2010). Moreover, it has been proposed that dysfunctional precision-weighting might be a critical factor in schizophrenia and autism, in which the balance between the weight placed on priors and evidence would be skewed toward the priors in the former and toward the evidence in the latter (Adams et al., 2013; Lawson et al., 2014, 2017). Thus, the concept of precision or confidence appears to be a central aspect of generating and using internal models, crucial in determining our experience through its influence on perception and attention.

Nevertheless, the concept of confidence or precision is somewhat elusive and has been rarely operationalized in a clear way in deviance detection studies. So far, it seems unclear how to measure confidence and investigate it with a simple paradigm that is also applicable to clinical settings. The aim of this report is to propose a simple manipulation that taps into precision or confidence based on the most common design to investigate deviance detection, the oddball paradigm, allowing us to investigate the hypothesis that sensory deviance detection signals are precision weighted.

In the typical oddball paradigm used to study deviance detection, two stimuli are presented with differing probabilities; an infrequent "deviant" stimulus is interspersed among the repeating presentation of the frequent "standard" stimulus. When the electrophysiological responses elicited by the deviant are compared to those elicited by the standard, a negative deflection can be observed on the difference waveform in the 100-200 ms latency range: the mismatch negativity (MMN; Näätänen, 1992). Thus, the MMN signals the detection of a change in the sensory stream. Since the discovery of the MMN, thousands of studies have used variations of the oddball paradigm, applying the MMN to study a wide range of issues in basic and clinical research, proving to be a powerful tool to study brain function (Näätänen et al., 2007, 2011, 2012). For the MMN to continue to be so useful, our understanding of the underlying MMN-generating process and significance must continue to be updated and evolve (Winkler, 2007).

Indeed, there has been a substantial progression on the explanatory theories regarding the type of computation indexed by the MMN-generating process. Initially, the sensory memory trace hypothesis proposed that each incoming stimulus is compared with the trace of the preceding stimuli stored in sensory memory and that MMN is elicited when the incoming stimulus differs (Näätänen, 1992). An alternative explanation proposed that the MMN is the result of the differential state of refractoriness or adaptation of the neural populations responding to the standard and deviant stimulus, with the standard population being more refractory due to the high rate of responses to the repeating standard, and thus eliciting a diminished response ("release from refractoriness," Näätänen, 1990, 1992), or "N1 adaptation hypothesis" (Jääskeläinen et al., 2004; May and Tiitinen, 2010) compared to the deviant. Currently, it is generally acknowledged that refractoriness differences underlie part of the effects measured in most of the classic deviance detection studies unless this aspect is properly controlled (Näätänen et al., 2005; Escera and Malmierca, 2014). Nevertheless, the predominant view is that there exists a unique deviance detection process indexed beyond refractoriness differences (the "true" MMN). Building up on this idea, the sensory memory trace hypothesis evolved into considering the trace against which each incoming stimulus is compared more of an abstract representation of a regularity, rather than a literal trace of the standard stimulus. The idea of regularity representations facilitated a transition from memory-based to prediction-based explanations, proposing that the comparison is not to a memory trace, but rather to a prediction generated on the basis of the regularity. Perhaps the currently best accepted view of the MMN is the model adjustment hypothesis, which also highlights the predictive model, proposing that the MMN-generating process has a direct role in the building of the predictive internal representation itself, rather than simply signaling deviance detection (Winkler and Czigler, 1998; Winkler, 2007). In this view, the MMN reflects the updating of the internal representation on the basis of how well the incoming stimuli match the predictions generated by the predictive model. However, while these last models stress the predictive aspect, they did not define how specifically the predictive representation is formed and applied. More recently, MMN has been interpreted from the predictive coding perspective as a manifestation of PE (Garrido et al., 2009; Wacongne et al., 2011; Lieder et al., 2013;

Schröger et al., 2015; Stefanics et al., 2018), placing the MMN-generating process within a wider conceptualization of the brain as a Bayesian inference system (Knill and Pouget, 2004; Friston, 2010) and thus providing a detailed explanation of the computations involved in the underlying inference process.

The different MMN models emphasize different aspects when it comes to understanding exactly what the *deviance* in deviance detection is, and thus outlining the factors that might influence MMN elicitation and amplitude. From a rather simple frequentist perspective of the classic oddball paradigm, the deviance associated with an event relates to its improbability, given a prediction of the occurrence of all possible events. Thus, in this view, the differential processing of deviant stimuli is determined exclusively by their low probability. This interpretation fits well with the N1-adaptation hypothesis, in which the effects would be due solely to differential base rate probability of the standard and deviant. However, from a Bayesian perspective PE (and thus MMN) reflects a violation of expectations, and can be related in a straightforward manner to the concept of Bayesian surprise (Ostwald et al., 2012). Bayesian surprise quantifies how incoming data affects an observer, by measuring the difference between the observer's beliefs before and after receiving the new data. New data that is difficult to integrate into the current explanatory model (i.e., the observer's beliefs) requires that significant changes are made to the model, thus yielding a high value of Bayesian surprise (Itti and Baldi, 2009). This perspective dissociates the amount of PE (surprise) elicited by a stimulus from its probability of occurrence, and also fits well with the model adjustment hypothesis of MMN (Winkler, 2007). The Bayesian perspective on surprise also stresses the importance of the observer's beliefs: when the observer cannot make confident predictions, any event holds little surprise value, no matter how improbable it is by itself.

In predictive coding models of brain function, confidence in the predictions derived from the internal model is tied to the concept of precision. Predictive coding proposes that the prediction error signal is weighted by an estimate of its expected precision, which inversely relates to the prediction error's variability (Feldman and Friston, 2010). This precision-weighting mechanism allows adjusting the relative weights of prior beliefs and sensory evidence in the inference process considering contextual factors, such as the amount of noise. Thus, the magnitude of sensory deviance detection signals elicited by a highly improbable deviant stimulus should reflect the confidence (precision), such that it should be down-weighted when contextual factors lead to highly variable signals. In other words, a highly improbable event will elicit less surprise when the situation does not allow constructing an internal model that reliably predicts the stimulation.

In sum, modern perspectives on the MMN-generating process place the concept of confidence or precision as a central parameter in the elicitation of MMN. However, until quite recently, among the myriad of studies on MMN there have been surprisingly very few that directly addressed this aspect. Nevertheless, classic MMN literature has shown that the MMN is modulated by factors that reflect the clarity or the certainty of a change (Fitzgerald and Todd, 2020). First, MMN will only be elicited to deviants presented with a probability of 0.30 or below (Kujala et al., 2007), and MMN amplitude increases with decreasing probabilities of the deviant (Näätänen, 1990, 1992). It is well-established that the MMN is larger for deviants that are more physically different (Winkler et al., 1992; Tiitinen et al., 1994; Amenedo and Escera, 2000; Daikhin and Ahissar, 2012), differ in more dimensions (Schröger and Wolff, 1998) or are more discriminable (Sams et al., 1985) from the standard (Näätänen, 1990, 1992). Much less research has focused on exploring the impact of the way the regularity is presented, that is, the characteristics of the standards rather than the deviants. Nevertheless, there is evidence indicating that the stability or strength of the regularity, or the amount of evidence gathered to support it, affects MMN amplitude. MMN increases after a greater number of repetitions of the standard (Baldeweg et al., 2004; Costa-Faidella et al., 2011a,b), after a longer period of stable regularity (Todd et al., 2011) or when the rate of standard repetitions is higher (with shorter ISIs; Pekkonen et al., 1995). Importantly, not only the amount of evidence collected for the regularity but also the clarity of this evidence plays a role. In this sense, factors that diminish the information extracted from the standard attenuate MMN (e.g., backward masking, Winkler and Näätänen, 1992), and introducing some variability in the specific characteristics of the repeating standard stimulus also decreases the amplitude of the MMN (Winkler et al., 1990).

All in all, although there is evidence indicating that confidence or precision may play an important role in the MMN-generating process, a simple dedicated paradigm is lacking that would allow to measure the effects of precision understanding the MMN as an index of a Bayesian inference process. Such a paradigm should allow isolating confidence without being confounded by refractoriness, which is tied to the deviant probability. Moreover, a clear operational definition of confidence applied to the oddball paradigm is missing to facilitate research in this aspect and hopefully lead to a better understanding of the MMN-generating process.

To investigate the influence of precision in sensory deviance detection signals, we propose a new oddball paradigm in which we vary the confidence on the model (inferred from the regularity established by the repetition of the standard stimulus), by manipulating the stability of the standard stimulus, while holding the deviant probability constant. To isolate effects of precision not confounded by refractoriness differences, we focus on the analysis of the deviant stimuli, which should elicit a precision-weighted PE signal reflecting the deviance detection process. If the MMN reflects the probability of the deviant stimulus, responses to the deviant should not differ between conditions. On the contrary, if it is a prediction error signal weighted by the confidence given by the overall variability of the stimulation, we would expect the amplitude of the deviant responses to be graded by the probability of the standard tone.

MATERIALS AND METHODS

Participants

Twenty-five healthy volunteers with no self-reported history of neurological, psychiatric, or hearing impairment and with

normal or corrected-to-normal visual acuity participated in the experiment. From this sample, five participants had to be excluded due to problems during the recording session ($N = 2$) or large artifacts in the Electroencephalogram (EEG) signal ($N = 3$), resulting in a final sample of 20 participants included in the study (mean age: 34.5 years; age range: 21–55 years; 8 males; all right-handed). All volunteers gave written informed consent in accordance with the guidelines of the Clinical Research Commission of the Hospital Universitari Institut Pere Mata and the Ethics Committee of the Institut d'Investigació Sanitària Pere Virgili before their participation and after the procedures were explained to them. The study conformed to the Code of Ethics of the World Medical Association (Declaration of Helsinki) and was approved by the Clinical Research Commission of the Hospital Universitari Institut Pere Mata, the Drug Research Ethics Committee of the Institut d'Investigació Sanitària Pere Virgili and the Bioethics Committee of the University of Barcelona. Recordings were performed at the Hospital Universitari Institut Pere Mata.

Auditory Stimuli

Eleven pure tones (44.1 kHz sampling rate; 50 ms duration; 5 ms hanning windowed rise/fall ramps) of different frequencies corresponding to musical notes, from A4 as the lowest pitch and Eb7 as the highest, spaced in steps of 3 semitones (440; 523.25; 622.25; 739.99; 880; 1046.5; 1244.51; 1479.98; 1760; 2093; and 2489.02 Hz), were generated with Matlab (R2020a; Mathworks) and delivered binaurally via Sony MDR-ZX110 headphones at 70 dB SPL using Psychtoolbox-3 functions implemented in Matlab environment [Psychophysics Toolbox Version 3 (PTB-3)] (Brainard, 1997; Pelli, 1997; Kleiner et al., 2007).

Sound Sequences

Auditory stimuli were arranged in four separate sequences (see **Figure 1A**), each containing 1650 pure tones delivered randomly at 333 ms SOA. Each sequence constituted one experimental block (i.e., one condition; ca. 9 min duration). Sequences differed mainly in the probability of appearance of the 880 Hz tone [from now on termed Standard (S)]: Oddball, p(S) = 10/11; High confidence, p(S) = 7/11; Low confidence, p(S) = 4/11 and Random (no tone repetition allowed), p(S) = 1/11. The probability of appearance of the 1046.5 Hz tone [from now on termed Deviant (D)] was kept at p(D) = 1/11 in all sequences. The remaining nine tones were presented as equiprobable fillers (from 440 to 2489.02 Hz, spaced in 3 semitone steps, excluding the D and S tones) with a combined probability of appearance of p(fillers) = 1−[p(S) + p(D)]. Each sequence was created by concatenating 150 microsequences of 11 tones (150*11 = 1650), generated according to the required characteristics. If a microsequence started with the same tone as that appearing at the previous microsequence ending (except for the S tone in the Oddball, High confidence and Low confidence sequences), a different microsequence was generated to avoid repetition. Albeit acknowledging that the S/D terms may not be appropriate for a sequence such as the Random one, in which all 11 tones are presented equiprobably, we decided to follow the traditional terminology of human auditory ERP studies on deviance detection (Näätänen, 1992; Näätänen et al., 2007) for consistency with past literature, readability, and because it reflects best our experimental manipulation of interest: the parametric variation of S probability.

Procedure

During the EEG recording session, participants sat in a comfortable chair in a sound-attenuated room and listened passively to the four sound sequences, delivered in random order, while reading a book (or a magazine or newspaper) of their own choosing. The total duration of the recording session was 40 min approximately (4 blocks × 9 min + pauses), plus EEG recording preparation (around 20 min).

EEG Recording and Preprocessing

EEG was continuously recorded from 16 Ag/AgCl electrodes and digitized at a sampling rate of 500 Hz by a BrainVision V-AMP amplifier (Brain Products, Germany) using the BrainVision Recorder version 1.21.0303 (Brain Products, Germany) acquisition software. Eleven electrodes were mounted in a nylon cap (EasyCap, Germany) at standard locations according to the international 10-20 system (Fp1, Fp2, F3, Fz, F4, T3, C3, Cz, C4, T4, Pz); additionally, two electrodes were positioned over the left and the right mastoids (M1 and M2, respectively), and three electrodes were used to record the electrooculogram [one placed below the left eye (VEOG); the remaining two placed at the outer canthi of the eyes (HEOG)]. The ground electrode was placed at AFz and the common reference electrode at the tip of the nose. All impedances were kept below 5 kΩ during the whole recording session.

Data preprocessing was performed offline using EEGlab v2021.0 software (Delorme and Makeig, 2004) running on Matlab R2020a. Data were bandpass filtered between 1 and 40 Hz (Kaiser window; β = 5.65; transition bandwidth = 0.5 Hz). Periods contaminated by non-stereotyped muscle artifacts were rejected by visual inspection. Independent component analysis decomposition was applied using the SOBI algorithm (Belouchrani and Cichocki, 2000). Independent components related to blinks, horizontal eye movements and heart rate, identified on the basis of their scalp topography and time course (Jung et al., 2000), were removed. After eliminating VEOG and HEOG channels from the set, artifact corrected data were cut in epochs from −0.1 to 0.3 s, time-locked to each auditory stimulus onset, and baseline corrected from −0.1 to 0 s. Epochs containing improbable data 3 SD above or below the mean probability distribution of values across all epochs were excluded (EEGlab's function *pop_jointprob.m*). Epochs corresponding to the D tone and the closest preceding S tone were selected for further analyses. Across participants, the mean (and SD) of the number of included trials per condition was: Oddball, D tone, 134.4 trials (7.2), S tone, 135.3 trials (5.7); High confidence, D tone, 135.9 trials (5.6), S tone, 136.3 trials (5.2); Low confidence, D tone, 133.95 trials (9.7), S tone, 133.4 trials (6.5); Random, D tone, 135.45 trials (4.7), S tone, 135.4 trials (5.7). No significant differences were found between the number of trials used in each condition (D tone: Kruskal-Wallis test, $\chi^2 = 0.5$, $p > 0.5$, df = 3; S tone: Kruskal-Wallis test, $\chi^2 = 2.35$, $p > 0.1$, df = 3). Data

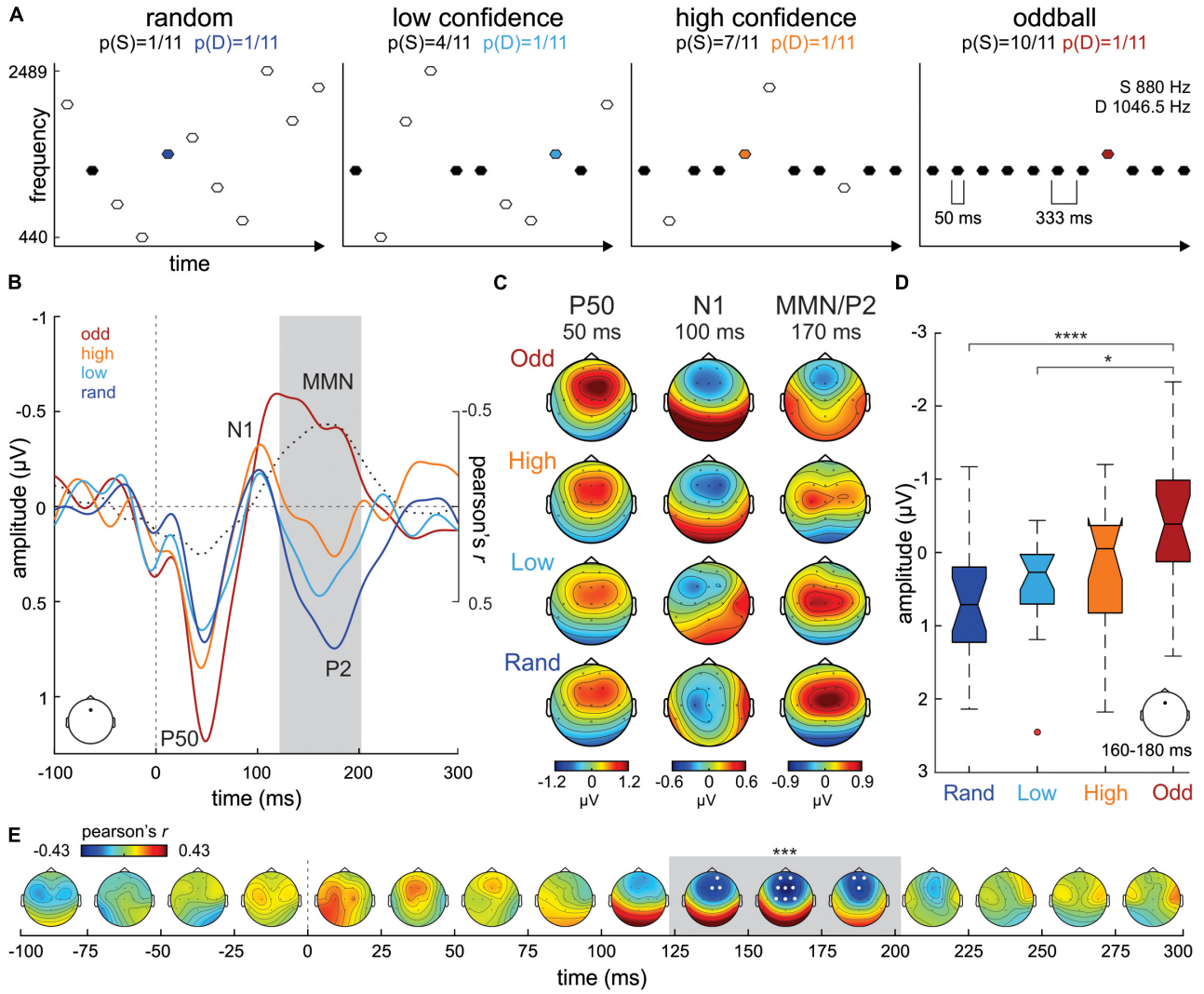

FIGURE 1 | (A) Experimental design. **(B)** ERP waveforms from Fz electrode evoked to D stimuli in the Oddball (odd; *dark red*), High confidence (high; *orange*), Low confidence (low; *cyan*) and Random (rand; *dark blue*) conditions. Correlation values (Pearson's *r*) between S tone probability and D tone ERP amplitudes at each time point are plotted in a dotted black line. The gray shaded area marks the temporal extent of the significant cluster of correlation values (122–202 ms). **(C)** P50, N1 and MMN/P2 scalp potential distribution maps per condition separately. **(D)** Boxplot series illustrating the distribution of mean amplitude ERP values extracted from Fz around the maximum correlation peak (170 ms) in our sample of participants, separately per condition. The boxplots represent the median value (middle line), the interquartile range (full box) and the extreme values (whiskers; outliers are plotted as separate dots). Significance of *post hoc* tests: $^{****}p < 0.001$; $^{*}p < 0.05$. **(E)** Time-electrode evolution of Pearson's *r*-values. The gray shaded area marks the temporal extent (122–202 ms) of the significant ($^{***}p < 0.005$) cluster of correlation values, while the white dots (electrodes) denote its spatial extent.

was then converted to fieldtrip format (Oostenveld et al., 2011), epochs were averaged separately per participant, tone type and condition and the resulting ERPs were lowpass filtered at 25 Hz with a zero-phase forward and reverse 6th order Butterworth IIR filter (hamming window). Difference waves (DW) were computed by subtracting, per participant and condition, the S tone ERP from the D tone ERP.

EEG Analyses

To investigate the influence of precision on deviance detection signals, we focused on the analysis of the D stimulus under different levels of precision, with the hypothesis that ERP amplitudes to the D tone would be modulated by the probability of the S tone. We computed a correlation analysis (Pearson's correlation) introducing the probability of the S tone as the independent variable (i.e., predictor; 10/11, 7/11, 4/11, 1/11 corresponding to the *Oddball*, *High confidence*, *Low confidence* and *Random* conditions, respectively) and the ERP amplitudes to the D tone (in the 4 experimental conditions) as the dependent variable. In order to overcome the problem of multiple comparisons over electrodes ($n = 13$) and time points (from −0.1 to 0.3 s; 200-time points at 500 Hz sampling rate), a mass-univariate, two-dimensional (time, electrode) cluster-based correlation analysis was conducted,

performed using a non-parametric randomization procedure (Maris and Oostenveld, 2007; in Fieldtrip, *ft_timelockstatistics* function with the options *cfg.statistic* = *"correlationT"* and *cfg.type* = *"Pearson"*). Neighboring electrodes were defined by the distance separating each other in a 2D projection of the montage, centering a 2.5 cm radius circle at each electrode and selecting those electrodes falling within. A minimum of two nearby electrodes was set per cluster. Correlation coefficient T-statistics were then computed at each time point and electrode (two-tailed) with the non-parametric Monte Carlo method. The Monte Carlo significance probability (*p*-value) was determined by calculating the proportion of 2D samples from 20,000 random partitions of the data that resulted in a larger test statistic than those on the observed test statistic. Then, clusters were created by grouping adjacent 2D points exceeding a significance level set to 0.05. The weighted cluster mass (Hayasaka and Nichols, 2004) was taken as the cluster-level statistic. The significance probability of the clusters was assessed with the described non-parametric Monte Carlo method. Values of $p < 0.05$, corrected for two-tailed tests, were considered significant. For each significant cluster we report its temporal spread, cluster statistic and *p*-value. To facilitate comparability of our results to previous MMN deviance detection studies, we complemented the analyses performed on D stimuli, analyzing the modulation caused by the probability of the S tone on the S tone ERP itself and on the D-S DW, following exactly the same statistical approach. However, note that differences in the S responses between conditions do not only reflect differences in precision, but also differences in refractoriness or adaptation as the manipulation of precision entails the manipulation of the S stimulus repetition rate. Therefore, we base our conclusions on the analysis of the D stimuli, whose probability was held constant across conditions.

RESULTS

Grand-average ($N = 20$) ERP waveforms evoked to the D tone (1046.5 Hz; probability of appearance in the sequence = 1/11) in the *Random*, *Low confidence*, *High confidence* and *Oddball* conditions, extracted from a frontocentral electrode (Fz), are illustrated in **Figure 1B**. As expected, the tone evoked prototypical P50 (ca. 50 ms) and N1 (ca. 100 ms) auditory ERP components in all conditions. A gradient in the ERP amplitude, becoming more negative with increasing S tone (880 Hz) probability across conditions (1/11, 4/11, 7/11 and 10/11 for the *Random*, *Low confidence*, *High confidence* and *Oddball* conditions, respectively), can be appreciated between ca. 120 and 200 ms, a time range consistent with that of MMN/P2 auditory ERPs. The scalp potential distribution maps of these ERP components are plotted in **Figure 1C** for each condition separately.

A mass-univariate correlation analysis between the probability of the S in the different experimental conditions (independent variable) and the amplitude of the ERP to the D tone (dependent variable), corrected for multiple comparisons in time and space (i.e., number of electrodes) using a cluster-based approach, yielded a significant fronto-central negative cluster between 122 ms and 202 ms ($wcm = -247.48$; $p < 0.005$; see **Figure 1E**), peaking at Fz electrode at 170 ms (*Pearson's* $r = -0.43$; see **Figure 1B**), corroborating the observation that D tone ERP amplitudes become more negative as S probability increases. This result was supported by a further confirmatory non-parametric statistical analysis on the mean ERP amplitudes at Fz extracted from each subject in a 160 to 180 ms time window (20 ms around the correlation peak; Kruskal-Wallis test, $\chi^2 = 16.59$, $p < 0.001$, df = 3; see **Figure 1D**). *Post hoc* tests corrected for multiple comparisons (Tuckey-Kramer) revealed that D ERP amplitudes at Fz during that time range were significantly more negative in the *Oddball* condition than in the *Random* ($p < 0.001$) and in the *Low confidence* ($p < 0.05$) conditions.

In order to evaluate the modulation that increasing a tone probability has on the activity evoked to that tone itself, the activity evoked to the S tones was submitted to the very same analysis. Grand-average ERP waveforms evoked to the S tone (880 Hz) in the Random, Low confidence, High confidence and Oddball conditions, extracted from Fz, are illustrated in **Figure 2A**. A gradient in the N1 amplitude (ca. 110 ms) can be observed, becoming less negative with increasing probability, as well as a reduced P50 (ca. 45 ms) in the Oddball condition as compared to the rest. The scalp potential distribution maps of these ERP components are plotted in **Figure 2B** for each condition separately.

However, these observations were not supported by statistical analyses, as the mass-univariate correlation analysis performed between the probability of the S in the different experimental conditions (independent variable) and the amplitude of the ERP to the S tone (dependent variable), corrected for multiple comparisons in time and space (i.e., number of electrodes) using a cluster-based approach, yielded no significant clusters.

For completeness, we submitted the DW ERPs (D ERP – S ERP) to the same analysis. Grand-average DW ERPs in the Random, Low confidence, High confidence and Oddball conditions, extracted from Fz, are illustrated in **Figure 3A**. As expected from the activity patterns elicited to the D and S tones, the DWs exhibit an increase in positivity around the P50 time range (ca. 40 ms) with increasing S tone probability, as well as a prominent MMN (ca. 140 ms) in the Oddball condition. The negativity at the MMN time range gradually increases with increasing S tone probability. The scalp potential distribution maps of both DW peaks are plotted in **Figure 3B** for each condition separately.

The mass-univariate correlation analysis between the probability of the S in the different experimental conditions (independent variable) and the amplitude of the DW ERP (dependent variable), corrected for multiple comparisons in time and space (i.e., number of electrodes) using a cluster-based approach, yielded a significant central-frontocentral positive cluster between −6 ms and 58 ms ($wcm = 166.71$; $p < 0.01$; see **Figure 3D**), peaking at Fz electrode at 38 ms (Pearson's $r = 0.43$; see **Figure 3A**), and a significant frontocentral negative cluster between 108 ms and 190 ms ($wcm = -234.54$; $p < 0.005$; see **Figure 3D**), peaking at Fz electrode at 142 ms (Pearson's $r = -0.42$; see **Figure 3A**). These results corroborate the observations that DWs increase in positivity at the P50

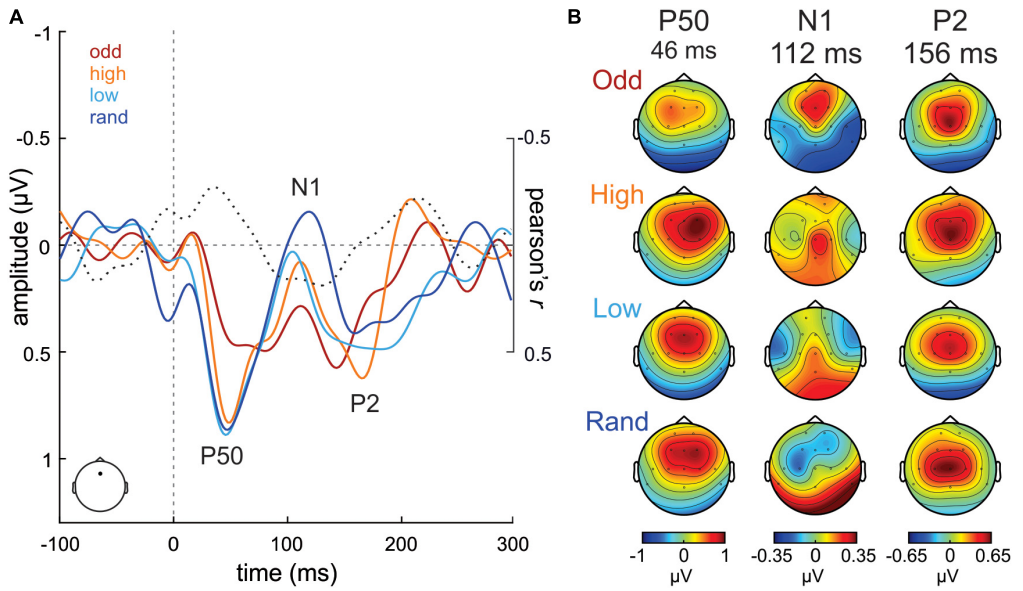

FIGURE 2 | (A) ERP waveforms from Fz electrode evoked to S stimuli in the Oddball (odd; dark red), High confidence (high; orange), Low confidence (low; cyan) and Random (rand; dark blue) conditions. Correlation values (Pearson's r) between S tone probability and S tone ERP amplitudes at each time point are plotted in a dotted black line. **(B)** P50, N1, and P2 scalp potential distribution maps per condition separately.

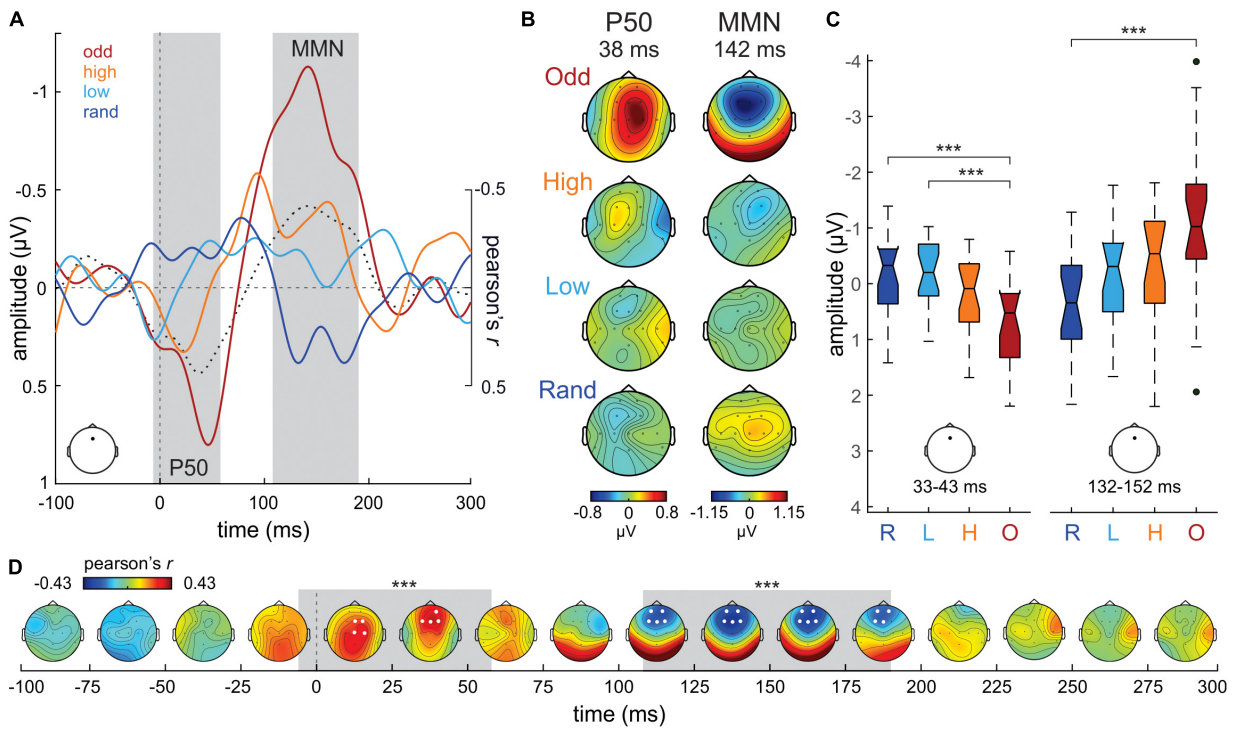

FIGURE 3 | (A) Difference waveforms (D ERP—S ERP) from Fz electrode in the Oddball (odd; dark red), High confidence (high; orange), Low confidence (low; cyan) and Random (rand; dark blue) conditions. Correlation values (Pearson's r) between S tone probability and DW ERP amplitudes at each time point are plotted in a dotted black line. The gray shaded areas mark the temporal extent of the significant clusters of correlation values (–6–58 ms; 108 to 190 ms). **(B)** P50 and MMN time range scalp potential distribution maps per condition separately. **(C)** Boxplot series illustrating the distribution of DW mean amplitude values extracted from Fz around the maximum correlation peaks (38 ms; 142 ms) in our sample of participants, separately per condition and P50/MMN time ranges. The boxplots represent the median value (middle line), the interquartile range (full box) and the extreme values (whiskers; outliers are plotted as separate dots). Significance of *post hoc* tests: ***$p < 0.005$. **(D)** Time-electrode evolution of Pearson's *r*-values. The gray shaded areas mark the temporal extent (–6–58 ms; 108–190 ms) of the significant (***$p \leq 0.005$) clusters of correlation values, while the white dots (electrodes) denote their spatial extent.

time range and increase in negativity at the MMN time range with increasing S tone probability. Further confirmatory non-parametric statistical analyses on the mean DW amplitudes at Fz extracted from each subject confirmed these findings: P50 time range, 33–43 ms time window (10 ms around the correlation positive peak), Kruskal-Wallis test, $\chi^2 = 15.49$, $p < 0.005$, df = 3; see **Figure 3C**; MMN time range, 132–152 ms time window (20 ms around the correlation negative peak), Kruskal-Wallis test, $\chi^2 = 14.26$, $p < 0.005$, df = 3; see **Figure 3C**. *Post hoc* tests corrected for multiple comparisons (Tuckey-Kramer) revealed that DW ERP amplitudes at Fz during the P50 time range were significantly more positive in the Oddball condition than in the Random ($p < 0.005$) and in the Low confidence ($p < 0.005$) conditions. DW amplitudes during the MMN time range were significantly more negative in the Oddball condition than in the Random ($p < 0.005$) condition.

DISCUSSION

Predictive coding models propose that sensory event-related brain potentials reflect the transmission of precision-weighted PE from lower to higher areas of the sensory hierarchy. According to this view, electrophysiological deviance detection signals like the MMN reflect the greater amount of PE elicited by the deviant (mispredicted) compared to the standard (predicted) stimuli (Friston, 2005; Garrido et al., 2009). Moreover, the gain of the PE is adjusted on the basis of an estimation of its precision, whereby more variable (uncertain) contexts lead to lower confidence and down-weighted PE signals compared to more stable (certain) contexts. To test whether the amplitude of sensory evoked responses reflecting PE varies as a function of uncertainty, we recorded ERPs elicited by 1046.5 Hz tones presented with $p = 0.1$ and manipulated the degree of variability of the rest of the sounds of the sequence, which were always drawn from a pool of 10 tones ranging between 440 and 2489.02 Hz. We found that the amplitude of the sensory response evoked by a low probability sound correlates linearly with the variability of the sound sequence in which it is embedded. Specifically, the lower the variability, the more negative the evoked response recorded over frontocentral electrodes between 122 and 202 ms. This gradual increase in negativity in the D tone ERP resulted in an MMN response in the D-S difference waves which decreased linearly with decreasing S tone probability. These results provide strong support for the idea that evoked potentials in the time range of the MMN reflect precision-weighted PE.

Traditionally, the MMN has been considered to be automatic and tied to sensory memory, thus operating on short time scales (< 30 s, Winkler et al., 2002) and reflecting local probability statistics (Fitzgerald and Todd, 2020). However, evidence has accumulated indicating that MMN is influenced by higher-order factors such as prior experience, foreknowledge through instruction (Frost et al., 2018), first impression biases (Todd et al., 2011, 2013) and attention (Auksztulewicz and Friston, 2015). These findings challenge the classic views on the computations underlying the MMN, centered on relatively simple mechanisms of deviance detection and regularity extraction, and push toward a broader conceptualization of the MMN as an index of more sophisticated learning processes in a world of sensory uncertainty in which precision plays a key role (Mathys et al., 2011; Fitzgerald and Todd, 2020).

In order to better understand the processes indexed by the MMN, here we have proposed a paradigm studying the impact of precision on sensory deviance detection focusing on the analysis of the D stimulus responses. We have chosen the term precision to refer to our manipulated variable. However, different terms relating to this idea (precision, confidence, uncertainty, variability, signal-to-noise ratio, predictability, context, second-order predictions, etc.) are used somewhat interchangeably in the literature, each stressing slightly different aspects. In general, they all relate to the hypothesis that, to cope with the many factors that limit the reliability of sensory information about the world, the brain encodes information probabilistically, in the form of probability distributions ("Bayesian coding hypothesis," Knill and Pouget, 2004). These distributions represent all possible values of any parameter, along with the associated probabilities for each value. Uncertainty typically refers to the width of the belief (or subjective probability) distribution (Ma and Jazayeri, 2014), and its inverse is the precision (Feldman and Friston, 2010). Thus, broader distributions (more variance) correspond to greater uncertainty and lower precision. Precision is also often defined as second-order predictions, or the predictions of context (Koelsch et al., 2019; Auksztulewicz and Friston, 2016), referring to contextual factors that influence predictability. That is, besides making a (first-order) prediction on content, the brain would make a (second-order) prediction, based on context, on how predictable an event is, or in other words, how likely it is that the content prediction will be correct (confidence). Therefore, uncertainty can also be defined as a measure of unpredictability or expected surprise (Feldman and Friston, 2010).

Altogether, the degree of variability (unpredictability) stands out as a crucial factor modulating sensory deviance detection, but variability can take myriad different forms. Indeed, different types of uncertainty have been proposed to drive different modulatory processes (Yu and Dayan, 2005), and, in principle, precision can refer to the belief distribution (the model), the predictions derived from it, the PE, or the stimulation itself. Logically, these are interrelated, as, for example, more variable contexts will lead to more uncertain predictions (Mathys et al., 2011). Nevertheless, both the precision of the prediction and the precision of the PE need to be considered to estimate the net effect of the sensory input on each observation (Kwisthout et al., 2017). In fact, the precision-weighted PE can be viewed as a Student's t-statistic, where to assess the significance of the difference between two distributions (the prediction and the observation) the difference in means (PE) is divided by its standard error (inverse variance or precision) (Feldman and Friston, 2010).

Hence, the question remains, what exactly does precision refer to? What types of variability or uncertainty specifically influence the magnitude of a deviance detection signal like the MMN? Given the multiple perspectives on how to define confidence, it seems necessary to empirically explore different types of manipulations to understand the significance of precision for the MMN.

The degree of predictability has been manipulated in many different ways in deviance detection studies. First of all, the very definition of the MMN as a deviance detection signal implies that it depends on predictability: only when the stimulation contains some type of statistical regularity that can be violated will there be the possibility to elicit an MMN. In fact, presenting the deviant sounds with the same probability embedded in a sequence of random (unpredictable) sounds (our Random condition) is an established control to isolate the MMN (Schröger and Wolff, 1996; Ruhnau et al., 2012). Indeed, Hsu et al. (2015) showed that relative to predicted stimuli, mispredicted stimuli (deviants violating the established regularity) elicited enhanced negative responses while unpredicted stimuli (presented in the absence of a rule) elicit attenuated responses.

Thus, the question is rather whether, when there is a statistical rule to be violated, the amplitude of the deviance detection signals depends on the degree of predictability. Previous studies have manipulated the strength of the rule by manipulating the number of consecutive repetitions of the standard presented immediately before the deviant (Baldeweg et al., 2004; Haenschel et al., 2005; Costa-Faidella et al., 2011a,b), or more generally the degree of repetitiveness of the sequence (Quiroga-Martinez et al., 2019, 2020) reporting greater MMN amplitudes with increased repetition. However, one concern with these types of studies is whether the effects observed reflect a modulation of the deviance detection process, or whether they reflect refractoriness differences.

The strength of the rule can also be weakened by introducing small variations in the characteristics of the repeating standard stimulus. Winkler et al. (1990) varied sound intensity across standard stimulus exemplars. In different blocks, the "substandards" covered a wider or narrower range of intensity values around a common mean. MMN elicited by intensity deviants decreased as the range of variation in the standard increased. In a similar design, Daikhin and Ahissar (2012) found that jittering the standard frequency reduced responses to frequency deviants, but only when the deviance magnitude was small. Importantly, in both these studies the deviants were defined by being outside the range of variation of the standard, thus adaptation differences could play a role in these effects as well, and the standard was always varied, thus no repetition rule was established.

We have proposed a parametric manipulation based on the stability of the standard stimulus, akin to a manipulation of signal-to-noise ratio, directly manipulating the strength of the rule (the rule being the standard tone and the noise being the rest of the tones). Aiming to investigate the effects of precision on the "true" MMN, or the part of the MMN which is due to predictive processes and not local adaptation or refractoriness mechanisms (i.e., repetition effects), we focused on the analysis of the responses to deviant stimuli with identical probability across the different standard stability conditions (a similar strategy to using a random control, Schröger and Wolff, 1996; Ruhnau et al., 2012). The results show a clear gradation of the D response with a time-course and scalp distribution compatible with the MMN. However, the MMN is typically extracted calculating the D-S difference wave, canceling out sensory responses and isolating the deviance detection signal. Therefore, the response elicited by the D stimulus cannot directly be considered an MMN. Both modulations of the D stimulus and the S stimulus responses affect the canonical MMN signal. In classic paradigms, ideally, the S and D responses are extracted from different conditions in a block design, so that they are elicited by the same physical stimulus under the two different roles. In our paradigm, the S and D tones are different physical stimuli. However, the mode of presentation of the D stimulus in our Random condition is identical to how the control S stimulus is presented in the well-established "many standards" or random control condition, used in previous studies to isolate the "true" MMN (Schröger and Wolff, 1996; Ruhnau et al., 2012). Therefore, the difference between the D ERP in the Oddball and the Random conditions is indeed the MMN response, and we can observe a clear gradual modulation of this response across the levels of our parametric precision manipulation.

Nevertheless, to provide a complete picture and for ease of comparison to the previous literature, we also analyzed the S stimulus responses, and found no significant correlation between the S tone ERP and the parametric precision manipulation. While this finding suggests that precision affects only the D and not the S responses, it should be interpreted with caution, as precision effects on the S responses might have been compensated with refractoriness effects, given the manipulation of the S stimulus probability across precision conditions. Thus, albeit precision can of course affect both S and D responses, and both effects would impact the MMN signal, practical issues regarding the design of the paradigm make it quite difficult to study both these aspects at the same time. Here we have focused on the investigation of the effects of precision on the deviance detection signal *per se*, which is elicited by the D, not the S stimulus, and contributes directly to the canonical MMN response.

In any case, again to facilitate comparison to previous studies, we also report the classic D-S difference waves, where the MMN can be clearly identified in the Oddball and the High confidence conditions, as expected. The modulations observed on the MMN response isolated in this way show the same pattern as the modulation observed on the D tone ERP in the MMN time window, with an additional earlier significant modulation affecting the P50 response. Again, given that the difference waves reflect both modulation of the S tone and the D tone ERPs and that the S tone ERP is also affected by refractoriness differences, this result should be interpreted with caution, and we prefer to refrain from making any firm conclusions based on the difference wave ERPs.

Thus, we have based our conclusions on the analysis of the D tone ERPs which had a fixed probability throughout the experiment. Despite their fixed probability, it could be argued that co-adaptation from nearby frequency channels could modulate deviant responses differentially across conditions (Jääskeläinen et al., 2004; May and Tiitinen, 2010; for a review of animal and human studies on stimulus-specific adaptation, see Escera and Malmierca, 2014). However, our results are inconsistent with this hypothesis, as co-adaptation in nearby frequency channels should render the responses to the deviant in the oddball condition smaller than in the rest of

experimental conditions. Instead, previous studies have shown that neuronal responses scale with the spectral distribution of auditory stimulation, a finding showing a dynamic variation in stimulus-specific adaptation, interpreted as adaptation to stimulus statistics (Herrmann et al., 2013, 2014). Indeed, several findings indicate that alphabet size (Winkler et al., 1992; Barascud et al., 2016; Auksztulewicz et al., 2017; Quiroga-Martinez et al., 2019, 2020) or the width of the distribution (Garrido et al., 2013; Larsen et al., 2020) of the stimulation sequence are reflected on neural signals, supporting the idea that variability in the stimulation (inverse precision) plays a role in the modulation of deviance detection. In our study, decreasing the confidence (from oddball to random) increases the spectral variability of the stimulation (i.e., tones of different frequencies become more probable), without broadening the spectral range of the sequence. As the low probability stimulus (D) falls at the center of the mean log spectral distribution of the stimulation (1046.5 Hz), the better the model representing the spectral distribution, the more reduced neural responses would be expected (Daikhin and Ahissar, 2012; Garrido et al., 2013) as the D tone becomes a prototype exemplar of the rule. Thus, encoding the distribution of stimulation features, such as tone frequency, could stand as a possible mechanism underlying precision-weighting of PE in variable contexts.

An interesting question is whether variability in one feature affects only deviance detection processes with respect to that feature, or whether reduced model confidence down-weights PE signals arising from violations of any of the stimulation parameters. Here, we have directly manipulated the predictability of the stimulus feature in which the deviant differs from the standard. However, confidence can also be manipulated varying the number of features that are predictable. Some findings suggest that variability in one feature does not affect deviance detection with regards to other features (Quiroga-Martinez et al., 2019, 2020). However, there is also evidence that manipulating the variability in one feature affects the detection of deviations in a second (stable) feature (Winkler et al., 1990). Notably, introducing temporal uncertainty (variability) reduces repetition suppression (Costa-Faidella et al., 2011a) and impairs the ability to detect new rules (Sohoglu and Chait, 2016). Thus, future studies using our paradigm could explore how the spectral variability manipulation across confidence levels affects responses to deviations in other features (e.g., duration or intensity deviants).

The strategies discussed so far modulated precision manipulating always low-level features of the stimulation; that is, physical differences between standards and deviants. However, predictability can also be increased by imposing additional higher-level rules or constraints. When participants are informed about the rules, the MMN is modulated (Frost et al., 2018; but see Koelsch et al., 2019 for an opposing argument). Moreover, stimuli that violate a local rule elicit smaller PE signals if they at the same time conform to a global rule (Sussman et al., 1998; Wacongne et al., 2011). It should be noted that manipulating predictability by imposing a higher order rule, is not the same as directly making the single existing rule more or less noisy. Nevertheless, these studies show that information from different levels of the representation hierarchy is integrated and top-down information from higher levels seems to be able to readjust precision at lower levels. Similarly, recent studies have shown that the MMN is affected by the rule stability estimated over time scales that must necessarily involve higher-order structures. In these studies, volatility is manipulated having the standard and deviant change roles more or less rapidly throughout the stimulation sequence, showing that MMN is larger during more stable stimulation stretches (Todd et al., 2011, 2013; Dzafic et al., 2020).

All in all, studies manipulating predictability in one way or another have shown that deviance detection signals are higher in less variable (more predicable) conditions. However, in general, the studies discussed above made comparisons between certain vs. uncertain conditions, but did not show a gradation of different levels of uncertainty. Thus, it is interesting to understand whether deviance detection is a process that varies parametrically with precision whenever precision is manipulated through the degree of regularity. Alternatively, there could be an "all-or-none" turning point when a given predictive model of the stimulation is accepted as valid, and only from that point on is the system actually using it to make predictions. For example, in a study investigating the effects of deviance magnitude, Horváth et al. (2008) gradually manipulated the frequency distance between deviant and standard and argued that the "true" MMN (when adaptation is controlled) is categorical, an all-or-none process. We performed a gradual manipulation of the rule strength across 4 levels of uncertainty, and found that responses to the deviant scale with rule precision, pointing to a continuous process. Nevertheless, at a descriptive level, we also observed a possible qualitative change between the oddball and the high precision conditions. Topographically, the process that varied parametrically with precision was centrally distributed. However, careful observation of the topographies of the oddball condition suggests the presence of an overimposed frontocentral negativity in this condition only, that is already not observable in the high confidence condition. This change in topography could reflect the activation of frontal generators (Deouell, 2007), suggesting that highly precise PEs may reach higher hierarchical levels before they can be silenced. The presence or absence of filler tones might also represent an important qualitative change in the stimulation leading to different strategies in the deviance detection process. Nevertheless, on the classic D-S difference waves, a clear MMN response can be observed both for the Oddball and the High confidence conditions, while no MMN is elicited in the Random condition, as expected from previous studies, and the signal elicited by the Low confidence condition lies somewhere in between. This indeed seems to suggest that the signal reflects a continuous rather than an all or none underlying process, however, additional research is needed to clarify this point. Specifically, it could be interesting to add more confidence steps to the design to further evaluate the gradation of the responses, and to extend the electrode montage to be able to perform a reliable source analysis, or use a technique with a higher spatial resolution, that would allow dissociating multiple hypothetical contributing sources.

In conclusion, in our paradigm, we have tapped into precision by manipulating pitch predictability gradually, going from random frequencies within a limited range, to a strong

(low-level) repetition rule. However, contrary to other studies that have manipulated repetitiveness, we focus on the response to D sounds of equal probability, thereby avoiding adaptation confounds. In our study, decreasing repetitiveness of the S rule means increasing spectral variability, similarly to alphabet size or distribution width manipulations, but critically our D stimulus falls on the center of the distribution and the range of values was equal across conditions, manipulating only the repetitiveness of the S within this range. We show that gradually lowering the precision of the pitch rule, gradually weakens responses to pitch deviants. The results support the view that sensory responses to the D sound are a manifestation of precision-weighted PE, in the context of a Bayesian inference process. However, as we have reviewed, there are various ways to define precision and manipulate it at multiple levels. Further research is needed to clarify whether all these effects reflect the same underlying process or not.

With this paradigm, we hope to demonstrate a viable, gradual manipulation of precision in the investigation of prediction and prediction errors in the auditory modality, which addresses the "true" MMN controlling for adaptation. Experimental manipulations tapping onto precision can be powerful tools to explore predictive processing and learning and their dysfunctions, and can be used to test the hypothesis of aberrant precision-weighting in schizophrenia and autism (Adams et al., 2013; Lawson et al., 2014, 2017; Haarsma et al., 2020). We believe our paradigm can shed some light on the concept of precision and the precision-weighting of prediction error signals in the Bayesian inference process, contributing to continuously advance the understanding of the MMN-generating process toward a broader conceptualization of the MMN as a signal of sophisticated learning processes in a world of sensory uncertainty.

DATA AVAILABILITY STATEMENT

The raw data supporting the conclusions of this article will be made available by the authors, without undue reservation.

ETHICS STATEMENT

The studies involving human participants were reviewed and approved by the Clinical Research Commission of the Hospital Universitari Institut Pere Mata, Drug Research Ethics Committee of the Institut d'Investigació Sanitària Pere Virgili and Bioethics Committee of the University of Barcelona. The patients/participants provided their written informed consent to participate in this study.

AUTHOR CONTRIBUTIONS

ISM, JC-F, and CE conceptualized and designed the paradigm. JC-F programmed the task and analyzed the data. ZL acquired the data. JC-F and ISM wrote the first version of the manuscript. CE, ZL, and EV revised the manuscript. CE and EV supervised the work. All authors contributed to the article and approved the submitted version.

FUNDING

This work was supported by the Spanish Ministry of Science and Universities (PSI2017-85600P and RYC-2013-12577 projects) and the MDM-2017-0729-18-2 Maria de Maeztu Center of Excellence (MINECO-FEDER), the 2017SGR-974 Excellence Research Group of the Generalitat de Catalunya, and the ICREA Acadèmia Distinguished Professorship awarded to CE. This project has received funding from the European Union's Horizon 2020 Research and Innovation Program under the Marie Skłodowska-Curie grant agreement no. 712949 (TECNIOspring PLUS) to ZL.

ACKNOWLEDGMENTS

We would like to thank Juanita Todd for helpful suggestions during the design of the protocol.

REFERENCES

Adams, R. A., Stephan, K. E., Brown, H. R., Frith, C. D., and Friston, K. J. (2013). The Computational Anatomy of Psychosis. *Front. Psychiatry* 4:47. doi: 10.3389/fpsyt.2013.00047

Amenedo, E., and Escera, C. (2000). The accuracy of sound duration representation in the human brain determines the accuracy of behavioural perception. *Eur. J. Neurosci.* 12, 2570–2574.

Auksztulewicz, R., Barascud, N., Cooray, G., Nobre, A. C., Chait, M., and Friston, K. (2017). The Cumulative Effects of Predictability on Synaptic Gain in the Auditory Processing Stream. *J. Neurosci.* 37, 6751–6760. doi: 10.1523/JNEUROSCI.0291-17.2017

Auksztulewicz, R., and Friston, K. (2015). Attentional Enhancement of Auditory Mismatch Responses: a DCM/MEG Study. *Cereb. Cortex* 25, 4273–4283. doi: 10.1093/cercor/bhu323

Auksztulewicz, R., and Friston, K. (2016). Repetition suppression and its contextual determinants in predictive coding. *Cortex* 80, 125–140. doi: 10.1016/j.cortex.2015.11.024

Baldeweg, T., Klugman, A., Gruzelier, J., and Hirsch, S. R. (2004). Mismatch negativity potentials and cognitive impairment in schizophrenia. *Schizophr. Res.* 69, 203–217.

Barascud, N., Pearce, M. T., Griffiths, T. D., Friston, K. J., and Chait, M. (2016). Brain responses in humans reveal ideal observer-like sensitivity to complex acoustic patterns. *Proc. Natl. Acad. Sci. U. S. A.* 113, E616–E625. doi: 10.1073/pnas.1508523113

Belouchrani, A., and Cichocki, A. (2000). Robust whitening procedure in blind source separation context. *Electr. Lett.* 36, 2050–2053.

Brainard, D. H. (1997). The psychophysics toolbox. *Spatial Vis.* 10, 433–436. doi: 10.1163/156856897X00357

Costa-Faidella, J., Baldeweg, T., Grimm, S., and Escera, C. (2011a). Interactions between "what" and "when" in the auditory system: temporal predictability enhances repetition suppression. *J. Neurosci.* 31, 18590–18597.

Costa-Faidella, J., Grimm, S., Slabu, L., Díaz-Santaella, F., and Escera, C. (2011b). Multiple time scales of adaptation in the auditory system as revealed by human evoked potentials. *Psychophysiology* 48, 774–783.

Daikhin, L., and Ahissar, M. (2012). Responses to deviants are modulated by subthreshold variability of the standard. *Psychophysiology* 49, 31–42.

Delorme, A., and Makeig, S. (2004). EEGLAB: an open source toolbox for analysis of single-trial EEG dynamics including independent component analysis. *J. Neurosci. Methods* 134, 9–21. doi: 10.1016/j.jneumeth.2003.10.009

Deouell, L. Y. (2007). The frontal generator of the mismatch negativity revisited. *J. Psychophysiol* 21, 188–203. doi: 10.1027/0269-8803.21.34.188

Dzafic, I., Randeniya, R., Harris, C. D., Bammel, M., and Garrido, M. I. (2020). Statistical Learning and Inference Is Impaired in the Nonclinical Continuum of Psychosis. *J. Neurosci.* 40, 6759–6769. doi: 10.1523/JNEUROSCI.0315-20.2020

Escera, C., and Malmierca, M. S. (2014). The auditory novelty system: an attempt to integrate human and animal research. *Psychophysiology* 51, 111–123.

Feldman, H., and Friston, K. J. (2010). Attention, uncertainty, and free-energy. *Front. Hum. Neurosci.* 4:215. doi: 10.3389/fnhum.2010.00215

Fitzgerald, K., and Todd, J. (2020). Making Sense of Mismatch Negativity. *Front. Psychiatry* 11:468. doi: 10.3389/fpsyt.2020.00468

Friston, K. (2005). A theory of cortical responses. *Philos. Transac. R. Soc. Lond. Ser. B Biol. Sci.* 360, 815–836.

Friston, K. (2010). The free energy principle: a unified brain theory? *Nat. Rev. Neurosci.* 11, 127–138.

Frost, J. D., Haasnoot, K., McDonnell, K., Winkler, I., and Todd, J. (2018). The cognitive resource and foreknowledge dependence of auditory perceptual inference. *Neuropsychologia* 117, 379–388.

Garrido, M., Kilner, J., Stephan, K., and Friston, K. (2009). The mismatch negativity: a review of underlying mechanisms. *Clin. Neurophysiol.* 120, 453–463.

Garrido, M. I., Sahani, M., and Dolan, R. J. (2013). Outlier responses reflect sensitivity to statistical structure in the human brain. *PLoS Comput. Biol.* 9:e1002999. doi: 10.1371/journal.pcbi.1002999

Haarsma, J., Fletcher, P. C., Griffin, J. D., Taverne, H. J., and Ziauddeen, H. (2020). Precision weighting of cortical unsigned prediction error signals benefits learning, is mediated by dopamine, and is impaired in psychosis. *Mol. Psychiatry* doi: 10.1038/s41380-020-0803-8 Epub online ahead of print.

Haenschel, C., Vernon, D. J., Dwivedi, P., Gruzelier, J. H., and Baldeweg, T. (2005). Event-related brain potential correlates of human auditory sensory memory-trace formation. *J. Neurosci.* 25, 10494–10501. doi: 10.1523/JNEUROSCI.1227-05.2005

Hayasaka, S., and Nichols, T. E. (2004). Combining voxel intensity and cluster extent with permutation test framework. *Neuroimage* 23, 54–63. doi: 10.1016/j.neuroimage.2004.04.035

Herrmann, B., Henry, M. J., and Obleser, J. (2013). Frequency-specific adaptation in human auditory cortex depends on the spectral variance in the acoustic stimulation. *J. Neurophysiol.* 109, 2086–2096. doi: 10.1152/jn.00907.2012

Herrmann, B., Schlichting, N., and Obleser, J. (2014). Dynamic range adaptation to spectral stimulus statistics in human auditory cortex. *J. Neurosci.* 34, 327–331.

Horváth, J., Czigler, I., Jacobsen, T., Maess, B., Schröger, E., and Winkler, I. (2008). MMN or no MMN: no magnitude of deviance effect on the MMN amplitude. *Psychophysiology* 45, 60–69.

Hsu, Y.-F., Le Bars, S., Hämäläinen, J. A., and Waszak, F. (2015). Distinctive Representation of Mispredicted and Unpredicted Prediction Errors in Human Electroencephalography. *J. Neurosci.* 35, 14653–14660. doi: 10.1523/JNEUROSCI.2204-15.2015

Itti, L., and Baldi, P. (2009). Bayesian surprise attracts human attention. *Vision Res.* 49, 1295–1306. doi: 10.1016/j.visres.2008.09.007

Jääskeläinen, I. P., Ahveninen, J., Bonmassar, G., Dale, A. M., Ilmoniemi, R. J., Levänen, S., et al. (2004). Human posterior auditory cortex gates novel sounds to consciousness. *Proc. Natl. Acad. Sci. U. S. A.* 17, 6809–6814.

Jung, T. P., Makeig, S., Humphries, C., Lee, T. W., McKeown, M. J., Iragui, V., et al. (2000). Removing electroencephalographic artifacts by blind source separation. *Psychophysiology* 37, 163–178.

Kleiner, M., Brainard, D. H., Pelli, D., Ingling, A., Murray, R., and Broussard, C. (2007). What's new in Psychtoolbox-3. *Perception* 36, 1–16. doi: 10.1068/v070821

Knill, D., and Pouget, A. (2004). The Bayesian brain: the role of uncertainty in neural coding and computation. *Trends Neurosci.* 27, 712–719.

Koelsch, S., Vuust, P., and Friston, K. (2019). Predictive Processes and the Peculiar Case of Music. *Trends Cogn. Sci.* 23, 63–77. doi: 10.1016/j.tics.2018.10.006

Kujala, T., Tervaniemi, M., and Schröger, E. (2007). The mismatch negativity in cognitive and clinical neuroscience: theoretical and methodological considerations. *Biol. Psychol.* 74, 1–19. doi: 10.1016/j.biopsycho.2006.06.001

Kwisthout, J., Bekkering, H., and van Rooij, I. (2017). To be precise, the details don't matter: on predictive processing, precision, and level of detail of predictions. *Brain Cogn.* 112, 84–91. doi: 10.1016/j.bandc.2016.02.008

Larsen, K. M., Dzafic, I., Darke, H., Pertile, H., Carter, O., Sundram, S., et al. (2020). Aberrant connectivity in auditory precision encoding in schizophrenia spectrum disorder and across the continuum of psychotic-like experiences. *Schizophr. Res.* 222, 185–194. doi: 10.1016/j.schres.2020.05.061

Lawson, R. P., Mathys, C., and Rees, G. (2017). Adults with autism overestimate the volatility of the sensory environment. *Nat. Neurosci.* 20, 4–6. doi: 10.1038/nn.4615

Lawson, R. P., Rees, G., and Friston, K. J. (2014). An aberrant precision account of autism. *Front. Hum. Neurosci.* 8:302. doi: 10.3389/fnhum.2014.00302

Lieder, F., Daunizeau, J., Garrido, M. I., Friston, K. J., and Stephan, K. E. (2013). Modelling Trial-by-Trial Changes in the Mismatch Negativity. *PLoS Comput. Biol.* 9:e1002911. doi: 10.1371/journal.pcbi.1002911

Ma, W. J., and Jazayeri, M. (2014). Neural coding of uncertainty and probability. *Annu. Rev. Neurosci.* 37, 205–220. doi: 10.1146/annurev-neuro-071013-014017

Malmierca, M. S., Sanchez-Vives, M. V., Escera, C., and Bendixen, A. (2014). Neuronal adaptation, novelty detection and regularity encoding in audition. *Front. Syst. Neurosci.* 8:111. doi: 10.3389/fnsys.2014.00111

Maris, E., and Oostenveld, R. (2007). Nonparametric statistical testing of EEG- and MEG-data. *J. Neurosci. Methods* 164, 177–190. doi: 10.1016/j.jneumeth.2007.03.024

Mathys, C., Daunizeau, J., Friston, K. J., and Stephan, K. E. (2011). A Bayesian foundation for individual learning under uncertainty. *Front. Hum. Neurosci.* 5:39. doi: 10.3389/fnhum.2011.00039

May, P. J., and Tiitinen, H. (2010). Mismatch negativity (MMN), the deviance-elicited auditory deflection, explained. *Psychophysiology* 47, 66–122. doi: 10.1111/j.1469-8986.2009.00856.x

Näätänen, R. (1990). The role of attention in auditory information processing as revealed by event-related potentials and other brain measures of cognitive function. *Behav. Brain Sci.* 13, 201–288.

Näätänen, R. (1992). *Attention and Brain Function*. United States: Lawrence Erlbaum Associates, Inc..

Näätänen, R., Jacobsen, T., and Winkler, I. (2005). Memory-based or afferent processes in mismatch negativity (MMN): a review of the evidence. *Psychophysiology* 42, 25–32.

Näätänen, R., Kujala, T., Escera, C., Baldeweg, T., Kreegipuu, K., Carlson, S., et al. (2012). The Mismatch Negativity (MMN) - A unique window to disturbed central auditory processing in aging and different clinical conditions. *Clin. Neurophysiol.* 123, 424–458.

Näätänen, R., Kujala, T., Kreegippu, K., Carlson, S., Escera, C., Baldeweg, T., et al. (2011). The mismatch negativity: an index of cognitive decline in neuropsychiatric and neurological diseases and in aging. *Brain* 134, 3432–3450.

Näätänen, R., Paavilainen, P., Rinne, T., and Alho, K. (2007). The mismatch negativity (MMN) in basic research of central auditory processing: a review. *Clin. Neurophysiol.* 118, 2544–2590. doi: 10.1016/j.clinph.2007.04.026

Oostenveld, R., Fries, P., Maris, E., and Schoffelen, J.-M. (2011). FieldTrip: open Source Software for Advanced Analysis of MEG, EEG, and Invasive Electrophysiological Data. *Comput. Intell. Neurosci.* 2011:156869. doi: 10.1155/2011/156869

Ostwald, D., Spitzer, B., Guggenmos, M., Schmidt, T. T., Kiebel, S. J., and Blankenburg, F. (2012). Evidence for neural encoding of Bayesian surprise in human somatosensation. *Neuroimage* 62, 177–188. doi: 10.1016/j.neuroimage.2012.04.050

Pekkonen, E., Rinne, T., and Näätänen, R. (1995). Variability and replicability of the mismatch negativity. *Electroencephalogr. Clin. Neurophysio.l* 96, 546–554. doi: 10.1016/0013-4694(95)00148-R

Pelli, D. G. (1997). The videotoolbox software for visual psychophysics: transforming numbers into movies. *Spatial Vision* 10, 437–442. doi: 10.1163/156856897X00366

Quiroga-Martinez, D. R., Hansen, N. C., Højlund, A., Pearce, M., Brattico, E., and Vuust, P. (2020). Musical prediction error responses similarly reduced by predictive uncertainty in musicians and non-musicians. *Eur. J. Neurosci.* 51, 2250–2269. doi: 10.1111/ejn.14667

Quiroga-Martinez, D. R., Hansen, N. C., Højlund, A., Pearce, M. T., Brattico, E., and Vuust, P. (2019). Reduced prediction error responses in high-as compared

to low-uncertainty musical contexts. *Cortex* 120, 181–200. doi: 10.1016/j.cortex.2019.06.010

Ruhnau, P., Herrmann, B., and Schröger, E. (2012). Finding the right control: the mismatch negativity under investigation. *Clin. Neurophysiol.* 123, 507–512. doi: 10.1016/j.clinph.2011.07.035

Sams, M., Paavilainen, P., Alho, K., and Näätänen, R. (1985). Auditory frequency discrimination and event-related potentials. *Electroencephalogr. Clin. Neurophysiol.* 62, 437–448. doi: 10.1016/0168-5597(85)90054-1

Schröger, E., Marzecová, A., and SanMiguel, I. (2015). Attention and prediction in human audition: a lesson from cognitive psychophysiology. *Eur. J. Neurosci.* 41, 641–664. doi: 10.1111/ejn.12816

Schröger, E., and Wolff, C. (1996). Mismatch response of the human brain to changes in sound location. *Neuroreport* 7, 3005–3008.

Schröger, E., and Wolff, C. (1998). Attentional orienting and reorienting is indicated by human event-related brain potentials. *Neuroreport* 9, 3355–3358. doi: 10.1097/00001756-199810260-00003

Sohoglu, E., and Chait, M. (2016). Detecting and representing predictable structure during auditory scene analysis. *ELife* 5:e19113. doi: 10.7554/eLife.19113

Stefanics, G., Heinzle, J., Horváth, A. A., and Stephan, K. E. (2018). Visual Mismatch and Predictive Coding: a Computational Single-Trial ERP Study. *J. Neurosci.* 38, 4020–4030. doi: 10.1523/JNEUROSCI.3365-17.2018

Sussman, E., Ritter, W., and Vaughan, H. G. Jr. (1998). Predictability of stimulus deviance and the mismatch negativity. *Neuroreport* 9, 4167–4170.

Tiitinen, H., May, P., Reinikainen, K., and Näätänen, R. (1994). Attentive novelty detection in humans is governed by pre-attentive sensory memory. *Nature* 372, 90–92. doi: 10.1038/372090a0

Todd, J., Provost, A., and Cooper, G. (2011). Lasting first impressions: a conservative bias in automatic filters of the acoustic environment. *Neuropsychologia* 49, 3399–3405. doi: 10.1016/j.neuropsychologia.2011.08.016

Todd, J., Provost, A., Whitson, L., Cooper, G., and Heathcote, A. (2013). Not so primitive: context sensitive meta-learning about unattended sound sequences. *J. Neurophysiol.* 109, 99–105.

Wacongne, C., Labyt, E., van Wassenhove, V., Bekinschtein, T., Naccache, L., and Dehaene, S. (2011). Evidence for a hierarchy of predictions and prediction errors inhuman cortex. *Proc. Natl. Acad. Sci. U. S. A.* 108, 20754–20759.

Winkler, I. (2007). Interpreting the mismatch negativity. *J. Psychophysiol.* 21, 147–163. doi: 10.1027/0269-8803.21.34.147

Winkler, I., and Czigler, I. (1998). Mismatch negativity: deviance detection or the maintenance of the 'standard'. *Neuroreport* 9, 3809–3813.

Winkler, I., Korzyukov, O., Gumenyuk, V., Cowan, N., Linkenkaer-Hansen, K., Ilmoniemi, J., et al. (2002). Temporary and longer term retention of acoustic information. *Psychophysiology* 39, 530–534. doi: 10.1017/S0048577201393186

Winkler, I., and Näätänen, R. (1992). Event-related potentials in auditory backward recognition masking: a new way to study the neurophysiological basis of sensory memory in humans. *Neurosci. Lett.* 140, 239–242. doi: 10.1016/0304-3940(92)90111-J

Winkler, I., Paavilainen, P., Alho, K., Reinikainen, K., Sams, M., and Näätänen, R. (1990). The effect of small variation of the frequent auditory stimulus on the eventrelated brain potential to the infrequent stimulus. *Psychophysiology* 27, 228–235. doi: 10.1111/j.1469-8986.1990.tb00374.x

Winkler, I., Paavilainen, P., and Näätänen, R. (1992). Can echoic memory store two traces simultaneously? A study of event-related brain potentials. *Psychophysiology* 29, 337–349.

Yu, A., and Dayan, P. (2005). Uncertainty, neuromodulation, and attention. *Neuron* 46, 681–692. doi: 10.1016/j.neuron.2005.04.026

Conflict of Interest: The authors declare that the research was conducted in the absence of any commercial or financial relationships that could be construed as a potential conflict of interest.

frontiers in Human Neuroscience

ORIGINAL RESEARCH
published: 01 October 2021
doi: 10.3389/fnhum.2021.737230

Arousal State-Dependence of Interactions Between Short- and Long-Term Auditory Novelty Responses in Human Subjects

Kirill V. Nourski[1,2†], Mitchell Steinschneider[3,4†], Ariane E. Rhone[1], Rashmi N. Mueller[1,5], Hiroto Kawasaki[1] and Matthew I. Banks[6,7]*

[1] Human Brain Research Laboratory, Department of Neurosurgery, The University of Iowa, Iowa City, IA, United States, [2] Iowa Neuroscience Institute, The University of Iowa, Iowa City, IA, United States, [3] Department of Neurology, Albert Einstein College of Medicine, Bronx, NY, United States, [4] Department of Neuroscience, Albert Einstein College of Medicine, Bronx, NY, United States, [5] Department of Anesthesia, The University of Iowa, Iowa City, IA, United States, [6] Department of Anesthesiology, University of Wisconsin School of Medicine and Public Health, Madison, WI, United States, [7] Department of Neuroscience, University of Wisconsin School of Medicine and Public Health, Madison, WI, United States

OPEN ACCESS

Edited by:
Manuel S. Malmierca, University of Salamanca, Spain

Reviewed by:
Steven Eliades, University of Pennsylvania, United States
Sarah Eagleman, Stanford University, United States

***Correspondence:**
Kirill V. Nourski
kirill-nourski@uiowa.edu

† These authors have contributed equally to this work and share first authorship

Specialty section:
This article was submitted to Cognitive Neuroscience, a section of the journal Frontiers in Human Neuroscience

Received: *06 July 2021*
Accepted: *13 September 2021*
Published: *01 October 2021*

Citation:
Nourski KV, Steinschneider M, Rhone AE, Mueller RN, Kawasaki H and Banks MI (2021) Arousal State-Dependence of Interactions Between Short- and Long-Term Auditory Novelty Responses in Human Subjects. Front. Hum. Neurosci. 15:737230. doi: 10.3389/fnhum.2021.737230

In everyday life, predictable sensory stimuli are generally not ecologically informative. By contrast, novel or unexpected stimuli signal ecologically salient changes in the environment. This idea forms the basis of the predictive coding hypothesis: efficient sensory encoding minimizes neural activity associated with predictable backgrounds and emphasizes detection of changes in the environment. In real life, the brain must resolve multiple unexpected sensory events occurring over different time scales. The local/global deviant experimental paradigm examines auditory predictive coding over multiple time scales. For short-term novelty [hundreds of milliseconds; local deviance (LD)], sequences of identical sounds (/xxxxx/) are interspersed with sequences that contain deviants (/xxxxy/). Long-term novelty [several seconds; global deviance (GD)] is created using either (a) frequent /xxxxx/ and infrequent /xxxxy/ sequences, or (b) frequent /xxxxy/ and infrequent /xxxxx/ sequences. In scenario (a), there is both an LD and a GD effect (LDGD, "double surprise"). In (b), the global deviant is a local standard, i.e., sequence of identical sounds (LSGD). Cortical responses reflecting LD and GD originate in different brain areas, have a different time course, and are differentially sensitive to general anesthesia. Neural processes underlying LD and GD have been shown to interact, reflecting overlapping networks subserving the detection of novel auditory stimuli. This study examined these interactions using intracranial electroencephalography in neurosurgical patients. Subjects performed a GD target detection task before and during induction of anesthesia with propofol. Recordings were made from the auditory cortex, surrounding auditory-related and prefrontal cortex in awake, sedated, and unresponsive states. High gamma activity was used to measure the neural basis of local-by-global novelty interactions. Positive interaction was defined as a greater response to the double surprise LDGD condition compared to LSGD. Negative interaction was defined as a weaker response to LDGD. Positive interaction was more frequent than negative interaction and was primarily found in auditory cortex.

Negative interaction typically occurred in prefrontal cortex and was more sensitive to general anesthesia. Temporo-parietal auditory-related areas exhibited both types of interaction. These interactions may have relevance in a clinical setting as biomarkers of conscious perception in the assessment of depth of anesthesia and disorders of consciousness.

Keywords: auditory cortex, consciousness, general anesthesia, high gamma, iEEG, local/global deviant, predictive coding, propofol

INTRODUCTION

In everyday life, sensory stimuli that are predictable are not very ecologically informative. Accordingly, neural activity elicited by such stimuli is dampened (reviewed in Nelken, 2014; Pérez-González and Malmierca, 2014). Unexpected stimuli stand out against the background of predictable stimuli. The *novelty* of the unexpected stimuli represents changes in the environment that may be ecologically salient. These unexpected sounds elicit larger neural responses in auditory processing networks compared to those elicited by the background (reviewed in Grimm and Escera, 2012).

The considerations noted above form the foundation for the predictive coding hypothesis for sensory processing. Expectations based on past sensory events generate feedback predictions within higher order cortical regions. Prediction signals are transmitted back to sensory cortices, resulting in diminished responses to the predicted stimuli (Mumford, 1992; Bastos et al., 2012). When sensory inputs violate these predictions, feedforward error signals are carried via ascending sensory pathways to higher order areas, and the dynamic model of the environment is updated. Predictive coding leads to metabolically efficient sensory processing, wherein resources are preserved and allocated to identify potentially important new information associated with changes in the environment.

Predictive coding in the auditory domain can be studied by presenting a background of frequent, predictable sounds ("*standards*") and introducing infrequent, unpredictable sounds ("*deviants*") against this background. Deviant stimuli are expected to elicit enhanced neural responses compared to those evoked by the standard stimuli. The difference between the two neural responses constitutes a *deviance effect*.

In real-life situations, the brain does not process one prediction violation at a time. Instead, it must resolve layers of novel sensory events that occur over multiple time scales. In the auditory domain, the local/global deviant (LGD) paradigm (Bekinschtein et al., 2009) is a useful experimental tool to examine predictive coding mechanisms over two distinct time scales. In this paradigm, short-term novelty occurs over hundreds of milliseconds and is exemplified by presenting repetitive sounds, such as the vowel /ɑ/, and infrequently introducing a different sound, e.g., the vowel /i/ (**Figures 1A,B**). This short-term novelty is termed local deviance (LD).

The LGD paradigm also allows for investigation of novelty over longer time scales. For example, within a block of stimuli, repetition of a sequence of five identical vowels (e.g., /ɑɑɑɑɑ/) can be paired with occasional presentation of a sequence wherein the final vowel is replaced with another (e.g., /ɑɑɑɑi/). This leads to both the short-term novelty (LD) effect and a deviance effect over a longer time scale that is based on the change of the overall pattern of the five-vowel sequences, termed global deviance (GD).

In this example, there is both an LD and a GD effect when five identical vowels are replaced by an occasional sequence of five vowels with the last one different from the first four ("*double surprise*"). GD can also occur when the frequent sequence contains a local deviant, e.g., /ɑɑɑɑi/, and is occasionally replaced by a quintuple of five identical stimuli /ɑɑɑɑɑ/. Here, GD is not associated with LD, but instead is represented by a globally unexpected local standard.

Local deviance and GD effects can be measured using non-invasive methods such as electroencephalography (EEG) and magnetoencephalography (MEG) as differences between responses to standard and deviant stimuli (Bekinschtein et al., 2009; Recasens et al., 2014a,b). Results of source analysis of these responses suggest that different brain regions encode auditory novelty with distinct temporal profiles of neural activation (Recasens et al., 2014a,b). While EEG and MEG provide the necessary temporal resolution to identify neural activity associated with LD and GD, their spatial resolution is insufficient to resolve detailed patterns of activity within the auditory cortical hierarchy (Bekinschtein et al., 2009; Wacongne et al., 2011; Strauss et al., 2015).

Intracranial electroencephalography (iEEG) provides both the high spatial and temporal resolution needed to identify the neural correlates of novelty detection. Studies using iEEG have refined results of non-invasive studies by demonstrating that auditory novelty detection in an LGD paradigm engages multiple cortical regions at distinct time scales (King et al., 2013; El Karoui et al., 2015; Nourski et al., 2018a). The LD effect is associated with feedforward information flow from core (primary) auditory cortex to non-core auditory and auditory-related regions. By contrast, the GD effect appears to originate in posterior superior temporal gyrus (STG) and surrounding auditory-related areas, with subsequent propagation forward to prefrontal cortex and backward to core auditory cortex (Nourski et al., 2018a).

Recent non-invasive studies found evidence for interactions between LD and GD effects, suggesting that these two forms of deviance detection are not fully independent modes of auditory novelty processing (Shirazibeheshti et al., 2018; Kompus et al., 2020; Witon et al., 2020). *Local-by-global* (L × G) *interactions* can be measured by comparing responses to four stimulus conditions: LSGS, LSGD, LDGS and LDGD. Here, L and G denote local

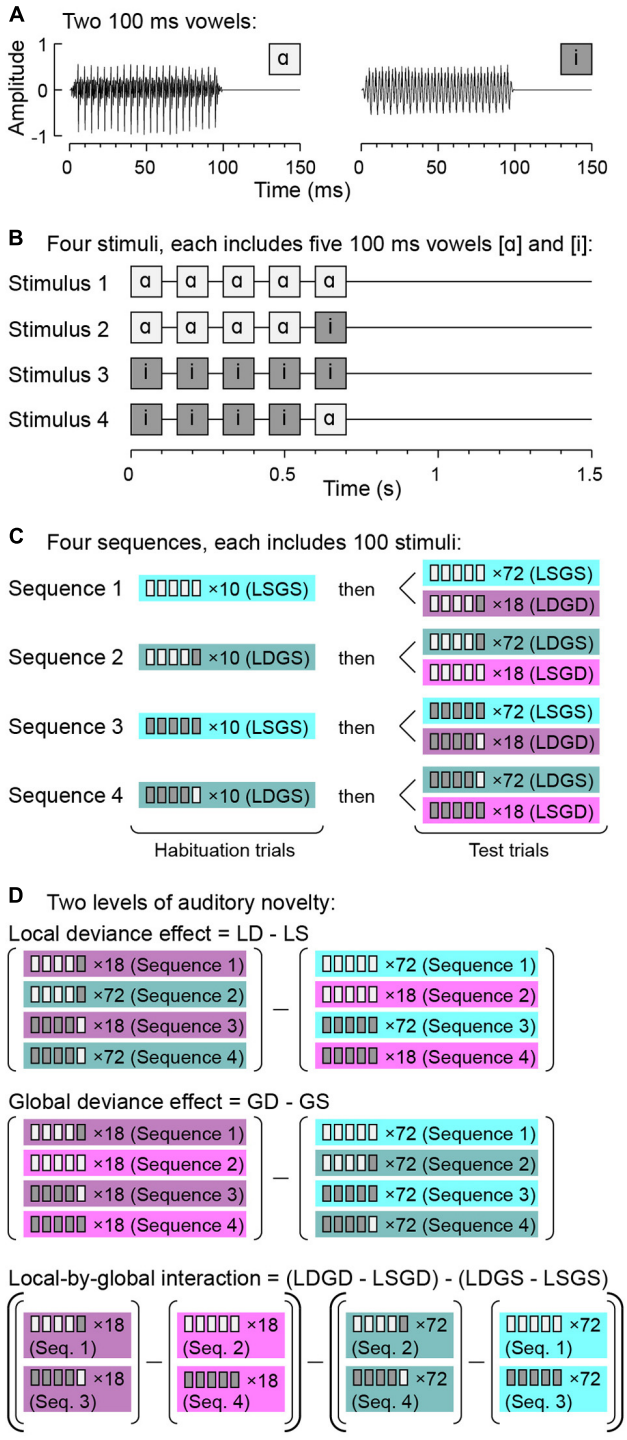

FIGURE 1 | Local/global deviant (LGD) experimental paradigm. **(A)** Waveforms of the two vowels/ɑ/and/i/used to construct the experimental stimuli. **(B)** Schematic of the four experimental stimuli. **(C)** Stimulus sequences. **(D)** Comparisons between responses to specific stimulus types to characterize LD and GD effects and L × G interactions. Note that in subject R413, a slightly modified paradigm was used, where each sequence included 110 stimuli. The 10-trial habituation sequence was followed by 80 GS and 20 GD test trials in this subject. GD, global deviant; GS, global standard; LD, local deviant; LS, local standard. Modified from Nourski et al. (2018a).

and global time scale, and S and D denote standard and deviant stimuli, respectively. Positive interaction is defined as a greater response to the double surprise LDGD condition compared to LSGD. Negative interaction is defined as a weaker response to the double surprise condition relative to LSGD.

Local-by-global interactions have been hypothesized to represent information flow between cortical networks that subserve short- and long-term novelty detection (Witon et al., 2020). Non-invasive studies have shown that neural responses to GD stimuli can be enhanced when these stimuli include LD (Wacongne et al., 2011; Shirazibeheshti et al., 2018). It is hypothesized that this increased response is based on the presence of a feedforward error signal provided by LD. Likewise, in the LSGD condition, the absence of this feedforward LD error signal can be expected to yield a diminished response to the LSGD stimulus.

A key consideration of auditory novelty detection is its modulation by arousal state. Within the predictive coding framework, the ongoing comparison of predictions and sensory observations is a fundamental feature of conscious sensory processing. Anesthetic-induced sedation and loss of consciousness (LOC) disrupt auditory predictive coding (Uhrig et al., 2016; Nourski et al., 2018b; Sanders et al., 2021). During anesthesia induced by propofol, LD effects are preserved within the auditory cortex when the subjects are unconscious, while GD effects are suppressed when subjects are sedated but still conscious (Nourski et al., 2018b).

The present work is the first iEEG study to investigate L × G interactions using the LGD paradigm. The goals of the study were four-fold: (1) Clarify the timing of positive and negative L × G interactions; (2) Identify the brain structures where these interactions occur; (3) Examine how these interactions are modulated during induction of general anesthesia with propofol; and (4) Differentiate attention- and task-related phenomena from those due to changes in arousal state.

These goals were addressed by using an active behavioral task which provided several advantages over a passive-listening setting. In a passive paradigm, absence of L × G interactions might simply be a function of inattention to the sound stimuli. Prevalence of high gamma GD effects is greater in an active paradigm compared to passive listening (Nourski et al., 2021b). Thus, it can be expected that L × G interactions would also be more prominent in an active task. Further, presence or loss of behavioral responses can serve as an additional criterion for defining the state of arousal. Finally, relating physiology and behavior helps identify neural activity contributing to task performance as opposed to less relevant neurophysiologic responses.

Cortical activity was measured in the high gamma iEEG band (70–150 Hz). High gamma is a surrogate of action potential firing in small neuronal populations. It provides a finer-grain spatial resolution compared to scalp EEG and intracranially recorded averaged evoked potentials (Steinschneider et al., 2008; Crone et al., 2011). In the present study, the gradual induction of general anesthesia allowed for a critically important comparison between sedated and unconscious states. Findings pertaining to sedation and unconsciousness may have translational relevance for the

TABLE 1 | Subject demographics and electrode coverage.

Subject[1]	Age	Sex[2]	Number of recording sites per ROI							Seizure focus
			Auditory cortex			Auditory-related	Prefrontal	Other	Total	
			HGPM	STP	STG					
R369	30	M	8	15	17	79	39	54	212	R medial temporal
L372	34	M	6	12	25	51	34	49	177	L temporal pole
R376	48	F	7	10	18	76	30	52	193	R medial temporal
R394	24	M	8	2	0	6	2	7	25	R medial temporal
R399	22	F	3	6	21	46	47	60	183	R temporal
L400	59	F	4	7	3	25	54	65	158	L medial temporal
R413	21	M	8	12	25	81	45	52	223	R medial temporal
Total number of recording sites			44	64	109	364	251	339	1171	

[1] *Letter prefix of the subject code denotes the side of electrode implantation over auditory cortex and the side of seizure focus (L = left; R = right).*
[2] *F = female; M = male.*

assessment of other altered states of arousal including sleep, delirium, and coma.

MATERIALS AND METHODS

Subjects

Study subjects were seven adult neurosurgical patients (three female, four male, age 21–59 years old, median age 30 years old) with medically refractory epilepsy. The patients had been implanted with intracranial electrodes to identify resectable seizure foci. Subjects' age, sex, electrode coverage, and seizure focus data are presented in **Table 1**. All subjects were native English speakers; all except one were right-handed and had left language dominance as determined by Wada tests (subject R413 was left-handed and right hemisphere-dominant).

All subjects underwent audiometric evaluation before the study, and none was found to have hearing deficits or word recognition scores sufficient to affect the findings presented in this study. Cognitive function, as determined by standard neuropsychological assessments, was in the average range in all subjects. Subject R394 had previously undergone a resection of a cavernoma in the anterior medial temporal lobe. The resection had spared cortex corresponding to all the brain regions of interests (ROIs) (see below) except for planum polare (PP). This subject had normal hearing and cognitive abilities and thus was included in the study.

The subjects were tapered off their antiepileptic drugs during the chronic monitoring and had their medication regimens reinstated to varying degrees at the end of the monitoring period, prior to the electrode removal and seizure focus resection surgery.

Stimuli and Procedure

Experiments were conducted in the operating room immediately prior to and during induction of general anesthesia for electrode removal and seizure focus resection surgery. The experiments were part of a series of studies on auditory novelty detection and resting state connectivity across task conditions and arousal states (Nourski et al., 2018a,b, 2021b,c; Banks et al., 2020). Auditory stimuli were quintuples of vowels /ɑ/ and /i/, presented in an LGD paradigm (Bekinschtein et al., 2009; Nourski et al., 2018a; **Figure 1**). The vowels were edited (duration 100 ms) from the steady-state vocalic portions of consonant-vowel stimuli /hɑd/ and /hid/, spoken by a female (fundamental frequency 232 and 233 Hz, respectively) (Hillenbrand et al., 1995). The vowels were normalized to the same root-mean-square amplitude and gated with 5 ms on/off ramps (**Figure 1A**). On each trial, four identical vowels, separated by 50 ms intervals, were presented, followed by either the same or different fifth vowel (**Figure 1B**). This within-quintuple difference constituted short term (local) deviance: /ɑɑɑɑɑ/ and /iiiii/ were LS stimuli, while /ɑɑɑɑi/ and /iiiiɑ/ were LD.

The stimuli were presented in blocks of four sequences, with the order of the sequences randomized across blocks (**Figure 1C**). In all subjects except R413, each sequence began with a recorded instruction that defined the task and the target (GD) stimulus to the subject, e.g., for Sequence 1: "This time, press the button when you hear this sound: /ɑɑɑɑi/. Once again, press the button when you hear this sound: /ɑɑɑɑi/." The instruction was followed by a habituation sequence of 10 trials that established the GS condition (e.g., /ɑɑɑɑɑ/ for Sequence 1), and then by 72 GS and 18 GD test trials, presented in a pseudorandom order. The difference in presentation frequency constituted the long term (global) deviance, and the identity of the GD stimulus changed across the four sequences within each block (**Figure 1D**). Note that the infrequent (GD) trials could have either five identical vowels (LSGD) or a different fifth vowel (LDGD). Likewise, the frequent (GS) trials either had the fifth vowel same or different as the first four (LSGS and LSGD, respectively). The intertrial interval varied within a Gaussian distribution (onset-to-onset mean 1500 ms, standard deviation 10 ms) to reduce heterodyning in the recordings secondary to the 60 Hz power line noise.

In subject R413, a simplified protocol was used, where instead of a recorded instruction, the task was explained beforehand to the subject by the researcher as follows: "Press the button every time you hear the sound sequence change." In this subject, each

10-trial habituation sequence was followed by 80 GS and 20 GD test trials. The duration of each experimental block was 11 min in all subjects.

Stimuli were presented by a TDT RZ2 processor (Tucker-Davis Technologies, Alachua, FL, United States) and delivered at a comfortable level (60–65 dB SPL) diotically via insert earphones (ER4B, Etymotic Research) enclosed in custom-fit earmolds. The subjects were instructed to operate the response button with the hand ipsilateral to the hemisphere from which recordings were made. This was done to minimize contributions to recorded neural responses from activity reflecting motor planning and execution, and somatosensory responses associated with the button press.

Each experiment included three or four 11-min blocks. The first block was presented immediately before administration of propofol. Following the completion of the first block, infusion of propofol was initiated at a rate of 50 μg/kg/min (Alaris pump, BD, Maplewood, MO, United States). Propofol was the sole sedative drug administered to the patients during the experimental period. The time course of induction of sedation followed by general anesthesia is shown for each subject in **Figure 2**. In all subjects except R413, the rate of infusion was increased every 10 min by 25 μg/kg/min, following the approach previously used by Nourski et al. (2017,2018b,2021b) and Banks et al. (2020). The duration of the infusion was 50 min with a maximum rate of 150 μg/kg/min. Three auditory stimuli blocks were presented during the 50 min. In subject R413, a simplified protocol was used, wherein the rate of infusion was 50 μg/kg/min for 20 min, followed by an increase to 150 μg/kg/min for another 20 min. An auditory stimulus block was presented during the final 11 min of each of these two 20-min periods. The infusions were supervised by an attending anesthesiologist using standard respiratory and hemodynamic monitoring. None of the infusions had to be interrupted or terminated for the patients' safety.

The depth of sedation was evaluated before and after each block using the Observer's Assessment of Alertness/Sedation (OAA/S) scale, the gold standard in assessing alertness in the clinical setting (Chernik et al., 1990). Responsiveness (calling the subject's name), speech (asking the subject to repeat the sentence, "The quick brown fox jumps over the lazy dog"), facial expression (the degree of facial relaxation), and eyes (the subject's ability to focus and ptosis) were all assessed and scored on a scale from 1 to 5. The composite OAA/S score, ranging from 5 ("alert") to 1 ("deep sleep"), was defined as the lowest level indicated by any of the four assessment categories.

For the purposes of analyses, three arousal states were defined in each subject: awake (W; before administration of propofol), sedated (S) and unresponsive (U). The letter "W" is used throughout the manuscript instead of "A" for "awake" to avoid the possibility of the abbreviated "A" being interpreted as "Anesthesia." The transition from OAA/S = 3 ("responsive to loud or repeated command") to OAA/S = 2 ("unresponsive

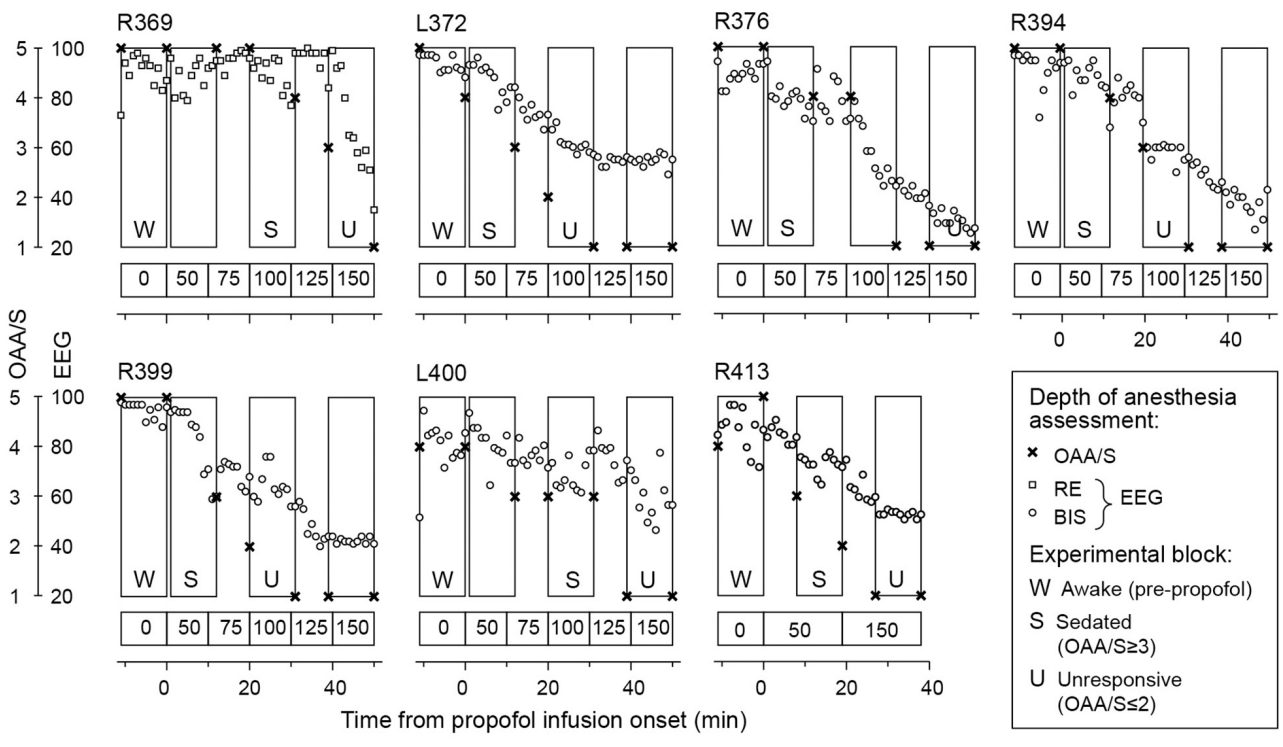

FIGURE 2 | Induction of general anesthesia. Observer's Assessment of Alertness/Sedation (OAA/S) scores (crosses) and electroencephalographic (EEG) sedation indices are plotted as functions of time. EEG-based sedation indices were response entropy [RE] in subject R369 and bispectral index (BIS) in all other subjects (open squares and circles, respectively). Rectangles denote 11-min LGD experimental blocks; letter labels indicate the three arousal states (W: awake, S: sedated, U: unresponsive). Propofol infusion rates are shown underneath each plot.

in the absence of mild prodding or shaking") (Chernik et al., 1990) was used as the threshold between sedation and LOC. LOC was thus approximated as the loss of responsiveness (Vanluchene et al., 2004; Nourski et al., 2018b; Banks et al., 2020). The depth of sedation was additionally assessed using EEG parameters: response entropy (RE) (E-ENTROPY module; Datex-Ohmeda, Madison, WI, United States) (Viertiö-Oja et al., 2004) in subject R369 and bispectral index (BIS) (BIS Complete 4-Channel Monitor; Medtronic, Fridley, MN, United States) (Gan et al., 1997) in all other subjects. The EEG parameters were recorded continuously throughout each experiment and were manually logged on a minute-by-minute basis.

Recording

Intracranial electrophysiological recordings were made using depth and subdural electrodes (Ad-Tech Medical, Oak Creek, WI, United States) implanted to identify potentially resectable seizure foci (Nagahama et al., 2018b). Electrode implantation, recording, and iEEG data analysis have been previously described in detail (Nourski and Howard, 2015). Depth electrode arrays (8–12 cylindrical macro contacts spaced 5 mm apart) targeting the superior temporal plane (STP) including Heschl's gyrus, were stereotactically implanted along the anterolateral-to-posteromedial axis of the gyrus. Depth electrodes which targeted insular cortex provided additional coverage of posteromedial portion of Heschl's gyrus (HGPM), planum temporale (PT), and PP. This configuration was clinically warranted, as it bracketed the suspected temporal lobe seizure foci for their accurate assessment (Nagahama et al., 2018a). Subdural strip and grid electrode arrays consisted of platinum-iridium disc contacts (2.3 mm exposed diameter, 5–10 mm contact-to-contact distance) embedded in a silicone membrane. They were implanted over lateral and ventral cerebral surfaces. A subgaleal electrode was used as a reference.

Reconstruction of the anatomical locations of implanted electrode contacts in individual subjects and their mapping onto a standardized set of coordinates was performed using FreeSurfer image analysis suite (Version 5.3; Martinos Center for Biomedical Imaging, Harvard, MA, United States) and in-house software. Subjects underwent T1-weighted whole-brain structural 3T magnetic resonance imaging (MRI) scans (resolution 1.0 mm) before electrode implantation and MRI and computerized tomography (CT) scans (resolution 1.0 mm) after implantation. Locations of the electrode contacts were obtained from post-implantation MRI and CT scans and projected onto pre-operative MRI scans using non-linear three-dimensional thin-plate spline morphing and intraoperative photography. The locations were then transformed into standard Montreal Neurological Institute (MNI) coordinates using linear co-registration to the MNI152 T1 average brain, as implemented in FMRIB Software library (Version 5.0; FMRIB Analysis Group, Oxford, United Kingdom). For recording sites in the left hemisphere, MNI x-axis coordinates (x_{MNI}) were multiplied by (−1) to map them onto the right-hemisphere common space.

The locations of recording sites were projected onto the right lateral hemispheric surface, STP, ventral and mesial views of the FreeSurfer average template brain (**Figure 3**). The electrode coverage in all subjects is summarized in **Table 1**. The following ROIs were identified, spanning the hierarchy of auditory cortical processing (a modification of the scheme used previously in Nourski et al., 2018a,b, 2021a,c; Banks et al., 2020):

(1) Core auditory cortex in the posteromedial portion of Heschl's gyrus (HGPM; $n = 44$ sites).
(2) Non-core auditory cortex in the STP ($n = 64$), including the anterolateral portion of Heschl's gyrus (HGAL; $n = 25$), PT ($n = 21$), and PP ($n = 18$).

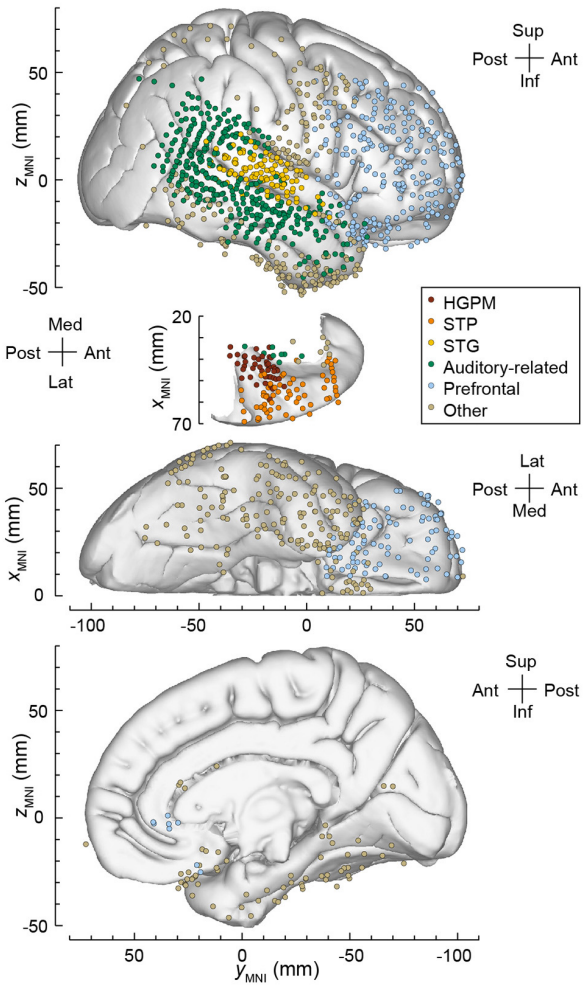

FIGURE 3 | Electrode coverage in all seven subjects. Locations of recording sites, color-coded according to the ROI, are plotted in MNI coordinate space and projected onto the right hemisphere of the Freesurfer average template brain for spatial reference. Left hemisphere MNI x-axis coordinates (x_{MNI}) were multiplied by –1 to map them onto the right-hemisphere common space. Projection is shown on the lateral, top-down (STP), ventral and mesial views **(top** to **bottom)**. Recording sites over orbital, transverse frontopolar, inferior temporal gyrus and temporal pole are shown in both the lateral and the ventral view. Sites in fusiform, lingual, parahippocampal gyrus and gyrus rectus are shown in both the ventral and medial view. Sites in the hippocampus ($n = 13$), amygdala ($n = 12$), frontal operculum ($n = 5$), parietal operculum ($n = 3$), substantia innominata ($n = 5$), putamen ($n = 1$), and uncus ($n = 1$) are not shown. HGPM, posteromedial portion of Heschl's gyrus; STP, superior temporal plane; STG, superior temporal gyrus.

(3) Non-core auditory cortex on the STG (n = 109), including its posterior (n = 72) and middle (n = 37) portions.
(4) Temporo-parietal auditory-related cortex (n = 364), including the posterior insula (n = 8), anterior STG (n = 17), superior temporal sulcus (upper bank, STSU: n = 12; lower bank, STSL: n = 19), and middle temporal (MTG; n = 187), supramarginal (SMG; n = 65), and angular (AG; n = 56) gyri.
(5) Prefrontal cortex (n = 251), including the inferior (IFG; n = 55), middle (MFG; n = 80), and superior (SFG; n = 15) frontal gyri, orbital (OG; n = 76) and transverse frontopolar gyri (TFG; n = 19), and anterior cingulate cortex (n = 6).

An additional 339 recording sites provided coverage of other brain areas, including the inferior temporal gyrus (ITG) (n = 62), temporal pole (n = 58), precentral (n = 44), postcentral (n = 30), parahippocampal (n = 21), fusiform gyrus (n = 20), gyrus rectus (n = 20), premotor cortex (n = 14), hippocampus (n = 13), amygdala (n = 12), anterior insula (n = 8), middle occipital gyrus (n = 6), superior parietal lobule (n = 6), frontal operculum (n = 5), substantia innominata (n = 5), cingulate gyrus (n = 4), parietal operculum (n = 3), lingual gyrus (n = 2), inferior occipital gyrus (n = 2), cuneus (n = 2), putamen (n = 1), and uncus (n = 1).

Assignment of recording sites to ROIs was based on anatomical reconstructions of electrode locations in each subject. For subdural arrays, it was informed by automatic parcelation of cortical gyri as implemented in the FreeSurfer image analysis suite (Destrieux et al., 2010, 2017). Heschl's gyrus was subdivided into HGPM and HGAL. The boundary between the two was defined physiologically based on the presence of phase-locked responses to click train stimuli and short-latency components in averaged evoked potentials. These features are characteristic of HGPM and are absent in HGAL (Brugge et al., 2009). STG was subdivided into posterior and middle non-core auditory cortex portions, and auditory-related anterior portion using the transverse temporal sulcus and ascending ramus of the Sylvian fissure as macroanatomical boundaries. For depth electrodes, ROI assignment was informed by MRI sections along sagittal, coronal, and axial planes. The insula was subdivided into the auditory-related posterior portion and anterior insular cortex (Zhang et al., 2019). Within cingulate gyrus, anterior cingulate cortex (as identified by automatic parcelation in FreeSurfer) was considered a prefrontal area and thus examined separately from the rest of cingulate cortex. Recording sites identified as seizure onset zones or those characterized by excessive noise, as well as depth electrode contacts located outside cortical gray matter, were excluded from analyses and thus are not listed in **Table 1**.

Behavioral (button presses) and iEEG data were recorded using the TDT RZ2 processor; iEEG data were amplified, filtered (0.7–800 Hz bandpass, 12 dB/octave rolloff) and digitized at a sampling rate of 2034.5 Hz.

Data Analysis

Analysis of data was performed using software written in MATLAB R2020a (MathWorks, Natick, MA, United States). Behavioral performance in the target detection task was characterized as accuracy (hit rate, i.e., the percentage of correctly detected target stimuli), sensitivity ($d' = Z_{hit}\text{-}Z_{false\ alarm}$, where Z is the inverse of the cumulative distribution function of the normal distribution) and reaction times (RTs). These metrics were computed separately for LDGD and LSGD trials in each awake and sedated block. Only button presses that occurred between the onset of the 5th vowel and the onset of the 1st vowel of the following trial were considered hits. Button presses that overlapped with the next non-target trial were considered false alarms. The behavioral results thus likely somewhat underestimated target detection rates and biased the RTs toward faster responses. Hit rates and d' values were compared between LDGD and LSGD trials across subjects using one-tailed Wilcoxon signed rank tests. RTs were compared between LDGD and LSGD trials using Wilcoxon rank sum tests. P-values were corrected for multiple comparisons using the false discovery rate (FDR) approach (Benjamini and Hochberg, 1995).

Analysis of iEEG data focused on power in high gamma band (70–150 Hz). Data were downsampled to 1000 Hz, denoised using demodulated band transform approach (Kovach and Gander, 2016) and bandpass-filtered (300th order finite impulse response filter, 70–150 Hz passband). Voltage deflections of the high gamma band-filtered signal that exceeded five standard deviations from the across-block mean for each recording site were considered artifacts. Trials that contained such deflections were excluded from further analysis. The high gamma signal was then squared and smoothed using a 50 ms running average window to obtain high gamma power. Power (μV^2) was used rather than voltage or dB-transformed event-related band power because response waveforms must be non-negative signals for the sign of the L × G interaction to be interpretable.

Responses were averaged across LSGS, LDGS, LSGD, and LDGD test trials separately (see **Figure 1D**, bottom row). L × G interactions were calculated as the difference of the differences of high gamma responses to the four stimulus types, i.e.,:

$$L \times G = (LDGD - LSGD) - (LDGS - LSGS)$$

Local-by-global interaction waveforms were baseline-corrected by subtracting the mean value over the 600 ms prior to the onset of the 5th vowel.

The statistical significance of L × G interactions was examined within the time interval between 0 and 800 ms following the onset of the 5th vowel. Significance was established using a non-parametric cluster-based permutation test (Maris and Oostenveld, 2007; Nourski et al., 2018a). The test statistic was based on grouping adjacent time points that exhibited L × G interactions. The cluster statistic for each recording site and experimental block was obtained by first computing t-values across all time points. At each time point, t-values were compared to a threshold value (the 1st percentile tail of the two-tailed T-distribution). Clusters were defined as consecutive time points for which the t-values exceeded the threshold, and the cluster-level statistic was computed as the sum of the t-values within each cluster. The p-values were calculated using permutation tests in which 10,000 random trial partitions were shuffled with respect to the four trial labels. Cluster-level statistics were calculated, and the largest cluster-level statistic was identified for

each partition. Monte Carlo p-values were calculated for each cluster based on the 10,000-sample distribution set of the test statistics. Interactions were considered significant at $p < 0.05$. Recording sites with at least one significant positive or negative L × G interaction cluster were considered as exhibiting the corresponding interaction type.

The spatial distribution of L × D interactions across the lateral hemispheric surface and the STP was visualized by plotting locations of sites characterized by significant positive or negative interactions in the MNI coordinate space and projecting them onto the right hemisphere of the FreeSurfer average template brain. ROIs were characterized in terms of the prevalence of positive and negative L × G interactions in each of the three arousal states. Prevalence was defined as the percentage of sites exhibiting a significant interaction in each arousal state. The onset latency of L × G interactions was defined as the beginning of the first significant cluster and calculated separately for positive and negative interactions. Onset latencies of positive interactions in the awake state were compared between HGPM, STP, STG, and auditory-related cortex using the Kruskal–Wallis test. For positive interaction, comparison of onset latencies in these ROIs between awake and sedated states was done using the Wilcoxon rank sum test. Likewise, for negative interaction, comparison of onset latencies between auditory-related and prefrontal cortex in the awake state was done using the Wilcoxon rank sum test. The overall time course of positive and negative interactions was visualized by plotting T-scores, averaged across sites that exhibited significant interactions, as functions of time after the 5th vowel onset.

RESULTS

Task Performance

All seven subjects performed the GD target detection task to varying degrees, as measured by hit rates, d' and RTs, during awake and sedated experimental blocks. The "double surprise" LDGD condition typically provided an advantage for the performance of the GD detection task compared to the LSGD target condition (**Figure 4**). In the awake state, the LDGD condition was associated with higher hit rates in six out of seven subjects (**Figure 4A**, top panel), though this improvement did not reach significance ($p = 0.055$). Sensitivity (d') for LDGD target trials was higher than for LSGD trials in five subjects (**Figure 4A**, middle panel), and the improvement was statistically significant ($p = 0.016$). Finally, the LDGD condition was associated with significantly faster behavioral responses in four subjects (R369: ΔRT = 263 ms, $p < 0.0001$; R376: ΔRT = 130 ms, $p = 0.00192$; R394: ΔRT = 216 ms, $p < 0.0001$; L400: ΔRT = 174 ms, $p = 0.00249$) (**Figure 4A**, bottom panel). Across all hit trials and subjects, the grand median RTs for LDGD and LSGD 420 and 516 ms, respectively.

Sedation with sub-hypnotic doses of propofol led to a deterioration of task performance (**Figure 4B**). Subjects R376 and R399 only had one and zero correct hit responses to LDGD

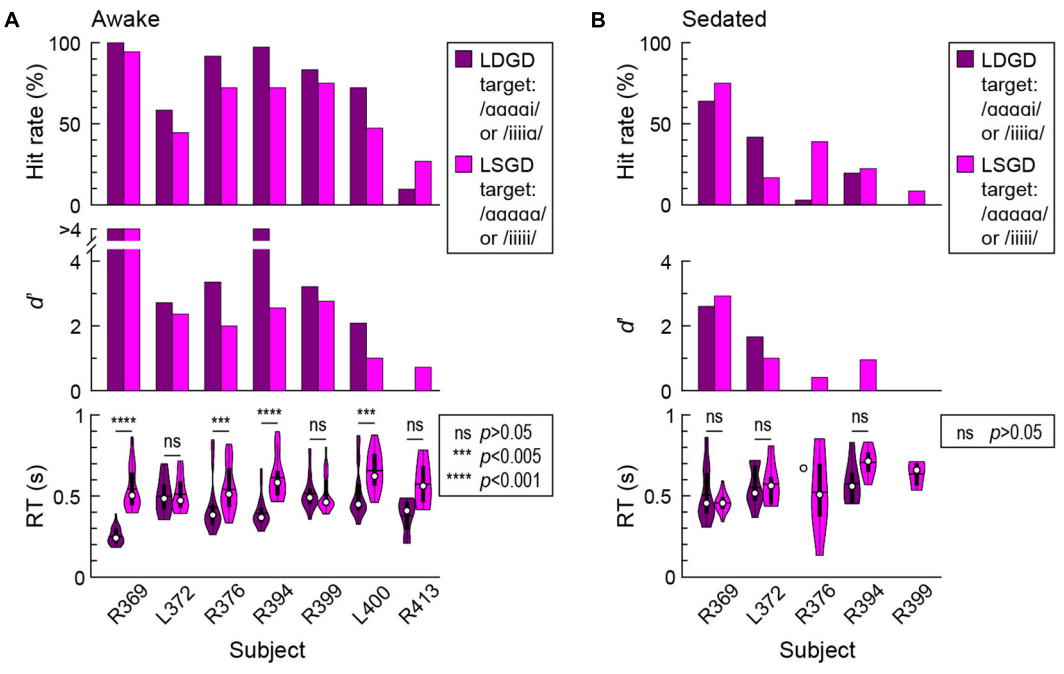

FIGURE 4 | Global deviance (GD) target detection task performance in the awake **(A)** and sedated **(B)** states. Summary of data from seven subjects. Hit rates (% correctly detected target stimuli), sensitivity (d') and RTs are plotted in the top, middle, and bottom panels, respectively. In the sedated state, subject R399 did not have correct hit responses to LDGD targets, and subjects L400 and R413 did not have correct hit responses to either LSGD or LDGD targets.

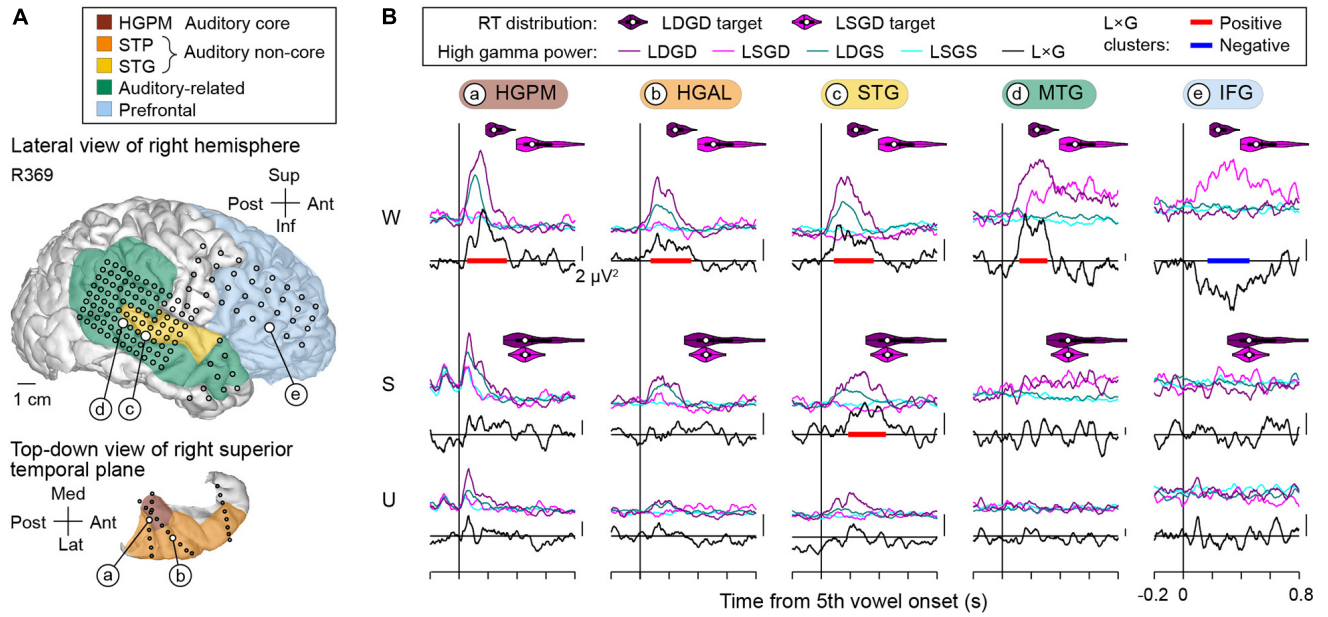

FIGURE 5 | L × G interactions during the induction of general anesthesia in a representative subject with right hemisphere electrode coverage (R369). **(A)** Lateral view of the right hemispheric surface and top-down view of the STP depicting electrode coverage. Colors represent different ROIs, circles represent recording sites. Larger white circles denote the locations of five representative recording sites (a–e). **(B)** High gamma responses to the final vowel of the LGD quintuplet stimulus recorded from the exemplary sites (a–e, left to right) and L × G interactions in awake, sedated, and unresponsive states (W, S, U; top to bottom). Across-trial average high gamma power envelopes are shown separately for the four stimulus conditions (LSGS, LDGS, LSGD, and LDGD; cyan, teal, magenta, and purple, respectively). Black lines denote L × G interaction time course, baseline-corrected by subtracting mean value over the 600 ms prior to the onset of the 5th vowel. Vertical scale bars correspond to 2 μV^2. Significant ($p < 0.05$) positive and negative L × G interaction clusters are shown as red and blue bars, respectively. RT distributions for LSGD and LDGD target stimuli are shown as magenta and purple violin plots, respectively. In each violin plot, a white circle denotes the median, a vertical line denotes the mean, a bar denotes *Q*1 and *Q*3, and whiskers show the range of lower and higher adjacent values (i.e., values within 1.5 interquartile ranges below *Q*1 or above *Q*3, respectively).

targets, respectively. Subjects L400 and L413 only had false alarm responses to both types of GD targets in the sedated state. None of the remaining three subjects exhibited a significant difference in RTs between LSGD and LDGD target trials. Sedation with propofol thus appeared to decrease the advantageous behavioral effect of "double surprise" provided by the LDGD condition in the awake state.

Electrophysiological Signatures of Local-by-Global Interactions

The use of subdural and depth arrays allowed for a comprehensive assessment of responses from multiple cortical regions comprising the auditory processing hierarchy. This assessment is exemplified by data from subject R369, who displayed the best task performance of all subjects (**Figure 5**). Coverage of the right hemispheric convexity by subdural electrode arrays is depicted along with a top-down view of the STP which illustrates the placement of depth arrays (**Figure 5A**). High gamma responses and L × G interactions at selected sites during awake (W), sedated (S), and unresponsive (U) states are shown in **Figure 5B**. As the main effects of LD and GD have been reported elsewhere (Nourski et al., 2018a,b), analyses presented below will focus solely on L × G interactions.

In subject R369, the awake state featured a *positive* L × G interaction within core auditory cortex (HGPM), surrounding auditory cortical areas (HGAL, lateral STG) and in auditory-related cortex (MTG) (**Figure 5B**, top row). Significant positive interaction (denoted by red bars in **Figure 5B**) emerged within 100 ms and peaked between 200 and 300 ms after the onset of the 5th vowel. By contrast, the IFG site was characterized by a *negative* L × G interaction, wherein LSGD stimuli elicited larger responses than LDGD beyond LD effect (blue bar in **Figure 5B**). This interaction developed later than the positive L × G interaction, emerging at around 200 ms after the 5th vowel onset in this example. The onset of both types of L × G interactions preceded the subjects' behavioral responses to the respective trials (see violin plots in **Figure 5B**). Sedation with propofol was associated with attenuation of L × G interactions. In the example shown in **Figure 5B** (middle row), the STG site was the only site that maintained a significant positive L × G interaction, while the negative interaction in the IFG site was absent. L × G interactions were abolished in the unresponsive state (see **Figure 5B**, bottom row).

Positive and negative L × G interactions were present in both hemispheres, as exemplified by data obtained from the left hemisphere in subject L372 (**Figure 6**). This subject exhibited below-average hit rates in the task and

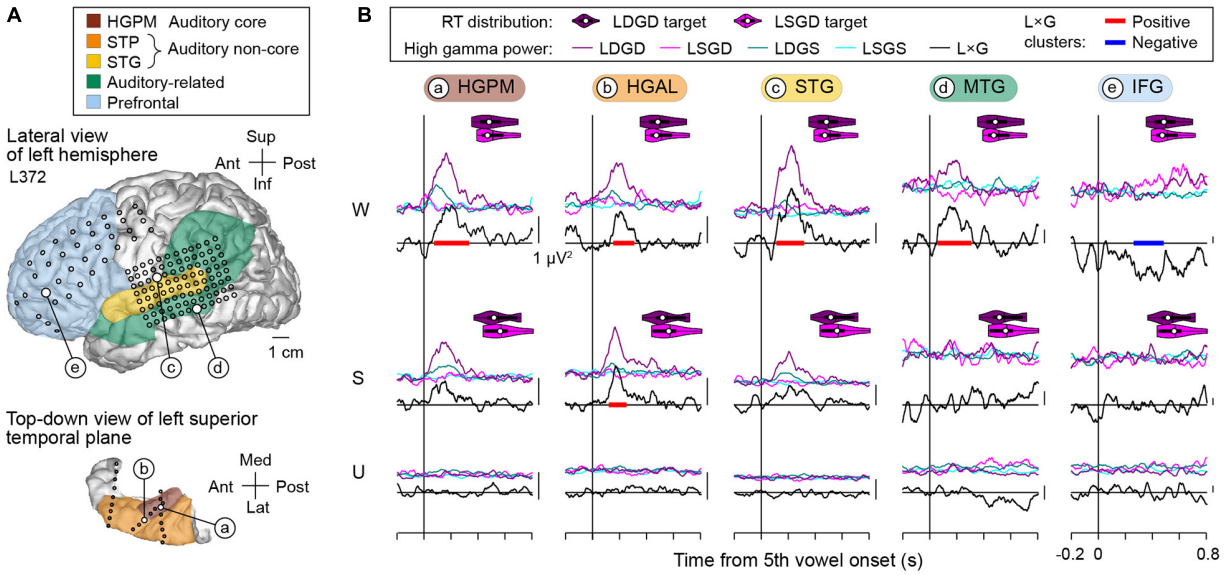

FIGURE 6 | L × G interactions during induction of general anesthesia in a representative subject with left hemisphere electrode coverage (L372). See caption of **Figure 5** for detail.

no significant RT difference between LSGD and LDGD. In the awake state, positive L × G interaction occurred in core, non-core auditory, and auditory-related cortex, and negative L × G interaction was identified in the IFG. As seen in the previous example, L × G interactions were strongly modulated by propofol. In the sedated and unresponsive state, there were no significant interactions except for a positive L × G interaction at the HGAL site in the sedated state.

The two examples above demonstrate positive and negative L × G interactions in both language-dominant and non-dominant hemisphere and in both above- and below-average task performers. Positive interaction preceded negative interaction and occurred at earlier stages within the cortical processing hierarchy. At all examined stages of cortical auditory processing, sedation with propofol strongly diminished these physiologic interactions, which were further attenuated in the unresponsive state.

Spatial Distribution and Time Course of Local-by-Global Interactions

The spatial distribution of L × G interactions across all subjects in the three states of arousal is summarized in **Figure 7**. The data were plotted in the MNI coordinate space and projected onto the right hemisphere of the FreeSurfer average template brain to allow for pooling of data from multiple subjects. Marked differences were present in the spatial distribution of positive and negative interactions. Only positive interaction was identified in the STP in the awake state. The auditory cortex on the lateral STG generally exhibited positive interaction whereas the surrounding auditory-related cortex exhibited both positive and negative interactions. Negative interaction was more common than positive in prefrontal cortex. In the three sites that featured both positive and negative interactions (a posterior STG and an MTG site in the awake state, and another posterior STG site in the sedated state), positive interaction preceded negative one. Increasing sedation by the administration of escalating doses of the propofol infusion led to a progressive decrease in the number of sites exhibiting L × G interactions. Eventually, when the unresponsive state was achieved, very few sites with significant interactions remained in the studied brain regions.

The distributions of L × G effects were examined with respect to responses to the vowel stimuli, LD and GD effects, as reported for this subject cohort in previous studies (**Figure 3B** in Nourski et al., 2021c and Figure 4 in Nourski et al., 2018b). In the awake state, sites that were responsive to the vowel stimuli yet exhibited no significant L × G interactions of either type, clustered in HGPM and PT. With sedation, there was an increased incidence of sites throughout the STP (except PP) and on the lateral STG. When the subjects became unresponsive, the prevalence of both types of L × G interaction markedly diminished compared to prevalence of responses to vowel stimuli both in the STP and on the lateral STG. Sites that exhibited a significant LD effect without a significant L × G interaction were present in all three studied arousal states, and their distribution (STP and lateral STG) was relatively consistent across the three states. Finally, sites that exhibited a significant GD effect without a significant L × G interaction mostly clustered in posterior auditory-related and prefrontal areas. With sedation, only a few such sites remained, reflecting a sharp decline in the prevalence of GD effect with sedation. In the unresponsive state, there were no sites that exhibited a significant GD effect and no L × G interaction.

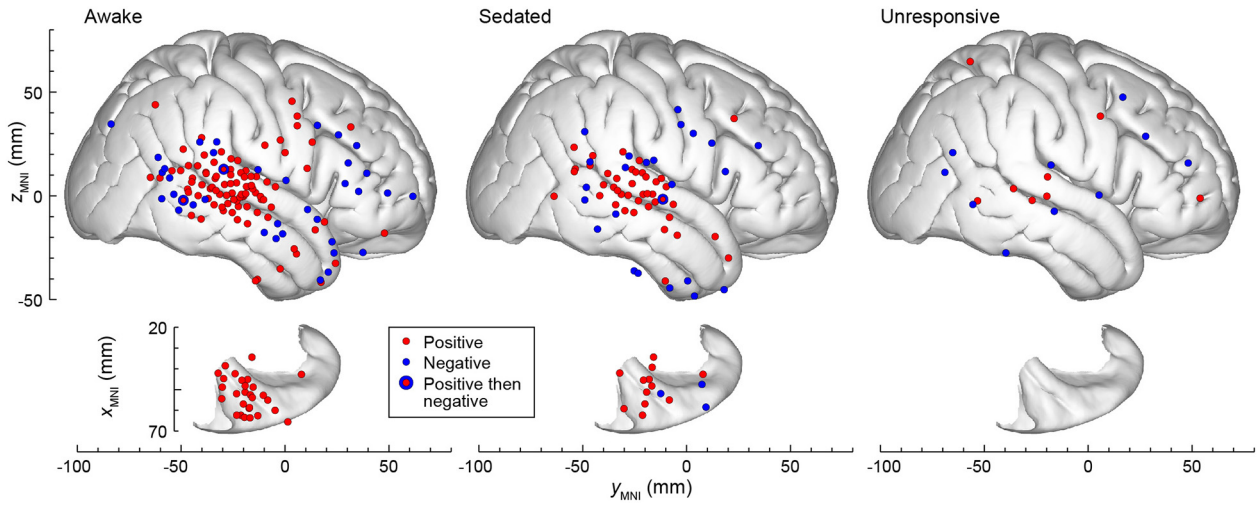

FIGURE 7 | The topography of L × G interactions across states of arousal. A summary of data from seven subjects, plotted in the MNI coordinate space and projected onto the right hemisphere of the FreeSurfer average template brain for spatial reference. Top-down views of the right superior temporal plane are plotted underneath side views of the right lateral hemispheric convexity and aligned along the y_{MNI} axis. Sites that exhibited positive and negative L × G interactions are depicted by red and blue symbols, respectively. Note that some sites in ventral prefrontal cortex (IFG and OG) appear over anterior STG when projected onto the template brain. Sites in the STSU and STSL are projected onto the lateral hemispheric convexity and thus appear to be over either STG or MTG.

The distribution of L × G interactions across ROIs, their onset latency and overall time course are examined in **Figure 8**. Overall, negative interaction was seen far less frequently than positive, as reflected in the different *y*-scales in **Figure 8A**. In the awake state, the prevalence of positive interaction was the highest in the canonical auditory cortex with prevalence in HGPM, STP, and STG of 45.5, 29.7, and 42.2%, respectively (**Figure 8A**, left panel). An intermediate response pattern with both positive and negative interactions was observed in the auditory-related cortex. The prevalence of negative interaction was greatest in the prefrontal and auditory-related cortex (5.58 and 5.49%, respectively) (**Figure 8A**, right panel). Sedation and loss of responsiveness were associated with a progressive decline in the prevalence of both types of interactions.

In the awake state, onset latencies of positive interaction were comparable between HGPM, STP, STG, and auditory-related cortex (median values 115, 108, 128, and 120 ms, respectively; $p = 0.210$, Kruskal–Wallis test) (**Figure 8B**, left panel). There was a significant increase in the onset latency of the positive L × G interaction between the awake and sedated states (median latencies 117 and 159 ms, respectively; $p = 0.000893$, Wilcoxon rank sum test) within the auditory and auditory-related cortex. Onset latencies of negative interaction were much longer than of positive interaction, with median values in auditory-related and prefrontal cortex of 441 and 335 ms, respectively. However, the difference between onset latencies in the two ROIs did not reach statistical significance in this limited data set ($p = 0.100$, Wilcoxon rank sum test) (**Figure 8B**, right panel). As even fewer sites exhibited this interaction in the sedated state (7 and 3 sites in auditory-related and prefrontal cortex, respectively), statistical inferences regarding latency were not feasible in this case.

The overall time course of positive and negative interactions is depicted in **Figure 8C**. The time course of both types of interactions was similar across the canonical auditory and auditory-related cortex in the awake and sedated states. This paralleled the similar onset latencies of positive interaction in these regions. The positive interaction peaked at around 200 ms and extended to around 400 ms after the onset of the final vowel. Negative interaction in auditory-related and prefrontal cortex had a slower time course.

Outside of core auditory cortex, there was variability in the prevalence of L × G interactions across subdivisions within each ROI (**Table 2**). Within the STP, PT exhibited the greatest prevalence of positive L × G interaction in the awake state (52.4%); negative interaction was not observed at all. By contrast, L × G interactions were virtually absent in PP. There was a progressive decrease in the prevalence of positive interaction from the posterior to middle to anterior STG (51.4, 24.3, and 5.88%, respectively). Negative interaction was very infrequent in all three subdivisions.

A marked difference in the prevalence of positive and negative interactions occurred outside of auditory cortex. The prevalence of positive and negative interactions in the awake state was similar in the three subdivisions of auditory-related cortex with extensive electrode coverage (MTG, SMG, and AG). This increase in prevalence of negative interaction culminated in the IFG. Of 55 sites in the IFG, where 2 (3.64%) sites showed positive interaction while 6 (10.9%, a two-fold increase compared to overall prevalence within prefrontal cortex) exhibited negative

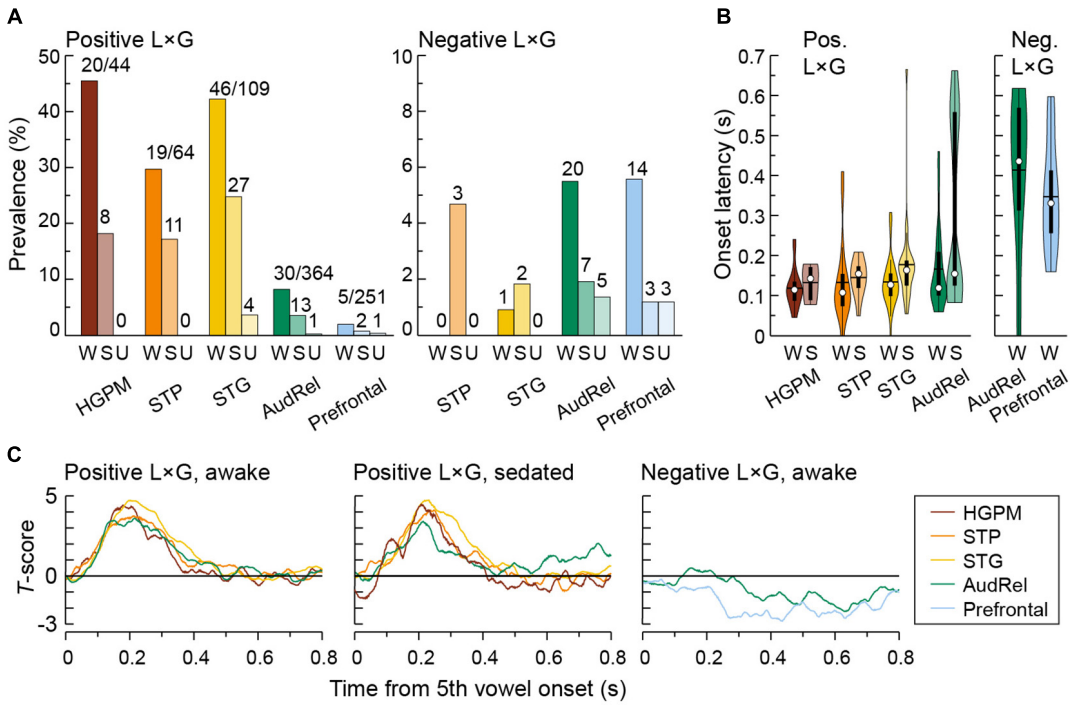

FIGURE 8 | Regional distribution and time course of L × G interactions. Summary of data from seven subjects. Colors represent ROIs, differently shaded bars and symbols represent measurements made in awake (W), sedated (S), and unresponsive (U) state (dark, medium, and light bar shading, respectively). **(A)** Percentages of sites with significant positive and negative L × G interactions (left and right panel, respectively). Numbers above bars indicate numbers of sites with significant L × G interactions. Note different *y*-scales in the left and right panel. **(B)** Onset latencies of positive and negative L × G interactions (left and right panel, respectively). In each violin plot, a white circle denotes the median, a horizontal line denotes the mean, a bar denotes *Q*1 and *Q*3, and whiskers show the range of lower and higher adjacent values (i.e., values within 1.5 interquartile ranges below *Q*1 or above *Q*3, respectively). The latency distributions for negative L × G interaction are only shown for the awake state, as very few sites exhibited this interaction in the sedated state (7 and 3 sites in auditory-related and prefrontal cortex, respectively), making statistical inferences impractical. **(C)** Time course of L × G interactions. *T*-scores averaged across sites that exhibited significant interactions are plotted as functions of time after the 5th vowel onset. In panels **(B,C)**, positive L × G interaction in prefrontal cortex and negative L × G interaction in canonical auditory cortex (HGPM, STP, and STG) are not shown due to their paucity in the respective regions.

interaction. None of the 34 recording sites in the SFG and TFG had either type of interaction. The highest percentage of interactions in other areas examined was in the precentral gyrus. Here, 8 out of 44 sites (18.2%) showed a positive interaction, while only one site displayed negative interaction in the awake state.

The regional distribution of L × G interactions presented in detail in **Table 2** is graphically summarized in **Figure 9**. Here, ROIs are color-coded based on the prevalence of positive and negative interactions in the awake state. Caution must be exercised when extrapolating the prevalence of these interactions in each ROI. First, it should not be assumed that interactions are homogenously distributed throughout each ROI, especially outside canonical auditory cortex (cf. **Figure 7**). Second, the prevalence was calculated based on limited sample sizes in several of the ROIs (cf. **Table 2**). Thus, this graphical summary warrants conservative interpretation. Still, it is evident that positive L × G interaction primarily occurred in the auditory cortex on the STP, lateral STG (except rostral areas PP and STGA), and precentral gyrus. By contrast, negative interaction primarily occurred within the IFG, and became progressively less prevalent at more dorsal and rostral prefrontal areas. Finally, multiple auditory-related ROIs exhibited both types of interaction.

DISCUSSION

Summary of Findings

The present study extends previous findings of auditory novelty processing (Nourski et al., 2018a,b, 2021b,c) by specifically examining neural responses that reflect interactions of LD and GD in the LGD paradigm. Identifying where and when these interactions occur provides insight into how the brain manages to simultaneously analyze multiple levels of novelty, as encountered in typical sound environments. Changes in these interactions may be relevant for understanding altered auditory novelty detection in states of reduced arousal. These considerations elevate L × G interactions from a purely experimental observation to a biologically relevant phenomenon.

The main finding of this study is that different brain regions are associated with positive and negative L × G interactions (see **Figure 9**). Positive interaction occurs in the canonical

TABLE 2 | Numbers and percentages of sites with significant positive and negative L × G interactions across arousal states.

ROI	n_{total}	Positive L × G interaction						Negative L × G interaction					
		W		S		U		W		S		U	
		n	%	*n*	%	*n*	%	*n*	%	*n*	%	*n*	%
HGPM	**44**	**20**	**45.5**	**8**	**18.2**	**0**	**0**	**0**	**0**	**0**	**0**	**0**	**0**
STP	**64**	**19**	**29.7**	**11**	**17.2**	**0**	**0**	**0**	**0**	**3**	**4.69**	**0**	**0**
HGAL	25	7	28	5	20	0	0	0	0	1	4	0	0
PT	21	11	52.4	5	23.8	0	0	0	0	0	0	0	0
PP	18	1	5.56	1	5.56	0	0	0	0	2	11.1	0	0
STG	**109**	**46**	**42.2**	**27**	**24.8**	**4**	**3.67**	**1**	**0.972**	**2**	**1.83**	**0**	**0**
Posterior STG	72	37	51.4	19	26.4	2	2.78	1	1.39	2	3.78	0	0
Middle STG	37	9	24.3	8	21.6	2	5.41	0	0	0	0	0	0
Auditory-related	**364**	**30**	**8.24**	**13**	**3.57**	**1**	**0.275**	**20**	**5.49**	**7**	**1.92**	**5**	**1.37**
Anterior STG	17	1	5.88	0	0	0	0	1	5.88	0	0	0	0
STSU	12	4	33.3	0	0	0	0	3	25	0	0	0	0
STSL	19	4	21.1	1	5.26	0	0	1	5.26	0	0	0	0
MTG	187	9	4.81	4	2.14	1	0.535	9	4.81	3	1.6	2	1.07
SMG	65	6	9.23	4	6.15	0	0	3	4.62	3	4.62	1	1.54
AG	56	5	8.93	3	5.36	0	0	3	5.36	1	1.79	2	3.57
Prefrontal	**251**	**5**	**1.99**	**2**	**0.797**	**1**	**0.398**	**14**	**5.58**	**3**	**1.2**	**3**	**1.2**
IFG	55	2	3.64	0	0	0	0	6	10.9	2	3.63	1	1.82
MFG	80	1	1.25	1	1.25	0	0	4	5	1	1.25	2	2.5
SFG	15	0	0	0	0	0	0	0	0	0	0	0	0
OG	76	1	1.32	1	1.32	1	1.32	3	3.95	0	0	0	0
TFG	19	0	0	0	0	0	0	0	0	0	0	0	0
Other	**339**	**21**	**6.19**	**3**	**0.885**	**3**	**0.885**	**7**	**2.06**	**19**	**5.6**	**2**	**0.59**
Inferior temporal g.	62	3	4.84	1	1.61	0	0	0	0	5	8.06	1	1.61
Temporal pole	58	2	3.45	1	1.72	0	0	0	0	2	3.45	0	0
Precentral g.	44	8	18.2	0	0	0	0	1	2.27	3	6.82	0	0
Postcentral g.	30	1	3.33	0	0	0	0	1	3.33	2	6.67	0	0
Parahippocampal g.	21	0	0	0	0	0	0	1	4.76	1	4.76	0	0
Fusiform g.	20	1	5	0	0	1	5	0	0	1	5	0	0
G. rectus	20	0	0	0	0	0	0	0	0	3	15	0	0
Premotor cortex	14	1	7.14	0	0	1	7.14	0	0	0	0	1	7.14
Hippocampus	13	0	0	0	0	0	0	1	7.69	0	0	0	0
Amygdala	12	0	0	0	0	0	0	0	0	0	0	0	0

ROI subdivisions that had electrode coverage of <10 sites are not shown.

AG, angular gyrus; g., gyrus; HGAL, anterolateral Heschl's gyrus; HGPM, posteromedial Heschl's gyrus; IFG, inferior frontal gyrus; L × G, local-by-global; MFG, middle frontal gyrus; MTG, middle temporal gyrus; OG, orbital gyrus; PP, planum polare; PT, planum temporale; ROI, region of interest; S, sedated; SFG, superior frontal gyrus; SMG, supramarginal gyrus; STSL, lower bank of the superior temporal sulcus; STSU, upper bank of the superior temporal sulcus; STG, superior temporal gyrus; TFG, transverse frontopolar gyrus; U, unresponsive; W, awake.

auditory cortex and, to a lesser degree, in the precentral gyrus (areas shaded in red in **Figure 9**). Negative interaction primarily occurs in the prefrontal cortex, more specifically in IFG (shaded blue in **Figure 9**) and, to a lesser extent, MFG and OG. Auditory-related areas are associated with both types of interaction (shaded purple in **Figure 9**). Behaviorally, GD is more salient when paired with the feedforward error signal associated with LD ("double surprise"). This is manifested as an enhancement in performance on the GD target detection task. By contrast, GD is less salient when where is no feedforward error signal. Paradoxically, the LSGD condition, which produces smaller responses in auditory cortex, can elicit larger responses in higher-order cortical regions particularly within prefrontal cortex. The physiologic profile for the LSGD combination is characterized by longer onset latencies and parallels the greater task difficulty as measured by lower hit rates and *d'*, and longer RTs.

Relationship to the Literature

In the original report introducing the LGD paradigm, no interactions were observed between LD and GD effects as measured by event-related potentials (Bekinschtein et al., 2009). This negative result has been subsequently attributed due to a non-standard method used to measure the interactions

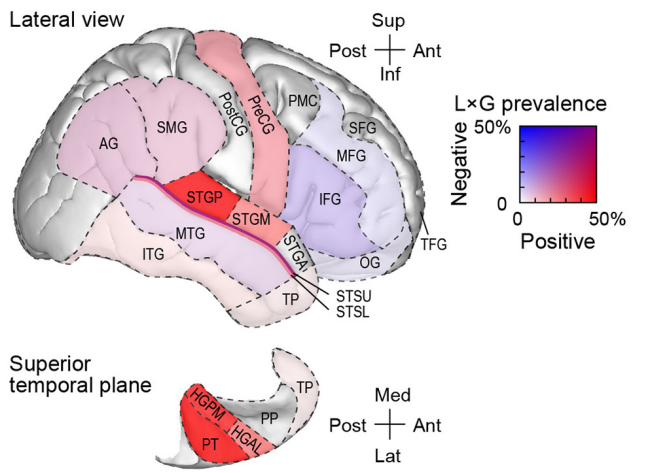

FIGURE 9 | Schematic of regional distribution of L × G interactions in the awake state. ROIs are color-coded according to prevalence of positive and negative interactions. For ROIs where only a single site exhibited a significant interaction (PP, STGA, PostCG, and PMC), prevalence estimates are not shown. See text and **Table 2** for details. AG, angular gyrus; HGAL, anterolateral Heschl's gyrus; HGPM, posteromedial Heschl's gyrus; IFG, inferior frontal gyrus; L × G, local-by-global; MFG, middle frontal gyrus; MTG, middle temporal gyrus; OG, orbital gyrus; PMC, premotor cortex; PP, planum polare; PreCG, precentral gyrus; PostCG, postcentral gyrus; PT, planum temporale; ROI, region of interest; SFG, superior frontal gyrus; SMG, supramarginal gyrus; STSL, STSU, lower and upper bank of the superior temporal sulcus, respectively; STGA, STGM, STGP, posterior, middle, and anterior superior temporal gyrus, respectively; TFG, transverse frontopolar gyrus; TP, temporal pole.

(Shirazibeheshti et al., 2018). An additional factor could be the use of the event-related potential as a response metric instead of a rectified signal (e.g., EEG power) (cf. Witon et al., 2020). The current study provides direct evidence for positive and negative L × G interactions by measuring high gamma power in iEEG recordings. The focus on high gamma activity was motivated by its high spatial specificity (Crone et al., 2011) and its interpretation as a surrogate for action potential firing within neuronal populations (Steinschneider et al., 2008).

A theoretical framework that accounts for the interactive component of the LGD paradigm has been proposed by Witon et al. (2020). In this framework, three phases of auditory novelty processing are envisioned. The early phase (100–150 ms) is characterized by detection of LD in the auditory cortex and includes the pre-attentive component of stimulus-specific adaptation (SSA) (Ulanovsky et al., 2003; Fishman and Steinschneider, 2012). The late phase (400–600 ms) is characterized by conscious attention-dependent detection of GD that is carried out by higher-order areas such as the IFG (Nourski et al., 2018a). Finally, the intermediate phase (250–350 ms) is postulated to represent bidirectional information exchange between the auditory cortex and IFG that underlies L × G interactions (Witon et al., 2020). Positive interaction as measured by intracranially recorded high gamma activity emerges earlier than that detected by the scalp EEG study of Witon et al. (2020) but otherwise overlaps with the intermediate processing phase. This interaction localizes to multiple areas within the auditory cortex and extends into adjacent auditory-related areas.

The onset latencies of responses to sound tend to increase along the auditory hierarchy, with the shortest latencies being in the core auditory cortex in HGPM (Nourski et al., 2014). This progressive increase in latency has been interpreted to reflect feedforward information flow from lower to higher auditory cortical regions (Nourski et al., 2021a). LD effects follow this feedforward latency pattern (Nourski et al., 2018a). Interestingly, this sequential increase in latency was not observed when examining positive L × G interaction along the auditory cortical hierarchy. Onset latencies of this interaction were similar across the auditory and auditory-related cortex. The reasons for this similarity in latency are unclear. It may be necessary to examine effective connectivity patterns to address this issue.

This iEEG study confirms the existence of a negative L × G interaction within the inferior frontal cortex, as first demonstrated by Witon et al. (2020) using scalp-recorded EEG. In the current study using iEEG, negative interaction was also observed in other areas of prefrontal cortex (MFG, OG). Another novel finding of his study was the prominence of negative interaction in auditory-related cortex (see **Table 2**). This effect was widespread and occurred in areas strongly associated with canonical auditory cortex (e.g., STSU) as well as higher-order associative regions (e.g., AG).

Unfortunately, onset latency data were not adequate to address whether the origin of negative interaction was within the prefrontal cortex and if this interaction was then transmitted to the auditory-related cortex via feedback connections. The median and mean latencies were shorter in the prefrontal compared to auditory-related cortex. However, the overall distributions of onset latencies were not significantly different between the two ROIs (at $p = 0.10$). Given the relative paucity of negative interaction, this question will have to be addressed by a future study employing a larger cohort of subjects with comprehensive electrode coverage of the relevant cortical regions.

Effects of Propofol-Induced Sedation and Unresponsiveness

The principal effect of propofol is the attenuation of L × G interactions, with a greater effect on negative interaction. This effect is consistent with the previously reported results obtained during recovery from propofol-induced sedation (Shirazibeheshti et al., 2018; Witon et al., 2020). The use of a novel slow induction protocol in the present study allowed for a comparison between the sedated and unresponsive states. Both positive and negative interactions were attenuated by propofol upon sedation and were essentially abolished upon LOC.

Previous work has shown loss of GD effects (measured by combining LSGD and LDGD trials) at subhypnotic doses of propofol when subjects were sedated, but still responsive (Nourski et al., 2018b). This study indicates that extension of the LGD paradigm into the clinical realm using scalp-recorded data could focus on the positive L × G interaction. By

contrast, given the greater sensitivity of the negative interaction to subhypnotic doses of propofol, negative interaction would likely be of a more limited utility in assessing pathologic states of consciousness.

Mechanisms of Novelty Detection and Local-by-Global Interactions Across the Auditory Processing Hierarchy

Local deviance effects measured in the LGD paradigm are closely related to mismatch negativity (MMN) (Näätänen and Alho, 1995). Two mechanisms have been proposed as contributing to MMN (and, by proxy, to the LD effect). These are (1) SSA, which refers to the attenuation of responses to the repetition of the same stimuli (Fishman, 2014); and (2) A higher-level process that reflects stored neuronal memory of acoustic patterns which have been established by repeated sounds (Näätänen et al., 2005). SSA is present in the ascending auditory pathways (Malmierca et al., 2009; Antunes et al., 2010; Richardson et al., 2013) and the primary auditory cortex (Ulanovsky et al., 2003; Farley et al., 2010; Fishman and Steinschneider, 2012). It can occur in the anesthetized state (Duque and Malmierca, 2015) and operates even when a single token stimulus precedes a subsequent token. To identify acoustic patterns made up of multiple tokens, deviance detection must occur over longer temporal intervals (Ulanovsky et al., 2004). The regions surrounding primary auditory cortex have been shown to operate over progressively longer temporal intervals and thus conform to this requirement (Sharpee et al., 2011).

The finding that LSGD stimuli elicited larger responses than to LDGD in higher-order brain areas, but not auditory cortex, was unexpected given that the fifth vowel is the same as the first four. It would be expected that SSA would lead to a diminished response to the fifth vowel in the LSGD condition. Therefore, the larger responses to LSGD stimuli must be based on additional mechanisms beyond SSA.

Global deviance effects result from integration of sensory inputs over longer temporal intervals than that required for LD detection. The mechanisms for GD detection likely engage broader cortical networks of auditory working memory and parallel that seen in the multiscale processing of human speech. For example, a study that examined processing of narrated stories at the word, sentence, and paragraph level identified brain regions associated with the processing of speech over these respective temporal scales (Lerner et al., 2011). There was a progressive activation of ever-higher level auditory and auditory-related cortical regions which paralleled the processing of speech at the three levels of increasing complexity. The highest degree of activation involved in processing at the paragraph level occurred in prefrontal and parietal networks. In a similar manner, GD effects also require integration of information over long temporal windows and engage prefrontal and parietal regions (Nourski et al., 2018a, 2021b). Outside the canonical auditory cortex, regions in the auditory processing hierarchy operate over the progressively longer time scales required to detect long-term novelty within sound patterns (Ulloa et al., 2008; Farbood et al., 2015).

Caveats and Limitations

A key concern regarding iEEG studies carried out in neurosurgical patients with epilepsy is that the experimental subjects are not entirely representative of a healthy population. With regards to the present study, consistent effects were observed across subjects despite differences in seizure disorder histories, antiepileptic medication regimens, and the location of seizure foci. Importantly, the findings of the present study are comparable to results obtained previously in healthy subjects using the same experimental paradigm and similar analyses of non-invasive recordings (Shirazibeheshti et al., 2018; Witon et al., 2020).

The variability of the effects of propofol in individual subjects represents a caveat specific to this investigation. Although the time course of the induction of general anesthesia varied across subjects, the arousal states were not defined by a specific dose or plasma concentration of propofol. Instead, arousal states were defined using the OAA/S, which is considered the gold standard for assessing awareness in the clinical setting (Chernik et al., 1990; Vanluchene et al., 2004).

Finally, for several reasons, the nature of the study precluded formal assessment of possible relationships between task performance and the electrophysiological L × G interaction profiles. First, L × G interaction–the neural response metric considered in the present study–is defined as the difference of differences between averaged responses to the four types of stimuli, i.e., (LDGD−LSGD)−(LDGS−LSGS). This complicates identification of relationships between behavioral performance and this particular facet of neural activity on a single-trial level. The relatively small subject sample (seven participants) with variable electrode coverage and the overall relatively low prevalence of significant L × G interactions also limited our ability to directly assess the relationship between physiology and behavior. Continuing this experimental paradigm in additional subjects will be required to formally address this important question.

Future Directions and Clinical Implications

Key future experiments will include examining LGD effects during sedation and unresponsiveness induced by different anesthetic drugs with different cellular mechanisms of action. In addition to the studies that use anesthetics to probe LGD effects and their interactions, future work will examine the systems-level mechanisms of LGD detection during stages of natural sleep. The translational relevance of this work will be enhanced by combining intracranial and scalp-recorded activity to relate changes in scalp-recorded potentials to their intracranial sources. This will be important to improve prognostic accuracy in patients with disorders of consciousness (e.g., delirium and coma) which are a major problem in current neurologic practice.

DATA AVAILABILITY STATEMENT

The raw data supporting the conclusions of this article will be made available by the authors, without undue reservation.

ETHICS STATEMENT

The studies involving human participants were reviewed and approved by University of Iowa Institutional Review Board. The patients/participants provided their written informed consent to participate in this study.

AUTHOR CONTRIBUTIONS

KN, MS, and MB: conception and design of the work. KN, RM, HK, and MB: acquisition of data. KN, MS, AR, and MB: analysis and interpretation of data. KN and MS: drafting the work. AR, RM, HK, and MB: editing the work. All authors provided approval for publication of the content and agreed to be accountable for all aspects of the work in ensuring that questions related to the accuracy or integrity of any part of the work are appropriately investigated and resolved.

FUNDING

This study was supported by grants NIH R01-DC04290, R01-GM109086, and UL1-RR024979.

ACKNOWLEDGMENTS

We thank Haiming Chen, Bradley Hindman, Christopher Kovach, Phillip Gander, and Beau Snoad for help with data collection and analysis, and Matthew Howard for his oversight and support of this work.

REFERENCES

Antunes, F. M., Nelken, I., Covey, E., and Malmierca, M. S. (2010). Stimulus-specific adaptation in the auditory thalamus of the anesthetized rat. *PLoS One* 5:e14071. doi: 10.1371/journal.pone.0014071

Banks, M. I., Krause, B. M., Endemann, C. M., Campbell, D. I., Kovach, C. K., Dyken, M. E., et al. (2020). Cortical functional connectivity indexes arousal state during sleep and anesthesia. *Neuroimage* 211:116627. doi: 10.1016/j.neuroimage.2020.116627

Bastos, A. M., Usrey, W. M., Adams, R. A., Mangun, G. R., Fries, P., and Friston, K. J. (2012). Canonical microcircuits for predictive coding. *Neuron* 76, 695–711. doi: 10.1016/j.neuron.2012.10.038

Bekinschtein, T. A., Dehaene, S., Rohaut, B., Tadel, F., Cohen, L., and Naccache, L. (2009). Neural signature of the conscious processing of auditory regularities. *Proc. Natl. Acad. Sci. U.S.A.* 106, 1672–1677. doi: 10.1073/pnas.0809667106

Benjamini, Y., and Hochberg, Y. (1995). Controlling the false discovery rate: a practical and powerful approach to multiple testing. *J. R. Stat. Soc. Series B Stat. Methodol.* 57, 289–300.

Brugge, J. F., Nourski, K. V., Oya, H., Reale, R. A., Kawasaki, H., Steinschneider, M., et al. (2009). Coding of repetitive transients by auditory cortex on Heschl's gyrus. *J. Neurophysiol.* 102, 2358–2374. doi: 10.1152/jn.91346.2008

Chernik, D. A., Gillings, D., Laine, H., Hendler, J., Silver, J. M., Davidson, A. B., et al. (1990). Validity and reliability of the observer's assessment of alertness/sedation scale: study with intravenous midazolam. *J. Clin. Psychopharmacol.* 10, 244–251.

Crone, N. E., Korzeniewska, A., and Franaszczuk, P. J. (2011). Cortical γ responses: searching high and low. *Int. J. Psychophysiol.* 79, 9–15. doi: 10.1016/j.ijpsycho.2010.10.013

Destrieux, C., Fischl, B., Dale, A., and Halgren, E. (2010). Automatic parcellation of human cortical gyri and sulci using standard anatomical nomenclature. *Neuroimage* 53, 1–15. doi: 10.1016/j.neuroimage.2010.06.010

Destrieux, C., Terrier, L. M., Andersson, F., Love, S. A., Cottier, J. P., Duvernoy, H., et al. (2017). A practical guide for the identification of major sulcogyral structures of the human cortex. *Brain Struct. Funct.* 222, 2001–2015. doi: 10.1007/s00429-016-1320-z

Duque, D., and Malmierca, M. S. (2015). Stimulus-specific adaptation in the inferior colliculus of the mouse: anesthesia and spontaneous activity effects. *Brain Struct. Funct.* 220, 3385–3398. doi: 10.1007/s00429-014-0862-1

El Karoui, I., King, J. R., Sitt, J., Meyniel, F., Van Gaal, S., Hasboun, D., et al. (2015). Event-Related potential. time-frequency, and functional connectivity facets of local and global auditory novelty processing: an intracranial study in humans. *Cereb. Cortex.* 25, 4203–4212. doi: 10.1093/cercor/bhu143

Farbood, M. M., Heeger, D. J., Marcus, G., Hasson, U., and Lerner, Y. (2015). The neural processing of hierarchical structure in music and speech at different timescales. *Front. Neurosci.* 9:157. doi: 10.3389/fnins.2015.00157

Farley, B. J., Quirk, M. C., Doherty, J. J., and Christian, E. P. (2010). Stimulus-specific adaptation in auditory cortex is an NMDA-independent process distinct from the sensory novelty encoded by the mismatch negativity. *J. Neurosci.* 30, 16475–16484. doi: 10.1523/JNEUROSCI.2793-10.2010

Fishman, Y. I. (2014). The mechanisms and meaning of the mismatch negativity. *Brain Topogr.* 27, 500–526. doi: 10.1007/s10548-013-0337-3

Fishman, Y. I., and Steinschneider, M. (2012). Searching for the mismatch negativity in primary auditory cortex of the awake monkey: deviance detection or stimulus specific adaptation? *J. Neurosci.* 32, 15747–15758. doi: 10.1523/JNEUROSCI.2835-12.2012

Gan, T. J., Glass, P. S., Windsor, A., Payne, F., Rosow, C., Sebel, P., et al. (1997). Bispectral index monitoring allows faster emergence and improved recovery from propofol, alfentanil, and nitrous oxide anesthesia. BIS Utility Study Group. *Anesthesiology.* 87, 808–815. doi: 10.1097/00000542-199710000-00014

Grimm, S., and Escera, C. (2012). Auditory deviance detection revisited: evidence for a hierarchical novelty system. *Int. J. Psychophysiol.* 85, 88–92. doi: 10.1016/j.ijpsycho.2011.05.012

Hillenbrand, J., Getty, L. A., Clark, M. J., and Wheeler, K. (1995). Acoustic characteristics of American English vowels. *J. Acoust. Soc. Am.* 97(5 Pt 1), 3099–3111. doi: 10.1121/1.411872

King, J. R., Faugeras, F., Gramfort, A., Schurger, A., El Karoui, I., Sitt, J. D., et al. (2013). Single-trial decoding of auditory novelty responses facilitates the detection of residual consciousness. *Neuroimage.* 83, 726–738. doi: 10.1016/j.neuroimage.2013.07.013

Kompus, K., Volehaugen, V., Todd, J., and Westerhausen, R. (2020). Hierarchical modulation of auditory prediction error signaling is independent of attention. *Cogn. Neurosci.* 11, 132–142. doi: 10.1080/17588928.2019.1648404

Kovach, C. K., and Gander, P. E. (2016). The demodulated band transform. *J. Neurosci. Methods* 261, 135–154. doi: 10.1016/j.jneumeth.2015.12.004

Lerner, Y., Honey, C. J., Silbert, L. J., and Hasson, U. (2011). Topographic mapping of a hierarchy of temporal receptive windows using a narrated story. *J. Neurosci.* 31, 2906–2915. doi: 10.1523/JNEUROSCI.3684-10.2011

Malmierca, M. S., Cristaudo, S., Pérez-González, D., and Covey, E. (2009). Stimulus-specific adaptation in the inferior colliculus of the anesthetized rat. *J. Neurosci.* 29, 5483–5493. doi: 10.1523/JNEUROSCI.4153-08.2009

Maris, E., and Oostenveld, R. (2007). Nonparametric statistical testing of EEG- and MEG-data. *J. Neurosci. Methods* 164, 177–190. doi: 10.1016/j.jneumeth.2007.03.024

Mumford, D. (1992). On the computational architecture of the neocortex. II. The role of cortico-cortical loops. *Biol. Cybern.* 66, 241–251. doi: 10.1007/BF00198477

Näätänen, R., and Alho, K. (1995). Mismatch negativity–a unique measure of sensory processing in audition. *Int. J. Neurosci.* 80, 317–337. doi: 10.3109/00207459508986107

Näätänen, R., Jacobsen, T., and Winkler, I. (2005). Memory-based or afferent processes in mismatch negativity (MMN): a review of the evidence. *Psychophysiology* 42, 25–32. doi: 10.1111/j.1469-8986.2005.00256.x

Nagahama, Y., Schmitt, A. J., Nakagawa, D., Vesole, A. S., Kamm, J., Kovach, C. K., et al. (2018b). Intracranial EEG for seizure focus localization: evolving techniques, outcomes, complications, and utility of combining surface and depth electrodes. *J. Neurosurg.* 1–13. doi: 10.3171/2018.1.JNS171808 [Epub ahead of print].

Nagahama, Y., Schmitt, A. J., Dlouhy, B. J., Vesole, A. S., Gander, P. E., Kovach, C. K., et al. (2018a). Utility and safety of depth electrodes within the supratemporal plane for intracranial EEG. *J. Neurosurg.* 131, 772–780. doi: 10.3171/2018.4.JNS171812

Nelken, I. (2014). Stimulus-specific adaptation and deviance detection in the auditory system: experiments and models. *Biol. Cybern.* 108, 655–663. doi: 10.1007/s00422-014-0585-7

Nourski, K. V., and Howard, M. A. III (2015). Invasive recordings in the human auditory cortex. *Handb. Clin. Neurol.* 129, 225–244. doi: 10.1016/B978-0-444-62630-1.00013-5

Nourski, K. V., Banks, M. I., Steinschneider, M., Rhone, A. E., Kawasaki, H., Mueller, R. N., et al. (2017). Electrocorticographic delineation of human auditory cortical fields based on effects of propofol anesthesia. *Neuroimage* 152, 78–93. doi: 10.1016/j.neuroimage.2017.02.061

Nourski, K. V., Steinschneider, M., McMurray, B., Kovach, C. K., Oya, H., Kawasaki, H., et al. (2014). Functional organization of human auditory cortex: investigation of response latencies through direct recordings. *Neuroimage* 101, 598–609. doi: 10.1016/j.neuroimage.2014.07.004

Nourski, K. V., Steinschneider, M., Rhone, A. E., Kawasaki, H., Howard, M. A. III, and Banks, M. I. (2018a). Processing of auditory novelty across the cortical hierarchy: an intracranial electrophysiology study. *Neuroimage* 183, 412–424. doi: 10.1016/j.neuroimage.2018.08.027

Nourski, K. V., Steinschneider, M., Rhone, A. E., Kawasaki, H., Howard, M. A. III, and Banks, M. I. (2018b). Auditory predictive coding across awareness states under anesthesia: an intracranial electrophysiology study. *J. Neurosci.* 38, 8441–8452. doi: 10.1523/JNEUROSCI.0967-18.2018

Nourski, K. V., Steinschneider, M., Rhone, A. E., Krause, B. M., Kawasaki, H., and Banks, M. I. (2021b). Cortical responses to auditory novelty across task conditions: an intracranial electrophysiology study. *Hear. Res.* 399:107911. doi: 10.1016/j.heares.2020.107911

Nourski, K. V., Steinschneider, M., Rhone, A. E., Krause, B. M., Mueller, R. N., Kawasaki, H., et al. (2021c). Cortical responses to vowel sequences in awake and anesthetized states: a human intracranial electrophysiology study. *Cereb. Cortex* bhab168. doi: 10.1093/cercor/bhab168 [Epub ahead of print].

Nourski, K. V., Steinschneider, M., Rhone, A. E., Kovach, C. K., Banks, M. I., Krause, B. M., et al. (2021a). Electrophysiology of the human superior temporal sulcus during speech processing. *Cereb. Cortex* 31, 1131–1148. doi: 10.1093/cercor/bhaa281

Pérez-González, D., and Malmierca, M. S. (2014). Adaptation in the auditory system: an overview. *Front. Integr. Neurosci.* 8:19. doi: 10.3389/fnint.2014.00019

Recasens, M., Grimm, S., Capilla, A., Nowak, R., and Escera, C. (2014a). Two sequential processes of change detection in hierarchically ordered areas of the human auditory cortex. *Cereb. Cortex* 24, 143–153. doi: 10.1093/cercor/bhs295

Recasens, M., Grimm, S., Wollbrink, A., Pantev, C., and Escera, C. (2014b). Encoding of nested levels of acoustic regularity in hierarchically organized areas of the human auditory cortex. *Hum. Brain Mapp.* 35, 5701–5716. doi: 10.1002/hbm.22582

Richardson, B. D., Hancock, K. E., and Caspary, D. M. (2013). Stimulus-specific adaptation in auditory thalamus of young and aged awake rats. *J. Neurophysiol.* 110, 1892–1902. doi: 10.1152/jn.00403.2013

Sanders, R. D., Casey, C., and Saalmann, Y. B. (2021). Predictive coding as a model of sensory disconnection: relevance to anaesthetic mechanisms. *Br. J. Anaesth.* 126, 37–40. doi: 10.1016/j.bja.2020.08.017

Sharpee, T. O., Atencio, C. A., and Schreiner, C. E. (2011). Hierarchical representations in the auditory cortex. *Curr. Opin. Neurobiol.* 21, 761–767. doi: 10.1016/j.conb.2011.05.027

Shirazibeheshti, A., Cooke, J., Chennu, S., Adapa, R., Menon, D. K., Hojjatoleslami, S. A., et al. (2018). Placing meta-stable states of consciousness within the predictive coding hierarchy: the deceleration of the accelerated prediction error. *Conscious. Cogn.* 63, 123–142. doi: 10.1016/j.concog.2018.06.010

Steinschneider, M., Fishman, Y. I., and Arezzo, J. C. (2008). Spectrotemporal analysis of evoked and induced electroencephalographic responses in primary auditory cortex (A1) of the awake monkey. *Cereb. Cortex* 18, 610–625. doi: 10.1093/cercor/bhm094

Strauss, M., Sitt, J. D., King, J. R., Elbaz, M., Azizi, L., Buiatti, M., et al. (2015). Disruption of hierarchical predictive coding during sleep. *Proc. Natl. Acad. Sci. U.S.A.* 112, E1353–E1362. doi: 10.1073/pnas.1501026112

Uhrig, L., Janssen, D., Dehaene, S., and Jarraya, B. (2016). Cerebral responses to local and global auditory novelty under general anesthesia. *Neuroimage* 141, 326–340. doi: 10.1016/j.neuroimage.2016.08.004

Ulanovsky, N., Las, L., and Nelken, I. (2003). Processing of low-probability sounds by cortical neurons. *Nat. Neurosci.* 6, 391–398. doi: 10.1038/nn1032

Ulanovsky, N., Las, L., Farkas, D., and Nelken, I. (2004). Multiple time scales of adaptation in auditory cortex neurons. *J. Neurosci.* 24, 10440–10453. doi: 10.1523/JNEUROSCI.1905-04.2004

Ulloa, A., Husain, F. T., Kemeny, S., Xu, J., Braun, A. R., and Horwitz, B. (2008). Neural mechanisms of auditory discrimination of long-duration tonal patterns: a neural modeling and fMRI study. *J. Integr. Neurosci.* 7, 501–527. doi: 10.1142/s021963520800199x

Vanluchene, A. L., Struys, M. M., Heyse, B. E., and Mortier, E. P. (2004). Spectral entropy measurement of patient responsiveness during propofol and remifentanil. A comparison with the bispectral index. *Br. J. Anaesth.* 93, 645–654. doi: 10.1093/bja/aeh251

Viertiö-Oja, H., Maja, V., Särkelä, M., Talja, P., Tenkanen, N., Tolvanen-Laakso, H., et al. (2004). Description of the entropy algorithm as applied in the Datex-Ohmeda S/5 entropy module. *Acta Anaesthesiol. Scand.* 48, 154–161. doi: 10.1111/j.0001-5172.2004.00322.x

Wacongne, C., Labyt, E., van Wassenhove, V., Bekinschtein, T., Naccache, L., and Dehaene, S. (2011). Evidence for a hierarchy of predictions and prediction errors in human cortex. *Proc. Natl. Acad. Sci. U.S.A.* 108, 20754–20759. doi: 10.1073/pnas.1117807108

Witon, A., Shirazibehehsti, A., Cooke, J., Aviles, A., Adapa, R., Menon, D. K., et al. (2020). Sedation modulates frontotemporal predictive coding circuits and the double surprise acceleration effect. *Cereb. Cortex* 30, 5204–5217. doi: 10.1093/cercor/bhaa071

Zhang, Y., Zhou, W., Wang, S., Zhou, Q., Wang, H., Zhang, B., et al. (2019). The roles of subdivisions of human insula in emotion perception and auditory processing. *Cereb. Cortex* 29, 517–528. doi: 10.1093/cercor/bhx334

Conflict of Interest: The authors declare that the research was conducted in the absence of any commercial or financial relationships that could be construed as a potential conflict of interest.

frontiers in Human Neuroscience

ORIGINAL RESEARCH
published: 29 October 2021
doi: 10.3389/fnhum.2021.734231

Predictability-Based Source Segregation and Sensory Deviance Detection in Auditory Aging

*Christiane R. Neubert[1], Alexander P. Förstel[2], Stefan Debener[2] and Alexandra Bendixen[1]**

[1] Cognitive Systems Lab, Faculty of Natural Sciences, Institute of Physics, Chemnitz University of Technology, Chemnitz, Germany, [2] Neuropsychology Lab, Department of Psychology, Carl von Ossietzky University of Oldenburg, Oldenburg, Germany

When multiple sound sources are present at the same time, auditory perception is often challenged with disentangling the resulting mixture and focusing attention on the target source. It has been repeatedly demonstrated that background (distractor) sound sources are easier to ignore when their spectrotemporal signature is predictable. Prior evidence suggests that this ability to exploit predictability for foreground-background segregation degrades with age. On a theoretical level, this has been related with an impairment in elderly adults' capabilities to detect certain types of sensory deviance in unattended sound sequences. Yet the link between those two capacities, deviance detection and predictability-based sound source segregation, has not been empirically demonstrated. Here we report on a combined behavioral-EEG study investigating the ability of elderly listeners (60–75 years of age) to use predictability as a cue for sound source segregation, as well as their sensory deviance detection capacities. Listeners performed a detection task on a target stream that can only be solved when a concurrent distractor stream is successfully ignored. We contrast two conditions whose distractor streams differ in their predictability. The ability to benefit from predictability was operationalized as performance difference between the two conditions. Results show that elderly listeners can use predictability for sound source segregation at group level, yet with a high degree of inter-individual variation in this ability. In a further, passive-listening control condition, we measured correlates of deviance detection in the event-related brain potential (ERP) elicited by occasional deviations from the same spectrotemporal pattern as used for the predictable distractor sequence during the behavioral task. ERP results confirmed neural signatures of deviance detection in terms of mismatch negativity (MMN) at group level. Correlation analyses at single-subject level provide no evidence for the hypothesis that deviance detection ability (measured by MMN amplitude) is related to the ability to benefit from predictability for sound source segregation. These results are discussed in the frameworks of sensory deviance detection and predictive coding.

Keywords: auditory scene analysis, foreground-background separation, predictive coding, elderly listeners, temporal processing, Electroencephalography (EEG), mismatch negativity (MMN)

OPEN ACCESS

Edited by:
Juanita Todd,
The University of Newcastle, Australia

Reviewed by:
Chia-Hsiung Cheng,
Chang Gung University, Taiwan
Zsófia Anna Gaál,
Hungarian Academy of Sciences (MTA), Hungary

****Correspondence:***
Alexandra Bendixen
alexandra.bendixen@physik.tu-chemnitz.de

Specialty section:
This article was submitted to Cognitive Neuroscience, a section of the journal Frontiers in Human Neuroscience

Received: *30 June 2021*
Accepted: *08 October 2021*
Published: *29 October 2021*

Citation:
Neubert CR, Förstel AP, Debener S and Bendixen A (2021) Predictability-Based Source Segregation and Sensory Deviance Detection in Auditory Aging. Front. Hum. Neurosci. 15:734231. doi: 10.3389/fnhum.2021.734231

INTRODUCTION

Hearing is a daily life challenge as the auditory system needs to disentangle the incoming sound mixture into meaningful streams by linking sounds belonging to one source together, and separating sounds belonging to different sources (Bregman, 1990). Sound segregation ability and the ability to track a particular sound source (e.g., a speaker) across time in a concurrent acoustic mixture is crucial to follow the target stream while ignoring background noise (e.g., other speakers, cafeteria noise). In most listeners, these auditory processes work surprisingly smoothly. The prevailing theoretical framework for explaining the ease with which listening in such complex environments works, is predictive coding (Friston, 2005; Winkler et al., 2009; Kanai et al., 2015). The core idea is that sound sources tend to behave regularly (predictably) over time, and once the brain has formed a predictive model for the emission pattern of a given sound source, this source can be tracked over time and separated from other sources without effort (Bendixen, 2014; Schröger et al., 2014; Winkler and Schröger, 2015), and even without attention (Sussman et al., 1999, 2007). As simple and elegant as this explanation seems, recent work has pointed toward some unresolved issues related to the predictive-coding account of auditory perception (Denham and Winkler, 2017; Heilbron and Chait, 2018). Both reviews reiterate the concern that detecting the predictability of a sound source does not imply forming actual predictions about this sound source, and that the underlying neural mechanisms are not entirely clear. Furthermore, the evidence for the brain's capacity to detect the predictability of a sound source often comes from indirect measures, using the logic of occasionally violating the otherwise predictable pattern and measuring whether the brain responds to this violation (deviation) in a specific way (Schröger, 2007). Whether detecting a predictability violation (i.e., sensory deviance detection) and sensory prediction are indeed related, is notoriously difficult to demonstrate (Denham and Winkler, 2017; Heilbron and Chait, 2018).

In the current study, we set out to find a link between detecting predictability violations and using auditory predictability for sound source segregation. We addressed this question by exploiting inter-individual variability in those two capabilities, asking whether listeners whose auditory system detects deviants more readily (as evidenced by corresponding brain responses) can also use predictability more easily for segregating sound sources from one another (as evidenced by listening success in a challenging task with auditory background interference). We chose a sample of listeners aged 60–75 years, for two main reasons. First, we expect to find more inter-individual variability in this sample than in young individuals (Alain et al., 2006), which increases the statistical power for finding a relation between deviance detection and predictability-based source segregation if there is such a relation. Second, previous studies have pointed toward a need for explaining elderly listeners' apparent deficits in complex sensory deviance detection (Getzmann and Näätänen, 2015; Rimmele et al., 2015) as well as in predictability-based source segregation (Rimmele et al., 2012a). Accordingly, providing evidence for such a relation would contribute to a better understanding of elderly listeners' difficulties with complex acoustic scenes (Alain et al., 2006).

To study predictability-based source segregation, we capitalized on prior work showing that spectrotemporal regularities support auditory stream segregation (Bendixen et al., 2010; Andreou et al., 2011; Sohoglu and Chait, 2016; Aman et al., 2021). Specifically, it is easier to segregate interleaved auditory streams when one or all of them contain spectrotemporal regularities (patterns). This has been demonstrated when the stream carrying the regularities is relevant to the listeners' task (Rimmele et al., 2012a; Aman et al., 2021) and also when the listener tries to ignore this stream (Andreou et al., 2011; Rimmele et al., 2012a). Evidence on whether this capacity to use regularities for stream segregation is preserved in elderly listeners is controversial: On the one hand, Rimmele et al. (2012a) suggest that elderly listeners can make use of predictability-based stream segregation when the stream carrying the regularity is task-relevant (see their Exp. 1), but not—at least not for all forms of regularity—when the regular stream is task-irrelevant and needs to be ignored (see their Exp. 2). Specifically, they found an age-related impairment in using an isochronous regularity in a background sound stream for ignoring this stream while performing a difficult foreground listening task. Rimmele et al. (2012a) interpret their findings in a predictive-coding framework by suggesting that spectrotemporal regularities stabilize auditory stream segregation and that the different levels of task relevance lead to different mechanisms of processing the regularities. On the other hand, de Kerangal et al. (2021) recently showed that the ability to track sources in an acoustic scene based on their regularities is largely preserved in elderly listeners. In their study, all streams were task-relevant, and the specific listening task was different from the one used by Rimmele et al. (2012a). The current study closely followed the task and design of Rimmele et al. (2012a) to assess whether elderly listeners' impairment in using background regularities for stream segregation can be replicated.

Besides this replication attempt, a key aspect of the current study—as denoted above—was to relate each individual listener's capability to use background regularities for stream segregation with their ability to extract such regularities. Regularity extraction was measured indirectly via the elicitation of specific brain responses by regularity violations. The key indicator was the mismatch negativity (MMN) component of the event-related brain potential (ERP) extracted from the participant's electroencephalogram (EEG). The MMN is a component elicited by sensory events that violate some previously established regularity (Näätänen et al., 1978; for reviews, see e.g., Näätänen et al., 2007; Garrido et al., 2009; Fitzgerald and Todd, 2020). MMN can thus be used as an indirect indicator of regularity extraction (Schröger, 2005). It is elicited even without attention to the stimuli carrying the regularities and violations (e.g., Näätänen et al., 1993; Winkler et al., 2005). MMN is elicited by violations of simple rules (such as repetition of stimulus properties), but also of more abstract regularities such as certain patterns in which sounds are arranged (Zachau et al., 2005; for a review see Paavilainen, 2013). The MMN component is characterized by a frontocentral negativity with polarity inversion at the

mastoids when using nose reference (Näätänen et al., 2001, 2005). Numerous studies have investigated MMN in elderly listeners, and many of them have found that its amplitude is attenuated and its peak latency is prolonged with aging (Alain and Woods, 1999; Cooper et al., 2006; Näätänen et al., 2011; Rimmele et al., 2012b; Cheng et al., 2013; Bartha-Doering et al., 2015; Getzmann and Näätänen, 2015).

To the best of our knowledge, no study has yet investigated whether MMN elicited by auditory regularity violations in elderly listeners shows a systematic relation with their ability to use regularities for stream segregation. We used the same spectrotemporal pattern as Rimmele et al. (2012a) to measure both auditory processes in the same listeners. We expected a significant correlation between MMN amplitude (as a proxy of auditory regularity extraction) and behavioral benefit from regular vs. random background sounds (as a proxy of regularity-based stream segregation). Finding such a correlation would strengthen the notion that extracting predictability and using predictability for decomposing acoustic mixtures are closely related processes, and would inform predictive-coding accounts of auditory perception.

MATERIALS AND METHODS

Participants

30 volunteers aged 60–75 years participated in the study (17 female, 13 male; 29 right-handed, 1 left-handed; mean age 67.8 years, SD 4.1 years). All participants' behavioral data were analyzed. Due to substantial artifacts in the EEG, two participants' data were excluded from ERP data analysis (both participants were female; mean age of the remaining sample: 68.1 years, SD 4.1 years). The study was approved by the Ethics Committee of the University of Oldenburg. According to the Declaration of Helsinki, each participant gave written informed consent prior to the beginning of the experiment after all procedures had been explained. Participants received a modest financial compensation (8 €/h) for their participation.

Experimental Stimuli and Apparatus

Sounds were created with Matlab (R2012b) and the stimulus delivery was controlled using the Psychophysics Toolbox extension for Matlab (Psychtoolbox 3.0.10). Instructions, visual cues during the training phase and the movie were presented on a wall-mounted TFT monitor. A Soundblaster X-Fi Audio interface was used to generate the audio signals. It was connected to a Tucker-Davis attenuator in bypass mode, which in turn was connected to a Denon PMA 510AE amplifier. Sounds were delivered via a pair of Cambridge Audio S30 speakers, positioned approximately 1.5 m away from the participant on both sides of the TFT monitor in the experimental room. Participants sat comfortably inside an electrically and acoustically shielded chamber while performing the experimental tasks.

Stream Segregation Part (Active Task)

Following Rimmele et al. (2012a), the behavioral task was set up such that two auditory streams were interleaved and that listeners had to perform a task (intensity deviant detection) in one of them (the "A" stream), while the other one (the "B" stream) interfered with the task. This interference was caused by random intensity variation in the "B" stream, which obscured the intensity regularity in the "A" stream and thus impeded deviance detection as long as tones from the "A" and "B" stream were perceptually integrated. Accurate task performance thus required perceptual segregation of streams A and B; in turn, task performance gives an indirect measure of stream segregation (see Micheyl and Oxenham, 2010; Andreou et al., 2011; Rimmele et al., 2012a; for the same measurement logic). Specifically, the stimulus set consisted of short sinusoidal tones with a duration of 60 ms, including 5 ms half-raised cosine on- and offset ramps. The stimuli had three different frequencies: 370 Hz ("low"), 440 Hz ("mid"), and 554 Hz ("high"), presented in rapid succession such that they can be interpreted as concurring streams "A" (high tones) and "B" (low and mid tones, see **Figure 1**). The task-relevant stream A was presented with a level of 60 dB(C-weighted) for standards, while the level of rare intensity deviants (10% of the stimuli in stream A) was increased by 10 dB. Deviants were randomly placed with the restriction of 1,500 ms minimum distance between any two deviants. The stimulus onset of the tones in stream A was pseudo-randomized and therefore unpredictable. The stimuli in stream A were presented with 80% occurrence probability uniformly distributed between any two tones of stream B, always leaving at least 15 ms silence between all tones to avoid simultaneous presentation. The task-irrelevant stream B consisted of mid and low tones, whose spectrotemporal predictability varied with the experimental condition. Level of tones in stream B varied randomly in both conditions (55–75 dB(C) in 1 dB steps). This value range was chosen to interfere with the deviant detection task as soon as stream segregation would fail. In the predictable condition, stream B followed an isochronous low-low-mid order with a constant SOA of 283 ms. In the random condition, stimuli in stream B were not presented in a spectrotemporal pattern; instead, the SOA was randomly chosen from three discrete values (160, 270, or 420 ms), and tone frequencies were randomly chosen from the different frequency values (370 or 440 Hz). Mean SOA was equal to the predictable condition, and the proportion of different frequency values was also kept identical to the predictable condition (i.e., twice as many low tones as mid tones).

In both conditions, participants were instructed to indicate intensity deviants (targets) in stream A with a mouse click. To control for laterality effects, half of the participants answered with the index finger of the right hand, the other half answered with the index finger of the left hand. The total number of deviant tones per condition (predictable or random) was 255, distributed to three blocks per condition. Each block had a duration of approximately 5 min. In the six blocks, the two conditions were presented in an alternating scheme, with the starting condition counterbalanced across participants.

Regularity Extraction Part (Passive-Listening Task)

In the regularity extraction part, only stream B (low and mid tones) of the predictable condition from the stream segregation part was presented. Instead of the standard low-low-mid triplet,

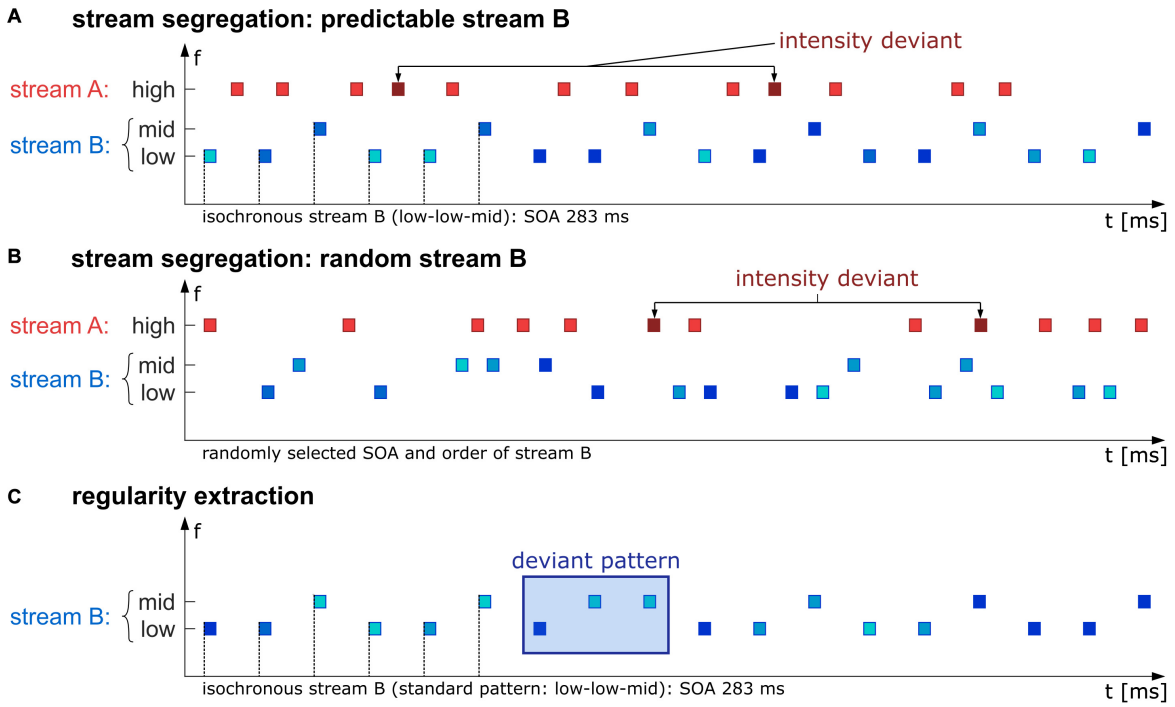

FIGURE 1 | Schematic illustration of the stimulus paradigm. In the first experimental part, participants were instructed to detect intensity deviants (probability in sequence 10%, deviants are 10 dB higher in level than standards) in a high-frequency stream A (red rectangles). The task-irrelevant stream B (blue rectangles) was presented in either an isochronous (SOA 283 ms) and therefore predictable low-low-mid pattern **(A)** or random in the chosen SOA (160, 270, or 420 ms) and frequency (either low or mid, **B**). The second experimental part was a passive listening condition in which just the B stream was presented (isochronous, SOA 283 ms) containing standard low-low-mid triplets which were rarely interrupted by a deviant low-mid-mid triplet with probability of 17% **(C)**. SPL levels in stream B across all conditions **(A–C)** varied between 55 and 75 dB illustrated by different blue hues.

a rule-breaking low-mid-mid triplet was interspersed with 17% probability. These deviant triplets were expected to elicit an MMN. During the passive-listening part, participants watched an emotionally neutral excerpt of a muted documentary. The measurement lasted 15 min, without breaks, including 180 deviant low-mid-mid triplets.

Procedure

Before the main experiment started, participants completed a four-level training procedure with increasing difficulty. In level 1, only the task-relevant stream A was presented, and visual support was given (a white square indicating the occurrence of a deviant tone). In level 2, stream A was presented alone without visual aid. In level 3, both streams (A and B) were presented with visual support for the deviant tone in stream A. In level 4, both streams were presented without visual aid; the procedure was thus identical to the experimental blocks. The training blocks lasted 1 min each and could be repeated if necessary (level 4 was always repeated at least once). Training was finished when performance reached a stable level and the participant had notably understood the task. After EEG preparation, one additional training block (level 4) was presented to refresh the knowledge of the task.

The main experiment consisted of two parts with EEG recordings throughout. First, participants completed the behavioral experiment (stream segregation part). Second, they were presented with the stimuli of the regularity extraction part while watching the silent documentary. After removing the EEG cap, the pure-tone audiogram (*via* Siemens Unity II audiometer and Sennheiser HAD-200 headphones) was measured at octave frequencies between 125 Hz and 8 kHz for both ears. To measure speech-in-noise comprehension, the Oldenburg Sentence Test (OLSA,[1] Wagener et al., 1999b) was administered, using the adaptive procedure at a noise level of 65 dB SPL (presented with calibrated Siemens CD 310 F free field speakers). In addition, participants filled questionnaires on demographic variables, and they completed the Mehrfachwahl-Wortschatz-Intelligenztest (MWT-B, Lehrl, 1977) as a short screening for verbal intelligence.

The whole experimental session lasted between 2.5 and 3.5 h, including all tests and tasks, electrode application and removal as well as breaks for the participants.

Electroencephalogram Recording

EEG data were continuously recorded using a BrainAmp amplifier system (BrainProducts, Gilching, Germany) with passive Ag/AgCl electrodes from 96 scalp positions using an infracerebral electrode cap with an equidistant electrode layout (Easycap, Herrsching, Germany). The horizontal

[1]https://www.hoertech.de/en/devices/olsa.html

electrooculogram (EOG) was measured with electrodes placed at the outer canthi of the left and right eye. The vertical EOG was obtained from separate electrodes placed below the left and right eye and from two electrodes above the eyes that were inserted in the electrode cap. The reference electrode was placed at the tip of the nose. EEG and EOG signals were amplified and recorded with a sampling rate of 500 Hz, applying an analog filter with 250 Hz low pass and 0.0159 Hz high pass (time constant 10 s).

Data Analysis

Hearing Tests

To calculate an aggregate measure for the peripheral hearing status, the average of the measured thresholds in the audiogram from 0.125 to 8 kHz across both ears was calculated (average hearing loss, AHL). To measure speech comprehension, the OLSA result yields the signal-to-noise ratio at which 50% of the speech material is still understood (50% speech recognition threshold in dB SNR). Pearson correlation coefficients were calculated for correlations between age and AHL (**Figure 2A**), age and OLSA (**Figure 2B**), as well as AHL and OLSA (**Figure 2C**).

Behavioral Data

During the stream segregation part, participants' responses and response times were recorded. Using signal detection theory, the sensitivity index d' was calculated separately for the two conditions (predictable, random). The d' calculation was adapted to account for the rapid stimulus presentation (Bendixen and Andersen, 2013). Specifically, if two consecutive button presses occurred within less than 50 ms from one another, the second one was marked as an accidental key press, and only the first one was counted for the analysis. All responses that occurred within 0.1–1.2 s after a target (intensity deviant onset) were counted as hits. Note that response windows between two targets never overlapped due to the minimal distance between two deviant stimuli of 1.5 s. All remaining button presses (i.e., those that were not counted as hits or accidental presses) were classified as false alarms. The proportion of hits was calculated by dividing the number of hits by the number of targets. The proportion of false alarms was adapted to the rapid stimulus presentation in the following way (Bendixen and Andersen, 2013): Conceptually, the experimental block duration was separated into response windows of 1.1 s duration (the defined response window for targets), and the number of false alarms was divided by the number of such windows in which false alarms could occur (i.e., without response windows for targets; for detailed methods see Bendixen and Andersen, 2013). Afterward the sensitivity index was calculated [d' = z(pHits)—z(pFA)] with z transformation by the inverse of the normal cumulative distribution function. To solve the problem that 100 or 0% hits or false alarms would result in plus or minus infinity, all proportion values were transformed

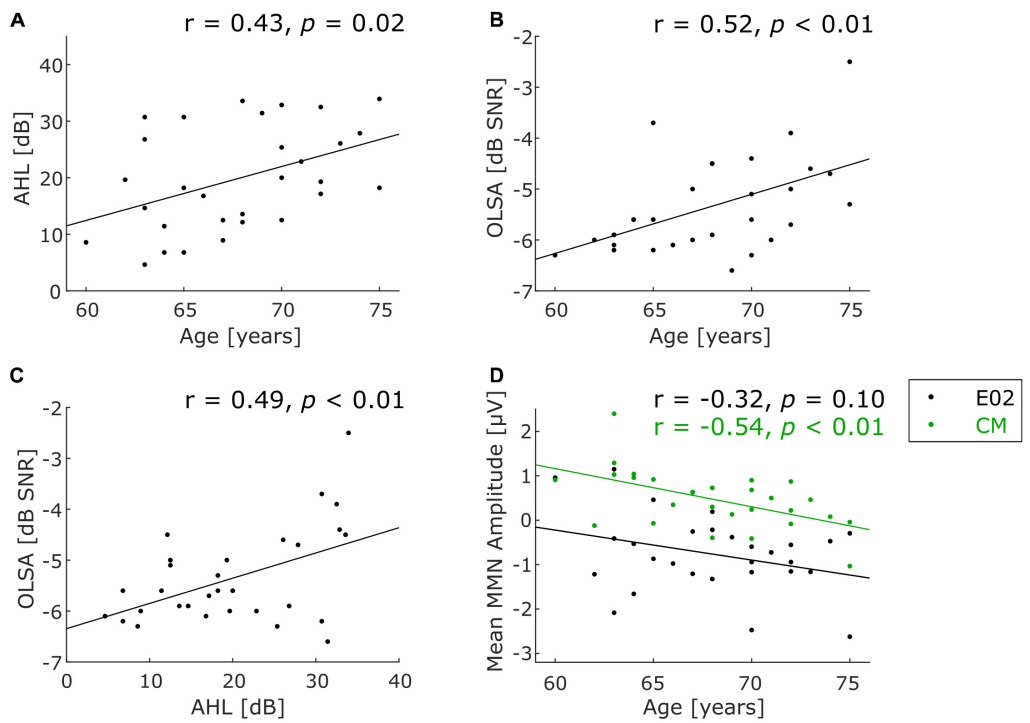

FIGURE 2 | Scatterplots for characterizing the participant sample. **(A)** Correlation of age and peripheral hearing status, **(B)** correlation of age and speech-in-noise comprehension, **(C)** correlation of the hearing tests with one another, **(D)** correlation of age and deviance detection measured by MMN at frontocentral electrode position (E02, black dots) and common mastoids (CM, green dots). Note that only 28 participants were included for the latter correlation (see text for details). Significantly positive correlations indicate that higher age is associated with higher average hearing loss (**A**, $p = 0.02$) and with worse speech-in-noise comprehension (**B**, $p < 0.01$). Moreover, higher average hearing loss is associated with worse speech-in-noise comprehension (**C**, $p < 0.01$). A significant negative correlation between MMN amplitude and age only for CM shows less positive amplitudes with increasing age (**D**, green line, $p < 0.01$).

by adding 0.5 to the individual hit and false alarm numbers and dividing the resulting score by the number of target or false alarm intervals adding one interval (Hautus, 1995). Due to this transformation and the finite number of targets and non-target intervals, a maximum d' sensitivity score of 6.01 would be achieved with perfect performance in each condition.

Sensitivity indices d' were statistically analyzed by two-tailed *t*-tests against zero separately for each conditions (predictable, random, see **Figure 3A**). They were compared between the two conditions with a paired-sample two-tailed *t*-test. To quantify a possible advantage (i.e., higher d' score) in the predictable relative to the random condition, the benefit Δd' was calculated, subtracting d' of the random condition from d' of the predictable condition. To analyze correlations between benefit and possible contributing factors like age, regularity extraction ability (measured by MMN), peripheral hearing status (AHL), and speech-in-noise comprehension (OLSA), Pearson correlation coefficients were calculated.

Reaction times were calculated separately for each condition in the stream segregation part (**Figure 3B**) and compared against each other with a paired-sample two-tailed *t*-test.

Electroencephalogram Pre-processing

Data analysis was carried out with Matlab R2020b (The MathWorks Inc., Natick, United States) and the toolbox EEGLAB (Delorme and Makeig, 2004) version 14.1.1b. EEG data were decomposed into independent components (independent component analysis, ICA) with the extended Infomax algorithm (Bell and Sejnowski, 1995). Prior to and only for the purpose of ICA, data were high-pass filtered with a Kaiser-windowed sinc finite impulse response (FIR) filter (cutoff frequency: 1 Hz, filter order: 9056, Kaiser β: 5.65326, transition bandwidth: 0.2 Hz, maximal passband ripple: −60 dB), and artificial consecutive epochs of 1 s length containing non-stereotypical artifacts (as identified by eeglab's rejkurt and jointprob functions with thresholds of 3 STD) were rejected. The independent components were saved in an untreated dataset (i.e., without the 1-Hz filter and the epoch rejection), and artifact-related component activity comprising eye movements, eye blinks, cardiac signals, muscle noise, and line noise were identified according to independent judgments by two of the authors (CN, AB). Subsequently, EEG data were filtered with a 0.1–30 Hz bandpass FIR filter (Kaiser-windowed, filter order: 9056, Kaiser β: 5.65326,

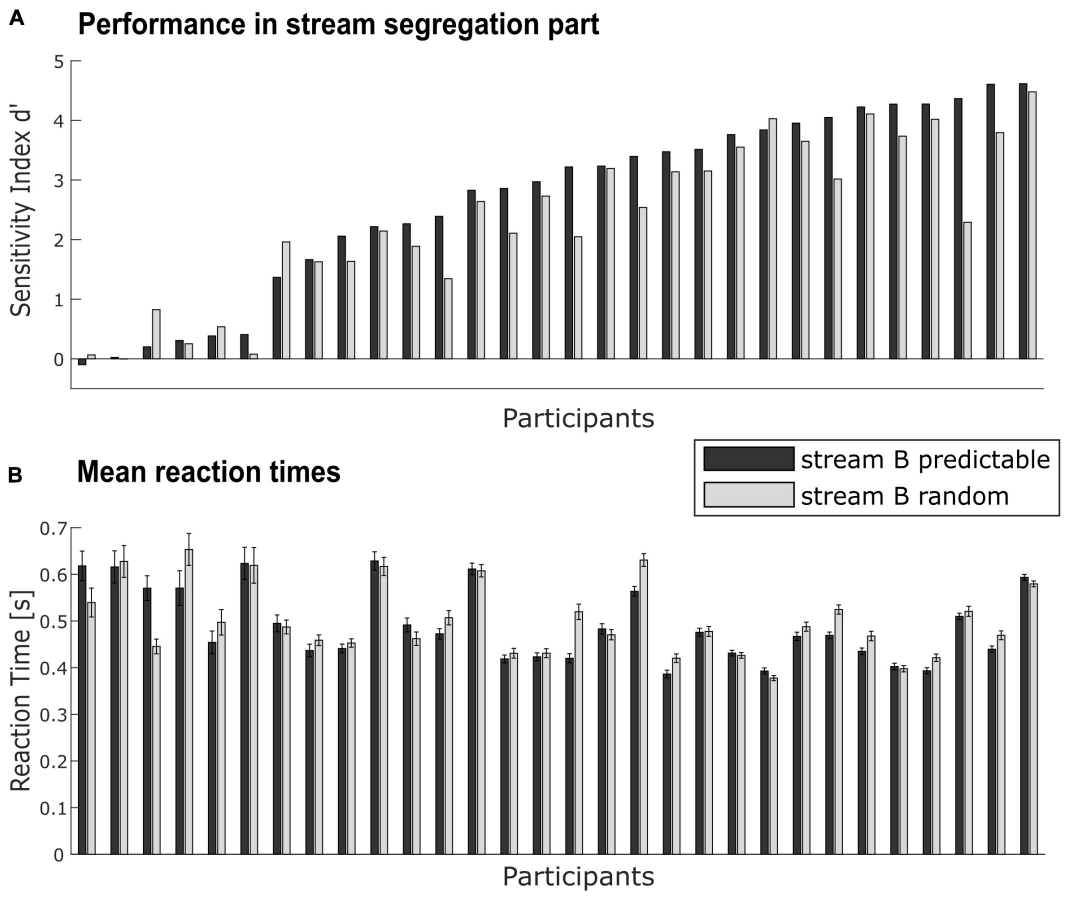

FIGURE 3 | Individual performance in the target detection task. **(A)** Performance for each participant (*N* = 30) as measured by sensitivity d' for predictable (black bars) and random conditions (gray bars). **(B)** Mean reaction times to detected targets in the task-relevant stream for each participant in both conditions (notation as in **A**). Error bars indicate the standard error in each condition within the participant. Data in both panels is sorted by performance in the predictable condition.

transition bandwidth 0.2 Hz, passband ripple: −60 dB). In some participants, few channels (maximum 3) with high amounts of residual artifact were replaced by using spherical interpolation. Epochs of 950 ms duration, including a 100 ms pre-stimulus interval used for baseline correction, were extracted from −100 to 850 ms relative to stimulus onset of the second stimulus in the low-low-mid standard triplet or the second tone in the low-mid-mid deviant triplet. With 850 ms post-stimulus, the epochs comprised exactly three tones. Epochs with amplitude changes exceeding 100 μV on any channel were rejected from further analysis. This left two participants with less than 70% artifact-free epochs; the corresponding datasets were excluded from further ERP analysis (see above). The remaining datasets showed an average data loss of 7.0% in the passive listening condition, with 621–878 remaining epochs per participant (Mean = 817, *SD* = 59) for standard triplets, and 129–180 remaining epochs (Mean = 167, *SD* = 13) for deviant triplets.

Event-Related Brain Potentials

Data from the remaining 28 participants were used to form grand-average ERPs per stimulus type (standard or deviant triplet) in the regularity extraction part of the experiment. Difference waves were calculated by subtracting the average ERP for each participant elicited by standard stimuli from that elicited by deviant stimuli. The difference wave of the grand-average ERP was examined at the frontocentral electrode E02, which is located on the midline between Fz and FCz (**Figure 4A**), and at the average of the mastoids (common mastoids, CM, **Figure 4B**). These are typical locations to quantify the auditory MMN component (Näätänen et al., 2007). The difference wave was tested for statistically significant deviations from zero by means of a sample-wise running *t*-test throughout the whole epoch window (i.e., from 0 to 850 ms), correcting for multiple comparisons via the false discovery rate (FDR, Benjamini and Hochberg, 1995). After confirming a significant frontocentral negativity with this procedure, the negativity was further characterized by using the average voltage in a latency range from 428 to 496 ms after the onset of the second tone in the triplet. This latency range was chosen to start with the first sample of the longest number of consecutively significant samples at E02 in the FDR-thresholded running *t*-test (428 ms), to cover the frontocentral peak in the grand-average difference

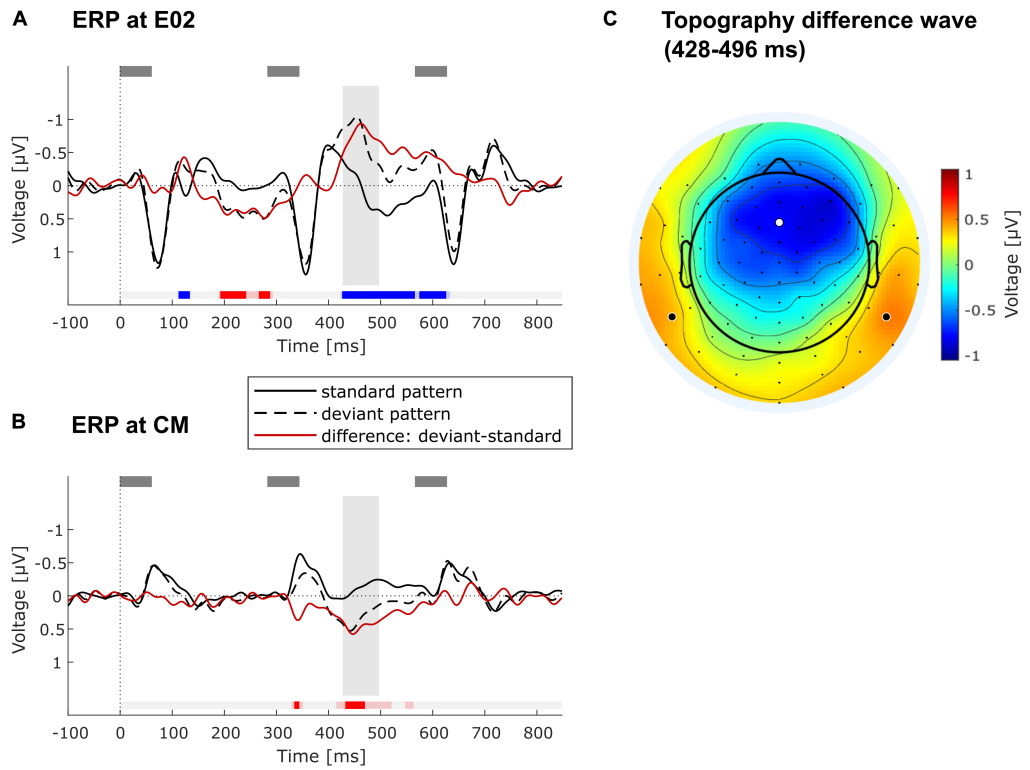

FIGURE 4 | ERP results. **(A)** Grand-average ERPs at frontocentral electrode position E02 across all included participants (*N* = 28) elicited by standard (solid black line) and deviant triplets (dashed black line) as well as their difference wave (red line). Gray rectangles above denote the tones. Timepoint 0 refers to the onset of the second tone in low-low-mid (standard) or low-mid-mid triplet (deviant). Blue/red markings under the ERPs indicate significant negative/positive deviation of the difference wave from zero as determined in running *t*-test with FDR-correction of the alpha level. Faint blue/red markings show significant negative/positive deviation with alpha level $p < 0.05$ (without correction). The gray vertical rectangle highlights the chosen time window (428–496 ms) around the peak of the negativity in the difference wave. **(B)** Grand-average ERPs at common mastoids (CM) across all included participants (*N* = 28). All markings, rectangles and lines have the same meaning as in **(A)**. **(C)** Topography of the difference wave in the chosen time window (428–496 ms), showing a frontocentral negativity with polarity inversion at the mastoids. The white dot indicates the location of E02 used for the ERP plot in **(A)**. Bold black dots show channel locations of left and right mastoid (both were averaged for ERP plot in **B**).

wave (462 ms), and to extend symmetrically to the other side of the peak (496 ms). It should be noted that peak-picking procedures are being criticized for their circularity ("double dipping") (Kriegeskorte et al., 2009; Luck and Gaspelin, 2017). In the current case, we chose the latency range (428–496 ms) *after* having determined that a significant negativity was elicited for every data sample in that range, and we used it for individual MMN amplitude quantification and for studying the scalp topography (**Figure 4C**).

RESULTS

Hearing Status and Verbal Intelligence

Average hearing loss (AHL) values across all frequencies ranged from 4.64 to 33.93 dB (Mean = 19.88 dB, *SD* = 9.14 dB), indicating wide variance from participants with almost normal thresholds to participants with considerable peripheral hearing loss. A significant correlation between AHL and age was observed ($r = 0.43$, $p = 0.02$, $N = 30$; see **Figure 2A**), indicating that peripheral hearing ability decreased with increasing age within our sample spanning 15 years of age. To exclude a confounding effect of hearing status on task performance, AHL in the frequency range in which the experimental stimuli were presented (370–554 Hz) was specifically examined. As a proxy, AHL values for 250 and 500 Hz were averaged, yielding a mean AHL of 5.42 dB (*SD* = 6.83 dB, range −7.5 to 20 dB). This indicates relatively preserved hearing at the frequencies of the auditory stimuli.

OLSA results ranged from −6.6 to −2.5 dB SNR (Mean = −5.36 dB SNR, *SD* = 0.93 dB SNR). This suggests a mild to moderate impairment in understanding speech in noise relative to the expected average threshold of young normal-hearing subjects at −7.1 dB SNR (Wagener et al., 1999a). Note that numerically lower—more negative—values indicate better performance. Speech-in-noise thresholds were significantly worse (i.e., less negative) with increasing age ($r = 0.52$, $p < 0.01$, $N = 30$; **Figure 2B**). Moreover, AHL correlated significantly with speech-in-noise comprehension ($r = 0.49$, $p < 0.01$, $N = 30$; **Figure 2C**).

All participants scored at or well above the population average on the verbal intelligence test MWT-B (verbal IQ range 97–145, mean IQ: 127), which rules out occurrences of major cognitive decline in the sample.

Behavioral Data: Performance and Predictability-Based Performance Benefit

Performance as evaluated by the sensitivity index d' scores ranged from −0.10 to 4.62 in the predictable condition (Mean = 2.69, *SD* = 1.52) and from 0 to 4.48 in the random condition (Mean = 2.35, *SD* = 1.33). The variation across participants was large (see **Figure 3A**), with some participants performing very well (note that performance without misses and false alarms would lead to a d' maximum of 6.01) and other participants with d' near zero failing to handle the target detection task above chance level. On average, performance in both conditions was significantly above chance [predictable condition: $t(29) = 9.69$, $p < 0.001$; random condition: $t(29) = 9.66$, $p < 0.001$].

Performance in the predictable condition was significantly better than in the random condition, $t(29) = 3.39$, $p < 0.01$. This implies that at group level, participants can benefit from the spectrotemporal regularity in the task-irrelevant background for performing the foreground task. At single-subject level, not all participants showed the same amount of benefit (or a benefit at all): Δd' values ranged from −0.62 to 2.08 (Mean = 0.34, *SD* = 0.54).

Mean reaction times (see **Figure 3B**) to detected targets in the task-relevant stream did not differ between conditions [$t(29) = -1.25$, $p = 0.22$; predictable condition: Mean = 0.49 s, *SD* = 0.08 s; random condition: Mean = 0.50 s, *SD* = 0.08 s].

Event-Related Brain Potential Data: Deviance Detection

FDR-corrected running *t*-tests of the difference wave (deviant minus standard) at the frontocentral electrode position E02 show significant negative and positive deflections in several time ranges, of which the longest one was taken for further statistical analysis (see **Figure 4A**). It consists in a pronounced negativity in a late time range, starting from 428 ms after the onset of pattern-violating second tone (low-*mid*-mid instead of low-low-mid). The topography of this late component (measured from 428 to 496 ms) shows a frontocentral negativity with inversed polarity at the mastoids (**Figures 4B,C**), which is consistent with a generator of this component in auditory cortex (Näätänen et al., 2007). The negativity was identified as an MMN (see below for discussion). Individual MMN amplitudes at the frontocentral electrode location E02 in the time window 428–496 ms varied widely from −2.62 to 1.15 μV (Mean = −0.77 μV, *SD* = 0.87 μV; mean amplitude was significantly negative at group level: $t(27) = -4.65$, $p < 0.001$). No significant correlation between frontocentral MMN amplitude and age was found ($r = -0.32$, $p = 0.10$, $N = 28$, black dots in **Figure 2D**). Individual MMN amplitudes at common mastoids (CM) varied in the chosen time window from −1.03 to 2.40 μV (Mean = 0.47 μV, *SD* = 0.66 μV; mean amplitude was significantly positive at group level: $t(27) = 3.78$, $p < 0.001$). MMN amplitudes at common mastoids were found to significantly correlate with age ($r = -0.54$, $p < 0.01$, $N = 28$, green dots in **Figure 2D**), with less positive MMN amplitudes associated with increasing age. The correlations between MMN amplitude and age at E02 and CM do not qualitatively change when controlling for AHL.

Correlations Between Predictability-Based Performance Benefit, Deviance Detection, and Auxiliary Data

Correlation analyses were carried out in search of underlying factors for the wide variation in the predictability-based

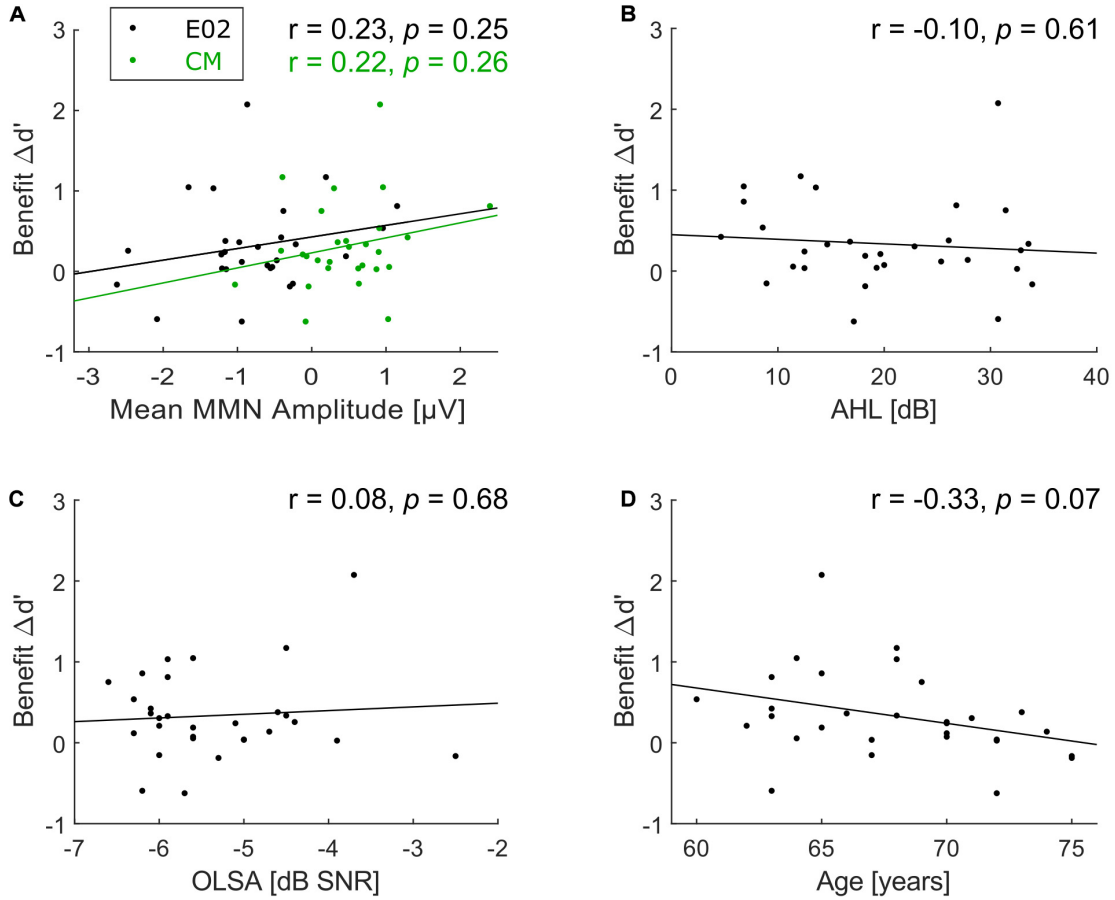

FIGURE 5 | Scatterplots of correlations with benefit. **(A)** Correlation between benefit Δd' and mean MMN amplitude at frontocentral electrode position E02 (black dots) and common mastoids (CM, green dots; note that just 28 participants were included for both correlations), **(B)** between benefit Δd' and average hearing loss (AHL), **(C)** between benefit Δd' and speech-in-noise comprehension, and **(D)** between benefit Δd' and age. No significant correlations with benefit Δd' were found.

performance benefit (Δd'). No significant correlation was observed between Δd' (as a measure of predictability-based performance benefit) and MMN amplitude (as a measure of deviance detection capacities) at E02, $r = 0.23$, $p = 0.25$, $N = 28$ (**Figure 5A**, black dots) and CM, $r = 0.22$, $p = 0.26$, $N = 28$ (**Figure 5A**, green dots). There was also no correlation between benefit and AHL ($r = -0.10$, $p = 0.61$, $N = 30$, **Figure 5B**) nor between benefit and speech-in-noise comprehension ($r = 0.08$, $p = 0.68$, $N = 30$, **Figure 5C**).

Examining the correlation of benefit and age suggests that there could be a trend toward lower benefit with increasing age ($r = -0.33$, $p = 0.07$; **Figure 5D**), though it does not meet the conventional alpha level of 5% (and much less a Bonferroni-corrected alpha level of 1% to compensate for the five correlation coefficients computed for benefit). This numerical association of benefit and age could reflect a spurious trend, or it could indicate a real effect measured with too low power given the relatively small sample size ($N = 30$). To separate between these two possibilities, we retrieved the data of all 16 participants (mean age = 65.9 years, $SD = 4.0$ years) from the elderly group of Experiment 2 by Rimmele et al. (2012a). The current experimental design is highly similar to Experiment 2 of Rimmele et al. (2012a), thus their data were re-analyzed in terms of Δd' benefit as in the current study by subtracting d' in the random condition from d' in their isochronous condition (corresponding to the predictable condition here). A joint correlation analysis based on data from both studies (**Figure 6**) revealed no significant correlation between age and benefit ($r = -0.14$, $p = 0.34$, $N = 46$), which suggests that the trend in the current experimental data was indeed spurious.

Further Control Analyses

Importantly, Rimmele et al. (2012a) had found no significant benefit for elderly participants in the isochronous condition (Mean d' = 2.55, $SD = 0.70$) relative to the random condition (Mean d' = 2.41, $SD = 0.74$). In order to identify reasons for the apparent discrepancy with the current result, a *post hoc* independent-samples *t*-test was performed to compare the Δd' results from Rimmele et al. (2012a) with the current data. Δd' was numerically higher in the current study (Mean = 0.34, $SD = 0.54$) than in the previous study (Mean = 0.13, $SD = 0.32$), but this difference was not statistically significant [$t(44) = 1.38$,

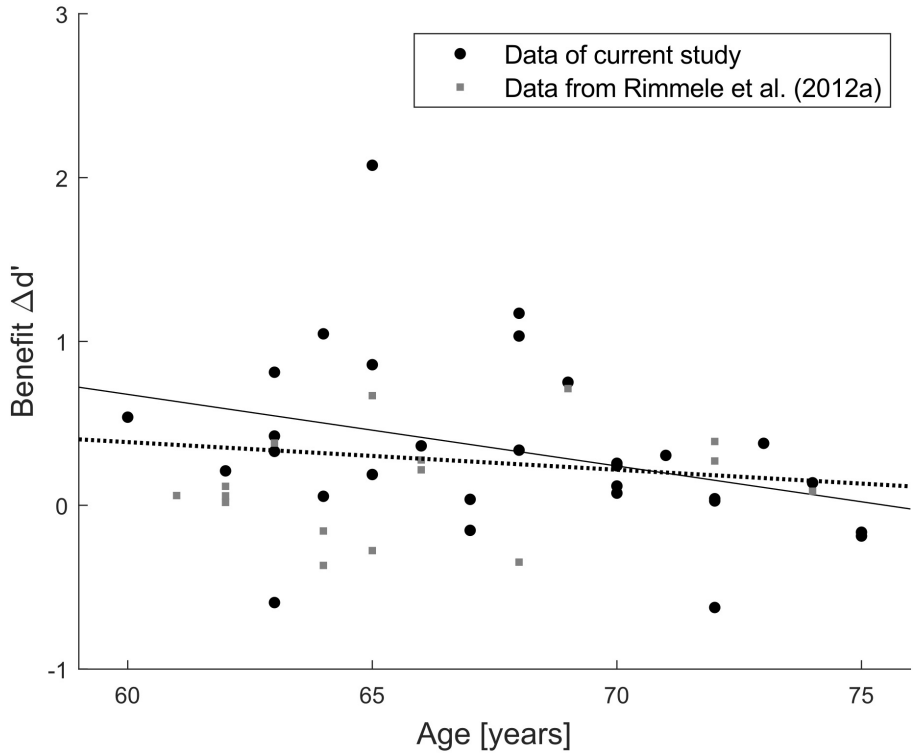

FIGURE 6 | *Post hoc* joint analysis of two independent participant samples. Scatterplot of the relation between age and benefit Δd' for performance in the predictable/isochronous minus random condition. Each dot refers to one individual data point (black dots: current study, gray squares: Exp. 2 in Rimmele et al., 2012a). Solid line indicates correlation in the current study ($r = -0.33$, $p = 0.07$, $N = 30$), dotted line indicates correlation in the combined data ($r = -0.14$, $p = 0.34$, $N = 46$).

$p = 0.17$]. Again, a joint analysis of both datasets showed that Δd' is significantly different from zero across both groups of elderly participants [Mean = 0.27, $SD = 0.48$, $t(45) = 3.71$, $p < 0.001$].

The lack of significant correlation of behavioral benefit (Δd') with any other measured variable (**Figure 5**) led us to examine the robustness of Δd' measurement, to rule out that measurement error underlies the absence of correlation. We assessed the robustness of the measurement by calculating Δd' separately for each consecutive pair of blocks (i.e., subtracting d' in the first random block from d' in the first predictable block, etc.)[2] and determining Cronbach's alpha of the three Δd' estimates. Across our 30 listeners, Cronbach's alpha was modest (0.31). Examination of the individual data showed that one single listener exhibited excessive variation between blocks[3] whereas all others' data were much more consistent. Excluding this one listener's data increased Cronbach's alpha to a moderate level of 0.58. Given that Δd' is a difference score, 0.58 is an acceptable value, and it is considerably higher than the observed correlation of Δd' with any other measured variable.

[2]Note that this assignment is to some degree arbitrary since the blocks were not administered in a paired manner.

[3]We verified in a *post hoc* analysis that this listener's data (with its inconsistent estimates of the Δd' effect) did not affect the other analyses in any way. None of the correlations reported in the manuscript changed qualitatively when excluding this listener's data.

DISCUSSION

The current study was designed to measure elderly listeners' abilities to extract an auditory spectrotemporal regularity (as evidenced by MMN responses to regularity violations) and to use the same regularity for stream segregation (as evidenced by enhanced listening performance in a foreground stream when the regularity is embedded in the to-be-ignored background). We expected to find a correlation between MMN amplitude (regularity extraction) and behavioral benefit (regularity-based stream segregation). In contrast to our hypothesis, we did not observe such a correlation, although both abilities were clearly present at group level and inter-individual variability was substantial in both of them. The two abilities and the absence of their association are discussed in turn below.

Pattern Regularity Extraction in Elderly Listeners

To study whether elderly listeners can extract spectrotemporal patterns, we used MMN as an indirect measure of regularity extraction (Schröger, 2005). The "low-mid-mid" deviations from the "low-low-mid" pattern indeed elicited a significant ERP component whose topography is consistent with the auditory MMN component (Näätänen et al., 2001, 2005). The time-range of the MMN component was relatively late, with its peak at

462 ms relative to the onset of the deviant event (second tone in the triplet). MMN usually occurs at about 100–250 ms after deviation onset (Näätänen et al., 2007; Garrido et al., 2009). One possible reason for the late MMN is that the three stimuli of the tone pattern are perceptually bound into an auditory object and that the comparison of the sensory input with the expected template (whose mismatch leads to MMN) takes place after the last tone of the triplet. Relative to this third tone, the observed peak latency is 179 ms, which is well in line with the usual MMN latency (Näätänen et al., 2007; Garrido et al., 2009). Alternatively, an embedded regularity may be encoded in different ways (Horváth et al., 2001), not only in the form of a global pattern regularity ("low-low-mid is continuously repeated") but also in the form of a local transitional regularity ("a mid-tone is always followed by a low tone"). This transitional regularity is not violated until the third tone of the triplet, which explains the occurrence of a late MMN as well. Other alternatives are that the late negativity reflects the typical prolongation of MMN latency in elderly listeners (Cooper et al., 2006; Näätänen et al., 2011; Getzmann and Näätänen, 2015), or that this negativity is not the typical MMN but the late discriminative negativity (LDN) following MMN, which has been described mainly for children (e.g., Cheour et al., 2001), but also for adults when abstract regularities are employed (Zachau et al., 2005; Bendixen et al., 2012). Altogether, we conclude that the negativity peaking at 462 ms reflects an automatic violation detection process, in which the deviant triplet violates the formed prediction about the sensory input and the predictive model needs to be updated (Winkler and Czigler, 1998).

One may object that comparing ERPs to standard (low-low-mid) and deviant triplets (low-mid-mid) is not ideal due to the physical difference in the second tone (low vs. mid tone). In fact, a significant early difference between standard and deviant ERP traces emerged in the latency range of the N1 component at about 120 ms after onset of the physically different tone (see **Figure 4A**). To differentiate whether this N1 enhancement for the deviant triplet was due to the physical difference or reflects an early sign of "true" deviance detection (Näätänen et al., 2005), it would have been more advantageous to swap the role of deviant and standard triplets half-way during the passive listening condition. Yet although this has been a standard recommendation in auditory MMN research for many years, recent work on the so-called "primacy bias" (Todd et al., 2011, 2013, 2014; Fitzgerald and Todd, 2018) has established that swapping standard and deviant comes with significant reductions in the overall size of the MMN component. This is because a "lasting first impression" of stimulus probabilities and significance has been formed, reducing the MMN elicited by the deviant that was first experienced as a standard (Todd et al., 2011, 2013, 2014; Fitzgerald and Todd, 2018). Such higher-order effects (signifying predictive coding at different timescales) would reduce overall MMN amplitude and might introduce another source of inter-individual variability. This might have interacted with the aim to quantify pattern MMN on an individual basis in the current study. Importantly, even if the early (120 ms) negativity elicited by deviant relative to standard triplets was confounded by physical difference, it is highly unlikely that this translated to the negativity at 462 ms analyzed here, because the third tone in standard and deviant triplets was physically identical and the early modulation was much smaller than the late MMN.

To sum up, the ERP data from passive listening suggest that—at group level—elderly listeners extracted the pattern regularity and detected deviations from it. Finding this ability at group level is consistent with prior work on pattern regularity extraction in elderly listeners (Alain and Woods, 1999; Näätänen et al., 2011; Rimmele et al., 2012b; Getzmann and Näätänen, 2015). The respective abilities of the individual listeners (as quantified by MMN amplitude) showed a high amount of variation, which was later used to address the question of a possible direct relation with the ability of regularity-based stream segregation.

Note that evidence in favor of pattern regularity extraction in elderly listeners does not imply that this ability is *fully* preserved in elderly listeners: this conclusion would require comparison with a young-listener control group. Such a control group was not included in the current study because our focus was on examining differences *within* a group of elderly listeners (60–75 years), not on drawing comparisons across wide age ranges (∼25 years vs. ∼65 years, as in many other studies). Previous studies comparing widely different age groups have consistently found smaller frontocentral MMN amplitudes in elderly as compared to young listeners (Alain and Woods, 1999; Näätänen et al., 2011; Rimmele et al., 2012b; Getzmann and Näätänen, 2015). The fact that we did not find a correlation between frontocentral MMN amplitude and age in the current study (**Figure 2D**, black dots) does not contradict those prior observations, as one would expect the chronological age to play a more minor role in a sample spanning 15 years (60–75 years) than in samples spanning 40 years of age and more.

Indeed, the correlation between polarity-reversed MMN amplitude at the common mastoids and age was significant in our sample (**Figure 2D**, green dots). This might indicate that elderly listeners show impairments in the supratemporal but not frontal MMN generators for deviations of our pattern regularity (Giard et al., 1990; Opitz et al., 2002; Näätänen et al., 2007), or it may reflect a shift in the orientation of the superior temporal gyrus dipole (Deouell, 2007). Since our frontocentral MMN amplitude numerically shows an almost parallel trajectory with age as the mastoid MMN amplitude (**Figure 2D**: both tend to become less positive/more negative with age), the latter explanation seems more likely (see Baldeweg et al., 1999, for a similar observation where frontal MMN increase is paralleled by mastoid MMN decrease, though not in the context of aging). More specifically, it seems plausible that a change in orientation of the superior temporal gyrus dipole reduces MMN amplitudes at mastoid electrodes and increases MMN amplitudes at frontocentral electrodes at the same time. In contrast, a change in strength of the superior temporal gyrus dipole would reduce MMN amplitude at both electrode sites, and one would have to assume a parallel increase in strength of the frontal MMN source to account for the observation that MMN decreases with age at the mastoids while it tends to increase with age at frontocentral electrodes. While this would be a less parsimonious explanation, the current data should

not be over-interpreted regarding this issue, especially since the association of age and frontocentral MMN amplitude was not significant by conventional criteria. It is likewise difficult to relate this observation to other MMN studies investigating aging effects by comparing young and elderly listeners, because many studies report frontocentral MMN amplitudes that are directly referenced to the mastoid electrodes, or do not report mastoid data at all. Further studies examining possible dissociations between temporal and frontal MMN generators with age are required, especially in the context of pattern regularities.

Regularity-Based Stream Segregation in Elderly Listeners

In the active-listening part of the current study, elderly listeners showed better foreground task performance when a task-irrelevant background stream carried a spectrotemporal regularity than when it did not. This is in line with the predictive-coding account of auditory stream segregation (Winkler et al., 2009, 2012). It is consistent with prior work on regularity-based stream segregation in young listeners (Andreou et al., 2011; Rimmele et al., 2012a), and informative with respect to previously conflicting results on whether this translates to elderly listeners: While de Kerangal et al. (2021) showed that the ability to track sources in an acoustic scene based on their regularities is largely preserved in elderly listeners, Rimmele et al. (2012a) had found an impairment of elderly listeners in regularity-based stream segregation. Since the current study closely followed the task and design of Rimmele et al. (2012a), we can now exclude task differences to underlie the different findings. The discrepancy of the current results with those of Rimmele et al. (2012a) is most likely due to issues of statistical power, with only 16 elderly listeners taking part in the previous study, compared to 30 elderly listeners in the current one. Alternatively, a procedural difference lies in the more comprehensive task training in the current study, from which the elderly may have benefitted. *Post hoc* analyses showed that the size of the behavioral benefit from regularity-based stream segregation in the two studies was not significantly different (though numerically higher in the current study), and that the behavioral benefit was significant when jointly analyzing both datasets. This underlines the necessity of replication studies with sufficient statistical power (Maxwell et al., 2015).

The fact that regularity-based stream segregation (i.e., behavioral benefit) does not correlate with peripheral hearing status (**Figure 5B**) nor with speech-in-noise comprehension (**Figure 5C**) is consistent with the findings from de Kerangal et al. (2021) who likewise found no such relations. This similar pattern of results in both studies is important on a theoretical level because it implies that the investigated regularity-based processing of complex acoustic scenes cannot trivially be explained by physical confounds in the stimulus setup (which might, e.g., put listeners with better peripheral hearing at an advantage). Instead, regularity-based processing of complex acoustic scenes appears to capture an independent ability, which is important to further investigate. The predictive-coding framework (Friston, 2005; Friston and Kiebel, 2009; Kanai et al., 2015; Denham and Winkler, 2017; Heilbron and Chait, 2018) provides an important theoretical basis for characterizing this ability, and in turn for developing a full understanding of auditory scene analysis and mitigating possible deficits thereof.

We conclude that elderly listeners *can* benefit from regularity-based stream segregation, but it is not known yet whether they can benefit *to the same extent* as young listeners. Answering the latter question would require taking measurements from a group of young listeners for comparison, which—as discussed for pattern regularity extraction above—was not in the focus of the current study. In view of the modified conclusion about the general ability of elderly listeners to perform regularity-based stream segregation, it seems warranted to verify the age group difference in this ability reported by Rimmele et al. (2012a) in an independent replication study. Similar to the ability for pattern regularity extraction, the ability for regularity-based stream segregation did not correlate with chronological age (**Figures 5D**, **6**). Again, this does not rule out the existence of an age effect when comparing groups with a wider age range, as one would expect chronological age to dominate the results more when spanning a wider range. In any case, the observed strong inter-individual differences in the capacity to benefit from background regularity (both in the current and in the previous study) warrant further examination.

Relations Between Pattern Regularity Extraction and Regularity-Based Stream Segregation

The key hypothesis of the current study was that listeners whose auditory system detects deviants more readily (as evidenced by MMN during passive listening) can also use predictability more easily for segregating sound sources from one another (as evidenced by regularity benefits in the active-listening task). This was expected to show up as a correlation between MMN amplitude and behavioral benefit. However, no such correlation was observed (**Figure 5A**). Since the inter-individual variation in both measures was high (see **Figure 5A**), the failure to find a correlation cannot be explained by floor or ceiling effects, or lack of variance. We must consider the possibility that part of the variation in the single-participant values reflects measurement error rather than true differences in the underlying ability. However, regarding MMN amplitudes, excessive measurement error seems unlikely given the significant correlation of individual mastoid MMN with age. Regarding behavioral benefit, robustness of the measurement was quantified by a Cronbach's alpha of 0.58, which is considerably higher than the observed correlation of Δd' benefit with any other measured variable.

To put potential concerns about measurement error further into perspective, it is important to note that well-established findings on auditory aging were replicated in the current study, even within the narrow age range (spanning 15 years) relative to studies comparing participants across different age groups (young vs. elderly). Specifically, we found that higher chronological age was accompanied by a decline in peripheral hearing ability (**Figure 2A**), which is consistent with prior work (e.g., Gates and Mills, 2005; Glyde et al., 2013). Increasing

hearing thresholds challenge locating, detecting, discriminating, and comprehending sounds especially in complex acoustic environments, resulting in impaired speech comprehension (for a review see Pichora-Fuller and Souza, 2003; Martin and Jerger, 2005). In accordance with this, we confirmed that higher chronological age is accompanied by worse speech-in-noise comprehension (**Figure 2B**). The relation between peripheral hearing status and speech-in-noise comprehension, though significant, is far from being deterministic (**Figure 2C**). This underlines the partial independence of peripheral and central auditory processes (Plomp, 1978; Pichora-Fuller and Souza, 2003; Alain et al., 2006; Peelle and Wingfield, 2016). In any case, replication of these established findings in the current study rules out the possibility that severe measurement error masked inter-individual differences of relevant auditory abilities.

Other factors may help to understand the absence of a significant correlation between MMN amplitude and behavioral benefit. Before drawing premature conclusions on a putative dissociation between regularity extraction and regularity-based stream segregation, we should consider whether the two variables are valid indicators of the processes they are assumed to reflect. MMN is an indirect measure of regularity extraction (Schröger, 2005), though a dissociation between deviance detection and regularity extraction is unlikely under all current theoretical and modeling frameworks (Näätänen et al., 2007; Garrido et al., 2009; Fishman, 2014; Fitzgerald and Todd, 2020). A more imminent question is whether MMN *amplitude* gives a valid assessment of the strength or probability of deviance detection, or whether other processes may confound this measurement. Specifically, since we measured regularity extraction via MMN in a separate, passive-listening condition, MMN amplitude differences between participants may reflect different levels of attention to the sound stream while watching the silent documentary. Though attention effects on the MMN itself are small (Sussman, 2007), overlapping components such as the N2b (Novak et al., 1990) may confound the measurement and thereby artificially enhance the measured MMN amplitude. In fact, those participants who do not successfully disregard the irrelevant sound stream while focusing their attention on the video, might actually be those who also have trouble disregarding the task-irrelevant low-low-mid sound stream while focusing their attention on the task-relevant (A) stream. It may be the case that their negativity in the MMN latency range is counter-intuitively larger than those of many others because they fail to ignore the sound stream. This would be consistent with findings from cognitive aging in a wider sense, showing that the ability to inhibit task-irrelevant stimuli decreases with age across modalities and task types (e.g., Weeks and Hasher, 2018; Gaál et al., 2020). Interindividual differences in the ability to ignore task-irrelevant information ("resist interference") would be one explanation why no consistent relation between MMN amplitude and benefit was found at group level. Future studies should mitigate this concern by measuring regularity extraction and deviant detection ability while participants' auditory attention is more strongly controlled. It would also be advantageous to measure both abilities with the presence of the "A" sound stream.

Similarly, it could be questioned whether the behavioral benefit is a valid indicator of regularity-based stream segregation in every individual case. The underlying assumption is that more success in segregating the streams automatically translates into higher task performance. Yet this neglects the possibility that some participants may have trouble focusing their attention on the correct stream even when they succeed in segregating the streams (Gaeta et al., 2001; Healey et al., 2008; Horváth et al., 2009; Passow et al., 2012). Denham and Winkler (2017) summarize similarly conflicting results in their review article, stemming from the fact "that predictable sequences attract attention while also being easier to suppress." They go on to conclude that "the presence of both tendencies may allow the influence of predictability to be easily modulated according to intrinsic preferences, attentional set and task demands" (Denham and Winkler, 2017). This consideration addresses contradictory findings across different studies, but it is well conceivable that it also applies within one study: In the current case, intrinsic preferences of individual participants may have obscured a systematic relation at group level. Therefore, an independent measurement of participants' ability to focus on a given stream, and also to perform the task without the existence of a background stream, is needed to yield further insights into the involved processes. This would also tap more into related cognitive processes such as resistance toward interference, going beyond the very general cognitive screening in terms of verbal intelligence in the current study.

CONCLUSION

In conclusion, due to a lack of an association between MMN amplitude and behavioral benefit we cannot provide support for the theoretical notion that extracting predictability and using predictability for decomposing acoustic mixtures are closely related processes. However, our observations do not rule out the possibility that such a relation may exist. Further studies are needed to rule out alternative explanations and to characterize the involved processes in more detail. The fact that elderly participants are successful in auditory regularity extraction and regularity-based stream segregation at group level, and that substantial inter-individual variation can be captured in these abilities with the present paradigm, provides a promising basis for further explorations into the involved processes.

DATA AVAILABILITY STATEMENT

The raw data supporting the conclusions of this article will be made available by the authors, without undue reservation.

ETHICS STATEMENT

The studies involving human participants were reviewed and approved by the Ethics Committee of the University of Oldenburg. The participants provided their written informed consent to participate in this study.

AUTHOR CONTRIBUTIONS

AB, AF, and SD contributed to conception and design of the study. AF collected the data. CN and AF analyzed the data. AB and SD reviewed the data analysis. CN and AB wrote the first draft of the manuscript. All authors contributed to manuscript revision, read, and approved the submitted version.

FUNDING

This work was funded by the German Research Foundation (Deutsche Forschungsgemeinschaft, DFG, Cluster of Excellence 1077 "Hearing4all"). The publication of this article was funded by Chemnitz University of Technology.

REFERENCES

Alain, C., Dyson, B. J., and Snyder, J. S. (2006). "Aging and the perceptual organization of Sounds: A Change of Scene?" In *Handbook of Models for Human Aging*, (ed) C P Michael. Amsterdam: Elsevier. 759–769. doi: 10.1016/B978-012369391-4/50065-5

Alain, C., and Woods, D. L. (1999). Age-related changes in processing auditory stimuli during visual attention: evidence for deficits in inhibitory control and sensory memory. *Psychol. Aging* 14, 507–519. doi: 10.1037/0882-7974.14.3.507

Aman, L., Picken, S., Andreou, L. V., and Chait, M. (2021). Sensitivity to temporal structure facilitates perceptual analysis of complex auditory scenes. *Hear. Res.* 400:108111. doi: 10.1016/j.heares.2020.108111

Andreou, L. V., Kashino, M., and Chait, M. (2011). The role of temporal regularity in auditory segregation. *Hear. Res.* 280, 228–235. doi: 10.1016/j.heares.2011.06.001

Baldeweg, T., Williams, J. D., and Gruzelier, J. H. (1999). Differential changes in frontal and sub-temporal components of mismatch negativity. *Int. J. Psychophysiol.* 33, 143–148. doi: 10.1016/S0167-8760(99)00026-4

Bartha-Doering, L., Deuster, D., Giordano, V., Zehnhoff-Dinnesen, A., and Dobel, C. (2015). A systematic review of the mismatch negativity as an index for auditory sensory memory: From basic research to clinical and developmental perspectives. *Psychophysiology* 52, 1115–1130. doi: 10.1111/psyp.12459

Bell, A. J., and Sejnowski, T. J. (1995). An Information-maximization approach to blind separation and blind deconvolution. *Neural Comput.* 7, 1129–1159. doi: 10.1162/neco.1995.7.6.1129

Bendixen, A. (2014). Predictability effects in auditory scene analysis: a review. *Front. Neurosci.* 8:60. doi: 10.3389/fnins.2014.00060

Bendixen, A., and Andersen, S. K. (2013). Measuring target detection performance in paradigms with high event rates. *Clin. Neurophysiol.* 124, 928–940. doi: 10.1016/j.clinph.2012.11.012

Bendixen, A., Denham, S. L., Gyimesi, K., and Winkler, I. (2010). Regular patterns stabilize auditory streams. *J. Acoust. Soc. Am.* 128, 3658–3666. doi: 10.1121/1.3500695

Bendixen, A., Schröger, E., Ritter, W., and Winkler, I. (2012). Regularity extraction from non-adjacent sounds. *Front. Psychol.* 3:143. doi: 10.3389/fpsyg.2012.00143

Benjamini, Y., and Hochberg, Y. (1995). Controlling the false discovery rate: a practical and powerful approach to multiple testing. *J. Royal Stat. Soc. Ser. B* 57, 289–300. doi: 10.1111/j.2517-6161.1995.tb02031.x

Bregman, A. S. (1990). *Auditory Scene Analysis: The Perceptual Organization of Sound*. Cambridge, MA: MIT Press.

Cheng, C.-H., Hsu, W.-Y., and Lin, Y.-Y. (2013). Effects of physiological aging on mismatch negativity: A meta-analysis. *Int. J. Psychophysiol.* 90, 165–171. doi: 10.1016/j.ijpsycho.2013.06.026

Cheour, M., Korpilahti, P., Martynova, O., and Lang, A. H. (2001). Mismatch negativity and late discriminative negativity in investigating speech perception and learning in children and infants. *Audiol. Neuro-Otol.* 6, 2–11. doi: 10.1159/000046804

Cooper, R. J., Todd, J., McGill, K., and Michie, P. T. (2006). Auditory sensory memory and the aging brain: a mismatch negativity study. *Neurobiol. Aging* 27, 752–762. doi: 10.1016/j.neurobiolaging.2005.03.012

de Kerangal, M., Vickers, D., and Chait, M. (2021). The effect of healthy aging on change detection and sensitivity to predictable structure in crowded acoustic scenes. *Hear. Res.* 2021:108074. doi: 10.1016/j.heares.2020.108074

Delorme, A., and Makeig, S. (2004). EEGLAB: An open source toolbox for analysis of single-trial EEG dynamics including independent component analysis. *J. Neurosci. Methods* 134, 9–21. doi: 10.1016/j.jneumeth.2003.10.009

Denham, S. L., and Winkler, I. (2017). Predictive coding in auditory perception: challenges and unresolved questions. *Eur. J. Neurosci.* 51, 1151–1160. doi: 10.1111/ejn.13802

Deouell, L. Y. (2007). The frontal generator of the mismatch negativity revisited. *J. Psychophysiol.* 21, 188–203. doi: 10.1027/0269-8803.21.34.188

Fishman, Y. I. (2014). The mechanisms and meaning of the mismatch negativity. *Brain Topograp.* 27, 500–526. doi: 10.1007/s10548-013-0337-3

Fitzgerald, K., and Todd, J. (2018). Hierarchical timescales of statistical learning revealed by mismatch negativity to auditory pattern deviations. *Neuropsychologia* 120, 25–34. doi: 10.1016/j.neuropsychologia.2018.09.015

Fitzgerald, K., and Todd, J. (2020). Making sense of mismatch negativity. *Front. Psychiatry* 11:468. doi: 10.3389/fpsyt.2020.00468

Friston, K. (2005). A theory of cortical responses. *Philos. Trans. R. Soc. B Biol. Sci.* 360, 815–836. doi: 10.1098/rstb.2005.1622

Friston, K., and Kiebel, S. (2009). Predictive coding under the free-energy principle. *Philos. Trans. R. Soc. B Biol. Sci.* 364, 1211–1221. doi: 10.1098/rstb.2008.0300

Gaál, Z. A., Nagy, B., File, D., and Czigler, I. (2020). Older adults encode task-irrelevant stimuli, but can this side-effect be useful to them? *Front. Human Neurosci.* 14:569614. doi: 10.3389/fnhum.2020.569614

Gaeta, H., Friedman, D., Ritter, W., and Cheng, J. (2001). An event-related potential evaluation of involuntary attentional shifts in young and older adults. *Psychol. Aging* 16, 55–68. doi: 10.1037/0882-7974.16.1.55

Garrido, M. I., Kilner, J. M., Stephan, K. E., and Friston, K. (2009). The mismatch negativity: A review of underlying mechanisms. *Clin. Neurophysiol.* 120, 453–463. doi: 10.1016/j.clinph.2008.11.029

Gates, G. A., and Mills, J. H. (2005). Presbycusis. *Lancet* 366, 1111–1120. doi: 10.1016/S0140-6736(05)67423-5

Getzmann, S., and Näätänen, R. (2015). The mismatch negativity as a measure of auditory stream segregation in a simulated "cocktail-party" scenario: Effect of age. *Neurobiol. Aging* 36, 3029–3037. doi: 10.1016/j.neurobiolaging.2015.07.017

Giard, M. H., Perrin, F., Pernier, J., and Bouchet, P. (1990). Brain generators implicated in the processing of auditory stimulus deviance: a topographic event-related potential study. *Psychophysiology* 27, 627–640. doi: 10.1111/j.1469-8986.1990.tb03184.x

Glyde, H., Cameron, S., Dillon, H., Hickson, L., and Seeto, M. (2013). The effects of hearing impairment and aging on spatial processing. *Ear Hear.* 34, 15–28. doi: 10.1097/AUD.0b013e3182617f94

Hautus, M. J. (1995). Corrections for extreme proportions and their biasing effects on estimated values of d'. *Behav. Res. Methods Inst.Comp.* 27, 46–51. doi: 10.3758/BF03203619

Healey, K., Campbell, K., and Hasher, L. (2008). "Cognitive aging and increased distractibility: Costs and potential benefits," in *Progress in Brain Research*, eds W. S. Sossin, J. C. Lacaille, V. F. Castellucci, and S. Belleville (Amsterdam: Elsevier), 353–363. doi: 10.1016/S0079-6123(07)00022-2

Heilbron, M., and Chait, M. (2018). Great expectations: is there evidence for predictive coding in auditory cortex? *Neuroscience* 389, 54–73. doi: 10.1016/j.neuroscience.2017.07.061

Horváth, J., Czigler, I., Birkás, E., Winkler, I., and Gervai, J. (2009). Age-related differences in distraction and reorientation in an auditory task. *Neurobiol. Aging* 30, 1157–1172. doi: 10.1016/j.neurobiolaging.2007.10.003

Horváth, J., Czigler, I., Sussman, E. S., and Winkler, I. (2001). Simultaneously active pre-attentive representations of local and global rules for sound sequences in the human brain. *Cogn. Brain Res.* 12, 131–144. doi: 10.1016/S0926-6410(01)00038-6

Kanai, R., Komura, Y., Shipp, S., and Friston, K. (2015). Cerebral hierarchies: Predictive processing, precision and the pulvinar. *Philos. Trans. R. Soc. B Biol. Sci.* 370:20140169. doi: 10.1098/rstb.2014.0169

Kriegeskorte, N., Simmons, W. K., Bellgowan, P. S., and Baker, C. I. (2009). Circular analysis in systems neuroscience: The dangers of double dipping. *Nat. Neurosci.* 12, 535–540. doi: 10.1038/nn.2303

Lehrl, S. (1977). *Mehrfachwahl-Wortschatz-Test (MWT-B)*. Furth: Straube.

Luck, S. J., and Gaspelin, N. (2017). How to get statistically significant effects in any ERP experiment (and why you shouldn't). *Psychophysiology* 54, 146–157. doi: 10.1111/psyp.12639

Martin, J. S., and Jerger, J. F. (2005). Some effects of aging on central auditory processing. *J. Rehab. Res. Dev.* 42, 25–44. doi: 10.1682/JRRD.2004.12.0164

Maxwell, S. E., Lau, M. Y., and Howard, G. S. (2015). Is psychology suffering from a replication crisis? what does "failure to replicate". Really Mean?. *Am. Psychol.* 70, 487–498. doi: 10.1037/a0039400

Micheyl, C., and Oxenham, A. J. (2010). Objective and subjective psychophysical measures of auditory stream integration and segregation. *J. Assoc. Res. Otolaryngol.* 11, 709–724. doi: 10.1007/s10162-010-0227-2

Näätänen, R., Gaillard, A. W. K., and Mäntysalo, S. (1978). Early selective-attention effect on evoked potential reinterpreted. *Acta Psychol.* 42, 313–329. doi: 10.1016/0001-6918(78)90006-9

Näätänen, R., Jacobsen, T., and Winkler, I. (2005). Memory-based or afferent processes in mismatch negativity (MMN): A review of the evidence. *Psychophysiology* 42, 25–32. doi: 10.1111/j.1469-8986.2005.00256.x

Näätänen, R., Kujala, T., Kreegipuu, K., Carlson, S., Escera, C., Baldeweg, T., et al. (2011). The mismatch negativity: An index of cognitive decline in neuropsychiatric and neurological diseases and in ageing. *Brain* 134, 3435–3453. doi: 10.1093/brain/awr064

Näätänen, R., Paavilainen, P., Rinne, T., and Alho, K. (2007). The mismatch negativity (MMN) in basic research of central auditory processing: A review. *Clin. Neurophysiol.* 118, 2544–2590. doi: 10.1016/j.clinph.2007.04.026

Näätänen, R., Paavilainen, P., Tiitinen, H., Jiang, D., and Alho, K. (1993). Attention and mismatch negativity. *Psychophysiology* 30, 436–450. doi: 10.1111/j.1469-8986.1993.tb02067.x

Näätänen, R., Tervaniemi, M., Sussman, E. S., Paavilainen, P., and Winkler, I. (2001). "Primitive intelligence" in the auditory cortex. *Trends Neurosci.* 24, 283–288. doi: 10.1016/S0166-2236(00)01790-2

Novak, G. P., Ritter, W., Vaughan, H. G., and Wiznitzer, M. L. (1990). Differentiation of negative event-related potentials in an auditory discrimination task. *Electroencephalography Clin. Neurophysiol.* 75, 255–275. doi: 10.1016/0013-4694(90)90105-S

Opitz, B., Rinne, T., Mecklinger, A., Von Cramon, D. Y., and Schröger, E. (2002). Differential contribution of frontal and temporal cortices to auditory change detection: FMRI and ERP results. *NeuroImage* 15, 167–174. doi: 10.1006/nimg.2001.0970

Paavilainen, P. (2013). The mismatch-negativity (MMN) component of the auditory event-related potential to violations of abstract regularities: a review. *Int. J. Psychophysiol.* 88, 109–123. doi: 10.1016/j.ijpsycho.2013.03.015

Passow, S., Westerhausen, R., Wartenburger, I., Hugdahl, K., Heekeren, H. R., Lindenberger, U., et al. (2012). Human aging compromises attentional control of auditory perception. *Psychol. Aging* 27, 99–105. doi: 10.1037/a0025667

Peelle, J. E., and Wingfield, A. (2016). The neural consequences of age-related hearing loss. *Trends Neurosci.* 39, 486–497. doi: 10.1016/j.tins.2016.05.001

Pichora-Fuller, M. K., and Souza, P. E. (2003). Effects of aging on auditory processing of speech. *Int. J. Audiol* 42, 11–16. doi: 10.3109/14992020309074638

Plomp, R. (1978). Auditory handicap of hearing impairment and the limited benefit of hearing aids. *J. Acoust. Soc. Am.* 63, 533–549. doi: 10.1121/1.381753

Rimmele, J., Schröger, E., and Bendixen, A. (2012a). Age-related changes in the use of regular patterns for auditory scene analysis. *Hear. Res.* 289, 98–107. doi: 10.1016/j.heares.2012.04.006

Rimmele, J., Sussman, E. S., Keitel, C., Jacobsen, T., and Schröger, E. (2012b). Electrophysiological evidence for age effects on sensory memory processing of tonal patterns. *Psychol. Aging* 27, 384–398. doi: 10.1037/a0024866

Rimmele, J., Sussman, E. S., and Poeppel, D. (2015). The role of temporal structure in the investigation of sensory memory, auditory scene analysis, and speech perception: A healthy-aging perspective. *Int. J. Psychophysiol.* 95, 175–183. doi: 10.1016/j.ijpsycho.2014.06.010

Schröger, E. (2005). The mismatch negativity as a tool to study auditory processing. *Acta Acust. United Acust.* 91, 490–501.

Schröger, E. (2007). Mismatch negativity: A microphone into auditory memory. *J. Psychophysiol.* 21, 138–146. doi: 10.1027/0269-8803.21.34.138

Schröger, E., Bendixen, A., Denham, S. L., Mill, R. W., Bőhm, T. M., and Winkler, I. (2014). Predictive regularity representations in violation detection and auditory stream segregation: From conceptual to computational models. *Brain Topograp.* 27, 565–577. doi: 10.1007/s10548-013-0334-6

Sohoglu, E., and Chait, M. (2016). Detecting and representing predictable structure during auditory scene analysis. *Elife* 5:e19113. doi: 10.7554/eLife.19113

Sussman, E. S. (2007). A New View on the MMN and attention debate: the role of context in processing auditory events. *J. Psychophysiol.* 21, 164–175. doi: 10.1027/0269-8803.21.34.164

Sussman, E. S., Horváth, J., Winkler, I., and Mark, O. (2007). The role of attention in the formation of auditory streams. *Percept. Psychophys.* 69, 136–152. doi: 10.3758/BF03194460

Sussman, E. S., Ritter, W., and Vaughan, H. G. (1999). An investigation of the auditory streaming effect using event-related brain potentials. *Psychophysiology* 36, 22–34. doi: 10.1017/S0048577299971056

Todd, J., Heathcote, A., Whitson, L. R., Mullens, D., Provost, A., and Winkler, I. (2014). Mismatch negativity (MMN) to pitch change is susceptible to order-dependent bias. *Front. Neurosci.* 8:180. doi: 10.3389/fnins.2014.00180

Todd, J., Provost, A., and Cooper, G. (2011). Lasting first impressions: A conservative bias in automatic filters of the acoustic environment. *Neuropsychologia* 49, 3399–3405. doi: 10.1016/j.neuropsychologia.2011.08.016

Todd, J., Provost, A., Whitson, L. R., Cooper, G., and Heathcote, A. (2013). Not so primitive: Context-sensitive meta-learning about unattended sound sequences. *J. Neurophysiol.* 109, 99–105. doi: 10.1152/jn.00581.2012

Wagener, K., Brand, T., and Kollmeier, B. (1999a). Development and evaluation of a German sentence test Part III: Evaluation of the Oldenburg sentence test. *Zeitschrift Für Audiologie* 38, 86–95.

Wagener, K., Kühnel, C., and Kollmeier, B. (1999b). Entwicklung und Evaluation eines Satztests für die deutsche Sprache Teil I: Design des Oldenburger Satztests. *Zeitschrift Für Audiologie* 38, 4–15.

Weeks, J. C., and Hasher, L. (2018). Older adults encode more, not less: evidence for age-related attentional broadening. *Aging Neuropsychol. Cogn.* 25, 576–587. doi: 10.1080/13825585.2017.1353678

Winkler, I., and Czigler, I. (1998). Mismatch negativity: Deviance detection or the maintenance of the "standard.". *NeuroReport* 9, 3809–3813. doi: 10.1097/00001756-199812010-00008

Winkler, I., Czigler, I., Sussman, E. S., Horváth, J., and Balázs, L. (2005). Preattentive binding of auditory and visual stimulus features. *J. Cogn. Neurosci.* 17, 320–339. doi: 10.1162/0898929053124866

Winkler, I., Denham, S. L., Mill, R. W., Bőhm, T. M., and Bendixen, A. (2012). Multistability in auditory stream segregation: a predictive coding view. *Philos. Trans. Royal Soc. Lon. Ser B Biol. Sci.* 367, 1001–1012. doi: 10.1098/rstb.2011.0359

Winkler, I., Denham, S. L., and Nelken, I. (2009). Modeling the auditory scene: predictive regularity representations and perceptual objects. *Trends Cogn. Sci.* 13, 532–540. doi: 10.1016/j.tics.2009.09.003

Winkler, I., and Schröger, E. (2015). Auditory perceptual objects as generative models: Setting the stage for communication by sound. *Brain Lang.* 148, 1–22. doi: 10.1016/j.bandl.2015.05.003

Zachau, S., Rinker, T., Körner, B., Kohls, G., Maas, V., Hennighausen, K., et al. (2005). Extracting rules: Early and late mismatch negativity to tone patterns. *NeuroReport* 16, 2015–2019. doi: 10.1097/00001756-200512190-00009

Conflict of Interest: The authors declare that the research was conducted in the absence of any commercial or financial relationships that could be construed as a potential conflict of interest.

frontiers in Human Neuroscience

ORIGINAL RESEARCH
published: 03 November 2021
doi: 10.3389/fnhum.2021.747769

The Brain Tracks Multiple Predictions About the Auditory Scene

*Kelin M. Brace and Elyse S. Sussman**

Department of Neuroscience, Albert Einstein College of Medicine, Bronx, NY, United States

The predictable rhythmic structure is important to most ecologically relevant sounds for humans, such as is found in the rhythm of speech or music. This study addressed the question of how rhythmic predictions are maintained in the auditory system when there are multiple perceptual interpretations occurring simultaneously and emanating from the same sound source. We recorded the electroencephalogram (EEG) while presenting participants with a tone sequence that had two different tone feature patterns, one based on the sequential rhythmic variation in tone duration and the other on sequential rhythmic variation in tone intensity. Participants were presented with the same sound sequences and were instructed to listen for the intensity pattern (ignore fluctuations in duration) and press a response key to detected pattern deviants (attend intensity pattern task); to listen to the duration pattern (ignore fluctuations in intensity) and make a button press to duration pattern deviants (attend duration pattern task), and to watch a movie and ignore the sounds presented to their ears (attend visual task). Both intensity and duration patterns occurred predictably 85% of the time, thus the key question involved evaluating how the brain treated the irrelevant feature patterns (standards and deviants) while performing an auditory or visual task. We expected that task-based feature patterns would have a more robust brain response to attended standards and deviants than the unattended feature patterns. Instead, we found that the neural entrainment to the rhythm of the standard attended patterns had similar power to the standard of the unattended feature patterns. In addition, the infrequent pattern deviants elicited the event-related brain potential called the mismatch negativity component (MMN). The MMN elicited by task-based feature pattern deviants had a similar amplitude to MMNs elicited by unattended pattern deviants that were unattended because they were not the target pattern or because the participant ignored the sounds and watched a movie. Thus, these results demonstrate that the brain tracks multiple predictions about the complexities in sound streams and can automatically track and detect deviations with respect to these predictions. This capability would be useful for switching attention rapidly among multiple objects in a busy auditory scene.

Keywords: auditory attention, task switching, pattern detection, mismatch negativity (MMN), event-related potentials (ERPs), neural entrainment

OPEN ACCESS

Edited by:
Manuel S. Malmierca, University of Salamanca, Spain

Reviewed by:
Gábor Péter Háden, Hungarian Academy of Sciences (MTA), Hungary
Philipp Ruhnau, University of Central Lancashire, United Kingdom

****Correspondence:***
Elyse S. Sussman
elyse.sussman@einsteinmed.org

Specialty section:
This article was submitted to Cognitive Neuroscience, a section of the journal Frontiers in Human Neuroscience

Received: *26 July 2021*
Accepted: *05 October 2021*
Published: *03 November 2021*

Citation:
Brace KM and Sussman ES (2021) The Brain Tracks Multiple Predictions About the Auditory Scene. Front. Hum. Neurosci. 15:747769. doi: 10.3389/fnhum.2021.747769

INTRODUCTION

It has long been appreciated that the excitability of the cortex oscillates in a rhythmic fashion (Bishop, 1932). Attention is adaptive, capable of following the fluctuations in the rhythmic structure of speech and music in a dynamic fashion (Large and Jones, 1999). Although many different oscillatory bands have been implicated in neuronal processing, this study focused on lower frequency oscillations, particularly related to attention. These low frequency oscillations are inherently present in the brain. The alignment of low frequency oscillations to external stimuli has been posited as a possible method of attentional selection (Lakatos et al., 2008; Schroeder and Lakatos, 2009).

The brain's response to sound stimulation can reflect the rhythmic structure and is thought to be a mechanism of selective attention (Lakatos et al., 2008; Schroeder and Lakatos, 2009; Calderone et al., 2014). Moreover, entrainment to stimulus presentation rate is positively correlated with behavioral detection (Large and Jones, 1999; Elhilali et al., 2009; Xiang et al., 2010), and expectation of rhythm has been shown to improve behavioral performance (Dowling et al., 1987). There is evidence of primate primary auditory cortical entraining to rhythmic stimuli after the stimuli have ended, indicating that these are not just evoked responses (Lakatos et al., 2013). Amplitude modulation of sounds is also reflected in the cortical response (Draganova et al., 2002). Attention to a target rhythm within a masking sequence can enhance neural entrainment to the target, originating from the auditory cortex. Performance on a target task is correlated with the strength of neural entrainment (Elhilali et al., 2009). Selective entrainment occurs more strongly to the attended rhythm when multiple possible rhythms are present (Costa-Faidella et al., 2017).

In the current study, we recorded an electroencephalogram (EEG) to investigate how the brain entrains to the rhythm of sounds when there are multiple possible rhythmic interpretations that can be extracted from a single sound stream. Specifically, we tested how attention drives entrainment to the two different rhythms by using a switching paradigm that requires a different task goal associated with each distinct rhythm perception.

To further assess processing associated with rhythmic perception, we used two dependent measures of the event-related brain potentials (ERPs), the mismatch negativity (MMN), and the P3b components that reflect processing of the deviant. The MMN, which is generated within auditory cortices (Tiitinen et al., 1993), provides an ideal tool for simultaneously assessing the brain's response to the attended and the unattended sound rhythms in the sequence (Sussman et al., 2014). Thus, MMN elicitation can be used to assess the representation of different rhythmic regularities maintained in auditory memory (Moldwin et al., 2017). The MMN system represents pattern regularities in a sequence of sounds (the "standard"; Sussman, 2007) and indexes detection of the violation of those regularities (the "deviant"; Schröger et al., 1992; Sussman et al., 1998, 2014; Picton et al., 2000; Näätänen et al., 2001; Takegata et al., 2001; Winkler et al., 2003; Sussman, 2007; Paavilainen, 2013; Pannese et al., 2015). The P3b component was used to evaluate task-related performance. The P3b component is associated with volitional control and its amplitude and latency are affected by task difficulty in dual task situations (Norman and Bobrow, 1975; Isreal et al., 1980; Kok, 2001). For example, task interference is associated with the elicitation of smaller P3b amplitude and longer P3b latency. Thus, the P3b component can be used together with behavioral indices of performance to assess cognitive demands.

The overarching goal of the current study was to gain a better understanding of complex sound perception by investigating the way in which sounds are represented in auditory memory during task performance when multiple rhythmic interpretations can be perceived from one sound stream. The current experiment incorporated elements of a task-switching paradigm along with manipulation of rhythmic attention. The paradigm was inspired by the methodology used in Costa-Faidella et al. (2017). The sound sequences contained two non-overlapping rhythms created by patterns in different tone features, a tone intensity pattern and a tone duration pattern. The task focused on detecting a pattern deviant in the respective feature (intensity pattern deviant or duration pattern deviant). The targets were unique deviants within the intensity and duration patterns to elicit MMN based on its respective standard pattern. In this way, we were able to assess both the brain representation of the standard rhythms by examining neural entrainment to the rhythm of the standard and deviant detection by examining elicitation of the MMN. We predicted that when participants performed repeated trials of the same task, there would be evidence of strong neural entrainment to the target rhythm, and an MMN elicited by the attended pattern deviants. We further predicted that the entrainment to the unattended, irrelevant rhythm (intensity pattern when attending duration, and duration pattern when attending intensity) would be attenuated or absent, which would likely preclude the MMN response. Additionally, because it was a switching paradigm, we expected some behavioral switch cost (e.g., lower hit rate or longer response time) when participants alternated between tasks. Finally, because we set up a competition between stimulus-driven rhythmic perceptions, we expected that there may be neural evidence of competition between the tasks.

MATERIALS AND METHODS

Participants

Twenty-four adults aged 22–41 years (median age 27.5, 11 males) were included in this study. All participants passed a hearing screening (25 dB HL or better for 500, 1,000, 2,000, and 4,000 Hz) and had no self-reported history of psychiatric or neurologic disorder. The study was carried out in accordance with the Code of Ethics of the World Medical Association (Declaration of Helsinki). Written consent was obtained from all participants after the study was explained to them. The protocol and informed consent documents were approved by the Institutional Review Board at Albert Einstein College of Medicine, Bronx, NY where the study was conducted.

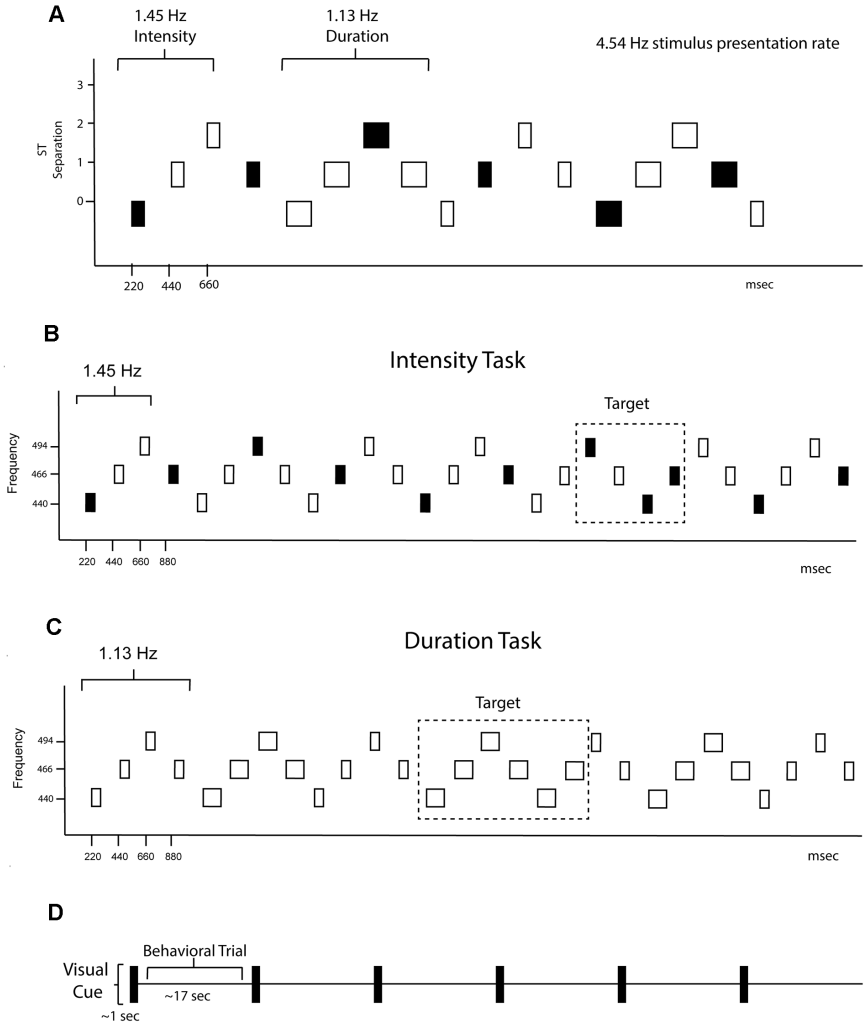

FIGURE 1 | Experimental protocol. **(A)** Schematic of the overall stimulus paradigm. The X-axis shows the timing in milliseconds and the Y-axis shows the frequency separation in semitones (ST). The rectangles represent the tones. The fill represents intensity, with black representing louder intensity tones and the white softer intensity tones, and the width of the rectangle represents tone duration. Both intensity and duration patterns were presented randomly within the stimulus blocks and are demarcated with the rhythm of each denoted. The global rhythm of the tones in the sequence was 4.54 Hz. **(B)** Intensity task. Only the intensity rhythm is displayed. The standard 4-tone intensity pattern was loud-soft-soft-loud, and had a rhythm of 1.51 Hz. The task was to keep the standard pattern in mind and press the response key when the pattern deviant (loud-soft-**loud**-loud) was detected. Thus, the button press was time-locked to the 3rd tone of the pattern where a louder tone came when a softer tone was expected. The frequency of the tones is displayed on the y-axis. The tone duration changes were irrelevant to the intensity task. **(C)** Duration Task. Only the duration rhythm is displayed. The standard 8-tone duration pattern was short-short-short-short-long-long-long-long, and had a rhythm of 1.13 Hz. The task was to keep the standard pattern in mind and press the response key when the pattern deviant (long-long-long-long-**long**-long) was detected. Thus, the button press was time-locked to the 5th long tone of the deviant pattern where a shorter tone was expected. The frequency of the tones is displayed on the y-axis. The tone intensity changes were irrelevant during the duration task. **(D)** Protocol schematic. A visual cue the words "intensity task" or "duration task" (depicted in time as a black rectangle) was presented on the screen for 1 s instructing participants what task to do. Sounds were presented randomly between 15–20 s, comprising one trial. Six trials of "intensity task" or "duration task" were presented randomly throughout each of the 20 blocks.

Stimuli

A graphical representation of the sound sequence is shown in **Figure 1**. Stimuli consisted of pure tones presented binaurally through insert earphones with a constant stimulus onset asynchrony (SOA) of 220 ms. Every sequence consisted of a repeating four-tone frequency pattern in a set order 440 Hz—466.16 Hz—493.88 Hz—466.16 Hz (**Figure 1A**). There was one semitone separation between each successive tone, facilitating perceptual integration (Bregman, 1990). Eight tones created the duration pattern (**Figure 1B**), with four longer duration tones (200 ms each) followed by four shorter tones (100 ms each). Three tones created the intensity pattern (**Figure 1C**), one loud tone (85 dBA) followed by two soft tones (70 dBA; calibrated with a Brüel and Kjær® sound level meter with an artificial ear). The resulting sequence from superimposing these patterns was perceptually ambiguous, with listeners able to hear either the rhythm of the intensity pattern (1.45 Hz)

or the rhythm of the duration pattern (1.13 Hz). There were 12 total individual tones used in the sequences that accounted for all possible combinations of frequency (low/middle/high), duration (long/short), and intensity (loud/soft).

Randomly occurring violations in both the intensity and duration patterns (deviants) occurred for 15% of intensity pattern triplets, the standard *loud-soft-soft* pattern was replaced with *loud-soft-**loud*** (**Figure 1B**); and 15% of duration patterns, the standard *long-long-long-long-short-short-short-short* pattern was replaced with *long-long-long-long-**long-long**-short-short* (**Figure 1C**). The infrequent deviants served as targets during one half of the experiment and irrelevant deviants in the other half.

Procedures

The two conditions, *Attend Visual* condition and *Attend Auditory* were conducted on two separate days. Participants were alternately assigned to start with one of the conditions and completed the other condition when they returned to the laboratory approximately 2 weeks later. In the *Attend Visual* condition, participants passively listened to the sound sequences while watching a closed-captioned movie (chosen from our video library). Ten 6-min sound sequences were presented, with each sequence having 1,458 stimuli (72 intensity deviants, 54 duration deviants).

In the *Attend Auditory* condition, participants listened to the sounds to identify the intensity and duration patterns and their deviants. The same set of sound sequences were used in both the *Attend Visual* condition and the *Attend Auditory* conditions but in a differently randomized order (20 sound sequences in all). A brief practice session was provided prior to the recording session. Participants were instructed about what sound patterns to listen for and were shown a visual depiction of the target patterns. Participants were then presented with a graded series of sound sequences to acquaint them with the task. First, they were presented with either the intensity or the duration pattern by itself (practicing one feature at a time with the order alternated across participants) and were instructed to identify the repeating pattern and press a response key when they heard violations to the pattern. Second, they were presented with the intensity or duration pattern along with the frequency modulation and asked to do the same task. Then, finally, they had the intensity, frequency, and duration modulations present and were told to focus on their target feature pattern (intensity or duration) and perform the same task they had been doing and ignore any other tone variations. After successfully training for one pattern feature task, they trained for the alternative task. 60% correct was used as the criterion used for both the intensity and the duration tasks to proceed to the EEG recording session. Two participants were excluded prior to data collection based on this practice criterion.

During the EEG recording, 20 differently randomized sequences were presented, each sequence having six trials of 15–20 s in length. Every trial was preceded by a visual stimulus that stayed on the monitor for 1 s to indicate which task intensity or duration patterns were to be performed on the next trial (**Figure 1D**). Only one of the tasks was performed for the duration of each trial. The total silent time between trials, including the visual stimulus, was 1.85 s. The time constant for decay of streaming bias is 1.42 s (Beauvois and Meddis, 1997). Thus, streaming bias persisted between trials. The tasks were split 50–50% among the trials so that on half of the trials participants performed the intensity task and half of the trials the duration pattern task. Task switching was also randomized so that half of the trials were "switching" trials (going from intensity task to duration task and vice versa) and half were "repeat" trials (repeating the same task as the previous trial). These two contingencies were orthogonal; thus one-quarter of trials were duration task switched (*Duration Switch*), one quarter were duration task repeated (*Duration Repeat*), one quarter were intensity task switched (*Intensity Switch*), and one quarter were intensity task repeated (*Intensity Repeat*). Regardless of which instruction was given, intensity and duration deviants were present in all trials, so participants needed to isolate and attend to one feature pattern (the *targets*) and ignore the distracting feature pattern (*non-targets*).

Participants sat in a comfortable chair in a sound-attenuated booth. The duration of one session, of which there were two occurring on separate days, was approximately 2 h, which included consenting, hearing screen, cap placement, task practice, task performance, and breaks.

Data Analysis

Behavioral Responses

Target responses were calculated for Intensity and Duration deviants separately within a "switch" trial and a "repeat" trial for the four trial types: *Duration Switch, Duration Repeat, Intensity Switch, and Intensity Repeat*. A button press was considered correct when it fell within 100–900 ms from target onset. Reaction time (RT) was calculated as the mean RT of the correct responses. Hit rate (HR) was calculated as the number of correct button presses divided by the total number of target stimuli. A false alarm was considered a button press to a non-target deviant. The false alarm rate (FAR) was calculated as the number of button presses made within the response window for non-target deviants divided by the total number of non-target deviants. There was no overlap in the response windows. HR, RT, and FAR were reported separately for each trial type.

To evaluate task-switching effects, which are generally observed very soon after the switch, we separately analyzed the HR and RT to the first target in each of the trials from the remaining targets.

EEG Recording and Data Reduction

Continuous EEG was recorded using a 32-channel electrode cap with the 10–20 international electrode placement system. An electrode placed at the base of the nose was used as the reference and the P09 electrode was used as the ground. Impedances were below 5 kΩ. EEG and EOG were sampled at a rate of 500 Hz using a bandpass filter of 0.05–100 Hz and a gain of 1,000 (Neuroscan Synamps amplifier, Compumedics Corp, El Paso, Texas). ERPs were extracted from the continuous EEG

files. After applying a 0.1–30 Hz bandpass filter (using a finite impulse response filter with zero phase shift and a roll-off slope of 24 dB/octave), EEG data for each subject were separated into 700 ms epochs, including a 100-ms pre-stimulus interval. Ocular artifact correction was performed for an individual when excessive blinking resulted in the exclusion of more than 20% of trials. For three participants who had excessive eye-blink activity, ocular artifact reduction was conducted to perform the correction using Neuroscan EDIT software. This Singular Value Decomposition transform method is used to identify the blink component. From the continuous EEG, a file is created that reflects the spatial distribution of the blink and then used to remove the blink. The blink-corrected data were then baseline-corrected across the whole epoch (the mean was subtracted at each point across the epoch). After baseline correction, artifact rejection criteria were set to ±75 mV. On average, 87% of all trials were included in the analysis. Condition-matched deviant epochs and standard epochs were grouped accordingly then baseline corrected to the pre-stimulus period and averaged to create individual mean waveforms. Deviant epochs that contained a correct button press were marked as "Correct" and averaged together, incorrect responses were omitted from this averaged waveform. Individual mean averages were then averaged to create grand-mean waveforms. The grand-mean standard waveform was subtracted from the grand-mean deviant waveform from the same condition, yielding a grand-mean difference waveform used to identify ERP components. The mean latency of the MMN component in each condition was determined using the Neuroscan program to find the maxima between 100–300 ms at the left mastoid (LM) electrode in the grand mean difference waveform. LM was used to avoid overlap of attention components. The unattended deviants, both duration and intensity, showed a clear double peak, and both of these peaks were quantified. For the P3b component, the maxima were determined between 300–600 ms at the Pz electrode. The peak latency of each ERP component in the grand mean waveform was used as the center to obtain a 50 ms interval used to assess the amplitude of the MMN component and a 60 ms window to obtain the mean for each individual for the P3b component. MMN area was quantified as the area between the Fz electrode and the averaged mastoid electrodes [(LM + RM)/2] and P3b was quantified as the area under the Pz electrode.

To perform the frequency analysis to visualize the entrainment to the rhythm, regions around targets were removed from the continuous file (100 ms pre and 1,000 ms after) to remove contributions from target response and motor activity. A high pass filter at 0.5 Hz was used. Eyeblink correction was performed using Neuroscan LDR. Matching trials were concatenated and fast FFT was performed on the resultant continuous file. Frequency power was measured at the target rhythms (1.13 Hz for duration pattern and 1.45 Hz for intensity pattern) and the stimulus presentation rate (4.45 Hz and 9.10 Hz for the 1st harmonic). The normalized power was determined by dividing the power at a given frequency by the average power of the surrounding frequencies ±1 Hz, excluding the other target frequency (i.e., the average surround power for the 1.13 Hz frequency did not include 1.45 Hz and vice versa).

Statistical Analyses

Behavioral Analyses

For HR and RT, separate repeated measures analysis of variance (rmANOVA) was performed with factors of task (Intensity/Duration), switching (switch/repeat), and primacy (first target/other targets). FAR was calculated using a two-way rmANOVA with factors of task and switching.

ERP Component Analyses

The first analysis determined the significant presence of the MMN and P3b components using a one-sided, one sample *t*-test to confirm that the amplitude was significantly greater than zero. The second analysis then compared the amplitude/latency of the ERP components across stimulus types and conditions. *Attend Auditory* condition: A four-way rmANOVA was used to compare the amplitude of the MMN with factors deviant type (Intensity vs. Duration), peak (First peak vs. Second peak), attention (attended vs. unattended), and switching (task switch vs. task repeat). "Attended" refers to MMNs elicited by the target stimuli and "unattended" refers to MMNs elicited by the non-target deviants. A second analysis was used to compare the unattended mean amplitude of the MMNs elicited by non-tartgets in the *Attend Auditory* condition to the mean amplitude MMNs elicited by deviants in the *Attend Visual* condition. A rmANOVA with factors of deviant type (Intensity/Duration), peak (First peak/Second peak), and trial type (Switch, Repeat, Attend Visual) was calculated.

P3b amplitude was compared using factors of task type (Intensity/Duration,) switching (task switch/task repeat), and electrode (Fz/Cz/Pz). Normal neural entrainment was analyzed with rmANOVA with factors of task type (Intensity/Duration) switching (task switch/task repeat), and rhythm (duration rhythm/intensity rhythm/stimulus rhythm/harmonic rhythm). A second analysis for neural entrainment was performed to compare the *Attend Auditory* conditions to the *Attend Visual* condition using rmANOVA with factors of conditions (Duration Switch/Duration Repeat/Intensity Switch/Intensity Repeat/Attend Visual) and rhythm(duration rhythm/intensity rhythm/stimulus rhythm/harmonic rhythm).

For all ANOVA calculations, where data violated the assumption of sphericity, degrees of freedom were corrected using Greenhouse-Geisser estimates of sphericity. Corrected *p* values are reported. For *post hoc* analyses, Tukey HSD for repeated measures was conducted on pairwise contrasts only when there were significant main effects or interactions. All statistical analyses were performed using Statistica software (Statsoft, Inc., Tulsa, OK, USA).

RESULTS

Behavior

Table 1 and **Figure 2** display the behavioral results.

Hit Rate

There was a main effect of the order on HR, with the first target of a block having a higher HR than the average of the rest of the targets ($F_{(1,23)} = 7.23$, $p = 0.01$, $\eta_p^2 = 0.24$). There was a main

TABLE 1 | Behavioral data.

Task	Hit rate		Reaction time (ms)		FAR
	First target	Other targets	First target	Other targets	All targets
Duration/Switch	0.78 (0.15)	0.76 (0.17)	532 (86)	543 (81)	0.020 (0.040)
Duration/Repeat	0.71 (0.20)	0.71 (0.20)	563 (82)	554 (79)	0.016 (0.023)
Intensity/Switch	0.86 (0.13)	0.83 (0.14)	449 (69)	470 (71)	0.027 (0.034)
Intensity/Repeat	0.85 (0.13)	0.82 (0.15)	453 (77)	473 (82)	0.021 (0.030)

Standard deviation is shown in parenthesis. ms, milliseconds; FAR, false alarm rate.

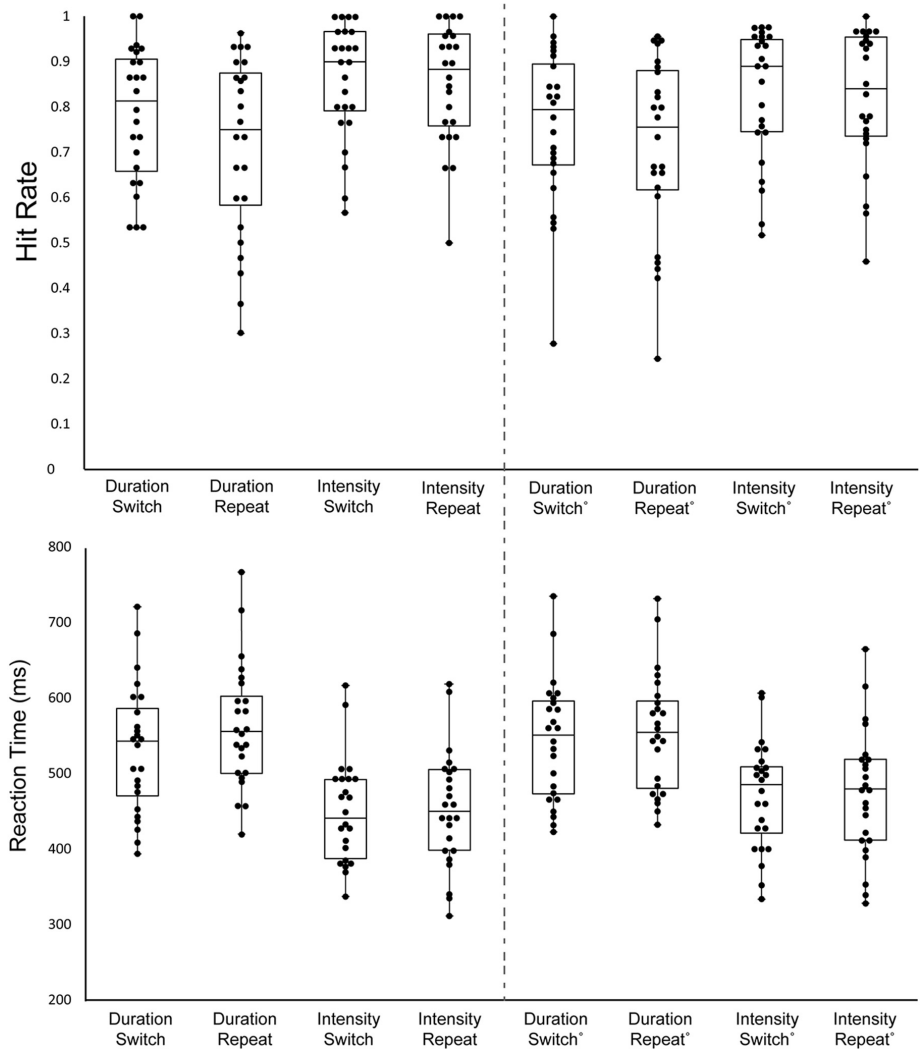

FIGURE 2 | Behavioral results. Hit Rate (HR; top graph) and Reaction Time (RT; bottom graph) are displayed for all stimulus types. Each black circle represents one individual. The upper whisker denotes the upper limit, the lower whisker denotes the lower limit, the upper bar represents the 3rd quartile, the middle bar represents the median, and the lower bar represents the 1st quartile. Each column shows a different stimulus type, indicating whether it was the Duration or the Intensity task and whether the trial was a Switch trial (the previous trial was the other task) or a Repeat trial (the same task repeated). The left columns 1–4 display the mean data of the first target of the trials and the right columns 5–8 display the mean of the remaining targets in the trials.

effect of task on HR, with a higher HR for the Intensity Task ($F_{(1,23)} = 8.71$, $p < 0.01$, $\eta_p^2 = 0.27$). Additionally, there was a main effect of switching, with switch trials having higher HR than repeat trials ($F_{(1,23)} = 7.23$, $p = 0.01$, $\eta_p^2 = 0.24$). There was no interaction between order and task ($F_{(1,23)} = 0.66$, $p = 0.42$), between order and switching ($F_{(1,23)} = 0.89$, $p = 0.36$), between task and switching ($F_{(1,23)} = 3.29$, $p = 0.08$), or between order, task, and switching ($F_{(1,23)} = 1.84$, $p = 0.19$).

Reaction Time

There was a main effect of order on RT ($F_{(1,23)}$ = 13.13, $p < 0.01$, η_p^2 = 0.36) with the first target of the block having a shorter RT. There was also a main effect of task ($F_{(1,23)}$ = 45.58, $p < 0.01$, η_p^2 = 0.65), due to the shorter RT to intensity pattern targets than Duration pattern targets. Additionally, there was a main effect of switching ($F_{(1,23)}$ = 11.9, $p < 0.01$, η_p^2 = 0.34), with switch trials having a shorter RT than repeat trials. There was an interaction between order and task ($F_{(1,23)}$ = 14.59, $p < 0.01$, η_p^2 = 0.39). *Post hoc* calculation showed First Target-Duration>First Target-Intensity ($p < 0.01$), First Target-Duration> Later Targets-Intensity ($p < 0.01$) Later Targets-Duration>First Target-Intensity ($p < 0.01$), Later Targets-Intensity>First Target-Intensity ($p < 0.01$). This showed participants have a faster response to the first target for the intensity task when compared to later targets, but this does not hold true for the duration task. There was an interaction between, order and switching ($F_{(1,23)}$ = 5.03, p = 0.03, η_p^2 = 0.18). *Post hoc* calculation showed First Target-Repeat>First Target-Switch ($p < 0.01$), Later Targets-Switch>First Target-Switch ($p < 0.01$), Later Targets-Repeat>First Target-Switch ($p < 0.01$). Participants had the fastest response time to the first target after a task switch when compared to other target types. There was no interaction between task and switching ($F_{(1,23)}$ = 3.55, p = 0.07). There was a three-way interaction between order, task, and switching ($F_{(1,23)}$ = 5.23, p = 0.03, η_p^2 = 0.19). *Post hoc* analysis showed First Target-Duration-Repeat>First Target-Duration-Switch ($p < 0.01$), First Target-Duration-Switch>First Target-Intensity-Switch ($p < 0.01$), First Target-Duration-Switch>First Target-Intensity-Repeat ($p < 0.01$), Later Targets-Duration-Repeat>First Target-Duration-Switch ($p < 0.01$), First Target-Duration-Switch>Later Targets-Duration-Repeat ($p < 0.01$).

False Alarm Rate

False alam rate (FAR) did not differ as a function of the task being performed or whether it was a switch or repeat trial. There was no main effect of task ($F_{(1,23)}$ = 1.44, p = 0.24), no main effect of switching ($F_{(1,23)}$ = 3.73, p = 0.07), and no interaction between task and switching ($F_{(1,23)} < 1$, p = 0.90).

Event Related Brain Potentials

MMN

Table 2, **Figures 3** and **4** display the MMN results. MMNs were elicited by the first two tones of the intensity and duration deviant patterns for both attended (**Figure 3** labeled with arrows) and unattended (**Figure 4**, labeled with arrows) pattern deviants (determined by one-sample *t*-tests all $p < 0.05$). For example, when *long-long-long-long-short-short-short-short* pattern was replaced with *long-long-long-long-**long-long**-short-short*, detection of the deviant could occur at the 5th long tone but both of the longer duration tones were deviant within the 8-tone pattern. The second deviant tone of the unattended duration pattern when the intensity task was being performed was the only second deviant that did not elicit MMN (p = 0.13).

In the Attend Auditory Condition, the MMN amplitude elicited by intensity pattern deviants was larger than duration pattern deviants (main effect of deviant type, $F_{(1,23)}$ = 32.27, $p < 0.01$, η_p^2 = 0.79). MMN amplitude was larger for the attended compared to the unattended tone pattern features (main effect of attention, $F_{(1,23)}$ = 5.19, p = 0.03, η_p^2 = 0.18). MMNs elicited by the first two tones did not differ in amplitude (no main effect of the peak, $F_{(1,23)}$ = 0.05, p = 0.82, $\eta_p^2 < 0.01$), nor did it matter if it was a switch or repeat trial (no main effect of switching, $F_{(1,23)}$ = 0.64, p = 0.43, η_p^2 = 0.02). There was an interaction between peak and switching ($F_{(1,23)}$ = 7.27, p = 0.01, η_p^2 = 0.24). *Post hoc* calculations showed that this was due to the MMN to the second tone of the pattern being larger in the switch trials than the second peak of the repeat trials (p = 0.05). There was a significant three-way interaction between deviant type, peak, and attention ($F_{(1,23)}$ = 13.72, $p < 0.01$, η_p^2 = 0.37). *Post hoc* calculations showed that Duration-First Peak-Attended < Intensity-First Peak-Attended ($p < 0.01$), Duration-First Peak-Attended < Intensity-Second Peak-Attended (p = 0.01), Duration-First Peak-Attended < Intensity-Second Peak-Unattended ($p < 0.01$). There was a three-way interaction between deviant type, peak, and switching ($F_{(1,23)}$ = 8.30, $p < 0.01$, η_p^2 = 0.27). *Post hoc* analysis showed that the intensity MMN elicited by the second tone of the deviant pattern when it was a switch task was smaller in amplitude than the other intensity MMN peaks. There were no interactions between deviant type and peak ($F_{(1,23)} < 1$, p = 0.44), between deviant type and attention ($F_{(1,23)}$ = 0.99, p = 0.33), between peak and attention ($F_{(1,23)}$ = 2.48, p = 0.13) between deviant type and switching ($F_{(1,23)}$ = 2.07, p = 0.16), between attention and switching ($F_{(1,23)}$ = 0.68, p = 0.42), between deviant type, attention, and switching ($F_{(1,23)}$ = 0.27, p = 0.61), between peak, attention, and switching ($F_{(1,23)}$ = 3.68, p = 0.07), or between deviant type, peak, attention, and switching ($F_{(1,23)}$ = 1.29, p = 0.27).

TABLE 2 | ERP amplitudes.

Condition	Task	MMN component				P3b component	
		Dur 1	Dur 2	Int 1	Int 2	Duration	Intensity
Attend/Auditory	Duration/Switch	−0.72 (1.28)	−1.11 (1.57)	1.35 (1.19)	−2.43 (1.61)	6.68 (3.70)	–
Attend/Auditory	Duration/Repeat	−0.90 (0.92)	−1.34 (0.19)	−1.63 (1.23)	−1.53 (1.08)	6.01 (3.55)	–
Attend/Auditory	Intensity/Switch	−0.49 (0.83)	−0.45 (0.84)	−2.35 (1.47)	−1.87 (2.36)	–	3.10 (2.71)
Attend/Auditory	Intensity/Repeat	−0.47 (0.81)	−0.33 (1.03)	−2.29 (1.13)	−1.48 (2.57)	–	3.77 (2.73)
Attend/Visual	Watching movie	−0.59 (0.52)	−0.66 (0.67)	−1.05 (1.06)	−1.96 (0.94)	–	–

Standard deviation is shown in parentheses. Dur1, duration pattern deviant first peak; Dur2, duration pattern deviant second peak; Int1, intensity pattern deviant first peak; Int2, intensity pattern deviant second peak; – no ERP component elicited.

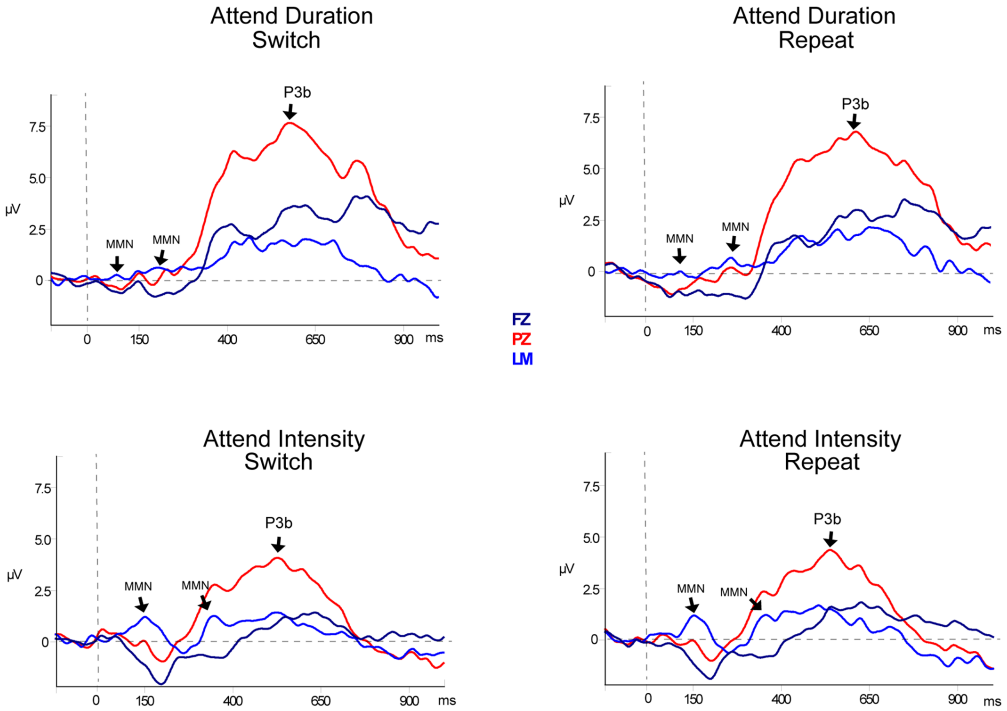

FIGURE 3 | Event-related potentials for target pattern deviants. Difference waveforms (deviant-minus-standard) are displayed for duration (top row) and intensity (bottom row) targets. Responses to the target during Switch trials are shown in the left column and responses to the targets during Repeat trials are shown in the right column. Responses recorded from Fz (dark blue solid line), the left mastoid (LM; light blue solid line), and Pz (red solid line) are overlain to demarcate both the mismatch negativity component (MMN) response and the P3b components. Significant components are denoted with an arrow and labeled. Two successive MMNs were elicited by two successive tones within the pattern deviants.

When all of the sounds were unattended, in the *Attend Visual* condition, as compared to when they were unattended in the *Attend Auditory* condition, intensity deviants elicited a larger amplitude MMN than duration deviants (the main effect of deviant type, $F_{(1,23)} = 47.82$, $p < 0.01$, $\eta_p^2 = 0.68$). The MMN elicited by the second tone of the pattern was larger in amplitude than the first (main effect of the peak, $F_{(1,23)} = 6.79$, $p = 0.02$, $\eta_p^2 = 0.23$). Unattended MMNs did not differ in amplitude as a function of whether auditory or visual was attended. There was no main effect of condition ($F_{(1,46)} = 0.64$, $p = 0.53$). There was a significant interaction between deviant type and peak ($F_{(1,23)} = 8.60$, $p < 0.01$, $\eta_p^2 = 0.27$). *Post hoc* showed Duration-First Peak < Intensity-First Peak ($p < 0.01$), Duration-First Peak < Intensity-Second Peak ($p < 0.01$), Duration-Second Peak < Intensity-First Peak ($p < 0.01$), Duration-Second Peak < Intensity-Second Peak ($p < 0.01$), and Intensity-First Peak < Intensity-Second Peak ($p < 0.01$). There was also an interaction between peak and condition ($F_{(1,46)} = 8.30$, $p < 0.01$, $\eta_p^2 = 0.26$). *Post hoc* calculation revealed that the 2nd MMN peak in the Attend Intensity and Attend Visual conditions were larger in amplitude than the MMNs in Attend Duration. There was no interaction between deviant type and condition ($F_{(1,46)} = 1.97$, $p = 0.15$). There was a three-way interaction between deviant type, peak, and condition ($F_{(1,46)} = 13.72$, $p < 0.01$, $\eta_p^2 = 0.37$). *Post hoc* calculations showed that the intensity MMN at the first peak was smaller in the Attend Visual condition than all of the other MMN peaks.

P3b Component

P3b amplitude was largest when performing the duration task (main effect of task, $F_{(1,23)} = 24.67$, $p < 0.01$, $\eta_p^2 = 0.52$). There was a significant main effect of electrode ($F_{(1,46)} = 65.77$, $p < 0.01$, $\eta_p^2 = 0.74$). *Post hoc* calculation showed Fz < Cz ($p < 0.01$) and Fz < Pz ($p < 0.01$). Amplitude did not differ between switching and repeat trials (no main effect of switching, $F_{(1,23)} = 0.18$, $p = 0.07$,). There was a significant interaction between deviant type and switching ($F_{(1,23)} = 6.15$, $p = 0.02$, $\eta_p^2 = 0.21$). *Post hoc* calculations showed that Duration Repeat<Duration Switch ($p < 0.01$), Intensity Repeat < Duration Repeat ($p < 0.01$), Intensity Switch < Duration Repeat ($p < 0.01$), Intensity Repeat < Duration Switch ($p < 0.01$), and Intensity Switch < Duration Switch ($p < 0.01$). There was a significant interaction between deviant type and electrode ($F_{(1,46)} = 15.5$, $p < 0.01$, $\eta_p^2 = 0.40$). *Post hoc* calculations show that the duration deviant P3b amplitude was larger than intensity deviant P3b at Cz and Pz electrodes, with no difference in amplitude between them at Fz. There was no interactions between switching and electrode ($F_{(1,46)} = 1.16$, $p = 0.32$, $\eta_p^2 = 0.05$), and or between deviant type, switching, and electrode ($F_{(1,23)} < 1$, $p = 0.67$).

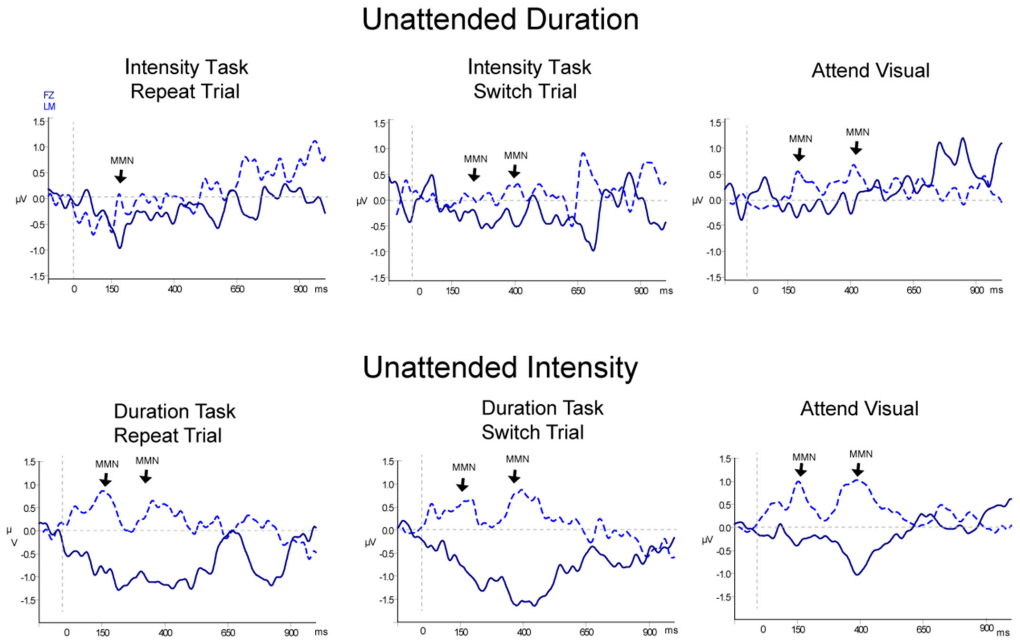

FIGURE 4 | Event-related potentials for non-target (unattended) pattern deviants. Difference waveforms (deviant-minus-standard) are displayed for duration (top row) and intensity (bottom row) non-targets. Responses to the non-targets during the Attend Auditory conditions: Repeat trials are shown in the left column and Switch trials are shown in the middle column, and responses to the non-targets in the Attend-Visual condition are displayed in the right column. The dark blue solid line displays the waveform recorded from the Fz electrode with the waveform at LM (light blue dashed line) overlain. Significant MMN components are denoted with an arrow pointed at LM and labeled. Two successive MMNs were elicited by two successive tones within the non-target pattern deviants, similarly as for the targets shown in **Figure 3**.

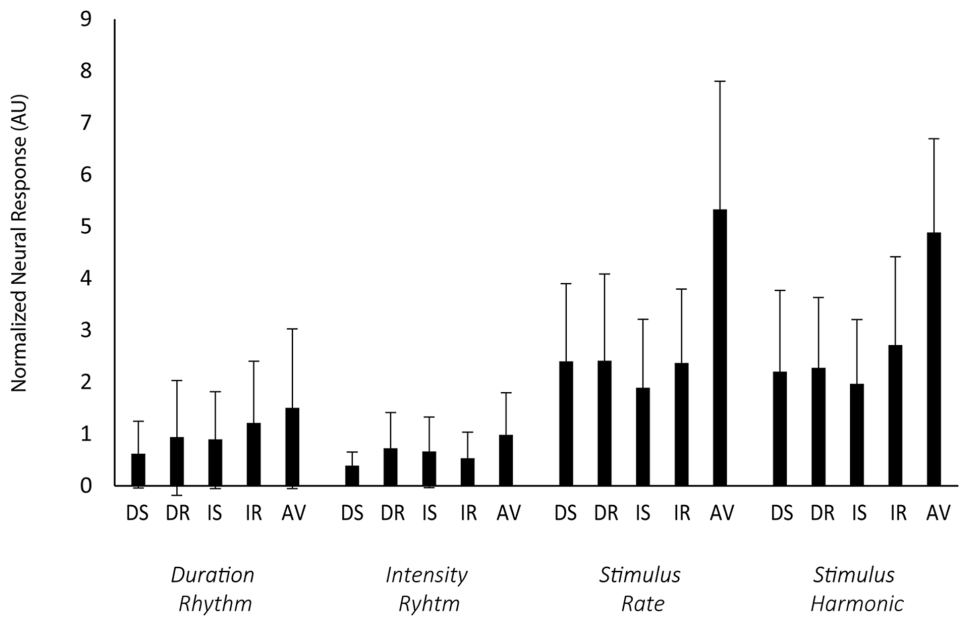

FIGURE 5 | Rhythmic entrainment. Rhythmic entrainment responses to the standard patterns are shown as the normalized neural response from the Cz electrode (y-axis), calculated as the square of the power of target frequency divided by the square of the average power in the surrounding 1 Hz frequency bin (excluding other target frequencies). Error bars display the standard deviation. Along the x-axis, the blue rectangles represent each task trial type (DS, duration switch trial; DR, duration repeat trial; IS, intensity switch trial; IR, intensity repeat trial; AV, attend visual stimuli). The sub x-axis is separated by duration rhythm (1.13 Hz), intensity rhythm (1.45), overall stimulus rate (4.45 Hz), and the first harmonic of the stimulus rate (9.10 Hz). The direction of attention had no effect on the strength of the responses. Attended rhythms in the Attend Auditory condition were not distinguished from unattended rhythms in the Attend Auditory condition.

Rhythmic Entrainment

Figure 5 shows the normalized neural responses to rhythmic entrainment. The raw data are presented in **Supplementary Figure 1** (**Supplementary Material**). Neural responses did not differ as a function of the task performed (no main effect of task ($F_{(1,23)} = 0.10$, $p = 0.75$). Repeat trials had greater normalized power than switching trials (main effect of switching $F_{(1,23)} = 5.97$, $p = 0.02$, $\eta_p^2 = 0.21$). There was also a main effect of rhythm, with the global stimulus rate and first harmonic (4.55 Hz and 9.10 Hz) both having greater power than the power of an individual feature pattern (1.14 Hz or 1.45 Hz; $F_{(3,69)} = 45.55$, $p < 0.01$, $\eta_p^2 = 0.66$). There was no interaction between task and switching ($F_{(1,23)} < 1$, $p = 0.41$), no interaction between task and rhythm ($F_{(3,69)} < 1$, $p = 0.41$), no interaction between switching and rhythm($F_{(3,69)} < 1$, $p = 0.74$), and no three-way interaction between task, switching, and rhythm ($F_{(3,69)} = 1.08$, $p = 0.036$).

There was a significant effect of condition ($F_{(4,92)} = 35.54$, $p < 0.01$, $\eta_p^2 = 0.61$). Power was greater in the *Attend Auditory* than *Attend Visual* condition. There was also a main effect of rhythm ($F_{(3,69)} = 61.45$, $p < 0.01$, $\eta_p^2 = 0.73$) with greater power to the global rhythm than either of the individual feature rhythms and interaction between condition and rhythm ($F_{(12,276)} = 6.67$, $p < 0.01$, $\eta_p^2 = 0.22$). The power in the global rhythms (4.55 Hz and 9.10 Hz) was greater when the auditory stimuli were attended, greater in the *Attend Auditory* than *Attend Visual*.

DISCUSSION

The current study varied rhythmic attention to two non-overlapping tone feature patterns to investigate how memory would represent sound patterns when multiple rhythmic interpretations could be perceived from a single sound stream. Although we expected that attending to one rhythm to perform a task would dampen the brain's response to the alternate rhythm, we found this not to be true. Evidence from neural entrainment to the target rhythm (the standard pattern) and by MMN elicited to pattern violations (deviance detection) demonstrated that both intensity and duration rhythms were maintained in memory irrespective of the direction of attention. The normalized power to the attended rhythm was not differentiated from the unattended rhythm and MMNs were elicited by pattern violations in the attended and unattended rhythms. Thus, attention to one pattern did not modulate the representation of the unattended, distracting pattern. Both patterns were tracked simultaneously in memory despite task goals.

Attention Effects and Multitasking

The presence of MMN, elicited by both of the pattern deviants, indicates that both feature patterns were distinctly represented in working memory. There were no amplitude differences in the MMN elicited in the *Attend Auditory* condition by attended targets and unattended auditory pattern deviants, and the *Attend Visual* condition to unattended deviants for both feature patterns. The MMN amplitude was larger for the intensity pattern deviants, suggesting the intensity task was either easier or more physically discriminable than the duration pattern deviants (Näätänen and Alho, 1995). Based on research with bistable visual stimuli, one might expect that maintaining one feature pattern to perform a task could suppress representation of the other feature pattern, to minimize task interference. However, that did not appear to be the case. Performing one task did not result in suppression of the alternative percept as MMNs were elicited by both attended feature pattern targets and by unattended feature pattern deviants. These results differ from our previous study (Costa-Faidella et al., 2017) that used a similar paradigm and found enhanced power to the attended rhythm compared to the unattended rhythm. However, there were some distinct differences that may explain the difference in our results. First, the Costa-Faidella et al. (2017) study did not use a switching paradigm, participants performed the same task in blocks of 12 trials before switching to another task. Second, the task did not involve pattern detection. Participants counted the number of stimuli occurring in the block. Finally, there were no pattern violations in the attended or unattended patterns. Selective entrainment was calculated based on tracking the attended pattern. Thus, one explanation for finding representation of both feature patterns (without enhancement of the attended) is that this was a switching task with participants alternating randomly 50–50% between doing the intensity pattern and duration pattern tasks within each stimulus block. As such, both percepts had to be "active" to efficiently perform the tasks when the unexpected visual cue instructed which pattern to attend to and detect deviants. Another explanation is that the pattern deviants themselves may have evoked some attentional (passive) awareness to the unattended pattern, which may have negated any enhancement to the attended. That is, the brain was multitasking between attended and unattended pattern deviance detection (Miller et al., 2015; Sussman, 2017; Symonds et al., 2020; Brace and Sussman, 2021).

One of the goals was to evaluate how attention modified sound representations of the standards and deviants. Thus, in addition to analyzing the brain response to the unattended standard and unattended deviant patterns when attention was directed to one of the two, we also recorded the brain response when attention was directed to watching a movie and neither pattern was attended, the sounds were irrelevant to the task. We expected to find a difference between the unattended feature patterns when comparing the *Attend Auditory* and *Attend Visual* conditions. However, this was not the case. Having no task with the sounds did not dampen the response to the unattended sounds compared to when one sound feature was attended, and one sound feature unattended. This indicates that attention to the sounds is not necessary for the two feature patterns to be simultaneously tracked and represented in working memory. MMNs of similar amplitudes and latencies were elicited by both of the unattended feature pattern deviants and entrainment to the individual rhythms was maintained in the *Attend Visual* condition. However, some further exploration may clarify the difference between having fluctuation in frequency, duration, and intensity occur simultaneously or

sequentially. In this experiment, we varied frequency, duration, and intensity parameters in sequential patterns of sounds. In realistic scenarios sounds sometimes vary simultaneously along multiple dimensions such as envelope, location, and other spectral components. Future studies may address how the auditory system tracks sequential vs. simultaneous variations of the auditory features.

Neural Entrainment

We were initially surprised to find no task-dependent enhancement of the target rhythm frequencies based on previous studies (Mesgarani and Chang, 2012; Costa-Faidella et al., 2017). The relative power to the individual feature rhythms did not differ for any of the attentional manipulations and there was no enhancement or suppression based on switch and repeat trials. It was clear through the rhythmic entrainment to the standard patterns, however, that there was maintenance of both simultaneously. This maintenance of the standard for both feature patterns is consistent with the MMN results of the study, with MMN amplitudes elicited by pattern deviants similarly to both patterns regardless of task demands. From this perspective, it is not surprising that both standard rhythms were similarly represented with equal power, unrelated to task demands. That is, finding entrainment to the rhythm of both standard patterns is consistent with finding MMNs elicited by attended and unattended pattern deviants.

Switch vs. Repeat Trials

HR was higher and RT shorter to the first target of the trial and higher after a task switch compared to the first target of the repeated trial. This is somewhat surprising on the surface based on task switching paradigms that commonly report a switching cost, lower HR, and longer RT, to the first trials after a task switch. However, our paradigm has not previously been used before and there are some differences that may distinguish the type of attention needed for preparing to perform one task or the other. A cue is provided to initiate the task that is then repeated through several trials before another cue is presented to either repeat or switch the task set. Thus, vigilance at the beginning of the trial may be greater when switching task is set than when repeating. This may explain why the initial trial of the repeat blocks showed a performance "cost." The readiness may have been biased toward switching tasks whenever a visual cue was presented and maintaining the task set may have taken more adjustment time. Another possibility is that because it is a bistable stimulus sequence, one sequence can be perceived in two different ways depending on what you focus on, maintaining one of the two possible percepts may take more effort if there is a propensity for spontaneous switching during the presentation of a seconds-long sequence. In this view, switching tasks would be easier to do than maintaining the previous task because maintaining one perceptual organization involves overcoming the propensity to switch to the other percept. This might have resulted in a longer RT or more missed trials for repeat trials. Performing the same task repeatedly with bistable stimuli may be more difficult than switching between the two percepts when the stimuli are ambiguous (Denham et al., 2013).

Another explanation addresses the difference in processing between the cue and the task (Allport and Wylie, 1999; Grange and Houghton, 2010). For the current paradigm, the time interval from the visual cue to the first target may be long enough that there is no interference between processing the cue and the time it takes participants to switch task sets. The silent period between trials may also have facilitated the ease of switching tasks. Additionally, the P3b amplitude did not distinguish switch vs. repeat trials, which may be consistent with the distinction between these phases, with no task interference. The P3b amplitude differed between tasks, with a smaller P3b amplitude for the intensity task, consistent with the interpretation that the intensity task was easier than the duration task and thus required less effort to perform (Kok, 2001).

CONCLUSION

The most critical finding of this experiment, shown by evidence from the standard and the deviant patterns, was that multiple, independent sound feature patterns (duration and intensity) were processed simultaneously despite the deployment of attention to task switching, task repeating, or watching a movie. The two neural indices that demonstrated this were: (1) neural entrainment to the standard patterns; and (2) the MMN components elicited by pattern deviants. Neural representations were similarly robust despite the direction of attention or task load. Normalized power to the rhythm of the standard attended feature patterns was similar to the rhythm of the standard unattended feature patterns. Additionally, the MMN was elicited by task-based feature pattern deviants with a similar amplitude as MMNs elicited by unattended feature patterns that were unattended because they were not the target pattern or because the participant ignored the sounds and watched a movie. Thus, the present data demonstrate a high level of adaptability and flexibility of the auditory system to navigate complex scenes when there are competing sound events. Results suggest a type of "multitasking" of the auditory system between attended and unattended sounds. That is, attending to one sound event does not negate representation of other sound events. This ability to track both attended and unattended regularities may be a crucial process involved in task-switching in complex sound environments.

DATA AVAILABILITY STATEMENT

The raw data supporting the conclusions of this article will be made available by the authors, without undue reservation.

ETHICS STATEMENT

The study was carried out in accordance with the Code of Ethics of the World Medical Association (Declaration of Helsinki). Written consent was obtained from all participants after the study was explained to them. The protocol and informed consent documents were approved by the Institutional Review Board at

Albert Einstein College of Medicine, Bronx, NY where the study was conducted.

AUTHOR CONTRIBUTIONS

KB: conceptualization, data curation, formal analysis, investigation, methodology, and writing—original draft. ES: conceptualization, formal analysis, funding acquisition, methodology, supervision, visualization, writing—review and editing. All authors contributed to the article and approved the submitted version.

FUNDING

This work was supported by the National Institutes of Health (NIH) (grant #R01 DC004263) and by the National Institute of General Medical Sciences (NIGMS) Medical Scientist Training Program grant (T32GM007288). The content is the sole responsibility of the authors and does not necessarily represent the views of the NIH. This work was submitted in partial fulfillment of the requirements for the degree of Doctor of Philosophy in the Graduate Division of Medical Sciences, Albert Einstein College of Medicine, New York (KB).

ACKNOWLEDGMENTS

We thank Jean DeMarco for assistance with data collection.

SUPPLEMENTARY MATERIALS

The Supplementary Material for this article can be found online at: https://www.frontiersin.org/articles/10.3389/fnhum.2021.747769/full#supplementary-material.

REFERENCES

Allport, A., and Wylie, G. (1999). "Task-switching: positive and negative priming of task-set," in *Attention, Space and Action: Studies in cognitive neuroscience*, eds G. W. Humphreys, J. Duncan, and A. Treisman (Oxford: Oxford University Press.), 273–296.

Beauvois, M. W., and Meddis, R. (1997). Time decay of auditory stream biasing. *Percept. Psychophys.* 59, 81–86. doi: 10.3758/bf03206850

Bishop, G. H. (1932). Cyclic changes in excitability of the optic pathway of the rabbit. *Am. J. Physiol.* 103, 213–224. doi: 10.1152/ajplegacy.1932.103.1.213

Brace, K. M., and Sussman, E. S. (2021). The role of attention and explicit knowledge in perceiving bistable auditory input. *Psychophysiology* 58:e13875. doi: 10.1111/psyp.13875

Bregman, A. S. (1990). *Auditory Scene Analysis: the Perceptual Organization of Sound*. Cambridge, MA: MIT Press.

Calderone, D. J., Lakatos, P., Butler, P. D., and Castellanos, F. X. (2014). Entrainment of neural oscillations as a modifiable substrate of attention. *Trends Cogn. Sci.* 18, 300–309. doi: 10.1016/j.tics.2014.02.005

Costa-Faidella, J., Sussman, E. S., and Escera, C. (2017). Selective entrainment of brain oscillations drives auditory perceptual organization. *Neuroimage* 159, 195–206. doi: 10.1016/j.neuroimage.2017.07.056

Denham, S. L., Gyimesi, K., Stefanics, G., and Winkler, I. (2013). Perceptual bistability in auditory streaming: How much do stimulus features matter? *Learn. Percept.* 5, 73–100. doi: 10.1556/lp.5.2013.suppl2.6

Dowling, W. J., Lung, K. M. T., and Herrbold, S. (1987). Aiming attention in pitch and time in the perception of interleaved melodies. *Percept. Psychophys.* 41, 642–656. doi: 10.3758/bf03210496

Draganova, R., Ross, B., Borgmann, C., and Pantev, C. (2002). Auditory cortical response patterns to multiple rhythms of AM sound. *Ear Hear.* 23, 254–265. doi: 10.1097/00003446-200206000-00009

Elhilali, M., Xiang, J., Shamma, S. A., and Simon, J. Z. (2009). Interaction between attention and bottom-up saliency mediates the representation of foreground and background in an auditory scene. *PLoS Biol.* 7:e1000129. doi: 10.1371/journal.pbio.1000129

Grange, J. A., and Houghton, G. (2010). Cue-switch costs in task-switching: cue priming or control processes? *Psychol. Res.* 74, 481–490. doi: 10.1007/s00426-009-0270-y

Isreal, J. B., Chesney, G. L., Wickens, C. D., and Donchin, E. (1980). P300 and tracking difficulty: evidence for multiple resources in dual-task performance. *Psychophysiology* 17, 259–273. doi: 10.1111/j.1469-8986.1980.tb00146.x

Kok, A. (2001). On the utility of P3 amplitude as a measure of processing capacity. *Psychophysiology* 38, 557–577. doi: 10.1017/s0048577201990559

Lakatos, P., Karmos, G., Mehta, A. D., Ulbert, I., and Schroeder, C. E. (2008). Entrainment of neuronal attentional selection. *Science* 320, 110–113. doi: 10.1126/science.1154735

Lakatos, P., Musacchia, G., O'Connel, M. N., Falchier, A. Y., Javitt, D. C., and Schroeder, C. E. (2013). The spectrotemporal filter mechanism of auditory selective attention. *Neuron* 77, 750–761. doi: 10.1016/j.neuron.2012.11.034

Large, E. W., and Jones, M. R. (1999). The dynamics of attending: How people track time-varying events. *Psychol. Rev.* 106, 119–159. doi: 10.1037/0033-295X.106.1.119

Mesgarani, N., and Chang, E. F. (2012). Selective cortical representation of attended speaker in multi-talker speech perception. *Nature* 485, 233–236. doi: 10.1038/nature11020

Miller, T., Chen, S., Lee, W. W., and Sussman, E. S. (2015). Multitasking: effects of processing multiple auditory feature patterns. *Psychophysiology* 52, 1140–1148. doi: 10.1111/psyp.12446

Moldwin, T., Schwartz, O., and Sussman, E. S. (2017). Statistical learning of melodic patterns influences the brain's response to wrong notes. *J. Cogn. Neurosci.* 29, 2114–2122. doi: 10.1162/jocn_a_01181

Näätänen, R., and Alho, K. (1995). Mismatch negativity—a unique measure of sensory processing in audition. *Int. J. Neurosci.* 80, 317–337. doi: 10.3109/00207459508986107

Näätänen, R., Tervaniemi, M., Sussman, E., Paavilainen, P., and Winkler, I. (2001). 'Primitive intelligence' in the auditory cortex. *Trends Neurosci.* 24, 283–288. doi: 10.1016/s0166-2236(00)01790-2

Norman, D. A., and Bobrow, D. G. (1975). On data-limited and resource-limited processes. *Cogn. Psychol.* 7, 44–64. doi: 10.1016/0010-0285(75)90004-3

Paavilainen, P. (2013). The mismatch-negativity (MMN) component of the auditory event-related potential to violations of abstract regularities: a review. *Int. J. Psychophysiol.* 88, 109–123. doi: 10.1016/j.ijpsycho.2013.03.015

Pannese, A., Herrmann, C. S., and Sussman, E. (2015). Analyzing the auditory scene: neurophysiologic evidence of a dissociation between detection of regularity and detection of change. *Brain Topogr.* 28, 411–422. doi: 10.1007/s10548-014-0368-4

Picton, T. W., Alain, C., Otten, L., Ritter, W., and Achim, A. (2000). Mismatch negativity: different water in the same river. *Audiol. Neurootol.* 5, 111–139. doi: 10.1159/000013875

Schroeder, C. E., and Lakatos, P. (2009). Low-frequency neuronal oscillations as instruments of sensory selection. *Trends Neurosci.* 32, 9–18. doi: 10.1016/j.tins.2008.09.012

Schröger, E., Näätänen, R., and Paavilainen, P. (1992). Event-related potentials reveal how non-attended complex sound patterns are represented by the human brain. *Neurosci. Lett.* 146, 183–186. doi: 10.1016/0304-3940(92)90073-g

Sussman, E. S. (2007). A new view on the MMN and attention debate the role of context in processing auditory events. *J. Psychophysiol.* 21, 164–175. doi: 10.1027/0269-8803.21.34.164

Sussman, E. S. (2017). Auditory scene analysis: an attention perspective. *J. Speech Lang. Hear. Res.* 60, 2989–3000. doi: 10.1044/2017_JSLHR-H-17-0041

Sussman, E. S., Bregman, A. S., and Lee, W. W. (2014). Effects of task-switching on neural representations of ambiguous sound input. *Neuropsychologia* 64, 218–229. doi: 10.1016/j.neuropsychologia.2014.09.039

Sussman, E., Ritter, W., and Vaughan, H. G., Jr. (1998). Predictability of stimulus deviance and the mismatch negativity. *Neuroreport* 9, 4167–4170. doi: 10.1097/00001756-199812210-00031

Symonds, R. M., Zhou, J. W., Cole, S. L., Brace, K. M., and Sussman, E. S. (2020). Cognitive resources are distributed among the entire auditory landscape in auditory scene analysis. *Psychophysiology* 57:e13487. doi: 10.1111/psyp.13487

Takegata, R., Paavilainen, P., Näätänen, R., and Winkler, I. (2001). Preattentive processing of spectral, temporal and structural characteristics of acoustic regularities: a mismatch negativity study. *Psychophysiology* 38, 92–98. doi: 10.1017/S0048577201991243

Tiitinen, H., Alho, K., Huotilainen, M., Ilmoniemi, R. J., Simola, J., and Näätänen, R. (1993). Tonotopic auditory cortex and the magnetoencephalographic (MEG) equivalent of the mismatch negativity. *Psychophysiology* 30, 537–540. doi: 10.1111/j.1469-8986.1993.tb02078.x

Winkler, I., Teder-Sälejärvi, W. A., Horváth, J., Näätänen, R., and Sussman, E. (2003). Human auditory cortex tracks task-irrelevant sound sources. *Neuroreport* 14, 2053–2056. doi: 10.1097/00001756-200311140-00009

Xiang, J., Simon, J., and Elhilali, M. (2010). Competing streams at the cocktail party: exploring the mechanisms of attention and temporal integration. *J. Neurosci.* 30, 12084–12093. doi: 10.1523/JNEUROSCI.0827-10.2010

Conflict of Interest: The authors declare that the research was conducted in the absence of any commercial or financial relationships that could be construed as a potential conflict of interest.

Publisher's Note: All claims expressed in this article are solely those of the authors and do not necessarily represent those of their affiliated organizations, or those of the publisher, the editors and the reviewers. Any product that may be evaluated in this article, or claim that may be made by its manufacturer, is not guaranteed or endorsed by the publisher.

frontiers in Human Neuroscience

MINI REVIEW
published: 05 November 2021
doi: 10.3389/fnhum.2021.704668

Sensory Attenuation in the Auditory Modality as a Window Into Predictive Processing

*Fabian Kiepe, Nils Kraus and Guido Hesselmann**

Psychologische Hochschule Berlin (PHB), Berlin Psychological University, Berlin, Germany

Self-generated auditory input is perceived less loudly than the same sounds generated externally. The existence of this phenomenon, called Sensory Attenuation (SA), has been studied for decades and is often explained by motor-based forward models. Recent developments in the research of SA, however, challenge these models. We review the current state of knowledge regarding theoretical implications about the significance of Sensory Attenuation and its role in human behavior and functioning. Focusing on behavioral and electrophysiological results in the auditory domain, we provide an overview of the characteristics and limitations of existing SA paradigms and highlight the problem of isolating SA from other predictive mechanisms. Finally, we explore different hypotheses attempting to explain heterogeneous empirical findings, and the impact of the Predictive Coding Framework in this research area.

Keywords: sensory attenuation, predictive processing, temporal control, temporal prediction, identity prediction, sense of agency (SoA)

OPEN ACCESS

Edited by:
István Winkler, Hungarian Academy of Sciences (MTA), Hungary

Reviewed by:
Maria Pyasik, University of Verona, Italy
Bence Neszmélyi, Hungarian Academy of Sciences (MTA), Hungary

****Correspondence:***
Guido Hesselmann
g.hesselmann@gmail.com

Specialty section:
This article was submitted to Cognitive Neuroscience, a section of the journal Frontiers in Human Neuroscience

Received: *03 May 2021*
Accepted: *14 October 2021*
Published: *05 November 2021*

Citation:
Kiepe F, Kraus N and Hesselmann G (2021) Sensory Attenuation in the Auditory Modality as a Window Into Predictive Processing. Front. Hum. Neurosci. 15:704668. doi: 10.3389/fnhum.2021.704668

INTRODUCTION

Sensory Attenuation (SA) describes the phenomenon that self-initiated sensory input is perceived with a lesser intensity than the same sensations generated externally (Hughes et al., 2013a; Pyasik et al., 2021). While many of us might have caught ourselves not noticing repeatedly clicking a ballpoint pen or tipping on the table, we perceive those sounds as noisy and intrusive when generated by another person (Klaffehn et al., 2019). The ability to differentiate one's own action-related auditory signals from externally generated sounds not only aids movement coordination but can also inform us of potential threats (Myers et al., 2020).

For the scope of this review, we will focus on two major approaches that have been brought forward in order to explain SA following self-initiated action. Classical forward models of SA (Blakemore et al., 1999, 2002; Synofzik et al., 2008) propose that for self-initiated actions, the designated structures of the motor system are in constant exchange with each other, not only generating motor commands but also creating efference copies of these commands. These efference copies allow the brain to predict the resulting changes in sensory inputs caused by the intended behavior and subsequently subtract predicted from actual changes in sensory inputs, canceling out the sensory consequences of self-initiated behavior (Bays et al., 2008). The proposed main function of SA in these models is to anticipate and cancel the sensory effects of movement (Miall and Wolpert, 1996), thereby enabling the differentiation of self-initiated from externally caused changes in sensory inputs. Depending on the specific implementation

of forward models, this information is subsequently used to make attributional judgments and facilitate a sense of agency (e.g., Synofzik et al., 2008). However, in recent years this view of SA has been challenged by applications of the broader theory of predictive processing.

PREDICTIVE PROCESSING

Predictive processing suggests that, not only for self-generated action but in general, we constantly make use of prior information in order to generate predictions about upcoming changes in sensory input in the form of a generative model (Friston et al., 2016). Possible deviations in actual sensory evidence from the predicted inputs (prediction errors) are used to update the current model and inform predictions in subsequent processing. This continuous Bayesian updating scheme enables inference of hidden states causing changes in the environment by comparing changes in predicted with actually detected sensory inputs, providing the basis for intero- as well as exteroception (Seth et al., 2012). During this process, the brain is constantly aiming at maximizing model evidence (i.e., to increase the utility of the predictive model) by minimizing prediction error and surprise. Further, the principle of active inference within predictive processing states that motor behavior plays an important role in achieving this (Parr et al., 2021). Self-initiated action herein serves the purpose of altering one's physical surroundings so that received sensory inputs match the predicted ones, thereby minimizing prediction errors. By informing involved systems about the desired state, predictions are the driving force for resulting self-initiated movements. Beforehand, however, there is a crucial time interval wherein the predicted outcome and the actual sensory input are yet to match. During this period, the signals stemming from self-initiated behavior are attenuated, signaling that these stimuli stem from self-actions (Aru, 2019). SA specifically would arise from lowering the precision of anticipated sensory events, being equivalent to drawing away attentional resources from these inputs (Brown et al., 2013).

The differences in the two portrayed explanatory frameworks may seem negligible when trying to explain everyday phenomena of sensory attenuation, but they bear important implications for the explanation of partially conflicting results in scientific research on SA. It is important to note that the two models make different assumptions over the function of SA in auditory perception. In forward models, SA enables the differentiation between externally and internally caused sensory signals. Information from motor regions in the brain is, therefore, a necessary condition for SA in forward models, since all self-generated auditory signals will be caused by motor activity. However, in predictive processing, motor information is only the expected precision (i.e., predictability) of a stimulus rendering it valuable in further processing (Friston, 2013). Therefore, predictive processing would imply attenuation of all anticipated sensory stimuli, independent of whether a self-initiated motor response was the perceived cause. Note, however, that an internally planned motor response is an especially reliable source of information rendering its anticipated auditory consequences unusually precise, thus facilitating SA. It follows that SA would be present in all expected stimuli but especially pronounced in expected self-generated ones.

In contrast to forward models, predictive coding does not conceive SA as a result of reafference cancellation. Rather, attenuation of expected signals is a logical conclusion from the imperative to minimize surprise and allocate attention and processing resources to unexpected stimuli since those are most effective in model updating. Importantly, this framework stresses the usefulness of predictive information on self-generated movements in creating a sense of agency (Kahl and Kopp, 2018). It does, however, not imply that sensory attenuation would necessarily follow from this. Looking at forward models, on the other hand, it is not apparent why self-generated signals should be attenuated, rather than amplified or distorted in any other fashion, since the predictive signal mainly serves the function of enabling differentiation between self and other. SA alone is likely insufficient in providing this information since an attenuated self-generated stimulus is subjectively hardly distinguishable from the same externally produced stimulus presented with less intensity (Burin et al., 2017). Alternatively, in order to differentiate between self and other generated stimuli, the perceptual systems could rely on a sense of *otherness*, as is present when hearing ones' own voice on tape, rather than attenuated processing.

In what follows, we will try to further disentangle the specific implications of both explanatory approaches and identify the strengths and weaknesses by comparing their potential to explain several recent empirical findings. Note that reasons for contradicting results might also stem from the wide variety of methods used, as well as from the lack of a single coherent theoretical framework.

STUDYING SENSORY ATTENUATION IN THE AUDITORY DOMAIN

Typical setups in behavioral SA research consist of a two-phase comparison task that either contains an externally triggered stimulus or a self-initiated stimulus (**Figure 1**). This stimulus is then compared to a consecutive second, often identical, stimulus. For the auditory domain, the participants usually produce a sound by keypress. Consecutively, the identical stimulus reappears without the participant's action, i.e., generated by a computer or another person. Thereafter, participants must compare or rate the volume of self-initiated vs. externally generated stimuli (Reznik et al., 2015). Participants then typically rate the self-initiated sound significantly lower in volume, compared to the externally generated signal (Reznik et al., 2015; Myers et al., 2020). Attenuation effects are not only studied using subjective measurements of perception but also in neuronal recordings of early stimulus-evoked brain activity. Studies using Electroencephalogram (EEG) or magnetoencephalogram (MEG) for example do not have to rely upon delayed behavioral responses reporting subjective attenuation effects that potentially are subject to post perceptual judgment biases, but in principle offer real time measures of auditory perception. They also provide further benefit in that they offer a measure of SA in

no-report paradigms, in which participants are asked to passively perceive a (potentially cued) sound-isolating SA from effects of motor planning and execution. In EEG studies that nevertheless do involve a self-initiated action, ERPs are typically corrected for motor behavior components. Such studies have revealed a reduction in amplitude of auditory event-related potentials (ERP; N1 and P2) when initiating endogenous sounds, such as speaking or blowing air, compared to externally generated auditory stimuli (Ford et al., 2007; Mifsud and Whitford, 2017).

CONFOUNDS OF TEMPORALITY

There are mainly two temporal mechanisms influencing the effect of SA: temporal predictability and temporal control. Temporal predictability describes the ability to predict the point in time at which a sensory event will occur. Temporal control, on the other hand, defines the ability to control the time of the stimulus onset through one's own behavior (Hughes et al., 2013a). When contrasting different explanatory models for SA, empirically disentangling the respective contributions of temporal predictability and control to SA becomes an especially important tool. Predictive processing considers the predictability of a stimulus central to its potential to elicit attenuated processing, and while direct control over stimulus appearance certainly should enhance predictability, it is not conceived as a mandatory requirement for SA. Forwards models, however, posit self-initiated motor behavior as a necessary requirement for SA, while making no assumptions over the role of predictability alone.

One effective tool to manipulate temporal predictability is delaying the onset of the stimulus. Several studies have shown attenuated N1 components despite (randomized) stimulus onset delays of up to 1,000 ms, suggesting that SA is not dependent on temporal predictability alone (Lange, 2011; van Elk et al., 2014; Klaffehn et al., 2019).

Recent studies tried to further disentangle the individual contributions of temporal control and temporal predictability to SA. Kaiser and Schütz-Bosbach (2018) demonstrated that significant attenuation of N1 to an auditory stimulus takes place when it is highly predictable but not self-generated and only passively perceived. They further show that N1 is not attenuated but elevated for trials in which participants were asked to press a button in reaction to a cue (thereby self-initiating the tone) compared to when they were asked to passively perceive the same cue. This not only stresses the relative importance of predictability compared to self-initiation for SA but also illustrates the shortcomings of forward models to explain SA when no motor behavior takes place. However, Klaffehn et al. (2019) found only a small influence of temporal predictability (manipulated by a 750 ms progress bar leading up to the stimulus) on P2 but not N1 amplitudes. Looking only at self-initiated actions, N1 showed strong attenuation effects to tones that were played immediately compared to when they were temporally delayed (750 ms) and preceded by a progress bar. Moreover, by implementing cued trials (visual stimuli indicating the timing of auditory stimulus onset) and uncued trials (random visual stimuli unrelated to auditory stimulus onset or action), Harrison et al. (2021) could isolate the effects of temporal predictability and temporal control and found that both mechanisms do independently contribute to attenuation. Note that in this study, temporal control had the usual facilitating effect on SA in the P2, but looking at the N1 effect patterns were reversed with higher temporal control leading to reduced attenuation of the ERP. The authors summarize that taken together, both factors (temporal predictability and temporal control) do not sufficiently explain the observed overall effect size of SA. These findings thus further highlight the rather strong relative importance of self-initiation on SA, potentially surpassing its contribution to the temporal predictability of a stimulus alone. Establishment and replication of the finding that self-initiation contributes more to SA than facilitating the (temporal) predictability of a stimulus would question the inherent logic of predictive processing models.

CONFOUNDS OF IDENTITY PREDICTION

Identity prediction describes the ability to predict the identity of the stimulus, based on self-initiated behavior (motor-based identity prediction) or other cues (non-motor-based identity prediction; Hughes et al., 2013a). Consistent with motor-based and prediction-based models, several studies show that motor identity prediction regulates SA (Hughes et al., 2013a). As for factors of temporal predictability, the question of whether and how non-motor-based identity prediction significantly contributes to SA can help us evaluate the utility of forward models. Since in those models prediction of subsequent changes of sensory inputs is solely based on motor-based efference copies, non-motor-based identity prediction should not contribute to SA. In predictive processing theories, not only self-generated action but also external information gathered across all sensory domains contributes to the prediction of subsequent sensory inputs, rendering identity prediction a useful mechanism contributing to SA (Talsma, 2015).

By studying the effect of self-initiated action on SA in trials of varying stimulus qualities, several experiments show significantly enhanced SA for motor identity prediction. Hughes et al. (2013b), for example, taught participants specific action-sound combinations and found significantly stronger N1 attenuation for stimuli that were coherent with previously learned contingencies, compared to non-coherent action-sound combinations. Baess et al. (2008) compared trials where the pitch of self-initiated sounds was constant (1,000 Hz), and thus predictable, with trials where the pitch was randomized (400–1,990 Hz), and thus unpredictable for participants. When the identity of the sound could be predicted, SA was significantly increased, compared to when it was not. The effect could further be isolated from self-generation of the stimulus in a passive listening paradigm, where identity could only be predicted on the basis of the previous tones (non-motor-based identity prediction; Lange, 2009). This poses a challenge to classical (or, auxiliary) forward models of SA, according to which predictions are solely based on efference copies of motor commands (Pickering and Clark, 2014). According to alternative specifications of forward models, however, SA is not simply a reflection of the efference

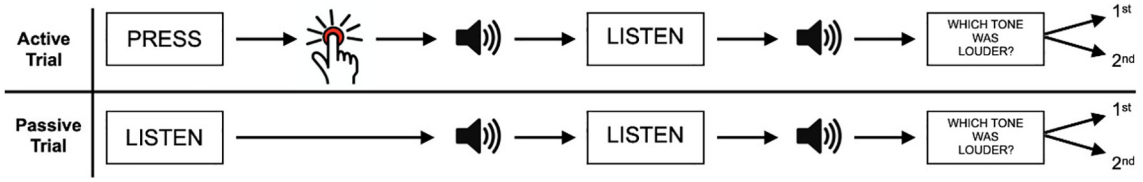

FIGURE 1 | A typical experimental setup examining sensory attenuation in the auditory paradigm. In active trials, participants have to self-initiate a sound (e.g., through a button press) and compare its volume to an externally generated sound. In passive trials, both sounds are generated externally. Adapted from Reznik et al. (2015). Copyright (2015) by Reznik et al.

copy. Specifically, the prediction of sensory outcomes in these models can be based on efference copies as well as on learned sensory associations (Pickering and Clark, 2014).

Dogge et al. (2019b), however, could only find a weak influence of identity prediction on SA, and no difference in influence between motor and non-motor identity prediction in forced choice tasks measuring different ERPs. Taken together, it seems that identity prediction, in general, can enhance SA, but cannot solely account for it. Further, motor-based identity predictions alone cannot account for the majority of the SA results (Horváth, 2015; Dogge et al., 2019b).

ATTENTION VS. PREDICTION

If SA relies entirely on motor-based prediction, attention towards a specific stimulus, which cannot be predicted, should not alter the overall effect of SA (Wiese, 2016). Indeed, several studies investigating attention-based explanations of SA suggest that attention effects may not be sufficient in explaining attenuation of self-generated actions and that both effects might be additive rather than intertwined with each other (Saupe et al., 2013). No significant differences in auditory ERP attenuation were found if attention was allocated towards non-auditory sensory input, motor behavior, or auditory stimuli (Timm et al., 2013; Neszmélyi and Horváth, 2021). However, other studies could show that attention increases sensory processing in SA paradigms, even outweighing the effects of SA in certain cases. In a sound detection task, Cao and Gross (2015) asked participants to attend to a specific target sound. Although there were no differences between the presented tones with regard to temporal predictability, attention towards a specific sound led to less SA, compared to the other tones. It is, however, difficult to disentangle the respective contributions of attention and prediction to SA, since attention generally should facilitate predictive abilities (Alink and Blank, 2021). While both mechanisms, attention and prediction, are thought to aid perception, their relationship is still up to debate (Schröger et al., 2015).

While prediction has been shown to decrease N1 and P1 components in auditory perception thus attenuating early auditory perception, attention was found to increase the perception of sensory inputs (Lange, 2013; Schröger et al., 2015). The heterogeneity of SA results, and the issues of temporality and identity prediction, might stem from difficulties in isolating these opposing mechanisms (Lange, 2013). But how do prediction and attention interact? Several studies show that attention to stimuli often results in elevated ERPs (N1 and P2) to those stimuli. However, if participants are instructed to execute a certain movement (e.g., a keypress), attention might be mainly allocated towards that action, drawing away attentional resources from subsequent perceptual processing. In auditory tasks, in which participants are instructed to solely listen and not to move, attention can be distributed fully towards the stimulus (Horváth, 2015). The heterogeneity of SA study results might thus stem from differences in attention orienting, depending on the study's design.

In a series of recent experiments, participants were instructed to press a button in a virtual environment during an auditory forced choice task. This allowed the researchers to detach tactile feedback from motor behavior (Fritz et al., 2021). Results suggest that SA for auditory stimuli only occurs if attention is oriented towards a different stimulus (e.g., tactile input deriving from the preceding movement), and away from the auditory modality. In a sound detection task by Reznik et al. (2015), the influence of sound intensity on SA was examined. Their study showed that for self-initiated tones with high intensity, the volume was attenuated. However, for self-initiated tones with low intensity, the volume was enhanced, suggesting that, for sounds with near-threshold volume, attention may be drawn towards these stimuli. Similar phenomena can also be observed in studies examining learned behavior. If certain action-stimulus combinations are learned, its perception of the stimulus is easier to predict. Therefore, attention can be oriented elsewhere. In an auditory forced choice task measuring EEG, Dogge et al. (2019b) could only observe attenuation of self-triggered stimuli if the connection between action and effect was trained properly beforehand, during a sufficient acquisition phase.

Attenuating expected stimuli at least partly dependent on the altered allocation of attention is also hypothesized in some predictive processing approaches to SA (Chennu et al., 2016; Wiese, 2016; Dogge et al., 2019a). According to predictive coding, attention is conceived as synaptic gain control, thereby regulating the precision of prediction errors at all levels of cortical processing (Chennu et al., 2016). Prediction on the other hand is thought of as top-down information flow including specific contents as well as precision, mediating the response of lower processing levels to incoming sensory evidence. These two processes would therefore be naturally interdependent,

considering that prediction can influence synaptic gain at lower processing levels to specific inputs. Note, however, that additional mechanisms have been brought forward describing how prediction could lead to SA, other than modulating attention (Schröger et al., 2015; Alink and Blank, 2021).

SENSE OF AGENCY

Another mechanism possibly influencing SA is the Sense of Agency (SoA). It describes the individual's awareness of control over self-initiated actions (Jeannerod, 2003). The efficient differentiation between internally and externally generated changes of sensory inputs might be a crucial component for the development of a coherent SoA. With disturbed agency being one of the explanations for schizophrenia symptoms, neurophysiological studies compared attenuation effects between healthy individuals and patients with diagnosed schizophrenia. They found reduced N1 attenuation for self-initiated behavior in schizophrenic patients (Ford and Mathalon, 2012).

A widely accepted connection between SA and SoA, however, has not been established yet. While SA appears to take place in low-level processing and in the first 200 ms after stimulus onset, SoA requires a higher and potentially later level of processing (Dewey and Knoblich, 2014; Wolpe and Rowe, 2014; Wen et al., 2019). Moreover, differences in study results might be explained by the difficulty of measuring SoA (Haggard and Chambon, 2012).

In a study by Timm et al. (2016), SoA was manipulated by altering learned delays for certain action-sound combinations. During an acquisition phase, participants learned that, after button press, the sound succeeds following a fixed delay (e.g., 200 ms). The test phase included trials with shortened delays (e.g., 0 ms), causing participants to perceive that the sound preceded their action, resulting in a lack of agency. Results showed that N1 attenuation for self-initiated sounds is not dependent on agency judgments. However, P2 attenuation appears to correlate with participants' SoA. Other observations underline the difficulty of placing SoA into motor-based forward models. Weiss et al. (2011) compared perceived subjective loudness of self- vs. other-initiated tones, and subdivided the trials into "interactive" and "individual" trials: interactive (1. self-generated, but other-initiated; 2. other-generated, but self-initiated) and individual (3. self-initiated and generated; 4. other-initiated and generated). During the interactive trials, the participants interacted with the experimenter (through taps on the shoulder) to trigger the stimuli. During the individual trials, there was no interaction between the participants and the experimenter. Significant differences in SA were found between all conditions including SoA (self-generated, but other initiated; other-generated, but self-initiated; self-initiated and generated) and the condition not containing SoA (other-initiated and generated), suggesting that having an SoA over specific actions affects perception. Interestingly, attenuation was strongest in the condition in which the button press was self-generated but other-initiated. This suggests that while SoA can influence SA, it might not be the only mechanism responsible for attenuation effects. Rather, it appears that an additional source informing us about incoming information (e.g., another person tapping us on our shoulder) helps us to successfully predict sensory input (Weiss et al., 2011).

Other studies showed that, although sounds were always generated by the participants themselves, there were differences in SA depending on their belief in agency. Desantis et al. (2012), for example, could show that framing participants into believing that another person triggered the stimuli had an influence on SA, although the sounds were always triggered by the participants themselves. Participants rated the volume of sounds they believed to be self-initiated as lower than the sounds they believed to be externally generated. Borhani et al. (2017) let the participants decide in which pitch range (low or high) the sound stimulus should appear, and showed that the belief of free choice alone can alter SA. These studies underpin the effects of SoA on SA, which are difficult to explain by motor-based forward models. If the motor command, and thus its efference copy, stays the same throughout all trials, there should not be differences in SA based on differences in SoA alone, according to forward models. While motor-based forward models mainly suggest SoA to be formed after stimulus onset, several studies could show that SoA can be influenced by mechanisms prior to action outcomes, like motor intention, the belief of agency, and free choice over designated action effects (Haggard and Chambon, 2012). As stated above, predictive processing additionally emphasizes the importance of predictive information for creating SoA (Kahl and Kopp, 2018). In line with the studies discussed above, this framework also omits the necessity that SA develops as a consequence of SoA, or *vice versa* (Burin et al., 2017). Rather, attenuation of expected signals may be the result of the imperative to reduce surprise and therefore reduced allocation of attention to predicted stimuli.

SUMMARY

Focusing on auditory studies, this review summarized recent developments in SA research and discussed the strengths and weaknesses of two major theoretical frameworks, forward models and predictive processing. Results of current studies examining the confounding effects of temporality indicate that while temporal predictability and control indeed influence attenuation effects, other mechanisms must be included to explain SA (Kaiser and Schütz-Bosbach, 2018; Harrison et al., 2021). Studies investigating the role of identity prediction could show SA based on learned associations rather than motor- vs. externally-generated behavior (Schröger et al., 2015; Dogge et al., 2019b). These results suggest SA to be a result of attention orienting based on the prediction that is not necessarily dependent upon motor behavior (Schröger et al., 2015; Chennu et al., 2016; Wiese, 2016; Dogge et al., 2019a). By manipulating attention orientation, multiple studies showed that, while self-initiated motor behavior is a reliable predictor, it does not necessarily lead to SA. Similarly, several studies observed the importance of cues prior to and after stimulus onset for the sense of agency and stated its impact on, but not its necessity for the development of SA.

Classical forward models depend on motor commands to predict and subsequently attenuate sensory inputs, thereby

giving the agent the possibility to differentiate between self- and other generated stimuli, and thus facilitating a sense of agency. These models cannot account for several phenomena of SA that were observed independent from motor behavior, the strong role of attention in SA, as well as the influence of agency beliefs on SA prior to stimulus onset. Predictive processing, on the other hand, states that we constantly make use of prior information, either self- or externally-generated, in order to create predictions about upcoming changes in sensory input in the form of a generative model (Friston et al., 2016). In this framework, only the predictability of a stimulus should determine its potential to elicit SA. This partially contradicts a consistent finding throughout the literature, namely that even when a stimulus is reliably predicted by external cues, self-generation of a motor behavior does still individually contribute a significant part to SA effects. Although self-initiated action serves as a reliable predictor for generating inferences, further research is needed to elucidate its central role in SA, leaving room for new explanatory hybrid models (Dogge et al., 2019a). Such models combine the existence of an efference-copy-based forward model with a global predictive mechanism. The forward model in this approach is still based only on motor action, potentially providing more efficient processing of contingencies that are especially reliable since they are self-initiated as well as deeply learned and reinforced over a time course of years, such as the production and perception of one's own voice. The global predictive mechanism on the other hand would provide a more flexible and adaptive tool in order to anticipate newly learned contingencies in an ever-changing environment. Further studies testing the assumption of differential processing of motor and non-motor-based predictive information is certainly needed to elucidate the utility of such hybrid models.

AUTHOR CONTRIBUTIONS

FK, NK, and GH wrote the manuscript. All authors contributed to the article and approved the submitted version.

REFERENCES

Alink, A., and Blank, H. (2021). Can expectation suppression be explained by reduced attention to predictable stimuli? *Neuroimage* 231:117824. doi: 10.1016/j.neuroimage.2021.117824

Aru, J. (2019). "From aliens to invisible limbs: the transitions that never make it into conscious experience," in*Transitions Between Consciousness and Unconsciousness*, 1st edition, G. Hesselmann (New York: Routledge), 148–162.

Baess, P., Jacobsen, T., and Schröger, E. (2008). Suppression of the auditory Nl event-related potential component with unpredictable self-initiated tones; evidence for internal forward models with dynamic stimulation. *Int. J. Psychophysiol.* 70, 137–143. doi: 10.1016/j.ijpsycho.2008.06.005

Bays, P. M., Wolpert, D. M., Haggard, E. P., Rosetti, Y., and Kawato, M. (2008). "Predictive attenuation in the perception of touch," in *Sensorimotor Foundations of Higher Cognition* (Oxford Scholarship Online), 339–358. doi: 10.1093/acprof:oso/9780199231447.003.0016

Blakemore, S. J., Frith, C. D., and Wolpert, D. M. (1999). Spatio-temporal prediction modulates the perception of self-produced stimuli. *J. Cogn. Neurosci.* 11, 551–559. doi: 10.1162/089892999563607

Blakemore, S. J., Wolpert, D. M., and Frith, C. D. (2002). Abnormalities in the awareness of action. *Trends Cogn. Sci.* 6, 237–242. doi: 10.1016/s1364-6613(02)01907-1

Borhani, K., Beck, B., and Haggard, P. (2017). Choosing, doing and controlling: implicit sense of agency over somatosensory events. *Psychol. Sci.* 28, 882–893. doi: 10.1177/0956797617697693

Brown, H., Adams, R. A., Parees, I., Edwards, M., and Friston, K. (2013). Active inference, sensory attenuation and illusions. *Cogn. Process.* 14, 411–427. doi: 10.1007/s10339-013-0571-3

Burin, D., Battaglini, A., Pia, L., Falvo, G., Palombella, M., and Salatino, A. (2017). Comparing intensities and modalities within the sensory attenuation paradigm: preliminary evidence. *J. Adv. Res.* 8, 649–653. doi: 10.1016/j.jare.2017.08.001

Cao, L., and Gross, J. (2015). Attention wins over sensory attenuation in a sound detection task. *PLoS One* 10:e0136585. doi: 10.1371/journal.pone.0136585

Chennu, S., Noreika, V., Gueorguiev, D., Shtyrov, Y., Bekinschtein, T. A., and Henson, R. (2016). Silent expectations: dynamic causal modeling of cortical prediction and attention to sounds that weren't. *J. Neurosci.* 36, 8305–8316. doi: 10.1523/JNEUROSCI.1125-16.2016

Desantis, A., Weiss, C., Schütz-Bosbach, S., and Waszak, F. (2012). Believing and perceiving: authorship belief modulates sensory attenuation. *PLoS One* 7:e37959. doi: 10.1371/journal.pone.0037959

Dewey, J. A., and Knoblich, G. (2014). Do implicit and explicit measures of the sense of agency measure the same thing? *PLoS One* 9:e110118. doi: 10.1371/journal.pone.0110118

Dogge, M., Custers, R., and Aarts, H. (2019a). Moving forward: on the limits of motor-based forward models. *Trends Cogn. Sci.* 23, 743–753. doi: 10.1016/j.tics.2019.06.008

Dogge, M., Hofman, D., Custers, R., and Aarts, H. (2019b). Exploring the role of motor and non-motor predictive mechanisms in sensory attenuation: perceptual and neurophysiological findings. *Neuropsychologia* 124, 216–225. doi: 10.1016/j.neuropsychologia.2018.12.007

Ford, J. M., and Mathalon, D. H. (2012). Anticipating the future: automatic prediction failures in schizophrenia. *Int. J. Psychophysiol.* 83, 232–239. doi: 10.1016/j.ijpsycho.2011.09.004

Ford, J. M., Roach, B. J., Faustman, W. O., and Mathalon, D. H. (2007). Synch before you speak: auditory hallucinations in schizophrenia. *Am. J. Psychiatry* 164, 458–466. doi: 10.1176/ajp.2007.164.3.458

Friston, K. (2013). Life as we know it. *J. R. Soc. Interface.* 10:20130475. doi: 10.1098/rsif.2013.0475

Friston, K., FitzGerald, T., Rigoli, F., Schwartenbeck, P., O Doherty, J., and Pezzulo, G. (2016). Active inference and learning. *Neurosci. Biobehav. Rev.* 68, 862–879. doi: 10.1016/j.neubiorev.2016.06.022

Fritz, C., Flick, M., and Zimmermann, E. (2021). Sensory attenuation for external events is produced by a competition for attentional resources. *bioRxiv* [Preprint]. 1–21. doi: 10.1101/2021.07.08.451581

Haggard, P., and Chambon, V. (2012). Sense of agency. *Curr. Biol.* 22, R390–R392. doi: 10.1016/j.cub.2012.02.040

Harrison, A. W., Mannion, D. J., Jack, B. N., Griffiths, O., Hughes, G., and Whitford, T. J. (2021). Sensory attenuation is modulated by the contrasting effects of predictability and control. *Neuroimage* 237:118103. doi: 10.1016/j.neuroimage.2021.118103

Horváth, J. (2015). Action-related auditory ERP attenuation: paradigms and hypotheses. *Brain Res.* 1626, 54–65. doi: 10.1016/j.brainres.2015.03.038

Hughes, G., Desantis, A., and Waszak, F. (2013a). Mechanisms of intentional binding and sensory attenuation: the role of temporal prediction, temporal control, identity prediction and motor prediction. *Psychol. Bull.* 139, 133–151. doi: 10.1037/a0028566

Hughes, G., Desantis, A., and Waszak, F. (2013b). Attenuation of auditory N1 results from identity-specific action-effect prediction. *Eur. J. Neurosci.* 37, 1152–1158. doi: 10.1111/ejn.12120

Jeannerod, M. (2003). The mechanism of self-recognition in human. *Behav. Brain Res.* 142, 1–15. doi: 10.1016/s0166-4328(02)00384-4

Kahl, S., and Kopp, S. (2018). A predictive processing model of perception and action for self-other distinction. *Front. Psychol.* 9:2421. doi: 10.3389/fpsyg.2018.02421

Kaiser, J., and Schütz-Bosbach, S. (2018). Sensory attenuation of self-produced signals does not rely on self-specific motor predictions. *Eur. J. Neurosci.* 47, 1303–1310. doi: 10.1111/ejn.13931

Klaffehn, A. L., Baess, P., Kunde, W., and Pfister, R. (2019). Sensory attenuation prevails when controlling for temporal predictability of self- and externally generated tones. *Neuropsychologia* 132:107145. doi: 10.1016/j.neuropsychologia.2019.107145

Lange, K. (2009). Brain correlates of early auditory processing are attenuated by expectations for time and pitch. *Brain Cogn.* 69, 127–137. doi: 10.1016/j.bandc.2008.06.004

Lange, K. (2011). The reduced N1 to self-generated tones: an effect of temporal predictability? *Psychophysiology* 48, 1088–1095. doi: 10.1111/j.1469-8986.2010.01174.x

Lange, K. (2013). The ups and downs of temporal orienting: a review of auditory temporal orienting studies and a model associating the heterogeneous findings on the auditory N1 with opposite effects of attention and prediction. *Front. Hum. Neurosci.* 7:263. doi: 10.3389/fnhum.2013.00263

Miall, R. C., and Wolpert, D. M. (1996). Forward models for physiological motor control. *Neural Netw.* 9, 1265–1279. doi: 10.1016/s0893-6080(96)00035-4

Mifsud, N. G., and Whitford, T. J. (2017). Sensory attenuation of self-initiated sounds maps onto habitual associations between motor action and sound. *Neuropsychologia* 103, 38–43. doi: 10.1016/j.neuropsychologia.2017.07.019

Myers, J. C., Mock, J. R., and Golob, E. J. (2020). Sensorimotor integration can enhance auditory perception. *Sci. Rep.* 10:1496. doi: 10.1038/s41598-020-58447-z

Neszmélyi, B., and Horváth, J. (2021). Action-related auditory ERP attenuation is not modulated by action effect relevance. *Biol. Psychol.* 161:108029. doi: 10.1016/j.biopsycho.2021.108029

Parr, T., Limanowski, J., Rawji, V., and Friston, K. (2021). The computational neurology of movement under active inference. *Brain* 144, 1799–1818. doi: 10.1093/brain/awab085

Pickering, M. J., and Clark, A. (2014). Getting ahead: forward models and their place in cognitive architecture. *Trends Cogn. Sci.* 18, 451–456. doi: 10.1016/j.tics.2014.05.006

Pyasik, M., Ronga, I., Burin, D., Salatino, A., Sarasso, P., Garbarini, F., et al. (2021). I'm a believer: illusory self-generated touch elicits sensory attenuation and somatosensory evoked potentials similar to the real self-touch. *Neuroimage* 229:117727. doi: 10.1016/j.neuroimage.2021.117727

Reznik, D., Henkin, Y., Levy, O., and Mukamel, R. (2015). Perceived loudness of self-generated sounds is differentially modified by expected sound intensity. *PLoS One* 10:e0127651. doi: 10.1371/journal.pone.0127651

Saupe, K., Widmann, A., Trujillo-Barreto, N. J., and Schröger, E. (2013). Sensorial suppression of self-generated sounds and its dependence on attention. *Int. J. Psychophysiol.* 90, 300–310. doi: 10.1016/j.ijpsycho.2013.09.006

Schröger, E., Marzecová, A., and SanMiguel, I. (2015). Attention and prediction in human audition: a lesson from cognitive psychophysiology. *Eur. J. Neurosci.* 41, 641–664. doi: 10.1111/ejn.12816

Seth, A. K., Suzuki, K., and Critchley, H. D. (2012). An interoceptive predictive coding model of conscious presence. *Front. Psychol.* 2:395. doi: 10.3389/fpsyg.2011.00395

Synofzik, M., Vosgerau, G., and Newen, A. (2008). Beyond the comparator model: a multifactorial two-step account of agency. *Conscious. Cogn.* 17, 219–239. doi: 10.1016/j.concog.2007.03.010

Talsma, D. (2015). Predictive coding and multisensory integration: an attentional account of the multisensory mind. *Front. Integr. Neurosci.* 9:19. doi: 10.3389/fnint.2015.00019

Timm, J., SanMiguel, I., Saupe, K., and Schröger, E. (2013). The N1-suppression effect for self-initiated sounds is independent of attention. *BMC Neurosci.* 14:2. doi: 10.1186/1471-2202-14-2

Timm, J., Schönwiesner, M., Schröger, E., and SanMiguel, I. (2016). Sensory suppression of brain responses to self-generated sounds is observed with and without the perception of agency. *Cortex* 80, 5–20. doi: 10.1016/j.cortex.2016.03.018

van Elk, M., Salomon, R., Kannape, O., and Blanke, O. (2014). Suppression of the N1 auditory evoked potential for sounds generated by the upper and lower limbs. *Biol. Psychol.* 102, 108–117. doi: 10.1016/j.biopsycho.2014.06.007

Weiss, C., Herwig, A., and Schütz-Bosbach, S. (2011). The self in social interactions: sensory attenuation of auditory action effects is stronger in interactions with others. *PLoS One* 6:e22723. doi: 10.1371/journal.pone.0022723

Wen, W., Kuroki, Y., and Asama, H. (2019). The sense of agency in driving automation. *Front. Psychol.* 10:2691. doi: 10.3389/fpsyg.2019.02691

Wiese, W. (2016). Action is enabled by systematic misrepresentations. *Erkenntnis* 82, 1233–1252. doi: 10.1007/s10670-016-9867-x

Wolpe, N., and Rowe, J. B. (2014). Beyond the "urge to move": objective measures for the study of agency in the post-Libet era. *Front. Hum. Neurosci.* 8:450. doi: 10.3389/fnhum.2014.00450

Conflict of Interest: The authors declare that the research was conducted in the absence of any commercial or financial relationships that could be construed as a potential conflict of interest.

Publisher's Note: All claims expressed in this article are solely those of the authors and do not necessarily represent those of their affiliated organizations, or those of the publisher, the editors and the reviewers. Any product that may be evaluated in this article, or claim that may be made by its manufacturer, is not guaranteed or endorsed by the publisher.

frontiers in Human Neuroscience

PERSPECTIVE
published: 19 November 2021
doi: 10.3389/fnhum.2021.721574

The Adaptation Model Offers a Challenge for the Predictive Coding Account of Mismatch Negativity

*Patrick J. C. May**

Department of Psychology, Lancaster University, Lancaster, United Kingdom

An unpredictable stimulus elicits a stronger event-related response than a high-probability stimulus. This differential in response magnitude is termed the mismatch negativity (MMN). Over the past decade, it has become increasingly popular to explain the MMN terms of predictive coding, a proposed general principle for the way the brain realizes Bayesian inference when it interprets sensory information. This perspective article is a reminder that the issue of MMN generation is far from settled, and that an alternative model in terms of adaptation continues to lurk in the wings. The adaptation model has been discounted because of the unrealistic and simplistic fashion in which it tends to be set up. Here, simulations of auditory cortex incorporating a modern version of the adaptation model are presented. These show that locally operating short-term synaptic depression accounts both for adaptation due to stimulus repetition and for MMN responses. This happens even in cases where adaptation has been ruled out as an explanation of the MMN (e.g., in the stimulus omission paradigm and the multi-standard control paradigm). Simulation models that would demonstrate the viability of predictive coding in a similarly multifaceted way are currently missing from the literature, and the reason for this is discussed in light of the current results.

Keywords: adaptation, auditory cortex, mismatch negativity, MMN, N1, predictive coding, stimulus omission

OPEN ACCESS

Edited by:
Marta I. Garrido,
The University of Melbourne, Australia

Reviewed by:
Chun-Yu Tse,
City University of Hong Kong,
Hong Kong SAR, China
Alessandro Tavano,
Max Planck Institute, Germany

***Correspondence:**
Patrick J. C. May
p.may1@lancaster.ac.uk

Specialty section:
This article was submitted to Cognitive Neuroscience, a section of the journal Frontiers in Human Neuroscience

Received: *07 June 2021*
Accepted: *11 October 2021*
Published: *19 November 2021*

Citation:
May PJC (2021) The Adaptation Model Offers a Challenge for the Predictive Coding Account of Mismatch Negativity. Front. Hum. Neurosci. 15:721574. doi: 10.3389/fnhum.2021.721574

INTRODUCTION

Change detection in the brain is studied by using the oddball paradigm where sporadically presented deviant stimuli are mixed in among often-repeating standard stimuli. The brain tends to respond weakly to standards and vigorously to deviants. In event-related potential (ERP) and field (ERF) measurements, the mismatch negativity (MMN) is defined as the difference in the respective responses elicited by deviants and standards. Despite the simplicity of this technical definition, there is nothing simple nor self-evident about the MMN. This is because it reflects two fundamental aspects of brain function: the flair for representing the world in terms of patterns, and the ability to pick out pattern-breaking events that carry the promise of salience. Butler (1968) originally described the differential between the standard and deviant N1 ("V") responses and explained in terms of neuronal habituation which selectively suppresses those neurons tuned to the standard. Näätänen et al. (1978) named this differential the MMN and suggested that it reflects the operation of sensory memory. Näätänen (1990, 1992) proposed a model of two-tier processing where the adherence of the stimulus to a repeating pattern is evaluated in a dedicated MMN generator, and where the suppression of the N1 happens in a separate generator which registers stimulus

onsets. A rival explanation, the so-called adaptation model, is similar to Butler's interpretation and suggests that suppressive effects within auditory cortex can account for the MMN and that the MMN is part of a modulated N1 response (May et al., 1999, 2015; Jääskeläinen et al., 2004; May and Tiitinen, 2010; Fishman, 2014). It is unclear what the physiological mechanisms of cortical adaptation/suppression are, but a likely candidate is short-term synaptic depression, STSD (Wehr and Zador, 2003, 2005). This has decay times up to several seconds, which coincides with the time constants of stimulus-specific adaptation (SSA) measured intracortically (Ulanovsky et al., 2003, 2004).

The MMN has edged its way toward mainstream neuroscience, helped along by its new-found role as a prime specimen of predictive coding (PC). This posits that perception is essentially an inference problem which the brain solves by constructing "generative models" to explain the causes of the sensory input (Rao and Ballard, 1999; Friston, 2005, 2010; Bastos et al., 2012). Such models sit at the top of the brain's processing hierarchy and generate prediction signals that are passed down the hierarchy. At each level, these signals attempt to match the sensory signals making their way up the hierarchy. When this matching occurs, the successful prediction signal suppresses the sensory signal. If there is a mismatch between the two, the sensory signal remains unsuppressed and continues its upwards journey. Therefore, sensory responses inform the system that a prediction error has occurred and that the generative model needs updating. Perception is a process where error signals nudge generative models into forms which minimise the prediction error, thereby offering the best explanation of the sensory input. In this framework, the repetition suppression of the N1 response to the standard is due to a dampening of the sensory signal by a successful prediction signal (Auksztulewicz and Friston, 2016) and the MMN to the deviant is a prediction error signal (Garrido et al., 2009; Wacongne et al., 2012; Chennu et al., 2013; Lieder et al., 2013a,b; Rentzsch et al., 2015; Carbajal and Malmierca, 2018; Fong et al., 2020).

The rise of PC as an explanation of the MMN has been heralded by a number of studies which point to evidence in favour of PC and against the adaptation model (e.g., Wacongne et al., 2012; Lieder et al., 2013a; Fitzgerald and Todd, 2020). Here, we revisit this issue and consider the viability of PC obliquely: I present the modern version of the adaptation model and a variety of simulations which produce MMN responses, including some that might pose a challenge for PC.

THE ADAPTATION MODEL COMES IN VANILLA AND CHOCOLATE

There are two varieties of adaptation model. Its most common form is also the traditional and most simplistic one. It builds on the premise that neurons that are repetitively stimulated become less responsive. The traditional model takes a unit-centric view by extrapolating this behaviour to event-related responses. The MMN is explained by the populations tuned to the standard being more adapted than those tuned to the deviant. The response to the stimulus is then a bottom-up process where the sensory signal drives the neural population to respond with a magnitude that depends on the adaptation level. Further, it is assumed that adaptation on both the unit and the population level depends on one aspect only: the time series of the specific stimulus to which the population is tuned. Thus, other stimuli used in the paradigm do not affect the responsiveness of the population. This traditional adaptation model is unconvincing (Fitzgerald and Todd, 2020): It can't explain the mismatch response to stimulus omissions (Yabe et al., 1997, 1998), because the responses of the model require a sensory signal. Also, it fails to explain the MMN to unexpected stimulus repetitions (Wacongne et al., 2012) because stimulus repetition supposedly always leads to more adaptation and a weaker response.

The traditional adaptation model can be operationalised to produce predictions of evoked responses. For example, Lieder et al. (2013a) formulated the adaptation hypothesis as exponentially adapting and recovering frequency channels and found that the experimental data favoured a model based on PC. Moreover, this idea of isolated adapting frequency channels is the basis for the multi-standard control paradigm (Schröger and Wolff, 1996; Jacobsen and Schröger, 2001). Here, the oddball condition is complemented by a control condition where the standards are replaced by several different stimuli equiprobable with the deviant. Because the presentation rate of the deviant is identical across the two conditions, the level of adaptation, according to the traditional adaptation model, should also be identical. Therefore, if the response to the deviant is stronger in the oddball condition than in the multi-standards control condition, this is taken as unequivocal proof that adaptation cannot explain the MMN, and that the MMN must therefore reflect something more. The multi-standard control condition has produced plenty of evidence that apparently refutes the adaptation model (for a review, see May and Tiitinen, 2010). It has recently become popular in animal electrophysiology where it is used for demonstrating that mismatch responses cannot be explained in terms of stimulus-specific adaptation (e.g., Harms et al., 2014; Kurkela et al., 2018) and that PC is therefore a more likely explanation (e.g., Parras et al., 2017).

There is a modern version of the adaptation model which bears but passing resemblance to its traditional counterpart. The acorn for this was planted by May et al. (1999) who argued that the frequency MMN can be explained as a modulated N1 response being generated on tonotopic maps with post-stimulus inhibition. The study used a computational model of auditory cortex where individual microcolumns interact with each other through lateral connections. This departure from the traditional adaptation model yielded a prediction, verified in EEG measurements, that the peak latency of the response to the deviant should have a non-monotonic dependence on the standard-deviance separation. This idea of modeling the auditory cortex as a system of interacting units (rather than isolated channels) was further developed by May and Tiitinen (2010) in their treatise on the adaptation model. These authors noted that the results which initially might appear to falsify the adaptation model are in fact consistent with this model. For example, the activity associated with the response to the standard has a different spatial distribution than the activity

underlying the MMN, (e.g., Rinne et al., 1999). Findings such as these have been used as evidence against the adaptation model as they appear to show that the generators of the MMN are separate from those of the N1 (for a review, see Näätänen et al., 2005). However, the adaptation model offers a simpler explanation in terms of variations in stimulus selectivity across cortical fields. For example, a field with broadly tuned neurons will respond similarly to the standard and deviant while, at the same time, a field with sharply tuned neurons will show stronger activation to the deviant. The spatial distribution of the responses elicited by the standard and deviant will therefore differ without implying the existence of a dedicated MMN generator (see sections 6.2 and 6.3 of May and Tiitinen, 2010). Further, one of the themes put forward by May and Tiitinen was that synaptic depression operating in the interconnected system of auditory cortex makes the system's responses highly context-dependent. This dependence shows up as MMN responses of various kinds as well as stimulus selectivity on the single-unit level. Staying on this theme, May and Tiitinen (2013) introduced a computational model that structurally copies the gross anatomy of the auditory cortex and where the synapses are modulated by STSD. Simulations showed that this system performs temporal binding, with individual columns exhibiting combination sensitivity similar to that found in monkey auditory cortex (Rauschecker, 1997). This sensitivity was found to be caused by the combination of STSD and the serial core-belt-parabelt structure of auditory cortex. In further simulations (May et al., 2015), the model replicated single-unit forward masking and SSA (Ulanovsky et al., 2003, 2004) as well as forward facilitation (Brosch et al., 1999; Brosch and Schreiner, 2000). Further, the model reproduced repetition suppression of the N1 (Lü et al., 1992) as well as several types of MMN. These were the frequency MMN (Tiitinen et al., 1994), MMN to "abstract" sound features (Korzyukov et al., 2003), and the MMN to small changes in complex tone sequences (Näätänen et al., 1993), where the latter two types are classed as evidence for "primitive intelligence" of auditory cortex (Näätänen et al., 2001). The success of the model in being able to recreate such a wide variety of phenomena was found to be a consequence of STSD. Removing STSD also abolished SSA, masking, facilitation, combination sensitivity, N1 adaptation, and the MMN.

THE ADAPTATION MODEL IN ACTION: SIMULATION METHODS

Original simulations of the modern version of the adaptation model were carried out to demonstrate that it reproduces those types of MMN which previously have been taken as evidence against the adaptation hypothesis. Importantly, these MMN responses, both empirically observed and simulated, might pose a challenge for the PC model as currently formulated. The model here is a modification of that of auditory cortex introduced in May and Tiitinen (2013) and May et al. (2015). It has a hierarchical structure with feedforward and feedback connections between cortical fields. However, the resemblance to PC stops here, there being no separate prediction and error units. Instead, as shown in **Figure 1A**, the dynamical unit of the model is a simplified description of the cortical column. Within each column, the excitatory and inhibitory neurons are treated as lumped populations described by mean-field state variables $u(t)$ and $v(t)$, respectively. These variables correspond to the membrane potential, and they are transformed into the mean firing rate through $g(x) = 1[x - \theta]\tanh[2(x - \theta)/3]$, where $\theta = 0.05$ is the threshold for firing and $1[.]$ is the Heaviside step function.

As depicted in **Figure 1B**, there are 208 cortical columns arranged into three core fields, eight belt fields, and two parabelt fields, with 16 columns per field (see Hackett et al., 2014). In addition, there is a 16-unit field where the excitatory populations represent the medial geniculate nucleus (MGN) of the thalamus and the inhibitory populations represent the surrounding thalamic reticular nucleus (for details, see Hajizadeh et al., 2019). There are therefore a total of 224 units. Fields are connected topographically to each other according to the anatomical results of Hackett et al. (2014). The signal progresses along the feedforward connections by first entering the MGN which then targets the three core fields, and these project to the surrounding belt fields, which in turn are connected to the two parabelt fields. These forward connections are reciprocated by feedback connections. Anatomically neighbouring fields are strongly interconnected while obliquely situated fields have fewer interconnections. The rostral parabelt field is interconnected with the anterior belt fields, and the caudal parabelt field connects with the posterior belt fields.

As illustrated in **Figure 1C**, the connectivity between the fields is expressed in the way the populations of excitatory neurons are connected to each other according to the 224×224 weight matrix $\mathbf{W}_{ee}$. The connections from the excitatory to the inhibitory neuron populations are defined by $\mathbf{W}_{ie}$, and the reciprocal connections are given by $\mathbf{W}_{ei}$. All column-to-column connections, both within and across fields, are assumed to be excitatory. The inhibitory populations make only local, short-range connections within the cortical column. Lateral inhibition across columns within a field is mediated by the excitatory population of each column exciting the inhibitory populations of neighbouring columns. The state equations are:

$$\tau_m \dot{\mathbf{u}}(t) = -\mathbf{u}(t) + \mathbf{W}_{ee}\mathbf{Q}(t) \cdot g[\mathrm{u}(t)] - \mathbf{W}_{ei}\mathbf{Q}(t) \cdot g[u(t)] + i_{aff}(t), \quad (1)$$

$$\tau_m \dot{\mathbf{v}}(t) = -\mathbf{v}(t)\,\mathbf{W}_{ie} g[\mathbf{u}(t)], \quad (2)$$

where $\boldsymbol{u}(t)$ and $\boldsymbol{v}(t)$ are vectors (224×1) of the state variables u and v, respectively, and $\tau_m = 30$ ms is the membrane time constant. The term $i_{aff}(t)$ represents afferent sensory input. This input is tonotopically organised into 16 frequency channels ($c_f = 1 \ldots 16$) which represent the activity of the inferior colliculus. This targets the MGN field through topographically organised connections so that each unit essentially represents a frequency channel. Because the various fields are topographically connected to each other, the cortical columns exhibit tonotopic organization in their responses, with the tuning curves becoming broader as one moves from MGN toward the parabelt. $\mathbf{Q}$ expresses STSD which drives adaptation. It is a diagonal 224×224 matrix where

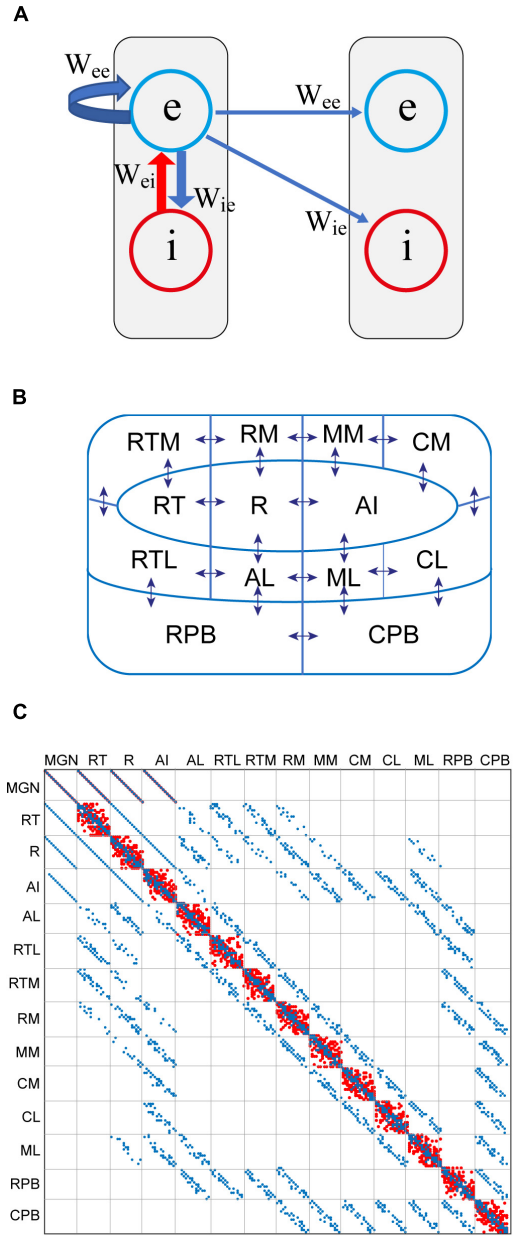

FIGURE 1 | A computational model of auditory cortex as a modern version of the adaptation model. **(A)** The basic functional unit of the model is the cortical column. This comprises a lumped description of the excitatory (e) and inhibitory (i) neuron populations. The e-population connects back to itself via feedback connections described in the weight matrix $\mathbf{W}_{ee}$. It also excites the excitatory populations of other columns. Lateral inhibition occurs through the e-population driving the i-population of neighbouring columns. **(B)** There are 208 cortical columns organised into three core fields (R, RT, AI), eight belt fields (AL, RTL, RTM, RN, MM, CM, CL, ML), and two parabelt fields (RPB, CPB). Neighbouring fields are strongly interconnected, as indicated by the arrows. The connections from RPB to RTM and RM as well as those from CPB to RM, MM, and CM are not shown. Abbreviation key: A – anterior (except for AI, primary auditory cortex), R – rostral, C – caudal, M – medial, L – lateral, T – temporal, PB – parabelt. **(C)** The weight matrices $\mathbf{W}_{ee}$ (blue) and $\mathbf{W}_{ie}$ (red) are overlayed. $\mathbf{W}_{ie}$ mediates lateral inhibition within each field. Long-range connections are found in $\mathbf{W}_{ee}$ only. Feedforward connections are below the diagonal, and feedback connections are above it.

the diagonal elements are described by the 224-element vector $\mathbf{q}(t)$ of synaptic efficacies:

$$\dot{\mathbf{q}}(t) = -\frac{\mathbf{q}(t)\, g[\mathbf{u}(t)]}{\tau_o} + \frac{1-\mathbf{q}(t)}{\tau_{rec}}, \quad (3)$$

where the first r.h.s. term describes the fast onset of STSD and the second term encapsulates the slow recovery. Note that STSD is assumed to depend on the presynaptic firing rate only, and therefore all the connections originating from the same column are modulated by the same element of $\mathbf{q}$ (hence $\mathbf{q}$ is a 224-element vector). There are two time constants: τ_o is the onset time constant (100 ms in cortex, 20 ms in MGN), and τ_{rec} is the time constant of recovery. The recovery time constant was treated as a free variable, justified by N1 recovery being highly subject-specific (Lü et al., 1992; Ioannides et al., 2003). The respective values of τ_{rec} across Experiments 1–5 described below were: [1.2, 1.2, 1.2, 1.7, 1.4] s.

The MEG signal is to a large extent generated by dendritic current flowing in the apical dendrites of cortical pyramidal neurons (Hämäläinen et al., 1993). In the model, the MEG is approximated by spatially summing the excitatory input currents to the excitatory neuron populations, that is, the second term on the r.h.s. of Eq. 1 (for a detailed description, see Hajizadeh et al., 2019). In the summation, the contribution from each connection is weighted according to connection type, with the weights being [−2,1,1] for feedforward, feedback, and intra-field connections, respectively.

Five experiments were carried out with the following oddball stimulation:

Experiment 1 – Standard stimuli (duration 50 ms, frequency channel c_f = 7) were presented with a stimulus onset interval (SOI) of 100 ms and omitted with 10% probability (parameters from Yabe et al., 1998). Each stimulus omission was treated as the deviant when calculating the ERF.

Experiment 2 – The standard stimulation was a series of tones (duration 50 ms, SOI 500 ms) which alternated in c_f frequency between 6 and 9. Occasionally, the tone with c_f = 6 was repeated (p = 5%). Comparisons were made between the ERF response elicited by the c_f = 6 tone in these two cases.

Experiment 3 – In the "global deviance" setup, two types of stimuli were used: a sequence of five identical tones ("xxxxX"; duration 50 ms, SOA 150 ms, c_f = 5) and a sequence "xxxxY" that was otherwise the same as xxxxX except that the fifth tone (c_f = 12) differed in frequency from the first four tones and was therefore a "local" deviant. These stimuli were presented in two conditions: one where xxxxY was the standard (p = 75%) and xxxxX was the "global" deviant (p = 15%), and one where these roles were reversed. In addition, the blocks contained occasional four-tone sequences (p = 10%). The sequences were separated by silent 850-ms periods. The parameters are from Wacongne et al. (2011).

Experiment 4 – Standards (c_f = 9, p = 90%) and deviants (c_f = 10, p = 10%) were presented in the oddball paradigm (tone duration 50 ms, SOI = 500 ms). In a separate multi-standard control condition, the standards were randomly replaced with equiprobable tones of different frequencies (c_f = 4…13, p = 10% for each).

Experiment 5 – Standards (c_f = 6, p = 80%) and deviants (c_f = 9, p = 20%) were presented as a series of anisochronous stimuli (duration 300 ms). The silent interval between consecutive tones varied randomly between 200 and 1,000 ms (flat distribution). The parameters are from Schwartze et al. (2011).

In all experiments, simulations comprised at least 400 presentations per condition. The responses to standards and deviants were averaged separately. The resulting ERFs were baseline-corrected (100 ms) and highpass filtered at 1 Hz.

THE ADAPTATION MODEL IN ACTION: SIMULATION RESULTS

Simulation results shown in **Figure 2** demonstrate that the modern version of the adaptation model reproduces those types of MMN which previously have been taken as evidence against the adaptation hypothesis.

Experiment 1 – The *omission MMN* is shown in **Figure 2A**. Due to the fast stimulus presentation rate, the standards (blue curve) produce no discernible responses. The occasional omission elicits a prominent response (red) which, apart from a late peak latency, resembles the observations of Yabe et al. (1998).

Experiment 2 – Tones alternating in frequency served as the standard stimulation. Occasionally alteration was replaced by stimulus repetition. As shown in **Figure 2B**, this results in a *stimulus repetition MMN*, as was found in simulations of the PC model of Wacongne et al. (2012).

Experiment 3 – Two types of sequences served as stimuli: five identical tones (xxxxX), and four identical tones followed by a "local" frequency deviant (xxxxY). **Figure 2C** shows the responses to the xxxxX sequence in two conditions: (1) It was the "global" standard stimulus, representing an expected repetition of the fifth tone. (2) It was the global deviant stimulus among xxxxY standards, therefore constituting an *unexpected stimulus repetition*. The global unexpectedness of the stimulus causes a late, "higher-order" MMN response, as observed by Wacongne et al. (2011).

Experiment 4 – **Figure 2D** shows the results where the multi-standard control condition was utilised. The deviant in the oddball condition elicits a larger response (red) than it does in the control condition (black). This is surprising given that we are viewing the behaviour of the adaptation model.

Experiment 5 – **Figure 2E** shows the results due to oddball stimulation. The frequency deviants (red) elicit stronger responses than the standards (blue). The twist here is that the presentation of the stimuli is anisochronous, with the stimulus onset intervals (SOIs) being random.

To summarise, the adaptation model produces a wide variety of MMNs which have been used as arguments against the adaptation hypothesis (Experiments 1–4). It is beyond the current scope to explore in detail what is generating the MMN in each experiment. As explained in May et al. (2015), SSA on the single-unit level is only part of the explanation, with tuning to stimulus features also playing a major role. Omission responses (Experiment 1) are to be expected as resonance effects, given that interacting excitatory and inhibitory neural populations are dynamically equivalent to driven oscillators with damping (May and Tiitinen, 2001; Hajizadeh et al., 2019, 2021). In addition, the omission response could be enhanced or even caused by high-pass filtering acting on the sudden, omission-related drop in the sustained activity which is elicited by fast-rate stimulation (May and Tiitinen, 2010). As for the multi-standard control results, these arise from the cortical columns being interconnected rather than acting as isolated frequency channels. Therefore, the response of each column depends not only on the stimulation rate (which would be required for the multi-standard control condition to be valid), but it is also modulated by lateral connections and the pattern of synaptic depression over the entire network, as established by the previous stimulation (May and Tiitinen, 2010). This means, for example, that columns that respond selectively to the standard-deviant combinations in the oddball condition respond less vigorously when this pattern is no longer dominant in the multi-standard condition, where the deviant is preceded by multiple different stimuli (May, 2017). This issue will be addressed in more detail in a separate paper.

ADAPTATION, PREDICTIVE CODING, OR A BIT OF BOTH?

It is time to reconsider what we mean by the adaptation model of MMN. The traditional model posits that adaptation is merely the repetition suppression of individual isolated neural populations. This version is really just a straw man that we should abandon because the brain does not contain isolated populations. A modern, updated adaptation model can be encapsulated thus: There is no process, mechanism, cortical area, or set of pathways that is dedicated to MMN generation, functionally separate from the rest of auditory cortex. Instead, the physiological mechanism that causes repetition suppression of neural responses (e.g., of the N1), is the *same* as that which makes the MMN happen. The candidate for this mechanism is STSD, which on its own might seem low-level because it causes transient weakening of synaptic connections. However, the effect of these synaptic modulations on the system level is profound. This is because synaptic depression happens in the context of an intricately interconnected, hierarchically organised network containing both excitation and inhibition. The stimulation at any one time point leaves, via STSD, a slowly decaying, highly malleable imprint on the functional structure of auditory cortex, that is, on the multitude of synaptic strengths by which the auditory cortex neurons are connected to each other. This functional structure keeps evolving and, at any time point, represents a weighted integration of all the stimulation that has occurred in a time window stretching seconds into the past. Temporarily weakened excitatory connections thus contribute to an attenuated response if they belong to an excitatory feedback loop triggered by the incoming stimulation, but they can contribute to an enhanced response if the activated circuit drives inhibition. The response of a neuron in auditory cortex thus intertwines the effect of the stimulus with the effect of the stimulation history and in this way is specific to both stimulus and history.

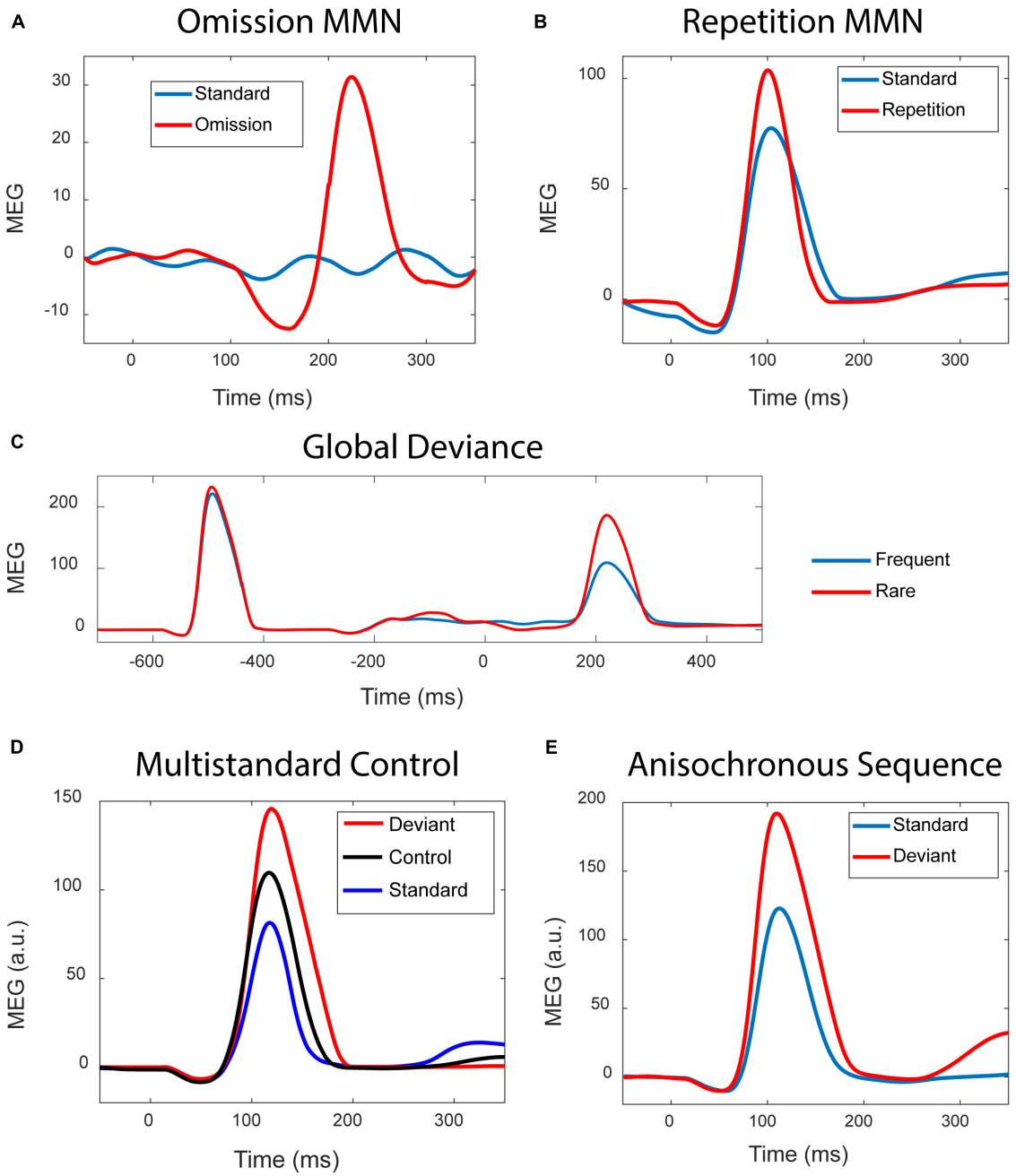

FIGURE 2 | Simulation results. **(A)** Standard stimuli presented at a fast rate (blue curve) elicit no discernible response, whereas the occasional stimulus omission (red curve) results in a prominent MMN. **(B)** Occasionally repeating a tone (red) in a sequence of alternating tones (blue) results in an MMN. **(C)** The blue curve is the response to a sequence xxxxX of five tones presented as a global standard, and the red curve is the response elicited by the same xxxxX as an infrequent global deviant. When the sequence is a global deviant, the ending of the sequence elicits a much stronger response than when it is a global standard. Zero time indicates the onset of the fifth tone. **(D)** In the classic oddball paradigm, frequency deviants (red) elicit a stronger response than the standards (blue). The response to the deviants is also stronger than the response elicited by the same deviants when these are presented as part of a random sequence of tones, in the so-called multi-standard control condition (black). **(E)** Standards (blue) and deviants (red) were presented as a series of anisochronous stimuli where the SOI varied randomly.

Therefore, repetition suppression is only one *of many* possible consequences of synaptic depression. These consequences show up as context sensitivity and, perhaps counterintuitively, as forward enhancement, depending on stimulation history (see May and Tiitinen, 2013; May et al., 2015). While STSD is a root cause of MMN, it plays a far wider role, enabling the gamut of other dependencies on stimulation history. Thus, there is nothing low-level about adaptation: while it is detected by using stimulus

repetition – the simplest and the most boring of stimulation paradigms – it reflects a fundamental mechanism whereby the auditory cortex is able to keep track of the past in a way which informs the way it responds to the present.

The version of the adaptation model used here has a hierarchical structure in terms of the core, belt, and parabelt, and in the above simulations, the feedback connections are all excitatory. However, in contrast to the PC model, there is no requirement for the feedback to be exclusively inhibitory, and neither does it have to be exclusively excitatory; in either case (not shown here), the model of auditory cortex is able to generate MMN responses. The model suggests that the functional significance of the hierarchical structure of the auditory cortex lies in the way it modulates temporal binding. Namely, simulation results suggest that the time window over which combination sensitive responses occur increases as one moves up the core-belt-parabelt hierarchy (May and Tiitinen, 2013; May et al., 2015; Westö et al., 2016).

"Adaptation model" is somewhat of a misnomer because the object of modelling is *not* the MMN but, rather, the auditory cortex. Indeed, other modelling studies have similarly linked STSD in auditory cortex to SSA (Mill et al., 2011; Yarden and Nelken, 2017; Kudela et al., 2018) and to combination sensitivity (Lee and Buonomano, 2012; Goudar and Buonomano, 2015). Also, the current auditory cortex model is by no means complete. It lacks input from, for example, the inferior frontal cortex (IFC), which is known to contribute to the MMN response generated in auditory cortex (e.g., Rinne et al., 2005; Tse et al., 2018; Lui et al., 2021). The simulations can be taken as a demonstration that the "local" processing happening in auditory cortex is sufficient for the generation of MMN. There is no need to postulate a top-down generative model outside auditory cortex. However, it is still perfectly possible, even within the AM framework, that IFC and other areas have a modulatory role in shaping the MMN. Further, although mimicking the gross anatomy of auditory cortex, the model is an extremely simplified description, and it lacks, for example, long-term dynamics such as Hebbian learning. Nevertheless, it is noteworthy that such a simple model can mimic the behaviour of auditory cortex in so many ways and levels of observation.

Can PC claim similar success? Certainly, the results from Experiments 1–3 can be explained in terms of PC, as was done in the modelling work of Wacongne et al. (2012). However, explaining the omission MMN (Experiments 1 and 3) is not straightforward because there is no sensory signal for the prediction signal to suppress. Why, then, would there be an error signal? Wacongne and colleagues suggested that in this case, the MMN could reflect the activity of the prediction signal itself. This explanation is problematic because this signal should then be visible also when the prediction is successful, so that we would measure MMNs to standards too. Instead, as in the above simulation, the observed omission response tends to be more prominent than the responses to the standards (Yabe et al., 1997, 1998). Further, how does the generative model at the top of the hierarchy actually emerge? On this question, PC accounts are abstract and conceptual. For example, Wacongne and colleagues implemented the generative model as a set of delay lines which keep the stimulus-elicited signal in memory for precisely the right time so that the signal can then be recycled back as a top-down inhibitory prediction signal that coincides with the next stimulus. Noting that this delay-line scheme is unrealistic, the authors speculated that the generative model might in fact be due to parts of cortex acting like an echo state network. This is fair, and it will probably be a tremendous task to construct a mechanistic explanation of how the brain creates, on the fly, generative models to attempt to fit whatever the world is throwing at it. Even though the brain could be adept at doing this, given its pattern generating abilities, the generative model nevertheless currently plays the role of *deus ex machina* in PC theory. The existence of the generative model enthroned atop the hierarchy is assumed rather than explained. Research has concentrated on testing whether sensory responses are compatible with the PC view, and it remains unaccounted for how the past evidence is actually transformed into a projection of what the future most likely holds. One exception is the study by Friston and Kiebel (2009) where the generative model was a pair of Lorenz attractors offering an abundance of priors which could recover the hidden state of similar attractors driving the input. The input in this case was simulated bird song, which has a precise frequency and time structure. Thus, the requirement for the generative model was the ability to provide prediction signals with the right intricate timing. But how would such a precise system fare when the input arrives at random times, such as in Experiment 5 and in the MMN experiment of Schwartze et al. (2011)? This consideration is different from the one concerning precision weighting of the error signal. Rather, it concerns what form the actual generative model should take. By what mechanism would the generative model know when to employ temporal precision and when not to? Further, with repetitive stimulation, the N1 amplitude depends strongly on SOI: the rate of growth is strongest for shortest SOIs (<1 s) before levelling off with longer SOIs. This behaviour is easily replicated by the adaptation model (May et al., 2015). From a PC perspective, one would need to explain why the performance of the generative model deteriorates the fastest when modelling the regularity should be the easiest.

The physiological evidence for PC is mixed, and the theory has been criticized for being difficult to falsify (Walsh et al., 2020) – something the adaptation model also suffers from. There is thin evidence for the proposed separateness of neurons representing predictions and prediction errors (Heilbron and Chait, 2018) and it is unclear how PC might correlate with perception (Denham and Winkler, 2020). Therefore, while Bayesian inference seems to be a computational principle of the brain, the actual implementation of it is uncertain, with PC being one among many candidates (Rescorla, 2021). Perhaps a reformulated version of Bayesian inference incorporating the adaptation model might be worth considering. The pattern of STSD could be seen as a posterior model for sensory stimuli, though of course not a generative one. A separate version of the model will exist on each level of the hierarchy, updating itself based on local information. In this view, the MMN can still be seen as an error signal, but one perhaps targeting a generative

model on the highest level of attention and action selection. It is possible that the brain uses local adaptation and PC in tandem but for different purposes: One the one hand, adaptation might be central to bottom-up change detection which drives involuntary attention shifts and is expressed in the MMN. On the other hand, PC might be the top-down mechanism which suppresses *task-irrelevant* signals in auditory cortex according to a generative model. This model would selectively describe those signals that need to be filtered out and this selection would be a function of the attentional set rather than just signal probability. Evidence for this kind of top-down, attention-related inhibition of sensory processing can be found in the visual system in the case of visual marking (Watson and Humphreys, 1997; Braithwaite and Humphreys, 2003, 2007), and it could be present in the auditory system also.

CONCLUSION

It is too early to discard the adaptation model as an explanation of deviance detection as revealed in the MMN. Its modern version is able to reproduce a wide variety of MMN responses as well as intracortical results. PC as currently formulated provides a mostly conceptual explanation, and therefore it is difficult to contrast the relative successes of these models. Whilst the adaptation model is incomplete and it lacks the normative power and elegance of predictive coding, there are challenges ahead before the PC can match the adaptation model on a mechanistic level.

DATA AVAILABILITY STATEMENT

The original contributions presented in the study are included in the article. The simulation code is available at https://github.com/pjcmay/ACtx-Model. Further inquiries can be directed to the corresponding author.

AUTHOR CONTRIBUTIONS

PM programmed and ran the simulations, prepared the figures, made the tea, and wrote the manuscript.

ACKNOWLEDGMENTS

I am grateful to and grateful for the Department of Psychology, Lancaster University, Lancaster, United Kingdom, and the Leibniz Institute for Neurobiology, Magdeburg, Germany, and colleagues thereof, who made this work possible. I thank Ms. Nina Härtwich, M.Sc., for helping me comment the Matlab code. A special thank you to Dr. Jason Braithwaite for our eye-opening discussions about PC and stimulus selection in visual cortex.

REFERENCES

Auksztulewicz, R., and Friston, K. (2016). Repetition suppression and its contextual determinants in predictive coding. *Cortex* 80, 125–140. doi: 10.1016/j.cortex.2015.11.024

Bastos, A. M., Usrey, W. M., Adams, R. A., Mangun, G. R., Fries, P., and Friston, K. J. (2012). Canonical microcircuits for predictive coding. *Neuron* 76, 695–711. doi: 10.1016/j.neuron.2012.10.038

Braithwaite, J. J., and Humphreys, G. W. (2003). Inhibition and anticipation in visual search: evidence from effects of color foreknowledge on preview search. *Percept. Psychophys.* 65, 213–237. doi: 10.3758/bf03194796

Braithwaite, J. J., and Humphreys, G. W. (2007). Filtering items of mass distraction: top-down biases against distractors are necessary for the feature-based carry-over to occur. *Vis. Res.* 47, 1570–1583. doi: 10.1016/j.visres.2007.02.019

Brosch, M., and Schreiner, C. E. (2000). Sequence sensitivity of neurons in cat primary auditory cortex. *Cereb. Cortex* 10, 1155–1167. doi: 10.1093/cercor/10.12.1155

Brosch, M., Schulz, A., and Scheich, H. (1999). Processing of sound sequences in macaque auditory cortex: response enhancement. *J. Neurophysiol.* 82, 1542–1559. doi: 10.1152/jn.1999.82.3.1542

Butler, R. A. (1968). Effect of changes in stimulus frequency and intensity on habituation of the human vertex potential. *J. Acoust. Soc. Am.* 44, 945–950. doi: 10.1121/1.1911233

Carbajal, G. V., and Malmierca, M. S. (2018). The neuronal basis of predictive coding along the auditory pathway: from the subcortical roots to cortical deviance detection. *Trends Hear.* 22, 1–33. doi: 10.1177/2331216518784822

Chennu, S., Noreika, V., Gueorguiev, D., Blenkmann, A., Kochen, S., Ibáñez, A., et al. (2013). Expectation and attention in hierarchical auditory prediction. *J. Neurosci.* 33, 11194–11205. doi: 10.1523/JNEUROSCI.0114-13.2013

Denham, S. L., and Winkler, I. (2020). Predictive coding in auditory perception: challenges and unresolved questions. *Eur. J. Neurosci.* 51, 1151–1160. doi: 10.1111/ejn.13802

Fishman, Y. I. (2014). The mechanisms and meaning of the mismatch negativity. *Brain Topogr.* 27, 500–526. doi: 10.1007/s10548-013-0337-3

Fitzgerald, K., and Todd, J. (2020). Making sense of mismatch negativity. *Front. Psychiatry* 11:468. doi: 10.3389/fpsyt.2020.00468

Fong, C. Y., Law, W., Uka, T., and Koike, S. (2020). Auditory mismatch negativity under predictive coding framework and its role in psychotic disorders. *Front. Psychiatry* 11:557932. doi: 10.3389/fpsyt.2020.557932

Friston, K. (2005). A theory of cortical responses. *Philos. Trans. R. Soc. Lond. B Biol. Sci.* 360, 815–836. doi: 10.1098/rstb.2005.1622

Friston, K. (2010). The free-energy principle: a unified brain theory? *Nat. Rev. Neurosci.* 11, 127–138. doi: 10.1038/nrn2787

Friston, K., and Kiebel, S. (2009). Attractors in song. *New Math. Nat. Comput.* 5, 1–32. doi: 10.1142/S1793005709001209

Garrido, M. I., Kilner, J. M., Stephan, K. E., and Friston, K. J. (2009). The mismatch negativity: a review of underlying mechanisms. *Clin. Neurophysiol.* 120, 453–463. doi: 10.1016/j.clinph.2008.11.029

Goudar, V., and Buonomano, D. V. (2015). A model of order-selectivity based on dynamic changes in the balance of excitation and inhibition produced by short-term synaptic plasticity. *J. Neurophysiol.* 113, 509–523. doi: 10.1152/jn.00568.2014

Hackett, T. A., de la Mothe, L. A., Camalier, C. R., Falchier, A., Lakatos, P., Kajikawa, Y., et al. (2014). Feedforward and feedback projections of caudal belt and parabelt areas of auditory cortex: refining the hierarchical model. *Front. Neurosci.* 8:72. doi: 10.3389/fnins.2014.00072

Hajizadeh, A., Matysiak, A., Brechmann, A., König, R., and May, P. (2021). Why do humans have unique auditory event-related fields? Evidence from computational modeling and MEG experiments. *Psychophysiology* 58:e13769. doi: 10.1111/psyp.13769

Hajizadeh, A., Matysiak, A., May, P., and König, R. (2019). Explaining event-related fields by a mechanistic model encapsulating the anatomical structure of auditory cortex. *Biol. Cybern.* 113, 321–345. doi: 10.1007/s00422-019-00795-9

Hämäläinen, M., Hari, R., Ilmoniemi, R. J., Knuutila, J., and Lounasmaa, O. V. (1993). Magnetoencephalography—theory, instrumentation, and applications

to non-invasive studies of the working human brain. *Rev. Mod. Phys.* 65, 413–497. doi: 10.1103/RevModPhys.65.413

Harms, L., Fulham, W. R., Todd, J., Budd, T. W., Hunter, M., Meehan, C., et al. (2014). Mismatch negativity (MMN) in freely-moving rats with several experimental controls. *PLoS One* 9:e110892. doi: 10.1371/journal.pone.0110892

Heilbron, M., and Chait, M. (2018). Great Expectations: is there evidence for predictive coding in auditory cortex? *Neuroscience* 389, 54–73. doi: 10.1016/j.neuroscience.2017.07.061

Ioannides, A. A., Popescu, M., Otsuka, A., Bezerianos, A., and Liu, L. (2003). Magnetoencephalographic evidence of the interhemispheric asymmetry in echoic memory lifetime and its dependence on handedness and gender. *Neuroimage* 19, 1061–1075. doi: 10.1016/s1053-8119(03)00175-7

Jääskeläinen, I. P., Ahveninen, J., Bonmassar, G., Dale, A. M., Ilmoniemi, R. J., Levänen, S., et al. (2004). Human posterior auditory cortex gates novel sounds to consciousness. *Proc. Natl. Acad. Sci. U. S. A.* 101, 6809–6814. doi: 10.1073/pnas.0303760101

Jacobsen, T., and Schröger, E. (2001). Is there pre-attentive memory-based comparison of pitch? *Psychophysiology* 38, 723–727.

Korzyukov, O. A., Winkler, I., Gumenyuk, V. I., and Alho, K. (2003). Processing abstract auditory features in the human auditory cortex. *Neuroimage* 20, 2245–2258. doi: 10.1016/j.neuroimage.2003.08.014

Kudela, P., Boatman-Reich, D., Beeman, D., and Anderson, W. S. (2018). Modeling neural adaptation in auditory cortex. *Front. Neural Circuits* 12:72. doi: 10.3389/fncir.2018.00072

Kurkela, J., Lipponen, A., Kyläheiko, I., and Astikainen, P. (2018). Electrophysiological evidence of memory-based detection of auditory regularity violations in anesthetized mice. *Sci. Rep.* 8:3027. doi: 10.1038/s41598-018-21411-z

Lee, T. P., and Buonomano, D. V. (2012). Unsupervised formation of vocalization-sensitive neurons: a cortical model based on short-term and homeostatic plasticity. *Neural Comput.* 24, 2579–2603. doi: 10.1162/NECO_a_00345

Lieder, F., Daunizeau, J., Garrido, M. I., Friston, K. J., and Stephan, K. E. (2013a). Modelling trial-by-trial changes in the mismatch negativity. *PLoS Comput. Biol.* 9:e1002911. doi: 10.1371/journal.pcbi.1002911

Lieder, F., Stephan, K. E., Daunizeau, J., Garrido, M. I., and Friston, K. J. (2013b). A neurocomputational model of the mismatch negativity. *PLoS Comput. Biol.* 9:e1003288. doi: 10.1371/journal.pcbi.1003288

Lü, Z. L., Williamson, S. J., and Kaufman, L. (1992). Human auditory primary and association cortex have differing lifetimes for activation traces. *Brain Res.* 572, 236–241. doi: 10.1016/0006-8993(92)90475-o

Lui, T. K., Shum, Y. H., Xiao, X. Z., Wang, Y., Cheung, A. T., Chan, S. S., et al. (2021). The critical role of the inferior frontal cortex in establishing a prediction model for generating subsequent mismatch negativity (MMN): a TMS-EEG study. *Brain Stimul.* 14, 161–169. doi: 10.1016/j.brs.2020.12.005

May, P., and Tiitinen, H. (2001). Human cortical processing of auditory events over time. *Neuroreport* 12, 573–577. doi: 10.1097/00001756-200103050-00028

May, P., Tiitinen, H., Ilmoniemi, R. J., Nyman, G., Taylor, J. G., and Näätänen, R. (1999). Frequency change detection in human auditory cortex. *J. Comput. Neurosci.* 6, 99–120. doi: 10.1023/a:1008896417606

May, P. J. C. (2017). A re-evaluation of the multi-standard control condition for the existence of a genuine MMN. *Psychophysiology* 54:s9. doi: 10.1111/psyp.12925

May, P. J. C., and Tiitinen, H. (2010). Mismatch negativity (MMN), the deviance-elicited auditory deflection, explained. *Psychophysiology* 47, 66–122. doi: 10.1111/j.1469-8986.2009.00856.x

May, P. J. C., and Tiitinen, H. (2013). Temporal binding of sound emerges out of anatomical structure and synaptic dynamics of auditory cortex. *Front. Comput. Neurosci.* 7:152. doi: 10.3389/fncom.2013.00152

May, P. J. C., Westö, J., and Tiitinen, H. (2015). Computational modelling suggests that temporal integration results from synaptic adaptation in auditory cortex. *Eur. J. Neurosci.* 41, 615–630. doi: 10.1111/ejn.12820

Mill, R., Coath, M., Wennekers, T., and Denham, S. L. (2011). A neurocomputational model of stimulus-specific adaptation to oddball and Markov sequences. *PLoS Comput. Biol.* 7:e1002117. doi: 10.1371/journal.pcbi.1002117

Näätänen, R. (1990). The role of attention in auditory information processing as revealed by event related potentials and other brain measures of cognitive function. *Behav. Brain Sci.* 13, 201–288.

Näätänen, R. (1992). *Attention and Brain Function*. Hillsdale, NJ: Erlbaum.

Näätänen, R., Gaillard, A. W., and Mäntysalo, S. (1978). Early selective-attention effect on evoked potential reinterpreted. *Acta Psychol.* 42, 313–329. doi: 10.1016/0001-6918(78)90006-9

Näätänen, R., Jacobsen, T., and Winkler, I. (2005). Memory-based or afferent processes in mismatch negativity (MMN): a review of the evidence. *Psychophysiology* 42, 25–32. doi: 10.1111/j.1469-8986.2005.00256.x

Näätänen, R., Schröger, E., Karakas, S., Tervaniemi, M., and Paavilainen, P. (1993). Development of a memory trace for a complex sound in the human brain. *Neuroreport* 4, 503–506. doi: 10.1097/00001756-199305000-00010

Näätänen, R., Tervaniemi, M., Sussman, E., Paavilainen, P., and Winkler, I. (2001). "Primitive intelligence" in the auditory cortex. *Trends Neurosci.* 24, 283–288. doi: 10.1016/s0166-2236(00)01790-2

Parras, G. G., Nieto-Diego, J., Carbajal, G. V., Valdés-Baizabal, C., Escera, C., and Malmierca, M. S. (2017). Neurons along the auditory pathway exhibit a hierarchical organization of prediction error. *Nat. Commun.* 8:2148. doi: 10.1038/s41467-017-02038-6

Rao, R. P., and Ballard, D. H. (1999). Predictive coding in the visual cortex: a functional interpretation of some extra-classical receptive-field effects. *Nat. Neurosci.* 2, 79–87. doi: 10.1038/4580

Rauschecker, J. P. (1997). Processing of complex sounds in the auditory cortex of cat, monkey, and man. *Acta Otolaryngol. Suppl.* 532, 34–38. doi: 10.3109/00016489709126142

Rentzsch, J., Shen, C., Jockers-Scherübl, M. C., Gallinat, J., and Neuhaus, A. H. (2015). Auditory mismatch negativity and repetition suppression deficits in schizophrenia explained by irregular computation of prediction error. *PLoS One* 10:e0126775. doi: 10.1371/journal.pone.0126775

Rescorla, M. (2021). Bayesian modeling of the mind: from norms to neurons. *Wiley Interdisc. Rev. Cogn. Sci.* 12:e1540. doi: 10.1002/wcs.1540

Rinne, T., Gratton, G., Fabiani, M., Cowan, N., Maclin, E., Stinard, A., et al. (1999). Scalp-recorded optical signals make sound processing in the auditory cortex visible? *NeuroImage* 10, 620–624. doi: 10.1006/nimg.1999.0495

Rinne, T., Degerman, A., and Alho, K. (2005). Superior temporal and inferior frontal cortices are activated by infrequent sound duration decrements: an fMRI study. *Neuroimage* 26, 66–72. doi: 10.1016/j.neuroimage.2005.01.017

Schröger, E., and Wolff, C. (1996). Mismatch response of the human brain to changes in sound location. *Neuroreport* 7, 3005–3008. doi: 10.1097/00001756-199611250-00041

Schwartze, M., Rothermich, K., Schmidt-Kassow, M., and Kotz, S. A. (2011). Temporal regularity effects on pre-attentive and attentive processing of deviance. *Biol. Psychol.* 87, 146–151. doi: 10.1016/j.biopsycho.2011.02.021

Tiitinen, H., May, P., Reinikainen, K., and Näätänen, R. (1994). Attentive novelty detection in humans is governed by pre-attentive sensory memory. *Nature* 372, 90–92. doi: 10.1038/372090a0

Tse, C. Y., Yip, L. Y., Lui, T. K., Xiao, X. Z., Wang, Y., Chu, W., et al. (2018). Establishing the functional connectivity of the frontotemporal network in pre-attentive change detection with Transcranial Magnetic Stimulation and event-related optical signal. *Neuroimage* 179, 403–413. doi: 10.1016/j.neuroimage.2018.06.053

Ulanovsky, N., Las, L., Farkas, D., and Nelken, I. (2004). Multiple time scales of adaptation in auditory cortex neurons. *J. Neurosci.* 24, 10440–10453. doi: 10.1523/JNEUROSCI.1905-04.2004

Ulanovsky, N., Las, L., and Nelken, I. (2003). Processing of low-probability sounds by cortical neurons. *Nat. Neurosci.* 6, 391–398. doi: 10.1038/nn1032

Wacongne, C., Changeux, J. P., and Dehaene, S. (2012). A neuronal model of predictive coding accounting for the mismatch negativity. *J. Neurosci.* 32, 3665–3678. doi: 10.1523/JNEUROSCI.5003-11.2012

Wacongne, C., Labyt, E., van Wassenhove, V., Bekinschtein, T., Naccache, L., and Dehaene, S. (2011). Evidence for a hierarchy of predictions and prediction errors in human cortex. *Proc. Natl. Acad. Sci. U. S. A.* 108, 20754–20759. doi: 10.1073/pnas.1117807108

Walsh, K. S., McGovern, D. P., Clark, A., and O'Connell, R. G. (2020). Evaluating the neurophysiological evidence for predictive processing as a model of perception. *Ann. N. Y. Acad. Sci.* 1464, 242–268. doi: 10.1111/nyas.14321

Watson, D. G., and Humphreys, G. W. (1997). Visual marking: prioritizing selection for new objects by top-down attentional inhibition of old objects. *Psychol. Rev.* 104, 90–122. doi: 10.1037/0033-295x.104.1.90

Wehr, M., and Zador, A. M. (2003). Balanced inhibition underlies tuning and sharpens spike timing in auditory cortex. *Nature* 426, 442–446.

Wehr, M., and Zador, A. M. (2005). Synaptic mechanisms of forward suppression in rat auditory cortex. *Neuron* 47, 437–445. doi: 10.1016/j.neuron.2005.06.009

Westö, J., May, P. J., and Tiitinen, H. (2016). Memory stacking in hierarchical networks. *Neural Comput.* 28, 327–353. doi: 10.1162/NECO_a_00803

Yabe, H., Tervaniemi, M., Reinikainen, K., and Näätänen, R. (1997). Temporal window of integration revealed by MMN to sound omission. *NeuroReport* 8, 1971–1974. doi: 10.1097/00001756-199705260-00035

Yabe, H., Tervaniemi, M., Sinkkonen, J., Huotilainen, M., Ilmoniemi, R. J., and Näätänen, R. (1998). Temporal window of integration of auditory information in the human brain. *Psychophysiology* 35, 615–619. doi: 10.1017/s0048577298000183

Yarden, T. S., and Nelken, I. (2017). Stimulus-specific adaptation in a recurrent network model of primary auditory cortex. *PLoS Comput. Biol.* 13:e1005437. doi: 10.1371/journal.pcbi.1005437

Conflict of Interest: The author declares that the research was conducted in the absence of any commercial or financial relationships that could be construed as a potential conflict of interest.

frontiers in Human Neuroscience

ORIGINAL RESEARCH
published: 10 February 2022
doi: 10.3389/fnhum.2021.794654

Dynamics of Oddball Sound Processing: Trial-by-Trial Modeling of ECoG Signals

Françoise Lecaignard[1,2], Raphaëlle Bertrand[1,2], Peter Brunner[3,4,5], Anne Caclin[1,2], Gerwin Schalk[5] and Jérémie Mattout[1,2]*

[1] Lyon Neuroscience Research Center, CRNL, INSERM, U1028, CNRS, UMR 5292, Lyon, France, [2] University Lyon 1, Lyon, France, [3] Department of Neurosurgery, Washington University School of Medicine, St. Louis, MO, United States, [4] Department of Neurology, Albany Medical College, Albany, NY, United States, [5] National Center for Adaptive Neurotechnologies, Albany, NY, United States

Recent computational models of perception conceptualize auditory oddball responses as signatures of a (Bayesian) learning process, in line with the influential view of the mismatch negativity (MMN) as a prediction error signal. Novel MMN experimental paradigms have put an emphasis on neurophysiological effects of manipulating regularity and predictability in sound sequences. This raises the question of the contextual adaptation of the learning process itself, which on the computational side speaks to the mechanisms of gain-modulated (or precision-weighted) prediction error. In this study using electrocorticographic (ECoG) signals, we manipulated the predictability of oddball sound sequences with two objectives: (i) Uncovering the computational process underlying trial-by-trial variations of the cortical responses. The fluctuations between trials, generally ignored by approaches based on averaged evoked responses, should reflect the learning involved. We used a general linear model (GLM) and Bayesian Model Reduction (BMR) to assess the respective contributions of experimental manipulations and learning mechanisms under probabilistic assumptions. (ii) To validate and expand on previous findings regarding the effect of changes in predictability using simultaneous EEG-MEG recordings. Our trial-by-trial analysis revealed only a few stimulus-responsive sensors but the measured effects appear to be consistent over subjects in both time and space. In time, they occur at the typical latency of the MMN (between 100 and 250 ms post-stimulus). In space, we found a dissociation between time-independent effects in more anterior temporal locations and time-dependent (learning) effects in more posterior locations. However, we could not observe any clear and reliable effect of our manipulation of predictability modulation onto the above learning process. Overall, these findings clearly demonstrate the potential of trial-to-trial modeling to unravel perceptual learning processes and their neurophysiological counterparts.

Keywords: single-trial analysis, predictive coding, mismatch negativity, Bayesian learning, general linear model, Bayesian model reduction

OPEN ACCESS

Edited by:
Manuel S. Malmierca, University of Salamanca, Spain

Reviewed by:
Sumie Leung, Swinburne University of Technology, Australia
Alejandro Tabas, Technical University Dresden, Germany

****Correspondence:***
Françoise Lecaignard
francoise.lecaignard@inserm.fr

Specialty section:
This article was submitted to Cognitive Neuroscience, a section of the journal Frontiers in Human Neuroscience

Received: *13 October 2021*
Accepted: *07 December 2021*
Published: *10 February 2022*

Citation:
Lecaignard F, Bertrand R, Brunner P, Caclin A, Schalk G and Mattout J (2022) Dynamics of Oddball Sound Processing: Trial-by-Trial Modeling of ECoG Signals. Front. Hum. Neurosci. 15:794654. doi: 10.3389/fnhum.2021.794654

INTRODUCTION

Recent computational models of perception address sound processing in oddball paradigms as the learning of regularities that pertain to the repetition of an acoustic pattern (typically a single tone in the basic form of oddball sequences, i.e., the *standard* stimuli). The corollary that follows is then to view mismatch responses elicited by unexpected *deviant* sounds as indexing surprise processing. In particular, the Mismatch Negativity (MMN; Näätänen et al., 1978) has been suggested to reflect a prediction error (Friston, 2005). This model of the MMN leverages on complex underlying (Bayesian) computations that raise the practical question of their neuronal implementation (Knill and Pouget, 2004). Deciphering these processes is a topic of intense research, both at the physiological (Garrido et al., 2009b; Auksztulewicz and Friston, 2016; Carbajal and Malmierca, 2018) and cognitive (Winkler, 2007; Heilbron and Chait, 2018) levels.

An important aspect that computational models of perception have put forward is the influence of the acoustic context onto sound processing in oddball paradigms, that is, as we shall see, explicitly formalized in popular predictive coding implementation (Friston, 2005; Spratling, 2016). Interestingly, this is in line with recent MMN findings which emphasized the importance of the ordering of experimental conditions (Fitzgerald and Todd, 2020; Todd et al., 2021), pointing out the need for refining our understanding of mismatch responses.

Surprise or prediction errors play a key role in perceptual inference and learning (Friston, 2009). Importantly, they are thought to drive belief updating in a context dependent manner. In other words, the context determines the relevance of a given prediction error, and whether it should be filtered out or accounted for by promoting some adaptation (Adams et al., 2013; Mathys et al., 2014). In the Bayesian framework, this context dependent modulation naturally emerges in the form of a precision weight. And surprise takes the more refined form of a precision-weighted prediction error (Bastos et al., 2012). Should the precision or confidence be low (e.g., in a noisy environment), the learning triggered by a new sound should be lessened to avoid irrelevant updates of the internal model. On the contrary, a high precision will amplify the prediction error, and yield a larger belief update.

The precision weighting account of contextual influences has led to manipulations of the statistical structure of oddball sequences to test specific predictions about the ensuing modulations of the MMN. In Garrido et al. (2013), auditory stimulations were sampled from a Gaussian distribution; larger amplitudes were measured at the MMN latency in response to outlier sounds when the distribution variance was reduced. This finding speaks to the precision of standard prediction, an aspect that has also been investigated recently using a different manipulation (SanMiguel et al., 2021). In this study, sound sequence comprised multiple tones occurring randomly, with two of them playing the role of deviants and standards, respectively. The proportion of standards in the sequence was manipulated while keeping deviant probability constant and larger deviant response at the MMN latency was reported in the more stable condition where standards were more frequent. Several studies also manipulated the predictability of sound sequences (Chennu et al., 2013; Recasens et al., 2014; Auksztulewicz and Friston, 2015; Lecaignard et al., 2015; Dürschmid et al., 2016; Auksztulewicz et al., 2017, 2018). In short, predictability has been associated with reduced brain responses, in line with expected smaller precision-weighted prediction errors (Lecaignard et al., 2015). However, enhanced brain activity has also been reported in predictability conditions (Barascud et al., 2016; Southwell et al., 2017). Together, these reports call for further investigations to shed light onto the computational mechanisms at play and their neurophysiological underpinnings. The current electrocorticographic (ECoG) study was intended to contribute to this effort.

Specifically, a closer look at the putative effect of predictability provides a plausible explanation for the above apparent contradictory findings. Indeed, predictability has a two-fold and opposite effect on prediction error and its precision, respectively. It is expected to decrease the former (as an unsurprising environment contributes to a more accurate prediction of future sensations) but to increase the latter (as a structured context provides more reliable prediction errors). An important aspect is that both computational variables depend upon the temporal structure of the sensory input sequence, but precision weight (or inverse variance) pertaining to second order statistics (in contrast with prediction pertaining to first-order ones) is expected to be optimized over a slower timescale (Mathys et al., 2014). As a consequence, averaging methods like traditional event-related potential (ERP) approaches will likely be unable to reveal the contribution of their respective dynamics onto brain activity, even if these dynamics become separable due to a predictability manipulation. To circumvent this issue, attempts have been made that consisted of comparing the mismatch responses obtained in the beginning and end of oddball sequences (Fitzgerald and Todd, 2018; Todd et al., 2021).

Alternatively, trial-by-trial analysis, pertaining to the examination of the single-trial activity elicited by single sounds, enables the direct examination of such dynamics. In a previous study using simultaneous EEG and MEG recordings, we coupled a predictability manipulation of an oddball paradigm with a single-trial data modeling approach (Lecaignard et al., 2021b). Trial-by-trial activity was found to be best predicted by a Bayesian learning model of the deviant probability and this model revealed a modulation of learning by sequence predictability, suggesting an automatic adaptation of sensory processing to the statistical structure of the auditory stream. This adaptation could be captured by a model parameter that determines the influence of past experience onto perceptual inference. The larger value we found under predictability can be interpreted as a larger memory span that fits well with the fact that the more structured the sound sequence, the more past information is integrated to make predictions These findings and few others speak to the plausibility of perceptual models engaged in oddball processing and the trial-by-trial fluctuations they prescribe (Ostwald et al., 2012; Lieder et al., 2013; Stefanics et al., 2014; Meyniel et al., 2016; Sedley et al., 2016; Weber et al., 2020).

We designed the present ECoG study around two objectives: first, we aimed at testing the reproducibility of the recent EEG-MEG single-trial findings, considering the youth of this field of research, and the methodological challenge on which it is based, i.e., the sensitivity of single-trial data to noise. We here expect ECoG data to refine the spatio-temporal characterization of perceptual learning because of its excellent spatial and temporal resolution. Second, to refine the description of cognitive process(es) engaged during the passive processing of sound, we propose a novel approach combining a general linear model (GLM) with advanced Bayesian methods for model comparison (Bayesian model reduction, Friston et al., 2016, 2018) to compare a learning regressor with non-learning ones. Using a GLM approach, competing cognitive hypotheses are no longer tested as mutually exclusive (as was the case in our prior EEG-MEG study) and we could examine where and when their related regressor each contributes to the observed data in a flexible way. It is interesting to note that this investigation, because it involves both dynamic and static models (learning and non-learning, respectively) also amounts to addressing the potential of the still little used single-trial modeling. In short, if dynamic models were found unlikely based on current data, single-trial modeling would appear too complex to reveal constant effects for which averaging methods like evoked potential analysis are perfectly relevant. Analysis of data from four implanted patients with ECoG electrodes over the temporal lobe provides substantial evidence for Bayesian learning in the brain and promotes single-trial modeling to further characterize auditory processing in the light of perceptual inference and predictive coding. Surprisingly, no clear evidence for the expected adaptation of learning under predictability could be disclosed.

MATERIALS AND METHODS

Participants

Six patients (P1, P2, P3, P4, P5, and P6) with pharmacologically intractable epilepsy participated in this study at Albany Medical Center (Albany, NY, United States). They underwent pre-surgical monitoring with temporary placement of electrocorticographic grids over frontal, parietal, and temporal cortices. Four of the six patients (P2, P4, P5, and P6) were also assessed with intracranial depth electrodes located over temporal regions; analysis of the related data is not included in the present study. All patients provided informed consent for participating in the study, which was approved by the Institutional Review Board of Albany Medical College and the Human Research Protections Office of the United States Army Medical Research and Materiel Command. **Table 1** summarizes the patients' clinical profiles. Cortical views with electrode overlay are provided in **Supplementary Figure S1**.

As explained in the experimental procedure section below, each patient received auditory stimuli divided into four runs during a single session. Two patients however followed a different scheme: patient P1 underwent two sessions (day 2 and day 5 after surgery) as well as patient P6 who received two runs in a first session (day 1) and six runs in a second one (day 2).

TABLE 1 | Clinical profiles of participants.

Subject	Age	Sex	Seizure focus	#grids	#strips	#electrodes
P1	69	M	Right temporal	1	11	92
P2	33	M	Left temporal	1	5	224
P3	51	M	Left temporal	1	6	126
P4	36	F	Right temporal	1	8	92
P5	27	F	Left temporal	2	4	93
P6	31	M	Left temporal	2	10	122

The number of electrodes refers to contacts included in the current analysis (distant from epileptogenic foci, without electrical or mechanical artifacts).

Given that they did not report having noticed the statistical manipulation of the sound sequences (see below), and in order to take advantage of most of these data, we included them all in our subsequent analyses (we hereafter refer to these datasets by P1a, P1b, P6a and P6b, respectively). However, no data from patient P1 or from P6a survived our selection criterion (see below). Hence, only session P6b was included for subsequent analysis. For full transparency, we included the analysis of P6a as **Supplementary Material** (**Supplementary Figure S2**). Regarding patient P3, our analyses identified only one responsive location; we decided not to include the data in the study, and provide the related findings in **Supplementary Material** (**Supplementary Figure S3**). In summary, the present work relies on four datasets: P2, P4, P5, and P6b.

Recordings

Implanted subdural grids (from PMT Corp., Chanhassen, MN, United States) were approved for human use and consisted of platinum-iridium electrodes (4 mm diameter, 2.4 mm exposed) that were embedded in silicone and spaced 6–10 mm from each other in five patients (P1, P3, P4, P5, and P6) and 3 mm in subject P2. Reference and ground were subdural electrodes distant from the epileptogenic area. Grid placement and duration of ECoG monitoring were determined to meet the requirements of the clinical evaluation.

Recordings were conducted at the patient bedside using BCI2000 (Schalk et al., 2004; Schalk and Mellinger, 2010[1]). Electrocorticographic signals were amplified using a 256-channel g.HIamp biosignal acquisition device (g.tec, Graz, Austria) and digitized at a sampling rate of 1200 Hz.

Sensor co-registration with cortical anatomy involved pre-operative magnetic resonance imaging (MRI) scans and post-operative computed tomography images (CT; Kubanek and Schalk, 2015), and was achieved using SPM8[2]. **Supplementary Figure S1** shows for each patient the resulting estimates of 3D stereotactic coordinates overlaying cortical brain mesh extracted from individual MRI scans using FreeSurfer[3].

Experimental Procedure

Each patient underwent one recording session with four runs, except for patients P1 and P6 who received two sessions

[1]https://www.bci2000.org

[2]https://www.fil.ion.ucl.ac.uk/spm/

[3]http://surfer.nmr.mgh.harvard.edu

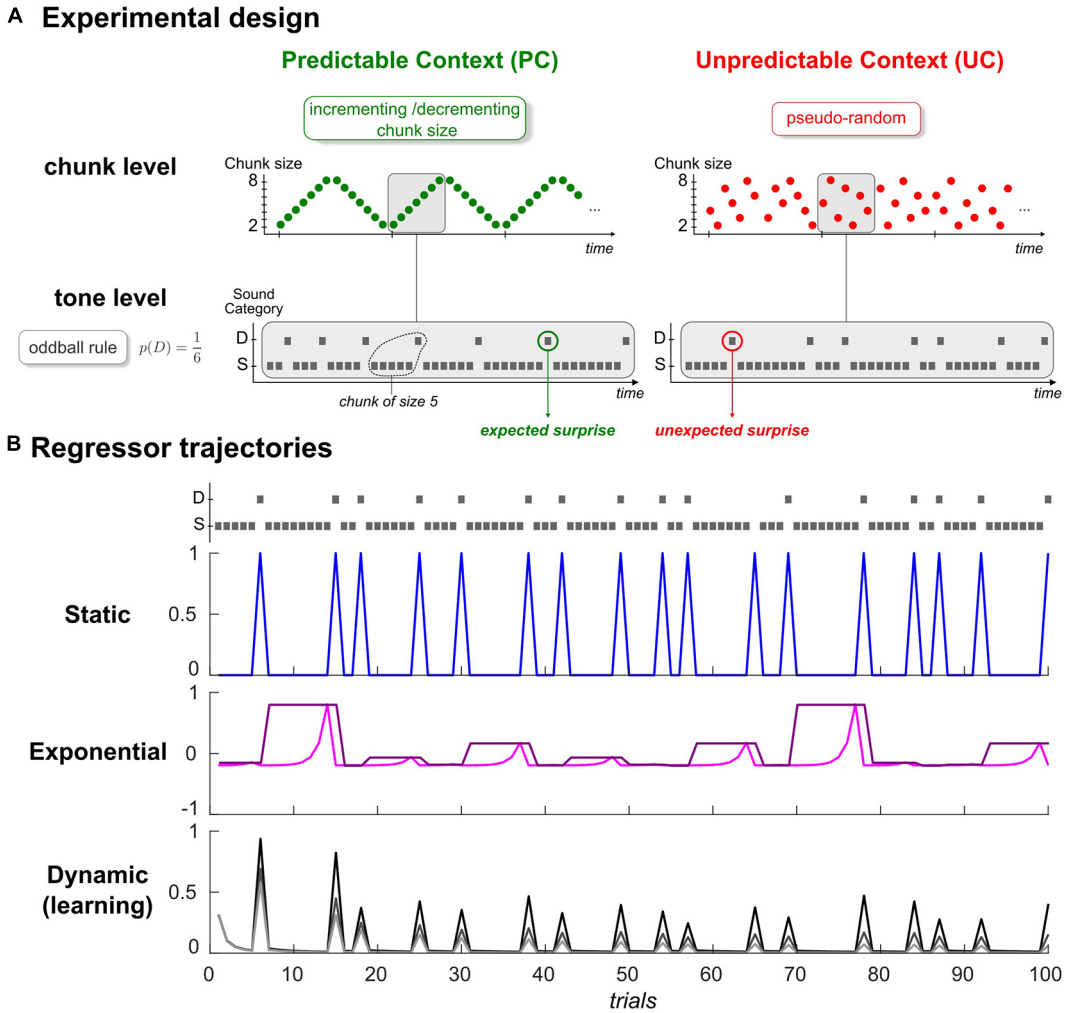

FIGURE 1 | (A) Experimental Design. Schematic view of the predictability manipulation (chunk level) applying to typical oddball sound sequences (tone level). Predictable context (left, green) involves cycles of ordered transitions between segments of repeating standards (chunks), which become shuffled in the Unpredictable context (right, red). Average deviant probability remains the same in both contexts (p = 1/6). Gray rectangles delineate an exemplary cycle for both sequences. S: Standard, D: Deviant. **(B)** Examples of regressors for the static (top), exponential (middle), and dynamic (bottom) categories. Each trajectory was simulated with the first 100 tones of one subject in context UC, depicted in the upper panel following the standard/deviant representation in panel **(A)**. In the static category, deviant regressor is shown in blue (standard regressor is not displayed for convenience, as it mirrors deviant regressor). Exponential rank and chunk size regressors are presented in pink and purple, respectively. Regarding the learning regressor, three examples of Bayesian Surprise trajectories are provided, and were generated from different time constant values (parameter τ in (Eq. 3); 10,20 and 50: from dark to light gray).

separated by 3 days (four runs each) and 1 day (two and six runs), respectively.

Brain activity was recorded during an auditory oddball paradigm originally developed by our group (Lecaignard et al., 2015) and slightly modified here (see **Figure 1A**). Participants were instructed to ignore the sounds and watch a silent movie of their choice with subtitles. Each session lasted ∼50 min, including short breaks between runs. In the previous EEG-MEG study (Lecaignard et al., 2015), subjects were asked at the end of the experiment, to report to which extent they had been following the instruction to ignore the sounds and whether they had noticed the different sound attributes. Here, given the constraints related to the patients' condition and the acquisitions conducted in a clinical context, these verifications were validated orally but we could not have an precise description of the participants' sensory experience.

Auditory sequence in every run consisted of sounds (70 ms duration, 500 ms interstimulus interval) with repeating *standard* (500 Hz or 550 Hz) and unexpected frequency *deviants* (550 Hz or 500 Hz, occurrence probability p = 1/6). As shown in **Figure 1A**, in the predictable context (PC), deviants were delivered according to an incrementing-decrementing rule applied to the size of repeating standard segments (or chunks) while they were pseudo-randomly distributed among standards in the unpredictable context (UC). We considered specific controls for the number of standards between two deviants

in context UC to ensure that despite their differing statistical structure, both sequence types (UC, PC) had the same deviant probability and the same distribution of chunk size (varying from 2 to 8 standards). Each context (UC, PC) was delivered in two runs to enable reversing the role of the two sounds (500 Hz/550 Hz; standard/deviant). Further details about stimuli and sequences can be found in Lecaignard et al. (2015). We used BCI2000 to deliver the acoustic stimuli that were presented binaurally through headphones.

Data Processing

We used the MNE software for electrophysiological analysis (Gramfort et al., 2013) for raw data conversion to BIDS format[4] and data preprocessing. Continuous recordings were band-pass filtered using a zero-phase finite impulse response (FIR) filter with Hann window in the 0.5–100 Hz band, notch-filtered at 60 Hz, 120 Hz, 180 Hz, and 240 Hz using a zero-phase FIR notch filter (stop band width at each frequency = 6 Hz) to remove the power line harmonics artifacts, and downsampled to 400 Hz. We excluded electrodes close to epileptogenic zones or electrodes whose ECoG signals were clearly artifactual based on visual inspection of the power spectral density. Time segments with obvious noise from electrical, mechanical or muscular origin were also rejected. Electrocorticographic recordings were referenced to the common averaged reference (CAR). We then extracted 600-ms-long epochs around the onset of the auditory stimuli (-100 to 500 ms around stimulus onset). Trial rejection was based on a peak-to-peak (maximum–minimum amplitude within epochs) threshold procedure applied to ECoG data: for each subject (except P2, see below), we first calculated for each location the distribution of peak-to-peak amplitudes over epochs. Next, at the level of the group of locations, we calculated the global distribution of mean values as well as that of outliers (two standard deviations from the mean). We rejected locations if their mean was found outlying the global mean (we call them as *bad* sensors). For the remaining locations, we used the outlier amplitude of the global outlier distribution as the threshold above which data segments were next rejected. The overall approach yielded the following threshold and rejection percentage: (364 uV; 26%), (330 uV; 19%), and (722 uV; 21%) for patients P4, P5, and P6b, respectively. In patient P2, data were contaminated by a lot of spikes; hence, we applied a threshold of 500 uV and obtained 39% of trial rejection. Regarding the datasets that were excluded, we obtained (586 uV; 16%), (461 uV; 16%), (742 uV; 13%), and (552 uV; 18%) in P1a, P1b, P3 and P6b, respectively. CAR referencing applied to the resulting sensor set.

We next applied a 2–20 Hz pass-band filter (zero-phase FIR) to continuous data, downsampled to 200 Hz for data reduction purpose and extracted the 600-ms epochs around the accepted trials resulting from the above-mentioned procedure. Finally, artifact-free and baseline-corrected epochs ([−100 +500] ms corresponding to $N_s = 120$ time samples) were exported into SPM12[2].

[4]https://bids.neuroimaging.io/

Rationale of the Modeling Approach

In order to test Bayesian learning as the perceptual model the brain would use when exposed to oddball sounds, as well as its automatic modulation under predictability (as we found using EEG-MEG), we considered a modeling framework based on advanced Bayesian methods and applying to single-trial activity. We here introduce to the overall procedure, which is depicted in **Figure 2**.

Single-trial activity here corresponds to the signals measured at ECoG sensors and induced by the presentation of a single stimulus. Single-trial signals are naturally relevant to investigate the functional interpretation of trial-by-trial fluctuations, that should reflect the updates of computational (learning) quantities if the brain was to entertain such learning. In this paper, the notion of dynamics refers to the temporal dependencies that take place over the time-course of the experiment (meaning that trial order matters). Considering that time-dependent influence is also critical for learning, we refer to dynamic or learning process equivalently. Dynamic processes differ from static ones where in this case past experience is not accounted for in stimulus processing. It should be noticed that the dynamic-based examination of brain activity is not possible using typical evoked responses, as the averaging of single-trial content is precisely meant to get rid of the dynamic information. In the following, we will refer to trial-by-trial dynamics (or trajectory) as the time series extracted over one or multiple experimental run(s) at a particular sensor and a particular peri-stimulus sample. And we will call data point the spatio-temporal location where it is measured (one sensor, one peri-stimulus sample). An example is illustrated in **Figure 2** (panel "Single-trial responses"). In the present work, there were $N_t = 672$ single trials per run, that each involves a 600 ms temporal window ($N_s = 120$ peri-stimulus samples). In total, for each participant, $N_c \times N_s$ trial-by-trial time series contributed to the present findings, with N_c the number of good channels (retained after artifact rejection).

The above-cited trial-by-trial modeling studies that have been conducted using oddball paradigms confronted brain signals (single-trial dynamics) with several model predictions that each reflected a possible account of sound processing (Ostwald et al., 2012; Lieder et al., 2013; Stefanics et al., 2014; Meyniel et al., 2016; Sedley et al., 2016; Weber et al., 2020; Lecaignard et al., 2021b). Typically, each model was treated separately and Bayesian model comparison (Penny et al., 2010) was then employed to select which one was more likely to have generate the observed data. Here, we considered a different approach based on a GLM in order to evaluate the contribution of each cognitive account to the data, in a way that does not preclude a mixture of several ones (thanks to the linear combination). We expected this scheme, because it is more flexible, to provide a finer spatio-temporal description of the mechanisms underlying oddball sound processing.

As can be seen in **Figure 2** and as will be described in Section "Statistical Model," we first considered a GLM comprising six different regressors (each detailed below) and that we call the "full model." For each participant (P2, P4, P5 and P6b), it was fitted to the trial-by-trial activity extracted at each data

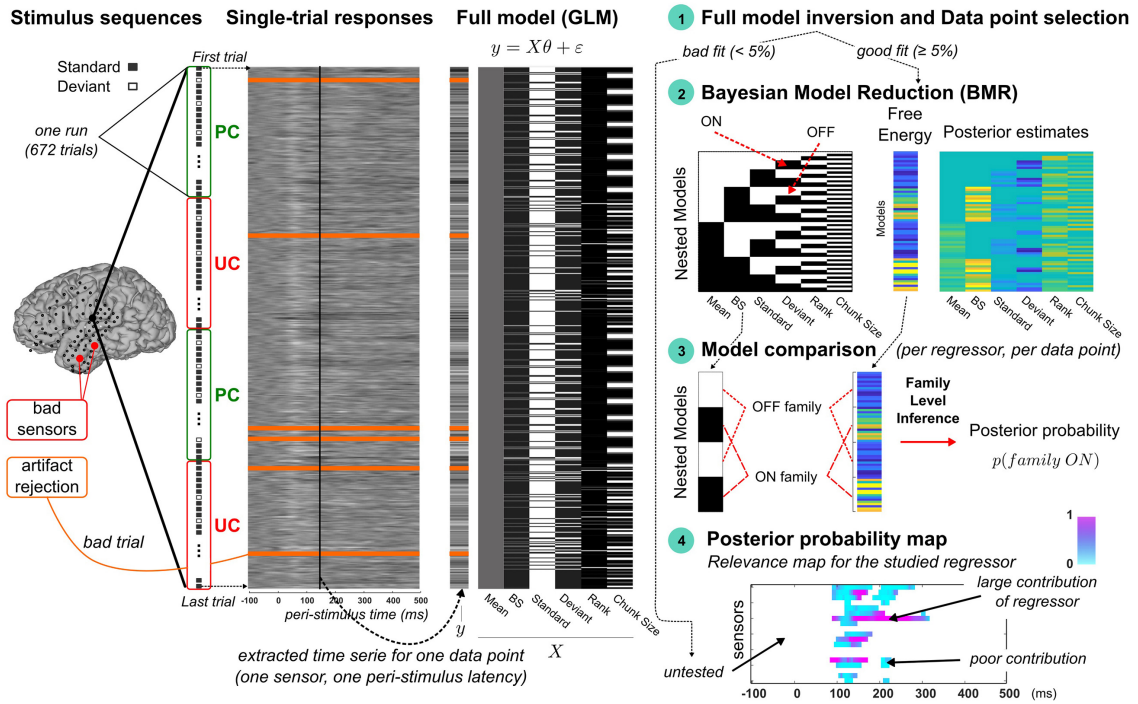

FIGURE 2 | Overview of the trial-by-trial modeling approach. From **left** to **right**. **Stimulus sequences:** Four illustrative runs of an experimental session are represented vertically with standard and deviant indicated by gray and white squares, respectively, and UC and PC contexts delineated by red and green rectangles, respectively. Electrocorticographic sensor overlay on a brain cortical surface (from participant P5) indicates the sensors classified as bad (red) and those retained for the modeling (black). **Single-trial responses:** 2D map of single-trial activity (uV) measured at the highlighted sensor on the brain surface (large black dot). Each row represents the 600 ms epoch of signal elicited by a stimulus of the oddball sequence (first and last trials are shown with dotted arrows). Bad trials (orange lines) are included in the modeling as trial order matters in dynamic processes (the related noisy signal is not accounted for). **Full model (GLM):** an example of design matrix (X) is provided (right) showing typical regressor trajectories (columns) over trials (rows). Data to be fitted (y) pertains to the trial-by-trial time series extracted at a particular latency (vertical black line overlaying the 2D single-activity map). **Step 1, Full model fitting and selection of data points:** data point is found responsive to the full model if goodness of fit is larger than 5%. In this case, the model comparison procedure (steps 2 to 4) is performed. **Step 2, Bayesian model reduction:** left panel (model space): each model (row) corresponds to a nested version of the full model obtained by switching ON (black) and OFF (white) the different regressors. Bottom row represents the full model (all regressors are ON). Right panel: BMR is applied to each nested model to derive the free energy and posterior estimates of model parameters. **Step 3, Model comparison:** for each regressor, two families are compared using family-level inference (Penny et al., 2010). The ON family (indicated here for the dynamic regressor, with BS denoting the Bayesian Surprise) includes all the ON models (black) with associated free energies as indicated with the dotted red lines. The OFF family is defined similarly based on the OFF models (white). **Step 4, Posterior probability map:** Posterior probability of the ON family is then computed at each responsive data point to derive a spatio-temporal map of the regressor's relevance. At each sensor (*y*-axis) and each peri-stimulus latency (*x*-axis), color intensity (from blue to pink) reflect the posterior probability (in [0, 1]). White points corresponds to untested data points due to an unreliable fitting of the full model (unresponsive data point). All maps in this figure are shown with arbitrary color scales.

point (defined in space and time at all good sensors and all peri-stimulus samples). If the resulting goodness of fit was acceptable (according to a criterion described in Section "Data Point Selection"), the data point was considered as model responsive and included for subsequent analysis. The latter aims at identifying the regressor(s) responsible for such responsiveness and rests on steps 2 to 4 of our methodological framework depicted in **Figure 2** (right panel). In step 2, we considered alternative models of the full one, obtained by switching ON and OFF the contributions of all regressors; we employed Bayesian Model Reduction (BMR; Friston et al., 2016) to derive efficiently specific Bayesian quantities that are necessary for the model comparison that comes next. Precisely, model comparison (step 3) was then conducted for each regressor independently at the level of families of models, grouping models where the regressor of interest is present (we will refer to the ON family) and models where it is not (the OFF family). Using family-level inference (Penny et al., 2010), we obtained the posterior probability of the ON family which quantifies how likely the regressor is to have contributed to the data (note that the sum of the ON and OFF family posterior probabilities is equal to 1). Applying this scheme (step 1 to step 3) to all data points (step 4) yields a spatio-temporal description of the regressor's relevance. Such posterior probability map (referring to the ON family) could be computed for each regressor. For sake of clarity, the notion of model will now refer to the GLMs (the full or nested variants) and we will use the term "regressor" to mention the different accounts of sensory processing that we test (some of them were tested as separate "models" in the above-mentioned trial-by-trial studies). This terminology emphasizes the fact that current alternative accounts are not tested as competing in this work.

This modeling approach was first applied to data in both contexts (UC and PC, four runs) to examine sensory processing and test it as Bayesian learning. This analysis is called *GLM analysis* and is described in Section "Assessing Dynamic, Static, and Exponential Contributions (*GLM Analysis*)." We then addressed the adaptation of sensory processing (of Bayesian learning in particular) under predictability in a second analysis (*Predictability analysis*) described in Section "Automatic Context Adaptation of Sound Processing (*Predictability Analysis*)." In this case, we first inverted data in context UC (two runs) to derive estimates of model parameters and these were next used as priors for model inversion in context PC (two runs). In this way, the ON family for one regressor gathers models where its related coefficient could depart from UC prior. The resulting posterior probability map (step 4) thus smartly indicates where and when the cognitive account of sensory processing associated to the regressor is shaped by predictability.

Statistical Model

We considered a general linear model (GLM) of the form:

$$y = h_0 X_0 + h^{BS}_{dyn} X^{BS}_{dyn} + \sum_{i\in\{std,dev\}} h^i_{static} X^i_{static} + \sum_{i\in\{rnk,cs\}} h^i_{exp} X^i_{exp} + \varepsilon \quad (1)$$

Where y is the trial-by-trial time series measured at a given ECoG location and a particular peristimulus time sample across all trials (for each subject, for each sensor, for each run and for each of the $N_s = 120$ samples spanning the [−100 +500] ms epoch, y is a vector of size $N_t = 672$ trials). All parameters of the linear combination (denoted h^*_*) are defined as Gaussian random variables and ε is a Gaussian measurement noise. Regressors (X^*_*) all consist in trial-wise trajectories, each representing a candidate explanatory factor (**Figure 1B**). First term in equation (Eq. 1) corresponds to the mean factor, with X_0 being a unit vector. Below, we present the five regressors that we aimed to assess, and that we grouped in three categories:

• *Dynamic regressor* (X^{BS}_{dyn})

This category involves a learning regressor deriving from an internal generative model that assumes that the brain learns from each stimulus presentation the probability μ to have a deviant to predict the next stimulus category U (with $U_k = 1$ in the case of trial k corresponding to a deviant and $U_k = 0$ in the case of a standard). We define $U \sim Bern\ (\mu)$ with *Bern* the Bernoulli distribution, and $\mu \sim Beta\ (\alpha,\ \beta)$ with α and β the parameters of the *Beta* distribution corresponding to deviant and standard counts at trial k, respectively (Eq. 3). Regressor reflects a precision-weighted prediction error at every sound of the oddball sequence, which expresses as a Bayesian Surprise (BS; Ostwald et al., 2012). In short, BS quantifies the belief updating on μ as it corresponds to the Kullback-Leibler divergence between the prior and the posterior $\mathcal{B}eta$ distributions over μ. At trial k, following the observation of sound input U_k, it writes:

$$BS(U_k) = \log\left(\frac{\Gamma(\alpha_{k-1}+\beta_{k-1})}{\Gamma(\alpha_k+\beta_k)}\right) + \log\left(\frac{\Gamma(\alpha_k)}{\Gamma(\alpha_{k-1})}\right) + \log\left(\frac{\Gamma(\beta_k)}{\Gamma(\beta_{k-1})}\right) + (\alpha_{k-1}-\alpha_k)\left[\psi(\alpha_{k-1}) - \psi(\alpha_{k-1}+\beta_{k-1})\right] + (\beta_{k-1}-\beta_k)\left[\psi(\beta_{k-1}) - \psi(\alpha_{k-1}+\beta_{k-1})\right] \quad (2)$$

Where Γ and ψ are the Gamma and Digamma Euler functions, respectively. Internal states α, β are updated as well as X^{BS}_{dyn} is augmented as follows:

$$\begin{cases} \alpha_{k+1} = U_k + e^{-\frac{1}{\tau}}\alpha_k \\ \beta_{k+1} = (1-U_k) + e^{-\frac{1}{\tau}}\beta_k \\ X_{dyn,k+1} = BS\left(U_k, \alpha_k, \beta_k, \tau\right) \end{cases} \quad (3)$$

Full description of the model is provided in our previous EEG-MEG work (Lecaignard et al., 2021b). As can be seen from equation (Eq. 3) and in **Figure 1B** (lower panel), standard and deviant counts vary with model parameter τ, a time constant that enables controlling the relative influence of past events in belief updating. It can be viewed as the size of the temporal integration window (or memory span). In our previous EEG-MEG study, a more predictable sequence was found to yield an increase in τ, which is consistent with the idea that the more regular or structured the sensory environment, the more one should rely on past events to form predictions. In the following, since regressor X^{BS}_{dyn} is the only one to be both dynamic and the output of a generative learning model, it will be called the *dynamic* or the *learning* regressor equivalently.

• *Static regressors* (X^{std}_{static}, X^{dev}_{static})

We here include two regressors to classify trials according to the actual sensory input (a standard or a deviant sound). X^{std}_{static} equals 1 at every occurrence of a standard stimulus, and 0 at every occurrence of a deviant stimulus. X^{dev}_{static} is the complementary of X^{std}_{static} (it is equal to 1-X^{std}_{static}). Although their respective trajectory is not constant (**Figure 1B**, upper panel), we consider these two regressors as static in the sense that they do not incorporate any time dependency but simply capture stimulus category. They are similar to the 'change detection' regressors defined in previous MMN modeling studies (Lieder et al., 2013; Stefanics et al., 2018; Lecaignard et al., 2021b). They indeed get close to the actual definition of the MMN and the way (averaged) oddball responses are traditionally computed, although typical studies usually discard the first standard following a deviant or even sometimes all standards but the one just preceding a deviant, precisely to get rid of time-dependent (dynamic) effects.

• *Exponential regressors* (X^{rank}_{exp}, X^{cs}_{exp})

Introducing this additional category was motivated by well-established MMN findings, namely that standard responses decrease over stimulus repetitions (Grill-Spector et al., 2006) and that the MMN amplitude increases as the number of standards preceding a deviant (chunk size) increases (Sams et al., 1983).

Note that these inter-trial modulations cannot be predicted by the above static regressors (X^{std}_{static}, X^{dev}_{static}), but could coincide with the predictions from the above dynamic (learning) factor, as was found in Lecaignard et al. (2021b). However, for a fair examination of brain signal dynamics in relation to these MMN findings, we considered two additional regressors accounting for standard repetition effects and deviant history, while not reflecting some output from a specific cognitive process. They concern the rank of stimulus repetition, where at trial k, $rank\,(U_k)$ is defined as the within-chunk number of presentation of current stimulus U_k, and chunk size, where $cs\,(U_k)$ is the size of the current chunk. Both rank and chunk size can take n values in the 2–8 range (they are defined ad-hoc as no generative model is involved here). We used exponential rather than linear factors because of recent EEG findings in the visual modality that showed that these regressors clearly best explain the repetition-suppression effect and its modulation by the number of standard repetitions (Stefanics et al., 2020). Thus, we defined regressors X^{rank}_{exp} and X^{cs}_{exp} as the normalized mean-centered exponential function of trial rank and trial chunk size, respectively. At trial k, we have:

$$\begin{cases} X^{rank}_{exp}\,(U_k) = \dfrac{\exp\left(rank\,(U_k)\right) - \ 1/n \sum_{i=1}^{n} \exp(rank\,(i))}{\exp(\max(rank\,(U)))} \\ X^{cs}_{exp}\,(U_k) = \dfrac{\exp\left(cs\,(U_k)\right) - \ 1/n \sum_{i=1}^{n} \exp(cs\,(i))}{\exp(\max(cs\,(U)))} \end{cases} \tag{4}$$

It should be noticed that since deviant is of rank 1, the only way to account for different brain responses to deviant and standard following a deviant is to involve a mixture of the rank regressor with either the chunk size or the static regressors (our modeling procedure is precisely equipped to test such hypothesis). As can be seen in **Figure 1B**, the rank regressor (middle panel, pink trace) shows a possible dynamics for the expected standard-to-standard variations (as amplitude increases over repetitions, we would expect a negative posterior estimate for coefficient h^{rank}_{exp}) that differs from the BS one (lower panel). Similarly, chunk size regressor (purple) assigns different amplitude to deviants depending on local past experience. The two exponential factors thus enable testing a conservative approach as the learning factor will now be proved explanatory only if it captures trial-wise fluctuations that are not captured by these more traditional factors (May and Tiitinen, 2010).

In sum, our model (that we denote as the full model) enables mixing competing trial-based covariates to refine the spatio-temporal description of cognitive processes engaged during the current oddball sequence exposure. The static category contrasts with the other two as related regressors X^{std}_{static} and X^{dev}_{static} are not equipped to capture time-dependent or trial order effects. Besides, the dynamic and exponential categories differ in their predictions of inter-trial fluctuations: dynamic regressor X^{BS}_{dyn} is computed as the output of a generative model implementing the learning of stimulus regularities whereas the exponential regressors are not directly computationally interpretable (X^{rank}_{exp} and X^{cs}_{exp} do not map onto cognitive mechanism). In the following, we provide in detail the modeling approach that we used to assess the contribution of each regressor over space and time to the ECoG data.

Assessing Dynamic, Static, and Exponential Contributions (*GLM Analysis*)

This first analysis aims at characterizing sensory processing during an oddball sequence (whatever the predictability manipulation, considering both contexts UC and PC), and testing in particular the Bayesian learning of deviant probability that we could evidence previously using EEG and MEG (Lecaignard et al., 2021b). We evaluate the relevance of each linear regressor (n = 6; X^{BS}_{dyn}, X^{std}_{static}, X^{dev}_{static}, X^{rank}_{exp}, X^{cs}_{exp} and $X_0 = 1$) to account for trial-to-trial fluctuations. Each evaluation involves nested versions of the full model, that we compare using Bayesian model comparison and family-level inference (Penny et al., 2010).

First, we here describe the model space for this *GLM analysis*, followed by a description of model inversion. Next, we present the family-level inference procedure performed for each regressor to assess its contribution to the observed data. Finally, we provide the details of two additional studies that were conducted to refine our analysis. The first one is based on simulated data and aims at controlling the ability of our approach to separate models (to infer the *true* generative model). The second consists in replicating the GLM analysis without including the learning regressor to test the specificity of its trial-by-trial dynamics compared to those of exponential regressors.

Model Space

Recently, a novel approach proved efficient to test the relevance of GLM factors, that frames this question in terms of model comparison (Friston et al., 2016, 2018). Precisely, for each regressor, we consider two GLM: one where the regressor is present (or switched ON) and one where it is absent (or switched OFF), using non-null and null coefficient h^*_* in equation (Eq. 1), respectively. Applying the ON/OFF scheme to all regressors, we could build a model space with all possible combinations ($N_m = 2^6 = 64$ models), depicted in **Figure 2** (right panel). As we shall see, evaluating the relevance of one regressor amounts to comparing in a Bayesian model comparison fashion the 32 models where it is ON with the 32 other ones where it is OFF (**Figure 2**, panel "Model Comparison").

Model Inversion

First, we fitted the full model to the ECoG signals in both contexts PC and UC, for each retained data point (that is, for each of the $N_s = 120$ peri-stimulus time sample of each accepted sensor). We used a Variational Bayes (VB) scheme implemented in the VBA toolbox (Daunizeau et al., 2014). Gaussian prior distributions were employed for every coefficient parameter, all with zero mean and non-null variance ($h^*_* \sim \mathcal{N}(0,5)$). We use a similar Gaussian prior for the learning parameter ($log(\tau) \sim \mathcal{N}(2,5)$). Data involved UC and PC runs (two runs per condition) and inversion was achieved in the following fashion: each run ($N_t = 672$ trials) was treated independently (model fit always starts with the above-mentioned priors) but posterior estimate

of each regressor coefficient accounts for the entire set (the four runs). Bad trials were ignored to avoid contaminating model fit with noisy signals but corresponding stimuli still entered model dynamics as they were observed by the brain. At convergence of the VB scheme, model inversion provides the Free Energy approximation of the log-model evidence (Friston et al., 2007), the percentage of explained variance afforded by the model (denoted $R2$) and the posterior distributions of model parameters (τ, h_0, h^{BS}_{dyn}, h^{std}_{static}, h^{dev}_{static},h^{rank}_{exp}, h^{cs}_{exp}). Data point selection was based on full model responsiveness, defined using a threshold on R2 (5%; more details about data selection is provided in Section "Data Point Selection"). Next, regarding the 63 nested models, we employed Bayesian Model Reduction (BMR; Friston et al., 2016) to derive analytically the (reduced) free energy and posterior estimates for each model from those obtained with the full model inversion. BMR affords a great gain in terms of computational resource (only the full model is to be inverted) and has been shown to provide better results than VB nested model inversions that involve iterative optimization procedure, with possibly the undesirable issue of local minima convergence (Friston et al., 2018). In practice, for each switched-OFF regressor, prior distribution of the corresponding regression coefficient was set to $h^*_* \sim \mathcal{N}(0,0)$ with the null variance forcing posterior estimate to stick to the null prior mean. Prior distribution for the switched-ON regressors was equal to ($h^*_* \sim \mathcal{N}(0,5)$).

Family-Level Inference

For each regressor, model comparison relied on family-level inference to compare the ON and OFF families of models, defined by grouping the 32 ON models and the 32 OFF models, respectively (**Figure 2**, panel "Model comparison"). Family comparison was based on the $N_m = 2^6$ free energies described above (full and reduced values). Applying the softmax function to these free energies enables computing the posterior probability of the ON family. The larger the ON posterior probability, the more likely the corresponding regressor contributes to the observed data. We performed ON/OFF family comparison for each regressor to derive the 6 ON posterior probabilities. They enabled us to examine the relevance of each corresponding hypothesis for sensory processing. Importantly, this scheme (6 ON/OFF family comparisons) was performed independently at every responsive peri-stimulus time point at every good electrode, in the aim to finely describe spatio-temporally oddball processing on a single-trial basis. For sake of clarity, the notation "family X^*_* = ON" will be used in what follows to differentiate between families when necessary.

Finally, Bayesian model averaging (BMA; Penny et al., 2006) provides the posterior estimates of model parameters averaged across model space (with model-evidence weighting based on the full and reduced free energies).

Model Separability (Simulation Study)

We investigated the ability of the above-mentioned procedure to recognize the respective contribution of each regressor, in particular with the present case of single-trial signals (as will be seen, the full model inversion yields rather low goodness-of-fit). To do so, we considered BMA posterior estimates of regressor coefficients measured at a particular time point on one electrode in a given participant. The full model was used with these values to generate 100 datasets, each made of two runs per context (UC and PC) using the exact stimulus sequences delivered to that patient. Critically, Gaussian noise was added to the synthetic data and its variance was adjusted so that the percentage of variance explained by the full model when inverting this synthetic set was of the same order of magnitude as the one measured with the real data. Values of R2 (from observed and synthetic data inversion) as well as measurement noise precision are provided in **Table 2**. We refer to these simulated data as the *full* data with regard to their generative model. We then generated another 100 datasets using only a dynamic contribution (τ, h_0, h^{BS}_{dyn} were equal to the BMA values while h^{std}_{static}, h^{dev}_{static}, h^{rank}_{exp} and h^{cs}_{exp} were set to 0); we refer to them as the *learning* data. Last, we generated 100 datasets using only static and exponential contributions (h^{std}_{static}, h^{dev}_{static}, h^{rank}_{exp} and h^{cs}_{exp} were equal to the BMA values while h^{BS}_{dyn} was set to 0); we refer to them as the *non-learning* data. Each of the 300 datasets was confronted to our procedure (full model inversion, BMR and family-level inference). Within each generative model case (*full*, *learning*, *non-learning*), we conducted family model comparison for each regressor. We used a random-effect (RFX) model (Penny et al., 2010) to treat independently each of the 100 simulations.

We applied this scheme to three data points in particular (**Figure 3A**) at which we found strong evidence for both standard and learning (case 1, a posterior temporal electrode in P5 at 130 ms), for learning only (case 2, posterior temporal electrode in P5 at 180 ms), and for standard only (case 3, posterior temporal electrode in P4 at 150 ms). Values of R2 and BMA estimates of τ, h^{BS}_{dyn} and h^{std}_{static} obtained from real data fitting are provided in **Table 2**. Applying the above-described modeling procedure to the resulting synthetic datasets, we would conclude in favor of model separability afforded by our modeling approach if for each case we could select the true regressor(s) *and* reject the null ones in the *full, learning* and *non-learning* RFX analyses.

The selected values for noise precision yielded R2 values that were found on average over simulations close to the observed data value, suggesting that we succeeded in generating similar conditions of data fitting between predicted and observed conditions (**Table 2**). For each case, RFX family inference (**Figure 3D**) indicated that contributions from dynamic and standard regressors could be retrieved when present in the true model (posterior exceedance probability = 1.0). In all three cases however, the different posterior probabilities for family $X^{BS}_{\text{dyn}} = ON$ obtained over simulations showed values between 0.4 and 1.0 (**Figure 3C** and **Table 2**). It is important to acknowledge this variability and keep in mind that real data inversion could well yield a posterior probability value within that range. Regarding the *learning* data, very poor goodness-of-fit was found over simulations (mean R2 = 0.2%) in case 3. This was expected as these data were generated with no contribution from the dynamic regressor. We obtained similar results with the *non-learning* data in case 2 (mean R2 = 0.2%). Importantly, as can be seen in **Figure 3**, *learning* and *non-learning*

TABLE 2 | Parameters and results obtained in the simulation study.

	ECoG inversion			Simulations		Full	Learning	Non-learning
				Noise precision		0.004	0.004	0.004
Case 1	**R2**		14.7	**R2 (mean)**		13.0	6.9	2.0
	Pp	X^{BS}_{dyn} / X^{std}_{static}	> 0.99 / 0.86	X^{BS}_{dyn}	**Pp range**	0.4–1.0	0.4–1.0	0.0–0.1
	BMA	$log(\tau)$	3.853		**RFX**	1.0	1.0	0.0
		h^{BS}_{dyn}	–0.128	X^{std}_{static}	**Pp range**	0.3–0.7	0.0–0.0	0.0–1.0
		h^{std}_{static}	0.006		**RFX**	1.0	0.0	1.0
				Noise precision		0.003	0.003	0.003
Case 2	**R2**		12.6	**R2 (mean)**		12.2	12.1	0.2
	Pp	X^{BS}_{dyn} / X^{std}_{static}	> 0.99 / 0.002	X^{BS}_{dyn}	**Pp range**	0.4–1.0	0.4–1.0	0.0–0.0
	BMA	$log(\tau)$	2.870		**RFX**	1.0	1.0	0.0
		h^{BS}_{dyn}	–0.094	X^{std}_{static}	**Pp range**	0.0–0.0	0.0–0.0	0.0–0.0
		h^{std}_{static}	0.000		**RFX**	0.0	0.0	0.0
				Noise precision		0.002	0.002	0.002
Case 3	**R2**		15.9	**R2 (mean)**		16.1	0.2	16.4
	Pp	X^{BS}_{dyn} / X^{std}_{static}	0.15 / > 0.99	X^{BS}_{dyn}	**Pp range**	0.0–0.1	0.0–0.1	0.0–0.1
	BMA	$log(\tau)$	2.761		**RFX**	0.0	0.0	0.0
		h^{BS}_{dyn}	0.000	X^{std}_{static}	**Pp range**	0.0–1.0	0.0–0.0	0.0–1.0
		h^{std}_{static}	0.026		**RFX**	1.0	0.0	1.0

*Three simulation analyses (Case 1, Case 2 and Case 3) were performed using different model parameter values inferred from ECoG data (see **Figure 3A**). For each case (rows), specific findings from ECoG inversion are provided (left): explained variance of full model fitting (R2) expressed as percentage, family ON posterior probability (Pp) for the learning and standard regressors, and BMA estimates of model time constant (τ), learning and standard regressor coefficients. Simulation results obtained from fitting the synthetic datasets generated with the full, learning, and non-learning GLM are provided (right). Measurement noise precision corresponds to the inverse variance of the Gaussian noise added to the synthetic data. R2 corresponds to the average over the 100 simulations. Pp range: minimum and maximum posterior probability values of family ON observed over the 100 simulations. RFX: posterior exceedance probability of family ON resulting from model comparison performed over the 100 simulations. X^{BS}_{dyn}, X^{std}_{static}, h^{BS}_{dyn}, h^{std}_{static} and τ correspond to GLM parameters described in the main text.*

data inversions yielded RFX family comparison that always indicated strong evidence for the true contributing regressor and poor evidence for the non-contributing ones. Overall, these findings demonstrate the reliability of this scheme (full model inversion, BMR and family-level inference) for single trial data analysis.

Specificity of the Bayesian Surprise Dynamics

The learning regressor was found necessary to account for trial-by-trial data in a spatially restricted but robust fashion (posterior probability of ON family ≥ 0.9), while the exponential ones could be clearly rejected. To better understand this effect, we next examined the specificity of the BS time course over trials in comparison to the exponential ones (**Figure 1B**). In other words, we assessed whether the exponential contributions could provide a better fit when taking the learning factor out of the model (in this way, we derive a model space comparable to the one used in the study by Stefanics et al. (2020), where the exponential model was found winning). We thus ran another time the ON/OFF family comparison (**Figure 2**, step 3) for each regressor and at each responsive data point, over the subset of model space where X^{BS}_{dyn} was absent ($N_m = 32$). Increased evidence for the $X^{rank}_{exp} = ON$ and $X^{cs}_{exp} = ON$ families would indicate the relevance of a dynamic trajectory, be it exponential or learning-based. On the contrary, similar rejection of exponential regressors as when learning is present would point to the BS specificity and strengthen the finding of a contribution of the learning regressor.

Automatic Context Adaptation of Sound Processing (*Predictability Analysis*)

This second analysis pertains to the modulatory effect of predictability on learning, an effect measured at the group-level using EEG-MEG recordings. In this previous work, we considered a learning model that expresses as the present GLM (Eq. 1) reduced to the X_0 and the X^{BS}_{dyn} contributions. Each context (UC, PC) was treated separately and we tested for a difference in the resulting posterior estimates using an ANOVA. Such a predictability effect could be observed at the group-level as a difference in the posterior estimates of the learning parameter τ between contexts (we found $\tau_{PC} > \tau_{UC}$).

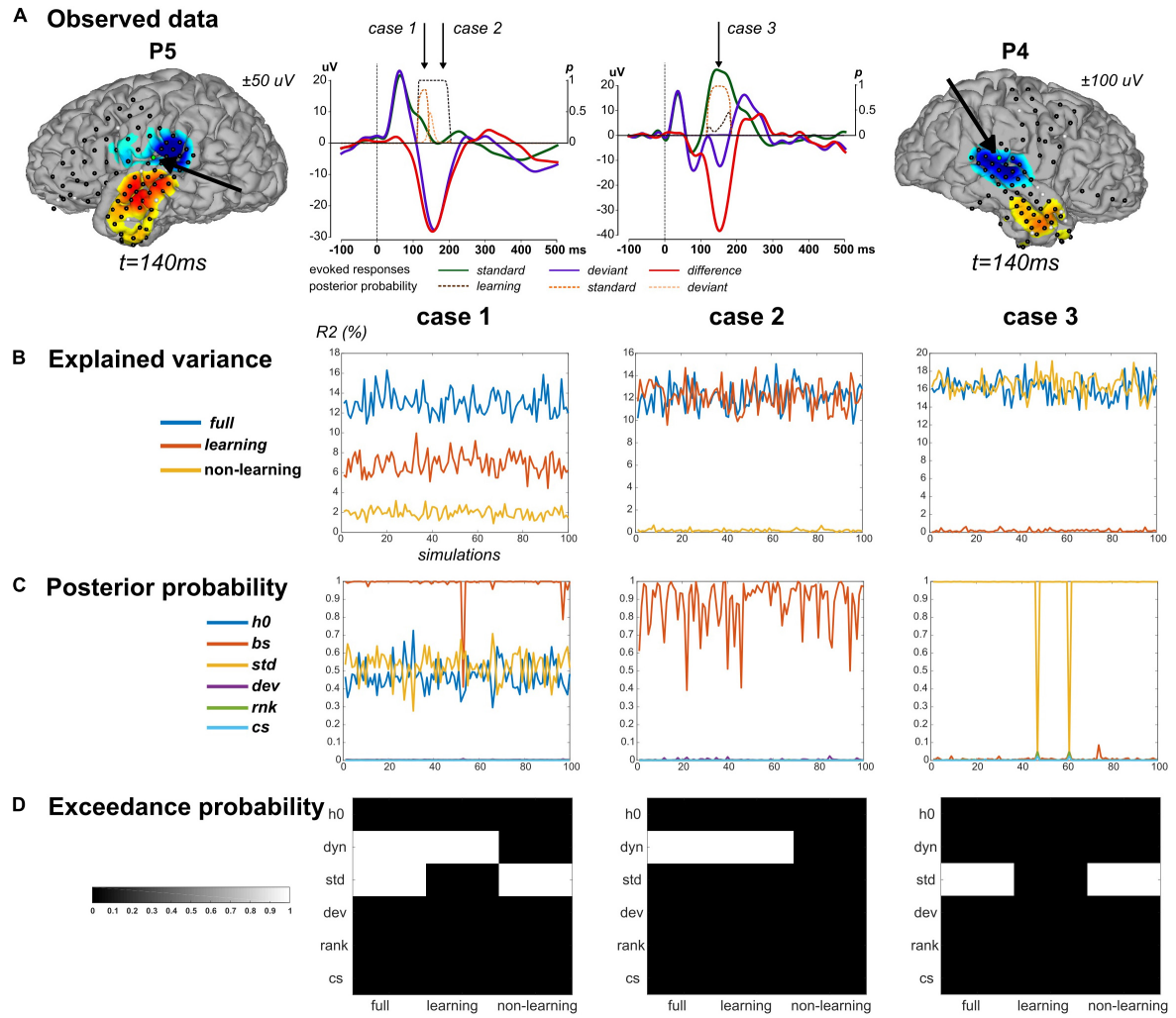

FIGURE 3 | Simulation findings. **(A)** Simulations were based on parameter values inferred from ECoG data fitting. Three cases were considered. Case 1 and Case 2 concern one sensor in P5, highlighted on the cortical surface (same display as in **Figure 5A**). Corresponding evoked responses at this sensor (average response across contexts UC and PC), for standard (green), deviant (purple) stimuli, and their difference (red), and posterior probabilities at peri-stimulus samples for the learning (brown), standard (orange) and deviant (yellow) regressors suppress (color code provided on the figure). Case 3 derived from one sensor in P4 (right). Cases are presented in columns in panels **(B–D)**. **(B)** Percentage of explained variance when fitting the full model to 100 simulated data (*x*-axis) generated from the full (blue), learning (red) and non-learning (yellow) models. **(C)** Posterior probability of each regressor (following the legend provided) for each simulated data with the full model. **(D)** Posterior exceedance probability for each regressor (*y*-axis) computed from family-level inference (RFX) performed over the 100 simulations generated from the full, learning and non-learning models (*x*-axis).

Here, to assess the difference in auditory processing between the two contexts, we adopt a different procedure inspired from typical analysis using dynamic causal models, where one experimental condition is defined as the basic process performed by the brain while the other condition is treated as perturbing this basic state (Garrido et al., 2009a; Kiebel et al., 2009). The strength of such approach lies in the fact the identification of specific model parameter(s) that capture(s) the difference between conditions is itself informative about the mechanisms behind such different processing. Not only this approach accounts very well for the expected predictability effect that we seek (an automatic adaptation of typical oddball processing through the modulation of the learning process) but also, from a methodological perspective, testing it can be handled very nicely with the ON/OFF family-level inference procedure deployed in the *GLM analysis*.

Precisely, we here started fitting only the UC data using the same priors as defined in the previous section, and the resulting estimates of model parameters (regressor coefficients and learning parameter τ) enabled to characterize a baseline for oddball processing. These values were next used as priors to fit the GLM with the PC data; here again the full model was inverted using a variational approach and the nested ON/OFF models were treated using BMR. The ON/OFF family comparison scheme was applied to model parameters (this time including τ) in context PC. Importantly, since priors were no longer null

(depending on UC data), the ON/OFF family comparison now enables testing the conformity/departure from priors resulting from the posterior estimates after fitting UC data, which speaks to the absence/presence of predictability effect. In sum, we here assess whether model parameters (the regressor coefficients, and the learning rate τ) in context PC should depart from baseline (UC) value in order to account for learning in a predictable context.

In more detail, we restricted the analysis to data points where evidence for learning was supported in the previous analysis. We chose a threshold of 0.75 on family $X^{BS}_{\text{dyn}} = ON$ posterior probability to that aim. For a fair examination of all predictability effects, we also included data points showing evidence for other contributing regressors (using the same threshold on posterior probability). In sum, all data points showing at least one regressor (except mean regressor X_0) for which posterior probability of the ON family was larger than threshold was included in the present analysis.

Starting with context UC, we applied the procedure described in **Figure 2** (step 1 to step 3) to derive BMA posterior estimates for every regressor coefficient. To obtain a fine estimate of the learning parameter in that context, we used those posterior estimates as priors over corresponding parameters in a dedicated inference where ($h_* \sim \mathcal{N}(\mu_{h*,BMA},5)$) while keeping an uninformative log-normal prior over the learning parameter itself ($log(\tau) \sim \mathcal{N}(2, 5)$). The resulting posterior mean estimates were then used as prior means for subsequent inversions in context PC. Regarding prior variance, an important distinction was made between the learning and static investigations. For the former, we expected predictability to affect learning parameter but not the regressor coefficient. This is because τ is an evolution parameter involved in the learning process (it shapes the effect of learning over trials) while h^{BS}_{dyn} is an observation parameter used to map hidden activity (here the BS) onto actual measurements (at the sensor level). Contrary to the evolution parameter, this observation one is meant to capture biophysical properties of the data generative process that are unrelated to the cognitive processes at play. This led us to set the following prior variance (for convenience, notation h^{BS}_{dyn} has been reduced to *dyn* in subscripts):

$$\begin{aligned} \sigma_\tau &= \begin{cases} 5 & if\ X^{BS}_{dyn} = ON \\ 0 & otherwise \end{cases} \\ \sigma_{dyn} &= 0 \end{aligned} \tag{5}$$

For regressors X^{std}_{static}, X^{dev}_{static}, X^{rank}_{exp}andX^{cs}_{exp}, which do not include any evolution parameter but a single observation one (h^*_*), prior variances were set as follows:

$$\sigma* = \begin{cases} 5 & if\ X^*_* = ON \\ 0 & otherwise \end{cases}$$

Similarly, we did not allow for offset parameter h_0 to vary between contexts, considering the prior distribution $h_0 \sim \mathcal{N}(\mu_{0,BMA}, 0)$.

Following full model inversion in PC using these adjusted prior distribution, the BMR and family-level inference procedure (**Figure 2**, steps 2, 3) was performed to assess the relevance of the evolution (τ) and observation (h^*_*) parameters. This procedure was run separately for each parameter category. For the evolution parameter τ, at every data point that showed a significant learning effect in the previous GLM analysis ($p(X^{BS}_{\text{dyn}} = ON) \geq 0.75$), family-level inference was run over a model space with 2 models (τ being ON/OFF). Regarding the observation parameters, similarly we selected data points that showed at least a significant contribution of the static or the exponential models in the previous GLM analysis. As the number of these effects varies from one data point to another, the model space was therefore specific to each of them (it comprises 2^n models with n the number of free parameters or, equivalently, the number of significant effects at that particular data point).

We also considered testing the predictability effect on the MMN component, as a significant reduction under context PC was measured at the group-level using each EEG and MEG modality separately (Lecaignard et al., 2015, 2021b). To that aim, at the individual level, we focused on post-stimulus time points in 100 and 200 ms where the MMN could be identified in all participants (**Figure 5B**). For each sensor that exhibited a learning effect in the *GLM analysis* (posterior probability larger than 0.75) at least in one of these time points, we averaged the [100 200] ms data for each accepted single trials. The resulting values were then examined using an unbalanced two-way ANOVA with a factor of stimulus type (standard, deviant) and a factor of context (UC, PC) in MATLAB (R2017b, The MathWorks Inc.).

Data Point Selection

Electrocorticographic grids provide a large number of electrodes, in particular high-density grids such as the one used with P2. For the sake of tractable computations as well as not to draw conclusions out of very poor model fits, we restricted the above analysis to ECoG electrodes with a fair amount of explained variance. Indeed, single-trial modeling approaches are quite recent, with no established standard regarding the expected explained variance contrary to more conventional ERP analysis. In a recent ECoG study (Sedley et al., 2016), a linear model composed of learning-based regressors (surprise, prediction error and precision trajectories) was applied to time-frequency data and resulted in an explained variance of the order of 2% or less, across subjects and electrodes. Here we selected data points based on the percentage of explained variance when fitting the full model to the pooled UC and PC data. Inspection of R2 values obtained at each sample, each sensor (**Figure 4A**) shows that R2 reached values up to 37.2%.

We further computed the individual evoked responses to standard and deviant sounds, and their difference exhibiting the MMN. Overlaying R2 time series on these responses (resulting from model inversions at each peri-stimulus time sample) revealed that maximum R2 values did coincide with electrodes and latencies showing the MMN (**Figure 4B**). Based on this

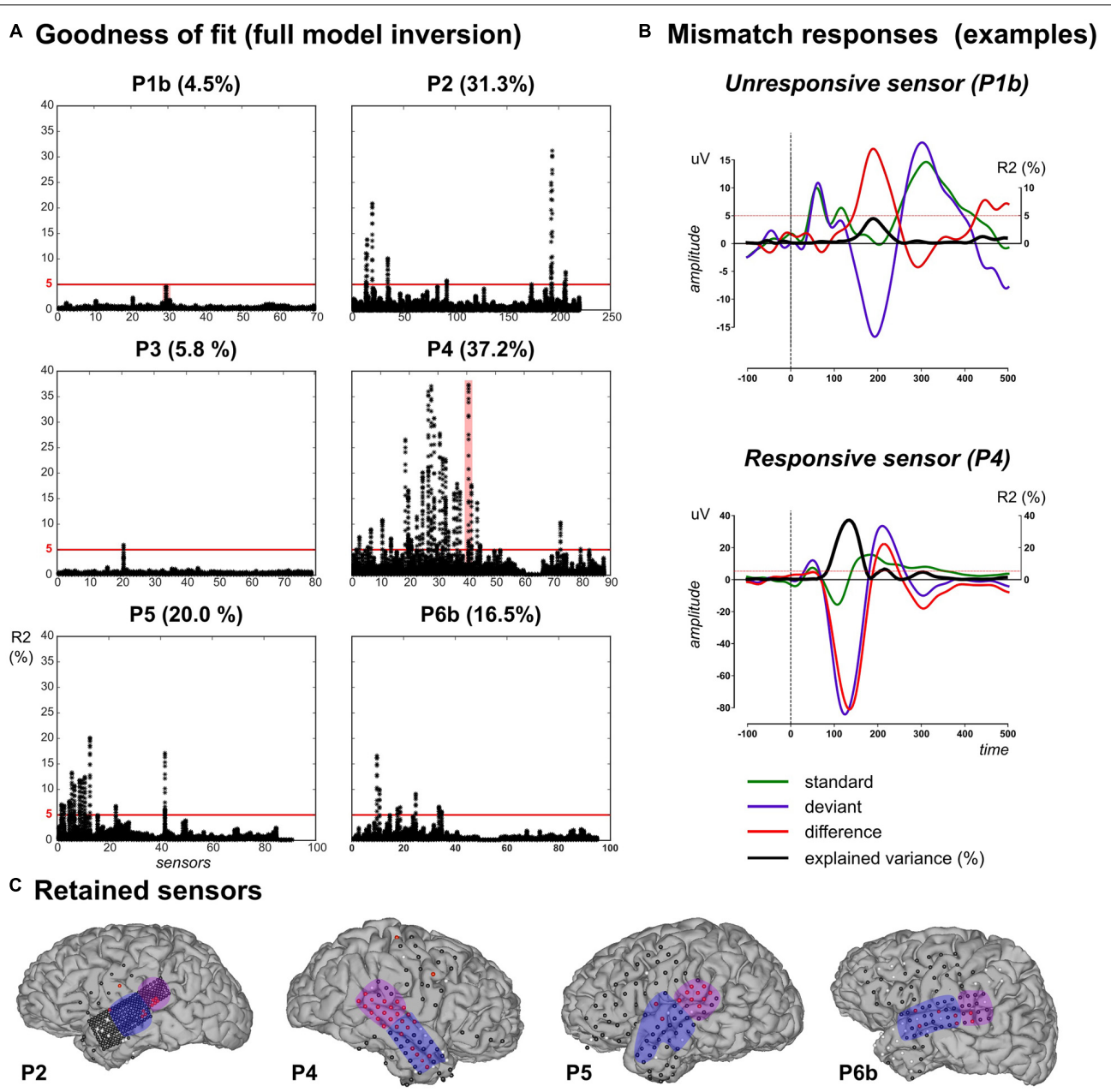

FIGURE 4 | Data selection based on goodness-of-fit in the full model inversion. **(A)** For each patient, explained variance (R2 percentage value) measured at each sensor (*x*-axis) for each peri-stimulus sample inversion ($N_s = 120$ black dots covering the [–100, 500] ms epoch per sensor). **(B)** Evoked responses elicited by standard (green), deviant (purple) and their difference (red) for two unresponsive (in P1b, upper plot) and responsive (in P4, lower plot) sensors. These two sensors are highlighted (red shaded areas) in panel **(A)**. Black trace indicates the R2 time-course. Red horizontal lines indicate the 5% threshold. **(C)** Cortical surface with sensor overlay in the four patients included in the present work. Selected sensors based on R2 thresholding are depicted in red, unresponsive and bad (rejected) sensors are in black and white, respectively. The present findings were measured in the anterior (blue) and posterior (purple) temporal regions.

qualitative investigation, we decided to apply an R2 threshold of 5% for data selection. This value resulted in the rejection of all data from P1a and P1b. In patient P3, only one electrode proved above-threshold (5.8%; over 4 consecutive time samples from 180 to 195 ms, see **Supplementary Material**). Finally, 10, 28, 11, 18, and 7 sensors fulfilled the selection criterion for patients P2, P4, P5, P6a, and P6b, respectively.

The above-described simulation study could confirm the validity of this data selection procedure with a 5% threshold for explained variance to separate models reliably.

All selected electrodes were found distributed over temporal regions (except for one parietal sensor in P4). In the following, for convenience, we present the results on those electrodes, which we split into two groups:

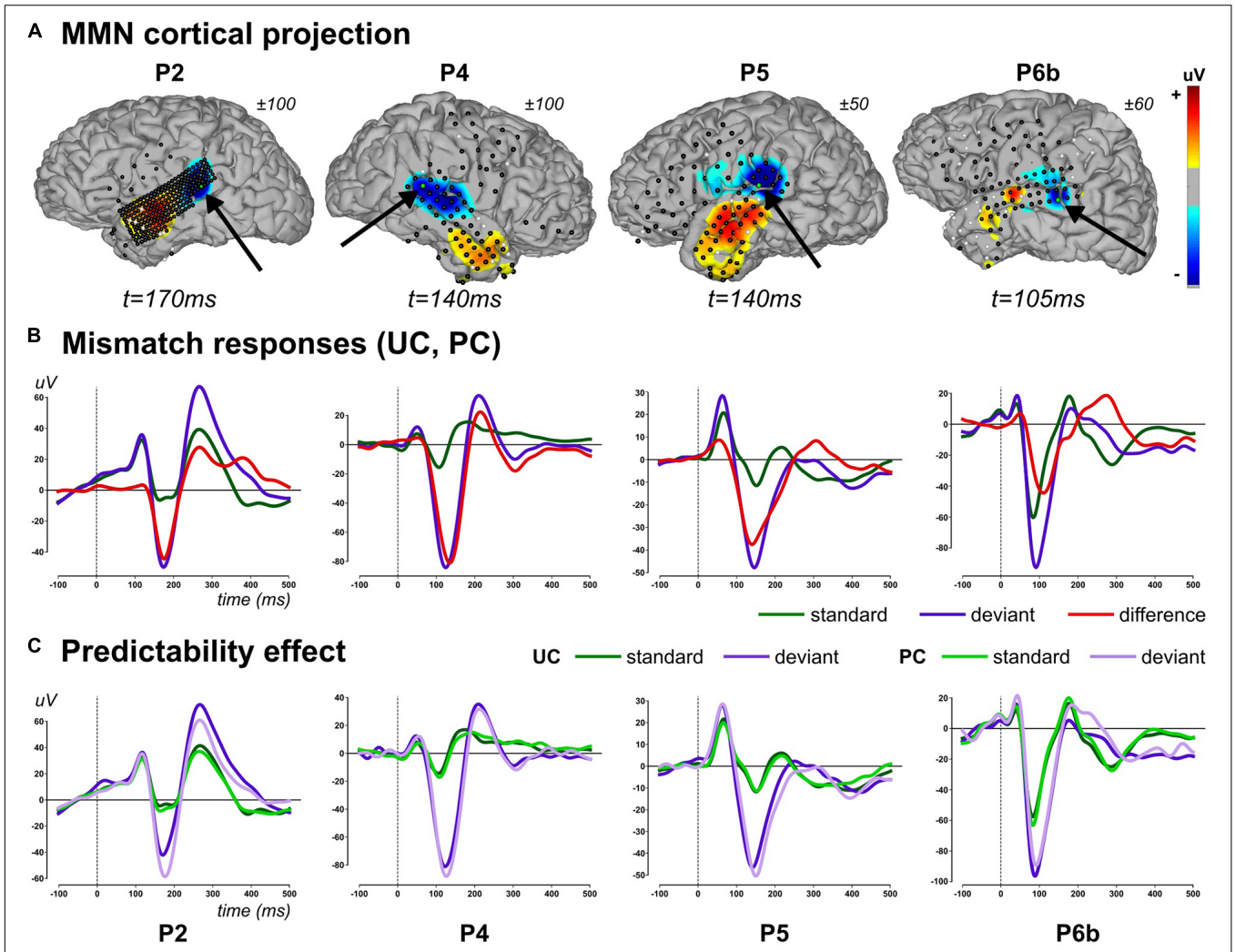

FIGURE 5 | Mismatch evoked responses (2–20Hz). **(A)** Projection of difference responses (deviant–standard) around the MMN peak onto cortical surface (linear projection based on sensor-to-mesh distance), for each patient (columns). Latency and amplitude range are provided for each patient. Sensor overlay: black and white dots represent good and bad sensors, respectively. For each cortical map, black arrow points to a relevant electrode (green dot) showing an MMN, whose evoked activity is provided in lower panel. **(B)** Average evoked activity across contexts (UC and PC) for standard (all of them including those of rank 1), deviant stimuli, and their difference for each patient (column), at a particular electrode (highlighted in panel **A**). **(C)** Evoked standard and deviant responses at the same electrode in context UC and PC. Panels **(B,C)**: traces are baseline corrected (–100 to 0 ms) and follow the color code provided.

the anterior and the posterior part of the temporal lobe, respectively (**Figure 4C**).

RESULTS

We report findings measured in four patients (P2, P4, P5, and P6b), first identifying the relevant explanatory variables and their spatio-temporal mapping (*GLM analysis*), and then testing for the effect of our experimental manipulation (*Predictability analysis*). Typical evoked responses to standard (occurring at any position within a chunk) and deviant stimuli as well as their differences are shown in **Figure 5B**, along with standard and deviant waveforms measured in each context separately (UC, PC) in **Figure 5C**.

Results in both sections below were obtained from selected data points (see "Materials and Methods" section). We do not report findings regarding the constant regressor (coefficient h_0 in Eq. 1); they are provided as **Supplementary Material** (**Supplementary Figure S4**).

GLM Analysis

Responsive data points (R2 $\geq$ 5%) were all found in the post-stimulus interval, at samples exhibiting the MMN in the following time windows: 145–325 ms in P2, 100–335 ms in P4 (one anterior temporal sensor showed also later responsiveness in 405–470 ms), 115–290 ms in P5, and 90-215 ms in P6b. We start by presenting the family-level inference results obtained with the ECoG data (UC and PC contexts) in the aim to assess the presence of each regressor in the GLM. We next show the effect of

switching off the contribution of the dynamic regressor onto the estimated contribution of the static and exponential covariates in order to test if the latter could compensate for the BS absence due to the alternative dynamics they entail (**Figure 1B**).

GLM Analysis (*Fitting UC and PC Data*)

Figure 6 shows the posterior probability of families $X^{BS}_{\text{dyn}} = ON$, $X^{std}_{\text{static}} = ON$, and $X^{dev}_{\text{static}} = ON$ measured at responsive time points in the anterior and posterior temporal clusters. In the anterior region, there were 4, 11, 2, and 5 responsive sensors (showing at least one sample with full model inversion R2 $\geq$ 5%) in P2, P4, P5, and P6b, respectively. Across the four subjects, the learning regressor (X^{BS}_{dyn}) was not found relevant at most responsive data points (median value of posterior probability: 0.09), with only three data points showing posterior probability larger than 0.5 (one sensor in P2, from 230 to 235 ms, $p > 0.78$; one sensor in P6b at 130 ms, $p = 0.81$). In contrast, strong evidence for the standard regressor (X^{std}_{static}) was measured predominantly (median value = 0.72). Posterior probability was found larger than 0.9 over at least one time point in 2/4, 7/11, and 2/5 sensors in P2, P4, and P6b, respectively (depicted in blue in **Figure 6A**). Regarding the deviant regressor (X^{dev}_{static}), posterior probability median was found equal to 0.26; data points showing values exceeding 0.9 could be found in P4 (one sensor at 425 ms), P5 (one sensor from 135 to 150 ms) and P6b (2 electrodes, from 210 to 215 ms, and from 190 to 205 ms, respectively) (depicted in green in **Figure 6A**). Concerning the exponential covariates (X^{rank}_{exp}, X^{cs}_{exp}), they both showed low posterior probabilities across patients. Regarding X^{rank}_{exp}, maximum posterior probability did not exceed 0.29 in all patients, but P6b (0.87 at 170 ms). Similarly, maximum posterior probability of X^{cs}_{exp} was smaller than 0.39 in all patients, but P2 (0.85 at one sensor, from 265 to 270 ms).

In the posterior temporal clusters, we report 4, 15, 9, and 2 responsive electrodes in P2, P4, P5, and P6b, respectively. No clear evidence supporting family $X^{BS}_{\text{dyn}} = ON$ was found in P2 (maximum value of 0.83, at one sensor from 200 to 215 ms) but in P4, P5, and P6b (each with maximum value of 1.0; 5/15, 8/9, and 2/2 electrodes above 0.9, respectively; depicted in red in **Figure 6B**). Across subjects, this learning effect was spanning from 85 to 215 ms (one sensor in P4 also showed posterior probability larger than 0.9 from 140 to 270 ms). For the static category, P4 showed 7/15 sensors with posterior probability larger than 0.9 over at least one time point but this effect was not found in the other three patients: maximum probability for $X^{std}_{\text{static}} = ON$ was equal to 0.72, 0.86, and 0.72 in P2, P5 and P6b, respectively. Regarding the deviant regressor, its contribution was found relevant in 1/4 sensor in P2 ($p > 0.92$ from 155 to 185 ms) and 3/15 sensors in P4 ($p > 0.91$ from 125 to 135 ms; $p = 0.95$ at 130 ms; $p > 0.98$ from 150 to 155 ms) but not in P5 and P6b (maximum posterior probability of 0.72 in both cases). In patient P4, 3 electrodes revealed learning and static effects (depicted in purple and cyan in **Figure 6B**) but not occurring at the same latency. For the exponential models, two patients disclosed an effect for $X^{rank}_{\text{exp}} = ON$: in P2, posterior probability was larger than 0.94 in 3/4 sensors from 165 to 185 ms, and in P5, it was larger than 0.91 in 1/9 sensor from 150 to 170 ms. No evidence could be suggested in P4 and P6b as maximum values were equal to 0.19 and 0.02, respectively. For family $X^{cs}_{\text{exp}} = ON$, posterior probabilities were all measured below 0.64, 0.06, 0.37 and 0.01 in P2, P4, P5 and P6b, respectively.

Specificity of Bayesian Surprise Dynamics

As the above findings supported the learning of the deviant probability (hence a dynamic process) in the posterior temporal region, we next examined if the exponential regressors (X^{rank}_{exp} and X^{cs}_{exp}) would be sufficient to capture this dynamics or whether the proposed learning dynamics would still be required to better explain the data.

Results are shown in **Figure 7**. First, it should be noticed that in P2, family-level inference for each regressor (except X^{BS}_{dyn}) revealed similar results as the full model space analysis (this can be seen for X^{std}_{static} and X^{dev}_{static} by comparing posterior probability maps between **Figures 6**, **7**). This is because data in this patient did not support the learning model (poor evidence for $X^{BS}_{\text{dyn}} = ON$). Based on findings in P4, P5 and P6b where it was found relevant, we see that the exponential hypothesis could be rejected: across these patients, median posterior probability was equal to 0.005 and 0.004 for families $X^{rank}_{\text{exp}} = ON$, and $X^{cs}_{\text{exp}} = ON$, respectively. On the contrary, the absence of learning contribution tend to increase the estimated contribution of the static family, as median posterior probability increases from 0.26 to 0.61, and from 0.14 to 0.55 for the standard and deviant regressor, respectively (over P4, P5, and P6b). However, this increase remains limited as when focusing on data points with strong learning evidence ($p(X^{BS}_{\text{dyn}} = ON) \geq 0.9$), these median values were found to change from 0.07 to 0.33 and from 0.03 to 0.40 for the standard and the deviant regressor, respectively.

Predictability Effect

In this second analysis, we test the hypothesis of an automatic adaptation of sound processing in the predictable context. We first report the analysis of the MMN component, followed by a presentation of the single-trial modeling findings.

In the [100 200] ms window, there was 1, 6, 9, and 3 sensors in participants P2, P4, P5 and P6b, respectively, that showed a posterior probability of family $X^{BS}_{\text{dyn}} = ON$ larger than 0.75 over at least one time point. The ANOVA revealed a significant main effect of stimulus type (standard, deviant) in all sensors in all participants ($p < 0.0001$). Without correcting p-values for multiple tests performed over sensors, no significant main effect of the factor context (UC, PC) could be observed in P2, P5 and P6b (P2: $F(1,1638) = 0.99$, $p = 0.34$; P5 (larger effect across the 9 sensors): $F(1,2163) = 3.39$, $p = 0.07$; P6b (larger effect across the 3 sensors): $F(1,3195) = 4.96$, $p = 0.03$). In P4, there were 5 out 6 sensors that disclosed a significant reduction of amplitude in context PC (smaller effect across the 5 sensors: $F(1,1987) = 8.42$, $p<0.004$; non-significant sensor: $F(1,1987) = 0.49$, $p = 0.48$). The stimulus type by context interaction, which corresponds to the predictability effect on the MMN, was not supported by any sensors in all participants (P2: $F(1,1638) = 0.94$, $p = 0.32$; P4

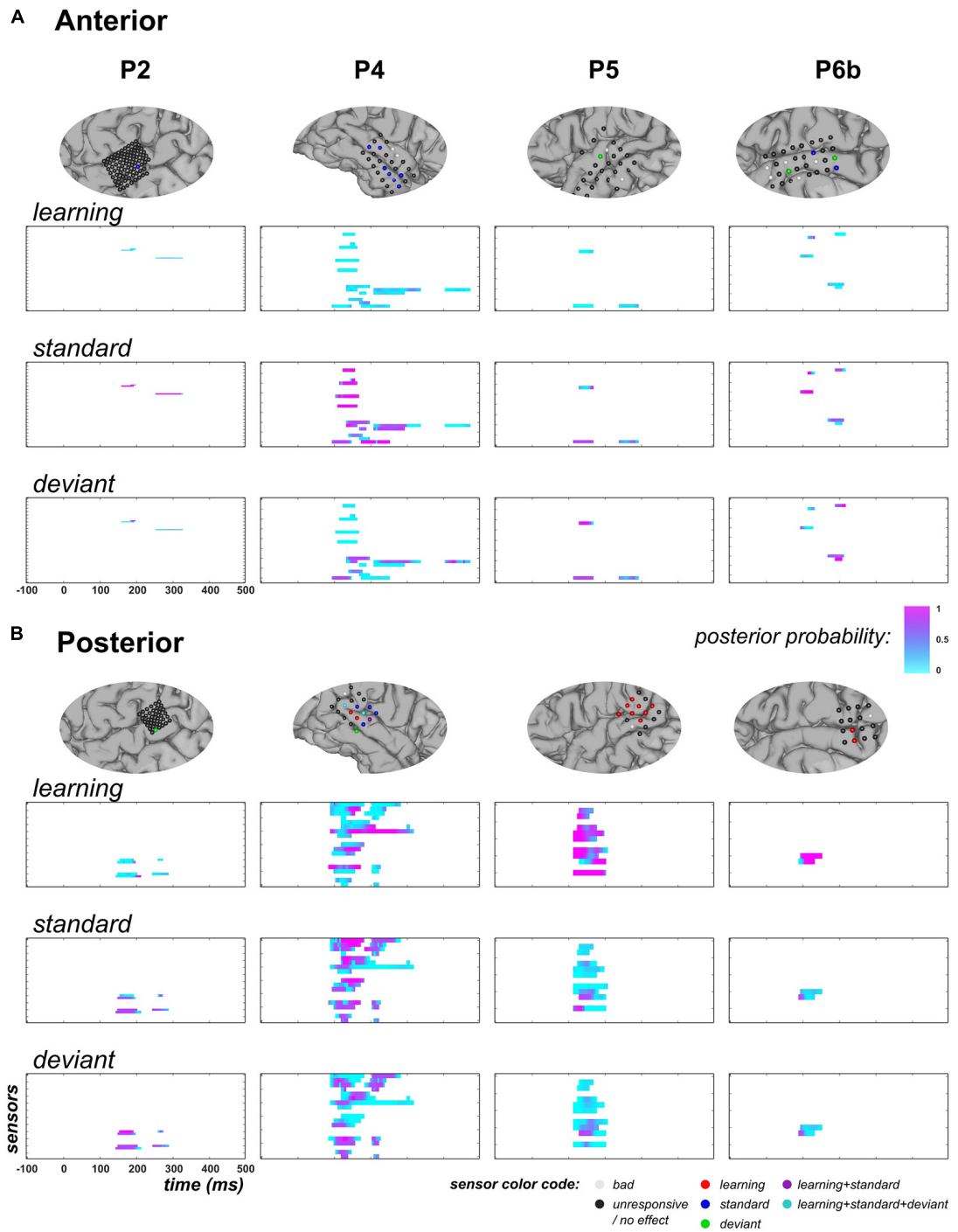

FIGURE 6 | GLM findings at temporal electrodes (across contexts, UC and PC). **(A)** Anterior overlay. Top row: for each subject (columns), zoomed view of cortical mesh with anterior temporal electrodes (following the clustering depicted in blue in **Figure 4C**). Electrodes exhibiting a posterior probability larger than 0.9 in the 50–250 ms time window (at least one sample) for one or multiple regressors are colored following the code provided at the bottom right of the figure. Rows 2 to 4: family-level inference for regressor X^{BS}_{dyn}, X^{std}_{static}, and X^{dev}_{static}, respectively. Each graph represents the posterior probability of family X^{*}_{*} = ON, measured at each peri-stimulus sample. **(B)** Posterior overlay. Same display, with electrodes in posterior clusters (purple cluster in **Figure 4C**).

(larger effect across the 6 sensors): $F(1,1987) = 2.42$, $p = 0.12$; P5 (larger effect across the 9 sensors): $F(1,2163) = 2.23$, $p = 0.14$; P6b (larger effect across the 3 sensors): $F(1,3195) = 3.35$, $p = 0.07$). The latter finding fits well with the similar difference (deviant-standard) traces obtained in contexts UC and PC represented in **Figure 5C**.

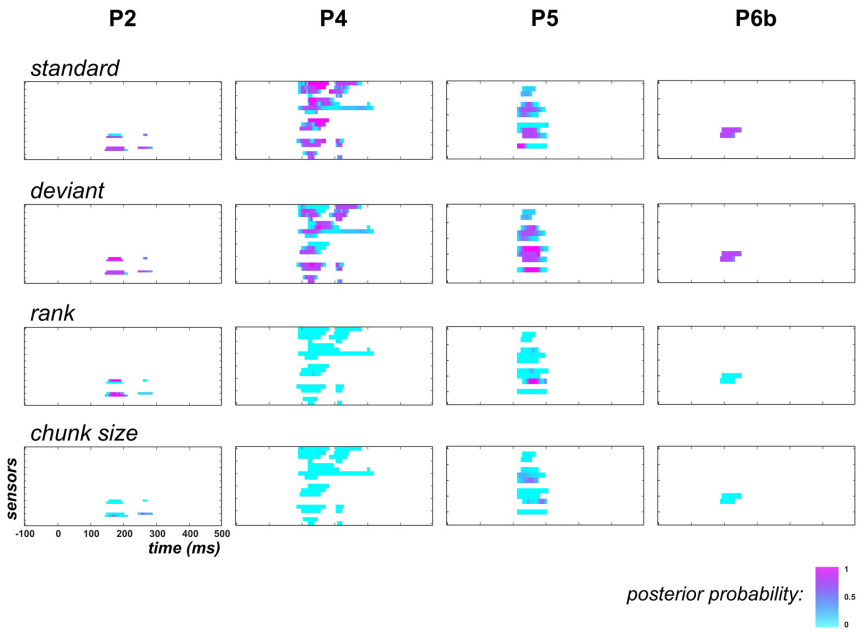

FIGURE 7 | Family-level inference in posterior temporal region when learning is removed from the GLM (UC and PC). Following the display in **Figure 6**, each individual map shows the posterior probability at posterior temporal sensors and at each peri-stimulus time point for families X^{std}_{static} = ON (**top row**), X^{dev}_{static} = ON (upper central), X^{rank}_{exp} = ON (**lower central**) and X^{cs}_{exp} = ON (**bottom**).

TABLE 3 | Selection of data points for the Predictability analysis.

Subjects	Selected data points	Sensors	Time windows	Learning	Standard	Deviant	Rank	Chunk size
P2	48	7	155–320	5	22	7	21	2
P4	186	19	85–455	67	117	15	0	0
P5	81	11	115–200	69	6	6	6	0
P6b	33	7	100–215	19	8	6	1	0

*Selection was based on findings in the GLM analysis shown in **Figure 6**: all data points that disclosed a posterior probability larger than 0.75 in at least one regressor (except mean regressor X_0) was included in the Predictability analysis. For each participant (rows), columns 2 to 4 provides the number of selected data points, their spatial extent (number of sensors involved) and their temporal extent (in ms). Columns 5 to 9 specify the number of selected data points that involved the corresponding regressor (multiple regressor effects could occur at the same peri-stimulus latency).*

The single-trial modeling analysis is based on the GLM and ON/OFF family-level inference scheme employed in the *GLM analysis*. Here it was adjusted at the level of prior definition to test if model parameters depart from the values inferred in the UC context when the GLM (and nested variants) is fitted to the PC data. We restricted this analysis to the significant covariate contributions identified by the above *GLM analysis* (based on a threshold of 0.75 on posterior probability). **Table 3** summarizes the resulting data point selection for each participant.

Results are presented in **Figure 8**.

First, regarding the predictability effect on learning, there was no data point to be tested in the anterior region, except one sensor in P2 from 230 to 235ms that here shows poor evidence for a predictability effect on τ (posterior probability lower than 0.5). Unexpectedly, in the posterior region where learning was previously found in P4, P5 and P6b, no clear evidence was observed in favor of a contextual modulation of parameter τ. Precisely, as can be seen in **Figure 8B**, maximum posterior probability of family $\tau = ON$ was equal to 0.5 in P2, 0.6 in P4, 0.9 in P5 (one electrode from 155 to 160 ms) and 0.5 in P6b.

For the static and exponential regressors, over the tested data points (columns 6 to 9, **Table 3**) we found low evidence supporting the modulation of their respective coefficient (h^*_*) by predictability. Indeed, family-level inference yielded posterior probabilities with median value over data points equal to 0.001 and 0.01 in the anterior and posterior region, respectively.

In sum, these results indicate that we here failed to reveal a predictability modulation of the MMN component and of the related perceptual learning as was evidenced at the group-level using EEG and MEG recordings (Lecaignard et al., 2021b).

DISCUSSION

We here presented results from single-trial ECoG data measured during the passive listening of oddball sequences with two

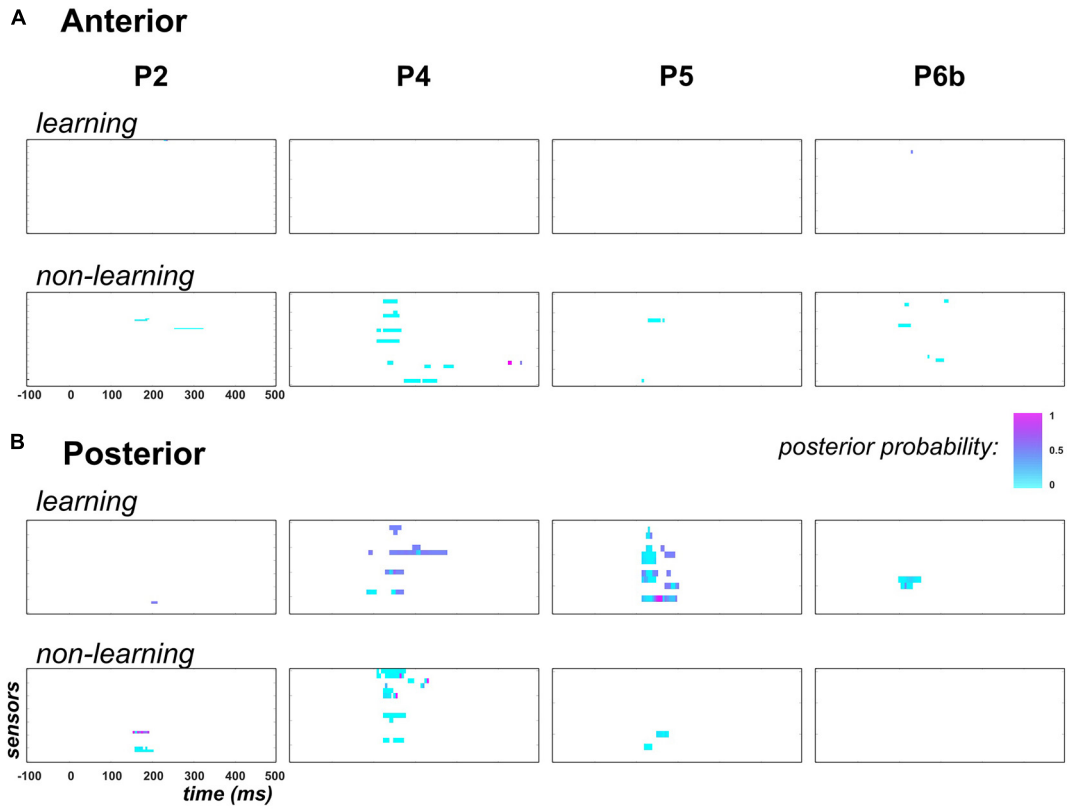

FIGURE 8 | Predictability findings (family-level inference in context PC). Following the display in **Figure 6**, each individual map shows the posterior probability measured at each peri-stimulus time point over anterior (panel **A**) and posterior (panel **B**) temporal electrodes. In each panel, top row (learning) shows results for family τ = ON: posterior probability here indicates how likely parameter τ differs across contexts PC and UC. Bottom row (non-learning) present similar results applied to the non-learning regressor coefficients (h^{std}_{static}, h^{dev}_{static}, h^{rank}_{exp} and h^{cs}_{exp}). Family-level inference for each parameter was conducted only at data points for which an effect for this parameter was found in the GLM analysis (posterior probability threshold of 0.75). For the non-learning maps, in the specific case where multiple effects could occur at the same data point in the GLM analysis, we present the largest posterior probability across these effects.

different levels of predictability. This study had two purposes. First, to test and refine the effects that we reported in a previous study using EEG-MEG recordings. In that respect, we do reproduce an important finding by showing that a cross-trial Bayesian learning model does predict some of the inter-trial fluctuations of temporal cortex activity, at the typical latency of the scalp MMN. However, we did not observe any difference in the learning parameter between the predictable and unpredictable contexts. The second related objective was methodological and concerned the relevance of single-trial analysis for the investigation of mismatch responses. We addressed this question by evaluating the respective explanatory power of dynamic and static predictors, respectively. Therefore we combined a GLM approach with a BMR strategy. Simulations indicated a sufficient model separability given our experimental design and validated this approach. When next applied to the ECoG data, it suggested a spatial dissociation whereby the dynamic account (Bayesian learning) could be measured mostly over the posterior part of the temporal lobe and the static one over anterior electrodes. Moreover, this analysis clearly concluded in favor of a Bayesian learning explanation over an exponential one. This demonstrates the sensitivity of single-trial model fitting and strengthens the computational view of trial-by-trial fluctuations as reflecting a trajectory of precision-weighted prediction errors.

Strengthened Evidence for Bayesian Learning During Oddball Processing

In this study, we pursued our investigation initiated with EEG-MEG recordings to shed light on perceptual learning processes and neurophysiological mechanisms during auditory oddball processing. In Stefanics et al. (2020), a similar GLM approach was employed and fitted to single-trial scalp EEG data, in the aim of investigating the repetition-suppression effect in the visual modality. Competing hypotheses were each framed as a separate GLM, that were all confronted to the data and next compared to each other using Bayesian model comparison. Here we appeal to a different methodology with a single GLM that enables mixing all hypotheses but whose respective contributions are then assessed using BMR and family-level inference. The strength of this approach is twofold. It is computationally very efficient and enables to compare many nested models. Furthermore, using a GLM approach alternative hypotheses are not strictly competing against each other in the sense that the putative most likely combination of models can be inferred given the data.

Our findings in 3 out of 4 patients present compelling evidence for Bayesian learning in posterior temporal sensors that also best show the classical MMN, between around 100 and 250 ms. Based on a posterior probability threshold of 0.9, it was measured in 5/15, 8/9, and 2/2 responsive sensors in P4, P5 and P6b, respectively. We thus succeeded in reproducing previous EEG-MEG findings, which support the view of auditory oddball processing as automatic perceptual learning (both studies involved passive listening). These results add to an emerging literature providing converging evidence from single-trial data analysis in similar experimental settings (Ostwald et al., 2012; Lieder et al., 2013; Stefanics et al., 2018; Weber et al., 2020) and more generally during sensory processing (Iglesias et al., 2013; Meyniel, 2020) where regularity learning in a context-dependent fashion is involved.

An important contribution of our study is that we succeeded in enriching this interpretation, as we here demonstrate the reliability of the explanatory power of learning dynamics (a Bayesian Surprise trajectory). This was achieved in a straightforward fashion by conducting an additional family-level inference analysis restricted to models in which the dynamic (learning) regressor was switched off. Increased evidence for the exponential regressors in this case was fairly expected, as these are the only ones that provide a time-dependent, though somewhat arbitrary, trajectory. In this way, we get closer to the model comparison performed in the study by Stefanics et al. (2020), that involved exponential, static and linear trends, but no learning model. Their study focused on the repetition-suppression effect that consists in the robust reduction of brain response amplitudes over stimulus repetition; a mechanism that is thought to participate to the MMN (Malmierca and Auksztulewicz, 2020). The authors found the exponential explanatory variable to outperform the other models. Several other studies provided similar evidence. At the neuronal level, using intracellular recordings, it was shown to account for the attenuation of the evoked discharge of visual cortical neurons (Sanchez-Vives et al., 2000). Regarding mismatch processing, plausible MMN modulations could be simulated using an exponential function, as in an attenuation model of the auditory N1 component (May and Tiitinen, 2010) or in a generative model operating at the neuronal level (Wacongne, 2016). None of these studies included a (Bayesian) learning explanatory factor. In contrast, the present analysis clearly speaks against this computational hypothesis as we measured poor evidence in favor of the rank and chunk size exponential regressors. Our findings favor such perceptual learning processes over simpler exponential accounts as the latter alternatives were clearly rejected by the data. These results fit with previous fMRI results obtained in a visual cue-association task (Iglesias et al., 2013) where a Bayesian learning model was selected over a simpler (Rescorla-Wagner) learning rule. Taken together, these findings demonstrate the informational value afforded by single-trial content, long considered as noise.

Spatially Distinct Processes in the Temporal Cortex

Stimulus-responsive electrodes were located predominantly in the temporal region. Interestingly, the GLM analysis highlighted the spatial specificity of cognitive processes. Neurophysiological correlates of perceptual learning were located in posterior temporal electrodes whereas electrodes best distinguishing between standard and deviant stimuli, at the latency of the classical MMN, were located in the anterior part. Note that the static category was also found to correlate with posterior electrode signals, but to a far lesser extent than the dynamic one. These two functional clusters correspond to the electrode subsets that showed an MMN (**Figure 5A**).

The mapping of the Bayesian learning process onto posterior electrodes is in line with previous EEG-MEG findings (Lecaignard et al., 2021b). The fusion of these non-invasive observations optimized the reconstruction of the cortical generators of mismatch responses, including the MMN and an earlier component peaking at approximately 70 ms after the deviant onset (Lecaignard et al., 2021a). In the superior temporal plane, we found a bilateral contribution from the primary auditory cortex (Heschl's gyrus), followed by a more anterior bilateral involvement of the planum polare. Bayesian learning was associated with both generators after fitting the single-trial cortical activity reconstructed at these cortical sites.

At the anterior cluster, we found large evidence for the static family (in 3/4 patients). This effect was more visible in P4 (7/11 sensors), at a latency (around 135ms) where the cortical map of the MMN displays lower amplitudes in anterior regions compared to the posterior ones. This low signal-to-noise ratio in the anterior regions may explain a greater sensitivity to the static regressor than to the dynamic one (assuming that trial-by-trial fluctuations in the case of noisy data could be well explained by the rather simple static trajectories but not by the dynamic one which in this case would be rejected as too complex). However, the fact that P6b also shows an anterior standard effect while both spatial clusters (anterior and posterior) have similar (but reverse) amplitude at the MMN speak against this hypothesis. Nevertheless, this anterior static effect contrasts with our EEG-MEG findings where, in the planum polare, Bayesian learning was found to outperform a simple 'change detection' model (Lecaignard et al., 2021b). Further investigations are needed to reconcile these two findings.

Lack of Predictability Effect

We could not reproduce here our EEG-MEG findings regarding the automatic adaptation of Bayesian learning to changes in the predictability of the acoustic environment. Neither did we observe the consequence of such an adaptation onto the evoked responses (the visible tip of the iceberg; no MMN reduction was measured as reported using EEG and MEG). Furthermore and somewhat surprisingly, no modeling responsiveness was found at inferior frontal sites where MMN generators could be located in several studies (Rinne et al., 2000; Schönwiesner et al., 2007; Fulham et al., 2014; Auksztulewicz and Friston, 2015; Lecaignard et al., 2021a).

In the EEG-MEG study, adaptation of Bayesian learning was found to imply model time constant or memory span (learning parameter τ). A larger τ value was inferred from single-trial data in the predictable context. Here, since the *GLM analysis* provided

strong evidence for such Bayesian learning, we expected to measure a comparable predictability modulation. Several possible explanations are discussed below as to why we did not reproduce the EEG-MEG findings.

First, the present work relies on individual analysis of data in 4 patients while the previous study relied on a group-level inference from 20 subjects. It should be noticed that individual statistical analysis of the predictability effect on the MMN component (data not shown) yielded 13 out of 20 participants showing a significantly reduced MMN in context PC (an effect measured with EEG, MEG or both). The fact that this MMN modulation was not systematically visible at the individual level (7/20 subjects did not show the effect) suggests a large inter-individual variability that could arise from the difficulty to learn the subtle predictability manipulation in passive listening (this difficulty is here even more stronger with the present paradigm, as discussed below). In this ECoG study, the implicit learning of the statistical structure of sound sequences could also be influenced by the patients' condition.

Also, in patients P2 and P4, 39% and 26% of the trials were discarded due to artefacts (spikes and high frequency bursts of arguably muscle origin). We obtained different results in the two recording sessions acquired in P6 (P6a and P6b, separated by 1 day), and they strongly differ in their number of accepted trials (1097 and 3199, respectively). This likely speaks to the fact that single-trial data modeling requires highly informed signals to provide conclusive inference from subtle variations. This could be achieved in the EEG-MEG work by collecting a large amount of data by fusing complementary techniques (EEG, MEG) and also through a large number of participants. In the present case, although ECoG provides signals with excellent temporal and spatial resolution, individual datasets may be insufficient. Again, single-trial data analysis is a burgeoning methodology as compared to averaging methods (ERPs, oscillations) and empirical reports are therefore needed to strengthen and improve this approach.

Another aspect concerns the lack of superior frontal cortical coverage of ECoG arrays in the four participants. In our EEG-MEG study, the predictability modulation of the MMN was larger in space and time in EEG than in MEG (as can be seen in **Figure 1B**; Lecaignard et al., 2021b). This aspect led us assume a superior frontal generator whose radial orientation would poorly express on gradiometers (MEG is acknowledged to have a very low sensitivity to radial sources). Few studies have reported MMN generators in superior frontal cortex (Lappe et al., 2013), but we could confirm the contribution of this region to the predictability adaptation (this effect was measured over a fronto-temporal network). Here, none of the four patients presented electrodes located in those regions, and it cannot be excluded that such a predictability effect might have been observed if it had been the case.

Finally, a plausible explanation for not observing a predictability effect could be the slight change of paradigm that we implemented for this study. Indeed, here the predictable sequence was made of alternating cycles with incrementing and decrementing chunk sizes, respectively, while in our initial study, predictable sound sequences were composed of incrementing cycles only. This change was made to avoid the discontinuity at the end of each cycle (where a chunk of size 8 is followed by a chunk of size 2), which consists in a kind of rule violation (at the chunk level). However, the counterpart of this correction is a reduction of the saliency of the underlying statistical structure, making it possibly more difficult for the brain to learn implicitly and adapts accordingly. Here we are faced with the challenge inherent in investigating implicit sensory processing. Experimental manipulations should be salient enough to be processed, but subtle enough to avoid triggering explicit processing.

Perspectives

The present analyses were based on single-trial evoked responses in the 2–20 Hz frequency band, in the aim of testing the reproducibility of and refine spatio-temporally previous EEG-MEG findings. The great informational value of ECoG is evident here, in particular through the spatial functional distinction at the MMN latency. However, the benefit of ECoG also lies in its potential to reveal fine cognitive processes from spectral analysis (Moheimanian et al., 2021; Paraskevopoulou et al., 2021). Regarding oddball processing, an ECoG study addressed the computational role of specific bandwidths from single-trial data analysis in the auditory cortex (Sedley et al., 2016). Remarkably, they could relate the gamma, beta and alpha bands to surprise, prediction updates and precision, respectively. In another study (Dürschmid et al., 2016), a predictability manipulation of deviant occurrence was also employed. Significant mismatch evoked responses in the 1–20 Hz frequency band were found in frontal and temporal electrodes but were not found to be modulated by predictability. This predictability effect was only visible in the high gamma activity, in frontal regions. Putting aside the differences in the experimental design between the two studies, the absence of predictability effect on evoked responses fits our own observations in the present work. An important next step with our data will be to explore the computational correlates of spectral responses.

CONCLUSION

The original results presented here and obtained from ECoG data analysis provide further evidence for the implementation of implicit Bayesian inference processes dedicated to monitoring environmental auditory regularities. Such empirical evidence are essential in the effort to assess the computational underpinnings of perception, and to reveal the link between neurobiological mechanisms and cognitive algorithms such as predictive coding. Importantly, this study illustrates the great potential of single-trial data analysis to reveal subtle dynamic brain processes.

DATA AVAILABILITY STATEMENT

The raw data supporting the conclusions of this article will be made available by the authors, without undue reservation.

ETHICS STATEMENT

The studies involving human participants were reviewed and approved by the Institutional Review Board of Albany Medical College; Human Research Protections Office of the United States Army Medical Research and Materiel Command. The patients/participants provided their written informed consent to participate in this study. Written informed consent was obtained from the individual(s) for the publication of any potentially identifiable images or data included in this article.

AUTHOR CONTRIBUTIONS

FL, AC, and JM conceptualized and designed the paradigm. PB and RB programmed the task and acquired the data. PB provided clinical information. FL and JM designed the methodology. FL implemented the computer codes, analyzed the data, and wrote the manuscript. GS, AC, PB, and JM revised the manuscript. JM, PB, and GS supervised the work. All authors contributed to the article and approved the submitted version.

FUNDING

This work was conducted in the framework of the LABEX CeLyA ("Centre Lyonnais d'Acoustique," ANR-10-LABX-0060) and the LABEX CORTEX ("Construction, Cognitive Function and Repair of the Cortex," ANR-11-LABX-0042) of the Université de Lyon, within the program "Investissements d'avenir" (ANR-11-IDEX-0007; decision no. 2019-ANR-LABX-02) operated by the French National Research Agency (ANR). This work was also was supported by the NIH (R01-EB026439, U24-NS109103, U01-NS108916, P50-MH109429, and P41-EB018783), and the United States Army Research Office (W911NF-14-1-0440) and Fondazione Neurone.

ACKNOWLEDGMENTS

We would like to thank Lawrence Crowther, Ladan Moheimanian, and James Swift for their help during data acquisition. We acknowledge the CC-IN2P3 (https://cc.in2p3.fr/) for providing computing resources and services needed for this work.

SUPPLEMENTARY MATERIAL

The Supplementary Material for this article can be found online at: https://www.frontiersin.org/articles/10.3389/fnhum.2021.794654/full#supplementary-material

REFERENCES

Adams, R. A., Stephan, K. E., Brown, H. R., Frith, C. D., and Friston, K. (2013). The computational anatomy of psychosis. *Front. Psychiatry* 4:47. doi: 10.3389/fpsyt.2013.00047

Auksztulewicz, R., and Friston, K. (2015). Attentional enhancement of auditory mismatch responses: a DCM/MEG study. *Cereb. Cortex* 25, 4273–4283. doi: 10.1093/cercor/bhu323

Auksztulewicz, R., and Friston, K. (2016). Repetition suppression and its contextual determinants in predictive coding. *Cortex* 80, 125–140. doi: 10.1016/j.cortex.2015.11.024

Auksztulewicz, R., Barascud, N., Cooray, G. K., Nobre, A. C., Chait, M., and Friston, K. (2017). The cumulative effects of predictability on synaptic gain in the auditory processing stream. *J. Neurosci.* 37, 6751–6760. doi: 10.1523/jneurosci.0291-17.2017

Auksztulewicz, R., Schwiedrzik, C. M., Thesen, T., Doyle, W., Devinsky, O., Nobre, A. C., et al. (2018). Not all predictions are equal: "what" and "when" predictions modulate activity in auditory cortex through different mechanisms. *J. Neurosci.* 38, 8680–8693. doi: 10.1523/jneurosci.0369-18.2018

Barascud, N., Pearce, M. T., Griffiths, T. D., Friston, K., and Chait, M. (2016). Brain responses in humans reveal ideal observer-like sensitivity to complex acoustic patterns. *Proc. Natl. Acad. Sci. U.S.A.* 113, E616–E625. doi: 10.1073/pnas.1508523113

Bastos, A. M., Usrey, W. M., Adams, R. A., Mangun, G. R., Fries, P., and Friston, K. (2012). Canonical microcircuits for predictive coding. *Neuron* 76, 695–711. doi: 10.1016/j.neuron.2012.10.038

Carbajal, G. V., and Malmierca, M. S. (2018). The neuronal basis of predictive coding along the auditory pathway: from the subcortical roots to cortical deviance detection. *Trends Hear.* 22:2331216518784822. doi: 10.1177/2331216518784822

Chennu, S., Noreika, V., Gueorguiev, D., Blenkmann, A., Kochen, S., Ibáñez, A., et al. (2013). Expectation and attention in hierarchical auditory prediction. *J. Neurosci.* 33, 11194–11205. doi: 10.1523/jneurosci.0114-13.2013

Daunizeau, J., Adam, V., and Rigoux, L. (2014). VBA: a probabilistic treatment of nonlinear models for neurobiological and behavioural data. *PLoS Comput. Biol.* 10:e1003441. doi: 10.1371/journal.pcbi.1003441

Dürschmid, S., Edwards, E., Reichert, C., Dewar, C., Hinrichs, H., Heinze, H.-J., et al. (2016). Hierarchy of prediction errors for auditory events in human temporal and frontal cortex. *Proc. Natl. Acad. Sci. U.S.A.* 113, 6755–6760. doi: 10.1073/pnas.1525030113

Fitzgerald, K., and Todd, J. (2018). Hierarchical timescales of statistical learning revealed by mismatch negativity to auditory pattern deviations. *Neuropsychologia* 120, 25–34. doi: 10.1016/j.neuropsychologia.2018.09.015

Fitzgerald, K., and Todd, J. (2020). Making sense of mismatch negativity. *Front. Psychiatry* 11:468. doi: 10.3389/fpsyt.2020.00468

Friston, K. (2005). A theory of cortical responses. *Philos. Trans. R. Soc. B Biol. Sci.* 360, 815–836. doi: 10.1098/rstb.2005.1622

Friston, K. (2009). The free-energy principle: a rough guide to the brain? *Trends Cogn. Sci.* 13, 293–301. doi: 10.1016/j.tics.2009.04.005

Friston, K., Litvak, V., Oswal, A., Razi, A., Stephan, K. E., van Wijk, B. C. M., et al. (2016). Bayesian model reduction and empirical Bayes for group (DCM) studies. *Neuroimage* 128, 413–431. doi: 10.1016/j.neuroimage.2015.11.015

Friston, K., Mattout, J., Trujillo-Barreto, N., Ashburner, J., and Penny, W. D. (2007). Variational free energy and the Laplace approximation. *Neuroimage* 34, 220–234. doi: 10.1016/j.neuroimage.2006.08.035

Friston, K., Parr, T., and Zeidman, P. (2018). *Bayesian Model Reduction. arXiv preprint arXiv:1805.07092*.

Fulham, W. R., Michie, P. T., Ward, P. B., Rasser, P. E., Todd, J., Johnston, P. J., et al. (2014). Mismatch negativity in recent-onset and chronic schizophrenia: a current source density analysis. *PLoS One* 9:e100221. doi: 10.1371/journal.pone.0100221

Garrido, M. I., Kilner, J. M., Stephan, K. E., and Friston, K. (2009b). The mismatch negativity: a review of underlying mechanisms. *Clin. Neurophysiol.* 120, 453–463. doi: 10.1016/j.clinph.2008.11.029

Garrido, M. I., Kilner, J. M., Kiebel, S., and Friston, K. (2009a). Dynamic causal modeling of the response to frequency deviants. *J. Neurophysiol.* 101, 2620–2631. doi: 10.1152/jn.90291.2008

Garrido, M. I., Sahani, M., and Dolan, R. J. (2013). Outlier responses reflect sensitivity to statistical structure in the human brain. *PLoS Comput. Biol.* 9:e1002999. doi: 10.1371/journal.pcbi.1002999.s002

Gramfort, A., Luessi, M., Larson, E., Engemann, D. A., Strohmeier, D., Brodbeck, C., et al. (2013). MEG and EEG data analysis with MNE-Python. *Front. Neuroinform.* 7:267. doi: 10.3389/fnins.2013.00267

Grill-Spector, K., Henson, R., and Martin, A. (2006). Repetition and the brain: neural models of stimulus-specific effects. *Trends Cogn. Sci.* 10, 14–23. doi: 10.1016/j.tics.2005.11.006

Heilbron, M., and Chait, M. (2018). Great expectations: is there evidence for predictive coding in auditory cortex? *Neuroscience* 389, 54–73. doi: 10.1016/j.neuroscience.2017.07.061

Iglesias, S., Mathys, C. D., Brodersen, K. H., Kasper, L., Piccirelli, M., den Ouden, H. E. M., et al. (2013). Hierarchical prediction errors in midbrain and basal forebrain during sensory learning. *Neuron* 80, 519–530. doi: 10.1016/j.neuron.2013.09.009

Kiebel, S., Garrido, M. I., Moran, R., Chen, C. C., and Friston, K. (2009). Dynamic causal modeling for EEG and MEG. *Hum. Brain Mapp.* 30, 1866–1876. doi: 10.1002/hbm.20775

Knill, D. C., and Pouget, A. (2004). The Bayesian brain: the role of uncertainty in neural coding and computation. *Trends Neurosci.* 27, 712–719. doi: 10.1016/j.tins.2004.10.007

Kubanek, J., and Schalk, G. (2015). NeuralAct: a tool to visualize electrocortical (ECoG) activity on a three-dimensional model of the cortex. *Neuroinformatics* 13, 167–174. doi: 10.1007/s12021-014-9252-3

Lappe, C., Steinsträter, O., and Pantev, C. (2013). A beamformer analysis of MEG data reveals frontal generators of the musically elicited mismatch negativity. *PLoS One* 8:e61296. doi: 10.1371/journal.pone.0061296

Lecaignard, F., Bertrand, O., Caclin, A., and Mattout, J. (2021b). Neurocomputational underpinnings of expected surprise. *J. Neurosci.* doi: 10.1523/jneurosci.0601-21.2021

Lecaignard, F., Bertrand, O., Caclin, A., and Mattout, J. (2021a). Empirical Bayes evaluation of fused EEG-MEG source reconstruction: application to auditory mismatch evoked responses. *Neuroimage* 226:117468. doi: 10.1016/j.neuroimage.2020.117468

Lecaignard, F., Bertrand, O., Gimenez, G., Mattout, J., and Caclin, A. (2015). Implicit learning of predictable sound sequences modulates human brain responses at different levels of the auditory hierarchy. *Front. Hum. Neurosci.* 9:505. doi: 10.3389/fnhum.2015.00505

Lieder, F., Daunizeau, J., Garrido, M. I., Friston, K., and Stephan, K. E. (2013). Modelling trial-by-trial changes in the mismatch negativity. *PLoS Comp. Biol.* 9, 1–16. doi: 10.1371/journal.pcbi.1002911

Malmierca, M. S., and Auksztulewicz, R. (2020). Stimulus-specific adaptation. MMN and predictive coding. *Hear. Res.* 399:108076. doi: 10.1016/j.heares.2020.108076

Mathys, C. D., Lomakina, E. I., Daunizeau, J., Iglesias, S., Brodersen, K. H., Friston, K., et al. (2014). Uncertainty in perception and the hierarchical gaussian filter. *Front. Hum. Neurosci.* 8:825. doi: 10.3389/fnhum.2014.00825

May, P. J. C., and Tiitinen, H. (2010). Mismatch negativity (MMN), the deviance-elicited auditory deflection, explained. *Psychophysiology* 47, 66–122. doi: 10.1111/j.1469-8986.2009.00856.x

Meyniel, F. (2020). Brain dynamics for confidence-weighted learning. *PLoS Comp. Biol.* 16:e1007935. doi: 10.1371/journal.pcbi.1007935

Meyniel, F., Maheu, M., and Dehaene, S. (2016). Human inferences about sequences: a minimal transition probability model. *PLoS Comp. Biol.* 12:e1005260. doi: 10.1371/journal.pcbi.1005260

Moheimanian, L., Paraskevopoulou, S. E., Adamek, M., Schalk, G., and Brunner, P. (2021). Modulation in cortical excitability disrupts information transfer in perceptual-level stimulus processing. *Neuroimage* 243, 118498. doi: 10.1016/j.neuroimage.2021.118498

Näätänen, R., Gaillard, A. W., and Mäntysalo, S. (1978). Early selective-attention effect on evoked potential reinterpreted. *Acta Psychol.* 42, 313–329. doi: 10.1016/0001-6918(78)90006-9

Ostwald, D., Spitzer, B., Guggenmos, M., Schmidt, T. T., Kiebel, S., and Blankenburg, F. (2012). Evidence for neural encoding of Bayesian surprise in human somatosensation. *Neuroimage* 62, 177–188. doi: 10.1016/j.neuroimage.2012.04.050

Paraskevopoulou, S. E., Coon, W. G., Brunner, P., Miller, K. J., and Schalk, G. (2021). Within-subject reaction time variability: role of cortical networks and underlying neurophysiological mechanisms. *Neuroimage* 237, 118127. doi: 10.1016/j.neuroimage.2021.118127

Penny, W. D., Mattout, J., and Trujillo-Barreto, N. J. (2006). *Bayesian Model Selection and Averaging. Statistical Parametric Mapping: The Analysis of Functional Brain Images*. London: Elsevier.

Penny, W. D., Stephan, K. E., Daunizeau, J., Rosa, M. J., Friston, K., Schofield, T. M., et al. (2010). Comparing families of dynamic causal models. *PLoS Comp. Biol.* 6:e1000709. doi: 10.1371/journal.pcbi.1000709

Recasens, M., Grimm, S., Capilla, A., Nowak, R., and Escera, C. (2014). Two sequential processes of change detection in hierarchically ordered areas of the human auditory cortex. *Cereb. Cortex* 24, 143–153. doi: 10.1093/cercor/bhs295

Rinne, T., Alho, K., Ilmoniemi, R. J., Virtanen, J., and Näätänen, R. (2000). Separate time behaviors of the temporal and frontal mismatch negativity sources. *Neuroimage* 12, 14–19. doi: 10.1006/nimg.2000.0591

Sams, M., Alho, K., and Näätänen, R. (1983). Sequential effects on the ERP in discriminating two stimuli. *Biol. Psychol.* 17, 41–58. doi: 10.1016/0301-0511(83)90065-0

Sanchez-Vives, M. V., Nowak, L. G., and McCormick, D. A. (2000). Cellular mechanisms of long-lasting adaptation in visual cortical neurons in vitro. *J. Neurosci.* 20, 4286–4299. doi: 10.1523/jneurosci.20-11-04286.2000

SanMiguel, I., Costa-Faidella, J., Lugo, Z. R., Vilella, E., and Escera, C. (2021). Standard tone stability as a manipulation of precision in the oddball paradigm: modulation of prediction error responses to fixed-probability deviants. *Front. Hum. Neurosci.* 15:734200. doi: 10.3389/fnhum.2021.734200

Schalk, G., and Mellinger, J. (2010). *A Practical Guide to Brain–Computer Interfacing with BCI2000: General-Purpose Software for Brain-Computer Interface Research, Data Acquisition, Stimulus Presentation, and Brain Monitoring*. London: Springer.

Schalk, G., McFarland, D. J., Hinterberger, T., Birbaumer, N., and Wolpaw, J. R. (2004). BCI2000: a general-purpose brain-computer interface (BCI) system. *IEEE T Bio-Med Eng* 51, 1034–1043. doi: 10.1109/tbme.2004.827072

Schönwiesner, M., Novitski, N., Pakarinen, S., Carlson, S., Tervaniemi, M., and Näätänen, R. (2007). Heschl's gyrus, posterior superior temporal gyrus, and mid-ventrolateral prefrontal cortex have different roles in the detection of acoustic changes. *J. Neurophysiol.* 97, 2075–2082. doi: 10.1152/jn.01083.2006

Sedley, W., Gander, P. E., Kumar, S., Kovach, C. K., Oya, H., Kawasaki, H., et al. (2016). Neural signatures of perceptual inference. *eLife* 5:e11476. doi: 10.7554/elife.11476

Southwell, R., Baumann, A., Gal, C., Barascud, N., Friston, K., and Chait, M. (2017). Is predictability salient? A study of attentional capture by auditory patterns. *J. Math. Psychol.* 372:20160105. doi: 10.1098/rstb.2016.0105

Spratling, M. W. (2016). A review of predictive coding algorithms. *Brain Cogn.* 112, 92–97. doi: 10.1016/j.bandc.2015.11.003

Stefanics, G., Heinzle, J., Czigler, I., Valentini, E., and Stephan, K. E. (2020). Timing of repetition suppression of event-related potentials to unattended objects. *Eur. J. Neurosci.* 52, 4432–4441. doi: 10.1111/ejn.13972

Stefanics, G., Heinzle, J., Horváth, A. A., and Stephan, K. E. (2018). Visual mismatch and predictive coding: a computational single-trial ERP study. *J. Neurosci.* 38, 4020–4030. doi: 10.1523/jneurosci.3365-17.2018

Stefanics, G., Kremláèek, J., and Czigler, I. (2014). Visual mismatch negativity: a predictive coding view. *Front. Hum. Neurosci.* 8:666. doi: 10.3389/fnhum.2014.00666

Todd, J., Frost, J. D., Yeark, M., and Paton, B. (2021). Context is everything: how context shapes modulations of responses to unattended sound. *Hear. Res.* 399:107975. doi: 10.1016/j.heares.2020.107975

Wacongne, C. (2016). A predictive coding account of MMN reduction in schizophrenia. *Biol. Psychol.* 116, 68–74. doi: 10.1016/j.biopsycho.2015.10.011

Weber, L. A. E., Diaconescu, A. O., Mathys, C. D., Schmidt, A., Kometer, M., Vollenweider, F., et al. (2020). Ketamine affects prediction errors about statistical regularities: a computational single-trial analysis of the mismatch

negativity. *J. Neurosci.* 40, 5658–5668. doi: 10.1523/jneurosci.3069-19.2020

Winkler, I. (2007). Interpreting the mismatch negativity. *J. Psychophysiol.* 21, 147–163. doi: 10.1027/0269-8803.21.34.147

Conflict of Interest: The authors declare that the research was conducted in the absence of any commercial or financial relationships that could be construed as a potential conflict of interest.

Publisher's Note: All claims expressed in this article are solely those of the authors and do not necessarily represent those of their affiliated organizations, or those of the publisher, the editors and the reviewers. Any product that may be evaluated in this article, or claim that may be made by its manufacturer, is not guaranteed or endorsed by the publisher.

frontiers in Human Neuroscience

ORIGINAL RESEARCH
published: 11 February 2022
doi: 10.3389/fnhum.2022.758138

Overt Oculomotor Behavior Reveals Covert Temporal Predictions

Alessandro Tavano[1]* *and Sonja A. Kotz*[2,3]

[1] Department of Neuroscience, Max Planck Institute for Empirical Aesthetics, Frankfurt am Main, Germany, [2] Department of Neuropsychology and Psychopharmacology, Faculty of Psychology and Neuroscience, Maastricht University, Maastricht, Netherlands, [3] Department of Neuropsychology, Max Planck Institute for Human Cognitive and Brain Sciences, Leipzig, Germany

Our eyes move in response to stimulus statistics, reacting to surprising events, and adapting to predictable ones. Cortical and subcortical pathways contribute to generating context-specific eye-movement dynamics, and oculomotor dysfunction is recognized as one the early clinical markers of Parkinson's disease (PD). We asked if covert computations of environmental statistics generating temporal expectations for a potential target are registered by eye movements, and if so, assuming that temporal expectations rely on motor system efficiency, whether they are impaired in PD. We used a repeating tone sequence, which generates a hazard rate distribution of target probability, and analyzed the distribution of blinks when participants were waiting for the target, but the target did not appear. Results show that, although PD participants tend to produce fewer and less temporally organized blink events relative to healthy controls, in both groups blinks became more suppressed with increasing target probability, leading to a hazard rate of oculomotor inhibition effects. The covert generation of temporal predictions may reflect a key feature of cognitive resilience in Parkinson's Disease.

Keywords: predictions, temporal expectations, eye movements, Parkinson's disease, hazard rate

OPEN ACCESS

Edited by:
Adonis Moschovakis, University of Crete, Greece

Reviewed by:
Daniel Thomas Smith, Durham University, United Kingdom
Shlomit Yuval-Greenberg, Tel Aviv University, Israel

***Correspondence:**
Alessandro Tavano
alessandro.tavano@ae.mpg.de; alessandro.tavano.office@gmail.com

Specialty section:
This article was submitted to Cognitive Neuroscience, a section of the journal Frontiers in Human Neuroscience

Received: *13 August 2021*
Accepted: *14 January 2022*
Published: *11 February 2022*

Citation:
Tavano A and Kotz SA (2022) Overt Oculomotor Behavior Reveals Covert Temporal Predictions. Front. Hum. Neurosci. 16:758138. doi: 10.3389/fnhum.2022.758138

INTRODUCTION

Blinks are defined as the temporary closure (≈ 0.3 s) of both eyes via rapid movements of both the upper and lower lids: the closing and closed phases of the movement are extremely rapid (<0.1 s), while the opening phase is slower (≈ 0.2 s, Kwon et al., 2013). On average, healthy human adults blink every 3–5 s (≈ 12–20 blinks per minute, Fatt and Weissman, 1992). Blinks help preserve the integrity of the ocular surface (lubrication, shielding from light and dirt, relieving eye muscle fatigue, Hall, 1945). However, blink frequency far exceeds such basic physiological needs, and there is evidence that arousal and attention drive blink frequency to change depending on whether at any given moment sensory information processing can be chunked (Wascher et al., 2015), when a release of attention from external stimulation is required (Nakano et al., 2013), or when fulfilled expectations indicate the end of cognitive processing (Ichikawa and Ohira, 2004).

In general, spontaneous blink rates decrease when attention is directed to incoming, external stimuli, particularly during experimental trials (Van Opstal et al., 2016) and when sustained, continuous attention is required to successfully complete a task (Maffei and Angrilli, 2018). It is unclear whether the component of attention that modulates blinking probability is strictly under dopaminergic control (Maffei and Angrilli, 2018; Sescousse et al., 2018), but there is evidence that Parkinson's patients with dyskinetic symptoms often exhibit increased eye movement rates

(Karson, 1983), possibly as a consequence of intracortical dishibition (Stinear and Byblow, 2003; Ammann et al., 2020). Indeed, eye movement disorders may present one of the early symptoms of Parkinson's Disease onset (Jung and Kim, 2019). However, while the blinking rate is likely a confounded measure as it could be due to either attentional demands or fatigue (Maffei and Angrilli, 2018), the temporal distribution of blink movements or blink timing appears to be a reliable and unconfounded index of participants' engagement in a task (Ichikawa and Ohira, 2004; Nakano and Miyazaki, 2019).

Temporal attention is reflected in the hazard rate distribution, which normalizes true stimulus probability using the survival function, that is, the probability that the event has not yet occurred (Luce, 1986). Recent work showed that blinks and saccadic movements are suppressed (oculomotor inhibition) before the onset of predictable targets (Abeles et al., 2020). For uniformly distributed stimulus onset times, the perceived probability of target onset is assumed to monotonically increase as time elapses. It follows that blink probability at each target position should diminish with increasing temporal expectations. As cortical beta disorganization in Parkinson's disease has been associated with reduced sensitivity to temporal regularities (te Woerd et al., 2015), and the generation of temporal expectations has been linked to motor cortical activity (Morillon and Baillet, 2017), we tested the distribution of blinks in Parkinson's patients (PD) and a healthy control group (HC) matched for gender, age, and cognitive performance. All participants completed an auditory task which required detecting the onset of a target sound in a continuous attention mode. Auditory stimulation sequences were composed of the continuous repetition of four standard tones followed by a fifth non-target, deviant tone. All sounds were delivered using a fixed stimulus onset asynchrony interval (isochronous stimulation). Target sounds occurred rarely (20% of sequences) and unpredictably (randomized distribution) within the repeating sequence, equiprobably substituting a standard tone in either position 2, 3, or 4, hence giving rise to the hazard rate of response times (see stimulus structure section). We hypothesized that if the orienting of attention in time giving rise to expectations depends on the functional integrity of motor cortical, then the distribution of blinks in time in PD and HC should differentially reflect the temporal statistics of target onset. Specifically, we expected PD patients to be less efficient than HC in suppressing blinks with the increasing probability of target onset as attention moved from position 2 to position 4 within each sound sequence.

MATERIALS AND METHODS

Participants

The experiment was conducted at the Max Planck Institute for Human and Cognitive Brain Sciences in Leipzig (Germany). Sixteen participants diagnosed with Parkinson's Disease (PD, 9 males, 7 females) were selected (mean age = 63.9 years, SD = 6.8). Sixteen healthy adult individuals (Healthy controls, HC), matched in age (mean = 63.9 years, SD = 7.1) and gender, were also recruited from the Institute's database. Education level was also matched (PD, mean = 5.6 years, SD = 1.2; HC, mean = 5.7 years, SD = 1.3). HC participants self-reported no neurological or psychiatric disorders or therapies involving the central nervous system. All participants signed a written informed consent complying with the Declaration of Helsinki on human experimentation. The study was approved by the Ethics Committee of the University of Leipzig, Germany.

Neuropsychological Profile

The two experimental groups were also cognitively matched on a battery of neuropsychological tests (see **Table 1**, reporting means and standard deviations within parenthesis): Mini Mental Test (Tombaugh and McIntyre, 1992); Tower of London (Shallice, 1982); Trail Making Test A and B (Tombaugh, 2004); Working memory–Digit Span Forward, maximal N of numbers recalled [Wechsler, 1997, Backward, maximal N of numbers recalled (Wechsler, 1997). For all pairwise comparisons, all $ts_{(30)} \leq -0.73$, all $ps \geq 0.465$].

Clinical Profile

The average illness duration in participants with PD was 3.78 years (SD = 2.63), with only two participants having been diagnosed for more than 6 years (15 and 11 years). Most patients (11 out of 16) presented with both tremors and akinetic rigidity, while 3 presented solely with akinesia and 2 with tremors. The average Höhn and Yahr index (Höhn and Yahr, 1967) was 2.03 (SD = 0.53, range 1–3), suggestive of bilateral involvement preserved balance functions. Asymmetry in body symptoms was equally distributed (right side = 8). On the UPDRS motor scale (Goetz et al., 2007), the mean was 13.5 (SD = 5, range 7–21), indicative of minimal to mild slowness and movement abnormality. All participants with PD were pharmacologically treated, predominantly with Levodopa and Ergot-dopamine agonists.

Stimulus Structure

Stimuli were three 50-ms pure tones (5 ms rise/fall), organized into continuously repeating five-tone sequences, binaurally presented via loudspeakers at 80 dB SPL and generated using Matlab (version 7, Mathworks, Natick, MA). The five-tone sequence was composed of four standard tones followed by a non-target deviant tone (**Figure 1A**). Standards were 440 Hz in pitch (A4 on the equal tempered scale, presented 900 times, 75% global stimulus probability), non-target deviants were 494 Hz (B4, presented 240 times, 20% global stimulus probability). A rare target (349 Hz, F4, presented 60 times, 20% of sequences, 5% global stimulus probability) occurred equiprobably (1/3) at one among standard positions 2, 3, or 4. To detect a target, participants had to attentively listen to each incoming sequence, whether it contained a target or not; within each sequence, internal target probability was predicted to changed with elapsed time, generating a hazard rate distribution (**Figure 1B**, upper panel). Denoting the survival probability ("the event has not yet occurred") as 1-F(t), where F(t) is the cumulative distribution function, the hazard function is then: $h(t) = f(t)/(1-F(t))$. There was a maximum of one target per sequence, and minimally two successive sequences without targets before the next target-containing sequence. Stimulus sequences were

TABLE 1 | Neuropsychological results.

Group	Mini Mental State	Tower of London	Trail Making Test A and B	Digit Span Fw	Digit Span Bw
HC	29.12 (0.85)	16.18 (1.42)	A: 40.56 (12.06), B: 77.62 (25.32)	6.50 (1.00)	5.06 (0.89)
PD	28.87 (0.99)	15.43 (2.06)	A: 39.37 (12.21), B: 82.37 (32.49)	6.68 (1.04)	5.06 (1.39)

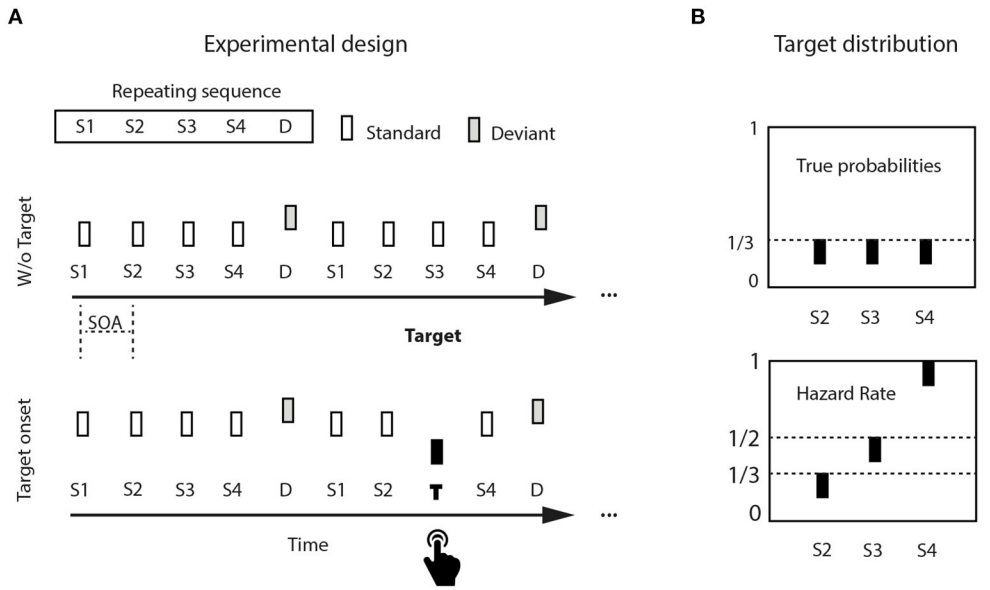

FIGURE 1 | Experimental design: **(A)** Pure tones were isochronously distributed in continuously repeating five-tone sequences, composed of four standard tones (440 Hz) and a final non-target deviant tone (494 Hz). Target tones were lower in pitch (349 Hz), and appeared in 20% of the sequences (= 5% of the tones). **(B)** Tones would appear equiprobably either in position two, three, or four within a sequence (upper left panel). Potential rare target position is used as a proxy for elapsed time. The hazard rate distribution increases target probability with target position (upper right panel).

delivered using Presentation© software (version 12.0, www.neurobs.com) running on a Windows PC.

Experimental Design

Participants sat in an electrically shielded, sound-attenuated chamber, and fixated a white cross on a black computer screen at a distance of 1 meter while listening to the auditory sequences. They responded to target tone onset by pressing a button on an external response box, using their preferred hand. Participants were unaware of target distribution, and were instructed to respond to the onset of target tones as accurately and fast as possible by pressing a button on a response box. They trained in a short block of 60 experimental randomly distributed tone sequences containing three targets. The training phase was repeated maximally once. If errors were made (Missing, False Alarm), the training block was repeated until no errors were detected. Experimental tone sequences were delivered with a constant 750-ms stimulus onset asynchrony (SOA), corresponding to a 1.34 Hz stimulus rate (three 5-min blocks).

EEG Recording

Electroencephalographic (EEG) data were collected using a 26 scalp Ag/AgCl electrode set (BrainAmp, 10–20 system): Fp1, Fpz, Fp2, F7, F3, Fz, F4, F8, FT7, FC3, FC4, FT8, T7, C3, Cz, C4, T8, CP5, CP6, P7, P3, Pz, P4, P8, O1, O2. Two external electrodes were placed at right and left mastoid sites, and four additional electrodes were placed at both eye canthi (leftLateral, rightLateral), and above and below the right eye (lowerVertical, upperVertical) to record eye movements (electrooculogram, EOG). An online reference was placed on the left mastoid and the sternum served as ground. Electrode impedance was kept below 5 KOhm. EEG/EOG sampling rate was set to 500 Hz, with online high-pass filtering at 0.01 Hz. The resulting continuous recordings were visually inspected and pruned from non-stereotypical artifacts or extreme voltage changes values. An Independent Component Analysis (ICA, Infomax algorithm, Bell and Sejnowski, 1995, as implemented in the EEGLAB toolbox, Delorme and Makeig, 2004) was performed on pruned, offline highpass-filtered at 1 Hz and lowpass-filtered at 45 Hz (Kaiser window, Beta 5.6533, filter order points 9056 and 184, transition bandwidth 0.2 and 10 Hz, respectively), standardized (z-score) continuous data. Using the SASICA toolbox for EEGLAB (Chaumon et al., 2015), ICs reflecting blinks/vertical eye movements and lateral eye movements were identified by a correlation threshold of 0.7 with bipolarized vertical and lateral EOG channels. The SASICA toolbox also identified ICs likely to reflect muscle artifacts, using autocorrelation (lag = 20 s), as well as those reflecting bad electrodes via a measure of focal

topography (threshold at 7 standard deviations relative to the mean across electrodes). The ICA results were then copied back to the pruned, standardized original continuous EEG data highpass-filtered at 0.1 Hz (lowpass 45 Hz). Eye-movement-related ICs, both vertical/blink-related and horizontal, ranged between 2 and 5 per participant, with at least a vertical/blink-related component per participant.

Blink Modeling

Blinks were individually modeled using the best signal selected out of a subset comprising the vertical EOG channel (both lowerV and upperV), a subset of frontal electrodes (in our case: Fp1, Fp2, Fz, F3, F4) and frontally focused independent components (ICs) representing blinks or vertical eye movements according to the Blinker toolbox pipeline (https://github.com/VisLab/EEG-Blinks; Kleifges et al., 2017). The Blinker algorithm first bandpasses the signal (1–20 Hz), then determines the intervals with an SD > 1.5 standard deviations above the signal mean (min interval = 50 ms, min separation between intervals = 50 ms). A fitting process follows by first finding specific landmarks for each blink interval, such as the maximal value within the interval, and the zero crossings immediately to the left and right of each max value, and then computing for each potential blink the best linear fits for the inner 80% of the up-stroke and down-stroke, respectively. The R^2 of left and right fit lines with the actual blink trajectory measures how close the potential blink is to a stereotypical blink. Then, the blink-amplitude ratio (BAR) is computed by dividing the average amplitude of the signal between the blink left and right zero crossings by the average amplitude of the positive portion of the signal comprised between the preceding blink right zero crossing and the current blink left zero crossing, as well as the current blink right zero crossing and the following potential blink right zero crossing (or end of signal if the current blink is the last one). Potential blinks with a BAR outside the range [3–20] are not included in the final computation ("used" signal, see below).

Next, Blinker determines "good" blinks (upStroke and downStroke R2 > 0.90), "better" blinks (upStroke and downStroke R2 > 0.95), and "best" blinks (up-stroke and down-stroke R2 > 0.98). To eliminate extraneous eye movements from actual blinks, two further criteria are satisfied: 1) The positive amplitude by velocity ratio (pAVR = 3), calculated from the left zero crossing to the maximal amplitude of each blink, distinguishes between the sharp rise of saccades (large velocity) and the more curved one proper to blinks; 2) The maximum amplitude distribution criterion eliminates blinks with low R^2 and with amplitude vastly away from the "best" blink median (Threshold = 5 robust standard deviations—1.48 times the median absolute deviation from the median—for "best" blinks, 2 for for "good" blinks). The resulting blinks constitute the "used" blinks set, which inform the analysis at an individual participant level (minimum number of blinks to stable estimates = 20).

Analysis of Blink Distributions

The Blinker pipeline was run on continuous, clean EEG datasets. One participant from the PD group was marked as an outlier as far as blink counts were concerned ($N = 556$) and thus was removed from further analysis, together which the gender- and age-matched HC participant. The final group was thus composed of 30 participants, 15 per group. Then, blink landmarks were copied back to the EEG trial structure, and finally epochs were extracted based on the repeating 5-tone sequences which did not contain a target (0–3,500 ms). This approach allowed analyzing the distribution of blinks in time as participants waited for a potential target, without any confounding effect from target onset. For each epoch, we marked the positions in time of blink maximal values (peaks), while the rest of the EEG data were zeroed out, obtaining vectors of blink peak distributions in time.

Participants were first compared for the total number of blinks (counts) and median blink-to-blink interval using a one-sided Wilcoxon rank sum test for equal medians, with the assumption that HC would outperform PD participants. The choice of a non-parametric statistical test was motivated by the non-gaussian distribution of blink counts (Kolmogorov-Smirnov test, all ps $< 1.645*10^{-15}$). Blink counts were subject to a robust regression analysis with bisquare weighting of the residuals (Matlab function *robustfit.m*), to asses the the relationship between HC and PD blink generators. The effect of age in driving blink counts was also tested, using both robust regression and Spearman correlation.

To assess the degree to which blink timing was sensitive to the auditory stimulus rate (1.34 Hz), blink epochs were concatenated into a single vector for each participant. A Fast Fourier Transform (FFT) analysis ($N = 8192$ data points, normalized dividing by N) was run on a hundred concatenated blink vector per participant in each group. The average peak power differences between HC and PD at sequence rate (0.267 Hz), stimulus rate (1.34 Hz), and first harmonic of the stimulus rate (2.67 Hz) were compared to their group threshold using a Wilcoxon signed rank test, and to each other using a one-sided Wilcoxon rank sum test (effect size $r = Z/\sqrt{Samplesize}$ for one sample/paired samples, $r = Z/\sqrt{Samplesize1 + Samplesize2}$ for independent samples).

Next, we turned to the analysis of median blink distributions within the repeating sequence. First, for each participant blink peak latencies were binned using a 20-ms bin size. Then, bin counts were normalized by the total number of blinks, and smoothed using a moving median of 5 bins. To obtain a measure of regularity in blink distribution across the repeating sequence, we employed the Nelder-Mead simplex direct search algorithm (Image Analyst, 2021) and optimized the search for the best fit for 5 Gaussian distributions on the median distributions across participants in each group, using a sigma of 20 and taking each tone interval's middle point as an initial guess for the mean or peak of each Gaussian. We then calculated the dissimilarity between HC and PD median histograms using χ^2 are a measure of distance: $\text{sum}((xi-yi)^2/(xi+yi))/2$. We tested the significance of the distance value using a bootstrapping approach (1,000 randomizations). Then, for each participant we collected the value at the each grand median fitted Gaussian peak within each sound interval, and compared them across groups using a series of Wilcoxon rank sum tests, FDR-corrected. Finally, by regressing blink frequency against the positional order of potential Target stimulus onset (positions 2, 3, and 4), we obtained peri-stimulus estimates of hazard rate effects in blink distributions—from **–300**

to + 300 ms relative to potential target onset -, which were tested for significance using a one-sample permutation test based on the t-statistic (Groppe et al., 2011; one-sided). Significance was determined for $p = 0.05$.

Probabilistic Saccade Estimation

As a partially independent measures of ocolomotor disorders in participants with PD, we resorted to calculating saccade probability and duration. An impairment in saccadic initiation, leading to a more variable onset of saccadic movements than matched healthy controls, has been shown to characterize patients PD from early on in the disease progression (Terao et al., 2011). Furthermore, saccade intrusions—characterized by involuntary saccades away and back to a fixation point, characterize oculomotor system functioning in PD (White et al., 1983), adding to variance in saccade probability distribution. We selected a probabilistic algorithm which detects saccades—as distinct from peri-blink saccadic movements—using an unsupervised training period (between 50 and 200 s), and uses expectation maximization to learn the parameters of Gaussian likelihood distributions for saccades (Toivanen et al., 2015; https://github.com/bwrc/eogert). Two parameters were selected: saccade probability for each detected event, and saccade duration. A Wilcoxon rank sum test was used to detect significant differences in mean variance between PD and HC.

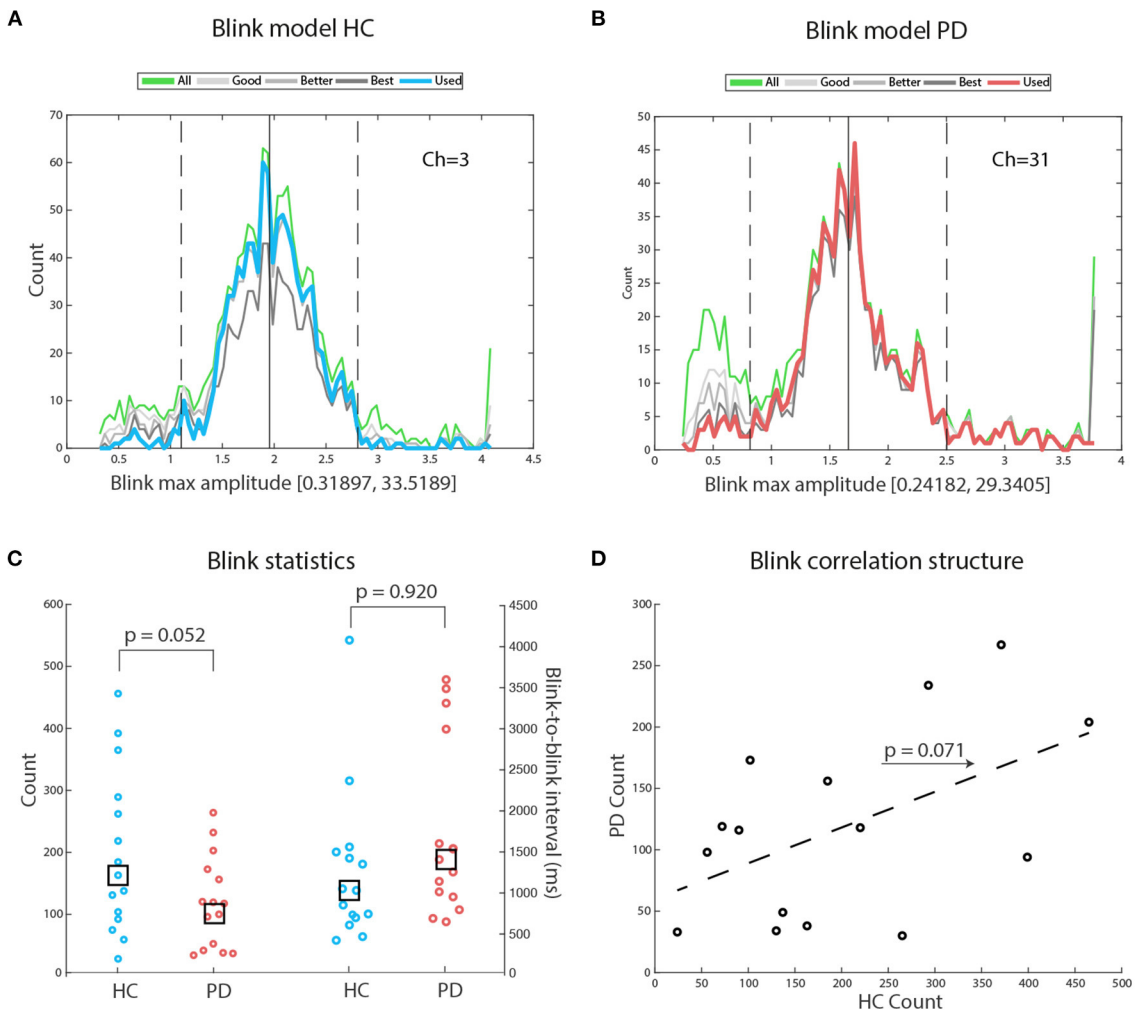

FIGURE 2 | Blink models: **(A)** Exemplary blink models for participant number 1 of the HC group. The green line depicts the amplitude distribution of all potential blinks: Amplitudes are measured in standard deviations, to avoid the confounding effects of differences in mean blink amplitudes across participants. Blink range on the x-axis: Notice that the right tail of the distribution is interrupted because most large amplitude values were outliers. The blue line depicts the blink distribution selected for further analysis. For details, see the Materials and Method section. **(B)** Exemplary blink models for participant #1 of the PD group. The red line depicts the blink distribution selected for further analysis. **(C)** There was a tendency to a significant difference favoring HC in total blink counts. There was no significant difference between HC and PD on mean interblink interval. Notice that the median interval is similar across groups. The largest median blink interval for both groups corresponds to physiological intervals. **(D)** A robust regression fit shows a tendency for matched participants from both groups to perform similarly, hinting at possible underlying common factors driving blink frequency.

RESULTS

Blink Models

Figures 2A,B display illustrative blink modeling results for participant number 1 of both groups. In both cases, the right tail of the distribution contains outliers that are eliminated based on the distance from the best blinks distribution (up-stroke and down-stroke R2 > 0.98). A Wilcoxon rank sum test of the difference between the number of blinks in HC and in PD failed to reach significance: $Z = 1.61$, $p = 0.052$, HC median number of blinks = 163, PD median number of blinks = 116. We then checked for the physiological realness of the interblink intervals, and found that values for both groups were comparably within expected values: HC median interblink interval = 1,037 ms (range: 650–3,638), PD median interblink interval = 1,419 ms (range: 422–4,125), $Z = -1.41$, $p = 0.920$. With the exception of one participant in each group, all medians were below 3,500 ms, likely reflecting the chunking effect of attention to the repeating tone sequence (see **Figure 2C**). The concentration of individual median values at the lower portion of the range suggests an attractive effect of stimulus rate on blink rate. A robust regression fit between HC blink counts and PD blink counts failed to reach significance [$t_{(13)} = 1.959$, $p = 0.071$] (see **Figure 2D**). When we averaged blink counts across groups and regressed the results against age in years, we found no significant fit (Spearman $\rho = -0.215$, $p = 0.503$), suggesting that in our samples age did not appear to be driving changes in blink frequencies.

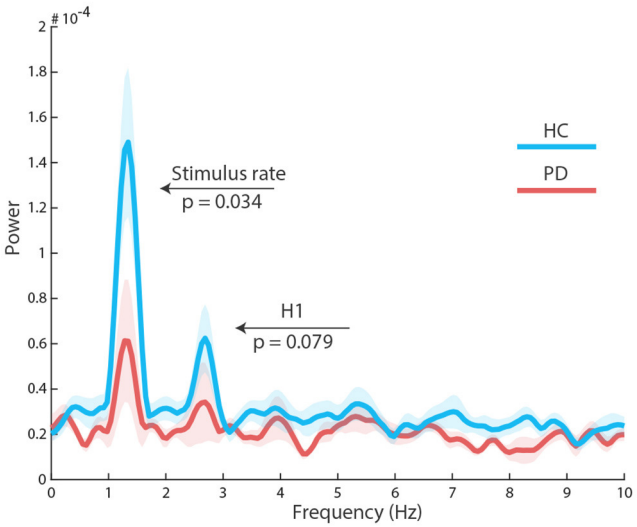

FIGURE 3 | Auditory regularities in the eyes: FFT results on concatenated epochs show a significant effect of stimulus rate in both groups, but larger for healthy control participants (blue line) than participants with Parkinson's Disease (red line). The first harmonic processes (H1) were not significant.

Blink Distribution Reflects Stimulus Structure

To explore how stimulus structure influenced the temporal distributions of blinks, we concatenated all selected epochs and submitted the resulting vector to a Fast Fourier Transform (FFT) analysis. Using a Wilcoxon signed rank test, we found a significant peak at stimulation frequency (1.34 Hz) in each group: HC, $Z = 2.89$, $p = 0.002$, $r = 0.74$ (reference power = $3*10^{-05}$); PD, $Z = 1.98$, $p = 0.047$, $r = 0.51$ (reference power = $2*10^{-05}$). However, there was a significant difference in peak power between the groups: HC median = $1.098*10^{-04}$, PD median = $4.644*10^{-05}$, $Z = 1.825$, $p = 0.034$, $r = 0.33$. There was no significant group peak, nor a group difference at the first harmonic of the stimulus rate (2.67 Hz): all ps ≥ 0.079. Similarly, there were no significant findings at the repeating sequence frequency (0.266 Hz): all ps ≥ 0.187 (see **Figure 3**).

Blink Rates Encode Temporal Predictions

The Nelder-Mead algorithm allowed us to optimally fit 5 Gaussians on the median of the median blink distributions for each group. For HC, the number of iterations was 719, with a mean residual of $6.447*10^{-4}$. For PD, the number of iterations was 1228, with a mean residual of $7.515*10^{-4}$ (see **Figures 4A,B**, respectively). We measured histogram similarity using χ^2 as a distance measure, and found that—globally—the distribution of blinks across the repeating sound sequence did not differ (distance = 1.494, $p = 0.73$, bootstrapping distribution, 1,000 repetitions). However, when we tested the differences in blink frequency (pristine values, that is before applying the moving-average smoothing) at fitted curve peak within each sound interval, using the fitted values for HC as reference also for participants with PD, we then found that the two groups differed in the S3 interval, that is at the center of the sequence (original $p = 0.007$, FDR $p = 0.01$), which corresponds also to the middle point in the attentive searchlight for a potential target onset (**Figure 4C**).

We then used a robust linear fit approach to calculate, for each peristimulus bin point, the slope of values across the onset of sounds at S2, S3, and S4. For both groups, we found a significant hazard-rate effect on blink frequency in the pre-stimulus period only (**Figure 4D**): all cluster Ts *leq* –2.79, all cluster ps *leq* 0.029; HC –220 to 200 ms, PD –180 ms; negative slopes indicate the amount of decrease with each potential Target interval. Pre-stimulus oculomotor activity became more inhibited with increasing waiting time across positions S2, S3, and S4.

Saccadic Movements

The similarity in blink temporal distribution between participants with PD and HCs becomes more relevant on the background of the significant difference between the two groups in saccadic movements estimated from electrooculographic data. Average saccade probability displyed larger variance in participants with PD (mean = 0.014) than in HCs (mean = 0.011): $Z = 2.13$, $p = 0.032$, $r = 0.54$. However, average saccade duration did not differ: $Z = 0.43$, $p = 0.663$. This suggests a disorder in saccade initiation in participants with PD, detectable

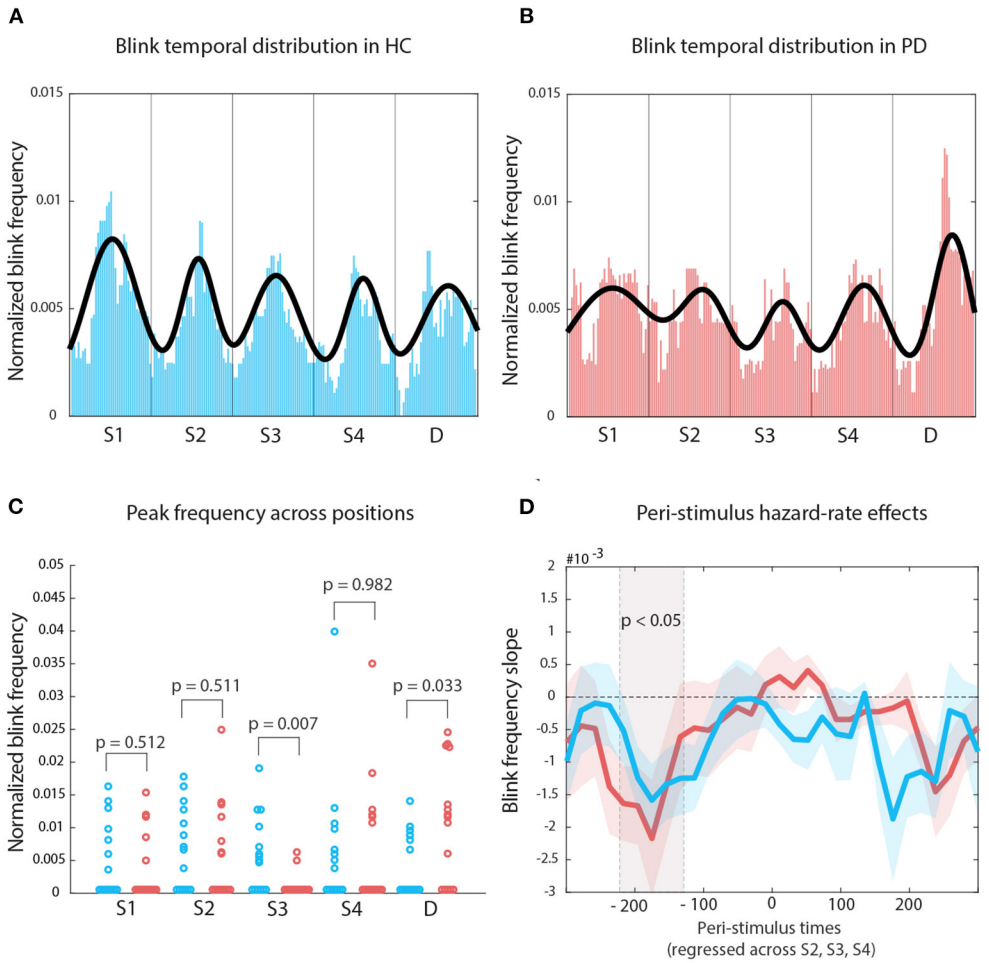

FIGURE 4 | Temporal organization of blink onset: **(A)** Median of blink frequency medians estimates across time for HCs. The Gaussian fit highlights the regularity in blink peak distribution following entrainment to stimulus regularity. **(B)** The same approach for PD participants displays a less organized structure. **(C)** The main difference between the two distribution lies with how blinks reflect the onset of S3. **(D)** The gray shade indicates mean blink frequency slopes for both HC and PD which display significant oculomotor inhibition effects; colored shaded areas indicate standard error of the mean.

even in the context of isochronous auditory stimulation driving entrainment in blink onset.

DISCUSSION

When stimulus statistics in the environment drive our attention toward the potential onset of a target event, changes occur at both central and autonomic nervous system levels, thereby modulating all motor effectors, not just those required to press a button. Indeed, recent work suggests that temporal predictions are reflected by eye movements, such as saccades and blinks (Abeles et al., 2020), that are partially under voluntary and partially under involuntary control. When we approach the probable onset time of a target event, ocular movements are suppressed, in order to avoid diverting attention to other stimuli (saccades) or suppressing sensory input (blinks). However, in everyday situations the uncertainty about when a target event will occur adds to the uncertainty about whether a target will occur at all. We tested whether oculomotor inhibition occurs for targets whose chance is globally very low (20%). Furthermore, by comparing the performance of healthy controls (HC) and gender- and age-matched Parkinson's Diseases (PD) patients, we measured the extent to which temporal predictions conveyed via oculomotor inhibition depend on general oculomotor fitness, which is impaired in PD. Overall, PD participants tended to produce less blinks than HCs, but the temporal organization of inter-blink-intervals is similar to that of healthy controls. Previous work showed that, in spontaneous blinking conditions and for a cohort between 40 and 89 years, mean blink amplitude and peak velocity decreased with age, but blink rate as such was not affected (Sun et al., 1997). In our case, age was not a significant factor in determining blink counts, although the effect of age on blink counts might have been overridden by the entraining effects of the stimulation structure.

We also found that inter-blink-intervals in both groups tend to follow the regular auditory stimulation rate (750 ms, 1.34 Hz, **Figure 3**), although HC outperformed participants with PD. This finding suggests that motor impairment in our sample of participants with PD, including oculomotor saccadic impairments, did not prevent the locking of blink frequency to stimulus statistics. However, oculomotor impairment in PD partially affected the organization of blink peak distribution (**Figures 4A–C**). Although the sequence-based distance between blink histograms for HC and PD was not significant, we found that in participants with PD blinks were significantly less likely to occur in response to the third sound of each repeating sequence. Previous work showed that spontaneous blinks in PD participants with mild and moderate severity were either abnormally reduced or increased relative to HC (Korosec et al., 2006). PD participants in that study displayed a more advanced motor impairment (UPDRS motor scale score) than in our patient sample, and participants were tested off medication, while the patients in our sample were tested on medication. The lack of an off medication condition is a limit to our findings, as it would have provided a test for blink entrainment. However, our study assesses oculomotor functionality within a continuous attention condition, that is under under stressful attentional demands (Maffei and Angrilli, 2018), suggesting resilience in patients' performance.

When we regressed blink probability across potential Target positions (S2, S3, S4), we found evidence of a hazard rate organization of blink onset probability in both groups. Oculomotor inhibition progressively increased while waiting for a potential target (**Figure 4D**). Importantly, as our analysis was run on the repeating sequences that did not contain a target, oculomotor inhibition was purely driven by cognitive expectancies for future target onset. The "hazard rate" of oculomotor activity is evident in the prestimulus period only, consistent with previous findings (Tavano et al., 2019; Abeles et al., 2020). Motor disorganization as a consequence of PD—at least in as far as it affects the oculomotor system—did not prevent the computation of evolving target probability in time, which is a key component of the processes generating temporal expectations. This likely preserves in patients a sufficient fit with the environment, whose statistics are inherently time-dependent.

DATA AVAILABILITY STATEMENT

The raw data supporting the conclusions of this article will be made available by the authors, without undue reservation.

ETHICS STATEMENT

The studies involving human participants were reviewed and approved by Ethics Committee of the University of Leipzig, Germany. The patients/participants provided their written informed consent to participate in this study.

AUTHOR CONTRIBUTIONS

AT and SK devised research hypothesis, wrote and revised draft, and approved submission. AT created scripts for data collection and analyzed data. Both authors contributed to the article and approved the submitted version.

ACKNOWLEDGMENTS

The authors wish to thank Ina Koch for data collection, Jana Kynast for the acquisition of neuropsychological data, and the two reviewers for helpful criticism. Patient data collection was supported by DFG KO 2268/3-1 to SK.

REFERENCES

Abeles, D., Amit, R., Tal-Perry, N., Carrasco, M., and Yuval-Greenberg, S. (2020). Oculomotor inhibition precedes temporally expected auditory targets. *Nat. Commun.* 11:3524. doi: 10.1038/s41467-020-17158-9

Ammann, C., Dileone, M., Pagge, C., Catanzaro, V., Mata-Marín, D., Hernández-Fernández, F., et al. (2020). Cortical disinhibition in Parkinson's disease. *Brain* 143, 3408–3421. doi: 10.1093/brain/awaa274

Bell, A.J., and Sejnowski, T.J. (1995). An information-maximization approach to blind separation and blind deconvolution. *Neural Comput.* 7, 1129–1159. doi: 10.1162/neco.1995.7.6.1129

Chaumon, M., Bishop, D.V., and Busch, N.A. (2015). A practical guide to the selection of independent components of the electroencephalogram for artifact correction. *J. Neurosci. Methods* 250, 47–63. doi: 10.1016/j.jneumeth.2015.02.025

Delorme, A., and Makeig, S. (2004). EEGLAB: an open source toolbox for analysis of single-trial EEG dynamics including independent component analysis. *J. Neurosci. Methods* 134, 9–21. doi: 10.1016/j.jneumeth.2003.10.009

Fatt, I., and Weissman, B.A. (1992). *Physiology of the Eye: An Introduction to the Vegetative Functions*. Boston, MA: Butterworth-Heinemann; Reed Publishing.

Goetz, C.G., Fahn, S., Martinez-Martin, P., Poewe, W., Sampaio, C., Stebbins, G.T., et al. (2007). Movement disorder society-sponsored revision of the unified Parkinson's disease rating scale (mds-updrs): process, format, and clinimetric testing plan. *Mov. Disor.* 22, 41–47. doi: 10.1002/mds.21198

Groppe, D.M., Urbach, T.P., and Kutas, M. (2011). Mass univariate analysis of event-related brain potentials/fields I. A critical tutorial review. *Psychophysiology* 48, 1711–1725. doi: 10.1111/j.1469-8986.2011.01273.x

Hall, A. (1945). The origin and purposes of blinking. *Br. J. Ophthalmol.* 29, 445–467.

Höhn, M. M., and Yahr, M. D. (1967). Parkinsonism: onset, progression and mortality. *Neurology* 17, 427–442. doi: 10.1212/wnl.17.5.427

Ichikawa, N., and Ohira, H. (2004). Eyeblink activity as an index of cognitive processing: temporal distribution of eyeblinks as an indicator of expectancy in semantic priming. *Percept. Mot. Skills* 98, 131–140. doi: 10.2466/pms.98.1.131-140

Image Analyst (2021). *Fit Multiple Gaussians*. Available online at: https://www.mathworks.com/matlabcentral/fileexchange/74408-fit-multiple-gaussians

Jung, I., and Kim, J.-S. (2019). Abnormal eye movements in parkinsonism and movement disorders. *J. Mov. Disord.* 12, 1–13. doi: 10.14802/jmd.18034

Karson, C. N. (1983). Spontaneous eye-blink rates and dopaminergic systems. *Brain* 106, 643–653. doi: 10.1093/brain/106.3.643

Kleifges, K., Bigdely-Shamlo, N., Kerick, S.,and Robbins, K.A. (2017). BLINKER: Automated extraction of ocular indices from EEG enabling large-scale analysis. *Front. Neurosci.* 11:12. doi: 10.3389/fnins.2017.00012

Korosec, M., Zidar, I., Reits, D., Evinger, C., and Vanderwerf, F. (2006). Eyelid movements during blinking in patients with Parkinson's disease. *Mov. Disord.* 21, 1248–1251. doi: 10.1002/mds.20930

Kwon, K. A., Shipley, R. J., Edirisinghe, M., Ezra, D. G., Rose, G., Best, S. M., et al. (2013). High-speed camera characterization of voluntary eye blinking kinematics. *J. R. Soc. Interface* 10:20130227. doi: 10.1098/rsif.2013.0227

Luce RC. *Response Times: Their Role in Inferring Elementary Mental Organization*. New York, NY: Oxford (1986).

Maffei, A., and Angrilli, A. (2018). Spontaneous eye blink rate: an index of dopaminergic component of sustained attention and fatigue. *Int. J. Psychophysiol.* 123, 58–63. doi: 10.1016/j.ijpsycho.2017.11.009

Morillon, B., and Baillet, S. (2017). Motor origin of temporal predictions in auditory attention. *Proc. Natl. Acad. Sci. U.S.A.* 114, E8913–E8921. doi: 10.1073/pnas.1705373114

Nakano, T., Kato, M., Morito, Y., Itoi, S., and Kitazawa S. (2013). Blink-related momentary activation of the default mode network while viewing videos. *Proc. Natl. Acad. Sci. U.S.A.* 110, 702–706. doi: 10.1073/pnas.1214804110

Nakano, T., and Miyazaki, Y. (2019). Blink synchronization is an indicator of interest while viewing videos. *Int. J. Psychophysiol.* 135, 1–11. doi: 10.1016/j.ijpsycho.2018.10.012

Sescousse, G., Ligneul, R., van Holst, R. J., Janssen, L. K., de Boer, F., Janssen, M., et al. (2018). Spontaneous eye blink rate and dopamine synthesis capacity: preliminary evidence for an absence of positive correlation. *Eur. J. Neurosci.* 47, 1081–1086. doi: 10.1111/ejn.13895

Shallice, T. (1982). Specific impairments of planning. *Phil. Trans. Royal Soc. London. B, Biol. Sci.* 298, 199–209. doi: 10.1098/rstb.1982.0082

Stinear, C. M., and Byblow, W. D. (2003). Role of Intracortical inhibition in selective hand muscle activation. *J. Neurophysiol.* 89, 2014–2020. doi: 10.1152/jn.00925.2002

Sun, W. S, Baker, R. S., Chuke, J. C., Rouholiman, B. R., Hasan, S. A., Gaza, W., et al. (1997). Age-related changes in human blinks. Passive and active changes in eyelid kinematics. *Invest. Ophtalmol. Vis. Sci.* 38, 92–99.

Tavano, A., Schröger, E., and Kotz, S. A. (2019). Beta power encodes contextual estimates of temporal event probability in the human brain. *PLoS ONE* 14:e0222420. doi: 10.1371/journal.pone.0222420

te Woerd, E. S., Oostenveld, R., Bloemde, B. R., Lange, F. P., and Praamstra, P. (2015). Effects of rhythmic stimulus presentation on oscillatory brain activity: the physiology of cueing in Parkinson's disease. *Neuroimage Clin.* 9, 300–309. doi: 10.1016/j.nicl.2015.08.018

Terao, Y., Fukuda, H., Yugeta, A., Hikosaka, O., Nomura, Y., Segawa, M., et al. (2011). Initiation and inhibitory control of saccades with the progression of Parkinson's disease? Changes in three major drives converging on the superior colliculus. *Neuropsychologia* 49, 1794–1806. doi: 10.1016/j.neuropsychologia.2011.03.002

Toivanen, M., Pettersson, K., and Lukander, K. (2015). A probabilistic real-time algorithm for detecting blinks, saccades, and fixations from EOG data. *J. Eye Mov. Res.* 8, 1–14. doi: 10.16910/jemr.8.2.1

Tombaugh, T. N. (2004). Trail making test A and B: normative data stratified by age and education. *Arch. Clin. Neuropsychol.* 19, 203–214. doi: 10.1016/S0887-6177(03)00039-8

Tombaugh, T. N., and McIntyre, N. J. (1992). The mini-mental state examination: a comprehensive review. *J. Am. Geriatr. Soc.* 40, 922–935. doi: 10.1111/j.1532-5415.1992.tb01992

Van Opstal, F., De Loof, E., Verguts, T., and Cleeremans, A. (2016). Spontaneous eyeblinks during breaking continuous flash suppression are associated with increased detection times. *J. Vis.* 16, 1–10. doi: 10.1167/16.14.21

Wascher, E., Heppner, H., Möckel, T., Kobald, S. O., and Getzmann, S. (2015). Eye-blinks in choice response tasks uncover hidden aspects of information processing. *EXCLI J.* 14, 207–1218. doi: 10.17179/excli2015-696

Wechsler, D. (1997). *Wechsler Adult Intelligence Scale*. San Antonio, TX: The Psychological Corporation.

White, O. B., Saint-Cyr, J. A., Tomlinson R. D., and Sharpe, J. A. (1983). Ocular motor deficits in Parkinson's disease: II. control of the saccadic and smooth pursuit systems. *Brain* 106, 571–587. doi: 10.1093/brain/106.3.571

Conflict of Interest: The authors declare that the research was conducted in the absence of any commercial or financial relationships that could be construed as a potential conflict of interest.

frontiers in Human Neuroscience

REVIEW
published: 03 March 2022
doi: 10.3389/fnhum.2022.787495

A Predictive Coding Framework for Understanding Major Depression

Jessica R. Gilbert, Christina Wusinich and Carlos A. Zarate Jr.*

Experimental Therapeutics and Pathophysiology Branch, National Institute of Mental Health, National Institutes of Health, Bethesda, MD, United States

Predictive coding models of brain processing propose that top-down cortical signals promote efficient neural signaling by carrying predictions about incoming sensory information. These "priors" serve to constrain bottom-up signal propagation where prediction errors are carried via feedforward mechanisms. Depression, traditionally viewed as a disorder characterized by negative cognitive biases, is associated with disrupted reward prediction error encoding and signaling. Accumulating evidence also suggests that depression is characterized by impaired local and long-range prediction signaling across multiple sensory domains. This review highlights the electrophysiological and neuroimaging evidence for disrupted predictive processing in depression. The discussion is framed around the manner in which disrupted generative predictions about the sensorium could lead to depressive symptomatology, including anhedonia and negative bias. In particular, the review focuses on studies of sensory deviance detection and reward processing, highlighting research evidence for both disrupted generative predictions and prediction error signaling in depression. The role of the monoaminergic and glutamatergic systems in predictive coding processes is also discussed. This review provides a novel framework for understanding depression using predictive coding principles and establishes a foundational roadmap for potential future research.

Keywords: major depression, predictive coding, mismatch negativity, reward processing, prediction errors, ventral striatum

OPEN ACCESS

Edited by:
Juanita Todd,
The University of Newcastle, Australia

Reviewed by:
Hideki Ohira,
Nagoya University, Japan
Benjamin Ely,
Albert Einstein College of Medicine, United States

****Correspondence:***
Jessica R. Gilbert
jessica.gilbert@nih.gov

Specialty section:
This article was submitted to Cognitive Neuroscience, a section of the journal Frontiers in Human Neuroscience

Received: *30 September 2021*
Accepted: *14 February 2022*
Published: *03 March 2022*

Citation:
Gilbert JR, Wusinich C and Zarate CA Jr (2022) A Predictive Coding Framework for Understanding Major Depression. Front. Hum. Neurosci. 16:787495. doi: 10.3389/fnhum.2022.787495

INTRODUCTION

The predictive coding framework suggests that the brain functions to minimize surprise and uncertainty by actively generating explanations for encountered stimuli (Friston, 2009). The framework is rooted in Bayesian probability theory and the so-called *Bayesian brain hypothesis* (Knill and Pouget, 2004) that conceptualizes perception as a constructive process that uses internal or generative models to encode prior beliefs about sensory inputs and their causes. Generative models help an individual formulate predictions about incoming sensory information that are tested against incoming sensory inputs and produce prediction errors. Prediction errors, in turn, are used by the brain to revise its model of the world by updating predictions in order to minimize

prediction errors (Friston, 2010). Recent work has extended these ideas to cognitive phenomena related to interoception (Seth, 2013), including the shaping of emotions (Seth and Friston, 2016; Clark et al., 2018) and the development of depression (Barrett et al., 2016; Kube et al., 2020).

Interoception, broadly defined as the sense of the physiological condition of the body (Craig, 2002), is proposed to be the sensory consequence of allostasis, the regulation of metabolism and bodily states (Barrett et al., 2016). Several recent reviews have focused on the role of predictive processes related to interoception in the etiology and pathophysiology of depression (Barrett and Simmons, 2015; Barrett et al., 2016; Stephan et al., 2016; Eggart et al., 2019). Rather than focusing on interoceptive processes, this review examines the electrophysiological and neuroimaging evidence regarding predictive coding deficits in exteroception in depression, focusing on sensory deviance detection and reward processing deficits that accompany major depressive disorder (MDD).

Bayesian models can be used to inform our understanding of neural and circuit-level dysfunction concomitant with psychiatric conditions such as MDD because they relate formal information-processing algorithms to underlying neural signals (O'Reilly et al., 2012). In current models of Bayesian brain updating, for example, predictions are thought to be carried by descending feedback from deep pyramidal cortical layers and to interact with ascending, feedforward prediction error signals from superficial cortical layers (Rao and Ballard, 1999; Friston and Kiebel, 2009; Bastos et al., 2012; Shipp et al., 2013). These prediction error signals serve to update an individual's expectations, with the precision or confidence placed in prediction errors associated with the synaptic gain or efficacy of superficial pyramidal cell signaling. From a theoretical standpoint, a model such as this can help elucidate cardinal differences between individuals with MDD and healthy participants because the fitting of experimental data to such a model can provide a mechanistic understanding of differences between groups. For example, such models could help an investigator test whether deficits in MDD are related to faulty internal generative models and resultant prediction error signaling associated with incoming sensory information. These models could also be used to make inferences about where prediction error signals originate in the cortex, and these regions can be probed to determine whether activity in a given region is associated with specific features of depressive symptomatology.

This review will highlight the electrophysiological and neuroimaging evidence for disrupted predictive processing in MDD, conceptually framing the discussion around Bayesian models of uncertainty and how disrupted generative predictions about the sensorium might lead to depressive symptomatology, including anhedonia and negative bias. This review will highlight studies of sensory deviance detection and reward processing in particular, describing research evidence for both disrupted predictions and prediction error signaling in MDD. Gaps in the literature where further research is warranted will also be discussed. Finally, the role of the monoaminergic and glutamatergic systems in generating these signals will be examined. This review provides a novel framework for understanding MDD using predictive coding principles and establishes a foundational roadmap for potential future research.

DISRUPTED SENSORY DEVIANCE DETECTION IN MAJOR DEPRESSIVE DISORDER

Sensory deviance detection—broadly defined as the ability to detect deviant stimuli while attending to a stream of incoming sensory information—is thought to reflect pre-attentive sensory processing (Schröger, 1998; Restuccia et al., 2006; Czigler, 2007). One technique for studying pre-attentive change detection involves using an oddball paradigm where a series of frequent stimuli (e.g., tones of a specific pitch "standard") are occasionally interrupted by less-frequent stimuli (e.g., tones of a higher pitch "deviant"). These kinds of paradigms have traditionally been collected using electrophysiological techniques such as electroencephalography (EEG) and magnetoencephalography (MEG) because the temporal components of event-related potentials (ERPs) generated in response to these stimuli have consistent response characteristics and well-documented neural generators (Garrido et al., 2009). In particular, a negative component in the event-related waveform is elicited by deviant relative to standard stimuli, which has been termed the mismatch negativity (MMN) response. The MMN response is considered an index of change detection processes (Näätänen et al., 2012) and, within a prediction coding framework, is thought to represent prediction error signaling (Friston, 2005). Generators of MMN electrophysiological signatures have been localized to primary and secondary auditory, visual, somatosensory, and olfactory cortices, and they have also been localized to higher-order regions, including the frontal cortex (Garrido et al., 2009).

Studies of the MMN response in MDD patients have reported mixed findings regarding waveform topographical changes accompanying MDD (see **Table 1**). The amplitude and latency of the characteristic MMN response—which occurs at approximately 100–250 ms after stimulus onset—has been measured in individuals with MDD relative to healthy participants. While some studies have reported that the MMN amplitude is attenuated in currently medicated and unmedicated MDD patients relative to healthy participants (Takei et al., 2009; Qiu et al., 2011; Qiao et al., 2013; Chen et al., 2015; Tseng et al., 2021), other studies have reported that the MMN amplitude is increased in unmedicated MDD patients (Kähkönen et al., 2007; He et al., 2010). Other studies found hemispheric asymmetries in the MMN response in MDD patients, with reduced MMN amplitudes in the right but not the left hemisphere in medicated MDD patients compared to healthy participants (Hirakawa et al., 2017). Furthermore, other studies reported MMN latency differences in MDD, with patients demonstrating slower peak MMN latencies than healthy participants (Qiao et al., 2013; Tseng et al., 2021). Finally, a small number of studies reported MMN amplitude changes for specific sensory features of oddball stimuli (e.g., timbre and tone duration), but not others (e.g., pitch, intensity, or location) in MDD patients (Mu et al., 2016; Tseng et al., 2021). Taken together, these findings provide

preliminary evidence that MDD is accompanied by an inability to accurately predict forthcoming sensory information, though significant inconsistencies exist with regard to whether the MMN amplitude is larger or smaller and whether it is shifted in time compared to healthy participants.

In addition to examining differences in MMN amplitudes and latencies, an important clinical question is whether differences in pre-attentive change detection are associated with depressive symptomatology in MDD. Several studies have examined whether changes in components elicited during an oddball task are associated with severity of depressive symptoms or other clinical measures of functional outcomes. For example, a recent study comparing both medicated and unmedicated MDD patients to healthy participants found that clinical measures of functional outcomes for MDD patients were associated with MMN source activity in regions including the anterior cingulate and the inferior and middle frontal gyri, though no significant differences in MMN amplitudes were noted in MDD patients compared to healthy participants (Kim et al., 2020). Other studies that did not source-localize MMN generators found no significant associations between severity of depressive symptoms and MMN amplitudes or latencies (He et al., 2010; Mu et al., 2016; Tseng et al., 2021), though earlier and later waveform components, such as the attenuation of the P1 (Kähkönen et al., 2007) and the amplitude of the P3a (Chen et al., 2015), have been associated with clinical characteristics such as severity of depressive symptoms and the number of depressive episodes reported by patients. The P1 is a positive ERP waveform component occurring approximately 100 ms after stimulus presentation and thought to reflect initial sensory attentional processing, while the P3a is a positive component occurring approximately 250–280 ms after stimulus presentation that localizes to fronto-central electrode sites and reflects attentional orienting and novelty detection processes. Taken together, the evidence suggests that gross changes in MMN response characteristics such as amplitude and latency are indeed associated with clinical measures reflecting the severity of depressive symptoms. Further research should continue to explore the relationship between source-localized generators of the MMN signal and depressive symptomatology, given that source-localized MMN response estimates in regions such as the anterior cingulate and inferior frontal gyrus could provide a stronger index of the severity of depressive symptoms compared to waveform characteristics alone.

Inconsistencies in MMN response findings in MDD may be due to several factors, including differences in the sensory modality under study, manipulations regarding what constitutes standard and deviant stimuli, sample sizes, and recruitment criteria for MDD samples. For example, some studies recruited drug-free patients only, while others included a mixture of medicated and unmedicated patients. Special caution should be exercised in interpreting studies where the samples include medicated patients, particularly those in which patients are taking selective serotonin reuptake inhibitors (SSRIs), the most widely prescribed antidepressants. This is because serotonin (5-hydroxytryptamine, 5-HT) is thought to play an important role in salience detection (see "Antidepressant Drugs and Predictive Processes," below). The heterogeneity of findings regarding deficits in the MMN response in MDD across studies may also be explained by the underlying heterogeneity of MDD symptomatology. For example, the MMN response has been hypothesized to index cognitive decline across different psychiatric disorders (Näätänen et al., 2012), suggesting that dysregulated sensory change detection, as indexed by the MMN response, might have prognostic importance in MDD.

As research expands our understanding of the sensory deviance detection deficits that accompany MDD, it is important to keep in mind the potential applications of this work. For example, a better understanding of the brain circuitry supporting prediction errors in sensory processing and their connectivity would improve our understanding of how feedforward and feedback signaling interact as well as illuminate the ways that these might be dysregulated in MDD. In addition, understanding the relationship between MMN signaling deficits and depression symptomatology could lead to the development of a simple, robust biomarker of symptom severity. Such work also fits within the larger Research Domain Criteria (RDoC) framework examing the relationship between neural circuitry disruption and dimensional symptomatology associated with mental disorders.

DISRUPTED REWARD PREDICTION AND PREDICTION ERROR SIGNALING IN MAJOR DEPRESSIVE DISORDER

Reinforcement learning, the process by which behavior is modified through experiences with reward and punishment, offers a theoretical framework for studying the neural circuity supporting decision making under conditions of uncertainty (Schultz, 2006). Several lines of evidence now suggest that dysfunctional reinforcement learning processes and dysregulated reward circuity might underlie some symptoms of MDD (Pizzagalli, 2014). Anhedonia, or hyposensitivity to rewards, is a cardinal symptom of MDD and is associated with worse outcomes, including poor treatment response and greater prevalence of suicidal thoughts and behaviors (Eshel and Roiser, 2010; Spijker et al., 2010; Pizzagalli, 2014; Vrieze et al., 2014; Winer et al., 2016; Yaseen et al., 2016; Loas et al., 2018). Negative bias—a hypersensitivity to punishment and a bias in expectation of negative events—is another common feature of MDD (Gotlib, 1983; Eshel and Roiser, 2010; Rouhani and Niv, 2019). It is worth noting that, though conceptualized distinctly, neural correlates of anhedonia and negative bias may overlap and mutually influence depressive symptoms and differences in reward processing.

Reinforcement learning paradigms using monetary incentives provide an avenue for modeling brain circuitry disruptions in reward processing associated with anhedonia and negative bias. During such tasks, discrepancies between an expected reward and a given reward produce reward prediction errors (RPEs). The neural correlates underlying belief updating, during which a participant alters their framework to make more accurate predictions to subsequent trials, can be examined.

Growing evidence suggests that key neural regions mediating RPE signaling include the lateral habenula, the ventral tegmental area (VTA), and the substantia nigra (Matsumoto and Hikosaka, 2007). The lateral habenula occupy a set of nuclei within the posterior-dorsal-medial region of the thalamus that are thought to have an important role in reward learning behavior [for a recent review of the circuity and functions of the lateral habenula, see Hu et al. (2020)]. The lateral habenula acts as a relay station by connecting the limbic forebrain with monoaminergic centers implicated in the pathophysiology of depression and has been proposed to participate in processing negatively valenced information (Yang et al., 2018b). Animal studies have demonstrated that lateral habenula neurons transmit RPEs in an inverted fashion (Matsumoto and Hikosaka, 2007, 2009a) and can suppress both activity in dopamine neurons (Christoph et al., 1986; Ji and Shepard, 2007) and motivated behaviors (Shumake et al., 2010; Friedman et al., 2011). While many lateral habenula neurons transmit information related to motivational salience (Matsumoto and Hikosaka, 2009b; Bromberg-Martin and Hikosaka, 2011), a subset of these neurons transmit information related to motivational value and exert control over selective positive RPE (i.e., signaling more reward than anticipated) and negative RPE (i.e., signaling less reward than anticipated) dopamine neurons (Matsumoto and Hikosaka, 2009b). Reward-related dopamine signals from the midbrain are broadcast to various regions of the cortex, including the striatum (particularly the nucleus accumbens), the prefrontal cortex, and the amygdala (Schultz, 2007; Niv and Montague, 2009).

Reward processing involves several distinct stages, and many studies have focused on the neural circuitry supporting the reward anticipation and feedback periods. Reward-related learning in particular is thought to occur through RPEs encoded by striatal dopamine signals (Schultz, 2016b). Several lines of evidence suggest that, compared to healthy participants, both medicated and unmedicated MDD patients have blunted RPE signaling within the ventral striatum during reward feedback (see **Table 2**; Zhang et al., 2013; Keren et al., 2018; Kumar et al., 2018), and EEG studies have consistently reported significant reductions in the feedback-related negativity (FRN) ERP component in medicated and unmedicated MDD patients compared to healthy participants (Keren et al., 2018). In addition,

TABLE 1 | Sensory deviance detection disruptions in MDD.

Authors	Major findings—MMN	Sample size and characteristics	Medication status	Methodology
Chen et al. (2015)	↓ MMN amplitude in first-episode and recurrent MDDs; no association between depression severity and MMN amplitudes; P3a amplitude negatively associated with depression severity in both MDD groups	45 first-episode MDD, 40 recurrent MDD, 46 HC	Medicated	EEG
Takei et al. (2009)	↓ MMN amplitude in MDDs; no association between depression severity and MMN amplitude/latency	14 MDD, 19 HC	Medicated	MEG
Hirakawa et al. (2017)	↓ MMN amplitude in MDDs in right but not left hemisphere, reduced MMN latencies in both hemispheres; no association between depression severity and MMN amplitude/latency	20 MDD, 36 HC	Medicated	MEG
Tseng et al. (2021)	↓ MMN amplitude and prolonged latency in first-episode/early stage MDDs for duration but not frequency deviants, ↓ MMN amplitude only for duration deviants in recurrent MDDs; no association between depression severity and MMN amplitude/latency	Meta-analysis of studies including 339 MDD, 343 HC	Mixed status	EEG and MEG
Qiao et al. (2013)	↓ MMN amplitude and prolonged latency in MDDs for increment but not decrement deviants; no association between depression severity and MMN amplitudes	20 first-episode MDD, 20 HC	Unmedicated	EEG
Qiu et al. (2011)	↓ MMN amplitude in MDDs for long-duration but not short-duration deviants; no association between depression severity and MMN amplitudes	24 first-episode MDD, 24 HC	Unmedicated	EEG
He et al. (2010)	↑ MMN amplitude in MDDs only compared to other groups; no association between depression severity and MMN amplitudes or latencies	22 MDD, 19 BPD, 22 comorbid MDD/BPD, 32 HC	Unmedicated	EEG
Kähkönen et al. (2007)	↑ MMN amplitude in MDDs for 10% but not 20% frequency change deviants in EEG but not MEG; P1 latency decrease negatively associated with depression severity	13 MDD, 12 HC	Unmedicated	EEG and MEG
Mu et al. (2016)	↑ MMN amplitude in MDDs for timbre but not pitch, location, intensity, slide, or rhythm deviants; no association between depression severity and MMN amplitudes or latencies	20 MDD, 20 HC	Unmedicated	EEG
Kim et al. (2020)	No differences in MMN amplitude between MDD and HC; ↓ MMN amplitude in BD compared to HC	27 MDD, 29 BD, 33 HC	Medicated	EEG

BD, bipolar depression; BPD, borderline personality disorder; EEG, electroencephalography; HC, healthy control; MEG, magnetoencephalography; MDD, major depression; MMN, mismatch negativity.

TABLE 2 | Reward prediction and prediction error disruptions in MDD.

Authors	Major findings—Reward signaling	Sample size and characteristics	Medication status	Methodology
Greenberg et al. (2015)	↓ RPE signal in right striatum in MDD; striatal PE-related signal associated with anhedonia severity	148 MDD, 31 HC	Unmedicated	fMRI
Keren et al. (2018)	↓ striatal activation during reward anticipation and blunted FRN response in MDD; longitudinal studies suggest these effects precede onset of depression in adolescents	Meta-analysis of 38 fMRI studies and 12 EEG studies	Mixed status	EEG and fMRI
Kumar et al. (2018)	↓ RPE signal in striatum in MDD; ↓ VTA-striatal connectivity during feedback; both striatal RPE signal blunting and habenula PPE signal associated with number of MDEs	25 MDD, 26 HC	Unmedicated	fMRI
Zhang et al. (2013)	↓ striatal activation during reward anticipation and feedback in MDD, ↑ activation in middle frontal gyrus and dorsal anterior cingulate during reward anticipation in MDD	Meta-analysis of studies including 341 MDD, 367 HC	Mixed status	fMRI
Rothkirch et al. (2017)	No differences in RPE signals in striatum and anterior insula; ↓ RPE signaling in orbitofrontal cortex in MDD; RPE signals in striatum and orbitofrontal cortex negatively associated with anhedonia severity	28 MDD, 30 HC	Unmedicated	fMRI
Rutledge et al. (2017)	No differences in RPE signals in striatum	32 MDD, 20 HC	Medicated	fMRI

EEG, electroencephalography; fMRI, functional magnetic resonance imaging; FRN, feedback-related negativity; HC, healthy control; MDD, major depression; MEG, magnetoencephalography; PE, prediction error; PPE, punishment prediction error; RPE, reward prediction error; VTA, ventral tegmental area.

some studies have suggested that VTA-striatal connectivity is blunted in response to reward feedback in unmedicated MDD patients compared to healthy participants (Kumar et al., 2018). However, other researchers have found seemingly contradictory results regarding RPE signaling in the striatum. For example, Rutledge and colleagues (2017) found that ventral striatum RPE signaling did not significantly differ between medicated MDD patients and healthy participants, while a recent review identified discrepancies in blunting or lack of blunting of ventral striatum signals during RPEs in MDD patients (Yaple et al., 2021). Taken together, a growing consensus suggests that MDD is accompanied by changes in dopaminergic signaling that affect reward-related outcomes in the striatum, though significant inconsistencies remain regarding whether the striatal activation is blunted or increased in MDD.

As with MMN response changes accompanying depression, an important clinical question is whether differences in striatal activity or other aspects of reward processing are associated with depressive symptomatology. Recent research suggests that blunting of striatal RPE signaling is associated with the number of depressive episodes reported by patients, indicating that MDD has an increasing impact on reward learning processes over time (Kumar et al., 2018). Similarly, signals in the habenula have also been correlated with the number of depressive episodes experienced by MDD patients (Kumar et al., 2018). A recent meta-analysis of studies using reward tasks in depression found that blunting of both striatal activation and the FRN response were associated with depressive symptomatology, though changes in the metrics that accompanied symptom severity did not reach levels that would be useful for clinical prediction (Nielson et al., 2021). Taken together, these findings suggest that RPE signaling deficits, as indexed by reductions in striatal activation and the FRN component of the M/EEG, are potentially useful biomarkers of MDD; nevertheless, more research is warranted to determine whether these brain circuitry changes may play a causal role in the development of depression (Nielson et al., 2021).

As previously noted in relation to the MMN response, inconsistencies in neurophysiological RPE findings in MDD may be due to a number of factors, including sample size and recruitment criteria, medication status, and differences in reward tasks and incentives and punishments. In addition, the heterogeneity of findings on RPEs in MDD may also be explained by underlying heterogeneity in MDD symptomatology. The severity of anhedonia, in particular, might be a useful construct for analyzing RPE signals in this context. One study that included anhedonia in its framework found that, for MDD patients, higher levels of anhedonia were associated with reduced RPE signals in the ventral striatum and medial orbitofrontal cortex (Rothkirch et al., 2017). Another study found that among those with and without an MDD diagnosis, severity of anhedonia moderated the relationship between reward expectancy and RPE signaling in ventral striatum; this suggests that those with worse symptoms of anhedonia may experience deficits in related aspects of reward learning regardless of diagnosis (Greenberg et al., 2015). Such subtyping work has also demonstrated that resting-state hyperconnectivity between thalamic and frontostriatal networks, including the reward-related circuitry discussed here, is associated with a depressive biotype characterized by increased anhedonia and psychomotor retardation (Drysdale et al., 2017).

As research in this area expands and our neuroscientific understanding of predictive coding deficits in depression is refined, it is important to consider the real-world applications of this work. For example, a better understanding of RPE signaling in reward tasks might increase our understanding of the neural processes that mediate anhedonia and negative bias, allowing the development of more refined and better targeted

pharmaceutical and psychotherapeutic interventions. Given the connection between altered reward learning and decision making processes, this research also has implications for suicide-related interventions (Dombrovski et al., 2013).

ANTIDEPRESSANT DRUGS AND PREDICTIVE PROCESSES

Presently, most approved antidepressant drugs target the monoaminergic system and regulate the reuptake, metabolism, or receptor pharmacodynamics of the neurotransmitters 5-HT and norepinephrine (also called noradrenaline). The typical onset of beneficial drug effects for these antidepressants takes several weeks (Quitkin et al., 1984; Gelenberg and Chesen, 2000), though mounting evidence suggests that earlier clinical and cognitive processing changes may help predict treatment outcomes (Katz et al., 1996; Harmer et al., 2009). More recently, the glutamatergic modulator ketamine has gained attention as a novel therapeutic that produces rapid-acting antidepressant effects in individuals with treatment-resistant MDD that manifest within hours of administration and last days (Zarate et al., 2006; Kishimoto et al., 2016). Concomitantly, in 2019 the FDA approved esketamine (the intranasally-administered *S*-enantiomer of ketamine) as an adjunctive treatment option for depression. This section explores the current state of the literature regarding the role of monoaminergic and glutamatergic [particularly via the N-methyl-D-aspartate (NMDA) receptor] signaling in predictive coding processes. Where appropriate, research evidence that highlights the effects of monoaminergic and glutamatergic antidepressant therapeutics on these processes in both MDD patients and healthy participants is also presented.

Monoaminergic Drugs

5-HT, norepinephrine, and dopamine are monoamines involved in a wide range of physiological and homeostatic processes. 5-HT, for example, has been implicated in a range of behaviors, including regulating the sleep-wake cycle and hormonal levels as well as influencing cognition, sensorimotor behaviors, and emotions (Jacobs and Azmitia, 1992). Norepinephrine has been implicated in regulating arousal and adapting network activity by influencing neuromodulatory neurons and peripheral arousal levels to support adaptive, flexible behavioral responses (Sara and Bouret, 2012).

Pre-attentive sensory processing research suggests that 5-HT is important for salience detection and potentially regulates the speed of change detection during sensory tasks (Kähkönen et al., 2005). In the primary visual cortex, for instance, the distribution of 5-HT-ergic axons appears to be highest in input layer IV of the cortex (Kosofsky et al., 1984; Morrison and Foote, 1986). In contrast, while 5-HT-ergic axons are consistently found in layer IV in primary auditory and somatosensory cortices, the distribution does not appear to be preferential (Wilson and Molliver, 1991a,b). Despite variability in the distribution of 5-HT-ergic axons across sensory modalities, studies have consistently shown that 5-HT modulates the salience of sensory inputs across modalities (Jacob and Nienborg, 2018). While the role of 5-HT in salience detection has been well documented, its role in the MMN response is less clear. In healthy participants, studies using acute tryptophan depletion (ATD)—which rapidly reduces the amino acid precursor of 5-HT and 5-HT metabolite concentrations in cerebrospinal fluid—have produced mixed findings. While some studies reported that ATD increased MMN amplitudes and reduced latencies (Kähkönen et al., 2005), other studies found either reduced MMN amplitudes (Ahveninen et al., 2002) or no differences in MMN responses following ATD (Leung et al., 2009). These discrepancies might be due to methodological differences in preprocessing approaches and other analytical techniques, including choices related to M/EEG source localization techniques (Fusar-Poli et al., 2006). In addition, while ATD is thought to reduce 5-HT release and subsequently blunt neurotransmission, there is no direct evidence that it decreases extracellular 5-HT concentrations. Caution is thus needed when interpreting its selective 5-HT effects (van Donkelaar et al., 2011).

The role of 5-HT in reward processing is less clear than for sensory deviance detection, and our current understanding derives from the observation that 5-HT has an opponent relationship with dopamine (Kapur and Remington, 1996; Daw et al., 2002). Phasic levels of dopaminergic activity are known to signal positive and negative RPEs related to how different the current reward is from ongoing predictions of long-running rewards (Schultz et al., 1997; Schultz, 2016b). Given the opponent relationship between dopamine and 5-HT, one theory regarding 5-HT's role in reward signaling is that phasic levels of 5-HT signal punishment prediction errors related to how different the current punishment is from ongoing predictions of future punishment (Daw et al., 2002). An extension of this model also accounts for how tonic 5-HT levels may represent the opportunity costs of waiting to avoid punishments (Cools et al., 2011). Studies using ATD and reward learning tasks in healthy participants have produced mixed findings, echoing studies that used MMN response tasks. One review of 36 studies that used ATD during reward learning tasks reported that lower 5-HT levels resulted in reduced sensitivity to punishments in nine of the 36 studies, with the authors noting that further research was warranted to clarify the role of 5-HT in reward tasks (Faulkner and Deakin, 2014). Similar caution should be used when interpreting results regarding 5-HT's role in reward processing, as previously discussed in relation to sensory deviance detection.

Research examining the role of norepinephrine in sensory processing indicates that it plays a complex modulatory role in sensory signaling (Jacob and Nienborg, 2018). Norepinephrine innervation in the somatosensory cortex is both uniform and dense across cortical layers (Morrison et al., 1982; Lewis et al., 1987). Unlike 5-HT, however, norepinephrine innervation in primary auditory and visual cortices is sparse across layers and virtually absent in layer IV (Foote and Pineda, 1993). Given the sparse distribution of norepinephrine receptors in auditory and visual cortices, norepinephrine's primary role in sensory processing appears to be in modulating NMDA receptor-mediated glutamate responses (Devilbiss and Waterhouse, 2000),

gating long-term plasticity (LTP) of glutamatergic synapses, and increasing the gain of local inhibitory synapses (Salgado et al., 2016). Because norepinephrine plays only an indirect role in sensory cortex signaling via modulation of glutamatergic mechanisms, little research has examined its specific role in sensory deviance detection.

While norepinephrine's role in sensory processing is understudied, recent work has begun to examine its role in reward-related tasks. In particular, recent evidence suggests that norepinephrine plays a role in modulating glutamatergic synapses in the nucleus accumbens, and that it might tune feedforward inhibition and impact reward-related circuitry as well as motivational states (Manz et al., 2021). Animal studies have also suggested that norepinephrine is associated with the amount of effort required to perform a reward task (here, force exerted on a grip in order to receive a reward) and that this effort is distinct from reward sensitivity (Varazzani et al., 2015; Borderies et al., 2020). While norepinephrine's role in reward-related tasks is also understudied, current findings suggest that it plays an important role in modulating motivation and effort levels. One particularly relevant area for future research regarding where motivation and effort influence reward-related behavior would be determining the opportunity costs associated with seeking or avoiding rewards and punishments. Perhaps norepinephrine and 5-HT operate synergistically in this regard to support motivated behaviors to continue to seek rewards or avoid punishments.

Given the proposed role of 5-HT and norepinephrine in predictive coding processes, it is useful to consider the effect of antidepressant drugs that target the monoaminergic system on sensory deviance detection and reward processing. While many previously reviewed studies of the MMN response and reward processing included medicated patients, the heterogeneity of medications and the inclusion of both medicated and unmedicated samples makes it difficult to tease apart the role that specific neurotransmitters may have played in predictive processing. Another way to approach this experimentally is to give antidepressant drugs to healthy participants. Such studies found that drugs such as escitalopram, the therapeutically-active *S*-enantiomer of citalopram [a highly selective serotonin reuptake inhibitor (SSRI)], increase MMN amplitudes in healthy participants (Oranje et al., 2008; Wienberg et al., 2010). In addition, research with citalopram using appetizing and aversive food picture stimuli found reduced ventral striatum and ventral medial/orbitofrontal cortex activation in healthy participants to appetizing foods such as chocolate (McCabe et al., 2010). Research with reboxetine, a norepinephrine reuptake inhibitor, found increased neural responses in the medial orbitofrontal cortex to the same appetizing foods (McCabe et al., 2010). One difficulty with using such dosing studies to inform our understanding of how predictive coding might be altered in MDD is that these antidepressants have a delayed onset of action of several weeks. Research on antidepressant drugs that selectively downregulate the 5-HT or norepinephrine transporter found that they produced a marked loss of binding sites for the targeted neurotransmitter over an overlapping 2–3 week time window corresponding with antidepressant efficacy (Frazer and Benmansour, 2002). Some drug studies have tried to account for this delay by having healthy participants take such drugs over several days (e.g., 7 days) (McCabe et al., 2010), while other studies have examined drug effects after only a single dose (Oranje et al., 2008; Wienberg et al., 2010). One study of the serotonin-norepinephrine reuptake inhibitor (SNRI) duloxetine in healthy participants used a 2-week daily dosing regimen and found increased ventral striatum responses during a reward task (Ossewaarde et al., 2011). Further work is needed using this longer-term dosing approach that overlaps with antidepressant response to the drug in order to better characterize the roles of 5-HT and norepinephrine in predictive coding processes. As a final point, recent research has begun to explore the antidepressant efficacy of "classic" 5-HT-ergic psychedelics including psilocybin and lysergic acid diethylamide-25 in MDD patients. Examining how such drugs impact both the MMN response and reward processing are promising directions for future research.

Finally, a new class of antidepressant drugs target dopamine, in addition to 5-HT and norepinephrine. Therefore, it is useful to consider the role of dopamine in predictive processes related to the MMN response and reward-related signaling. The role of dopamine in sensory signaling is understudied, though it is thought to play an important role in modulating human attention and arousal (Coull, 1998). Limited research examining the effects of haloperidol, a partially selective dopamine D2 receptor antagonist, demonstrated that drug administration did not affect the source location or amplitude of the MMN response in healthy participants, suggesting that dopamine does not have a role in sensory deviance detection processes *per se* (Kähkönen et al., 2002). However, the drug was found to influence the amplitude of the MMN response in healthy participants during a condition where participants selectively attended to one of two simultaneously presented auditory streams, suggesting that dopamine plays a specific role in the involuntary detection of task-irrelevant deviants (Kähkönen et al., 2001). Studies examining the MMN response in healthy participants following acute tyrosine/phenylalanine depletion also suggest that reducing dopamine neurotransmission has no effect on the MMN response (Leung et al., 2009). Taken together, these findings suggest that dopamine is not directly involved in predictive coding processes at the level of sensory inputs.

Much more is known about dopamine's role in reward processing and RPE signaling, as has been previously discussed (Matsumoto and Hikosaka, 2007; Schultz, 2007; Matsumoto and Hikosaka, 2009b; Schultz, 2016b). However, while animal models consistently demonstrate that dopamine signals code RPEs (Schultz, 2016a), research examining pharmacological manipulations of dopamine in healthy participants offer mixed findings. While dopamine antagonism has been demonstrated to consistently decrease reward learning, dopamine antagonism and dietary manipulations of dopamine offer mixed results (Webber et al., 2021). These discrepancies could be due to a number of factors including drug manipulations, dosing regimens, or the possibility that there is an optimal level of dopamine for reward-related learning, with increases beyond this level impairing

reward-related functioning (Vaillancourt et al., 2013). Further research is needed in this area to elucidate how changes in dopamine signaling concomitant with depression are associated with RPE signals.

Glutamatergic Drugs

Glutamate is the primary excitatory neurotransmitter in the brain and is important for regulating cortical excitability and experience-dependent synaptic plasticity and LTP. Glutamatergic signaling deficits have been widely reported in mood disorders including MDD (Choudary et al., 2005; Yüksel and Öngür, 2010; Bernard et al., 2011), and subanesthetic doses of the non-competitive NMDA receptor antagonist ketamine have been shown to rapidly reduce depressive symptoms (Zarate et al., 2006; Kishimoto et al., 2016). Antidepressant response to ketamine appears to rely on both high affinity antagonistic binding properties at the NMDA receptor and alpha-amino-3-hydroxy-5-methyl-4-isoxazolepropionic acid (AMPA) throughput modulation (Maeng et al., 2008; Zanos et al., 2016). In the context of predictive coding signaling, this is particularly relevant because AMPA and NMDA receptors may support distinct contributions to feedforward and feedback signaling. For example, in the visual system, AMPA receptors are primarily thought to propagate visual activity from lower to higher-order visual areas, while NMDA receptors modulate recurrent connections (Lumer et al., 1997; Dehaene et al., 2003; Self et al., 2012). Much of what is known about the NMDA receptor's role in the MMN response and reward processing comes from pharmacological ketamine studies.

Subanesthetic-dose ketamine has been used to model schizophrenia-like effects in healthy participants, and findings from these studies can inform our understanding of the NMDA receptor's role in sensory deviance detection. In healthy participants, ketamine administration consistently diminished auditory ERP amplitudes during drug infusion (Rosburg and Kreitschmann-Andermahr, 2016; Harms et al., 2021). Electrophysiological findings have also demonstrated that ketamine increases the latency of MMN responses in healthy participants (Umbricht et al., 2000; Kreitschmann-Andermahr et al., 2001), though its effect on amplitude is stronger than its effect on latency (Rosburg and Kreitschmann-Andermahr, 2016). In the context of the MMN response, ketamine administration was found to reduce frontal MMN amplitudes immediately post-infusion and again at 2 h post-infusion in MDD patients; furthermore, immediate change in MMN amplitude predicted antidepressant response (de la Salle, 2022). In contrast, other studies that used a roving auditory oddball task collected 3–4 h post-ketamine infusion in MDD patients found that ketamine administration increased MMN response, but only when all repetitions of the post-deviant tone were analyzed (Sumner et al., 2020). The same study found that feedforward connectivity from the primary auditory cortex to the inferior temporal cortex for the deviant tones was associated with antidepressant response. Taken together, the evidence suggests that ketamine administration consistently and acutely attenuates MMN amplitude and increases its latency in healthy participants, but that findings regarding how ketamine influences MMN response in MDD patients are mixed. Some of this discrepancy could be related to differences in the oddball task design or could be related to differences in the timing of MMN response measurements relative to ketamine administration. Additional work is needed to examine both acute and delayed ketamine effects on MMN response, particularly in unmedicated patients, in order to tease apart transient effects that result from NMDA receptor blockade from more delayed antidepressant effects that result from changes in synaptic efficacy.

Ketamine has also been administered to healthy participants during reward learning tasks. Results indicated that acute subanesthetic ketamine administration attenuated ventral striatum activation during reward anticipation (Francois et al., 2016). Additional research focused on ketamine's effects on reward processing in MDD patients, in part spurred by recent findings that ketamine blockade of NMDA receptor-dependent bursting activity in the lateral habenula mediated antidepressant response in animal models, with subsequent disinhibitory effects in downstream reward centers (Yang et al., 2018a; Cui et al., 2019). A recent study of unmedicated MDD patients currently in remission found that ketamine increased activation in the nucleus accumbens, putamen, insula, and caudate 2 h post-administration, during the reward feedback period (Kotoula et al., 2021). Another study of medicated MDD patients found that ketamine administration resulted in increased ventral striatum and orbitofrontal cortex activation during both the reward anticipation and feedback periods of a reward task administered 1 day post-infusion (Sterpenich et al., 2019). Taken together, these findings suggest that ketamine improves sensitivity to rewards as indexed by increased activation in the striatum and other reward-related circuitry, and that these effects might be mediated by changes in NMDA receptor-mediated bursting within the lateral habenula. Additional work is needed to examine how changes in activity within these reward-related regions post-ketamine may be associated with antidepressant response in MDD.

CONCLUSION

The predictive coding framework conceptualizes perception as a constructive process where internal generative models are used to predict incoming sensory inputs and their causes. MDD has traditionally been viewed as a disorder characterized by negative cognitive biases, and these biases could result in disrupted prediction error signaling within this framework. This paper reviewed the evidence for disrupted predictions in MDD in relation to both sensory deviance detection and reward processing and examined the role of 5-HT, norepinephrine, and NMDA receptor-mediated glutamate signaling in these predictive processes. While the evidence suggests that MDD is accompanied by changes in both sensory deviance detection and reward processing, much additional work is needed. Future studies should pay particular attention to medication status in MDD in order to control for the influence of

antidepressant drugs on effects of interest. More work is also needed to understand how cardinal symptoms of MDD such as anhedonia and negative bias are associated with reward-related neural processing in particular. Finally, additional studies are needed to understand how 5-HT, norepinephrine, and NMDA receptor-mediated glutamate signaling might synergistically support predictive signaling in both healthy participants and MDD patients.

AUTHOR CONTRIBUTIONS

All authors listed have made a substantial, direct, and intellectual contribution to the work, and approved it for publication.

FUNDING

Funding for this work was supported by the Intramural Research Program at the National Institute of Mental Health, National Institutes of Health (IRP-NIMH-NIH; ZIAMH002857). The NIH had no further role in study design; in the collection, analysis, or interpretation of data; in the writing of the report; or in the decision to submit the paper for publication.

ACKNOWLEDGMENTS

We thank the 7SE research unit and staff for their support. Ioline Henter (NIMH) provided invaluable editorial assistance.

REFERENCES

Ahveninen, J., Kähkönen, S., Pennanen, S., Liesivuori, J., Ilmoniemi, R. J., and Jääskeläinen, I. P. (2002). Tryptophan depletion effects on EEG and MEG responses suggest serotonergic modulation of auditory involuntary attention in humans. *Neuroimage* 16, 1052–1061. doi: 10.1006/nimg.2002.1142

Barrett, L. F., Quigley, K. S., and Hamilton, P. (2016). An active inference theory of allostasis and interoception in depression. *Philos. Trans. R. Soc. Lond. B Biol. Sci.* 371:20160011. doi: 10.1098/rstb.2016.0011

Barrett, L. F., and Simmons, W. K. (2015). Interoceptive predictions in the brain. *Nat. Rev. Neurosci.* 16, 419–429. doi: 10.1038/nrn3950

Bastos, A. M., Usrey, W. M., Adams, R. A., Mangun, G. R., Fries, P., and Friston, K. J. (2012). Canonical Microcircuits for Predictive Coding. *Neuron* 76, 695–711. doi: 10.1016/j.neuron.2012.10.038

Bernard, R., Kerman, I. A., Thompson, R. C., Jones, E. G., Bunney, W. E., Barchas, J. D., et al. (2011). Altered expression of glutamate signaling, growth factor, and glia genes in the locus coeruleus of patients with major depression. *Mol. Psychiatry* 16, 634–646. doi: 10.1038/mp.2010.44

Borderies, N., Bornert, P., Gilardeau, S., and Bouret, S. (2020). Pharmacological evidence for the implication of noradrenaline in effort. *PLoS Biol.* 18:e3000793. doi: 10.1371/journal.pbio.3000793

Bromberg-Martin, E. S., and Hikosaka, O. (2011). Lateral habenula neurons signal errors in the prediction of reward information. *Nat. Neurosci.* 14, 1209–1216. doi: 10.1038/nn.2902

Chen, J., Zhang, Y., Wei, D., Wu, X., Fu, Q., Xu, F., et al. (2015). Neurophysiological handover from MMN to P3a in first-episode and recurrent major depression. *J. Affect. Disord.* 174, 173–179. doi: 10.1016/j.jad.2014.11.049

Choudary, P. V., Molnar, M., Evans, S. J., Tomita, H., Li, J. Z., Vawter, M. P., et al. (2005). Altered cortical glutamatergic and GABAergic signal transmission with glial involvement in depression. *Proc. Natl. Acad. Sci. U.S.A.* 102, 15653–15658. doi: 10.1073/pnas.0507901102

Christoph, G., Leonzio, R., and Wilcox, K. (1986). Stimulation of the lateral habenula inhibits dopamine-containing neurons in the substantia nigra and ventral tegmental area of the rat. *J. Neurosci.* 6, 613–619. doi: 10.1523/JNEUROSCI.06-03-00613.1986

Clark, J. E., Watson, S., and Friston, K. J. (2018). What is mood? A computational perspective. *Psychol. Med.* 48, 2277–2284.

Cools, R., Nakamura, K., and Daw, N. D. (2011). Serotonin and dopamine: unifying affective, activational, and decision functions. *Neuropsychopharmacology* 36, 98–113. doi: 10.1038/npp.2010.121

Coull, J. T. (1998). Neural correlates of attention and arousal: insights from electrophysiology, functional neuroimaging and psychopharmacology. *Prog. Neurobiol.* 55, 343–361. doi: 10.1016/s0301-0082(98)00011-2

Craig, A. D. (2002). How do you feel? Interoception: the sense of the physiological condition of the body. *Nat. Rev. Neurosci.* 3, 655–666.

Cui, Y., Hu, S., and Hu, H. (2019). Lateral habenular burst firing as a target of the rapid antidepressant effects of ketamine. *Trends Neurosci.* 42, 179–191. doi: 10.1016/j.tins.2018.12.002

Czigler, I. (2007). Visual mismatch negativity. *J. Psychophysiol.* 21, 224–230.

Daw, N. D., Kakade, S., and Dayan, P. (2002). Opponent interactions between serotonin and dopamine. *Neural Netw.* 15, 603–616. doi: 10.1016/s0893-6080(02)00052-7

de la Salle, S. (2022). Electrophysiological correlates and predictors of the antidepressant response to repeated ketamine infusions in treatment-resistant depression. *Prog. Neuropsychopharmacol. Biol. Psychiatry* 115:110507. doi: 10.1016/j.pnpbp.2021.110507

Dehaene, S., Sergent, C., and Changeux, J.-P. (2003). A neuronal network model linking subjective reports and objective physiological data during conscious perception. *Proc. Natl. Acad. Sci. U.S.A.* 100, 8520–8525. doi: 10.1073/pnas.1332574100

Devilbiss, D. M., and Waterhouse, B. D. (2000). Norepinephrine exhibits two distinct profiles of action on sensory cortical neuron responses to excitatory synaptic stimuli. *Synapse* 37, 273–282. doi: 10.1002/1098-2396(20000915)37:4<273::AID-SYN4>3.0.CO;2-#

Dombrovski, A. Y., Szanto, K., Clark, L., Reynolds, C. F., and Siegle, G. J. (2013). Reward signals, attempted suicide, and impulsivity in late-life depression. *JAMA Psychiatry* 70, 1020–1030. doi: 10.1001/jamapsychiatry.2013.75

Drysdale, A. T., Grosenick, L., Downar, J., Dunlop, K., Mansouri, F., Meng, Y., et al. (2017). Resting-state connectivity biomarkers define neurophysiological subtypes of depression. *Nat. Med.* 23, 28–38.

Eggart, M., Lange, A., Binser, M. J., Queri, S., and Müller-Oerlinghausen, B. (2019). Major depressive disorder is associated with impaired interoceptive accuracy: a systematic review. *Brain Sci.* 9:131. doi: 10.3390/brainsci9060131

Eshel, N., and Roiser, J. P. (2010). Reward and punishment processing in depression. *Biol. Psychiatry* 68, 118–124.

Faulkner, P., and Deakin, J. F. W. (2014). The role of serotonin in reward, punishment and behavioural inhibition in humans: insights from studies with acute tryptophan depletion. *Neurosci. Biobehav. Rev.* 46, 365–378. doi: 10.1016/j.neubiorev.2014.07.024

Foote, S. L., and Pineda, J. A. (1993). Extrathalamic modulation of cortical function. *Annu. Rev. Neurosci.* 10, 67–95. doi: 10.1146/annurev.ne.10.030187.000435

Francois, J., Grimm, O., Schwarz, A. J., Schweiger, J., Haller, L., Risterucci, C., et al. (2016). Ketamine suppresses the ventral striatal response to reward anticipation: a cross-species translational neuroimaging study. *Neuropsychopharmacology* 41, 1386–1394. doi: 10.1038/npp.2015.291

Frazer, A., and Benmansour, S. (2002). Delayed pharmacological effects of antidepressants. *Mol. Psychiatry* 7, S23–S28. doi: 10.1038/sj.mp.4001015

Friedman, A., Lax, E., Dikshtein, Y., Abraham, L., Flaumenhaft, Y., Sudai, E., et al. (2011). Electrical stimulation of the lateral habenula produces an inhibitory effect on sucrose self-administration. *Neuropharmacology* 60, 381–387. doi: 10.1016/j.neuropharm.2010.10.006

Friston, K. (2005). A theory of cortical responses. *Philos. Trans. R. Soc. Lond. B Biol. Sci.* 360, 815–836.

Friston, K. (2009). The free-energy principle: a rough guide to the brain? *Trends Cogn. Sci.* 13, 293–301. doi: 10.1016/j.tics.2009.04.005

Friston, K. (2010). The free-energy principle: a unified brain theory? *Nat. Rev. Neurosci.* 11, 127–138. doi: 10.1038/nrn2787

Friston, K., and Kiebel, S. (2009). Predictive coding under the free-energy principle. *Philos. Trans. R. Soc. Lond. B Biol. Sci.* 364, 1211–1221. doi: 10.1098/rstb.2008.0300

Fusar-Poli, P., Allen, P., Mcguire, P., Placentino, A., Cortesi, M., and Perez, J. (2006). Neuroimaging and electrophysiological studies of the effects of acute tryptophan depletion: a systematic review of the literature. *Psychopharmacology* 188, 131–143. doi: 10.1007/s00213-006-0493-1

Garrido, M. I., Kilner, J. M., Stephan, K. E., and Friston, K. J. (2009). The mismatch negativity: a review of underlying mechanisms. *Clin. Neurophysiol.* 120, 453–463. doi: 10.1016/j.clinph.2008.11.029

Gelenberg, A. J., and Chesen, C. L. (2000). How fast are antidepressants? *J. Clin. Psychiatry* 61, 712–721. doi: 10.4088/jcp.v61n1002

Gotlib, I. H. (1983). Perception and recall of interpersonal feedback: Negative bias in depression. *Cogn. Ther. Res.* 7, 399–412. doi: 10.1016/j.jbtep.2009.03.001

Greenberg, T., Chase, H. W., Almeida, J. R., Stiffler, R., Zevallos, C. R., Aslam, H. A., et al. (2015). Moderation of the relationship between reward expectancy and prediction error-related ventral striatal reactivity by anhedonia in unmedicated major depressive disorder: findings from the EMBARC study. *Am. J. Psychiatry* 172, 881–891. doi: 10.1176/appi.ajp.2015.14050594

Harmer, C. J., Goodwin, G. M., and Cowen, P. J. (2009). Why do antidepressants take so long to work? A cognitive neuropsychological model of antidepressant drug action. *Br. J. Psychiatry* 195, 102–108. doi: 10.1192/bjp.bp.108.051193

Harms, L., Parras, G. G., Michie, P. T., and Malmierca, M. S. (2021). The Role of Glutamate Neurotransmission in Mismatch Negativity (MMN), a measure of auditory synaptic plasticity and change-detection. *Neuroscience* 456, 106–113. doi: 10.1016/j.neuroscience.2020.01.046

He, W., Chai, H., Zheng, L., Yu, W., Chen, W., Li, J., et al. (2010). Mismatch negativity in treatment-resistant depression and borderline personality disorder. *Prog. Neuropsychopharmacol. Biol. Psychiatry* 34, 366–371. doi: 10.1016/j.pnpbp.2009.12.021

Hirakawa, N., Hirano, Y., Nakamura, I., Hirano, S., Sato, J., Oribe, N., et al. (2017). Right hemisphere pitch-mismatch negativity reduction in patients with major depression: an MEG study. *J. Affect. Disord.* 215, 225–229. doi: 10.1016/j.jad.2017.03.046

Hu, H., Cui, Y., and Yang, Y. (2020). Circuits and functions of the lateral habenula in health and in disease. *Nat. Rev. Neurosci.* 21, 277–295. doi: 10.1038/s41583-020-0292-4

Jacob, S. N., and Nienborg, H. (2018). Monoaminergic neuromodulation of sensory processing. *Front. Neural Circuits* 12:51. doi: 10.3389/fncir.2018.00051

Jacobs, B. L., and Azmitia, E. C. (1992). Structure and function of the brain serotonin system. *Physiol. Rev.* 72, 165–229.

Ji, H., and Shepard, P. D. (2007). Lateral habenula stimulation inhibits rat midbrain dopamine neurons through a GABAA receptor-mediated mechanism. *J. Neurosci.* 27, 6923–6930. doi: 10.1523/JNEUROSCI.0958-07.2007

Kähkönen, S., Ahveninen, J., Jääskeläinen, I. P., Kaakkola, S., Näätänen, R., Huttunen, J., et al. (2001). Effects of haloperidol on selective attention: a combined whole-head MEG and high-resolution EEG study. *Neuropsychopharmacology* 25, 498–504. doi: 10.1016/S0893-133X(01)00255-X

Kähkönen, S., Ahveninen, J., Pekkonen, E., Kaakkola, S., Huttunen, J., Ilmoniemi, R. J., et al. (2002). Dopamine modulates involuntary attention shifting and reorienting: an electromagnetic study. *Clin. Neurophysiol.* 113, 1894–1902. doi: 10.1016/s1388-2457(02)00305-x

Kähkönen, S., Mäkinen, V., Jääskeläinen, I. P., Pennanen, S., Liesivuori, J., and Ahveninen, J. (2005). Serotonergic modulation of mismatch negativity. *Psychiatry Res.* 138, 61–74. doi: 10.1016/j.pscychresns.2004.09.006

Kähkönen, S., Yamashita, H., Rytsälä, H., Suominen, K., Ahveninen, J., and Isometsä, E. (2007). Dysfunction in early auditory processing in major depressive disorder revealed by combined MEG and EEG. *J. Psychiatry Neurosci.* 32, 316–322.

Kapur, S., and Remington, G. (1996). Serotonin-dopamine interaction and its relevance to schizophrenia. *Am. J. Psychiatry* 153, 466–476. doi: 10.1176/ajp.153.4.466

Katz, M. M., Koslow, S. H., and Frazer, A. (1996). Onset of antidepressant activity: reexamining the structure of depression and multiple actions of drugs. *Depress. Anxiety* 4, 257–267. doi: 10.1002/(SICI)1520-6394(1996)4:6<257::AID-DA1>3.0.CO;2-9

Keren, H., O'callaghan, G., Vidal-Ribas, P., Buzzell, G. A., Brotman, M. A., Leibenluft, E., et al. (2018). Reward processing in depression: a conceptual and meta-analytic review across fMRI and EEG studies. *Am. J. Psychiatry* 175, 1111–1120. doi: 10.1176/appi.ajp.2018.17101124

Kim, S., Baek, J. H., Shim, S.-H., Kwon, Y. J., Lee, H. Y., Yoo, J. H., et al. (2020). Mismatch negativity indices and functional outcomes in unipolar and bipolar depression. *Sci. Rep.* 10:12831. doi: 10.1038/s41598-020-69776-4

Kishimoto, T., Chawla, J. M., Hagi, K., Zarate, C. A., Kane, J. M., Bauer, M., et al. (2016). Single-dose infusion ketamine and non-ketamine N-methyl-d-aspartate receptor antagonists for unipolar and bipolar depression: a meta-analysis of efficacy, safety and time trajectories. *Psychol. Med.* 46, 1459–1472. doi: 10.1017/S0033291716000064

Knill, D. C., and Pouget, A. (2004). The Bayesian brain: the role of uncertainty in neural coding and computation. *Trends Neurosci.* 27, 712–719. doi: 10.1016/j.tins.2004.10.007

Kosofsky, B. E., Molliver, M. E., Morrison, J. H., and Foote, S. L. (1984). The serotonin and norepinephrine innervation of primary visual cortex in the cynomolgus monkey (*Macaca fascicularis*). *J. Comp. Neurol.* 230, 168–178. doi: 10.1002/cne.902300203

Kotoula, V., Stringaris, A., Mackes, N., Mazibuko, N., Hawkins, P. C. T., Furey, M., et al. (2021). Ketamine modulates the neural Ccorrelates of reward processing in unmedicated patients in remission from depression. *Biol. Psychiatry Cogn. Neurosci. Neuroimaging.* [Epub online ahead of print],. doi: 10.1016/j.bpsc.2021.05.009

Kreitschmann-Andermahr, I., Rosburg, T., Demme, U., Gaser, E., Nowak, H., and Sauer, H. (2001). Effect of ketamine on the neuromagnetic mismatch field in healthy humans. *Cogn. Brain Res.* 12, 109–116. doi: 10.1016/s0926-6410(01)00043-x

Kube, T., Schwarting, R., Rozenkrantz, L., Glombiewski, J. A., and Rief, W. (2020). Distorted cognitive processes in major depression: a predictive processing perspective. *Biol. Psychiatry* 87, 388–398. doi: 10.1016/j.biopsych.2019.07.017

Kumar, P., Goer, F., Murray, L., Dillon, D. G., Beltzer, M. L., Cohen, A. L., et al. (2018). Impaired reward prediction error encoding and striatal-midbrain connectivity in depression. *Neuropsychopharmacology* 43, 1581–1588. doi: 10.1038/s41386-018-0032-x

Leung, S., Croft, R. J., Guille, V., Scholes, K., O'neill, B. V., Phan, K. L., et al. (2009). Acute dopamine and/or serotonin depletion does not modulate mismatch negativity (MMN) in healthy human participants. *Psychopharmacology* 208, 233–244. doi: 10.1007/s00213-009-1723-0

Lewis, D., Campbell, M., Foote, S., Goldstein, M., and Morrison, J. (1987). The distribution of tyrosine hydroxylase-immunoreactive fibers in primate neocortex is widespread but regionally specific. *J. Neurosci.* 7, 279–290. doi: 10.1523/JNEUROSCI.07-01-00279.1987

Loas, G., Lefebvre, G., Rotsaert, M., and Englert, Y. (2018). Relationships between anhedonia, suicidal ideation and suicide attempts in a large sample of physicians. *PLoS One* 13:e0193619. doi: 10.1371/journal.pone.0193619

Lumer, E. D., Edelman, G. M., and Tononi, G. (1997). Neural dynamics in a model of the thalamocortical system. I. Layers, loops and the emergence of fast synchronous rhythms. *Cereb. Cortex* 7, 207–227. doi: 10.1093/cercor/7.3.207

Maeng, S., Zarate, C. A., Du, J., Schloesser, R. J., Mccammon, J., Chen, G., et al. (2008). Cellular mechanisms underlying the antidepressant effects of ketamine: role of α-amino-3-hydroxy-5-methylisoxazole-4-propionic acid receptors. *Biol. Psychiatry* 63, 349–352. doi: 10.1016/j.biopsych.2007.05.028

Manz, K. M., Coleman, B. C., Grueter, C. A., Shields, B. C., Tadross, M. R., and Grueter, B. A. (2021). Noradrenergic signaling disengages feedforward transmission in the nucleus accumbens shell. *J. Neurosci.* 41, 3752–3763. doi: 10.1523/JNEUROSCI.2420-20.2021

Matsumoto, M., and Hikosaka, O. (2007). Lateral habenula as a source of negative reward signals in dopamine neurons. *Nature* 447, 1111–1115. doi: 10.1038/nature05860

Matsumoto, M., and Hikosaka, O. (2009a). Representation of negative motivational value in the primate lateral habenula. *Nat. Neurosci.* 12, 77–84. doi: 10.1038/nn.2233

Matsumoto, M., and Hikosaka, O. (2009b). Two types of dopamine neuron distinctly convey positive and negative motivational signals. *Nature* 459, 837–841. doi: 10.1038/nature08028

McCabe, C., Mishor, Z., Cowen, P. J., and Harmer, C. J. (2010). Diminished neural processing of aversive and rewarding stimuli during selective serotonin

reuptake inhibitor treatment. *Biol. Psychiatry* 67, 439–445. doi: 10.1016/j.biopsych.2009.11.001

Morrison, J. H., and Foote, S. L. (1986). Noradrenergic and serotoninergic innervation of cortical, thalamic, and tectal visual structures in old and new world monkeys. *J. Comp. Neurol.* 243, 117–138. doi: 10.1002/cne.902430110

Morrison, J. H., Foote, S. L., O'connor, D., and Bloom, F. E. (1982). Laminar, tangential and regional organization of the noradrenergic innervation of monkey cortex: dopamine-β-hydroxylase immunohistochemistry. *Brain Res. Bull.* 9, 309–319. doi: 10.1016/0361-9230(82)90144-7

Mu, Z., Chang, Y., Xu, J., Pang, X., Zhang, H., Liu, X., et al. (2016). Pre-attentive dysfunction of musical processing in major depressive disorder: a mismatch negativity study. *J. Affect. Disord.* 194, 50–56. doi: 10.1016/j.jad.2016.01.028

Näätänen, R., Kujala, T., Escera, C., Baldeweg, T., Kreegipuu, K., Carlson, S., et al. (2012). The mismatch negativity (MMN) – A unique window to disturbed central auditory processing in ageing and different clinical conditions. *Clin. Neurophysiol.* 123, 424–458. doi: 10.1016/j.clinph.2011.09.020

Nielson, D. M., Keren, H., O'callaghan, G., Jackson, S. M., Douka, I., Vidal-Ribas, P., et al. (2021). Great expectations: a critical review of and suggestions for the study of reward processing as a cause and predictor of depression. *Biol. Psychiatry* 89, 134–143. doi: 10.1016/j.biopsych.2020.06.012

Niv, Y., and Montague, P. R. (2009). "Chapter 22 - Theoretical and empirical studies of learning," in *Neuroeconomics*, eds P. W. Glimcher, C. F. Camerer, E. Fehr, and R. A. Poldrack (London: Academic Press), 331–351.

Oranje, B., Jensen, K., Wienberg, M., and Glenthøj, B. Y. (2008). Divergent effects of increased serotonergic activity on psychophysiological parameters of human attention. *Int. J. Neuropsychopharmacol.* 11, 453–463. doi: 10.1017/S1461145707008176

O'Reilly, J. X., Jbabdi, S., and Behrens, T. E. J. (2012). How can a Bayesian approach inform neuroscience? *Eur J. Neurosci.* 35, 1169–1179. doi: 10.1111/j.1460-9568.2012.08010.x

Ossewaarde, L., Verkes, R. J., Hermans, E. J., Kooijman, S. C., Urner, M., Tendolkar, I., et al. (2011). Two-Week administration of the combined serotonin-noradrenaline reuptake inhibitor duloxetine augments functioning of mesolimbic incentive processing circuits. *Biol. Psychiatry* 70, 568–574. doi: 10.1016/j.biopsych.2011.03.041

Pizzagalli, D. A. (2014). Depression, stress, and anhedonia: toward a synthesis and integrated model. *Annu. Rev. Clin. Psychol.* 10, 393–423. doi: 10.1146/annurev-clinpsy-050212-185606

Qiao, Z., Yu, Y., Wang, L., Yang, X., Qiu, X., Zhang, C., et al. (2013). Impaired pre-attentive change detection in major depressive disorder patients revealed by auditory mismatch negativity. *Psychiatry Res.* 211, 78–84. doi: 10.1016/j.pscychresns.2012.07.006

Qiu, X., Yang, X., Qiao, Z., Wang, L., Ning, N., Shi, J., et al. (2011). Impairment in processing visual information at the pre-attentive stage in patients with a major depressive disorder: a visual mismatch negativity study. *Neurosci. Lett.* 491, 53–57. doi: 10.1016/j.neulet.2011.01.006

Quitkin, F. M., Rabkin, J. G., Ross, D., and Stewart, J. W. (1984). Identification of true drug response to antidepressants: use of pattern analysis. *Arch. Gen. Psychiatry* 41, 782–786. doi: 10.1001/archpsyc.1984.01790190056007

Rao, R. P. N., and Ballard, D. H. (1999). Predictive coding in the visual cortex: a functional interpretation of some extra-classical receptive-field effects. *Nat. Neurosci.* 2, 79–87. doi: 10.1038/4580

Restuccia, D., Marca, G. D., Valeriani, M., Leggio, M. G., and Molinari, M. (2006). Cerebellar damage impairs detection of somatosensory input changes. A somatosensory mismatch-negativity study. *Brain* 130, 276–287. doi: 10.1093/brain/awl236

Rosburg, T., and Kreitschmann-Andermahr, I. (2016). The effects of ketamine on the mismatch negativity (MMN) in humans – A meta-analysis. *Clin. Neurophysiol.* 127, 1387–1394. doi: 10.1016/j.clinph.2015.10.062

Rothkirch, M., Tonn, J., Köhler, S., and Sterzer, P. (2017). Neural mechanisms of reinforcement learning in unmedicated patients with major depressive disorder. *Brain* 140, 1147–1157. doi: 10.1093/brain/awx025

Rouhani, N., and Niv, Y. (2019). Depressive symptoms bias the prediction-error enhancement of memory towards negative events in reinforcement learning. *Psychopharmacology* 236, 2425–2435. doi: 10.1007/s00213-019-05322-z

Rutledge, R. B., Moutoussis, M., Smittenaar, P., Zeidman, P., Taylor, T., Hrynkiewicz, L., et al. (2017). Association of neural and emotional impacts of reward prediction errors with major depression. *JAMA Psychiatry* 74, 790–797. doi: 10.1001/jamapsychiatry.2017.1713

Salgado, H., Treviño, M., and Atzori, M. (2016). Layer- and area-specific actions of norepinephrine on cortical synaptic transmission. *Brain Res* 1641, 163–176. doi: 10.1016/j.brainres.2016.01.033

Sara, S. J., and Bouret, S. (2012). Orienting and reorienting: the locus Coeruleus mediates cognition through arousal. *Neuron* 76, 130–141. doi: 10.1016/j.neuron.2012.09.011

Schröger, E. (1998). Measurement and interpretation of the mismatch negativity. *Behav. Res. Methods Instrum. Comput.* 30, 131–145.

Schultz, W. (2006). Behavioral theories and the neurophysiology of reward. *Annu. Rev. Psychol.* 57, 87–115. doi: 10.1146/annurev.psych.56.091103.070229

Schultz, W. (2007). Multiple dopamine functions at different time courses. *Annu. Rev. Neurosci.* 30, 259–288. doi: 10.1146/annurev.neuro.28.061604.135722

Schultz, W. (2016b). Dopamine reward prediction-error signalling: a two-component response. *Nat. Rev. Neurosci.* 17, 183–195. doi: 10.1038/nrn.2015.26

Schultz, W. (2016a). Dopamine reward prediction error coding. *Dialogues Clin. Neurosci.* 18, 23–32. doi: 10.31887/DCNS.2016.18.1/wschultz

Schultz, W., Dayan, P., and Montague, P. R. (1997). A neural substrate of prediction and reward. *Science* 275, 1593–1599. doi: 10.1126/science.275.5306.1593

Self, M. W., Kooijmans, R. N., Supèr, H., Lamme, V. A., and Roelfsema, P. R. (2012). Different glutamate receptors convey feedforward and recurrent processing in macaque V1. *Proc. Natl. Acad. Sci. U.S.A.* 109, 11031–11036. doi: 10.1073/pnas.1119527109

Seth, A. K. (2013). Interoceptive inference, emotion, and the embodied self. *Trends Cogn. Sci.* 17, 565–573. doi: 10.1016/j.tics.2013.09.007

Seth, A. K., and Friston, K. J. (2016). Active interoceptive inference and the emotional brain. *Philos. Trans. R. Soc. Lond. B Biol. Sci.* 371:20160007. doi: 10.1098/rstb.2016.0007

Shipp, S., Adams, R. A., and Friston, K. J. (2013). Reflections on agranular architecture: predictive coding in the motor cortex. *Trends Neurosci.*36, 706–716. doi: 10.1016/j.tins.2013.09.004

Shumake, J., Ilango, A., Scheich, H., Wetzel, W., and Ohl, F. W. (2010). Differential neuromodulation of acquisition and retrieval of avoidance learning by the lateral habenula and ventral tegmental area. *J. Neurosci.* 30, 5876–5883. doi: 10.1523/JNEUROSCI.3604-09.2010

Spijker, J., De Graaf, R., Ten Have, M., Nolen, W. A., and Speckens, A. (2010). Predictors of suicidality in depressive spectrum disorders in the general population: results of the Netherlands Mental Health Survey and Incidence Study. *Soc. Psychiatry Psychiatr. Epidemiol.* 45, 513–521. doi: 10.1007/s00127-009-0093-6

Stephan, K. E., Manjaly, Z. M., Mathys, C. D., Weber, L. A. E., Paliwal, S., Gard, T., et al. (2016). Allostatic self-efficacy: a metacognitive theory of dyshomeostasis-induced fatigue and depression. *Front. Hum. Neurosci.* 10:550. doi: 10.3389/fnhum.2016.00550

Sterpenich, V., Vidal, S., Hofmeister, J., Michalopoulos, G., Bancila, V., Warrot, D., et al. (2019). Increased reactivity of the mesolimbic reward system after ketamine injection in patients with treatment-resistant major depressive disorder. *Anesthesiology* 130, 923–935. doi: 10.1097/ALN.0000000000002667

Sumner, R. L., Mcmillan, R., Spriggs, M. J., Campbell, D., Malpas, G., Maxwell, E., et al. (2020). Ketamine improves short-term plasticity in depression by enhancing sensitivity to prediction errors. *Eur. Neuropsychopharmacol.* 38, 73–85. doi: 10.1016/j.euroneuro.2020.07.009

Takei, Y., Kumano, S., Hattori, S., Uehara, T., Kawakubo, Y., Kasai, K., et al. (2009). Preattentive dysfunction in major depression: a magnetoencephalography study using auditory mismatch negativity. *Psychophysiology* 46, 52–61. doi: 10.1111/j.1469-8986.2008.00748.x

Tseng, Y.-J., Nouchi, R., and Cheng, C.-H. (2021). Mismatch negativity in patients with major depressive disorder: a meta-analysis. *Clin. Neurophysiol.* 132, 2654–2665. doi: 10.1016/j.clinph.2021.06.019

Umbricht, D., Schmid, L., Koller, R., Vollenweider, F. X., Hell, D., and Javitt, D. C. (2000). Ketamine-induced deficits in auditory and visual context-cependent processing in healthy volunteers: implications for models of cognitive deficits in schizophrenia. *Arch. Gen. Psychiatry* 57, 1139–1147. doi: 10.1001/archpsyc.57.12.1139

Vaillancourt, D. E., Schonfeld, D., Kwak, Y., Bohnen, N. I., and Seidler, R. (2013). Dopamine overdose hypothesis: evidence and clinical implications. *Mov. Disord.* 28, 1920–1929. doi: 10.1002/mds.25687

van Donkelaar, E. L., Blokland, A., Ferrington, L., Kelly, P. A. T., Steinbusch, H. W. M., and Prickaerts, J. (2011). Mechanism of acute tryptophan depletion: is it only serotonin? *Mol. Psychiatry* 16, 695–713. doi: 10.1038/mp.2011.9

Varazzani, C., San-Galli, A., Gilardeau, S., and Bouret, S. (2015). Noradrenaline and dopamine neurons in the reward/effort trade-off: a direct electrophysiological comparison in behaving monkeys. *J. Neurosci.* 35, 7866–7877.

Vrieze, E., Demyttenaere, K., Bruffaerts, R., Hermans, D., Pizzagalli, D. A., Sienaert, P., et al. (2014). Dimensions in major depressive disorder and their relevance for treatment outcome. *J. Affect. Disord.* 155, 35–41. doi: 10.1016/j.jad.2013.10.020

Webber, H. E., Lopez-Gamundi, P., Stamatovich, S. N., De Wit, H., and Wardle, M. C. (2021). Using pharmacological manipulations to study the role of dopamine in human reward functioning: a review of studies in healthy adults. *Neurosci. Biobehav. Rev.* 120, 123–158. doi: 10.1016/j.neubiorev.2020.11.004

Wienberg, M., Glenthoj, B., Jensen, K., and Oranje, B. (2010). A single high dose of escitalopram increases mismatch negativity without affecting processing negativity or P300 amplitude in healthy volunteers. *J. Psychopharmacol.* 24, 1183–1192. doi: 10.1177/0269881109102606

Wilson, M. A., and Molliver, M. E. (1991a). The organization of serotonergic projections to cerebral cortex in primates: regional distribution of axon terminals. *Neuroscience* 44, 537–553. doi: 10.1016/0306-4522(91)90076-z

Wilson, M. A., and Molliver, M. E. (1991b). The organization of serotonergic projections to cerebral cortex in primates: retrograde transport studies. *Neuroscience* 44, 555–570. doi: 10.1016/0306-4522(91)90077-2

Winer, E. S., Drapeau, C. W., Veilleux, J. C., and Nadorff, M. R. (2016). The association between anhedonia, suicidal ideation, and suicide attempts in a large student sample. *Arch. Suicide Res.* 20, 265–272. doi: 10.1080/13811118.2015.1025119

Yang, Y., Wang, H., Hu, J., and Hu, H. (2018b). Lateral habenula in the pathophysiology of depression. *Curr. Opin. Neurobiol.* 48, 90–96. doi: 10.1016/j.conb.2017.10.024

Yang, Y., Cui, Y., Sang, K., Dong, Y., Ni, Z., Ma, S., et al. (2018a). Ketamine blocks bursting in the lateral habenula to rapidly relieve depression. *Nature* 554, 317–322. doi: 10.1038/nature25509

Yaple, Z. A., Tolomeo, S., and Yu, R. (2021). Abnormal prediction error processing in schizophrenia and depression. *Hum. Brain Mapp.* 42, 3547–3560. doi: 10.1002/hbm.25453

Yaseen, Z. S., Galynker, I. I., Briggs, J., Freed, R. D., and Gabbay, V. (2016). Functional domains as correlates of suicidality among psychiatric inpatients. *J. Affect. Disord.* 203, 77–83. doi: 10.1016/j.jad.2016.05.066

Yüksel, C., and Öngür, D. (2010). Magnetic resonance spectroscopy studies of glutamate-related abnormalities in mood disorders. *Biol. Psychiatry* 68, 785–794. doi: 10.1016/j.biopsych.2010.06.016

Zanos, P., Moaddel, R., Morris, P. J., Georgiou, P., Fischell, J., Elmer, G. I., et al. (2016). NMDAR inhibition-independent antidepressant actions of ketamine metabolites. *Nature* 533, 481–486. doi: 10.1038/nature17998

Zarate, C. A. Jr., Singh, J. B., Carlson, P. J., Brutsche, N. E., Ameli, R., Luckenbaugh, D. A., et al. (2006). A randomized trial of an N-methyl-D-aspartate antagonist in treatment-resistant major depression. *Arch. Gen. Psychiatry* 63, 856–864. doi: 10.1001/archpsyc.63.8.856

Zhang, W.-N., Chang, S.-H., Guo, L.-Y., Zhang, K.-L., and Wang, J. (2013). The neural correlates of reward-related processing in major depressive disorder: a meta-analysis of functional magnetic resonance imaging studies. *J. Affect. Disord.* 151, 531–539. doi: 10.1016/j.jad.2013.06.039

Conflict of Interest: CZ was listed as a co-inventor on a patent for the use of ketamine in major depression and suicidal ideation; as a co-inventor on a patent for the use of (2R,6R)-hydroxynorketamine, (S)-dehydronorketamine, and other stereoisomeric dehydroxylated and hydroxylated metabolites of (R,S)-ketamine metabolites in the treatment of depression and neuropathic pain; and as a co-inventor on a patent application for the use of (2R,6R)-hydroxynorketamine and (2S,6S)-hydroxynorketamine in the treatment of depression, anxiety, anhedonia, suicidal ideation, and post-traumatic stress disorders. He has assigned his patent rights to the U.S. Government but will share a percentage of any royalties that may be received by the government.

The remaining author declares that the research was conducted in the absence of any commercial or financial relationships that could be construed as a potential conflict of interest.

Publisher's Note: All claims expressed in this article are solely those of the authors and do not necessarily represent those of their affiliated organizations, or those of the publisher, the editors and the reviewers. Any product that may be evaluated in this article, or claim that may be made by its manufacturer, is not guaranteed or endorsed by the publisher.

Advantages of publishing in Frontiers

OPEN ACCESS
Articles are free to read for greatest visibility and readership

FAST PUBLICATION
Around 90 days from submission to decision

HIGH QUALITY PEER-REVIEW
Rigorous, collaborative, and constructive peer-review

TRANSPARENT PEER-REVIEW
Editors and reviewers acknowledged by name on published articles

Frontiers
Avenue du Tribunal-Fédéral 34
1005 Lausanne | Switzerland

Visit us: www.frontiersin.org
Contact us: frontiersin.org/about/contact

REPRODUCIBILITY OF RESEARCH
Support open data and methods to enhance research reproducibility

DIGITAL PUBLISHING
Articles designed for optimal readership across devices

FOLLOW US
@frontiersin

IMPACT METRICS
Advanced article metrics track visibility across digital media

EXTENSIVE PROMOTION
Marketing and promotion of impactful research

LOOP RESEARCH NETWORK
Our network increases your article's readership